

## Construction and performance characterisation of the low-cost regenerators for travelling-wave thermoacoustic engines

Abdulrahman (Sayed) ABDULJALIL<sup>a</sup>, Zhibin YU<sup>a</sup>  
and Artur J. JAWORSKI<sup>a,\*</sup>

In a travelling wave thermoacoustic device, the regenerator sandwiched between a pair of (hot and cold) heat exchangers constitutes the so-called thermoacoustic core, where the thermoacoustic energy conversion from heat to acoustic power takes place. The temperature gradient along the regenerator caused by the two heat exchanges excites and maintains the acoustic wave in the resonator. The devices are called “travelling wave” because the phase angle difference between the pressure and velocity oscillation is close to zero in the regenerator. The regenerator is typically made of tortuous materials such as wire mesh screens, randomly packed spheres, porous ceramics and others. The flow and heat transfer processes taking place within these random geometries, are not well understood.

This paper presents the construction and testing of two new types of low-cost regenerators, which are made of steel wool and metal foam, respectively. The steel wool is uniformly pressed into a purpose built thin-walled “can” with carefully selected pressure to obtain the required porosity and equivalent hydraulic radius. The metal foam (see figure 1) can be carefully cut and also fits into the regenerator “can”. These regenerators are initially tested in a steady air flow in order to estimate their porosity, the pressure drop and the viscous dissipation. Subsequently, they are installed in a looped-tube travelling-wave thermoacoustic engine to test their performance. In addition, a more conventional ceramic regenerator of a regular geometry (with several hundred of square pores, see figure 2) is also tested to serve as a benchmark for the two low-cost regenerators. The testing includes the onset temperature difference (minimum temperature difference required to start the acoustic oscillation in an engine), the acoustic power output, thermal efficiency and the temperature profile along the regenerator. The detailed comparison will be presented.

<sup>a</sup> School of MACE, University of Manchester, PO BOX 88, Manchester M60 1QD, UK

\* Corresponding author, e-mail: [a.jaworski@manchester.ac.uk](mailto:a.jaworski@manchester.ac.uk); Tel: 01612754352; Fax: 08701307474



Figure 1 Metal foam regenerator



Figure 2 Ceramic regenerator

**When red blood cells tumble, swing and roll !**

Manouk Abkarian<sup>a</sup>, Magalie Faivre<sup>b</sup>, Annie Viallat<sup>b</sup>

We reveal that under moderate shear stresses ( $\sim 0.1$  Pa) red blood cells present an oscillation of their inclination («swinging») superimposed to the long-observed steady tanktreading motion<sup>1</sup>. A simple model based on a fluid ellipsoid surrounded by a viscoelastic membrane initially unstrained (shape memory) predicts all observed features of the movement, including swing characteristics (magnitude and period of cell inclination) and the critical shear stress of the transition towards the solid-like tumbling motion. Finally, we observe that the tumbling movement itself is unstable in time for shear stresses lower but close to the swinging transition. The axis of symmetry of the cells drifts towards the direction of the flow vorticity in time and faster for higher shear stresses, driving the cells in a typical stable «rolling» movement.

---

<sup>a</sup> laboratoire des Colloïdes Verres et Nanomatériaux, UMR 5587 CNRS/U. Montpellier II.

<sup>b</sup> Laboratoire Adhésion et inflammation, INSERM U600/ CNRS UMR 6212/ U. Méditerranée.

<sup>1</sup> M. Abkarian, M. Faivre and A. Viallat, *Phys. Rev. Lett.* **98(18)**: Art. No 188302 (2007).



## Dispersion of Four-Heavy-Particle Sets in Turbulent Flow using Kinematic Simulation

A. Abou El-Azm Aly\* and F. Nicolleau

We study the dispersion of four-heavy-heavy particle clusters (tetrahedron) in an isotropic and incompressible three-dimensional turbulent flow. The turbulent velocity field is generated using kinematic simulation, KS, which allows us to vary the inertial-range and to reach large values of the Reynolds number. We study the time evolution of the parameters characterizing the geometry, size and shape of the tetrahedron. Different initial separations between particles, inertial-ranges, Stokes numbers and particle drift velocities were considered. We found that the Reynolds number has no effect on the shape evolution of the tetrahedron provided that the initial distance between the particle is larger than the Kolmogorov length scale.

In figure 1 and 2, all the curves of  $\langle V \rangle$  and  $\langle I_2^{th} \rangle$  for a constant value of  $\Delta_0/L_1 = 0.032$  and  $\Delta_0/L_1 = 0.5$  approximately collapse for the different Reynolds numbers. This result was obtained for the same case of four-particle sets in diffusion, we can extend it to the four-heavy-particle set dispersion for Stokes numbers in the range of  $0.2 \leq St \leq 1$  at a zero drift velocity and drift velocities in the range  $0.2 \leq \gamma \leq 2$  at Stokes number  $St = 0.02$  and 2 for inertial ranges  $185 \leq k_N/k_1 \leq 2000$ .

\*Department of Mechanical Engineering, The University of Sheffield, Sheffield, United Kingdom.

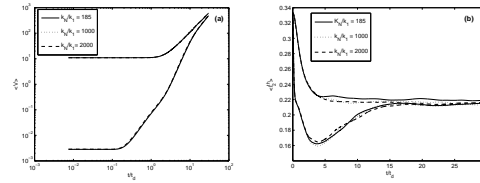


Figure 1: (a) Time evolution of the tetrahedron volume  $\langle V \rangle$ , (b) the tetrahedron shape factor  $\langle I_2^{th} \rangle$ , for an initial separation from top  $\Delta_0/L_1 = 0.5$  and bottom  $\Delta_0/L_1 = 0.032$ ,  $St=1$  and different Reynolds numbers.

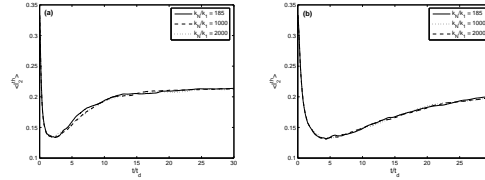


Figure 2: Time evolution of the tetrahedron shape factor  $\langle I_2^{th} \rangle$ , for an initial separation  $\Delta_0/L_1 = 0.032$  and (a)  $\gamma = 0.2$  (b)  $\gamma = 1$ , for different Reynolds numbers.

### Vibration and bounding wall structure effects on a flow in nano-channels

**Abramyan A.K.<sup>1</sup>, Mirantsev L.V<sup>2</sup>**

The results of molecular dynamics simulations of a fluid flow in flat nano - channels of the width  $\sim 10$  molecular diameters with vibrating walls has been presented. Both cases of crystalline and amorphous walls are considered. It is shown that these vibrations could have an essential influence on the structure and behaviour of the fluid in the nano – channels. The amorphous layer wall oscillations caused only the channel width changes (reduction and expanding) and the correspondent fluid density changes. No qualitative fluid structure changes were observed. The vibrations of the walls with crystalline structure strongly enhance a positional order in the fluid and give rise to a significant decrease in the fluid flow rate. It was found that in the first case (when the channel width reduces) the average flow rate in the channel 4.7 times less than it was in the channel with fixed walls, whereas in the second case (the channel width expands) the flow rate was 5.08 times more in comparison with the fixed wall channel. Whereas at the oscillations causing the channel width expansion the translation order attenuates at least in one of the near wall layers and the effective viscosity of the fluid contained in the channel decreases. Thus, switching from one type of the nano-channel wall oscillation to another the average flow rate in the channel can be changed by a factor of 20. Cases of the regularly located roughness and the irregular roughness have been studied. A fluid shear flow caused by a bounding wall steady motion parallel to the fixed wall in a flat nano-channel (Couette flow) has been investigated. For the case when the solid wall atoms are located at sites of the face-centered cubic crystal lattice and for disordered arrangement of these atoms (amorphous structure of the solid wall), the flow velocity profiles and the shearing tension acting on the walls at various temperatures and distances between them have been obtained. It has been shown that obtained flow velocity profiles and shearing tensions as well as the calculated values of effective fluid viscosity in the nano-channel are strongly dependent on the structure of its solid bounding walls. Corresponding values for the fluid effective viscosities at the Couette flow in the amorphous wall nano-channel are the following  $\eta = 7.3 \times 10^{-3} \text{ gcm}^{-1}\text{sec}^{-1}$  (at  $T^* = 2$ ) and  $\eta = 1.1 \times 10^{-2} \text{ gcm}^{-1}\text{sec}^{-1}$  (at  $T^* = 1.5$ ), and at the flow in the similar channel with crystal structure walls  $\eta = 1.1 \times 10^{-2} \text{ gcm}^{-1}\text{sec}^{-1}$  (at  $T^* = 2$ ) and  $\eta = 3.4 \times 10^{-2} \text{ gcm}^{-1}\text{sec}^{-1}$  (at  $T^* = 1.5$ ). The obtained values of viscosities are comparable with those that can be found in the literature. For example, the water viscosity at the room temperature  $\eta \approx 10^{-2} \text{ gcm}^{-1}\text{sec}^{-1}$

---

<sup>a</sup> <sup>b</sup> Institute of Problems of Mechanical Engineering RAS, V.O. Bolshoi 61, 199178, St. Petersburg, Russia

## Motion of an elliptic vortex ring

D. Adhikari<sup>a</sup> and T. T. Lim<sup>a</sup>

An elliptic vortex ring is known to be an unstable vortex ring due to its oscillatory deformation while propagating. In addition, a high aspect ratio elliptic vortex ring is known to deform to the point where the vortex ring breaks up into two smaller vortex rings. This inherent instability in the elliptic vortex ring hastens the onset of turbulence as compared to a circular vortex ring. Because of this, elliptic nozzle or orifice has been used in many applications to promote mixing in the fluid. While both theoretical and experimental studies of elliptic vortex rings have been conducted previously<sup>1,2</sup>, the behaviour of the vortex core during the deformation of the elliptic vortex ring remains unclear. Moreover, most of the experimental studies were conducted using flow visualization technique, which although gives useful visual information about the vortex core, do not provide any quantitative information about the velocity and vorticity fields.

In the present investigation, we focus our attention on the vorticity field during various stages of the vortex ring deformation. In particular, we are interested to find out whether the vortex core undergoes both stretching and compression during deformation. Experiments will be conducted in a water tank using elliptic nozzle of aspect ratios 1, 2 and 3. Obviously, the nozzle of aspect ratio of 1 represents a circular tube, and the results are included here for the purpose of comparison. The water tank is a modified version of the one used by Lim (1997)<sup>3</sup>, and the vortex ring generator consists of piston sliding inside a matching Plexiglas tube. When the piston is given an impulsive push, a slug of fluid ejects from the nozzle and rolls up to form a vortex ring. Both flow visualization and DPIV measurements will be conducted. The DPIV setup consists of a Nd-YAG pulsed laser (New Wave Solo PIV) as the illumination source and a Kodak Megaplug CCD camera (model ES 4.0, 2048 pixels x 2048 pixels) to capture the image data. Dantec® FlowMap adaptive cross correlation DPIV algorithm will be used to analyze the captured flow images.

---

<sup>a</sup> Department of Mechanical Engineering, National University of Singapore

<sup>1</sup> M.R. Dhanak & B.D. Bernardinis, *J. Fluid Mech.* **109**, 189 (1981)

<sup>2</sup> F. Hussain & H.S. Husain, *J. Fluid Mech.* **208**, 257 (1989)

<sup>3</sup> T.T. Lim, *Fluid Dyn. Res.* **21**, 47 (1997).

**Analysis of the potential risk associated to glowing embers in prescribed burning of felling debris in stands of hazel (*Corylus avellana*)**

E. Planas<sup>a</sup>, A. Àgueda<sup>a</sup>, M. Miralles<sup>b</sup>, E. Pastor<sup>a</sup> and Y. Pérez<sup>a</sup>

Many prescribed burnings of felling debris are executed each year either by fire-fighters or by agricultural workers. Usually they follow a burning protocol in order to assure that the residual glowing embers will not be able to start a fire during the next hours. However, from time to time, these prescribed burnings are the origin of forest fires.

The purpose of the work presented in this paper is to analyse the conditions — after the extinction procedure has been applied— that can lead the glowing embers to keep temperature high enough and sustained during a period of time (72 h) large enough, giving thus a potential threat of ignition of a new fire in the vicinity.

An analysis of the main variables affecting the glowing combustion has been done and a set of experimental tests has been conducted burning several piles of felling debris of stands of hazel (*Corylus avellana*). These tests have been performed in close collaboration with a specialized group of the Catalan fire-fighters (GRAF), in order to try diverse extinction procedures which could affect the behaviour of the residual glowing embers. Every pile burned was monitored during 72 hours using thermocouples and an infrared camera. Moreover, after 72 hours, an induced wind was created in some of the piles which still maintained high temperatures, in order to see the effect of wind on the combustion reactivation and also the potential distances reached by the embers swept along by the wind.

The results show that depending on the type of extinction applied and under certain situations, the piles can be revived in the presence of moderate winds and the glowing embers can reach considerable distances allowing the possibility of secondary fires, even 72 hours after extinction.

---

<sup>a</sup> Centre d'Estudis del Risc Tecnològic (CERTEC), Universitat Politècnica de Catalunya

<sup>b</sup> Grup de Recolzament d'Actuacions Forestals (GRAF), Direcció General de Prevenció, Extinció d'incendis i Salvaments, Departament d'Interior, Generalitat de Catalunya

## A fluid mechanical analysis of platelet aggregation in the thrombosis test tube

Takeshi Akinaga<sup>a</sup>, Masako Sugihara-Seki<sup>a</sup>,  
Tomoaki Itano<sup>a</sup> and Junichiro Yamamoto<sup>b</sup>

Platelets play a pivotal role in arterial thrombogenesis. A new instrument called the Görög Thrombosis Test (GTT) was designed to measure sequentially shear-induced platelet reactivity and thrombolysis from a non-anticoagulated blood sample. The test tube consists of a conical plastic tube and two perfectly round steel balls inside (Fig. 1). Flat thin spacers are placed between the inner surface of the conical tube and the round balls, so that there are narrow gaps between them. When a native blood is added to the tube, it flows downward due to the gravity, passes through the narrow gaps where high shear occurs, and exits in droplets into an adjacent collecting tube. The measurements of the time interval of sequential droplets allow to detect the reduction and arrest of the blood flow, which occurs probably due to the activation, aggregation and stabilized thrombus formation by shear-activated platelets.

As a basis to understand the initial mechanism of the platelet aggregation in the GTT tube, we have computed numerically the fluid flow through the tube and traced the trajectories of platelets which are evenly distributed upstream. At each instance, we calculated the distances between all adjacent platelets and examined the pairs of platelets whose distances are within 3.0  $\mu\text{m}$ . Since the size of the platelet is about 3.0  $\mu\text{m}$ , these pairs are expected to have a possibility to collide each other and form aggregations. A representative example of our results is shown in figure 2, which depicts the sites of possible formation of the platelet aggregation.

<sup>a</sup> Faculty of Physics, Kansai University.

<sup>b</sup> Faculty of Nutrition, Kobe Gakuin University.

<sup>1</sup> Yamamoto J. et al., *Blood Coagulation and Fibrinolysis* **14**, 31 (2003).

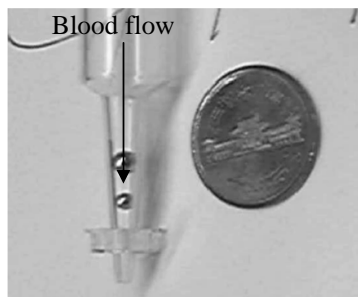


Figure 1: GTT tube compared with a 23mm diameter coin

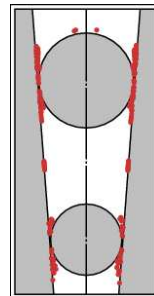


Figure 2: The sites of possible formation of the platelet aggregation are shown by red circles.

### The 3D structure of a dipole in shallow layers of fluid

R.A.D. Akkermans\*, L.P.J. Kamp\*, H.J.H Clercx\* and G.J.F. van Heijst\*

The canonical laboratory set-up to study two-dimensional (2D) turbulence is the electromagnetically driven shallow one- or two-fluid layer. The argument used here is that whenever the vertical length scale is much smaller than the horizontal length scale the flow is presumed to behave in a 2D fashion. However, this assumption disregards the presence of a strong non-uniform magnetic field used to electromagnetically force the flow, a vertical component of the Lorentz force, and, most importantly, it oversimplifies the structure of 3D recirculating flows.

We will address the above mentioned issues with an experimental and numerical study of one of the most elementary coherent structures found in 2D turbulence, the dipolar vortex. Stereoscopic-PIV measurements reveal the surprisingly persistent three-dimensionality of the shallow fluid layer flow, even when the forcing has been stopped (and the non-uniform magnetic field is inactive), and the remarkably complex 3D structure of the evolving dipole (see Fig. 1). Our 3D simulations reveal that these structures owe their existence not to friction with a no-slip bottom, not to free-surface deformations, nor to three-dimensionality introduced during the forcing phase but to the vertical confinement of the flow.

Complementary simulations on two-fluid layers show that the structures emerging in the post-forcing phase qualitatively show the same features as observed in our one-layer experiment.

Furthermore, we studied the tendency of relaxation towards a Poiseuille-like profile in the vertical direction, for the one- and two-fluid layers. It follows that these shallow flows do not relax to a Poiseuille-like profile on time scales that are relevant for experimental investigations on quasi-two-dimensional dipolar flows.

---

\*JM Burgerscentre & Fluid Dynamics Laboratory, Dept. of Applied Physics, Eindhoven University of Technology, P.O. Box 513, 5600 MB Eindhoven, Netherlands.

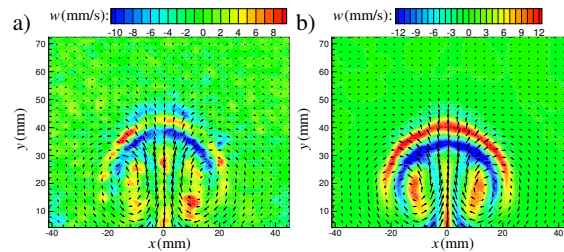


Figure 1: Experimentally (a) and numerically (b) obtained velocity fields after forcing phase of a dipolar vortex at mid-depth (vectors: horizontal velocity, colors: vertical velocity).

## Linear stability, transient growth and the role of viscosity stratification in compressible plane Couette flow

Meheboob Alam\*, M. Malik† and J. Dey‡

Both temporal<sup>1</sup> and spatial<sup>2</sup> linear stability characteristics, along with the non-modal transient energy growth, are investigated for compressible plane Couette flow with three-dimensional disturbances. The steady mean flow is characterized by a non-uniform shear-rate and a varying temperature-field across the wall-normal direction for a perfect gas with Sutherland's viscosity model. This flow is known to be linearly unstable to acoustic modes for a range of supersonic Mach numbers ( $M$ ). The dominant instability belongs to the “mode I” and “mode II” at low and moderate-to-high Mach numbers ( $M$ ), respectively. The inviscid spatial problem has been analysed by solving the compressible Rayleigh equation. A leading order viscous correction to the inviscid solution reveals that the neutral and unstable modes are destabilized by the no-slip enforced by viscosity. An analysis of perturbation energy reveals that the instability is primarily caused by an excess transfer of energy from mean-flow to perturbations. It is shown that the energy-transfer from mean-flow occurs close to the moving top-wall for “mode I” instability, whereas it occurs in the bulk of the flow domain for “mode II”.

For the transient growth analysis, the maximum amplification of perturbation energy over time,  $G_{\max}$ , is found to increase with increasing Reynolds number  $Re$ , but decreases with increasing Mach number  $M$ . This decrease of transient growth with increasing Mach number is shown to be tied to the decrease in the energy transferred from the mean flow which is tied to the sharp decay of “viscous” eigenfunctions with increasing  $M$ . In contrast to incompressible shear flows, we found that the streamwise-independent modes ( $\alpha = 0$ ) in the present flow *do not* follow the well-known scaling law:  $G(t/Re) \sim Re^2$ . It is shown that the linear stability operator can be partitioned into  $\mathcal{L} \sim \tilde{\mathcal{L}} + Re^2 \mathcal{L}_p$  under the Mack-transformation, and the dominance of the  $Re$ -dependent operator  $\mathcal{L}_p$  is shown to be responsible for the *invalidity* of the above quadratic scaling-law in compressible Couette flow. While the pure streamwise vortices are the optimal patterns at high Mach numbers (in contrast to incompressible Couette flow), the modulated streamwise vortices are the optimal patterns for low-to-moderate values of the Mach number. A reduced inviscid model, based on Ellingsen-Palm-type solution, has been shown to capture all salient features of transient energy growth of full viscous problem.

Lastly, the effect of *viscosity stratification*<sup>3</sup> on predicted instabilities is probed by considering two prototype mean flows: (a) the *uniform shear* flow with constant viscosity, and (b) the *non-uniform shear* flow with *stratified* viscosity. For both modal and non-modal instability, it is shown that the viscosity-stratification of the underlying mean flow would lead to a ‘delayed’ transition in compressible Couette flow.

---

\*Engineering Mechanics Unit, Jawaharlal Nehru Center, Bangalore 560064, India

†Department of Aerospace Engineering, IISc, Bangalore 560012, India

<sup>1</sup>Malik et al., *Phys. Fluids* **18**, 034103 (2006).

<sup>2</sup>Malik et al., *Phys. Fluids* (2008, under review).

<sup>3</sup>Malik et al., *Phys. Rev. E* **77** (2008, In press).

## Turbulent Flows over Rough Walls

M. Amir<sup>a</sup> and I.P. Castro<sup>a</sup>

Turbulent flows over smooth surfaces have been studied extensively for a long time but, despite their practical importance, less is known for flows over rough surfaces. It is commonly assumed that the wall roughness is a local effect that only affects the inner layer up to a distance of about 4 to 5 roughness heights. There is increasing evidence that this is not always true (e.g. Krogstad<sup>1</sup>) and, clearly, for sufficiently large surface protruberances it is intuitively most likely. There has never been a concerted effort to explore under what precise circumstances this 'classical' view is inadequate and what are then the distinguishing differences between the rough-surface and smooth-surface flow, for both external flows (boundary layers) and internal flows (pipes & channels). The purpose of the present study is therefore, to explore the limiting roughness height where outer layer similarity holds. Some initial remarks on the mean flow over many kinds of surface have already been published<sup>2</sup>.

The present experiments were conducted in a 'suck-down' wind tunnel whose working section is rectangular (0.6 x 0.9 m) and 4.5 m in length. The rough surface consisted of sixteen 5-mm elements having five different heights chosen from a normal distribution with a mean and standard deviation of 5 mm and 1.5 mm respectively. This roughness covered the entire floor of the wind tunnel and measurements were made using LDA. Data were obtained using a two-component Dantec fibre-optic probe mounted outside the tunnel at various locations downstream of the leading edge of the roughness and at various free-stream speeds. This led to a wide range of momentum thickness Reynolds numbers ( $1300 < Re_0 < 22000$ ). A wide range of the ratio of roughness element height to boundary-layer depth is also covered ( $0.04 < h/\delta < 0.16$ ). From these results, similarity of both the mean velocity and turbulence structure on rough and smooth walls is critically evaluated.

The results show the usual downward shift in the logarithmic region of the mean velocity profile, relative to the smoothwall baseline. At lower values of both  $Re_0$  and  $h/\delta$ , good agreement is noted between the rough wall velocity defect profiles and the smoothwall baseline in the inner layers of the rough wall flows, supporting the existence of outer-layer similarity. At higher values of  $h/\delta$ , the collapse becomes poor and noticeable differences are seen in the velocity defect profiles. Profiles of the streamwise Reynolds stress,  $\langle u'^2 \rangle$ , show that it is significantly augmented by roughness. A similar enhancement is also noted in profiles of the wall-normal Reynolds stress,  $\langle v'^2 \rangle$ , and the effects get stronger with increasing  $h/\delta$  at a fixed  $Re_0$ . When normalized using  $\mu^2_\tau$  (the friction velocity) the results show that significant increases in the wall-normal Reynolds stress penetrate well into the outer layer over the rough wall. These findings indicate that there may be a critical roughness height where wall similarity fails for this and probably other types of roughness.

<sup>a</sup> School of Engineering Sciences, University of Southampton, Southampton SO17 1BJ, UK

1 Krogstad et al., *J. Fluid Mech.* **245**, 599-617 (1992).

2 Castro IP, *J. Fluid Mech.* **585**, 469-485 (2007)



## Stochastic Modeling of Evaporating Turbulent Sprays

Gaurav Anand and Patrick Jenny\*

Polydispersed turbulent evaporating and reacting flows are complex two-phase flow phenomena occurring in many industrial processes. This phenomena is characterised by liquid fuel droplets dispersion, their evaporation, and the fuel vapour reaction with the oxidizer, all occurring interactively at the same time. Thus signifying the need for accurate prediction of the fuel droplets dispersion and their evaporation. In the present study, a framework for modeling two-phase evaporating flow is presented.

This framework employs an Eulerian-Lagrangian-Lagrangian approach<sup>1</sup>. For the continuous phase, a joint velocity-composition probability density function (PDF) method is used<sup>2</sup>. Opposed to other approaches, such PDF methods require no modeling for turbulent convection and chemical source terms. For the dispersed phase, the mass density function (MDF, density-weighted PDF)  $\mathcal{F}_p(x, V_p, D_p, \psi_p, V_s, \psi_s; t)$  of velocity, diameter, temperature, seen gas velocity and seen gas composition is calculated. This provides a unified formulation, which allows to consistently address the different modeling issues associated with such a system. Because of the high dimensionality, particle methods are employed to solve the PDF transport equations.

The above framework has been used to simulate the experimental results obtained by Sommerfeld and Qiu<sup>3</sup> for the evaporating iso-propyl alcohol spray. Figure (1) shows the preliminary comparison between the mean droplet diameter profiles obtained from the experiment and simulation. A good overall agreement is observed.

\*ETH Zurich, Zürich, Switzerland

<sup>1</sup>B. Naud, *PhD Thesis, Delft University of Technology*, (2003).

<sup>2</sup>P. Jenny and S. B. Pope, *J. Comp. Physics* **166**(2), 218 (2001).

<sup>3</sup>M. Sommerfeld and H. H. Qiu, *Int. J. of Heat and Fluid Flow* **19**, 10 (1998).

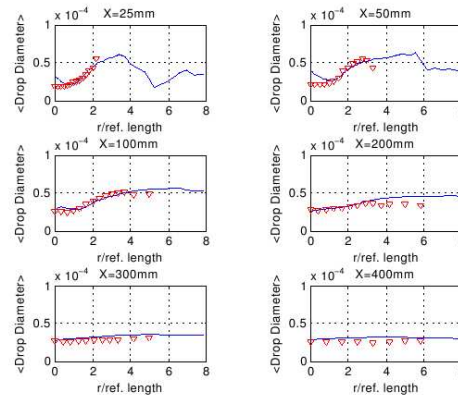


Figure 1: Experimental ( $\nabla$ ) and simulation (—) result for the evaporating spray

## Rotational force in insect flight

Jean-Yves Andro<sup>a</sup>, Laurent Jacquin<sup>b</sup>

This work aims at providing a new formulation for the rotational force of a pitching airfoil. Indeed rotational force has been identified as the source of significant transient forces in the context of insect flight<sup>1</sup>. Those transients are likely to be key mechanisms for the great performances of insects and so a special effort must be dedicated to its modelling for the design of future microdrones.

Rotational force used to be interpreted as an unsteady rotational circulation which is establishing around the airfoil so as to maintain the Kutta condition at the trailing edge during reversal motions<sup>2</sup>. With this formulation only valid for high Reynolds numbers and small amplitudes, the force is found to be proportional to the rotational rate and nil when the axis of rotation is located at the 75% chordwise position.

Nevertheless, extra low Reynolds numbers and large pitch amplitudes characteristic of insect flight induce large separation of the flow and vortex shedding at the trailing edge (see figure 1). So the rotational force must be revisited under those particular conditions. For this purpose we release 2D DNS simulations of a pitching flat plate at  $Re=100$ . A semi-empirical method associated with a parametric study has permitted to precise the evolution of the rotational force with the rotational rate and the location of the rotational axis. Isolating the rotational force from the quasi-steady contribution and the added mass contribution, we found that it is proportional to the square of the rotational rate and nil when the rotational axis is located at the 50% chordwise position.

The force induced by the trailing edge vortex and the associated flow separation can be seen as an inertial force based on the trailing edge velocity. This simplified model has been tested for a large range of frequencies, pitch amplitudes and Reynolds numbers. A good agreement with DNS results has been obtained (see figure 2).

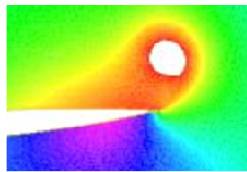


Figure 1: Pressure field during the vortex shedding at the trailing edge

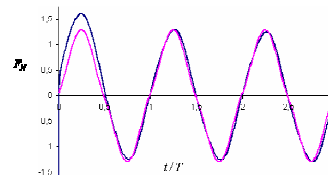


Figure 2: Comparison of DNS results and a simplified model for the instantaneous total force

<sup>a</sup> ONERA, centre de Meudon, France.

<sup>b</sup> ONERA, Centre de Meudon, France

<sup>1</sup> Dickinson et al., *Science* **284**, 1954 (1999).

<sup>2</sup> Sane & Dickinson, *The Journal of Experimental Biology* **205**, 1087 (2002).

## Anomalous transport in complex relaxation gas flows

V. V. Aristov<sup>a</sup>, A. A. Frolova<sup>a</sup> and S. A. Zabelok<sup>a</sup>

The flows for small spatial relaxation regions at scales of the mean free path described by the Boltzmann (or model) kinetic equation may demonstrate nontraditional features. Numerical solutions (and also analytical approximations) for the non-uniform relaxation problem (the boundary nonequilibrium distribution is accepted) for a one-component gas have shown that at some conditions the velocity and temperature gradients have the same signs as the appropriate nonequilibrium stress tensor components and heat fluxes respectively<sup>1</sup>. In the present paper we generalize the results to flows of a more complex gas media. This is stimulated, in particular, by applications of flows in microscale. The Unified Flow Solver (UFS)<sup>2</sup> for solving the Boltzmann equation and the model equation of BGK-type for mixtures<sup>3</sup> is used. In Fig.1 decrease of temperature corresponds to the negative heat flux (the binary mixture is used); the transfer of nonequilibrium stress demonstrates the analogous features. The role of different terms in the kinetic heat transfer is considered. One can note the qualitative agreement between solutions in Fig. 1 (the scale of relaxation zones by the model equation is smaller). The heat flux tends to zero in course of relaxation, with the negative flux allows the gas flow downstream to cool. The nonuniform relaxation problem is formulated for 2D flows. In this case a variant of the complex supersonic jet flow is simulated and the anomalous heat transfer is observed near the symmetry line. The influence of the inner degrees of freedom on the spatial relaxation of the molecular gas is also considered. The possibility of experimental verification with new methods<sup>4</sup> is discussed keeping in mind perspectives of heating or cooling the microscopic regions of a gas.

<sup>a</sup> Dorodnicyn Computing Centre of the Russian Academy of Sciences

<sup>1</sup> V.V. Aristov, *Phys. Letters A*, **250**, pp.354 (1998)

<sup>2</sup> Kolobov et al, *J. Comput. Phys.*, **223**, 2, 589 (2007)

<sup>3</sup> Andries et al, *J. Stat. Phys.*, **106**, 993 (2002)

<sup>4</sup> Fulton et al, *Nature. Physics*, **2**, 465, (2006)

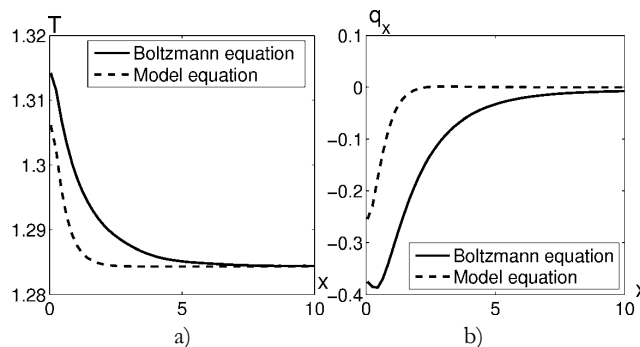


Figure 1. Profiles of temperature a) and heat flux b).

## Numerical study of solid cylinders moving freely in a viscous fluid

AUGUSTE Franck\*, FABRE David\*, MAGNAUDET Jacques\*

We consider the dynamics of cylindrical objects moving freely under the effect of buoyancy in a viscous fluid. The problem is investigated by means of direct numerical simulation using a code solving both the Navier-Stokes equations governing the flow in the frame of the body, and the generalized Kirchhoff-Kelvin equations governing the body motion<sup>1</sup>. The problem is characterised by three dimensionless parameters: the density ratio  $\frac{\rho_s - \rho_f}{\rho_f}$ , the body aspect ratio  $\chi$  and the Archimedes number  $Ar = \sqrt{\frac{r_{eq}^3 g |\rho_s - \rho_f|}{\rho_f \nu}}$ , where  $r_{eq}$  is a characteristic length scale of the body. We are especially concerned by the case  $\frac{|\rho_s - \rho_f|}{\rho_f} \approx 1\%$  and  $\chi \in [3 - 10]$  which was recently studied experimentally<sup>2</sup>. Our numerical results reveal an excellent agreement with these experiments and reproduce the regular oscillatory paths observed beyond a critical value of the Archimedes number. In addition, they provide evidence of the existence of new kinds of unsteady regimes existing at lower values of the Archimedes number.

\*Institut de Mécanique des fluides de Toulouse, Université Paul Sabatier

<sup>1</sup>G. Mougin & J. Magnaudet, *Int. J. Multiphase Flow* **28**, 1837-1851 (2002)

<sup>2</sup>P. Ern *et al.* *Phys. Fluids* **19**, 113302 (2007)

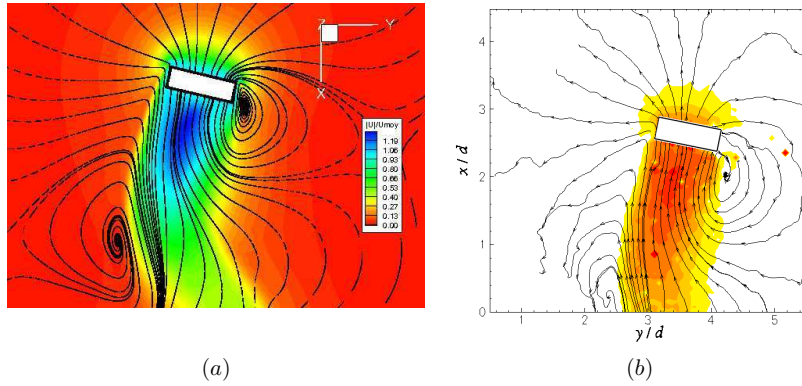


Figure 1: Flow around a zigzagging cylinder of aspect ratio  $\chi = 3$  (streamlines and velocity modulus). (a) : numerical simulation. (b) : PIV measurement.

## Mode competition in slowly varying flows

M. Avila\*, M. J. Belisle† J. M. Lopez ‡ F. Marques\* and W. S. Saric†

In slowly varying time-periodic flows the most unstable perturbations are not always periodic solutions of the equations of motion<sup>1</sup>. These flows are very sensitive to noise and imperfections. Here we consider the case of viscous fluid contained between two cylinders. The outer cylinder is held stationary, whereas the inner cylinder rotates harmonically about a zero-mean with

$$Re(t) = Re_a \sin(\omega t).$$

Centrifugal instability is triggered every half-period and results in secondary Taylor vortex flows<sup>2</sup>. In the high frequency regime, this instability is manifested by angular momentum jets erupting from the inner cylinder at a fixed axial location (Type B Taylor vortex flow). In the low frequency regime, the jets shift their locations by half the wavelength of the pattern when the inner cylinder reverses its direction of rotation (Type A Taylor vortex flow). These flows are initiated at synchronous bifurcations, have the same spatial symmetries, but are characterized by different spatio-temporal symmetries and axial wavenumber. Flows with precisely the same symmetries as A and B arise in other systems, such as the periodically driven cavity flow<sup>3</sup> and cylinder wake flows<sup>4</sup>, via analogous bifurcations in the transition from two-dimensional to three-dimensional flow.

We have experimentally and numerically investigated mode competition between states A and B in the neighborhood where they bifurcate simultaneously. In the idealized numerical model, the two flows have been found to coexist and be stable in a narrow region of parameter space. However, in the physical experiment, neither state has been observed in the coexistence region. Instead, we observe noise-sustained flows with irregular time-dependent axial wavenumber. Outside this region, for lower frequency only A is observed, and for higher frequency only B is observed, in good agreement with the numerical simulations and the Floquet stability analysis. This finding poses a fundamental question of interest in mode competition and pattern formation. In particular it is noteworthy that the wavenumber selection fails only in the mid-frequency coexistence region. For lower frequencies, where noise effects are expected to be more pronounced due to the long time that perturbations have to grow and decay, regular spatially and temporally periodic flows were in fact observed. It is thus of interest to determine the nature of the flows observed in the coexistence region, and in particular to determine if it is noise sustaining a mixed mode generated by a combination of A and B with a wide range of axial wavenumbers.

---

\*Departament de Física Aplicada, Univ. Politècnica de Catalunya.

†Department of Aerospace Eng., Texas A&M University.

‡Department of Mathematics and Statistics, Arizona State University.

<sup>1</sup>P. Hall, *J. Fluid Mech.* **126**, 357–368 (1983).

<sup>2</sup>Youd *et al.*, *J. Fluid Mech.* **487**, 367–376 (2003).

<sup>3</sup>Marques *et al.*, *Physica D* **189**, 247–276 (2004).

<sup>4</sup>Barkley & Henderson, *J. Fluid Mech.* **322**, 215–241 (1996).

# Numerical simulation of air flow in the human respiratory system based on a multi-model approach

L. Baffico\*, C. Grandmont† and B. Maury‡

We present numerical simulations of the air flow in the human bronchial tree obtained using a multi-model approach<sup>1,2</sup> (see figure below): in the upper part (first  $N$  generations) of the bronchial tree, 3D Navier–Stokes equations are used to model the fluid behaviour; in the distal part of the bronchial tree, a “condensation” technic, based on *Poiseuille* law and that leads to non-standard boundary conditions for the 3D fluid equations, is used to model the pressure drop in this zone; finally a chamber-piston-spring system is used to represent the alveolar zone. The piston displacement is governed by a forced harmonic oscillator differential equation. The external force applied to the piston, which represents the muscular forces exerted by the diaphragm and thoracic cage, drives the fluid flow in the bronchial tree.

A tetrahedral mesh of the upper bronchial tree, reconstructed from medical imagery, is used as the 3D fluid domain.

We discuss some implementation issues of this model, and we show how different choices of model’s parameters in the distal part modify the fluid behaviour in the 3D zone.

\*Laboratoire de Mathématiques N. Oresme, Université de Caen-Basse Normandie, F14032 Caen Cedex, France

†INRIA, REO project-team, INRIA Rocquencourt, F78153 Le Chesnay Cedex, France.

‡Laboratoire de Mathématiques, Université Paris-Sud, F91405 Orsay Cedex, France

<sup>1</sup>C. Grandmont et al., *Proceedings of the International Conference “New Trends in Continuum Mechanics 2003”*, 147 (2005).

<sup>2</sup>B. Maury et al., *ESAIM Proceedings* **14**, 115 (2005).

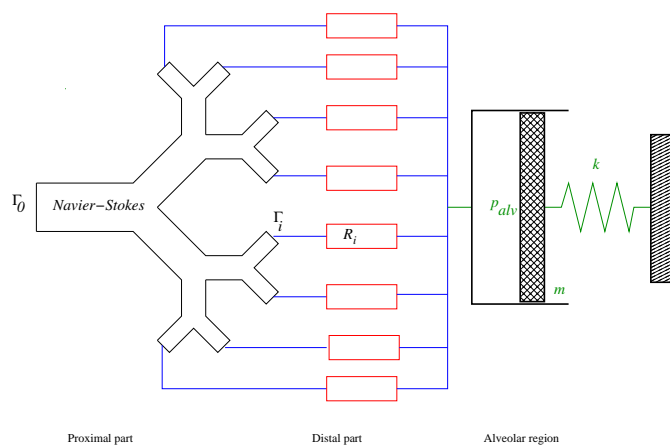


Figure 1: Multi-model of the respiration tree

### The Global Stability of the Jet in Crossflow

Shervin Bagheri\*, Philipp Schlatter\*, Dan S. Henningson\*,  
and Peter J. Schmid†

The global linear stability analysis of the jet in crossflow to three-dimensional perturbations is numerically investigated. At velocity ratio  $R = 3$ , defined as the ratio of free-stream velocity to jet velocity, the flow is globally linearly unstable. In this case, the temporal frequency of the most unstable global mode is in good agreement with the dominant intrinsic frequency associated with the jet shear-layer vortices observed in direct numerical simulation (DNS).

The DNS is based on spectral code of the flat-plate boundary layer, where the jet is enforced as a boundary condition with parabolic velocity distribution. A snapshot of the flow under consideration is shown in Figure 1a. Shear-layer vortices are continuously shed along the jet trajectory with a well-defined frequency. The baseflow for the stability analysis is a steady solution of Navier-Stokes, obtained by damping the unstable temporal frequencies using the selective frequency damping method<sup>1</sup>. Note that the 3D steady state is different from the time-averaged flow in terms of both the jet trajectory and the large-scale vortical structures; the steady state consists of a dominant counter-rotating vortex pair in the far field emerging from the near field vorticity of the shear layer (Figure 1b).

The large eigenvalue problem is solved using the ARPACK library and the linearized DNS as a time stepper. The most unstable mode shown in Figure 1b), takes the shape of a localized wavepacket, wrapped around the counter-rotating vortex pair. For the final contribution, higher velocity ratios is also considered, in order to explore the presence of a critical velocity ratio for global instability.

\*Linné Flow Centre, KTH Mechanics, Stockholm, Sweden

†LadHyX, CNRS-Ecole Polytechnique, Palaiseau, France.

<sup>1</sup>Åkervik et. al *Phys. Fluids* **18**

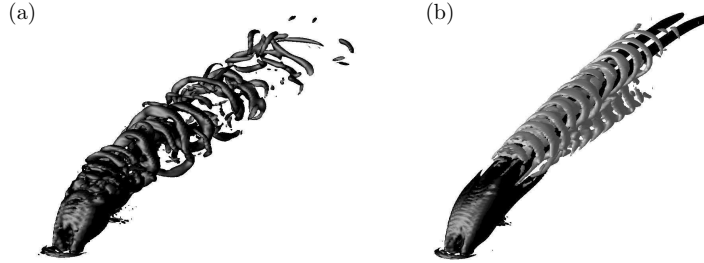


Figure 1: Isocontours representing the  $\lambda_2$  vortex-identification criterion. a) Snapshot of the flow for  $R = 3$ . b) The steady state in black isocontours and the most unstable global mode in gray. The crossflow is from lower left to upper right.

## Convective instability and transient growth in steady and oscillatory separated flows

Dwight Barkley\*, Hugh M. Blackburn†, Spencer J. Sherwin‡

We present a transient energy growth analysis of 2D and 3D optimal linear perturbations for steady flow over a backward-facing step, and steady and pulsatile flows in straight tubes with smooth axisymmetric contractions (stenoses). In each case, Reynolds numbers are considered well below the critical value for the onset of absolute instability. The analysis quantifies the transient linear response of the flows due to local convective instability downstream of the step edge or stenotic constriction. A typical result is shown in Figure 1 for the backward-facing step at  $Re = 500$ . The 2D linear transient energy growth is of order  $80 \times 10^3$  in this case. 3D optimal disturbances are broadly similar in shape to the 2D cases and the corresponding spanwise wavelengths are of order ten step heights. Nonlinearity is shown to have a stabilizing effect on the instability. For the stenotic flows, the global optimal disturbances about an initially axisymmetric state are three-dimensional with azimuthal wavenumber one, and arise as sinuous local convective instabilities in extended shear layers. For details see<sup>1 2 3</sup>

\*Mathematics Institute and Centre for Scientific Computation, University of Warwick.

†Department of Mechanical and Aerospace Engineering, Monash University.

‡Department of Aeronautics, Imperial College London

<sup>1</sup>Blackburn, Barkley et al, *J. Fluid Mech.* (in press 2008).

<sup>2</sup>Barkley, Blackburn et al, *Int. J. Numer. Meth. Fluids* (in press 2008).

<sup>3</sup>Blackburn, Sherwin et al, *J. Fluid Mech.* (in review).

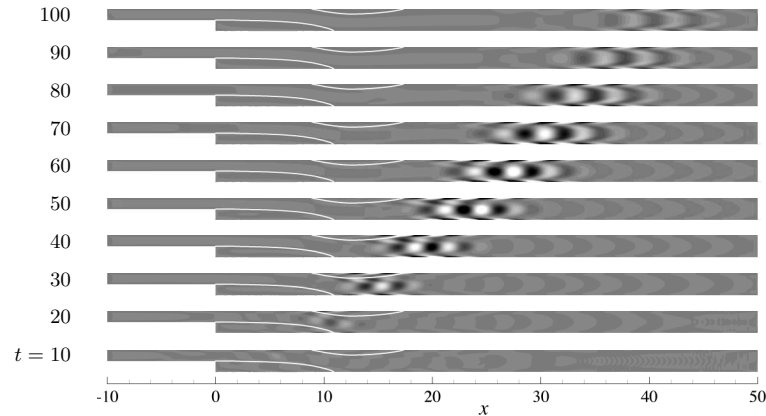


Figure 1: Time evolution of the optimal 2D linear perturbation in flow over a backward-facing step at  $Re = 500$ . Shown in grey is the vorticity field of the perturbation. Separating streamlines of the base flow are shown.



## The air-liquid flow in bifurcating networks of micro-channels

Yu Song\*, Michael Baudoin\*, Charles N. Baroud\* and Paul Manneville\*

We use microfluidic techniques to investigate the air-liquid flow in the pulmonary airway. The lung presents a bifurcating network where the relation between the mean diameters of successive branches can be described as  $d_{i+1} = 2^{-1/3}d_i$ <sup>1</sup>. The presence of liquid plugs in the airways introduces a nonlinear relationship between the pressure and the plug's capillary number:  $P = ACa + BCa^{2/3}$ , in which  $Ca = U\eta/\gamma$  is the capillary number and  $U$ ,  $\eta$ ,  $\gamma$  are the plug's velocity, the liquid viscosity and the surface tension, respectively. Here A and B depend on the surface tension, the geometry of the channel and the length of the liquid plug<sup>2</sup>.

The branching geometry introduces complex behaviour even in the case of a single plug. In our networks, we introduce a factor  $\rho$  to express the linear relation between cross-sections of successive generations in the bifurcating network  $s_{i+1} = \rho s_i$ , and provide a constant pressure drop between the first and the last generation. As the plug goes through successive divisions, its velocity increases before decreasing, as shown in figure 1a for a typical case. Meanwhile, the total flowrate changes according to the ratio of the cross-section as figure 1b. In both figures, the dotted line with squares corresponds to the case of the airway. As we can see, this linear model is similar to the pulmonary model.

Experimentally, we fabricate networks of micro channels in which we can inject liquid plugs and observe their transport, as shown in figure 2. We focus on the global statistical behaviour of the flow in the network, relying on experimental measurements to extract spatio-temporal patterns.

\*Laboratoire d'Hydrodynamique (LadHyX), Ecole Polytechnique, 91128 Palaiseau cedex, France.

<sup>1</sup>Weibel, *The pathway for oxygen*, 272 (1984).

<sup>2</sup>Ody et al., *J. Colloid Interface Sci.* **308**, 231 (2007).

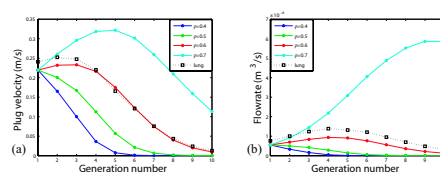


Figure 1: Computational results: (a) Plug velocity and (b) Network flowrate

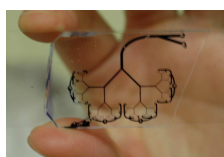


Figure 2: The network of micro channels for experiments

## Bioconvection in stratified environments

R. N. Bearon\*

Bioconvection is a fascinating phenomenon of fluid mechanics that is driven by the swimming motion of micro-organisms. Typically the velocity and spatial scale of the fluid motions are much larger than those associated with the swimming speed and size of an individual cell, resulting in rapid transport of cells and the formation of complex spatial patterns in cell concentration. Motile micro-algae are ubiquitous in aquatic systems, and understanding how they are spatially distributed at a wide range of length and time scales is an important ecological task. In order to make predictions about when and where bioconvection might occur, we need to understand how other physical factors, such as salinity stratification, will affect swimming behaviour, fluid flow, and the resultant spatial distribution of cells.

Motivated by laboratory experiments, I will present a linear stability analysis for the onset of bioconvection in a stable linear salinity gradient <sup>1</sup>. A continuum approximation for the cells is used, where the only effect of the cells on the fluid is their negative buoyancy. The bulk fluid velocity satisfies continuity and the Navier-Stokes equation under the Boussinesq approximation, with variation in fluid density due to salinity stratification and variation in cell concentration. The swimming behaviour of the cells is modeled as a constant upwards component combined with a diffusive component, calculated explicitly from individual-level observations of swimming trajectories <sup>2</sup>.

To obtain analytic results, a deep chamber is considered, where at equilibrium cells are concentrated in a thin boundary region. The ratio of chamber depth to boundary region depth is  $d \gg 1$ . Using matched asymptotic analysis, the critical value of the cell Rayleigh number,  $R_{crit}$ , for which the forcing due to a perturbation in cell concentration in the upper region drives flow is obtained. The effect of the salinity stratification depends on the salt Rayleigh number,  $R_s$ . If  $R_s^{1/6} = o(d)$ , the salinity gradient suppresses the vertical extent of the perturbation to the flow and salinity to a region of non-dimensional depth  $O(R_s^{-1/6})$ . The critical cell Rayleigh number is unaffected by the salinity gradient and is given at leading order by  $R_{crit} = 2d^3\delta$ , where  $\delta$  is the ratio of horizontal to vertical cell self-diffusion. If  $R_s^{1/6} = O(d)$ , the salinity gradient confines perturbations in the flow and salinity to the thin boundary region, and  $R_{crit}$  is specified as an algebraic function of  $R_s$ .

---

\*Department of Mathematical Sciences, University of Liverpool

<sup>1</sup>R. N. Bearon and D. Grünbaum, *Phys. Fluids* **18**, 12(2006).

<sup>2</sup>R. N. Bearon and D. Grünbaum, *J. Theor. Biol.* In Press

## The drag-out problem in liquid film theory, revisited

Eugene Benilov\*, Vladimir Zubkov\*

Many industrial coating processes can be modelled by a simple setting where an infinite sloping plate is being withdrawn from an infinite pool of a viscous liquid. Given that the plate's speed is constant and, eventually, a steady state is established, one usually needs to know the so-called *load*, i.e. the thickness of the liquid film that the plate carries away from the pool.

This classical problem was originally formulated by Derjaguin<sup>1</sup> in 1943. Assuming that the effects of inertia and surface tension are weak, he conjectured that the load is  $l = (\mu U / \rho g \sin \alpha)^{1/2}$ , where  $\rho$  and  $\mu$  are the liquid's density and viscosity,  $g$  is the acceleration due to gravity, and  $\alpha$  is the angle between the plate and the horizontal.

In the work presented, the above formula is derived from the Stokes equations under the assumption that the slope of the plate is small (without it, the formula is invalid). It is shown that the problem has infinitely many steady solutions, all of which are stable – but only one of these corresponds to Derjaguin's formula. This particular steady solution can only be singled out by matching it to a self-similar solution describing the non-steady upper part of the film. Interestingly, even though the region where the steady state has been established expands with time, the upper part of the film (with its thickness decreasing towards the 'tip') expands faster. As a result, the mean value of the film's thickness is 1.5 times smaller than the load.

We have also found a solution describing what happens if, after a certain period of time, the plate stops and the liquid films drains back into the pool.

---

\*Department of Mathematics, University of Limerick.

<sup>1</sup>Derjaguin, C. R. (*Dokl. Akad. Sci. URSS* **39**, 13 (1943)).

## Fluctuations, fronts, and stratification in sedimentation: experiments

Laurence Bergougnoux\*, Daniel Chehata Gómez\*,  
Élisabeth Guazzelli\*, John Hinch†

Although the sedimentation of non-Brownian particles at low Reynolds number can be considered as one of the simplest examples of suspension flow, it is still a challenging problem, still debated today. The difficulty lies in the long range nature of the multibody hydrodynamic interactions between particles and the coupling between these and the microstructure of the suspension.

While the average velocity of a suspension of spheres sedimenting in a viscous fluid can be successfully predicted theoretically <sup>1</sup>, the problem of velocity fluctuations is still unresolved. Analytical calculations for dilute random sedimenting suspensions predict that the size of the fluctuations diverges with the size of the container <sup>2 3</sup>. But no such divergence is seen in experiments <sup>4 5 6</sup>. There have been a number of arguments attempting to explain this screening of the fluctuations among which the idea that a vertical gradient in the mean concentration may suppress the diverging fluctuations <sup>7 8</sup>.

The objective of the present study is to examine experimentally how velocity fluctuations are screened and whether they are controlled by concentration gradients within the suspension.

---

\*IUSTI - CNRS UMR 6595, Polytech'Marseille.

†DAMTP, University of Cambridge.

<sup>1</sup>G. K. Batchelor, *J. Fluid Mech.* **52**, 245 (1972)

<sup>2</sup>R. E. Caflisch and J. H. C. Luke, *Phys. Fluids* **28**, 759 (1985)

<sup>3</sup>E. J. Hinch, in *Disorder and Mixing* edited by E. Guyon *et al.*, Kluwer Academic (1988)

<sup>4</sup>H. Nicolai and E. Guazzelli, *Phys. Fluids* **7**, 3 (1995)

<sup>5</sup>P. N. Segrè, *et al.*, *Phys. Rev. Lett.* **79**, 2574 (1997)

<sup>6</sup>É. Guazzelli, *Phys. Fluids* **13**, 1537 (2001)

<sup>7</sup>J. H. C. Luke, *Phys. Fluids* **11**, 754 (1999)

<sup>8</sup>P. J. Mucha *et al.*, *J. Fluid Mech.* **501**, 71 (2004)

CFD STUDY OF THE GAS CARRY-UNDER IN A GAS-LIQUID COMPACT CYCLONE (GLCC™)  
SEPARATOR USING A MIXTURE MODEL

Bienvenue Nkengue  
Erasmus Mundus Master in Mech. Eng. Program  
ETSEIB, Universitat Politècnica de Catalunya  
Barcelona, Spain  
[brahimsalaha@yahoo.fr](mailto:brahimsalaha@yahoo.fr)

Luis R. Rojas-Solórzano  
Dpto. de Conversión y Transporte de Energía  
Universidad Simón Bolívar  
Caracas, Venezuela. A.P. 89000  
[rrojas@usb.ve](mailto:rrojas@usb.ve)

---

ABSTRACT

A three-dimensional CFD study of the two-phase flow field in a Gas-Liquid Cylindrical Cyclone (GLCC) using the finite volume-based finite element method is presented. The numerical analysis was made for air-water mixtures at near atmospheric conditions, while both liquid and gas flow rates were changed. The two-phase flow behavior is modeled using an Eulerian-Eulerian approach, considering both phases as an interpenetrating continuum. This method computed the inter-phase phenomena by including a source term in the momentum equation to consider the drag between the liquid and gas phases. The gas-liquid flow is modeled using an inhomogeneous mixture model, in order to capture the interfacial effects associated to the general complex interfacial boundaries. Results are compared to experiments and to results from a bi-modal inhomogeneous particle model. The CFD technique here proposed, demonstrates to satisfactorily reproduce important features not easily depicted in experiments and not computed when using the particle model. Results show phase distributions and velocity profiles inside the GLCC, as well as the computed gas carry-under for different operating conditions.

## Non-linear evolution of a vortex pair in a stratified fluid

Axel Deloncle\*, Paul Billant\* and Jean-Marc Chomaz\*

We have performed high-resolution direct numerical simulations of the nonlinear evolution of a pair of counter-rotating vertical vortices in a stratified fluid for various high Reynolds numbers  $Re$  and low Froude numbers  $Fh$ <sup>1</sup>. As observed experimentally<sup>2</sup>, the vortices are bent by the zigzag instability producing high vertical shear (figure 1). We have found that there is no nonlinear saturation so that the exponential growth is stopped only when the viscous dissipation by vertical shear is of the same order as the horizontal transport, i.e. when  $Z_{\max}^h = O(Re)$  where  $Z_{\max}^h$  is the maximum horizontal enstrophy nondimensionalized by the vortex turn-over frequency. The zigzag instability therefore transfers directly the energy from large scales to the small dissipative vertical scales. However, for high Reynolds number, the vertical shear created by the zigzag instability is so intense that the minimum local Richardson number  $Ri$  decreases below a threshold around 1/4 and small-scale Kelvin-Helmholtz instabilities develop (figure 1). We show that this can only occur when  $ReF_h^2 > 340$ .

\*LadHyX, CNRS, École Polytechnique, F-91128 Palaiseau Cedex, France

<sup>1</sup>A. Deloncle et al., *J. Fluid Mech.* **599**, 229 (2008).

<sup>2</sup>P. Billant and J.-M. Chomaz *J. Fluid Mech.* **418**, 167 (2000).

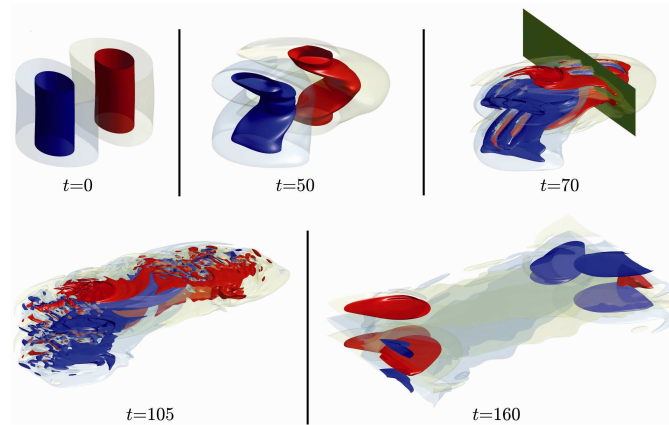


Figure 1: Vertical vorticity isosurfaces of the simulation for  $F_h = 0.66$  and  $Re = 3180$ . The two vortices, initially columnar, are bent by the zigzag instability ( $t = 50$ ). By  $t = 70$ , Kelvin-Helmholtz instabilities develop in the highly sheared region and produce small-scales structures ( $t = 105$ ). Smooth pancake vortices are eventually produced ( $t = 160$ ). Red and blue contours represent  $\pm 60\%$  of the vertical average of the maximum vertical vorticity in each horizontal plane. Transparent isosurfaces are the same for a 10% level.

## The initial flow caused by an inclined, accelerating wavemaker

John Billingham<sup>\*</sup>, David J. Needham<sup>†</sup>, Peter G. Chamberlain<sup>‡</sup>

We consider the initial, two-dimensional flow generated by the horizontal motion of a plane, rigid wavemaker into an initially stationary layer of inviscid fluid. The most interesting flows occur when the wavemaker is inclined towards the fluid. Using the method of matched asymptotic expansions for small times, we find that the flow develops in an inner and an outer region, with a jet forming in the inner region, but that this solution only exists when the wavemaker is sufficiently close to the vertical. At inclinations beyond a critical value, we include the effect of surface tension, with coefficient  $\sigma$ , in order to investigate how the solution breaks down as  $\sigma \rightarrow 0$ . We find that when the contact angle is such that the initial free surface is horizontal, capillary waves form, and pinch off a bubble at a finite time. For other contact angles, we have uncovered a rich asymptotic structure, one feature of which is the formation of a breaking gravity wave, unaffected by surface tension at leading order, that owes its existence purely to the initial curvature of the free surface and its effect on the subsequent flow. Another interesting feature is a finite waiting time, which occurs for contact angles less than  $45^\circ$ , during which the contact line is stationary before starting to move up the wavemaker.

---

<sup>\*</sup>School of Mathematical Sciences, University of Nottingham.

<sup>†</sup>School of Mathematics, University of Birmingham.

<sup>‡</sup>Department of Mathematics, University of Reading.

## Bending at the base of a dragged-out viscous thread

M. J. Blount\*, J. R. Lister\*

We consider steady flow of a slender viscous thread falling from a nozzle onto a moving horizontal belt. We analyse steady solutions in the asymptotic limit of a very slender thread. Previous analysis<sup>1</sup> of the problem has assumed the dominant force balance to be between gravity and viscous stretching, and has neglected the resistance that the thread has to bending. While the bending resistance is small for a slender thread, we show that its inclusion gives rise to a boundary-layer structure in which bending stresses become important only near the belt, where they support a vertical stress and allow the velocity and rolling conditions to be satisfied. The outer solution is analogous to a viscous catenary, with velocity fixed at the belt and at the nozzle. There are three asymptotic regimes, with distinct structures, corresponding to the cases that the belt speed is larger than, smaller than, or close to the velocity of a freely falling thread. The stability of the solutions within each regime is discussed, and the implications for the onset of meanders in the ‘fluid-mechanical sewing machine’ are explored.

---

\*ITG, DAMTP, University of Cambridge.

<sup>1</sup>Chiu-Webster, S. & Lister, J. R., *J. Fluid Mech.* **569**, 89 (2006).



## Hydraulic Flow through a Channel Contraction

Onno Bokhove\*

We will consider shallow water flows through a contraction, experimentally, analytically and numerically. In shallow flows in natural or man-made channels, a contraction geometry is not uncommon. It consists of a more or less uniform channel followed by a contraction of the channel into a nozzle where the width is minimal before the channel suddenly or gradually fans out again. Large variations in water flow discharges through such contracting channels may lead to dramatic changes in the flow state, including stowage effects with upstream moving surges. Such phenomena do occur when rivers overflow and the water is funneled underneath constricting bridges or through ravines.

We limit ourselves to study the states of water flow through an idealized experimental set-up with a sluice gate and an upstream horizontal channel of constant width  $b_0$  ending in a linear contraction of minimum width  $b_c$ . Experimentally, we observe upstream steady and moving bores/shocks, and oblique waves in the contraction, as single and multiple (steady) states, as well as a steady reservoir with a complex hydraulic jump in the contraction occurring in a small section of the  $b_c/b_0$  and Froude number parameter plane. One-dimensional hydraulic theory provides a comprehensive leading-order approximation, in which a turbulent frictional parameterization is used to achieve quantitative agreement. An analytical and numerical analysis is given for two-dimensional supercritical shallow water flows. It shows that the one-dimensional hydraulic analysis for inviscid flows away from hydraulic jumps holds surprisingly well, even though the two-dimensional oblique hydraulic jump patterns can show large variations across the contraction channel.

1. B. Akers and O. Bokhove, Hydraulic flow through a contraction: multiple steady states. Under revision *Phys. Fluids*, <http://eprints.eemcs.utwente.nl> (2008).

---

\*Dep. of Applied Mathematics, Univ. of Twente, The Netherlands. o.bokhove@math.utwente.nl



Figure 1: The structure of the 2D hydraulic jump in the contraction is akin to a Mach stem in a nozzle in gas dynamics. Top view. Oblique waves originate at the beginning of the contraction, and are joined by a “stem” roughly perpendicular to the walls.

## Dynamics of bubble pinch-off in a stagnant water pool

R. Bolaños-Jiménez\*, A. Sevilla\*, C. Martínez-Bazán\* and J.M. Gordillo†

We present an experimental and numerical study of the detachment of a gas bubble growing quasi-statically at a constant flow rate from a vertical nozzle placed at the bottom of a quiescent water pool. In particular we focus on the dynamics of the necking process and its dependence on the Bond number, defined as  $Bo = \rho g a^2 / \sigma$ , where  $a$  is the inner radius of the nozzle. The time evolution of the neck radius during the collapse process has been obtained by means of a high-speed digital video camera, using a microscopic lens which provides with spatial and temporal resolutions of  $5 \mu\text{m}/\text{px}$  and  $10 \mu\text{s}$  respectively, in the range of Bond numbers  $0.012 \leq Bo \leq 1.23$ . Our experimental data indicates that the asymptotic law recently obtained for the inviscid pinch-off of a bubble,  $\tau \propto r_0^2 \exp(-\log(r_0^2))^{1/2}$ , where  $\tau$  is the time to pinch-off, is never achieved down to about  $20 \mu\text{m}$ , suggesting an extremely slow approach to the asymptotic regime. However, we provide with a simple model based on the cylindrical Rayleigh-Plesset equation which closely reproduces the time evolution of both the minimum radius,  $r_0$ , and the associated local axial curvature,  $r_1$  (see Fig. 1(a)). The model, derived assuming slenderness of the local shape near the minimum radius, consists of a couple of ODEs for  $r_0$  and  $r_1$  which, in the limit of large Reynolds numbers and negligible gas effects, take the form  $-\log(r_0 r_1) d \log(r_0 \dot{r}_0)/ds + 1 - 2(1 - 2r_1 r_0)r_0/(r_0 \dot{r}_0)^2 = 0$ ,  $-\log(r_0 r_1) d \log(r_0 r_1)/ds - 1 + (1 - 2r_1 r_0)r_0/(r_0 \dot{r}_0)^2 = 0$ , with  $s = -\log(r_0)$ ,  $\dot{r}_0 = dr_0/dt$ . We propose a simple scaling law for the collapse time based on the good agreement among the experiments, the results obtained with a boundary integral numerical code and the model for the entire range of Bond numbers. Finally, we will present some preliminary data concerning the axial velocity of the Worthington jet entering the bubble after pinch-off (see Fig. 1(b)).

\*Área de Mecánica de Fluidos, Dep. Ingeniería Mecánica y Minera, Universidad de Jaén, Spain.

†Departamento de Ingeniería Aeroespacial y Mecánica de Fluidos, Universidad de Sevilla, Spain.

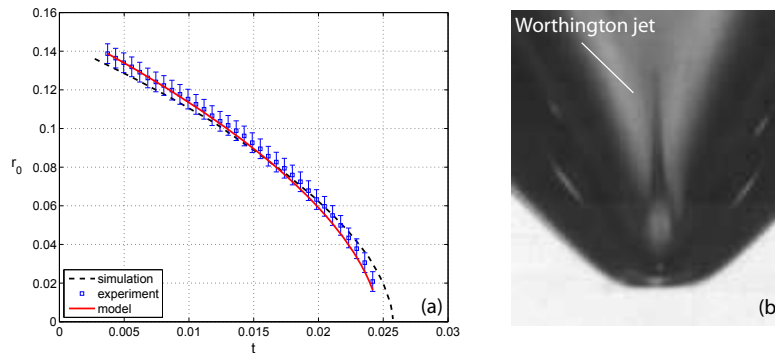


Figure 1: (a) Bubble collapse for  $Bo=0.9$ . (b) Worthington jet.

# Finite-difference high-order implementation of the immersed-boundary technique for the incompressible Navier-Stokes equations

Giuseppe Bonfigli\*

A novel implementation of the immersed-boundary technique is proposed for the solution of the incompressible Navier-Stokes equations in primitive variables. The standard formulation with direct imposition of the discrete continuity equation and Dirichlet boundary conditions at solid walls for the velocity is used<sup>1,2</sup>. Fourth-order finite differences on Cartesian staggered grids<sup>1</sup> are considered for spatial discretization, whereby adapted stencils including intersection points between grid lines and immersed boundary are introduced for derivation and interpolation at boundary-near points. Explicit schemes are considered for time integration (e.g. Adams-Bashforth, standard Runge-Kutta).

Procedures based on similar formulations of the Navier-Stokes equations have long been available in the literature<sup>1,2</sup>, but only recently immersed-boundary capabilities have been included by Peller et. al.<sup>3</sup> in the finite-volume context. By considering finite-difference discretization, we could easily achieve high-order accuracy, thus exploiting the advantages of Cartesian grids. Furthermore, using adapted stencils at boundary-near grid points the coupling between velocity and pressure induced by the implementation of the boundary conditions in the procedure by in Peller et. al.<sup>3</sup> could be removed. If explicit time integration is used, not only the pressure and the velocity, but also each single component of the velocity vector, may be computed in sequence, solving decoupled problems. We also mention that only coordinates of the intersection points between computational grids and boundary are needed in the numerical procedure, neither the normal direction to the boundary nor its curvature need to be computed.

Consistency and accuracy tests have been carried out solving the Navier-Stokes equations in the 2-d rectangular domain  $[-1, 1] \times [-1, 1]$  with exclusion of the circular region  $\{\underline{x} : |\underline{x}| < 0.2\}$ . Non-homogeneous boundary conditions have been imposed on  $|\underline{x}| = 0.2$  according to the immersed boundary technique and an unsteady volume-force has been added to the right-hand side of the momentum equation, so that

$$u_1 = \frac{\pi}{4}(1 - \cos(\pi x_1)) \sin(\pi x_2) \sin(\omega t), \quad u_1 = -\frac{\pi}{4} \sin(\pi x_1)(1 - \cos(\pi x_2)) \sin(\omega t),$$

$$p = \cos(\pi x_1) \cos(\pi x_2) \sin(\omega t)$$

was known to be the exact solution of the problem. Errors in the numerical solution have been found to be proportional to the fourth power of the grid step, in agreement with the nominal order of accuracy of the considered finite-difference stencils. Consistency with the accuracy of the used time-integration scheme was observed when varying the time step.

\*Institute of Fluid Dynamics, ETH Zurich.

<sup>1</sup>Harlow and Welch, *J. Comp. Phys* **8**, 2182 (1965).

<sup>2</sup>Bürger et. al., *J. Comp. Phys* **203**, 49 (2005).

<sup>3</sup>Peller et. al., *Int. J. Num. Meth. Fluids* **52**, 1175 (2006).

## Two-dimensional falling film flow along steep topography

V. Bontozoglou<sup>a</sup> and K. Serifi<sup>a,b</sup>

Steps are paradigms of steep wall topography. When a falling film flows along a step, both the flow field and the free surface shape are locally strongly modified. Such modification may be undesirable, as in film coating, or desirable as in heat/mass transfer intensification. Literature results refer mostly to the Stokes limit<sup>1,2,3</sup>, where surface tension balances gravity resulting in capillary features upstream of the step (a ridge before a step-in and a depression before a step-out).

We are presently investigating numerically the parametric evolution with inertia of vertical, steady film flow along isolated step-ins and step-outs. A Galerkin finite-element method<sup>4</sup> is used, with appropriate transformation of the flow domain and node clustering around the corner of the step, and the parametric range spanned includes Reynolds numbers  $Re \sim O(10^{-3}-10^2)$  and capillary numbers  $Ca \sim O(10^{-2}-10^1)$ .

The lengthscale of the capillary features upstream of a step-in or a step-out decreases uniformly with  $Re$ , in a way that is accurately predicted from an order-of-magnitude balance of gravity, capillary and inertia forces. The height of the capillary features first grows but then diminishes with increasing  $Re$ . Their disappearance occurs when inertia forces dominate capillary forces, and is accompanied by a displacement of the key dynamics from upstream to downstream of the step. In particular, the change in flow direction imposed by the step is accomplished at low  $Re$  by a capillary mechanism operating before the step, and at high  $Re$  by an inertial mechanism operating after the step. The essence of the latter is a low-pressure region developing behind the step, which is triggered by the pressure singularity at the edge.

At a step-out, a new downstream free surface feature appears at high enough  $Re$ , caused by liquid overshoot in the horizontal direction. The conditions for the onset of this inertial ridge are correctly predicted by an order-of-magnitude balance of gravity, capillary and inertia forces only when the parametric variation in the streamwise lengthscale is also taken into account. The height of the inertial ridge is shown to be restrained by capillary forces at low  $Re$  and by inertial forces (the low-pressure region) at high  $Re$ .

---

<sup>a</sup> Mechanical Engineering, University of Thessaly, Volos, Greece.

<sup>b</sup> Present address: Faculty of Applied Sciences, ULB, Brussels.

<sup>1</sup> Kalliadasis S., Bielarz C. & Homsy, G.M. *Phys. Fluids*, **12**, 1889 (2000).

<sup>2</sup> Mazouchi A. & Homsy G.M., *Phys. Fluids*, **13**, 2751 (2001).

<sup>3</sup> Gaskell P., Jimack P., Sellier M., Thompson H. & Wilson M., *J. Fluid Mech.*, **509**, 253 (2004).

<sup>4</sup> Malamataris N., Vlachogiannis M. & Bontozoglou V., *Phys. Fluids*, **14**, 1082 (2002).

## Global flow instability in a lid-driven cavity and circular cylinder cascade

V. B. L. Boppana\* and J. S. B. Gajjar\*

The main aim of the current work is to compute the global instability accurately in two classic flow problems - flow in a lid-driven cavity and flow past a circular cylinder cascade. This is accomplished using a new numerical technique which was implemented earlier successfully to compute the steady flow in the above two problems. See Gajjar and Azzam<sup>1</sup> for more details. The governing Navier-Stokes equations which are in terms of stream function and vorticity are discretized using a fourth-order central difference method in streamwise direction and Chebyshev collocation in the transverse direction. The normal mode approach of the linear stability analysis is used according to which the disturbance to the steady flow is taken proportional to  $\exp(\lambda t)$ . The resultant discrete form of the linearised Navier-Stokes equations is in the form of the generalized eigenvalue problem given by

$$\mathbf{A}\mathbf{u} = \lambda\mathbf{B}\mathbf{u}$$

and is solved using ARPACK<sup>2</sup>. In general with the standard discretization techniques, the matrices  $\mathbf{A}$  and  $\mathbf{B}$  are very large and sparse, and special techniques need to be adopted to solve the problem. In addition it is difficult to produce grid independent results. With the current numerical method, the problem size is significantly reduced and useful converged results have been obtained.

In the case of lid-driven cavity, three different aspect ratios are considered to study their effect on the critical Reynolds number. It was found that the flow undergoes Hopf bifurcation at the critical parameter. Similarly, for the flow past circular cylinder cascade, the primary wake instability is found to exhibit Hopf bifurcation at the critical Reynolds number. The study is done for various gap widths between the cylinders as well as for different outlet boundary locations. The former is to understand the blockage effect on the critical parameter and the latter is to find the minimum outlet location (for the chosen boundary conditions) in order to avoid the reflection of waves.

The interesting results that are obtained in these two flow problems for different cases as mentioned above will be presented.

---

\*School of Mathematics, University of Manchester.

<sup>1</sup>J. S. B. Gajjar and N. Azzam, *J. Fluid Mech.* **520**, 51 (2004).

<sup>2</sup>Lehoucq et al., *ARPACK User's guide, Solution of large-scale eigenvalue problems with implicitly restarted Arnoldi methods*. SIAM (1998).

## Superstability of surface nanobubbles

Bram Borkent\*, Holger Schönherr†, Stephan Dammer\*, Peichun Tsai\*,  
Julius Vancso† and Detlef Lohse\*

In recent years, numerous experiments revealed the existence of nanoscopic soft domains at the liquid-solid interface, see for instance Zhang *et al.*<sup>1</sup> and references therein. Most experiments employ atomic force microscopy (AFM)<sup>2</sup> but other techniques have been used as well. The most consistent interpretation of these experiments is that the soft domains, which resemble spherical caps with heights of the order of 10 nm and diameters of the order of 100 nm, are so-called *surface nanobubbles*, i.e., nanoscale gas bubbles located at the liquid-solid interface.

Surface nanobubbles are puzzling objects: due to their huge curvatures, surface tension should lead to rapid dissolution of the bubbles, but in practice they are stable for hours. Recently, we showed that surface nanobubbles, contrary to the expectation, do *not* act as nucleation sites for shock wave induced cavitation on surfaces, where a large tensile stress is created in the water<sup>3</sup> (Figure 1). This adds another puzzle to the nanobubble paradox.

In this paper we will address two issues: how is the liquid-air interface deformed by the mechanical forces of the AFM tip, i.e. what is the precise shape of the nanobubbles? To address this issue we created controlled nanobubbles - trapped in well-defined nanoholes - and compared them with AFM studies on conventional surface nanobubbles. The second question is: can we create nanobubbles which do nucleate? Again, we use nanobubbles trapped inside well-defined nanopits.

\*Physics of Fluids, Faculty of Science and Technology, University of Twente, P.O. Box 217, 7500 AE Enschede, The Netherlands.

†Materials Science and Technology of Polymers, Faculty of Science and Technology, University of Twente, P.O. Box 217, 7500 AE Enschede, The Netherlands.

<sup>1</sup>X.H. Zhang *et al.* *Langmuir* **22**, 5025 (2006).

<sup>2</sup>J. W. G. Tyrrell and P. Attard, *Phys. Rev. Lett.* **87**, 176104 (2001); A. C. Simonsen *et al.* *J. Colloid Interface Sci.* **273**, 291 (2004); M. Holmberg *et al.*, *Langmuir* **19**, 10510 (2003); A. Agrawal *et al.*, *Nano Lett.* **5**, 1751 (2005); S. Yang *Langmuir* **23**, 7072 (2007).

<sup>3</sup>B.M. Borkent *et al.* *Phys. Rev. Lett.* **98**, 204502 (2007)

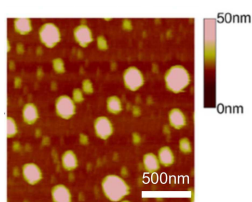


Figure 1: Surface nanobubbles on silanized silicon are present even after a large tensile stress has been applied to the liquid (picture taken from <sup>3</sup>)

## Deterministic Turbulence and Its Application

V.I. Borodulin<sup>a</sup>, Y.S. Kachanov<sup>a</sup> and A.P. Roschektayev<sup>a</sup>

The idea on existence of the deterministic (reproducible) wall turbulence was advanced recently<sup>1</sup> based on experimental data and on the concept on the universality of the turbulence production mechanisms in *transitional* and *turbulent* wall shear flows<sup>2</sup>. This idea has been substantiated experimentally<sup>3</sup> and resulted in creation of an efficient method for investigation of turbulent flows. The present work demonstrates an application of this method to investigation of LEBU-device effect on the instantaneous structure of a turbulent boundary layer.

The model, a flat plate equipped with wall bump producing adverse pressure gradient, was mounted in a test section of low-turbulence wind tunnel. The laminar-turbulent transition on the model was initiated (*not forced!*) by a special disturbance generator. Downstream of the generator a certain domain was found, where the flow was turbulent in accordance with common notions but still deterministic, reproducible, and coherent with initial disturbances. The flowfield  $U(x, y, z, t)$  in this domain was registered in absence and in presence of LEBU-devices, which showed up to 10% reduction of the skin friction. The comparison of two flowfields allows us to propose the following explanation of this effect.

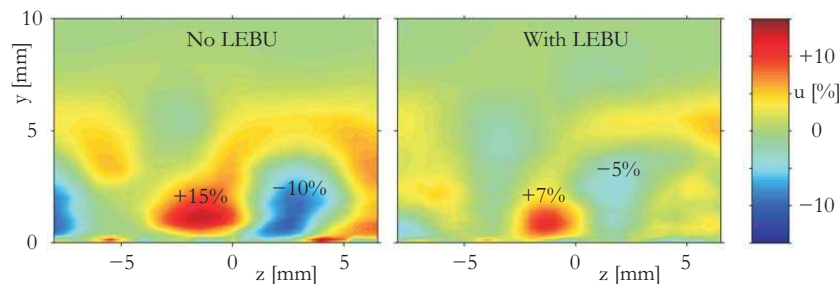
As was shown in previous experiments, the ring-like vortices generated continuously by  $\Lambda$ - (horseshoe) vortices and propagated near the boundary-layer edge, induce some strong perturbations in the near-wall region. This phenomenon is typical for both transitional and turbulent boundary layers<sup>2</sup>. The induced perturbations play a role of seeding in launching new coherent vortical structures. After (partial) destruction of the ring-like vortices by the LEBU-devices the near-wall domain appears to be less perturbed and the formation of new wall structures is blocked.

<sup>a</sup> Institute of Theoretical and Applied Mechanics, Novosibirsk, Russia.

<sup>1</sup> Borodulin et al., *Proc. Conf. Stability and Turbulence of Flows... Novosibirsk*, **X**, 27 (2005).

<sup>2</sup> Kachanov, *Recent Results in Laminar-Turbulent Transition*, **86**, 1 (2003).

<sup>3</sup> Borodulin et al., *Springer Proceedings in Physics*, **117**, 176 (2007).



An instance of  $u(y, z)$  demonstrating suppression of near-wall positive fluctuations.

Boundary layer thickness is about 5 mm, LEBU-device is at 4.2 mm.

## On hydrodynamic stability of the two-phase flow in a plane channel with a finite volume fraction of inclusions

Sergei Boronin<sup>a,b</sup>

Within the two-fluid approach<sup>1</sup> to modeling heterogeneous flows, the linear stability problem is formulated for the suspension flow in a plane channel. Both a non-zero particle velocity slip and a finite volume fraction of particles are taken into account. Corrections to the Stokes drag force (in the Brinkman form<sup>2</sup>) and to the bulk viscosity of suspension (Einstein's formula) due to a finite volume concentration of particles are used. The undisturbed flow is described by the parabolic velocity profile with no particle velocity slip and a uniform cross-channel profile of the particle volume concentration. The stability problem is reduced to an eigenvalue problem for an ordinary differential equation, which is solved numerically using the orthogonalization method. Effects of particles on the flow stability are governed by three dimensionless groups: the particle inertia parameter  $\beta$  (the ratio of the channel width to the particle velocity relaxation length), the particle volume concentration  $C_0$ , and the particle-to-fluid density ratio  $\eta$ . A parametric study is performed and the dependence of the critical Reynolds number on  $\beta$  is obtained for various magnitudes of  $\eta$  and  $C_0$  (Fig. 1). It is found that the critical Reynolds number is lower than that for the pure-fluid flow in the case of high-inertia particles ( $\beta \sim 1$ ) lighter than the fluid ( $\eta < 0.5$ ) and low-inertia particles ( $\beta \gg 1$ ) heavier than the fluid ( $\eta > 3.5$ ).

<sup>a</sup> Schlumberger Moscow Research, Russia.

<sup>b</sup> Institute of Mechanics, Lomonosov Moscow State University, Russia.

<sup>1</sup> F. E. Marble, *Ann. Rev. Fluid Mech.*, **1**, 397 (1970).

<sup>2</sup> H. C. Brinkman, *Appl. Sci. Res., Sec. A*, **1**, 27 (1947).

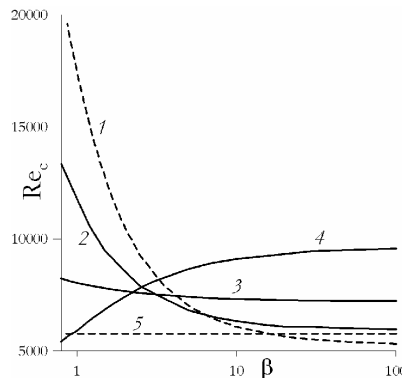


Figure 1: The critical Reynolds number  $Re_c$  vs. the particle inertia parameter  $\beta$  at the fixed mass concentration  $\eta C_0 = 0.1$ . Curve 1 – dusty-gas flow ( $\eta \gg 1$ ,  $C_0 \ll 1$ ), 2 –  $\eta = 3$ ,  $C_0 = 0.033$ ; 3 –  $\eta = 1$ ,  $C_0 = 0.1$ , 4 –  $\eta = 0.5$ ,  $C_0 = 0.2$ , 5 – pure-fluid flow.



## Bifurcations and coexisting solutions in cylindrical Rayleigh-Benard convection

Katarzyna Boróńska\*, Laurette S. Tuckerman†

In 1999, Hof et al.<sup>1</sup> described five different steady patterns observed experimentally in a cylindrical Rayleigh-Bénard convection cell at identical parameter values:  $Ra = 14200$ ,  $Pr = 6.7$ ,  $\Gamma \equiv \text{radius/height} = 2$  with insulating lateral boundaries. Our goal was to reproduce these patterns numerically, to ascertain their limits of existence and stability, and, where possible, to connect them to the trivial conductive branch.

We used a pseudospectral time-stepping code, adapted to carry out steady-state solving via Newton's method and linear stability analysis via Arnoldi's method<sup>2</sup>. We initialised simulations with the same small perturbation at different values of  $Ra$ , leading to different final convective patterns. These in turn served as initial conditions for both time integration and steady-state solving. In addition to reproducing the five steady states experimentally observed<sup>1</sup> at  $Ra = 14200$  – called mercedes, two-roll, three-roll, four-roll and torus – we also discovered a new time-dependent state, the rotating S. Over the range  $Ra \leq 30000$ , we calculated a total of fifteen branches of stable and unstable states. Of these, the two-torus ( $m = 0$ ), dipole ( $m = 1$ ), pizza ( $m = 2$ ) and marigold ( $m = 3$ ) branches bifurcate from the conductive branch. The four-roll branch bifurcates from the pizza branch, the three-roll branch from the dipole branch, and the mercedes, mitsubishi and cloverleaf branches from the marigold branch. Figure 1 shows the bifurcation diagram and representative states.

\*School of Computing, University of Leeds, United Kingdom

†PMMH-ESPCI-CNRS, France.

<sup>1</sup>B. Hof, G.J. Lucas, T. Mullin, *Phys. Fluids* **11**, 2815 (1999).

<sup>2</sup>C.K. Mamun & L.S. Tuckerman, *Phys. Fluids* **7**, 80 (1995).

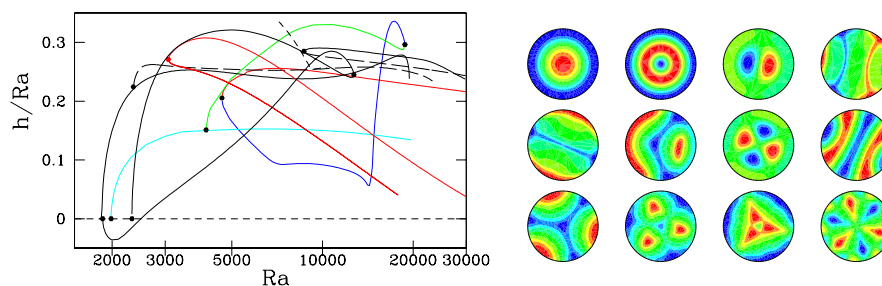


Figure 1: Bifurcation diagram (left) containing fifteen steady branches.

Row 1 (right): torus, two-torus, dipole, three-roll.

Row 2 (right): two-roll, CO, pizza, four-roll.

Row 3 (right): mercedes, cloverleaf, mitsubishi, marigold.

Not shown: unstable torus, two-torus and two-roll states.

### Flow control using hairy surfaces

Julien Favier\*, Antoine Dauptain†, Alessandro Bottaro‡

This communication presents a model of hairy media, using a homogenized approach, and its interaction with a fluid flow around a circular cylinder at Reynolds number  $Re < 200$  (Fig. 1). The capability of this surface to achieve shape adaptation in separated flows is investigated, and its benefits are discussed in the context of separation control.

To solve this fluid/structure interaction problem we use a partitioned approach based on the direct resolution of Navier-Stokes equations together with a non-linear set of equations describing the dynamics of the hairy surface. A volume force, estimated as the drag of a thick cluster of hair, provides the link between the fluid and the structure problems.

For the structure part, a subset of reference elements approximates the whole layer. The dynamics of these elements is governed by a set of equations based on the inertia, elasticity, interaction and dissipation effects of articulated rods<sup>1</sup>. For the coupling, experimental and theoretical results on flows going through densely packed arrays of cylinders are used to estimate the drag volume force<sup>2</sup>.

The configuration chosen is that of the flow past a circular cylinder, a simple and well documented test case. This communication shows quantitatively how a hairy surface coating can change the Strouhal number, the drag and the maximum lift for steady and unsteady laminar regimes. A parametric study will highlight the most efficient set of parameters (length of elements, density, flexibility, etc.) with respect to the control of boundary layer separation.

\*DICAT, University of Genoa, Italy

†DICAT, University of Genoa, Italy

‡DICAT, University of Genoa, Italy

<sup>1</sup>Lindström *et al.*, *Physics of Fluids* **19**, 113307 (2007).

<sup>2</sup>Howells *et al.*, *Journal of Fluid Mechanics* **355**, 163–192 (1998).

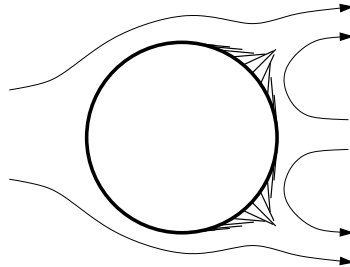


Figure 1: A cylinder half-coated with a hairy-like surface.

## Characterization of droplets entrainment in gas-liquid horizontal pipe flow

S. Boulesteix\*, P. Ern\* and F. Charru\*

The topic of this study is the entrainment of droplets which occurs in several regimes of gas-liquid pipe flow (including wavy-stratified and annular flows) because of the shear applied on the liquid layer by the faster gas stream. This phenomenon is of interest in many industrial processes, such as oil extraction, for it considerably increases mass and momentum transfer between the phases<sup>1</sup>.

The atomisation process at the interface of an air-water flow has been studied using a high-speed camera (6000 images per second). This allowed us to identify two main breakup mechanisms (see figure 1) responsible for the liquid fragmentation : bag and ligament breakups, which are also present in the case of a liquid drop suddenly exposed to a high velocity gas stream<sup>2</sup> and of the atomisation of a liquid jet by a faster coaxial gas stream<sup>3</sup>. Frequent occurrence of collisions between droplets, resulting in several fragments of smaller size than the mother drops, have been observed. Droplets sizes and velocities (obtained by digital image processing), which are key informations in the understanding and modelling of the atomisation process, will also be shown and discussed.

---

\*Institut de Mécanique des Fluides de Toulouse.

<sup>1</sup>B.J. Azzopardi, *Int. J. Multiphase Flow* **23**, 1 (1997).

<sup>2</sup>S.A. Krzeczowski, *Int. J. Multiphase Flow* **6**, 227 (1980).

<sup>3</sup>P. Marmottant and E. Villermaux, *J. Fluid Mech.* **498**, 73 (2004).

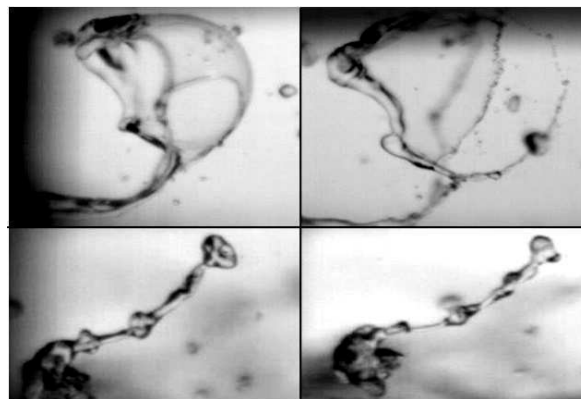


Figure 1: Examples of bag-breakup (top) and ligament breakup (bottom) mechanisms observed in the pipe.

## Impact of turbulent flow on large spherical roughness elements

C. Braun\*, M. García-Villalba\*, G. H. Jirka\* and W. Rodi\*

In the last years, highly turbulent flow over walls roughened by large roughness elements has been studied widely in order to gain insight into the structure of turbulence in such a flow and how to control it. However, most studies focused on the turbulent flow field only and did not consider the effect of the flow field on the roughness layer, but this effect is crucial for many aspects of engineering, e.g. for sediment transport in rivers. As a first step towards a deeper understanding of the complex interaction between a turbulent flow field and a mobile roughness layer, this contribution studies the impact of a turbulent flow field on fixed spherical roughness elements. As experimental and numerical facilities to study the problem with sufficiently high resolution became feasible only recently, few studies on the topic exist.<sup>1,2,3</sup>

Large eddy simulations were carried out of flow over three layers of spherical roughness elements in cubical packing at a particle Reynolds number of  $Re_* = u_* D / \nu = 550$ , where  $u_*$  is the friction velocity,  $D$  is the particle diameter and  $\nu$  is the kinematic viscosity. The simulations use a computational domain of  $48 D$  in streamwise,  $8 D$  in spanwise and  $7 D$  in vertical direction. The water-depth-to-roughness-height ratio is  $H/D = 4$ . Periodic boundary conditions are applied in streamwise and spanwise direction, the free surface condition is modelled by using the rigid-lid assumption on this surface. At the wall where the spheres are placed the no-slip condition is applied. The spherical roughness elements are discretised by employing the immersed boundary method of Uhlmann<sup>4</sup>. By this the flow field around the roughness elements is resolved. Forces on the particles can be obtained directly as result of the immersed boundary method. In the talk, time-averaged flow statistics are presented and compared with results of previous studies. Furthermore, statistical properties of the forces are analysed as well the correlation between flow structures and particle forces.

---

\*Institute of Hydromechanics, University of Karlsruhe, Karlsruhe, Germany.

<sup>1</sup> Hofland et al., *J. Hydr. Eng.* **131**(9), 770-781 (2005)

<sup>2</sup> Singh et al., *J. Hydr. Eng.* **133** (4), 386-398, (2007).

<sup>3</sup> Uhlmann and Fröhlich *H. Perf. Comp. Science & Eng.* '07, Stuttgart (HLRS), Springer, (2007).

<sup>4</sup> Uhlmann, *J. Comput. Phys.* **209**(2), 448-476 (2005).

## On a similarity solution in unsteady marginal separation

S. Braun\*, S. Scheichl\* and A. Kluwick\*

In this paper we investigate initial value problems associated with the high Reynolds number asymptotic theory of unsteady, marginally separated incompressible boundary layer flows. Special emphasis is placed on solutions which blow-up within finite time. To be specific, the evolution of the displacement function  $A(X, T)$  and the interaction pressure  $P(X, T)$ , governed by<sup>1,2</sup>

$$A^2 - X^2 + \Gamma = \int_X^\infty \frac{\partial^2 A / \partial \xi^2}{\sqrt{\xi - X}} d\xi - \int_{-\infty}^X \frac{\partial A / \partial T}{(X - \xi)^{1/4}} d\xi, \quad P = \frac{1}{\pi} \int_{-\infty}^\infty \frac{\partial A / \partial \xi}{X - \xi} d\xi, \quad (1)$$

is computed for well defined initial data  $A(X, T = T_0) = A_0(X)$ . Here  $X$ ,  $T$  and  $\Gamma$  denote the spatial coordinate in stream-wise direction, the time and a controlling parameter. As is well-known, steady solutions of (1) exist in the parameter range below a limiting value  $\Gamma_c$  only. Our analysis showed that any choice of  $A_0(X)$  associated with (i) (suitably forced) sub-critical,  $\Gamma < \Gamma_c$ , or alternatively (ii) super-critical,  $\Gamma > \Gamma_c$ , conditions which result in the formation of finite time singularities leads to similar terminal structures of  $A$  as  $X \rightarrow X_s$ ,  $T \rightarrow T_s$ . This suggests the existence of an unique self-similar behaviour close to the blow-up point  $(X_s, T_s)$ . Appropriate expansions<sup>2</sup>  $A \sim (T_s - T)^{-2/3} \hat{A}(\hat{X}) + \dots$ ,  $P \sim (T_s - T)^{-10/9} \hat{P}(\hat{X}) + \dots$  with the similarity variable  $X - X_s = (T_s - T)^{4/9} \hat{X}$  then give

$$\hat{A}^2 = \int_{\hat{X}}^\infty \frac{d^2 \hat{A}}{d\xi^2} \frac{d\xi}{\sqrt{\xi - \hat{X}}} - \frac{2}{3} \int_{-\infty}^{\hat{X}} \left( \hat{A} + \frac{2}{3} \xi \frac{d\hat{A}}{d\xi} \right) \frac{d\xi}{(\hat{X} - \xi)^{1/4}}. \quad (2)$$

Indeed, the solution  $\hat{A}(\hat{X})$  turns out to be unique, Fig. 1. Consequences of this important issue and the extension to cover locally three-dimensional flows will be addressed as well.

\*Institute of Fluid Mechanics and Heat Transfer, Vienna University of Technology, Austria.

<sup>1</sup>A.I. Ruban, *Izv. Akad. Nauk SSSR: Mekh. Zhidk. Gaza* **6**, 55 (*Fluid Dyn.* **17**, 860) (1983).

<sup>2</sup>F.T. Smith, *Aero. Q.* **33**, 331 (1982).

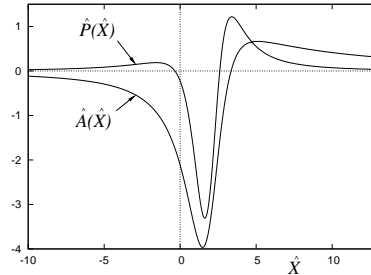


Figure 1: Unique blow-up structure in case of planar unsteady marginal separation.

### Wet granulates under shear

M. Brinkmann,\* S.E. Ebrahimpnazhad,\* J. Sakar,\* J. Vollmer,\* S. Herminghaus\*

Small amounts of a wetting liquid render sand a stiff and moldable material. Cohesion between wet grains is caused by the presence of capillary bridges forming at the points of contact. The finite strength of these liquid bonds is responsible for a transition from a quiescent to a fluidised state under applied shear stress. Accordingly, certain types of landslides and avalanches can be viewed as a fluidisation transition of wet grains under shear.<sup>1</sup>

The fluidisation transition is studied in a MD-type simulation of a two dimensional assembly of bidisperse discs under the action of a spatially heterogeneous external force. Capillary interaction is modelled as a short ranged, but hysteretic attractive force between discs, which repel each other with soft core potentials. Besides the fluidisation threshold we study the spatial and temporal distribution of granular temperature, shear rate, stress, local packing fraction, and density of capillary bridges in both the fluidised and the quiescent state. The local viscosity  $\eta$  of the fluidised state is dominated by the local packing fraction  $\rho$ , and diverges upon approaching the area fraction of randomly packed disks ( $\rho_c \approx 0.85$ ). Applying different types of soft core potentials and rupture scenarios of capillary bridges the fluidisation phase diagram is constructed in terms of the area fraction of grains and the driving force.

The energy lost in each rupture event constitutes an additional mechanism for energy dissipation being linear in the shear rate. As a consequence, there is a non-trivial cross over from a regime where dissipation is dominated by the hysteretic attractive forces to the common viscous dissipation in elastic hard core gases. In simulations where the shear rate is fixed by Lees-Edwards boundary conditions (rather than inducing shear by coupling to an external field) the viscous dissipation can lead to a temperature run-away. Consequently, granular temperature is a non-trivial thermodynamic variable: one needs a thermostat to follow the dynamics of the wet granulate.

---

\*MPI Dynamics & Self-Organization, Bunsenstr. 10, D-37073 Göttingen, Germany

<sup>1</sup>S. Herminghaus, *Adv. Phys.* **54**, 221 (2005).

## Hysteresis on the subcritical vortex dynamics in a von Kármán flow experiment

Alberto de la Torre\*, Montserrat A. Miranda\* and Javier Burguete\*

We present the experimental study of the dynamics of a flow created by two propellers rotating in opposite directions placed at both ends of a cylindrical cavity. A steady and symmetric mean flow appear for low and intermediate Reynolds numbers. The fluid is aspirated by the propellers near the axis, where it is ejected towards the cylindrical wall and the flow is closed at the equator:<sup>1</sup> Two symmetrical cells are created, each one rotating around the axis in the same direction of the nearest propeller. This flow can loose its stability breaking the azimuthal symmetry: steady equatorial vortices appear in the equator.

For larger Reynolds numbers ( $Re > 10^4$ ) the top-bottom symmetry is broken, and the relative sizes of the cells become different. Associated with this symmetry breaking, the vortices propagate around the azimuthal direction, either with a positive or negative velocity. This dynamics can be described using a very simple toy model with a subcritical bifurcation (see figure 1 and reference <sup>2</sup>). According to this model, a hysteresis should be present in the experiment, and it has been found for a very narrow parameter interval.

Three different time-scales are present in the experiment, associated with different phenomena, and the competition between this scales is responsible for the dynamical behavior of the vortices. Finally, this velocity field is evaluated as a potential flow to be used in dynamo experiments. The numerical results reveal that the presence of these vortices can affect dramatically the dynamo threshold<sup>3</sup>.

\*Dept. Física y Matemática Aplicada, Univ. Navarra, Irunlarrea 1, E-31008 Pamplona, Spain.

<sup>1</sup>C. Nore et al, *J. Fluid Mech.* **477**, 51 (2003).

<sup>2</sup>A. de la Torre et al., *Phys. Rev. Lett.* **99**, 054101 (2007).

<sup>3</sup>A. de la Torre et al., *Eur. Phys. J - ST* **146**, 313-320 (2007).

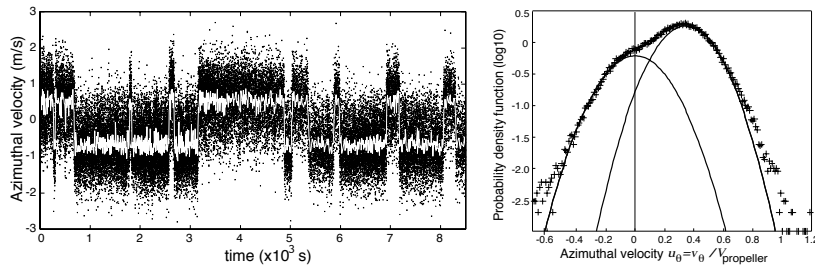


Figure 1: (a) temporal evolution of the instantaneous (black) and averaged (white) azimuthal velocity in the equator of the cylindrical cavity. Two states can be distinguished, one with positive and the other with negative mean velocities. (b) Histogram of one of these states, described using two gaussians.

## What Can Thermal Convection Teach Us about the Nature of Turbulence?

F. H. Busse\*

Thermal convection in a fluid layer heated from below provides a most convenient setting for the study of turbulence. The Rayleigh number  $R$  as the dimensionless measure of the temperature difference forcing convection is the main control parameter, but the Prandtl number is an important second parameter describing the ratio of the two nonlinearities governing the problem. The transition from simple to complex forms of flows can be followed either through numerical simulations of the with increasing  $R$  increasingly chaotic motions or through the study of sequences of subsequent bifurcations of periodic solutions of the basic equations. The latter solutions often exhibit the patterns that become visible as coherent structures in the turbulent version of the system. The theoretical findings are supported (and actually preceded) by laboratory experiments as will be demonstrated by a short movie. In the fully turbulent regime smaller scales of motion tend to act on larger scale flows in a diffusive fashion. This property supports the employment of eddy diffusivities for the description of turbulent processes. The physics underlying the eddy diffusivity concept manifests itself in the striking similarity exhibited between many atmospheric and oceanic dynamic phenomena and their counterparts in laboratory experiments. Thermal convection offers several examples for this aspect.

---

\*Institute of Physics, University of Bayreuth



## Global existence and regularity of a family of periodic incompressible Navier-Stokes flows

Miguel D. Bustamante\*, Edriss S. Titi† and Koji Ohkitani‡

We prove that a family of 3D incompressible Euler or Navier-Stokes flows defined in the periodic cube  $[0, L]^3$  with periodic boundary conditions can be reduced to an equivalent 2D flow. The family consists of flows that are initially invariant under the continuous symmetry  $(x, y, z) \rightarrow (x, y, z) + (s, s, s) \quad \forall s \in \mathbb{R}$ . The proof is constructive and maps any flow in the family into an equivalent 2D flow, known in the literature as a 2.5D flow<sup>1</sup> or a DiPerna-Majda's construction<sup>2</sup>, for which global (in time) existence and regularity is a known property.

Recently<sup>3</sup>, a 3D Navier-Stokes flow with a specially simple analytical initial condition was shown numerically to have a very tame behavior, with an energy dissipation  $\epsilon(t) = Re^{-1} \int_{[0, L]^3} |\boldsymbol{\omega}(\mathbf{x}, t)|^2 d\mathbf{x}$  that vanishes in the infinite-Reynolds number limit, i.e.,  $\lim_{Re \rightarrow \infty} \max_{t \in \mathbb{R}} \epsilon(t) = 0$ , contrary to the expected behavior  $\lim_{Re \rightarrow \infty} \max_{t \in \mathbb{R}} \epsilon(t) = \text{const.} \neq 0$ . In the present work we show that this flow belongs to the above-mentioned family, and thus its special properties can be understood from the regularity of the 2.5D flow associated with it.

In order to study the depletion of this flow in more detail, we compare the results in<sup>3</sup> with a new 2D numerical simulation of the associated 2.5D flow. We address also the problem of the inverse energy cascade by 3D numerical simulations of a forced Navier-Stokes flow in the family.

---

\*Mathematics Institute, The University of Warwick, UK.

†Department of Mathematics, and Department of Mechanical and Aerospace Engineering, University of California, Irvine, CA, USA, ALSO, Department of Computer Science and Applied Mathematics, Weizmann Institute of Science, Israel.

‡Department of Applied Mathematics, The University of Sheffield, UK.

<sup>1</sup>D. Montgomery and L. Turner, *Phys. Fluids* **25**, 345 (1982).

<sup>2</sup>R. J. DiPerna and A. J. Majda, *Commun. Math. Phys.* **108**, 667 (1987).

<sup>3</sup>K. Ohkitani, to appear in *Physica D, special issue EE250* (2008).

## Global frequency selection in a controlled wake

V. Parezanovic\*, and O. Cadot\*.

The experimental present study explores the effect of a control cylinder on the global frequency of a blunt bluff body wake at  $Re = 50000$ . When the control cylinder is located around the centre of the mean bubble recirculation region ( $x_c$  is the distance from the rear of the blunt bluff body), a significant frequency increase is found (without any drag modification). The mechanism for this frequency increase is revealed by means of a 2D DNS (see figures). When the frequency is large, there is a feedback effect of the vorticity created by the control cylinder on the primary sheets of opposite vorticity that is produced by the blunt bluff body. This feedback effect disappears when the control cylinder reaches the end of the recirculation bubble (at  $x_c = 0.76D$ ). We will present High speed PIV results from the experiment of the flow inside the bubble recirculation region with the control cylinder.

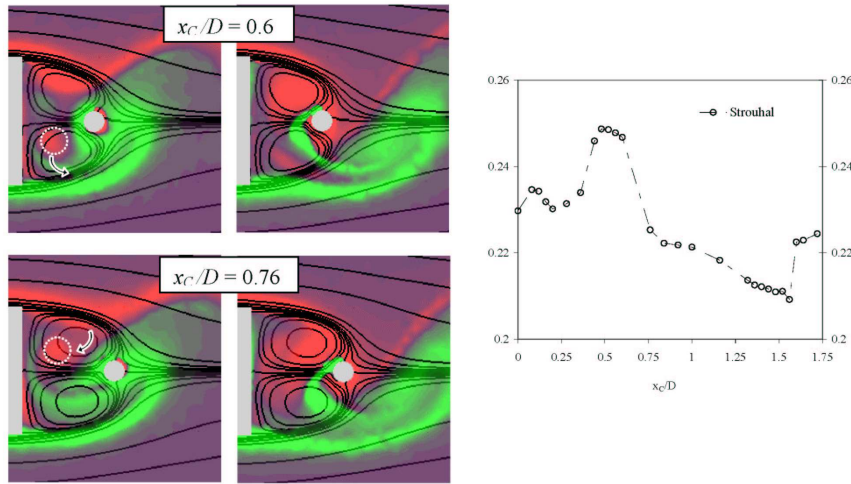


Figure 1: Vorticity fields for different positions (top and bottom) of the control cylinder for two consecutive times. Strouhal number vs. the distance  $x_c$  of the control cylinder from the rear of the bluff body

\*Unite de Mecanique, ENSTA, Chemin de la Huniere, Palaiseau, France

### Three-dimensional Floquet stability analysis of the wake of a confined circular cylinder

Simone Camarri\*, Flavio Giannetti†

The flow around a bluff body that is confined in a plane channel is characterized by several peculiarities if compared to the unconfined case. For instance, in the case of a symmetrically-confined circular cylinder, studied in detail by Sahin & Owens<sup>1</sup>, an asymmetric vortex shedding may occur or an asymmetric steady stable solution may exist for given combinations of the blockage ratio and the flow Reynolds number. Moreover, when alternate vortex shedding from the cylinder occurs, an inversion of the wake vortices takes place downstream of the cylinder (see, for instance, Zovatto & Pedrizzetti<sup>2</sup> and Camarri & Giannetti<sup>3</sup>). More precisely, vortices are alternately shed in the wake as in the unconfined case, i.e. if we imagine the flow to be from left to right, clockwise and counterclockwise vortices are shed from the upper and lower sides of the cylinder, respectively. However, at a certain distance along the wake, depending on both the Reynolds number and the blockage ratio, the trajectories of the two families of vortices intersect and, further downstream, their position with respect to the symmetry line is inverted, i.e. counterclockwise and clockwise vortices are positioned in the upper and lower half of the wake, respectively. This phenomenon persists also when three-dimensional fluctuations are present in the flow, as shown by Camarri et al.<sup>4</sup> for a square cylinder. To the authors' knowledge, the transition of this class of flows from a two-dimensional to a three-dimensional state has not been previously studied in the literature, in spite of the very peculiar configuration of the wake vortices. In particular, it might be interesting to study the analogies and the differences in the three-dimensional transition between the confined and the unconfined case and to highlight the role of the vortex inversion in this transition process.

In this work we consider the case of a symmetrically confined circular cylinder with an incoming Poiseuille flow, since this is a flow which has been largely studied in the literature. The three-dimensional transition of this flow is studied by a linear Floquet analysis, and the resulting unstable modes are analyzed and compared to those found for the unconfined case. Moreover, the critical Reynolds number for three-dimensional stability is found for different blockage ratios. This quantitative information may be useful since several two-dimensional numerical studies of the considered flow are described in the literature, sometimes at relatively large Reynolds numbers. An immersed-boundary technique and a second-order, staggered and centered finite-difference scheme, are used both for calculating the two-dimensional base flow and for performing the Floquet stability analysis. The unsteady equations are advanced in time using a third-order accurate Runge-Kutta scheme. The dominant Floquet multipliers are extracted by a Krylov subspace method.

\*Dip. Ingegneria Aerospaziale, University of Pisa.

†DIMEC, University of Salerno.

<sup>1</sup>Sahin and Owens, *Phys. Fluids* **16:5**, 1305 (2004).

<sup>2</sup>Zovatto and Pedrizzetti, *J. Fluid Mech.* **440**, 1 (2001).

<sup>3</sup>Camarri and Giannetti *J. Fluid Mech.* **574**, 169 (2007).

<sup>4</sup>Camarri et al., *Proceedings of the XVII Congress AIMETA*, 11-15 September 2005, Florence.

## Wall pressure fluctuations in non-equilibrium turbulent boundary layers: a multivariate wavelet analysis

Roberto Camussi<sup>a</sup>, Marc C. Jacob<sup>b</sup>, and Gilles Robert<sup>b</sup>

Pressure fluctuations induced at the wall by turbulent boundary layers play a major role in many physical problems of engineering interest since they contribute significantly to the generation of surface vibrations and noise radiation. Despite the large body of literature devoted to the study of wall pressure statistical properties, there is still some room for improvement in the field especially as far as the physical nature of the fluid dynamic events responsible for the observed pressure field statistics is concerned. This is an important issue from the practical viewpoint mainly to address suitable control strategies aimed at manipulating the flow structures and modifying the wall pressure behaviour.

The main objective of the present work is to provide a qualitative picture of the coherent events associated to the most strongly cross-correlated wall pressure events. Wall pressure data-bases obtained experimentally in two different laboratory flows are analyzed and properly post-processed in order to extract the desired information. A first data-base has been collected at the aerodynamic laboratory of the University *Roma Tre* (Italy). Measurements were taken by a microphone pair flush mounted at the wall of a shallow cavity installed within a low speed wind tunnel. A second data base analyzed was delivered from measurements performed within the anechoic wind tunnel of the Acoustics Centre of the *Ecole Centrale* of Lyon. In this case wall pressure fluctuations have been measured at the wall of a turbulent boundary layer in a channel which was geometrically modified to achieve a weak pressure gradient.

Due to the random nature of the pressure signals at the wall, data are statistically treated through conditional analyses based on the wavelet transform. The wavelet transform of single point velocity or pressure signals was successfully applied to track coherent structures in turbulent shear flows and to characterize their statistical properties<sup>1,2</sup>. The conditioning procedure proposed therein is instead based on the selection of events determined through the computation of a time-frequency localised equivalent of the Fourier Coherence, obtained by the application of a cross-wavelet transform to signal pairs.

A tracking algorithm is developed and conditional Probability Density Functions, conditionally averaged equivalents of Fourier spectral quantities, and ensemble averaged pressure time signatures are computed. In both the experiments it is found that the statistically predominant structures are sweep type events exhibiting bi-modal statistics and that the conditional Coherence function coincides with its non-conditional Fourier equivalent.

---

<sup>a</sup> Mechanical and Industrial Engineering Dept. (DIMI), University 'Roma 3', Rome, I-00146, Italy

<sup>b</sup> Centre Acoustique du LMFA, UMR CNRS 5509 – Ecole Centrale de Lyon – Université Claude-Bernard Lyon I, F-69134 Ecully Cedex, France

<sup>1</sup> R. Camussi, G. Guj, *J. Fluid Mech.* **348**, 177 (1997).

<sup>2</sup> R. Camussi, F. Di Felice, *Phys. Fluids* **18**, 035108-1 (2006).

## Transient Growth of Perturbations in an Expanding Pipe

Chris Cantwell\*, Dwight Barkley\* and Hugh Blackburn†

A numerical study of the growth of infinitesimal perturbations to flow in an axisymmetric expanding pipe has been conducted. This extends existing work on the backward-facing step<sup>1</sup>. Simulations have been undertaken using existing direct optimal growth analysis<sup>2</sup> techniques on a spectral element discretisation<sup>3</sup>. Figure 1 (top) shows a cut-away of the geometry of the expanding pipe under consideration.

Results are presented showing the magnitude of this growth against time over the range of Reynolds numbers  $Re = 20$  to  $Re = 300$ , as well as a comparison of growth in the first four azimuthal wavenumbers at fixed Reynolds number. The critical Reynolds number for the onset of growth in these first four wavenumbers is also determined. It is found that the maximum growth occurs in the azimuthal wavenumber  $k = 1$ . The  $k = 1$  initial perturbation leading to optimal growth at  $Re = 50$  is visualized in Figure 1 (bottom).

\*Mathematics Institute and the Centre for Scientific Computing, University of Warwick, UK

†Department of Mechanical and Aerospace Engineering, Monash University, Australia.

<sup>1</sup>H.M. Blackburn, D. Barkley, et al., *J. Fluid Mech.* (in press 2008)

<sup>2</sup>D. Barkley, H.M. Blackburn et al., *Int. J. Numer. Meth. Fluids* (in press 2008)

<sup>3</sup>H.M. Blackburn and S.J. Sherwin, *J. Comp. Phys* **179**(2), 759 (2004)

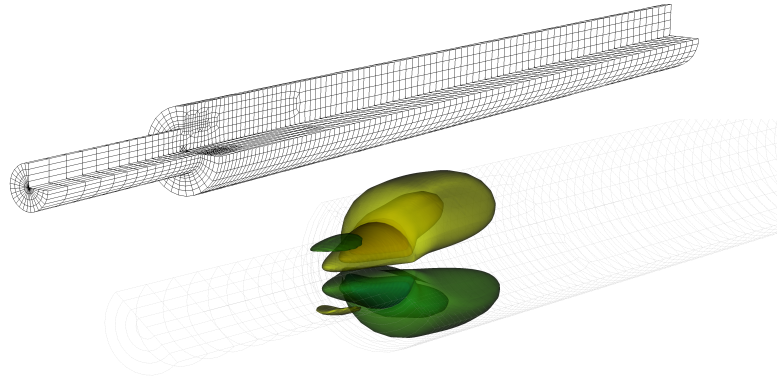


Figure 1: Expanding pipe geometry (top) with expansion ratio of two and step-height  $h$ , having an in-flow of  $10h$  and an out-flow of  $50h$ , and (bottom) isosurfaces of the axial velocity component for the initial perturbation leading to optimal energy growth in the  $k = 1$  azimuthal wavenumber.

# Numerical investigations of baker's map based chaotic mixers.

Philippe Carrière\*

Chaotic mixing generated by the separation/stacking mechanism, the key underlying concept in the baker's map, has motivated some studies in the literature. In a recent work<sup>1</sup>, it has been obtained that the steady, 3-D flow induced in a system like in figure 1.a leads, in the mean, to a lyapunov exponent close to  $\ln 2$  (as for the baker's map). Here, we present some complementary characterisations of the system and some preliminary results of a comparison exercise with other kinds of mixers as, for instance, the one proposed by Chen and Meiners<sup>2</sup> (see figure 1.b). As an illustration, a rather non-intuitive result is that, while the mixing behaviour may appear to differ in the details (figure 2), the mixer of Chen & Meiners also leads to a value of the lyapunov exponent very close to  $\ln 2$ .

\*Laboratoire de Mécanique des Fluides et d'Acoustique, CNRS-Université de Lyon; ECL-UCBL-INSa. Ecole Centrale de Lyon, 36 av. G. de Collongues, 69134 Ecully cedex, France.

<sup>1</sup>Ph. Carrière, *Phys. Fluids* **19**, 118110 (2007)

<sup>2</sup>H. Chen & J.-S. Meiners, *Appl. Phys. Lett.* **12**, 2193 (2004)

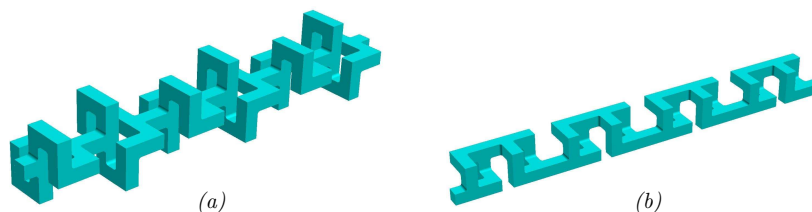


Figure 1: Examples of baker's map based chaotic mixers. (a): symmetric configuration as in Ref. 1. (b): asymmetric configuration proposed in Ref. 2.

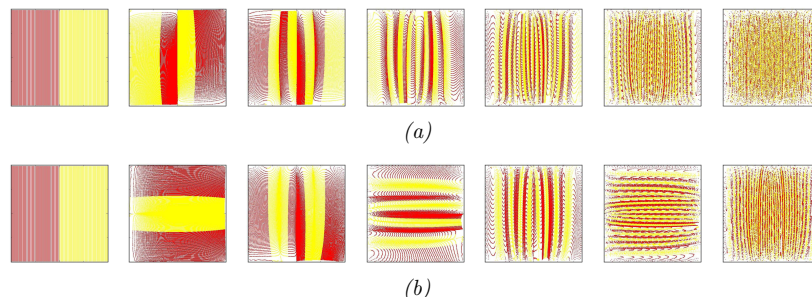


Figure 2: Mixing of non-diffusive tracers in successive cross-section planes for the corresponding mixers of figure 1.

## Multimode decomposition of a DNS signal into 3D Tollmien-Schlichting-like waves

Grégoire Casalis\*, Estelle Piot\*

This study deals with spatially growing perturbations in a laminar incompressible boundary layer on a flat plate without pressure gradient. The Blasius flow is distorted by a spanwise row of small roughness elements, and is consequently inhomogeneous in two directions : the wall-normal ( $y$ ) and spanwise ( $z$ ) directions. A Direct Numerical Simulation has been undertaken, see <sup>1</sup> to compute the disturbance created by the scattering of a travelling 2D Tollmien-Schlichting (TS) wave by the distorted base flow. The aim of the present study is to decompose the obtained disturbance into the linear eigenmodes of the base flow, extending a previous work, see <sup>2</sup>.

As the base flow is inhomogeneous in the  $y$  and  $z$  directions and assumed to be parallel, infinitesimal perturbations are sought at each streamwise ( $x$ ) location under the normal mode form :

$$\hat{q}(x, y, z, t) = q(y, z)e^{i(\alpha x - \omega t)} \quad (1)$$

where  $\omega$  is the frequency of the incoming 2D TS wave. Introducing this representation into the linearized Navier-Stokes equation yields a two-dimensional partial differential equations (PDE) system, which reads:

$$E \frac{\partial \mathbf{A}}{\partial y} + F \frac{\partial \mathbf{A}}{\partial z} = \mathcal{H}_1 \mathbf{A} + i\alpha \mathcal{H}_2 \mathbf{A} \quad (2)$$

where  $\mathbf{A}(y, z)$  is a vector function depending on the pressure and velocity components of the perturbation  $q$  and  $E$ ,  $F$ ,  $\mathcal{H}_1$  and  $\mathcal{H}_2$  are (12,12) matrices functions of the mean flow and  $\omega$ . The solutions of this PDE system are the eigenmodes of the base flow. It has been shown that they consist in three-dimensional TS-like waves<sup>3</sup>.

To decompose the DNS-computed disturbance into these eigenmodes, one has to use an orthogonality relationship leading to the evaluation of the amplitude of each mode. As the stability equations are nonself-adjoint, both sets of eigenfunctions of the direct and adjoint problems have to be used to allow the decomposition of the DNS disturbance into the normal modes. This biorthogonal eigenfunction system has been previously used in a two-dimensional boundary layer<sup>2</sup> (i.e. for a flow that is inhomogeneous in the streamwise direction only).

In the present work, such a method is extended and applied to the considered three-dimensional boundary layer (inhomogeneous in two directions). The validity of the obtained biorthogonality condition is checked on artificial combinations of the eigenmodes. Then, the DNS disturbance is decomposed into the eigenmodes, i.e. the amplitude of each eigenmode is computed. This is possible even if the pressure component of the DNS disturbance is unknown. Finally, the linear combination of the eigenmodes with the amplitudes previously computed is compared favorably with the DNS disturbance.

\*Aerodynamics and Energetics Modeling, ONERA, Toulouse, FRANCE

<sup>1</sup>A. Wörner, *PhD thesis*, Stuttgart, 2003.

<sup>2</sup>A. Tumin, *Phys. Fluids* **15**, 2525 (2003).

<sup>3</sup>E. Piot, et al. *Eur. J. Mech. B/Fluids* **accepted for publication**, (2008).

## Fast-rising cap bubbles with a toroidal bubbly wake

C. P. Caulfield<sup>\*</sup>, J. R. Landel<sup>†</sup>, C. Cossu<sup>‡</sup>

The prediction of the rise speed of large buoyant bubbles is a fundamental fluid mechanics problem relevant to a number of applications ranging from carbon sequestration technology to chemical engineering or astrophysics. Single large bubbles typically have a spherical cap shape with bubbles of larger volume rising faster than ones of smaller volume. However, except in exceptionally well-controlled and low-noise experiments, we demonstrate that the released gas splits into a leading cap bubble followed by a crown of satellite bubbles that can contain up to 50% of the total volume of the rising bubble system. We find in this more likely and realistic case that the leading bubble takes a reproducible lenticular shape and that the satellite bubbles rearrange in a characteristic toroidal crown. Contrary to intuition, this system of bubbles rises faster than a single cap bubble of the same total volume, suggesting that the crown of smaller bubbles reduces the drag of the total bubble system.

---

<sup>\*</sup>BP Institute & Department of Applied Mathematics & Theoretical Physics, University of Cambridge, U.K.

<sup>†</sup>Département de Mécanique, École Polytechnique, Palaiseau, France

<sup>‡</sup>Département de Mécanique, & Laboratoire d'Hydrodynamique (LadHyX), CNRS - École Polytechnique, Palaiseau, France



## How to stir turbulence

Hakki Ergun Cekli\* and Willem van de Water\*

The best way to create homogeneous and isotropic turbulence in a windtunnel is through using a grid. However, the achievable Reynolds numbers are small. Much stronger turbulence and much larger Reynolds numbers can be reached through active grids<sup>1</sup>. Our active grid is a regular grid of rods with attached vanes that can be rotated by servo motors. The control of the grid is such that at each instant the angle of each axis is prescribed, which allows us to correlate the state of the grid with the turbulence it creates. The active grid is placed at the beginning of the 8 m long,  $0.9 \times 1\text{m}^2$  area of the test section of our recirculating windtunnel. The turbulence properties are measured using an array of hot-wire anemometers.

The question is whether the grid should be operated periodically or randomly to produce the best turbulence; that is turbulence which is stationary and has the highest Reynolds number. Figure 1 illustrates that periodic stirring causes a strong response of the flow at the stirring frequency. Obviously, the imprint of random stirring is not visible in the turbulence spectrum, but such direct imprint may still be there. The key question then is whether the direct impression of the stirrer on the turbulence is broken by stirring randomly. This question will be answered by time-correlating the grid with the turbulence, that is: will the correlation decrease with increasing randomness? In our experiments the degree of randomness is varied by changing the motion parameters of the grid more or less randomly.

In the case of synchronised periodic motion of the grid, we have found preferred frequencies where the turbulence dissipation rate is optimal. We will discuss these results in terms of a resonant response of the turbulence.

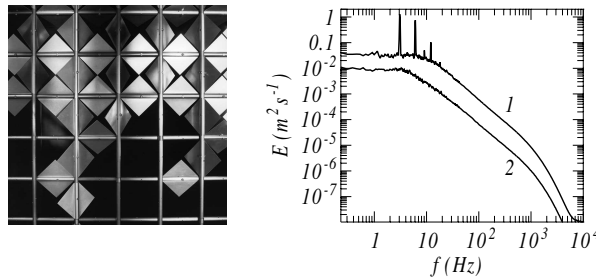


Figure 1: Left: photograph of the active grid. Right: curve 1: turbulence spectrum obtained by periodic stirring of the grid with frequency 3 Hz. The spectrum shows sharp peaks at the stirring frequency and its higher harmonics. Line 2: random stirring. For clarity, line 2 has been shifted down one decade.

\*Physics Department, Eindhoven University of Technology.

<sup>1</sup>H. Makita, *Fluid Dyn. Res.* **8**, 53 (1991); Ralph Savelsberg and Willem van de Water, *Phys. Rev. Lett.* **100**, 34501-34504 (2008)

## An erosion-deposition model for granular beds sheared by turbulent flows

F. Charru\*

Up to now, the bedload transport at the surface of granular beds is predicted from semi-empirical laws, giving the volumetric flow rate of the particles as a power law of the Shields number (dimensionless shear stress exerted by the fluid on the bed), with the shear stress calculated as if the bed were fixed. The accuracy of the predictions is mainly limited by the algebraic character of these transport laws, which ignore the effect of dimensionless parameters such as the particle Reynolds number, and also ignore any relaxation effect between the particle flux and the shear stress.

An improvement of the situation has been proposed recently for viscous flow, which describes the dynamics of the moving layer by a first-order partial derivative equation for the number  $n$  of moving particles per unit area (figure 1)

$$\frac{\partial n}{\partial t} = \dot{n}_e - \dot{n}_d - \frac{\partial(nU)}{\partial x}, \quad (1)$$

where  $\dot{n}_e$  is the erosion rate from the fixed bed,  $\dot{n}_d$  the deposition-rate, and  $U$  the mean particle velocity. A modelling of these three terms has been proposed, with the numerical coefficients determined from experiments<sup>1</sup>. It has been shown that when included in a stability analysis of the plane bed, this erosion-deposition model significantly improves ripple length predictions<sup>2,3</sup>.

We will present an extension of the model to turbulent flow. It will be shown that slightly different modellings of the erosion time involved in the erosion rate, lead to the slightly different versions of the classical transport laws. It will also be shown how weak dependences on the particle Reynolds number naturally arise in the transport law. The ‘Bagnold hypothesis’ according to which the fluid shear stress is reduced to the threshold on the fixed bed, will also be discussed in connection with recent work<sup>4</sup>.

\*Institut de Mécanique des Fluides de Toulouse, 31400 Toulouse, France

<sup>1</sup>F. Charru, H. Moulleron & O. Eiff *J. Fluid Mech.* **519**, 55–80 (2004).

<sup>2</sup>F. Charru & E. J. Hinch *J. Fluid Mech.* **550**, 111–121 (2006).

<sup>3</sup>F. Charru *Phys. Fluids* **18**, 121508 (2006).

<sup>4</sup>G. Parker, G. Seminara and L. Solari *Water Resour. Res.* **39**, 1183 (2003).

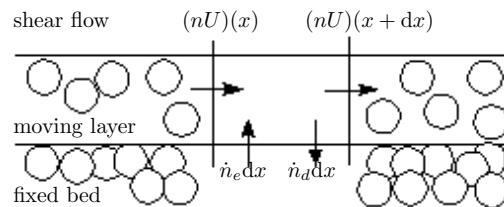


Figure 1: Sketch of the particle fluxes in a strip of the moving layer, of length  $dx$  and width unity.

## Morphological approach to the behavior of suspensions

Xavier Chateau\*

Estimates for the overall properties of suspensions of spherical particles in a fluid have been obtained by means of a morphologically representative pattern based approach. The suspension is described as a set of spherical inclusions (the particles) embedded in spherical shells of the suspending fluid with identical geometrical and mechanical properties. The patterns are isotropically distributed over the representative elementary volume of the suspension.

We showed that the new estimate fits the classical Krieger–Dougherty estimate for the viscosity of a Newtonian monodisperse suspension with a relative error less than 5 % for relative viscosity between 1 and 100.

We also computed the storage modulus  $G'$ , loss modulus  $G''$  and relative viscosity  $\eta$  as a function of the solid volumic fraction  $\varphi$  for a suspension of elastic particles in a viscous fluid (Figure 1, right). Interestingly, the theoretical estimates versus  $\varphi$  curves are very similar to the overall properties versus time curves experimentally measured on a bentonite after a strong preshear was applied to the material<sup>1</sup> (Figure 1, left). The observed behavior can be accounted for by assuming that aggregation of the clay particles results in an increase of the effective volume fraction  $\varphi$  as a function of time (the small particles form elastic aggregates). Then, the morphological model is also able to describe the liquid-solid transition of soft-jammed systems.

\*Université Paris Est, Institut Navier.

<sup>1</sup>G. Ovarlez et al, *Phys Rev. E* 76, 011406 (2007)

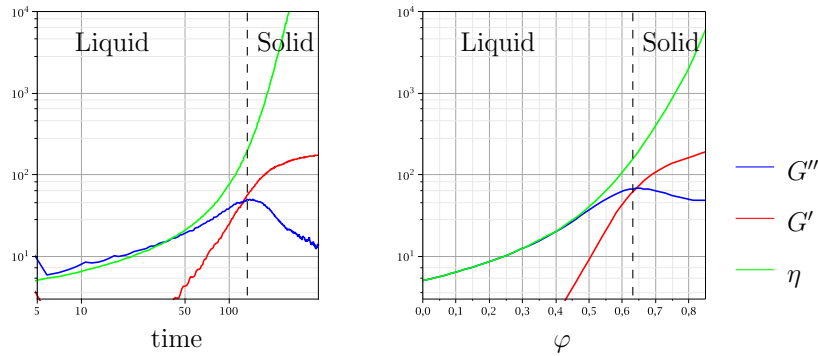


Figure 1: Comparison between the experimentally measured rheological properties of a bentonite suspension as function of time (left) and the morphological representative pattern based estimates of the overall properties of the suspension when the particles are elastic ( $G = 500$  Pa), the suspending fluid is purely viscous ( $\mu = 5$  Pa.s) and the close solid packing fraction is equal to 1.

### Experimental study of the amplitude dependencies of disturbance waves in annular two-phase flow using conditional averaging technique.

Cherdantsev A.V.<sup>a, b</sup>, Alekseenko S.V.<sup>a, b</sup>, Antipin V.A.<sup>a</sup>, Kharlamov S.M.<sup>a</sup> and Markovich D.M.<sup>a, b</sup>

Disturbance waves appear on the surface of liquid film sheared by high-velocity turbulent gas stream and represent large bulks of liquid with an amplitude several times greater than average film thickness. These waves are considered to be the main source of liquid entrainment into the core of gas stream. A tremendous amount of experimental works was devoted to studying the annular flow and disturbance waves properties<sup>1</sup>.

An important feature of this type of flow is that properties of different disturbance waves may vary greatly at the same flow parameters<sup>2</sup>. In most of the experimental works the influence of flow parameters on the average values and standard deviation of waves properties were investigated<sup>3</sup>. In other works, individual waves properties were studied<sup>4</sup>.

In the present work the assumption is made that all characteristics of a disturbance wave are generally defined by the wave's amplitude at constant flow parameters. Thus, to obtain the amplitude dependence of a certain characteristic of disturbance waves for given flow conditions, the whole range of disturbance waves amplitudes was separated into a set of narrow sub-ranges. Then all the waves with the amplitude belonging to the chosen sub-range were processed separately from the other waves to obtain the average value of the characteristic. Such quasi-deterministic approach gives more systematic and detailed information on the influence of flow parameters on the disturbance waves properties and evolution.

The downward air-water flow in a 15 mm diameter tube was investigated in the range of liquid Reynolds numbers 90-350 and superficial gas velocities 20-64 m/s using a set of flush-mounted conductivity probes. The amplitude dependence of disturbance waves velocity was shown to be the same for different distances from the inlet. Generalizing dependencies of waves velocity on amplitude, average shear stress and substrate thickness, were suggested. Using the velocity data, independence of waves spacing of superficial gas velocity was shown. Average profiles of disturbance waves of given amplitude were obtained. The linear dependency of disturbance waves steepness on their amplitude was observed, and universality of this dependence for different values of gas velocity was shown.

---

<sup>a</sup> Institute of Thermophysics, Siberian Branch of the Russian Academy of Science.

<sup>b</sup> Novosibirsk State University.

<sup>1</sup> Azzopardi. *Int. J. Mult. Flow*. **23**, 1 (1997).

<sup>2</sup> Hewitt, Hall Taylor. *Pergamon Press, Oxford* (1970).

<sup>3</sup> Chu, Dukler. *AIChE J.* **21**, 583 (1975).

<sup>4</sup> Thwaites et al. *Chem. Engng. Sci.* **31**, 481 (1989).

## Correction of multihole pressure probe measurements in velocity gradients

Valery Chernoray<sup>a</sup>, Johan Hjärne<sup>b</sup>

Multihole pressure probes are widely used as accurate, robust, and versatile flow-measuring instruments with numerous advantages over other flow measuring devices. Surprising though that a very few experimentalists, which use the multihole pressure probes in strong gradient fields, apply the spatial resolution and downwash velocity corrections.

In recent experiments performed at Chalmers<sup>1</sup> extensive measurements were performed using both the five-hole probes and cross hot-wires. During data analysis it was found that the crossflow velocity components measured by the five-hole pressure probes disagreed with those obtained using the cross hot-wires. Differences between these two measurement data sets were observed in zones of vane wakes and sidewall boundary layers where the velocity gradients are strong. Our subsequent research has revealed that a modified version of correction by Ligrani et al.<sup>2</sup> can be used to compensate for the 5-hole probe errors caused by the velocity gradients.

The results on the implementation and verification of the correction will be presented. The efficiency of the obtained correction is scrutinized through detailed side-by-side comparison with corresponding cross hotwire data. To our knowledge, such verification was not performed previously. This study demonstrates a very good efficiency and reliability of the correction, which lead to a significant improvement of the corrected velocity data. A very important fact is that the described correction is not found to over-correct and distort the data and can be used safely.

<sup>a</sup> Applied Mechanics, Chalmers University of Technology, 412 96 Gothenburg, Sweden.

<sup>b</sup> Aero and Thermo Dynamics, Volvo Aero Corporation, 461 81 Trollhättan, Sweden.

<sup>1</sup> Hjärne et al., *ASME paper* GT2007-27712 (2007).

<sup>2</sup> Ligrani et al., *Exp. Fluids*, **7**, 424 (1989).

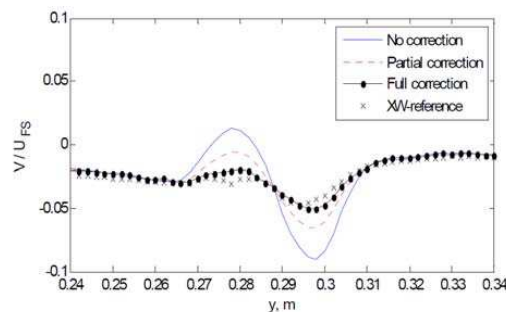


Figure 1: Effect of different parts of correction. Profiles of vertical velocity at  $x = 0.5C$  and  $z = -0.036$  m. Partial correction denotes correction for spatial resolution without downwash correction.

## Linear and non-linear transient behaviour of a separated flow

S. Cherubini<sup>\*†</sup>, F. Alizard<sup>\*</sup>, J.-C. Robinet<sup>\*</sup> and P. De Palma<sup>†</sup>

The non-modal transient behaviour of a two-dimensional separated boundary layer flow over a flat plate is investigated using a linear and a non-linear approach based on linear global eigenvalue analysis and DNS simulations. The base flow, as well as the unsteady solutions, are computed by integration of the two-dimensional incompressible Navier-Stokes equations. The separation is obtained by assigning a suction-and-blowing normal velocity profile at the upper boundary. The Reynolds number,  $Re = U_\infty L/\nu = 30000$ , where  $L = 0.05m$ , leads to an asymptotically linearly stable flow. Nonetheless, the non-normality of the Navier-Stokes operator could lead to a transient growth of the energy  $E(t)$ . In order to measure such an amplification we compute, by means of global mode decomposition, the initial perturbation leading to the maximum amplification<sup>1</sup>. The energy evolution of the optimal initial condition in a linear regime is computed by the global model and by a DNS simulation initialized with an optimal perturbation of amplitude  $10^{-8}$  (see Figure 1(a)). At short time, a very large transient growth of the perturbations is observed in the separated zone<sup>2</sup>, which reaches  $E(t)/E(0) \sim 10^8$ , while in the non separated zone the perturbations are damped. Furthermore, the flow shows a similar behavior when initialized by a white noise perturbation placed upstream or within the separated zone (see Figure 1(b)), namely in the region where the optimal initial energy is clustered as well. In order to compare the non-linear transient behaviour with the linear one, the optimal or random perturbation is injected on the base flow with an increasing amplitude equal to  $10^{-4}$ . As shown in Figure 1(c), the energy growth in the separated zone saturates<sup>3</sup>, reaching an earlier maximum of about  $10^7$ . Nonetheless, a further increase of energy is observed in the non separated zone, which could mean that the two-dimensional flow could be non-linearly convectively unstable though linearly stable. The same behaviour has been observed for lower Reynolds numbers, up till  $Re \sim 22000$ .

<sup>\*</sup>SINUMEF Laboratory, Arts et Métiers ParisTech, 151, Bd. de l'Hôpital 75013 Paris, France.

<sup>†</sup>DIMEG, Politecnico di Bari, Via Re David 200, 70125 Bari, Italy.

<sup>1</sup>L.N. Trefethen, M. Embree, *Princeton University Press* (2005).

<sup>2</sup>F. Alizard, J.-Ch. Robinet, *ICIAM* (2007).

<sup>3</sup>U. Ehrenstein and F. Gallaire, *submitted to JFM* (2007).

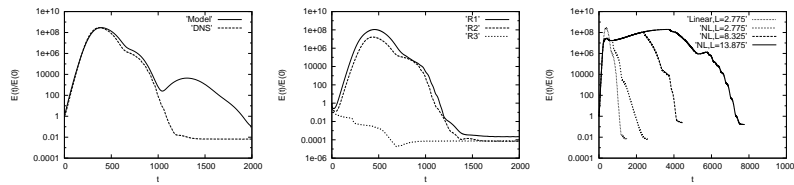


Figure 1: Evolution in time of the energy for different initial perturbations: (a) linearly optimal; (b) white noise, placed upstream (R1), within (R2), or downstream (R3) the bubble, in a linear regime; (c) non-linear, for different domain length.

## Liquid flows through nanopores: from hydrodynamic to atomistic motion

Mauro Chinappi\*, Francesco Picano\* and Carlo Massimo Casciola\*

Liquids confined in nanometer scale pores present features that can differ largely from the macroscopic case. At these scales the classical hydrodynamic description of fluid dynamics fails and the a new behaviour abruptly sets in as a distinctive signature of the nanofluidic regime <sup>1</sup>, for instance the density profile, far from being homogeneous, shows a strong layering near the walls and in the pore (Fig 1, left panel).

In this study the cross-over from hydrodynamic to atomistic motion in nanoscopic channels is investigated by means of many-body molecular dynamics simulations of a simple Lennard-Jones liquid for various pore geometries. The system is constituted by two liquid reservoirs connected by a nanopore. Both symmetric (cylindrical) and asymmetric (truncated conical) pores are analyzed. For pore diameter  $d$  of the order of the atom dimension  $\sigma$  the motion proceeds through the so called single-file motion, namely a concerted, sequential, motion of concomitant molecules along a chain, with no possibility of overtaking <sup>2</sup>. We show that in this case, for low forcing intensity, the mass flow rate scales as  $d^3$ . On the other hand for large  $d$  (i.e.  $d/\sigma \gg 1$ ) the system is expected to reach the hydrodynamic regime resulting in power four scaling of the mass flow rate. Direct comparison of molecular dynamics simulation with numerical solution of the Navier Stokes equation shows that the hydrodynamic behavior is reached for pore larger than a threshold diameter. The two different scaling laws give a complete description of the linear response (low forcing) of the system (Fig. 1, right panel). A systematic investigation of the non linear effects arising under strong load will be discussed to understand the validity limits for the hydrodynamic description.

\*Department of Mechanics and Aeronautics, "Sapienza" University of Rome, via Eudossiana 18, 00184, Rome, Italy

<sup>1</sup>Chinappi et al. *Phys. Rev. Lett.* **97**, 144509 (2006).

<sup>2</sup>Berezhkovskii et al. *Phys. Rev. Lett.* **89**, 64503 (2002)

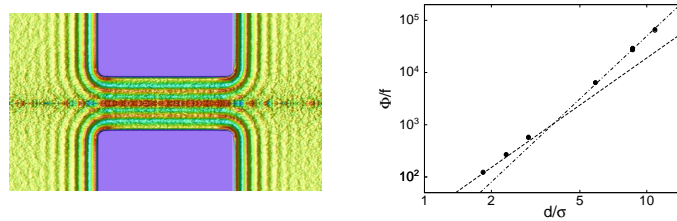
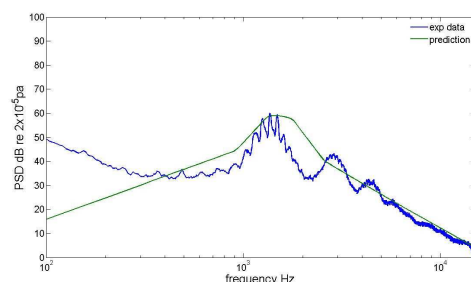


Figure 1: Left. Equilibrium density profile for a Lennard-Jones liquid in a narrow cylindrical pore Right. Linear regime. Mass flow rate  $\Phi$  as a function of the pore diameter  $d/\sigma$ . The two lines correspond to the  $d^3$  and  $d^4$  scaling.

## On the Surface Pressure Fluctuations and Tonal Noise Generated by Airfoil in Laminar Flows

Tze Pei Chong<sup>a</sup> and Phillip Joseph<sup>b</sup>

Because of its importance to wide range of applications (aircraft, turbomachinery and wind turbines), the study of airfoil noise is still ongoing in the research community. One of the frequently quoted noise problem that occurs in this area is the discrete frequency tone generated by convecting laminar and low Mach number flows to an airfoil inclined at small angles to the streams. Tonal noise up to 20-40dB above the background broadband levels have been reported in the literatures<sup>1-2</sup>. The widely accepted mechanism of tonal noise generation is related to the growth of laminar boundary layer extending up to the trailing edge at the pressure side of the airfoil. At moderate Reynolds numbers the growth of Tollmien-Schlichting instability waves at the pressure side will be amplified strongly with the inflectional profiles near the trailing edge<sup>2</sup>. By flow visualization the authors<sup>2</sup> found that these instabilities amalgamate with the regular von Karman vortex street and shed at the frequency of the tone. To further understand this mechanism and the noise source, an experiment program has been carried out in Southampton to characterize the relationship between the unsteady velocity fields in the boundary layer and wake and the surface pressure fluctuations near the trailing edge of an airfoil. The radiated airfoil noise will also be measured. The airfoil is a NACA0012 with chord length of 15cm and span 45cm, giving an aspect ratio of 3. The experiment is performed in a large anechoic chamber equipped with a newly built quiet and low turbulence blow down open jet wind tunnel<sup>3</sup>. The surface pressure fluctuations were measured by embedded miniature microphones and hot wire was used to measure the velocity fluctuations in the boundary layer and wake. Farfield noise was measured separately by B&K microphones and good repeatability was observed for the measured data. Aerodynamic and acoustic responses under the effects of Reynolds numbers and angle of attacks were also characterized at  $1-7 \times 10^5$  and  $0^\circ$ ,  $5^\circ$ ,  $10^\circ$  and  $15^\circ$  respectively. The measured airfoil noise is consistent with the classical prediction for all of the test cases<sup>4</sup>. Example of which is shown in Figure 1 for the power spectra density (PSD) with the airfoil inclined at  $5^\circ$  at jet velocity of 28.8m/s. Acquisition of the experimental data has been completed and data analyse is currently underway. It is hoped that the results can provide further insight into the hydrodynamic features of the airfoil that ultimately produce the tonal noise at different flow conditions.



**Fig. 1** Power spectra density of airfoil noise measured at 0.5m above the trailing edge at  $5^\circ$  AOA with jet velocity of 28.8m/s.

<sup>a,b</sup> ISVR, University of Southampton.

<sup>1</sup> Paterson, R., Vogt, P., Fink, M. and Munch, C., 1972, *J. Aircraft*, **10**, 296-302

<sup>2</sup> Nash, E., Lowson, M. and McAlpine, A., 1999, *JFM*, **382**, 27-61

<sup>3</sup> Chong, T. P., Joseph, P. and Davies, P.O.A.L., 2007, 13<sup>th</sup> AIAA Aeroacoustic Conference, Rome, Italy

<sup>4</sup> Brooks, T., Pope, D. and Marcolini, M., 1989, Tech. rep. NASA Reference Publication 1218



## Response of near-wall turbulent flow to temporal acceleration

Y M Chung<sup>\*</sup> and S Y Jung<sup>†</sup>

In the present work, we simulated an accelerated turbulent pipe flow using LES to investigate the delay effect on the near-wall turbulence<sup>1</sup>. In the present study, the simulations were started from a fully-developed turbulent pipe flow at  $Re_0 = 7000$ . And the mass flow rate was increased linearly<sup>2</sup> to a final Reynolds number  $Re_1 = 45200$ . Figure 1B) shows the development of the skin friction coefficient,  $C_f$ . The ramp-up can be divided into three different regimes: an initial stage, a transient stage, and a relaxation stage. The initial stage ( $7000 < Re < 19000$ ) denotes the gradual increase of  $C_f$  due to slower responses of turbulence than those of the mean velocity. During the transient stage ( $19000 < Re < 29000$ ), the turbulence production near the wall is vigorously enhanced, thus  $C_f$  is rapidly increased. In the relaxation stage ( $29000 < Re < 45200$ ), the turbulence approaches the pseudo-steady state near the wall and it is propagated from the wall to the centre of the pipe at a certain speed. The present results shown in Figure 1C) suggest that the enhanced anisotropy of the turbulence in the initial and transient stages will be a challenging problem to standard turbulence models, and RANS results will be included in the final manuscript.

<sup>\*</sup>School of Engineering, University of Warwick, U.K.

<sup>†</sup>St. Anthony Falls Laboratory, University of Minnesota, USA.

<sup>1</sup>Y.M. Chung, *Int. J. Numer. Meth. Fluids* **47**, 925 (2005).

<sup>2</sup>S. He, J.D. Jackson, *J. Fluid Mech.* **408**, 1 (2000).

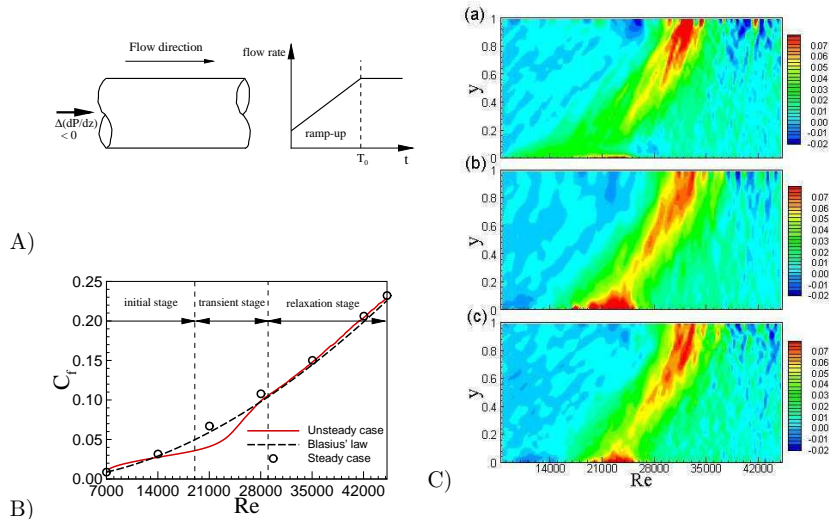


Figure 1: A) Schematic diagram, B) Skin friction coefficient, and C) Relative rate of changes of r.m.s. velocity fluctuations ( $u'$ ,  $v'$ , and  $w'$ ).

## Absolute Instability of Light Jets Emerging from Circular Injector Tubes

W. Coenen\*, A. Sevilla† and A. L. Sánchez\*

We present a numerical study of the spatiotemporal, inviscid linear instability of light jets emerging from round tubes for values of the Reynolds number,  $\text{Re}_j = \rho_j Q / (\pi a \mu_j) \gg 1$ , where  $Q$  is the volumetric flow rate,  $\rho_j$ ,  $\mu_j$  are, respectively, the jet density and viscosity, and  $a$  is the injection tube radius. The analysis focuses on the influence of the injector length  $l_t$  on the stability characteristics of the resulting jet, whose base velocity profile at the exit is computed in terms of the dimensionless tube length  $L_t = l_t / (\text{Re}_j a)$  by integrating the boundary-layer equations along the injector. Both axisymmetric ( $m = 0$ ) and helical ( $|m| = 1$ ) modes of instability are investigated for different values of the jet-to-ambient density ratio  $S = \rho_j / \rho_\infty < 1$ . For short tubes  $L_t \ll 1$  the base velocity profile at the tube exit is uniform except in a thin surrounding boundary layer of thickness  $\text{Re}_j^{-1/2} a$ . Correspondingly, the stability analysis reproduces previous results of uniform velocity jets, according to which the jet becomes absolutely unstable to axisymmetric modes for a critical density ratio  $S_c \simeq 0.66$ , and to first azimuthal modes for  $S_c \simeq 0.35$ . For tubes of increasing length the analysis reveals that both modes exhibit absolutely unstable regions for all values of  $L_t$  and small enough values of the density ratio. In the case of the first azimuthal mode  $|m| = 1$  we find a critical density ratio which increases monotonically with the injection tube length, reaching its maximum value  $S_c \simeq 0.5$  as the exit velocity approaches the parabolic profile for  $L_t \gg 1$ . In the case of axisymmetric modes  $m = 0$ , the critical density ratio achieves a maximum value  $S_c \simeq 0.9$  for  $L_t \simeq 0.04$  and then decreases to approach  $S_c \simeq 0.7$  for  $L_t \gg 1$ . The absolute growth rates in this limiting case of near-Poiseuille jet profiles are however extremely small for  $m = 0$ , in agreement with the fact that axisymmetric disturbances to the parabolic velocity profile are neutrally stable. As a result, for  $S < 0.5$  the absolute growth rate of the helical mode becomes larger than that of the axisymmetric mode for sufficiently large values of  $L_t$ , indicating that the helical mode prevails in the instability development of very light jets issuing from long injectors.

---

\*Área de Mecánica de Fluidos, Universidad Carlos III de Madrid.

†Área de Mecánica de Fluidos, Universidad de Jaén.

## Gas separation and bubble behavior at a woven screen

Michael Conrath<sup>\*</sup> and Michael Dreyer<sup>†</sup>

Gas-liquid two phase flows are widespread. In many applications the separation of both phases is necessary. Chemical reactors, water treatment devices or gas-free delivery of fluid and fuel are only some of them.

We have built an experiment that consists of a Dutch Twilled woven screen made of stainless steel in a vertical Plexiglass tube that can carry upward as well as downward flow. The screen is suspended perpendicular to the flow which is forced through it at variable strength. Controlled injection of air bubbles allows us to examine the ability of the screen to separate air and liquid. We present experimental data on the static bubble point, i.e. the pressure difference when the air breaks through the weave. This is related to the behavior of a single bubble that is trapped under the weave in upward flow. A theoretical prediction of the bubble shapes under various flow conditions is based on a shooting method and a simplified pressure distribution. Qualitatively, we report on the bubble behavior beyond the bubble point and in downward flow.

---

<sup>\*</sup>ZARM, University of Bremen.

<sup>†</sup>ZARM, University of Bremen.

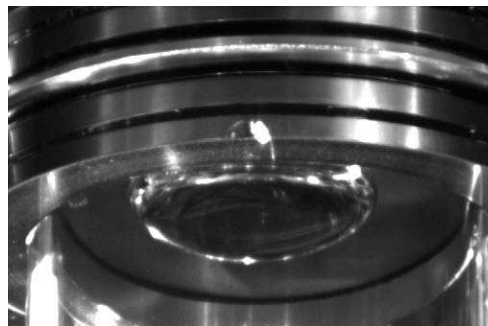


Figure 1: View on the bubble trapped under the screen.

## Mixing in Steady Flow in Small Amplitude Helical Pipes

Andrew N. Cookson\*, Spencer J. Sherwin\* and Denis J. Doorly\*

Small amplitude helical pipes have been proposed for use as arterio-venous shunts and bypass grafts<sup>1</sup>. Preliminary *in vivo* tests found that conventional grafts were completely occluded, whereas grafts constructed with helical pipes were not. Swirling flow and in-plane mixing induced by the geometry were hypothesised to be the mechanisms responsible<sup>1</sup>. Whether or not such geometry is proven to be beneficial, studying mixing in helical pipe flows is of basic interest.

Using an approximation to a helical geometry, a coordinate mapping could be used, thereby allowing the Navier-Stokes equations to be solved in a mapped domain using a spectral/hp element code (*Nektar*). The helical pitch was fixed at 6 pipe diameters ( $D$ ), and the helical radius varied from  $0.1D$  to  $0.5D$ . A physiologically appropriate Reynolds number of 250 was used for all cases. Mixing, through stirring, was examined by tracking passive, coloured particles using a high-order algorithm.

Slices of the particle trajectories, taken at integer multiples of the pitch length, reveal a double-vortex structure emerging with increasing helical radius, as shown in Figure 1(b). This is despite an in-plane velocity field of a single vortex for all the geometries considered, as indicated by the axial vorticity contours in Figure 1(a). We show that this discrepancy can be explained by a rotating reference frame, raising questions regarding the appropriate definition of a vortex for helical geometries, and other pipe flows in general. Figure 1(c) shows the effective velocity field in the cross-sectional plane, which is that acting on the particles, and thus explaining the trajectories in Figure 1(b). An information entropy measure<sup>2</sup> was applied to slices of the particle trajectories to quantify the mixing. These results show that the mixing increases sharply up to a helical radius of  $0.25D$ , but only slightly above this.

\*Department of Aeronautics, Imperial College London.

<sup>1</sup>Caro et al., *J. R. Soc. Interface.* **2**, 261 (2005).

<sup>2</sup>T. G. Kang, T. H. Kwon, *J. Micromech. Microeng.* **14**, 891 (2004).

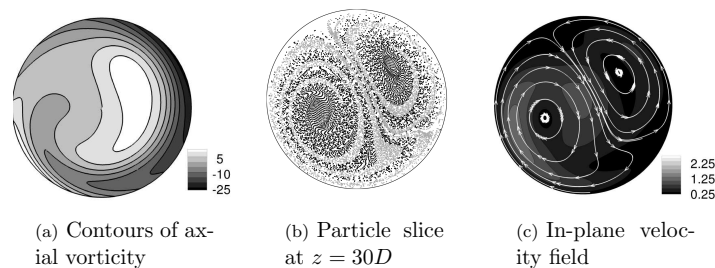


Figure 1: Results for a helical radius of  $0.25D$

## Natural ventilation of buildings: time-dependent flows in an emptying filling box in the presence of steady opposing wind

I. A. Coomaraswamy\*, C. P. Caulfield<sup>†\*</sup>

Natural ventilation - the harnessing of pressure differences caused by temperature variations and prevailing wind to drive airflow through interior spaces - can significantly reduce the energy consumption required to maintain thermal comfort within buildings. However, many time-dependent flow phenomena observed in naturally ventilated spaces remain poorly understood. We investigate reduced models of ventilation flows based on the “emptying filling box” approach of Linden *et al.*<sup>1</sup>.

We consider the stratification and flow produced by a turbulent plume rising from a point source of buoyancy at the base of a cuboidal enclosure, where the latter is ventilated by a windward opening at ceiling level and a leeward opening at floor level, so that prevailing wind acts to oppose buoyancy driven flow. Hunt & Linden<sup>2</sup> demonstrated that in such circumstances, multiple steady states exist above a critical wind strength. We develop a time-dependent model for this system by extending the approach of Kaye & Hunt<sup>3</sup> to incorporate the effects of opposing wind. Our model describes situations in which a two-layer stratification is maintained (with a clear interface between a hot upper layer and a cool lower layer of ambient air) as well as ones in which the whole interior is well-mixed.

Applying this model to an initial value problem - box filling with constant opposing wind - we predict the existence of a variety of transient phenomena and identify the final state obtained for any given wind strength  $W$  and effective vent size  $V$ . We observe that the interface can overshoot its equilibrium level by a significant proportion of the total box height before reaching its final state - a much larger proportion than the 3.7% seen in the absence of wind by Kaye & Hunt. In some cases, we see a well mixed transient before the stratified steady state is reached. However, we find that for regions of the  $W$ - $V$  parameter space where multiple equilibria can exist, the wind driven final state is always attained.

We perform laboratory experiments to verify our predictions, using salt-bath modelling along with shadowgraph and dye attenuation techniques for flow visualization. We discuss some simple improvements to our model, as well as potential implications of our results for the design of ventilation systems in real buildings.

---

\*Department of Applied Mathematics & Theoretical Physics, University of Cambridge, Centre for Mathematical Sciences, Wilberforce Road, Cambridge CB3 0WA, UK.

<sup>†</sup>BP Institute, University of Cambridge, Madingley Road, Cambridge CB3 0EZ, UK.

<sup>1</sup>Linden *et al.*, *J. Fluid Mech.* **212**, 309 (1990).

<sup>2</sup>Hunt & Linden, *J. Fluid Mech.* **527**, 27 (2005).

<sup>3</sup>Kaye & Hunt, *J. Fluid Mech.* **520**, 135 (2004).

## Optimal Amplification of Energy in Fluid-flow induced Flapping of a Thin Panel

Gennaro Coppola\*, Luigi de Luca†, Luigi Mongibello‡

The flapping of a thin streamlined and deformable body (panel) interacting with a fluid current is a physical phenomenon commonly observed in a variety of science and engineering situations<sup>1</sup>. In spite of a remarkable bulk of modern papers, the flow-induced flapping dynamics does not seem to be exhaustively studied in all its aspects.

The equation modelling the dynamical behaviour of a thin panel invested by a current, in terms of its transverse position  $\eta(\tau, s)$ ,  $\tau$  and  $s$  being the non dimensional time and streamwise coordinate, respectively, may be written in non dimensional form as:

$$\frac{\partial^2 \eta}{\partial \tau^2} = -\frac{\partial^4 \eta}{\partial s^4} - \Delta p + \frac{1}{2} \rho V^2 c_D \frac{\partial^2 \eta}{\partial s^2}$$

where inertia, bending elasticity, aerodynamic pressure and tension due to viscous shear stress effects are included. Following Theodorsen, the pressure jump can be modelled by the sum of the contributions of both a circulatory and a non circulatory potential as<sup>2</sup>:  $\Delta p = \rho V C_\gamma f(s) (\eta_\tau + V \eta_s) + \rho n(s) \eta_{\tau\tau}$ . The control parameters are  $\rho$ , the ratio of the fluid density to that of the panel with which it interacts, and  $V$ , the ratio of the fluid velocity to the velocity of the so called bending waves. Various BCs may be enforced at leading and trailing edges for the cases of clamped and/or free edges.

The non-normal character of the equation of motion has not yet been investigated (apart from some finite-dimensional models<sup>3</sup>), and this aspect constitutes, indeed, the subject of the present paper. For different values of the control parameters, as well as various BCs, it is shown that under subcritical conditions (i.e., before the occurrence of the flutter instability) the governing operator is non-normal. Within this context, it is found that the subcritical flapping dynamics is crucially governed by the first two eigenvalues, i.e the first two natural frequencies that converge to each other due to the flow interaction and experience a collision followed by a subsequent splitting, leading to instability at the critical conditions.

The energy optimal amplification exhibits a transient growth characterized by significantly large time-periodic oscillations. The period of such oscillations is related to the topology of the spectrum<sup>4</sup> and agrees strictly with the one of the periodic self-sustained global oscillations predicted via DNS of the unsteady dynamics of the panel. The physical relevance of the described oscillating behaviour is discussed as well.

---

\*Dept. of Energetics and Applied Thermodynamics, DETEC, Università di Napoli, Italy.

†Dept. of Aerospace Engineering, DIAS, Università di Napoli Federico II, Italy.

‡ENEA, C.R. Casaccia, Roma, Italy

<sup>1</sup>M.P. Paidoussis, *Fluid-Structure Interactions*, 2, Elsevier (2003)

<sup>2</sup>Argentina and Mahadevan, *Proc. Nat. Acad. Sci.* **102**, 1829 (2005).

<sup>3</sup>Schmid and de Langre, *ASME J. Appl. Mech.*, **70**, 894 (2003).

<sup>4</sup>Coppola and de Luca, *Phys.Fluids*, **18**, 078104-1 (2006).

## The effects of suction on the stability of the Bödewadt boundary layer

Natalie Culverhouse<sup>\*</sup> and Sharon O. Stephen<sup>\*</sup>

It has been noted from rotor-stator experiments that boundary layers are present on both the rotor and stator. Such experiments have observed that the boundary layer over the stator is the first to become unstable<sup>1</sup>. The stator can be modelled as an infinite stationary plane where fluid in the far field is rotating, known as the Bödewadt boundary layer. Experiments have successfully shown instabilities with the presence of crossflow vortices in the form of stationary spirals. From theoretical and experimental studies on the stability of boundary layers, it is well known that suction is used as a stabilising mechanism in many applications. An investigation into the effect of suction on the inviscid modes, as shown by<sup>2</sup>, in the Bödewadt boundary layer is discussed here. The study of<sup>3</sup> has shown analysis concerning the inviscid modes for the case of the rotating disc where no suction is applied. More recently the investigation of<sup>4</sup> has demonstrated that for the Bödewadt problem stationary spiral rolls can be described by linear inviscid theory. Here a large Reynolds number analysis is performed to study the stability of the Bödewadt boundary layer for the stationary modes when suction is applied using an asymptotic approach. As well as discussing the effects of suction on the effective velocity profile, eigenrelations are derived for neutral stability modes and solutions are found using numerical methods for various suction values.

---

<sup>\*</sup>School of Mathematics, University of Birmingham.

<sup>1</sup>Lingwood and Alfredsson, Proceedings of the IUTAM Symposium, Sedona, Arizona **24**, 409 (1999).

<sup>2</sup>Gregory et al., *Phil. Trans. R. Soc. Lond. A* **248**, 155 (1955).

<sup>3</sup>Hall, *Proc. R. Soc. Lond. A* **406**, 93 (1986).

<sup>4</sup>Mackerrill, *Phil. Trans. R. Soc. Lond. A* **363**, 1181 (2005).

### Resuspension by a droplet

Stuart B. Dalziel<sup>a</sup> and Martin M. Seaton<sup>b</sup>

The problem of a droplet of liquid impacting a rigid boundary has been studied extensively. The initial response of the droplet is essentially inviscid, with a conversion of the kinetic energy of the impact into radial kinetic energy and surface energy as the droplet distorts. If the impact is not too violent, the droplet will remain in one piece and attempt to contract back once all the kinetic energy is spent, but the degree of contraction is strongly affected by the wetting properties of the boundary.

In contrast, a droplet of a liquid impacting a layer of fine particles not only spreads out and distorts, but also transfers some of its kinetic energy to particle layer, both deforming the layer and ejecting particles. This process couples the essentially inviscid hydrodynamics within the droplet with ballistics within the particle layer.

Once the kinetic energy is spent, the droplet begins to contract. Even if the particles cannot support a tensile force to resist this, their wetting properties nevertheless play a role if they adhere to the surface of the droplet, rigidifying it to slow and limit the contraction.

Figure 1 illustrates the experimental observations that will be presented in this paper. Here we see the impact of a small droplet of water onto a bed of fine, essentially non-cohesive particles.

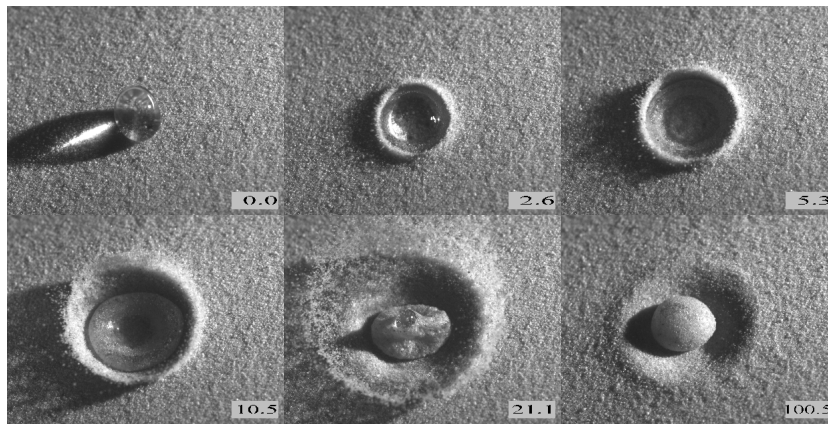


Figure 1: Impact of a droplet. Times are shown in milliseconds after the impact.

<sup>a</sup> Department of Applied Mathematics and Theoretical Physics, University of Cambridge.

<sup>b</sup> Department of Applied Mathematics and Theoretical Physics, University of Cambridge.  
Now at CERC Ltd., Cambridge



## Ignition by a hot gas stream

Joel Daou\* and Faisal Al-Malki\*

We consider a new class of solutions of the equations describing premixed combustion that we call *generalised flame balls* and their application to the problem of ignition by a hot gas stream. These solutions describe stationary spherical flames with a flow of hot inert gas, either a source or a sink, at the origin. Depending on the flow, these flames can have positive, zero, or negative propagation speeds with respect to the surrounding reactive mixture, with zero speeds characterising the classical Zeldovich flame balls. A full analytical description of the stationary solutions and their stability is provided, using a large-activation-energy asymptotic approach and a thermo-diffusive approximation. The results are complemented by a numerical study. The number and stability of the generalised flame balls are identified in various regions of the  $l$ - $M$ - $h_0$  space, where  $l$  is the (reduced) Lewis number, and  $M$  and  $h_0$  the flow rate and its enthalpy at the origin, respectively. It is typically found that, when the flow is a source, there is a critical maximum value of the source strength  $M_{max}$  depending on  $l$  and  $h_0$ , above which there are no stationary solutions, and below which two solutions characterising a small stable flame ball and a large unstable flame ball exist; the implications of these results to the problem of ignition by a hot inert gas are discussed. When the flow is a sink, however, there is typically a single unstable solution, except for sufficiently large values of the Lewis number and large negative values of  $M$ , where three flame balls exist, the medium one being stable. Finally, the relation between the flame speed, positive and negative, and the front curvature, small or large, is addressed.

---

\*School of Mathematics, University of Manchester.

## **Experimental evidence of internal solitary wave-induced global instability in shallow water benthic boundary layers**

**Peter A Davies<sup>a</sup>, Magda Carr<sup>a,b</sup>**

Experimental evidence is presented in support of the theoretical prediction of Diamessis & Redekopp (2006) for wave-induced vortex formation at the lower solid boundary of a shallow, two-layer, stably-stratified fluid system as a result of global instability. The time-dependent boundary layer induced by the propagation of a strongly non-linear internal wave of depression in shallow water is examined experimentally. Measurements of the velocity field close to the bottom boundary illustrate the generation of an unsteady boundary jet in the adverse pressure gradient region aft of the wave and the instability of this flow (as revealed by the appearance of coherent periodic vortex structures at the lower boundary) at sufficiently high values of the wave Reynolds number. The vortical structures are shown to extend into the water column and cause significant benthic turbulence. It is shown that global instability has a critical threshold dependent upon the Reynolds number of the flow and the amplitude of the wave. The critical amplitudes observed are approximately half those predicted by Diamessis & Redekopp (2006) indicating internal wave-induced benthic mixing may be even more prominent than previously thought.

---

<sup>a</sup> Department of Civil Engineering, University of Dundee

<sup>b</sup> School of Mathematics & Statistics, University of St Andrews

## Vortex dipole: free and strained evolution

Ivan Delbende<sup>\*†</sup> and Maurice Rossi<sup>\*‡</sup>

We present a numerical and theoretical study of the dynamics of a two-dimensional vortex dipole. The DNS is performed using a pseudo-spectral Fourier code in a large computational domain, so as to keep most of the vorticity shed behind by the dipole inside the computational domain. The initial condition consists of two small core Lamb–Oseen vortices with opposite circulations. We carefully extract the time evolution of variables such as dipole velocity, vortex core size, spacing, circulation and ellipticity. Moreover, a relation between ellipticity and the two-dimensional strain imposed by the companion vortex is proposed, which generalizes the relation obtained by Moore and Saffman<sup>1</sup> for the elliptical patches to structures with nonuniform vorticity.

The time evolution consists of several phases depending on the size of the vortex cores. The first phase is well documented: the core size  $a$  grows through viscous diffusion while the vortex spacing  $b$  and circulation remain constant. When the aspect ratio  $a/b$  is sufficiently large, the system enters a second phase with decreasing circulation and increasing core size and vortex spacing. Thereafter an asymptotic regime is reached; in this regime, the solution is not self-similar, but a solution can be found using a  $Re^{-1}$  expansion in the spirit of Moffatt et al.<sup>2</sup> and in agreement with numerical results. The overall dipole evolution can be theoretically predicted using three coupled phenomenological equations, which are capable to reproduce most of the features measured on the DNS.

In this asymptotic regime, the ellipticity tends towards the limit value 1.75, indicating that the 2D strain to vorticity ratio (tending towards 0.125) remains below the critical ratio 0.15 above which no more elliptical solution exists. However, in other situations such as 3D vortex reconnection, the potential flow induced by vortex curvature drives the two vortices towards each other. In the plane of closest approach normal to the vortex axis, the mutual 2D strain may then become super-critical, and diffusive stripping of vorticity is observed to turn to substantial filamentation (see figure), as observed experimentally for 2D strained monopoles and dipoles<sup>3</sup>.

<sup>\*</sup>Université Pierre et Marie Curie-Paris6, France

<sup>†</sup>LIMSI-CNRS, UPR3251, BP133, F-91403 Orsay Cedex

<sup>‡</sup>IJLRA-UPMC, UMR7190, F-75232 Paris Cedex 05

<sup>1</sup>Kida, *J. Phys. Soc. Japan* **50**, 3517 (1981).

<sup>2</sup>Moffatt, Kida and Ohkitani, *J. Fluid Mech.* **259**, 241 (1994).

<sup>3</sup>Paireau et al., *J. Fluid Mech.* **351**, 1 (1997); Trieling et al., *Phys. Fluids* **10**, 144 (1998).

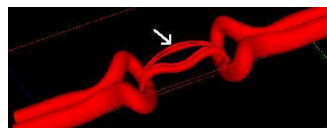


Figure 1: Ejection of vorticity (indicated by the arrow) during the reconnection of antiparallel vortices of equal strengths. Vorticity isosurface, three-dimensional DNS.

## Turbulence structure at an electrodeposition surface induced by jet arrays with random firing.

Delbos S\*, Weitbrecht V<sup>†</sup>, Bleninger T<sup>†</sup>, Grand PP\*,  
Chassaing E\*, Lincot D\*, Kerrec O\* and Jirka GH<sup>†</sup>

Electrochemical deposition processes in dilute aqueous solutions require well controlled homogenous turbulence pattern to achieve good quality and homogeneity of electrodeposited layer. The Institute for Research and Development on Photovoltaic Energy (IRDEP) is working on a Copper Indium diSelenide (CIS) electrodeposition process used to manufacture photovoltaic devices<sup>1</sup>. Flow properties within the electrodeposition reactor are of great importance to the layer quality, and hence photovoltaic conversion efficiency of the manufactured photovoltaic devices.

Laboratory studies were conducted in a cube-shaped reactor with the aim to generate and control homogeneous turbulence near the wall with zero mean primary flow and minimal mean secondary flow motions for achieving a homogeneous electrodeposition process. The turbulence is generated by a jet array, divided into 4 sectors consisting of 16 jets each; each sector can be activated separately.

Velocity measurements have been performed using a 2-D Laser Doppler Velocimetry (LDV) system to determine the mean and turbulent flow characteristics. The influence of the distance between jet array and deposition surface, as well as the influence of randomly activating the 4 jet sectors, will be discussed.

For continuous injection, and a reactor configuration where the individual jets merge before impinging with the deposition surface, strong, steady mean flow cells of the size of the reactor have been observed. A random firing<sup>2</sup> of the four jet sectors can suppress the steady mean flow and increase the turbulence. Random injection can increase the isotropy of the turbulence and increase the Root Mean Square (RMS) of the flow

Characteristic numbers of the flow, the isotropy ratio and secondary flow ratio, will be compared to the data of a similar turbulence-generating devices<sup>2</sup> (Grid-stirring devices, other jet arrays). The secondary flow ratio for the random firing system is lower than the ones found for grid-stirring devices. The study of power density spectra shows that random injection decreases the damping effect of the wall on turbulence.

The distance between the jet orifices and the deposition surface and the random activation of the jet sectors are important parameters for optimization of the jet array system. Both parameters combined with an optimized reactor configuration improve the deposition processes considerably. Resulting electrodeposition will be presented and clearly show a dramatic effect of these parameters on the quality of the electrodeposition.

---

\*Institute of Research and Development on Photovoltaic Energy, IRDEP (UMR 7174 EDF-CNRS-ENSCP), EDF R&D, 6, quai Watier, 78400 Chatou, France

<sup>†</sup>Institute for Hydromechanics, University Karlsruhe, Kaiserstr. 12, 76131 Karlsruhe, Germany

<sup>1</sup>Taunier et al., *Thin Solid Films* **480**, 526 (2005).

<sup>2</sup>Variano et al., *Experiment in Fluids* **37**, 613 (2004).

## APPLICATION OF THE CHIMERA METHOD FOR THE SIMULATION OF A SPHERE NEAR A WALL

T. Deloze<sup>a</sup>, Y. Hoarau<sup>a</sup> and J. Dusek<sup>a</sup>

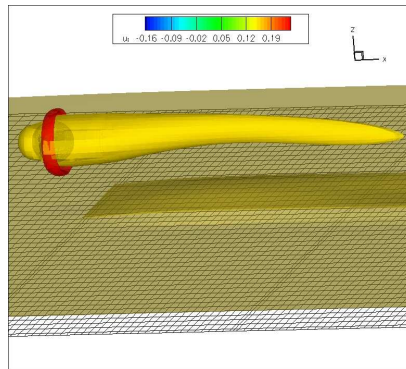
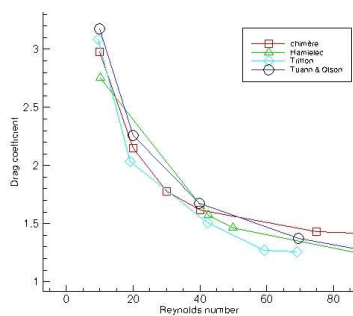
In a recent work in our group we studied the scenario of transition to chaos of a free sphere falling under gravity. We are now working on a free sphere falling in a tube. We are particularly interested in the ground effect induced by the wall on the sphere. The sphere is studied for its characteristics similar to macro particles and a lot of studies deal with flow around spheres. Zeng and al [1] showed that a fixed sphere placed in a flow very closed to a wall is submitted to a ground effect. Previously Segré and Silberger [2] showed experimentally small particules in a poiseuille flow reach an equilibrium position.

In this talk we will focus on the validation of the implementation of a chimera methodology in the NSMB solver and the first simulations of the flow around a sphere near a wall. The chimera overset scheme provides a simple solution for simulations of flows past complex or moving geometries. It consists in solving the equation on overlapping grids. We use a first-order interpolation to link data from one block to another. We have simulated the 2D cylinder and the fixed sphere near a wall for steady and unsteady flow. The results on the cylinder are consistent with the litterature and validate the implementation of this method. The first results on the sphere with a steady flow shows a ground effect in agreement with Zeng and al [1] and simulations have been extended to unsteady flow.

<sup>a</sup> Institut de Mécanique des Fluides et des Solides de Strasbourg - UMR 7507 Université Louis Pasteur / CNRS – 2 rue Boussingault 67000 Strasbourg FRANCE – deloze@imfs.u-strasbg.fr

<sup>1</sup> *J. of Fluid Mech.* Vol, **536** 1-25, 2005

<sup>2</sup> *J. of Fluid Mech.* Vol, **14** 136-157, 1962



Figures : drag coefficient versus Reynolds number for the 2D cylinder (right) and isovalues of velocity for a sphere at Re 400 and distance of wall 2.

## Discontinuities propagation in a pipe flow of suspension of motile microorganisms

Petr Denissenko\*, Sergei Lukaschuk†

On average, the bottom-heavy unicellular algae swim upwards (gravitaxis). In a downwelling pipe flow, gravitactic cells drift horizontally towards the pipe axis where they focuss into a visible thread<sup>1</sup>. When the cell concentration near the axis is large enough, the thread becomes unstable and downward propagating axisymmetric nodules occur. At sufficiently large cell concentrations the flow profile in a pipe significantly deviates from the parabolic<sup>2</sup>. Indeed, the general solution of Navier-Stokes equations for the stationary pressure-driven flow in a circular pipe contains two terms,  $w \propto r^2$  and  $w \propto \ln r$  for the axial velocity. Due to a singularity at  $r = 0$ , the logarithmic solution is usually omitted. This is not the case in a vertical pipe with the denser fluid located near the axis. Two linearly independent solutions require two parameters to define the flow profile. An introduction of an extra parameter opens the possibility for the wave-like disturbances to occur in the pipe.

A model of the flow in a pipe with the heavy (microorganism-laden) core at the axis is constructed. The obtained quasi-linear system of partial differential equations for the core cross-section and the core density is written in conservative form. The velocity of nodule propagation is calculated by applying the 1-dimensional conservation laws (Rankine-Hugoniot conditions) across the discontinuity.

\*School of Engineering, University of Warwick.

†Department of Engineering, University of Hull.

<sup>1</sup>J.O. Kessler, *Nature* **313**, 218 (1985).

<sup>2</sup>P. Denissenko and S. Lukaschuk, *Phys. Lett. A* **362**, 298 (2007).

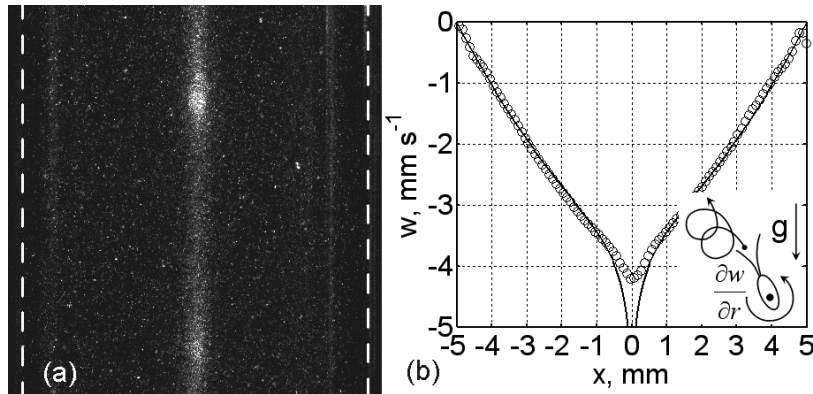


Figure 1: Nodules traveling downwards along the pipe axis (a); the axial velocity profile (b). The bottom-heavy microorganisms are focussed at the axis by the shear.

## Global optimal perturbation and transient growth over a backward facing step

G. Dergham<sup>†\*</sup>, D. Sipp<sup>\*</sup>, J.-C. Robinet<sup>†</sup> and L. Jacquin<sup>\*</sup>

This work deals with the linear transient growth developing over the separated flow resulting from a backward facing step.

The non-normality of the Navier Stokes equations is responsible for transients amplifications of perturbations that can lead to transition<sup>1</sup>. The question to know what is the perturbation leading to a maximum energy growth comes then naturally. The issue at stake is to know whether a flow is able to amplify existing noise.

We decided to focus on two-dimensional inhomogeneous flows with a recirculation bubble. Two geometries were studied: a classical backward facing step and a smooth rounded one<sup>2</sup>. We choose these flows because they are known to exhibit strong transient growths and because they represent a classical configuration in many applications.

The parameters of interest are the Reynolds number  $Re$  (based on the step height and the upstream velocity), the spanwise wavelength of the perturbations and the ratio of the boundary layer thickness over the step height.

We computed the base flow using a Newton method for Reynolds numbers where the flow is two-dimensionally stable, as shown in Figure 1(a). Then we looked for the optimal perturbation using two different methods. The first one is based on a continuous direct-adjoint approach using the iterative calculation of a gradient<sup>3</sup>. The second consists of the construction of a reduced order model based on a global mode basis<sup>4</sup>. The latter will underline the ability of a superposition of global modes to represent the linear dynamics of the flow. The solution of the reduced order model is eventually compared with the one obtained from the first method, considered as a reference (see Figure 1(b)).

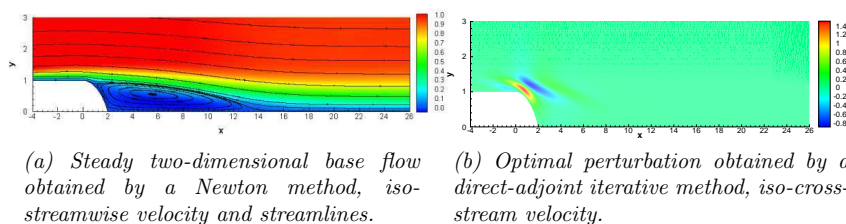


Figure 1: The case of a rounded backward facing step at  $Re = 400$ .

\*ONERA, Fundamental and Experimental Aerodynamics Department, 8 rue des vertugadins, 92190 Meudon, France.

<sup>†</sup>SINUMEF Laboratory, Arts et Métiers ParisTech, 151 Bd. de l'Hôpital, 75013 Paris, France.

<sup>1</sup>P. Schmid, *Ann. Rev. Fluid Mech.* (2007).

<sup>2</sup>J.-E. Wesfreid, ESPCI/PMMH, private communication.

<sup>3</sup>O. Marquet, D. Sipp, J.-M. Chomaz & L. Jacquin, *JFM* (2008).

<sup>4</sup>E. Åkervik, J. Höpfner, Uwe Ehrenstein & D. Henningson, *JFM* (2007).

## A generalization of Benjamins' theory for internal waves in deep fluid.

*Oleg G. Derzhó<sup>a</sup>, Roger Grimshaw<sup>b</sup>*

Solitary waves of permanent form propagating in a stratified fluid owe their existence to a balance between nonlinear wave steepening and linear wave dispersion. For waves of small but finite amplitude the nonlinearity is usually quadratic, and the coefficient in front of this quadratic term is determined by the specific profile of stratification. Higher order expansions in the wave amplitude may account for higher nonlinearities, however, such an approach is limited to waves that do not overturn. Overturning occurs at a certain finite critical wave amplitude at which the horizontal velocity approaches zero in a frame of reference moving with the wave, that is, a local critical point appears inside the flow. Above this critical amplitude the critical point evolves into a vortex core that moves with the wave.

In this contribution we describe a model for long large-amplitude internal solitary waves with a vortex core, propagating on a narrow layer of nearly uniformly stratified fluid embedded in an infinitely deep homogeneous fluid. The case of small but finite amplitude waves was first examined in the pioneering work by Benjamin (1966). We generalise his result for the case of large amplitude waves. A key observation that enables us to deal analytically with finite amplitude waves is that, for the case of nearly uniform stratification in the layer, the nonlinearity is weak even if the wave amplitude is large, in fact all non-overturning waves in the uniformly stratified environment are linear in the Boussinesq approximation. Thus the asymptotic procedure that uses an expansion parameter characterising the deviation of stratification from the uniform profile does not require smallness of the wave amplitude.

In this contribution we consider the case when wave amplitudes slightly exceed the critical amplitude and recirculation zone is formed inside the wave. Our main result is a new equation for the wave amplitude, which accounts for waves with amplitudes beyond the critical amplitude at which the incipient overturning occurs, and a vortex core appears inside the wave. The effect of the vortex core is to introduce into the amplitude equation an extra nonlinear term proportional to the  $3/2$  power of the difference between the wave amplitude and the critical amplitude. Thus the derived equation incorporates the nonlinearity arising due to the flow over the recirculation core, and the nonlinearity associated with the ambient stratification; the dispersion term, however, remains of the Benjamins' integral type. We note that the form of the extra term does not depend on the details of the stratification. We find that as wave amplitude increases above the critical amplitude, the wave broadens, which is in marked contrast to the case of small amplitude waves where sharpening of the wave crest normally occurs. Further, the wave speed is found to depend nonlinearly on the wave amplitude and the traditional linear dependence underestimates this speed. We show that the asymptote of the wave amplitude at infinity is still  $1/x^2$  as in the theory by Benjamin (1966) despite the fact that we predict quite different wave shapes in the middle part of the wave. The limiting form of the broadening wave is a deep fluid bore which does not exist in the small amplitude limit.

<sup>a</sup>*Institute of Thermophysics, Russian Academy of Sciences, Novosibirsk, Russia and Department of Physical Oceanography, Memorial University of Newfoundland, St. John's, Canada*

<sup>b</sup>*Department of Mathematical Sciences, Loughborough University, Loughborough, UK*



## A two-fluid model for violent aerated flows

Denys Dutykh<sup>\*</sup>, Frédéric Dias<sup>\*</sup> and Jean-Michel Ghidaglia<sup>\*</sup>

The purpose of this communication is to discuss the simulation of a free surface compressible flow between two fluids, typically air and water. We use a two fluid model with the same velocity, pressure and temperature for both phases. In such a model, the free surface becomes a thin three dimensional zone. The present model has at least three advantages: (i) the free-surface treatment is completely implicit; (ii) it can naturally handle wave breaking and other topological changes in the flow; (iii) one can easily vary the Equation of States (EOS) of each fluid (in principle, one can even consider tabulated EOS). Moreover, our model is unconditionally hyperbolic for reasonable EOS.

First, we present the physical context of our study <sup>1</sup>. Then, we introduce the governing equations and we give some rationales on the limit of this model to the classical free surface model. Finally, we present our numerical method based on a flux scheme <sup>2</sup> which is, in particular, constructed to model accurately impacts of waves on walls. Since our code is designed for unstructured meshes, it can easily treat complex geometries (for example, liquified natural gas carrier tank). This communication will conclude with the presentation of different simulation results on the sloshing of a liquid in a closed container.

---

<sup>\*</sup>Centre de Mathématiques et de Leurs Applications, École Normale Supérieure de Cachan, 61, Avenue du Président Wilson, 94235 Cachan France.

<sup>1</sup>G.N. Bullock et al., *Coastal Engineering*, **54**, 602 – 617 (2007).

<sup>2</sup>J.-M. Ghidaglia et al., *Eur. J. Mech. B/Fluids*, **20**, 841 – 867 (2001).

## some aspects of wildfire behaviour

John Dold\*

The presentation briefly reviews a number of aspects of bushfire or wildfire behaviour, as known experimentally and as has been or is currently being modelled theoretically. References are too numerous to be included in this abstract.

In essence, two chemical processes sustain a bushfire. Cellulose, the principal carbohydrate in vegetation, is pyrolysed (converted into a flammable vapour) at temperatures around 400°C; the other main constituents, hemicellulose and lignose, also pyrolyse, but more slowly or at a higher temperature. The pyrolysis vapour is then oxidised by the air, requiring temperatures above about 1000°C to maintain the reaction, but also releasing enough heat to raise the temperature adiabatically up to about 1700°C, if the vegetation is mainly dry cellulose.

Heat transfer from the flames maintains the pyrolysis, although moisture in the vegetation can greatly increase the amount of energy required for this to happen. Buoyancy of the hot combustion products along with wind and slope effects helps to determine the average shape of the flame. This, in turn, determines the rate of heat transfer to fresh vegetation (mostly through radiation) and hence the rate at which the leading edge of the fire spreads. The position of the trailing edge of the fire is largely determined by the residence time of the flame, or the time needed for the vegetation to fully pyrolyse. The total rate at which vegetation is pyrolysed between the leading and trailing edges, along with the exothermicity of the oxidation, determine the intensity or power of the bushfire per unit length of the fireline.

The nature of the heat transfer from the flame into the fresh vegetation is very important and it is relatively simple to show that different functional dependences on the intensity of the flame can cause a straight fireline either to evolve towards a steady rate of spread or to accelerate and grow indefinitely in intensity. The latter ‘eruptive’ or ‘blow-up’ form of behaviour is seen in practice and, sadly, often leads to fatalities when fires burn up canyons. It would appear to be partly caused by attachment of the flow associated with the fire-plume to a vegetated surface, as some recent experiments of fires burning up a sloping trench have demonstrated.

Very large fires can interact with the atmosphere in dramatic ways, generating storm-clouds even in dry atmospheres that would not normally support such clouds. The heat of the fire and, to some extent, the water released in oxidising carbohydrates in the vegetation, lead to this atmospheric instability. Convection due to such a pyrocumulus may help to generate ground-level winds that enhance the fire. Indeed, destructive tornados have been observed in such fire-storms. Smaller scale ‘fire-whirls’, containing a vortex of flame, are a fairly typical feature of many wildfires.

Another aspect that is sometimes observed in intense wildfires is the appearance of large flames where there really is no significant vegetation to burn, as reported by some experienced firefighters; in one instance, such flames spread with unusual colours over terrain that had already been burnt and should therefore have not been flammable at all. A possible cause for this is an accumulation of pyrolysis vapour that has somehow escaped unburnt from the original fire itself.

---

\*School of Mathematics, University of Manchester.

## Modelling of the interaction between a single bubble and a wall: Application to Ultrasound Contrast Agents

Benjamin Dollet\*, Michel Versluis<sup>†</sup>, Leen van Wijngaarden<sup>†</sup> and Detlef Lohse<sup>‡</sup>

Ultrasound Contrast Agents (UCA) are coated microbubbles, currently extensively studied to target endothelial cells, for local drug delivery. It is therefore important to distinguish free-floating bubbles from bubbles located close, or targeted to blood vessels. Experiments in our group, using ultra-high-speed imaging<sup>1</sup> combined with optical micromanipulation<sup>2</sup> enabled to study the response of a single UCA to ultrasonic pulses, as a function of its distance from a wall, showing that the wall hinders the radial oscillation of the bubble<sup>2</sup>, and that nonspherical oscillations are induced in an imaging plane perpendicular to the wall<sup>3</sup>. Here, we propose a theoretical study to understand the observed bubble behaviours.

We consider the hydrodynamic interaction of a single bubble with a wall, including all possible bubble motions: volumetric oscillations, translation, and nonspherical deformations. In the frame of potential flow theory, we use the series expansion of the velocity potential in powers of the separation ratio between the bubble radius and the distance of its center to the wall<sup>4</sup>. We subsequently match the potential flow to the viscous boundary layer along the wall. We derive the coupled equations of the bubble dynamics using a Lagrangian approach. We predict the bubble response to ultrasound, as a function of various parameters (applied frequency and amplitude, bubble size and coating, bubble/wall distance).

We show that our new model predicts a decrease of the resonance frequency as a bubble gets closer to a wall, in agreement with experiments. We reproduce correctly the observed decrease of oscillation amplitude for a bubble close to the wall, and we show that it is due to the coupling between oscillation and translation rather than to the friction in the boundary layer. The threshold for nonspherical oscillations is also discussed and compared to experimental measurements.

---

\*Institut de Physique de Rennes, Université Rennes 1, France and Physics of Fluids, University of Twente, The Netherlands.

<sup>†</sup>Physics of Fluids, University of Twente, The Netherlands.

<sup>1</sup>C. T. Chin, C. Lancée, J. Borsboom, F. Mastik, M. E. Frijlink, N. de Jong, M. Versluis, D. Lohse, *Rev. Sci. Instr.* **74**, 5026 (2003).

<sup>2</sup>V. Garbin, D. Cojoc, E. Ferrari, E. di Fabrizio, M. L. J. Overvelde, S. M. van der Meer, N. de Jong, D. Lohse, M. Versluis, *Appl. Phys. Lett.* **90**, 114103 (2007).

<sup>3</sup>H. J. Vos, B. Dollet, J. G. Bosch, M. Versluis, N. de Jong, *Ultrasound Med. Biol.* in press (2008).

<sup>4</sup>C. W. M. van der Geld, *J. Eng. Math.* **42**, 91 (2002).

## Intraventricular flow changes in an infarcted left ventricle

Federico Domenichini<sup>a</sup> and Gianni Pedrizzetti<sup>b</sup>

The cardiac diagnostic process is primarily based on the evaluation of myocardial mechanics while little is known about pathologic blood dynamics that is rarely considered to this purpose. The blood flow inside the left ventricle is known to be associated with the development of a vortex structure<sup>1</sup> that facilitates the redirection of the rapidly entering fluid toward the outflow track<sup>1</sup>. Little is known about the differences in the intraventricular blood flow under various conditions, as well as their relation with specific pathologies.

The flow inside the left ventricle is here analyzed in presence of an akinetic and dyskinetic myocardial motion as it would occur for a regional ischemic pathology. Ischemia is a primary systolic dysfunction caused by the partial or total occlusion of a coronary vessel, leading to a reduced blood perfusion in the corresponding myocardial muscular territory, and the following decrease of its contractile function. The objective is to support some physically-based evidence of the changes that occur in the intraventricular flow from healthy state to controlled pathologic condition.

The study is performed through three-dimensional numerical simulations of the flow in a model left ventricle<sup>2</sup>. Starting from healthy condition, the motion of the wall in the infarcted region is progressively reduced to simulate different degrees of the pathology. The governing equations are solved with a fractional step method in a bi-periodic computational box, using a mixed spectral – finite differences method. The presence of the ventricle wall is managed through a version of the Immersed Boundary method.

Results show that the presence of an anterior-inferior wall infarction leads to the shortening and weakening of the mitral jet that enters the cavity during the diastolic filling. A region of stagnating flow is found near the ventricle apex and in the region close to the ischemic wall. The results are in agreement with previous clinical findings based on the analysis of echographic images<sup>3</sup>. Such phenomena are also noticed for moderate degrees of the ischemic pathology and suggest a potential value of the study of the intraventricular flow to develop early diagnostic indicator.

---

<sup>a</sup> Dipartimento di Ingegneria Civile e Ambientale, University of Firenze.

<sup>b</sup> Dipartimento di Ingegneria Civile e Ambientale, University of Trieste.

<sup>1</sup> Pedrizzetti & Domenichini, *Phys. Rev. Lett.* **95**, 108101 (2005).

<sup>2</sup> Domenichini et al., *J. Fluid Mech.* **539**, 179 (2005).

<sup>3</sup> Beppu et al., *Circulation* **78**, 157 (1988).

## Flow control on a high thickness airfoil by a trapped vortex

R. S. Donelli\*, F. De Gregorio\* and P. Iannelli\*

This paper presents the experimental and numerical campaign aimed to investigate the potential benefits obtainable using a trapping vortex cell system on a high thickness airfoil to control flow separation. To ensure a high lift-to-drag ratio, wing of modern airplanes are thin and streamlined. However, the tendency to design commercial aircraft of ever-larger dimensions, or innovative configuration as Blended-Wing-Body airplanes requests innovative solution in the field of wing structures. In order to carry a larger load having thick wing would be beneficial. The drawback of this type of airfoils is a low efficiency due to a high value of the drag coefficient caused by the flow separation in the trailing edge region. At the end of 2005, VortexCell2050, an European funded research project, has been launched with the scope of investigate the possibility to control the flow separation using trapped vortex cavities and active control. Basic concept of the trapped vortex cavities is shown in figure 1. The flow otherwise separated is forced to remain attached by an intense vortex anchored in the cavity. A 2D model has been numerically investigated, designed and built in order to present clear and stable separation. PIV measurements have been performed in the low cost CT-1 open wind tunnel having test section sizes of 305x305x600 mm<sup>3</sup> and maximum speed of 55 m/s. This model has been mounted on the bottom of the wind tunnel as shown in Figure 2 (left side). An extensive experimental and numerical test campaign has been performed for investigating the aerodynamic characteristics of the test article and in particular the flow separation behaviour. PIV measurements and based RANS approaches solvers have been used. Successively a trapping vortex cavity has designed, built and installed on the model (figure 2 on the right). The cavity has been equipped with a blowing and suction system in order to try to stabilise the vortex in the cavity. All the trapping vortex cavity has been built with fully transparent material in order to allow the PIV measurements inside the cavity. The influence of the trapped vortex cell on the 2D airfoil model has been investigated. Numerical and experimental results have been compared and a description of these investigations and on the stabilization of the flow separation will be presented.

\*Italian Aerospace Research Centre (CIRA).



Figure 1: Trapped vortex concept.

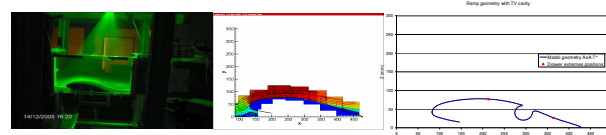


Figure 2: Experimental set-up and PIV field - Cavity geometry on the model.

## Aeroacoustics

Ann P Dowling<sup>a</sup>

Aeroacoustics is the study of noise generation by turbulent flow or by unsteady flows interacting with surfaces. It therefore involves integration of ideas from fluid mechanics and acoustics. The main motivation is to understand and hence reduce the noise from aircraft. Of course, aircraft engines are a major source of noise particularly emanating from the high-speed fans and also from the propulsive jets. However, on approach, the airframe of a modern jet generates just as much noise as the engines. This noise comes primarily from the unsteady airflow through high-lift devices, such as flaps and slats, and around the undercarriage.

Various aircraft noise sources will be reviewed in this talk. Our current understanding of the unsteady flows that contribute to this noise will be discussed, highlighting the areas where further research is required. Particular attention will be given to ways of integrating the near-field unsteady flow with the far-field sound. Jet noise will be taken as example to illustrate ways of doing that and how computational fluid dynamics can contribute.

The possibilities for manipulating flows to reduce the noise in the medium term will be discussed, together with more radical solutions for ultra low-noise aircraft in the longer term.

---

<sup>a</sup> *Department of Engineering, University of Cambridge*

## Subcritical and supercritical capillary channel flow

Aleksander Grah<sup>a</sup>, Joerg Klatte<sup>a</sup> and Michael E. Dreyer<sup>a</sup>

We will present numerical studies on capillary channel flow, based on results of the sounding rocket experiments TEXUS 41/42. The flow through a capillary channel is established by a gear pump at the outlet. The channel, consists of two parallel glass plates with width  $b = 25\text{mm}$ , gap  $a = 10\text{mm}$  and length  $l = 12\text{mm}$ . The meniscus of a compensation tube maintains a constant system pressure. Steady and dynamic pressure effects in the system force the surfaces to bend inwards<sup>2</sup>. A maximum flow rate is achieved when the free surface collapses and gas ingestion occurs at the outlet<sup>1</sup>. This critical flow rate depends on the channel geometry, the flow regime and the liquid properties. The aim of the experiments is the determination of the free surface shape and to find the maximum flow rate.

In order to study the unsteady liquid loop behaviour, a dimensionless transient model was developed. It is based on the unsteady Bernoulli equation, the unsteady continuity equation and geometrical conditions for the surface curvature and the flow cross-section. The pressure is related to the curvature of the free liquid surface by the dimensionless Gauss-Laplace equation with two principal radii.

The experimental and evaluated contour data shows good agreement for a sequence of transient flow rate perturbations<sup>3</sup>. The surface oscillation frequencies and amplitudes can be predicted with quite high accuracy.

The dynamic of the pump is defined by the increase of the flow rate in a time period  $\delta = \Delta Q / \Delta t$ . To study the unsteady system behavior in the “worst case”, we use a perturbations related to the natural frequency of the oscillating liquid.

In the case of steady flow at maximum flow rate, when the “choking” effect occurs, the surfaces collapse and cause gas ingestion into the channel. This effect is related to the Speed Index. At the critical flow rate the Speed Index reaches the value  $S_{ca} = 1$ , in analogy to the Mach Number.

For unsteady choking does not necessarily cause surface collapse. We show, that temporarily Speed Index values exceeding One may be achieved for a perfectly stable supercritical dynamic flow. As a supercritical criterion for the dynamic free surface stability we define a Dynamic Index  $D$  considering the local capillary pressure and the convective pressure, which is a function of the local velocity. The Dynamic Index is below One for stable flow while  $D = 1$  indicates surface collapse. This studies result in a stability diagram, which defines the limits of flow dynamics and the maximum unsteady flow rate. It may serve as a road map for open capillary channel flow control.

<sup>a</sup> ZARM (Center of Applied Space Technology and Microgravity), University of Bremen.

<sup>1</sup> Rosendahl et al., *J. Fluid Mech.* **518**, 187- 214 (2004).

<sup>2</sup> Rosendahl et al., *Exp. Fluids* **42**, 683-696 (2007).

<sup>3</sup> Grah et al., *J. Fluid Mech.* (accepted 2007).

## Similarity Solutions for Unsteady Gravity-driven Slender Rivulets

B. R. Duffy\*, Y. M. Yatim\*, S. K. Wilson\* and R. Hunt\*

Rivulets occur commonly in a wide range of geophysical, biological and industrial contexts. In the present study the lubrication approximation is used to analyse the unsteady gravity-driven flow of slender non-uniform rivulets on a plane inclined at an angle  $\alpha$  to the horizontal, as shown in figure 1. By adopting an analogous approach to that of Smith<sup>1</sup> and Duffy & Moffatt<sup>2</sup> in their analyses of steady rivulet flow, unsteady similarity solutions are obtained for both sessile rivulets (when  $0 < \alpha < \pi/2$ ) and pendent rivulets (when  $\pi/2 < \alpha < \pi$ ) and for both converging rivulets in  $x < 0$  and diverging rivulets in  $x > 0$ , where  $x$  denotes distance down the plane. Numerical and asymptotic methods are used to obtain detailed descriptions of the possible rivulets in each case. The similarity solution predicts that at any time  $t$  the rivulet widens or narrows according to  $|x|^{3/4}$  and thickens or thins according to  $|x|^{1/2}$  as it flows down the plane. At any station  $x$  the rivulet widens or narrows like  $|t|^{-1/4}$  and thickens or thins like  $|t|^{-1/2}$ . Cross-sectional profiles are ‘single-humped’ for sessile rivulets and either ‘single-humped’ or ‘double-humped’ for pendent rivulets.

\*Department of Mathematics, University of Strathclyde, 26 Richmond Street, Glasgow G1 1XH.

<sup>1</sup>P. C. Smith, *J. Fluid Mech.* **58**, 275 (1973).

<sup>2</sup>B. R. Duffy & H. K. Moffatt, *Euro. J. Appl. Math.* **8**, 37 (1997).

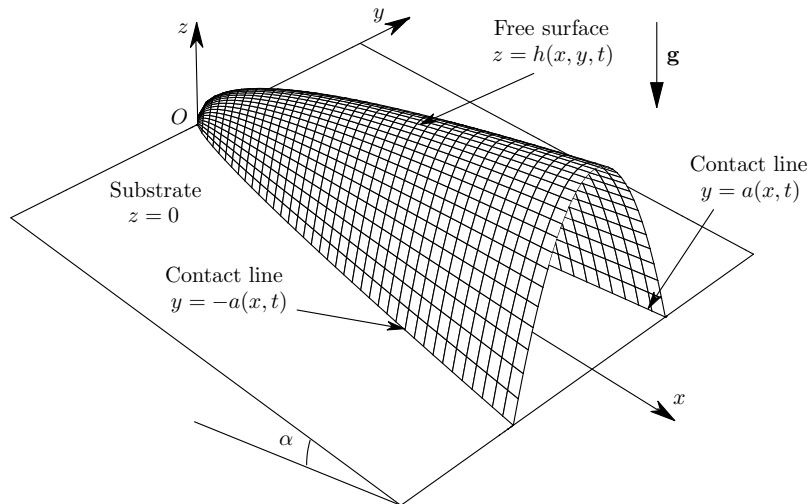


Figure 1: An unsteady slender rivulet on an inclined plane.



## Finite-amplitude solutions in transitional pipe flow

Y. Duguet\*, R.R. Kerswell†

Transition to turbulence in cylindrical pipe flow is governed by one single dimensionless parameter, the Reynolds number  $Re = UD/\nu^1$ . The reason for transition remains obscure due to the sensitivity of the linearly-stable laminar Hagen-Poiseuille flow to the shape and amplitude of disturbances. Here, using direct numerical simulation, we focus on short axially periodic pipes length  $L = 5D$ , with  $Re = 2875$ . In the related phase-space, we consider the phase-space boundary between the trajectories which relaminarise and those which become turbulent<sup>2</sup>. The dividing trajectories usually display a chaotic behaviour<sup>3</sup>. Quantification of the recurrences along those dividing trajectories reveals that they transiently approach unstable finite-amplitude solutions, invariably lower branch travelling waves. The laminar/turbulent boundary is a repeller when all finite-amplitude solutions sitting on it possess at least two unstable eigendirections. The use of a Newton-Krylov solver allows to identify those exact travelling waves solutions from the data, some of them being new solutions. A Hopf bifurcation of the most visited travelling wave solution occurs at  $Re = 1785$ . This indicates the existence of a relative periodic orbit of long period, which proves to be very unstable. This network of finite-amplitude solutions, with their homoclinic/heteroclinic connections, has direct implications on the transition phenomenon.

---

\*Department of Mechanical Engineering, KTH, Stockholm

†School of Mathematics, University of Bristol, Bristol, UK

<sup>1</sup>O. Reynolds, *Phil. Trans. Roy. Soc.*, 1883, **174**, 935-982

<sup>2</sup>Toh S., Itano, I. *J. Phys. Soc. Japan*, 2001, **70**, 703-716

<sup>3</sup>Schneider T.M. et. al., *Phys. Rev. Lett.*, 2007, **99**, 034502

### 3D effects on a monopolar vortex in a rotating shallow layer

M. Duran-Matute\*, R.R. Trieling\*, L.P.J. Kamp\* and G.J.F. van Heijst\*

It is generally believed that vertical confinement and rotation enforce two-dimensionality of flows. For a shallow flow the vertical velocities tend to be smaller than the horizontal velocities, whereas rotation makes the vertical derivatives of the velocity tend to zero (Taylor-Proudman theorem). It is the aim of this work to study numerically the effects of rotation and vertical confinement on a monopolar vortex in a shallow layer of fluid.

We solved the initial-value problem for the three-dimensional Navier-Stokes equations in cylindrical coordinates with azimuthal symmetry using the finite-element code COMSOL<sup>1</sup>. A Lamb-Oseen vortex was used as the initial condition for the horizontal flow. Three dimensionless parameters were varied: the Rossby number  $Ro = \omega_p/(2\Omega)$ , the Ekman number  $Ek = \nu/(2H^2)$  and the Reynolds number  $Re = \omega_p R^2/\nu$ , where  $\Omega$  is the rotation rate of the system,  $\omega_p$  is the initial peak vorticity,  $\nu$  is the kinematic viscosity,  $R$  is the radius of the vortex, and  $H$  is the depth of the fluid.

During the initial stage of the evolution, a vertical velocity profile develops to satisfy the no-slip boundary condition at the bottom, and a secondary motion is set up (figure 1). Different criteria are used to quantify the two-dimensionality of the flow, e.g. the ratio of the energies of the mean and the secondary flows, as well as the magnitude of the horizontal divergence.

The effect of rotation on a shallow flow is not straight forward. The degree of two-dimensionality of the flow, according to the criteria used, can be increased or decreased depending on the Ekman, Rossby, and Reynolds numbers.

\*Fluid Dynamics Laboratory, Eindhoven University of Technology.

<sup>1</sup>URL <http://www.comsol.com>

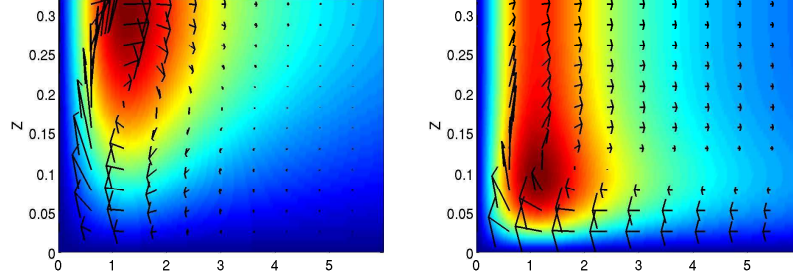


Figure 1: Typical velocity field of the vortex with  $Re = 100$ ,  $Ro = \infty$ ,  $Ek = \infty$  (left) and  $Re = 100$ ,  $Ro = 0.1$ ,  $Ek = 9.8 \times 10^{-3}$  (right). The vortex has a radius  $R = 1$  and the layer has a depth  $H = 0.32$ . The color represents the magnitude of the azimuthal velocity (zero in blue, and the maximum velocity in red). The arrows denote the radial and vertical velocity components.

## Velocity fluctuations from randomly oscillating spheres

Bruno Eckhardt, Juergen Buehrle \*

The velocity field of a slowly moving sphere is usually described by the Stokes field with its characteristic  $1/\text{distance}$  decay further away from the spheres. When this description is used for the velocity field induced by sedimenting particles, the slow decay is compensated by the rapid increase in the number of contributing particles, suggesting a divergence, or, in physical terms, a volume dependence of the fluctuations. However, when the time-dependence is taken into account, the velocity fields change character and fall off differently. We present results for a model where the particles undergo random velocity fluctuations. The inclusion of the time-dependent diffusional spreading of vorticity drastically changes the variations of the velocity fluctuations with distance. For a sphere with velocity fluctuations that uniformly cover a range in frequencies between  $\omega_{min}$  and  $\omega_{max}$ , the fluctuations decrease like  $1/r^2$  close to the sphere and up to distances  $\sqrt{\nu/\omega_{max}}$ , like  $1/r^4$  for distances up to  $\sqrt{\nu/\omega_{min}}$  and like  $1/r^6$  for even larger distances. When the motion from several particles can be superimposed, as in the case of a dilute sediment, the high frequency regularization prevents the fluctuation divergence expected from the time-independent equations. Among the direct and testable consequences of this argument are a prediction for the highest frequency of the velocity fluctuations which can occur, and a viscosity dependence and a  $\phi^{2/3}$  concentration dependence for the fluctuations.

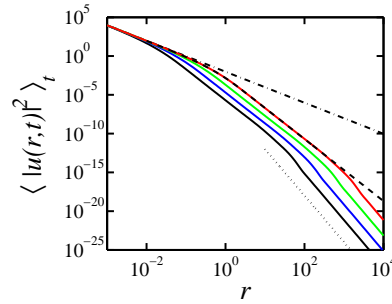


Figure 1: Velocity fluctuations for a randomly oscillating sphere. (a):  $x$ -component of the velocity as a function of the distance for viscosities  $\nu = 0.1$  (black),  $\nu = 1$  (blue),  $\nu = 10$  (green) and  $\nu = 100$  (red). The dot-dashed line shows the fluctuations as obtained from steady Stokes flow. The dashed line shows the prediction and the dotted line shows the  $1/r^6$ -decay. The highest frequency is  $10^6$  times the lowest frequency  $\omega_{min}$ .

\*Fachbereich Physik, Philipps-Universität Marburg, 35032 Marburg, Germany

## The role of singularities in hydrodynamics

Jens Eggers\*

If a tap is opened slowly, a drop will form. The separation of the drop is described by a singularity of the Navier-Stokes equation with a free surface. A drop spreading on a table develops a singular flow at the corner of the drop; spreading can occur only if the singularity is relieved at a microscopic length scale near the corner. Shock waves are singular solutions of the equations of ideal, compressible hydrodynamics.

These examples show that singularities are characteristic for the tendency of the hydrodynamic equations to develop small scale features spontaneously, starting from smooth initial conditions. Two properties are crucial for the understanding of singularities:

**Universality:** The local behaviour near the singularity is described by a unique solution, which contains no or very few adjustable parameters, independent of initial conditions. Thus the structure of the singularity imposes important constraints on the fashion in which a new object, such as a drop, may be born.

**Self-similarity:** As smaller and smaller scales are produced, the spatial structure of the solution remains the same, independent of scale. This invariance greatly simplifies the problem, so one is able to gain analytical insight into many highly nonlinear problems. Recently, it has emerged that some problems are more subtle in that they contain logarithmic corrections to purely self-similar behaviour. These corrections are however captured by the dynamics of a low-dimensional dynamical system, which describes changes to self-similar behaviour on a logarithmic time scale.

In this talk, I illustrate the mathematical structure of singularities with various physical examples. I show that singularities are vital to many engineering problems such as printing, painting, coating, and air entrainment. The focusing inherent in a singularity can be used to make small things, such as micron-sized fluid jets.

---

\*School of Mathematics, University of Bristol, University Walk, Bristol BS8 1TW, United Kingdom

# Low-frequency oscillations in a separating boundary-layer flow

Uwe Ehrenstein\* and François Gallaire†

There is general evidence that laminar detached boundary layers are likely to undergo two-dimensional low frequency oscillations known as 'flapping'<sup>1</sup>. However, the physical mechanisms at the origin of this type of instability are only partially understood. We readdress the low-frequency oscillations for an elongated separation bubble induced by a bump geometry. A quasi-Newton approach is used to determine steady states for Reynolds numbers above the critical value for global instability and previous conjectures<sup>2</sup> that topological flow changes are responsible for the overall instability are not confirmed. The flow dynamics is analysed by computing two-dimensional temporal eigenmodes of the linearized Navier-Stokes equations. An optimal perturbation dynamics is performed and the long-time disturbance dynamics is shown to exhibit a global cycle at low frequency. This global beating behaviour is interpreted as resulting from the superposition of eigenmodes which originate at the center of the bubble and become almost simultaneously unstable, while exhibiting equally spaced frequencies (cf. modes labelled (1)-(6) in figure 1c). The corresponding low-frequency oscillations are retrieved in the direct numerical simulation of the Navier-Stokes equations by starting with the optimal initial condition and the dynamics is shown to be similar to the self-sustained 'flapping' already reported for the same flow geometry<sup>3</sup>.

\*IRPHÉ, Université de Provence, 49, Rue Joliot-Curie, F-13384 Marseille Cedex 13, France.

†Lab. J. A. Dieudonné, Université de Nice-Sophia Antipolis, F-06108 Nice Cedex 02, France.

<sup>1</sup>Dovgal et al., *Prog. Aerospace Sci.* **30**, 61 (1994).

<sup>2</sup>Theofilis et al., *Phil. Trans. R. Soc. Lond. A* **358**, 3229 (2000).

<sup>3</sup>M. Marquillie & U. Ehrenstein, *J. Fluid Mech.* **490**, 169 (2003).

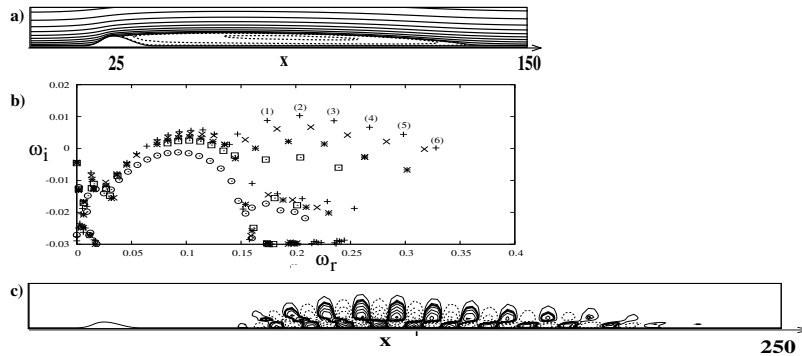


Figure 1: (a) Streamlines of flow state at  $Re = 590$ , bump height  $h = 2$ . (b) Eigenvalue spectrum at  $Re = 590$  for several bump heights  $h = 1.8$  (o),  $h = 1.85$  (□),  $h = 1.9$  (\*),  $h = 1.95$  (x),  $h = 2$  (+). (c) Streamwise velocity component of mode with eigenvalue labelled (3) in (b).

## Conglomerates of spheres falling steadily in a viscous fluid

Maria L. Ekiel-Jezewska\* and Eligiusz Wajnryb\*

In many biological, medical and industrial applications, it is of interest to predict theoretically what is the sedimentation velocity of small conglomerates of micro-particles under gravity in a fluid, and how the settling speed can be enhanced or decreased, by a suitable modification of the configuration, or directly by a change of the relative motion of the particles. This issue is especially important for mechanisms of effective swimming, recently intensively investigated for biological systems as well as for artificial micro- and nano-swimmers.

In this work, this problem is investigated for the simple model of a conglomerate made of three identical spheres under gravity in a low-Reynolds number flow. The accurate spherical multipole method of solving the Stokes equations is used, with the controlled high order of the truncation. The mobility problem is solved and velocities of all the particles are evaluated for systematically changed initial configurations of the sphere centers.

First, steady solutions of Stokesian dynamics are searched for numerically. The corresponding equilibrium configurations of three spheres are found and listed. For each of them, its collective translation as well as rotation of individual spheres are specified. All the equilibria with touching spheres are shown to be unstable. Unstable perturbations often correspond to separating a pair of touching spheres.

The results are also compared with the point-particle model. For touching spheres, such an approximation has to take into account additional constraint forces, which do not allow the points, which approximate the touching spheres, to change the interparticle distance.

A chain-like system, in which such separation is not allowed and each sphere *always* touches another one is important because of practical applications. Its dynamics is investigated separately and the only stable equilibrium configuration is found. Settling of a chain of beads, which are free to rotate around their line of centers is shown to differ significantly from the motion of a rigid chain at the same configuration.

---

\*Institute of Fundamental Technological Research, Polish Academy of Sciences, Świętokrzyska 21, 00-049 Warsaw, Poland.

### Curvature effects in Cartesian coordinates

G. El Khoury\*, H. I. Andersson†, B. Pettersen\*

Turbulent flows in curved channels are known to exhibit substantial asymmetries both in the mean flow and turbulence characteristics<sup>1, 2</sup>. These asymmetries are induced by the centrifugal force, which tends to enhance the turbulence level along the outer (concave) wall and reduce the turbulent agitation near the inner (convex) surface. In addition, pairs of counter-rotating secondary vortices may arise as a result of the centrifugal instability<sup>1</sup>. These flow phenomena have been observed in direct numerical simulations (DNS) of channel flow with weak<sup>1</sup> and moderate<sup>2</sup> curvature.

In the aforementioned studies, the simulations were based on the full Navier-Stokes equations expressed in a cylindrical coordinate system. In the present investigation we first rigorously derived a set of governing equations of motion in a Cartesian coordinate system with additional terms aimed to account for the major effects of streamline curvature. The resulting set of PDEs is valid to first order in the dimensionless curvature parameter  $\delta/R_c$ , where  $2\delta$  is the wall distance and  $R_c$  is the radius of curvature. We thereafter implemented this new set of PDEs in a conventional DNS code using Cartesian meshes. After having reproduced the results of Moser et al.<sup>1</sup> for weak curvature ( $\delta/R_c = 0.01$ ), we next considered a moderately curved channel with  $\delta/R_c = 0.05$ . The present results, as shown in figure 1, compare favourably with those of Nagata et al.<sup>2</sup> and the adequacy of our simplified approach is thereby justified. It is particularly rewarding that distinct pairs of counter-rotating streamwise-oriented vortices are observed in the simulated flow field.

\*Dept. of Marine Technology, Norwegian Univ. of Science and Technology.

†Dept. of Energy and Process Engineering, Norwegian Univ. of Science and Technology.

<sup>1</sup>Moser et al., *J. Fluid Mech.* **175**, 479 (1987).

<sup>2</sup>Nagata et al., *J. Turbulence* **5**, 017 (2004).

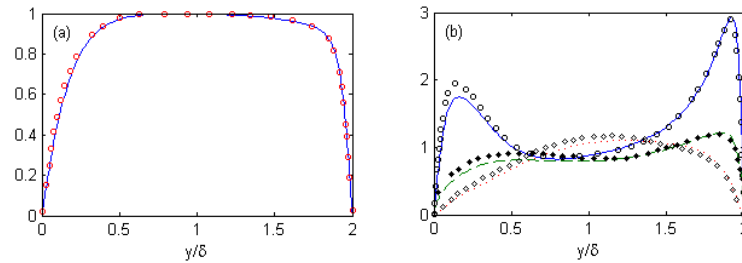


Figure 1: Turbulence statistics in a curved channel with  $\delta/R_c = 0.05$ . (a) Mean velocity  $U(y)$ . (b) Turbulence intensities  $u_{i,rms}$ . The symbols are DNS data from Nagata et al.<sup>2</sup>.

## Surface-roughness effects on droplet impact

Andrew Ellis<sup>\*</sup> and Frank Smith<sup>\*</sup>

This presentation addresses surface-roughness effects on droplet impact, with special application to the phenomenon of aircraft icing. When aircraft fly through adverse weather conditions ice can accumulate on parts of the structure, especially on the leading edge of a wing, which in turn can lead to a catastrophic loss in lift. One specific type of aircraft icing, known as SLD icing, is when super-cooled liquid water droplets of sizes greater than  $40\mu\text{m}$  strike the wing and freeze. Ice formation under SLD conditions is not fully understood and one key issue is the role of the underlying surface roughness of the iced wing on the droplet impact<sup>1</sup>.

Owing to the large Reynolds number involved, we examine in the present study the idealised case of high-speed inviscid impact of a water droplet on to a rough solid surface. The Weber and Froude numbers are also large and so surface tension and gravity can be neglected in a first approximation. Expressions for the contact point motion and free surface shapes are derived and solutions are presented for a range of roughness shapes. We also discuss the problem of determining the motion when there are many contact points over a rough surface. This can occur when the ice structure is sufficiently large that successive touchdowns of the free surface take place after the initial impact.

---

<sup>\*</sup>Department of Mathematics, UCL.

<sup>1</sup>Gent et al., *Phil. Trans. Roy. Soc. Lond. A* **358**, 2873 (2000).



## Flutter of a single flag or two parallel flags in uniform flow

Christophe Eloy\*, Lionel Schouveiler\*

When immersed in a uniform airflow, flexible plates can exhibit flutter instability above a critical value of the flow velocity. We have both investigated the flutter of a single flag clamped into a vertical mast and the coupled dynamics of two parallel flags. The figure displays the superimposed views of the flags over one flutter period  $T$ . The images are captured with a high-speed camera placed above the flags and the airflow of velocity  $U$  is blowing from top.

For a single flag of span  $H$ , the mode envelope depends mainly on its chord  $L$ . For short flags, a single-neck mode can be observed (similar to the shape of the two flags in the figure) while a double-neck mode is obtained for longer flags (not shown here). If two identical flags are placed side by side at a given separation distance  $d$ , different regimes of coupled flutter motion can be obtained as described in the figure caption.

A linear stability analysis is carried out in the limit of a potential flow<sup>1</sup>. Mode shapes are assumed to be one-dimensional (as observed in the experiments) but the flow is calculated in three dimensions. This stability analysis allows to predict the critical velocity, mode shapes and their frequencies which compare well with experimental measurements.

---

\*IRPHE, CNRS & Aix-Marseille Université, France.

<sup>1</sup>Eloy et al., *J. Fluids Struct.* **23**, 904 (2007).

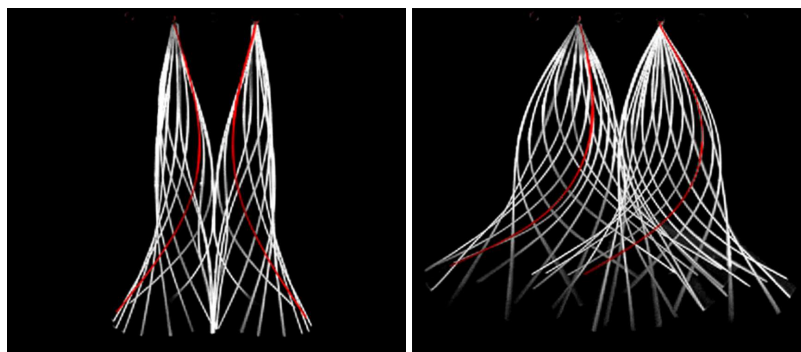


Figure 1: When the flow velocity  $U$  is increased and keeping all other parameters constant, we first observe an out-of-phase instability mode (left). Eventually a second bifurcation occurs giving rise to an in-phase flutter (right). In these figures, the first position has been colored in red to emphasize the phase relation between the two flags.

## Experimental investigation of the loads supporting the zigzag motion of freely rising axisymmetric bodies

P. Ern<sup>\*</sup>, P. C. Fernandes<sup>\*</sup>, F. Risso<sup>\*</sup> and J. Magnaudet<sup>\*</sup>

The forces and torques governing the zigzag motion of thick, slightly buoyant disks rising freely in a liquid at rest were determined by applying the generalized Kirchhoff equations to experimental measurements of the body motion performed for a single body-to-fluid density ratio  $\rho_s/\rho_f \approx 1$ . The evolution of the amplitude and phase of the various contributions to the hydrodynamic loads was studied as a function of the two control parameters: the body aspect ratio (the diameter-to-thickness ratio  $\chi = d/h$  ranges from 2 to 10) and the Reynolds number ( $100 < Re < 330$ ),  $Re$  being based on the rise velocity and diameter of the body. The results notably show a major influence of the aspect ratio on the relative magnitudes and phases. In parallel, time sequences of the velocity fields around the moving body were obtained using Particle Image Velocimetry. The differences observed between two bodies having contrasted aspect ratios ( $\chi = 3$  and  $\chi = 10$ ) were analyzed in relation with the evolution of the loads acting on the body and of the displacement and rotation of the body during a period of the zigzag. The phase difference between the vortical force and torque turns out to have a crucial influence on the path. Finally, the scaling of the amplitude and phase of the vortical loads was identified and used to propose an empirical model of the body motion valid for all the investigated cases.

---

<sup>\*</sup>Institut de Mécanique des Fluides de Toulouse, UMR CNRS/INPT/UPS 5502, Allée du Prof. C. Soula, 31400 Toulouse, France

## Laboratory experiments on atmospheric rotors

D.Etling<sup>a</sup>, A.Paci<sup>b</sup>, C.Knigge<sup>a</sup> and O.Eiff<sup>b</sup>

Stratified flows over obstacles have received much interest in the last decades within atmospheric or hydraulic contents. For the case of mountain lee waves it has been known for some time, that flow reversal can occur under the wave crests under special environmental conditions. These flows are called rotors and are characterized as very turbulent quasi two dimensional vortices with horizontal axis parallel to the mountain. Although many laboratory experiments have been performed for stratified flows over obstacles (e.g.”1”), not much work has been done on the rotor problem. This might be due to the fact, that conditions for rotor formation have been revealed only recently by numerical simulations (e.g.”2”). In fact it has been found, that rotor formation is favoured by an elevated density jump above the mountain top, which has not been considered in earlier laboratory experiments with continuous stratification.

We have performed experiments in the stratified towing tanks of CNRM at Meteo France at Toulouse. We used the same set up for a medium tank of 7 m length and a large tank of 22 m length as already used for lee wave experiments described in “1”. The main difference is the introduction of a neutrally stratified lower layer capped by a density jump under a continuous stratified upper layer. By varying the towing speed of the obstacle and the position of the density jump above the obstacle we were able to find the proper flow configurations with rotor formation . The results of about hundred experiments fitted quite well into the regime diagram on flow phenomena (lee waves, rotors, hydraulic jumps) obtained for similar density profiles in the numerical simulations “2”. We will present results on rotor formation by short video clips and streak line photographs and the related flow fields from PIV analysis.

---

<sup>a</sup> Institute of Meteorology and Climatology, University Hannover, Germany

<sup>b</sup> CNRM, Meteo France, Toulouse, France

<sup>1</sup> Eiff et al. Dyn.Atmos.Oceans **40**,71 (2005).

<sup>2</sup> Vosper, Q.J.R.Meteorol.Soc. 130, 1723 (2004).

## Symmetric and asymmetric shedding modes in the wake of axisymmetric objects.

FABRE David\*, AUGUSTE Franck\*, MAGNAUDET Jacques\*

The flow of a viscous flow past solid objects is characterised by successive bifurcations leading to various kinds of shedding modes. We use numerical simulation to study the case of fixed bodies with axial symmetry. The case of a sphere is well documented. A first bifurcation occurs for  $Re \approx 210$  (where  $Re$  is a Reynolds number based on the body diameter and the incoming velocity), and gives rise to a steady shedding mode characterised by a reflexional symmetry (figure *a*). A second bifurcation takes place for  $Re \approx 270$  leading to an unsteady mode (figure *b*). This mode also displays reflexional symmetry and can be termed a "zig-zig" mode as it is characterised by the shedding of hairpin vortices in a single direction. A different picture is observed in the case of a flat disk<sup>1</sup>. A first bifurcation is then found for  $Re \approx 116$ , leading to a steady mode similar to that observed with a sphere. However the second bifurcation, which occurs for  $Re \approx 121$ , leads to a shedding mode which breaks the reflexional symmetry (figure *c*). This mode can be termed a "yin-yang" mode because of the characteristic shape of the vorticity contours in the near wake. A third bifurcation occurs for  $Re \approx 139$ , leading to a shedding mode which recovers the reflexional symmetry. This mode can be described as a "zig-zag" mode as it is characterised by the shedding of hairpin vortices in alternate directions.

We show that these results can be explained by a simple nonlinear system describing the interaction of a steady mode and a Hopf mode in presence of  $O(2)$  symmetry<sup>2</sup>. We plan to extend the investigation to oblate spheroids and cylinders of finite thickness. Such bodies, which are intermediate between the sphere and the thin disk, will hopefully allow us to identify the geometrical property (curvature, thickness, edge for disks and cylinders) responsible for the selection between "yin-yang" and "zig-zig" modes.

\*Institut de Mécanique des fluides de Toulouse, Université Paul Sabatier

<sup>1</sup>F. Auguste *et al.*, *18ème Congrès français de mécanique*, Grenoble, 2007

<sup>2</sup>D. Fabre *et al.*, *Physics of fluids*, submitted (2008)

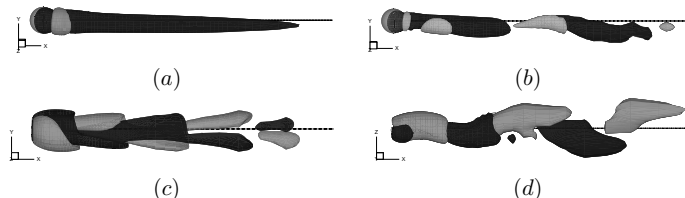


Figure 1: Shedding modes in the wake of axisymmetric objects (axial vorticity contours) : (a) steady mode for a sphere with  $R = 250$ , (b) "zig-zig" mode for a sphere with  $R = 280$ . (c) "yin-yang" mode for a flat disk with  $R = 123$ , (d) "zig-zag" mode for a flat disk with  $R = 150$ .

## Vortex analysis in the near wake behind a porous cylinder subject to blowing or suction

Bengt E.G. Fallenius\* and Jens H.M. Fransson\*

Recently, interest has been focused on the ability to manipulate the wake of bluff bodies to reduce drag, increase heat transfer or mixing, enhance combustion and prevent structural oscillations. Here, uniform blowing or suction through the surface of a porous cylinder has been studied. The flow rate through the cylinder surface is quantified by the parameter  $\Gamma = V/U_\infty \times 100$ , where  $V$  is the flow velocity through the cylinder surface and  $U_\infty$  is the free stream velocity. Positive and negative values of  $\Gamma$  are associated with blowing and suction, respectively. Experiments have been performed in the BL wind tunnel at KTH Mechanics on a cylinder with a diameter of  $D = 50$  mm and a surface made of a sintered plastic material. Here  $U_\infty = 1 \text{ m s}^{-1}$ , which corresponds to a diameter Reynolds number of 3 700. Smoke visualizations, surface pressure and hot-wire measurements as well as Particle Image Velocimetry (PIV) have been used to retrieve qualitative and quantitative flow information. A Matlab<sup>®</sup> program using a standard vortex detection algorithm has been developed for the PIV data, which provides statistical information about vortex sizes, strengths, location etc, when varying the blowing/suction rate. Small-scale vortices are identified by examining the areas in a high-pass filtered field where the local (2D) velocity gradient tensor has positive complex eigenvalues<sup>1</sup>, implying that the streamlines have a closed circular path. Vortex sizes, locations, strengths etc are stored, which makes a statistical examination of different quantities possible. It is found that even moderate levels of suction/blowing ( $|\Gamma| \leq 6.5$ ) have a large impact on the flow around the cylinder. Suction delays separation contributing to a narrower wake width, and a corresponding reduction in drag, whereas blowing shows the opposite behaviour. However, figure 1 shows that the size and strength of the vortices are nearly unchanged for different levels of suction, and the location where the highest probability of vortices to appear is close to the point of maximum back-flow ( $X_{BF}$ ) in the wake.

This work was financially supported by the Swedish Research Council and the Göran Gustafsson foundation.

\*Linné Flow Centre, KTH Mechanics, SE-100 44 Stockholm, Sweden.

<sup>1</sup>See e.g. Adrian et al., *Exp. Fluids* **29**, 275 (2000).

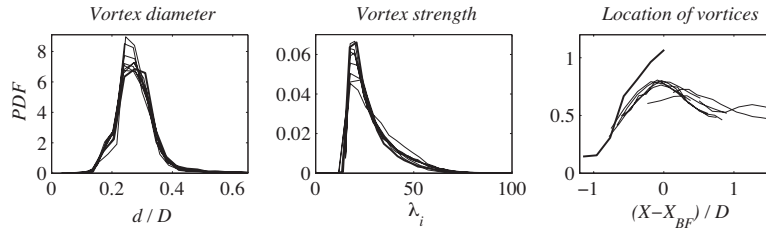


Figure 1: PDFs of the vortex diameter, the vortex strength and the streamwise position normalized with the point of maximum backflow are shown for suction levels in the range  $\Gamma = (0 : -6.5)$ . Bold line corresponds to the natural case ( $\Gamma = 0$ ).

## Analytical methods in biomicrofluidics

Fedosenko N.B<sup>a</sup>

In this moment microfluidics became a rapidly development area of fluid mechanics. Many interesting and very important applications of microfluidics lies in biotechnology. In microscale fluid dynamics became important such properties of the fluid as: rarefaction effects, viscous heating, electrokinetics, chemical and biochemical reaction with important role of surfaces, non-Newtonian effects and so on.

From one point of view we can't not take into the account all mentioned properties of the fluid. But in many typical biotechnological systems as membranes, drug delivery systems, proteomic reactors presents a such huge number of surfaces that our intentions became fruitless and imposable.

For that reason in designing biotechnological systems is very important to have an analytical or semi-analytical method that can calculate system in all and take into the account "microfluidics effects". Most knowing model is a lumped model. It is based on the equation like a Bernoulli's equation with additional item in the right side and also called Bernoulli's approach. This approach have a severe restricts and exists examples of uselessness of lumped model.

In this work is suggested an approach for analytical solution of incompressible flows equations for low Reynolds numbers and the properties of this solution is investigated. The results are used to investigating of microfluidics flows. And then extended to non-Newtonian fluids such as fluids with proteins that widely used in biomicrofluidics. The analytical solution of a boundary value problem for the Stokes is esteemed and suggested the solutions in a final form. The method of solution equations with the convective terms is offered. There the results obtained for the solution of equations like Stoke's equations directly used. For this purpose the special non-linear differential substitution of variables is offered. This differential substitution of variables sets a functional connection of the solution of a non-linear problem and solution of the conforming linear problem. The difference is, that the boundary conditions for linear (auxiliary) equations by a non-linear manner depend each on each. In this work the structure of relation of boundary conditions for (auxiliary) linear problem is offered. Then, by analogy with the solution of the Stokes problem, the analytical solution of this problem is obtained. After that with application of non-linear differential substitution of variables it is possible to obtain the solution of equations of incompressible viscose flows.

And after all we can extend our solution in semi-analytical form to estimate non-Newtonian fluids flows (for examples fluids with proteins) that play very important role in biomicrofluidics.

---

<sup>a</sup> Center for Advanced Studies, Saint-Petersburg State Polytechnical University

## An accelerated multigrid approach for time-integration of incompressible Navier-Stokes equations

Yuri Feldman<sup>a</sup>, Alexander Yu. Gelfgat<sup>a</sup>

Following a suggestion of using a direct linear system solver for stability analysis of steady state flows<sup>1</sup> we discuss a possible acceleration of 2D and 3D time-marching algorithms by implementation of a direct linear solver for the inner iteration of a multigrid approach.

The multigrid approach<sup>2-4</sup> is applied to unsteady incompressible Navier-Stokes equations. The semi-implicit second-order three-level scheme is used for the time integration. We use a correction scheme (CS) of Ref. 2 and a coupled line Gauss-Seidel smoother (CLGS)<sup>3</sup>. The line-wise smoother computes the pressure and the velocity corrections simultaneously over the entire row of finite volumes. This assembled equations system allows for an analytical solution. The modified method is extremely fast since it needs no more than  $O(5N)$  operations to compute the values of  $N$  corrections over the entire row for both 2D and 3D geometries. A typical  $V$ -cycle technique<sup>4</sup> is used for the multigrid iterations.

For test calculations we consider three dimensional lid-driven cavity flow as well as natural convection in rectangular and cubic cavities. The obtained lid-driven flow results agree carefully with solution reported in Ref. 5 for  $Re=10^3$  for various aspect and width ratios. We also considered the MIT2001 benchmark dealing with 8:1 thermally driven cavity flow<sup>6</sup> and convection in a laterally heated cubical enclosure as two representative 2D and 3D natural convection examples, respectively. The obtained periodical solution is in a good agreement with the results of Ref. 7. Several representative three-dimensional steady state flows within cubic thermally and lid-driven cavities are also reported. The characteristic CPU times consumed for a single time step per one node and per one CPU are of order  $5 \times 10^{-3}$  msec and  $10^{-2}$  msec for 2D and 3D calculations, respectively.

---

<sup>a</sup> School of Mechanical Engineering, Tel-Aviv University.

<sup>1</sup> A.Yu. Gelfgat, *Int. J. Numer. Meth. Fluids* **53**, 485 (2007).

<sup>2</sup> A. Brandt, *Math. Comput.* **31**, 333 (1977).

<sup>3</sup> MF. Paisley, *Int. J. Numer. Meth. Fluids* **30**, 441 (1999).

<sup>4</sup> Trottenberg et al., *Multigrid, Ac. Press, London*, (2001).

<sup>5</sup> S. Albensoeder, H.C. Kuhlmann *J. Comput. Phys.* **206**, 536 (2005).

<sup>6</sup> Christon et al., *Int. J. Numer. Meth. Fluids* **40**, 953 (2002).

<sup>7</sup> S. Xin, P. Le Quere, *Int. J. Numer. Meth. Fluids* **40**, 981 (2002).

## Analysis of the contribution of flow features to the global forces on a bluff body

L. Fiabane<sup>\*†</sup>, M. Gohlke<sup>\*</sup> and O. Cadot<sup>†</sup>.

The present study explores a new way of evaluation of fluid-dynamic forces on bluff bodies. The concern here is to determine the role of flow structures around a bluff body, particularly in their wake, and to link coherent structures in the vicinity of a bluff body (namely the vortices) to the forces acting on it. The aim is to have a more efficient exploitation of the data obtained from numerical simulations.

The main idea is to link the fluid-dynamic forces to the vorticity by using an exact formulation obtained from a budget equation and based on the impulse equation, as stated in recent papers (e.g. Noca et al.<sup>1</sup>). Furthermore, the boundary terms in that equation are discussed.

$$F(t) = \frac{d}{dt} \int_V \overline{\omega(t)} \wedge \vec{x} dV + \int_V \overline{u(t)} \wedge \overline{\omega(t)} dV + \oint_S \vec{n} \cdot \mathbf{\Upsilon}_i(t) dS$$

$$\mathbf{\Upsilon}_i(t) = \overline{\omega(t)}(\vec{x} \wedge \overline{u(t)}) - \overline{u(t)}(\vec{x} \wedge \overline{\omega(t)}) + \left( \vec{x} \cdot (\vec{\nabla} \cdot \mathbf{T}(t)) - \vec{x}(\vec{\nabla} \cdot \mathbf{T}(t)) + \mathbf{T}(t) \right)$$

Since the phenomena involved are rather complex, in a first step the study is undertaken on a two-dimensional case with the prospect to extend the same kind of method to three dimensions. Simulations are carried out on a two-dimensional academical geometry in an airflow at moderate Reynolds numbers (Re=100), which allows to consider the wake as two dimensional (see Sohankar et al.<sup>2</sup>).

Direct numerical simulations (DNS) were performed. Post-processing was done using a decomposition of the velocity into mean and fluctuating fields in order to compute and compare the contributions of each field on the mean aerodynamic forces (see the expression underneath).

$$\overline{u(t)} = \vec{U} + \overline{u'(t)} \text{ with } \langle \overline{u(t)} \rangle_t = \vec{U} \text{ and } \langle \overline{u'(t)} \rangle_t = 0$$

$$\langle F(t) \rangle_t = \int_V \vec{U} \wedge \vec{\Omega} dV + \int_V \langle \overline{u'(t)} \wedge \overline{\omega'(t)} \rangle_t dV + \oint_S \vec{n} \cdot \langle \mathbf{\Upsilon}_i(t) \rangle_t dS$$

Results are presented for cylinders with rectangular section of different aspect ratios. Here again, special caution is taken with boundary terms.

---

<sup>\*</sup>PSA Peugeot Citroen, Department of Research and Innovation, Velizy-Villacoublay, France.

<sup>†</sup>Unite de Mecanique, ENSTA, Chemin de la Huniere, Palaiseau, France

<sup>1</sup>Noca et al., *J. Fluids and Struct.* **13**, 551 (1999).

<sup>2</sup>Sohankar et al., *Physics of Fluids* **11,2**, 288 (1999).



## On the motion of a Taylor bubble rising at counter-current flow in a vertical channel.

B. Figueroa, J. Fabre\*

The regime of flow characterized by the formation of long, bullet-shaped bubbles that rise in the interior of pipes (known as Taylor<sup>1</sup> bubbles) was studied for the particular situation where the slugs rise while facing a (downwards) liquid velocity profile upstream the bubble nose. Some previous investigations like that of Martin<sup>2</sup>, Dukler et al.<sup>3</sup>, and later by Ha-Ngoc et al.<sup>4</sup> and Lu et al.<sup>5</sup>, suggest that above a critical counter-current mean velocity  $Um_c$ , the flow symmetry is broken and an increase in the bubble velocity  $V$  is observed.

A numerical code that solves the full incompressible (2D) Navier-Stokes equations using the VOF method<sup>6</sup> was used to carry on a series of numerical simulations at large Reynolds and Eötvös numbers. Two types of simulations were implemented during this study: first the mean velocity  $Um$  is set to a constant value, so Taylor bubbles evolve in time to reach their final rise velocity and shape. If the mean velocity does not exceed  $Um_c$ , the symmetric layout is stable, and the bubble adopts a symmetric final shape even if the initial shape is eccentric. Conversely, if the mean velocity is above  $Um_c$  the transition to the non-symmetric regime is observed. For the second type of simulations the mean velocity  $Um$  was varied with time.  $Um$  was increased beyond the critical value where the transition appears, and then decreased gradually to reach the initial conditions. The path followed in the  $Um - V$  plane shows evidence of a hysteresis cycle, as shown in figure 1, where the descending and ascending  $Um$  branches are labeled 'JADIM des/asc' (JADIM is the code acronym). Preliminary experimental results have shown a similar behavior for bubbles rising in circular tubes.

\*Institut de Mécanique des Fluides de Toulouse

<sup>1</sup>Taylor, G.I., *Proc Roy Soc London, Series A* **Vol. 201, No. 1065, 192-196**, (1950).

<sup>2</sup>Martin, C.S., *J. Fluids Eng.* **98, 715-22**, 169 (1976).

<sup>3</sup>Dukler A.E. et al., *Proceedings of the 3rd International Workshop on Two Phase Fundamentals, ICL, London*, 1-66 (1992).

<sup>4</sup>Ha-Ngoc, H., *Ph.D. Thesis, Institut National Polytechnique de Toulouse, France*, (2003).

<sup>5</sup>Lu, X., *J. Fluid Mech.* **568**, 173-192 (2006).

<sup>6</sup>Bonometti et al., *Int. J. Multiphase Flow* **33-2**, 109-133 (2007).

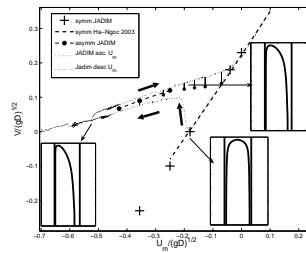


Figure 1: Dimensionless bubble velocity  $V/\sqrt{gD}$  vs. mean liquid velocity  $Um/\sqrt{gD}$ .

## On the logarithmic velocity profile in very rough open-channel flows

E. Florens\*, O. Eiff\*, F.Y. Moulin\*

In homogeneous rough boundary layers, the mean flow above the roughness sub-layer can be described by a logarithmic law with three parameters : the friction velocity  $u_*$ , the roughness length  $z_0$ , and the zero-plane displacement  $d$ . However, even in homogeneous situations without vertical confinement effects, which can arise in shallow free-surface flows, the methods to determine these three parameters yield inconsistent results. The discrepancies can be attributed in part to the limited data arising from the difficulties of measuring the turbulent flow within the canopy, especially the turbulent and the dispersive stresses. For example, Macdonald<sup>1</sup>, having access only to the mean velocity profiles, introduces a constraint based on mass conservation of the log-law to determine the parameter triplet. Cheng and Castro<sup>2</sup>, on the other hand, surmised that their turbulent shear stress measurements above the canopy extrapolated to the displacement height within the canopy are not too far from their direct  $u_*$  determination via drag force measurements. Nikora<sup>3</sup> suggested a conceptually simple method to determine the triplet based on the log-law without resorting to additional ad hoc constraints by fitting the mean strain of the log-region. However, in case of heterogeneous roughness distributions, secondary circulations or strong vertical confinement, deviations from the log-law are expected. Here, we investigate experimentally the effect of vertical confinement on the boundary layer structure and the determination of the parameter triplet. Turbulent velocity fields were measured above the canopy, as well as inside, yielding the turbulent and dispersive stresses. PIV measurements were performed in a  $20m \times 1.1m \times 0.5m$  glass-walled open-channel whose bottom was covered with 2 cm wide cubes arranged in a squared distribution yielding a planar and frontal densities of 0.19. The measurements were made in the fully-developed boundary layer for three vertical confinements. The complete vertical description of the flow field with double-averaging is used to compare Nikora's above-the-canopy log-law method and Cheng and Castro's extrapolation method with our results. The effect of vertical confinement on the log-law and its ability to yield consistent friction parameters will be discussed.

\*Institut de Mécanique des Fluides de Toulouse, France

<sup>1</sup>R.W. Macdonald, *Boundary Layer Met.* **97**, 25 (2000).

<sup>2</sup>H. Cheng and I.P. Castro, *Boundary Layer Met.* **104**, 229 (2002).

<sup>3</sup>V. Nikora et al., *River Flow 2002* **1**, 83 (2002).

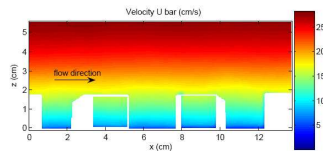


Figure 1: Mean velocity field over and inside a squared distribution of cubes

## Linear and nonlinear dynamics of axisymmetric waves in the hollow core vortex

J. Fontane\*, D. Fabre\* and P. Brancher\*

The dynamics of trailing vortices are under constant investigation during last decades since it is of considerable interest to reduce aircraft wakes and associated hazards to forthcoming planes. The isolated axisymmetric vortex is the commonly used simplest elementary model when considering such issue. Although asymptotically stable, recent studies have revealed its sensitiveness to specific perturbations, leading in some cases to considerable gains of energy<sup>1,2</sup>. Albeit of evident interest, the underlying mechanisms of energy growth are considered in the linear regime.

The nonlinear dynamics of such vortices need also to be considered in order to complete the picture. Rather than performing direct numerical simulations<sup>3</sup>, an interesting way to investigate it is to consider the nonlinear interactions of waves. This approach is motivated by the possible existence of resonance between wave components. For this purpose, the base flow model is simplified by considering the hollow core vortex. Arising naturally when a tank is drained (bath-tube vortex), it presents simpler dynamics than the Lamb-Oseen vortex as it only possesses two families of waves. This point is of crucial importance for the tractability of the problem.

In this work, the nonlinear temporal evolution of axisymmetric waves are investigated through numerical integration when the flow is submitted to various initial conditions (travelling or standing wave, pinching of the free surface, wave trains). We focus on wave trains as important energy exchanges between the main component and its sideband waves are observed (figure 1). This phenomenon is related to the Benjamin-Feir instability<sup>4</sup> (triadic resonance) occurring for wave trains on deep water.

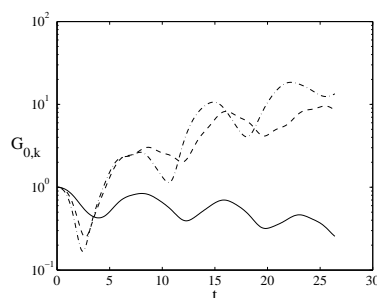


Figure 1: Energy Gain of the main component  $k = 1$  (—), the upper sideband wave  $k = 1.1$  (---) and the lower sideband wave  $k = 0.9$  (- -) for  $Re = 1000$  and  $We = \infty$ .

\*Institut de Mécanique des Fluides de Toulouse, France

<sup>1</sup>Antkowiak & Brancher, *Phys. Fluid* **16** (1), L1 (2004)

<sup>2</sup>Antkowiak & Brancher, *J. Fluid Mech.* **578**, 295 (2007)

<sup>3</sup>Takahashi, Ishii & Miyazaki, *Phys. Fluid* **17**, 035105 (2005)

<sup>4</sup>T.B. Benjamin & J.E. Feir *J. Fluid Mech.* **27**, 417 (1967)

## TIP SELECTION FOR THREE-DIMENSIONAL DENDRITES

M. R. Foster\*, S. Tanveer†

The speed of the tip of a slender, three-dimensional dendrite propagating into an undercooled melt has been determined in the laboratory, and in various computations<sup>1</sup>. However, the limit of vanishingly small surface energy presents serious difficulties for determination of that propagation rate. The exact zero-surface-energy Ivantsov solution, with its paraboloidal shape, determines only the product of tip speed and radius, but neither one explicitly. We formulate the evolution equation for the three-dimensional dendrite for small Peclet number (and hence, small undercooling). If  $\mathcal{B}$  is a dimensionless measure of the (small) surface energy, we find that, as in the two-dimensional case<sup>2</sup>, the asymptotic expansion of the solution for  $\mathcal{B} \rightarrow 0$  leads to no determination of the tip speed from conventional asymptotic techniques, because it is the transcendently small terms in that expansion that provide that determination. The evolution equation is analytically continued off the real line, and an inner equation is obtained, in a region of width  $\propto \mathcal{B}^{2/7}$  about the location of the curvature singularity closest to the real line. The inner equation turns out to be virtually the same as that for the two-dimensional case<sup>2,3</sup>. Its solution matches to the transcendently small portion of the solution on the real line, within a Stokes sector that includes a segment of that line. If  $\alpha$  is a measure of the four-fold anisotropy of the surface energy of the material, then we find that the inner problem is a nonlinear, second-order eigenvalue problem that relates a quantity  $\alpha/\mathcal{B}^{4/7}$  to the tip curvature.

In the two-dimensional case, that eigenvalue problem gives a set of tip speeds, the lowest of which appears to correspond to that observed; however, in this three-dimensional problem, we must permit small deviations from axisymmetry near the tip, arising from the anisotropy. That leads to, (1), a singularity location that is a function of the azimuthal angle,  $\phi$ , and, (2), an eigenvalue problem that is also azimuthally dependent. So, the procedure is to write the surface of the dendrite as

$$Z = -\frac{1}{2}r^2 + \sum_{n=1}^{\infty} \frac{a_n}{4n} r^{4n} \cos(4n\phi),$$

where  $-r^2/2$  is the paraboloid, and the second term is appropriate for a crystal with four-fold anisotropy. By satisfying the eigenvalue problem for all  $\phi$ , the set of coefficients  $\{a_n\}$  and the tip speed may be determined.

We present an approximate determination for these coefficients that retains only  $a_1$  and  $a_2$ , comparing our results with those reported previously<sup>4</sup>, in a work retaining only  $a_1$ . Finally, we compare both with the determination for a large number of terms, achieved by computational means.

---

\*Mathematical Sciences, Rensselaer Polytechnic Institute

†Mathematics, The Ohio State University

<sup>1</sup>See Kessler & Levine, *Phys. Rev. A* **33**, 7867 (1986), for example

<sup>2</sup>Tanveer, *Phys. Rev. A* **40**, 4756 (1989)

<sup>3</sup>Ben-Amar & Pomeau, *Europhys. Lett* **2**, 307 (1986)

<sup>4</sup>Brener & Melnikov, *JETP* **80** (1995)

## Experimental study of turbulent spot evolution in the ASBL\*

Jens H. M. Fransson<sup>†</sup>

Turbulent spots and their streamwise evolution play a major role in most transition scenarios. The appearance of turbulent spots in laminar boundary layers was first noted by Emmons,<sup>1</sup> who proposed a spot probability appearance model, which recently<sup>2</sup> has proven to work well for the free stream turbulence (FST) induced transition scenario. However, there are many fundamental questions still remaining unanswered, which are important in the striving after new transition prediction models.

In this experimental study the effect of Reynolds number on turbulent spot evolution has been studied while keeping the boundary layer thickness constant. This type of study can only be performed in the asymptotic suction boundary layer where uniform suction through the wall is applied creating a boundary layer which does not develop in space. The velocity profile in the ASBL can readily be derived as,

$$u(y) = U_\infty \{1 - e^{yV_w/\nu}\},$$

where  $U_\infty$ ,  $V_w$ , and  $\nu$  are the free stream velocity, the suction velocity ( $< 0$ ), and the kinematic viscosity, respectively. With the access of an analytic solution to the Navier–Stokes eq. for the ASBL case it is straight forward to calculate the displacement and the momentum thicknesses as  $\delta_1 = -\nu/V_w$  and  $\delta_2 = \delta_1/2$ , respectively, giving a constant shape factor,  $H_{12} = 2$ , independent of the suction velocity. The Reynolds number based on the displacement thickness, thus, becomes  $Re = -U_\infty/V_w$  allowing for  $Re$ -changes without necessarily changing the boundary layer thickness,  $\delta_{99} = \delta_1 \ln(100)$ . In the past very few experiments have been performed in ASBLs<sup>3</sup> due to the inherent difficulties in setting up this type of boundary layer experiment. These experiments were carried out in the MTL wind tunnel at KTH Mechanics. A porous plate ( $2250 \times 1000 \text{ mm}^2$ ) made of a sintered plastic material was used in order to allow for uniform surface suction. In a pre-study the material permeability was determined, which through Darcy’s law relates the pressure difference ( $\Delta p$ ) across the plate to the velocity through the porous material. In this way the suction velocity could be calculated simply by measuring  $\Delta p$  during the actual experiments. Here, a  $\Delta p$  of 18–19 Pa was maintained, implying that the displacement thickness was kept constant around  $\delta_1 = 1.45 \text{ mm}$ . Turbulent spots were generated by means of short pulsed wall-jets through one or two holes in the plate. The initial condition was further studied by changing the jet strength and the pulse duration. Finally, the effect of FST was studied using two different turbulence generating grids. The measurements were performed with hot-wire anemometry and considering all experimental cases over 387 000 spots were generated, which give a satisfied statistical convergence of the data at each measurement point. Streamwise (6 locations), spanwise (91) and wall-normal (30) traverses were done, giving a good spatial resolution of the spots which in turn allows for detailed data analyses to be presented.

\* Asymptotic Suction Boundary Layer.

<sup>†</sup>Linné Flow Centre, KTH Mechanics, SE-100 44 Stockholm, Sweden.

<sup>1</sup>Emmons, *J. Aero. Sci.* **18**, 490 (1951).

<sup>2</sup>Fransson et al., *J. Fluid Mech.* **527**, 1 (2005).

<sup>3</sup>Fransson and Alfredsson, *J. Fluid Mech.* **482**, 51 (2003).

## Coriolis effects in rotating Hele-Shaw cell.

Hermes Gadêlha\*, José A. Miranda† and Enrique Alvarez-Lacalle‡

A growing number of experimental and theoretical works has been addressing various aspects of the viscous fingering formation in rotating Hele-Shaw cells (see Fig. 1). However, only a few of them consider the influence of Coriolis forces. In this work, we approach the problem analytically and numerically. We use a modified Darcy's law including the exact form of the Coriolis effects to execute a mode-coupling analysis of the system. By imposing no restrictions on the viscosity contrast  $A$  (dimensionless viscosity difference) we go beyond linear stages, and examine the onset of nonlinearities. Our results indicate that when Coriolis effects are taken into account, an interesting interplay between the Reynolds number  $Re$  and  $A$  arises. This leads to important changes in the stability and morphological features of the emerging interfacial patterns. We contrast our mode-coupling approach with previous theoretical models proposed in the literature. Finally, boundary integral techniques are employed to simulate important interfacial behaviors at fully nonlinear stages (see Fig. 2).

\*Centre for Mathematical Biology, Mathematical Institute, University of Oxford, UK.

†Departamento de Física, Universidade Federal de Pernambuco, Brazil.

‡Universitat Politècnica de Catalunya, Spain.

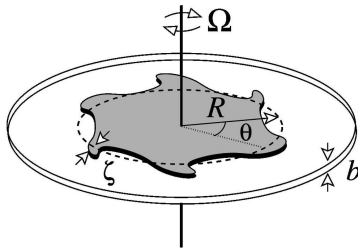


Figure 1: Sketch of a rotating Hele-Shaw cell of gap width  $b$  containing two immiscible, viscous fluids spinning with constant angular velocity around the  $z$  axis.

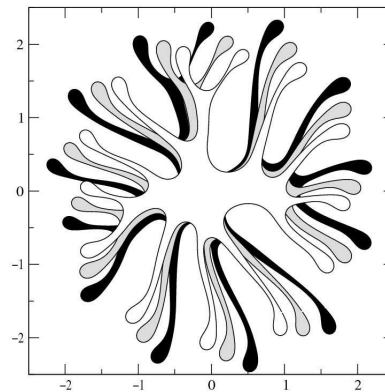


Figure 2: Numerical experiments showing the development of typical fingering patterns in a rotating Hele-Shaw cell when Coriolis effects are significant.

## Modelling Ciliary Driven Flows, with Application to The Lung and Development

Gaffney EA<sup>ad</sup>, Smith DJ<sup>bcd</sup>, Blake JR<sup>cd</sup>

Numerous physiological and patho-physiological factors are known to influence how waves of beating cilia protruding from the lung epithelium clear mucus from lung surfaces. While this clearance is an important innate defence mechanism of the airways, there is often insufficient data to quantitatively evaluate how such factors influence mucus transport<sup>1</sup>, motivating experimental and theoretical modelling studies. Here, we consider an in-vitro representation of the lung epithelium and airway surface liquid<sup>2</sup> in addition to the lung. Modelling predictions for the important biophysics of mucus flow in the lung are discussed together with the significance of mixing and diffusion when interpreting tracer transport within in-vitro representations of the lung surface.

We will also address the modelling of fluid flows induced by whirling cilia within the mouse embryo node, which is observed to induce initial left-right symmetry breaking in mouse development. The quantitative characterisation of this flow will allow one to test the biophysical foundations underlying hypothesised mechanisms for how nodal fluid dynamics induces asymmetric gene expression, a subject of intense scientific debate.

- 
- a Centre for Mathematical Biology, Mathematical Institute, University of Oxford, 24-29 St Giles', Oxford, OX1 3LB.
  - b Reproductive and Child Health, Medical School, University of Birmingham, Birmingham B15 2TT, UK.
  - c School of Mathematics, University of Birmingham, Edgbaston, Birmingham B15 2TT, UK.
  - d Centre for Human Reproduction Science, Birmingham Women's Health Care NHS Trust, Edgbaston, Birmingham B15 2TG, UK.

- 1 Donno et al, *Chest* **118**, 1142 (2000)
- 2 Matsui et al, *J. Clin. Invest.* **102**, 1125 (1998).

### Bifurcations in separated boundary layer flows.

J. S. B. Gajjar\*, R. P. Logue\*, A. I. Ruban\*

The manner in which a laminar separated flow becomes unstable is of immense interest not just from the technological perspective, but also from theoretical viewpoint. In many problems of practical interest, such as leading edge separation, the Reynolds is large and this it makes it difficult to compute the steady flow, if it exists, accurately and subsequently to study the instability of the flow. Full simulations of the Navier-Stokes equations are computationally very intensive and cannot resolve the important features unless very large grids are used, and this is not always feasible. Analytically, the model problems which have been studied are far removed from a real separated flow in which the flow is truly non-parallel, and conclusions about the stability of the flow based on making use of the parallel flow assumptions, are of dubious value for these non-parallel flows.

In our current work we have adopted the philosophy that it is possible to study the stability of a laminar separated flow by investigating the instability of the flow governed by the triple-deck and related equations. These equations arise from a self-consistent asymptotic analysis of the Navier-Stokes equations in the limit that the Reynolds number is large. The advantages of this approach are that it is possible to describe the separation process, but using reduced equations. In addition the stability characteristics can be more easily studied and important generic mechanisms more easily identified.

We have obtained the steady state solutions of the equations numerically using a number of different techniques including arc-length continuation. This enables one to compute stable and unstable branches.

The stability of the flow is examined by two methods. In one approach we look for small perturbations to the steady flow proportional to  $e^{\lambda t}$ . This gives rise to a set of linearised equations leading to a generalised eigenvalue problem after discretization. In the second approach the linearised unsteady equations are solved directly with forced and unforced perturbations and the stability of the flow investigated.

A number of different problems have been studied but two in particular, for which results will be presented include the subsonic flow past a convex corner, for which the interaction law is

$$\frac{\partial p}{\partial x} = -\frac{1}{\pi} \int_{-\infty}^{\infty} \frac{a_{ss}(s, t)}{s-x} ds,$$

and a second problem which concerns liquid layer flow over convex and concave corners for which

$$p = -sa - \frac{\partial^2 a}{\partial x^2},$$

see <sup>1</sup>, and where  $s$  is a parameter,  $p(x, t)$ ,  $a(x, t)$  are the pressure and displacement function respectively.

---

\*School of Mathematics, University of Manchester.

<sup>1</sup>Gajjar,(1987) *Computers & Fluids*, **15**, 337-360.



## Time-dependent subgrid scales in residual-based large eddy simulation of turbulent channel flow

Peter Gamnitzer\*, Volker Gravemeier\*,<sup>†</sup> and Wolfgang A. Wall\*

In large eddy simulation (LES), only the coarser scales of turbulent flows are resolved. A new approach to LES is based on the variational multiscale method (VMM). In a VMM, scales are separated a priori by variational projection rather than by filtering approaches, which are traditionally applied for LES<sup>1</sup>. Two types of VMMs for LES have been developed. On the one hand, a three-scale VMM for LES has been successfully applied to turbulent flow problems<sup>2,3</sup>. On the other hand, a (two-scale) residual-based VMM for LES was recently introduced<sup>4</sup>. The unresolved (fine) scales in the residual-based VMM are introduced into the equation for the resolved (coarse) scales via an approximate analytical solution of the unresolved scales.

This study investigates the effect of taking into account the time dependency of the unresolved scales in the aforementioned approximate analytical solution of the unresolved-scale problem. For stabilized finite element solutions of laminar flow problems, this extension was already shown to give better results<sup>5</sup> than the quasi-static approach, which neglects this time dependency. The residual-based VMM with time-dependent subgrid scales is presented in this talk, and the impact of the time dependency is studied for the well-known test case of turbulent channel flow. For time-integration, a generalized- $\alpha$  scheme is employed<sup>6</sup>. This time integration is used both for the solution of the resolved scales and for the approximate solution of the unresolved-scale problem. The latter is represented by ordinary differential equations. Results are presented from computations for various values of the Reynolds number, namely  $Re_\tau = 180$ ,  $Re_\tau = 395$  and  $Re_\tau = 590$ . Results from our numerical experiments are compared to reference calculations obtained with a quasi-static approximation of the unresolved scales and a computation based on a dynamic Smagorinsky model<sup>7</sup>.

\*Chair for Computational Mechanics, Technische Universität München.

<sup>†</sup>Emmy Noether Research Group "Computational Multiscale Methods for Turbulent Combustion"

<sup>1</sup>Sagaut, *Springer* (2006).

<sup>2</sup>Hughes et al., *Computing and Visualization in Science* **3**, 47 (2000).

<sup>3</sup>Gravemeier, *Archives of Computational Methods in Engineering - State of the Art Reviews* **13**, 249 (2006).

<sup>4</sup>Bazilevs et al., *Computer Methods in Applied Mechanics and Engineering* **197**, 173 (2007).

<sup>5</sup>Codina et al., *Computer Methods in Applied Mechanics and Engineering* **196**, 2413 (2007).

<sup>6</sup>Jansen et al., *Computer Methods in Applied Mechanics and Engineering* **190**, 305 (2000)

<sup>7</sup>Germano et al., *Physics of Fluids A* **3**, 1760 (1991)

## A moving mesh finite element method for two-phase flows with insoluble surfactants

Sashikumaar Ganesan<sup>\*</sup>, Lutz Tobiska<sup>†</sup>

A moving mesh finite element scheme using the arbitrary Lagrangian Eulerian (ALE) approach is presented to compute two-phase flows with insoluble surfactants. The immiscible two-phase flow is governed by the time dependent incompressible Navier-Stokes equations with piecewise constant material properties. The surfactant concentration over the moving interface is described by a scalar convection-diffusion equation with a source like term to account for the local changes in the interface area. These two equations are coupled through the surface tension, which may be a linear or non-linear function of surfactant concentration. A second order inf-sup stable finite element pair is used to discretize the Navier-Stokes equations. Further, the Laplace-Beltrami operator technique is used to handle the curvature term which allows to reduce one order of differentiation in the curvature approximation. Since an interface resolved mesh is used, high curvature and/or complex interfaces (see for *e.g.*, figure 1) can also be handled with this scheme. An excellent mass conservation (without any mass correction approach) is obtained for the fluid in each phase and for the surfactant over the interface. A number of 2D computations are performed to validate the proposed numerical scheme.

---

<sup>\*</sup>Institute for Analysis and Numerical Mathematics, Otto von Guericke University, Magdeburg.

<sup>†</sup>Institute for Analysis and Numerical Mathematics, Otto von Guericke University, Magdeburg.

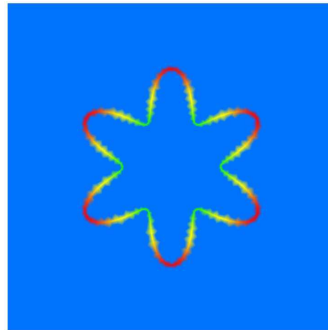


Figure 1: Nonuniform distribution of insoluble surfactant over an unequilibrium interface.

### Acoustically coupled pulsations and translation of two microbubbles in ultrasound

V. Garbin<sup>a</sup>, B. Dollet<sup>a,b</sup>, L. van Wijngaarden<sup>a</sup>, N. de Jong<sup>a</sup>, D. Lohse<sup>a</sup> and M. Versluis<sup>a</sup>

The application of microbubbles as a contrast agent in ultrasound medical imaging has motivated an even broader interest in investigating bubble phenomena. Here we study experimentally the acoustic coupling between microbubbles pulsating in an ultrasound field, which is known to produce a net attraction between two bubbles pulsating in phase, through the secondary Bjerknes force. This coupling can modify the acoustic response of a bubble through a change of its resonance frequency. Therefore, quantifying the interaction between bubbles is crucial for optimizing medical imaging protocols.

We selected two bubbles (BR-14 ultrasound contrast agents, Bracco Research S.A., Geneva) using optical tweezers<sup>1</sup>, and positioned the bubble pair away from the sample chamber wall, to prevent wall effects as viscous shear and acoustic reflections, thus allowing to quantify purely the interaction between bubbles. The ultra-high speed “Brandaris 128” imaging facility<sup>2</sup> was used to optically record the bubble dynamics at 15 million frames per second. From the optical measurements we tracked the instantaneous bubble radii and positions.

The ultra-high speed recordings revealed the alternately attractive-repulsive effect of the secondary Bjerknes force. The bubbles display small oscillations, with the same frequency as the driving ultrasound, around a position that slowly drifts, resulting in the net attraction observed for bubbles pulsating in phase.

We model the translation by writing a force balance for each bubble. A boundary condition of no-slip is assumed at the bubble interface, which is coated with a layer of lipid molecules to prevent dissolution or coalescence of the bubbles. Only those experiments where the bubbles retain their spherical symmetry are analyzed.

If the viscous drag is accounted for through the quasi-steady Stokes’ drag, the dissipation due to viscosity is largely underestimated. High-Reynolds number corrections (in our experiments  $Re \sim 5-10$ ) do not correctly account for the discrepancy. Instead, good agreement with the experimental observations is found if we account for the oscillatory character of the boundary layer that is developed (in the limits of small amplitude and high frequency of oscillations) through Stokes’ solution for an oscillating sphere, which also accounts for history force effects.

---

<sup>a</sup> Physics of Fluids, University of Twente, The Netherlands.

<sup>b</sup> Groupe de Matière Condensée et Matériaux, Université Rennes 1, France.

<sup>1</sup> V. Garbin et al., *Appl. Phys. Lett.* **90**, 114103 (2007)

<sup>2</sup> C.T. Chin et al., *Rev. Sci. Instrum.* **74**, 5026 (2003)

## Numerical investigation of gas bubbles rising in liquids

D. Gaudlitz\*, N. A. Adams\*

Bubbly flows occur in a large number of natural and technological processes, e.g. in chemical industry and in metallurgy. To improve the knowledge about physical mechanisms determining the motion and deformation of a gas bubble rising in a liquid we perform direct numerical simulations of such flows. Based on DNS data an analysis of the interaction between the bubble and its wake allows for a comprehensive interpretation of the observed steady and unsteady rising paths.

The Navier-Stokes equations for incompressible, non-reacting two-phase flows are discretized using a finite difference method on an equidistant Cartesian grid. For representing phase interfaces we have chosen the hybrid particle-level-set method<sup>1</sup>. This hybrid Eulerian-Lagrangian approach combines the computationally efficient reconstruction of interfaces given by the level-set method with the good conservation properties of marker-particle methods. A modified version of this method has been proposed in order to achieve higher accuracies in case regions of the interface, e.g. bubble skirts, become marginally resolved by the computational grid<sup>2</sup>.

For bubbles rising steadily on linear ascent paths we observed a toroidal vortex ring inside the closed laminar bubble wake, which agrees very well with the experimental findings. Air bubbles of a diameter  $d > 2.0$  mm rising in water can develop spiraling or zig-zagging paths. As in experiments, the periodic shedding of hairpin vortices in the bubble wake has been found to cause the zig-zagging motion of the bubble. Moreover, cascades of several interconnected hairpin vortices have been identified in the simulations, see Fig. 1. The bubble exhibits symmetric as well as asymmetric shape oscillations. The latter can be attributed to the periodic formation of new systems of hairpin vortices at the lower side of the bubble.

\*Institute of Aerodynamics, Technical University Munich.

<sup>1</sup>Enright et al., *J. Comput. Phys.* **183**, 83 (2002).

<sup>2</sup>Gaudlitz et al., *Computers & Fluids* (in press).

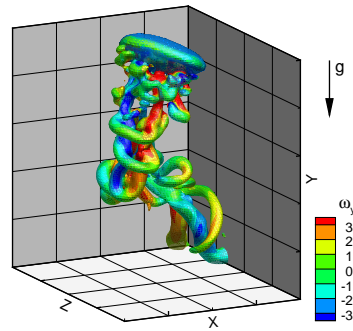


Figure 1: Instantaneous vortex structures ( $\lambda_2 = -1$ ) in the wake of a zig-zagging bubble.

## High-speed Jet Formation after Solid Object Impact

Stephan Gekle\*, José Manuel Gordillo†,  
Devaraj van der Meer\* and Detlef Lohse\*

A spectacular example of free surface flow is the impact of a solid object on a liquid: Upon impact a splash is created and a surface cavity (void) emerges. Its collapse creates an upwards and downwards jet at the pinch-off singularity and entrains a giant bubble<sup>1,2</sup>. The impact of a circular disc leads to an especially impressive jet.

Using sophisticated boundary-integral techniques including careful surface surgery we show that jet formation in the present context stands out from previously studied mechanisms such as bubble collapse near a wall, liquid droplet impact or bubbles rupturing near a free surface. Instead, the purely inertial focussing makes the present phenomenon more reminiscent of the very violent jet of fluidized metal observed during the collapse of "lined cavities" in military and mining operations<sup>3</sup>.

After impact, a cavity of several disc radii depth emerges (a). Hydrostatic pressure pushes the surface inward leading to the pinch-off of a large bubble halfway down the cavity (b). This pinch-off point constitutes a finite-time singularity with diverging radial velocity.

Immediately after closure, in (c) and (d), two fast sharp-pointed jets are observed shooting up- and downwards from the closure location, which by then has turned into a stagnation point surrounded by a locally hyperbolic flow pattern. This flow, however, is *not* the mechanism feeding the two jets. Our simulations show that only the inertial focussing of the liquid colliding at the base of the jet provides enough energy to eject the observed high-speed jets. The liquid contained in the jet is shown to originate exclusively from a thin layer straddling the surface of the original collapsing bubble.

\*Physics of Fluids, University of Twente, The Netherlands

†Mecánica de Fluidos, Universidad de Sevilla, Spain

<sup>1</sup>Bergmann et al., *Phys. Rev. Lett* **96**, 154505 (2006).

<sup>2</sup>Gekle et al., *Phys. Rev. Lett.* (in press).

<sup>3</sup>Birkhoff et al., *J. Appl. Phys.* **19**, 563 (1948).

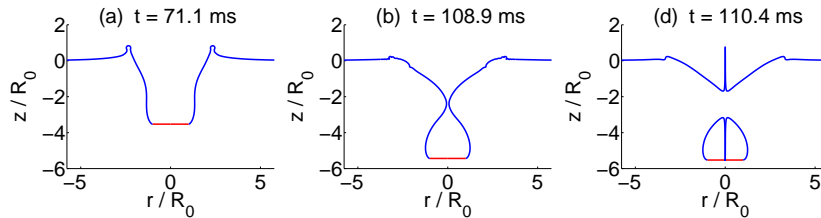


Figure 1: Surface profiles (blue) showing the cavity created after the impact of the disc (red) in (a), its collapse (b) and the two jets, (c) and (d). Note the extremely short time scale of jet formation: the jet grows above the original surface in only about 1% of the total time after impact. Units are normalized by the disc radius  $R_0 = 2$  cm, the impact speed is  $V_0 = 1$  m/s.

## Transition in Internally Heated Inclined Plane Parallel Shear Flows

S.C. Generalis\*, F.H. Busse†

This work is concerned with transitions in a viscous incompressible fluid bounded between two inclined parallel plates of infinite extent maintained at constant temperature when convection is generated by uniformly distributed internal heat sources. The study here is motivated partially by previous work<sup>1,2</sup> but primarily by the fact that the present problem has many important environmental and industrial applications. An example are heat sources produced in fluids in nuclear fusion reactors where liquid sodium is used to cool the hot plasma. Geophysical and planetary applications include the cases where heat is released by an electric current in a conductive fluid and internal heating has been studied in connection with the absorption of solar radiation in planetary atmospheres. In addition the present problem can be compared with Bénard convection<sup>3</sup>, where motions are driven by temperature differences across the fluid layer and not by homogeneous heating. The present study focuses on the plane parallel shear flow with a homogeneously distributed heat source with or without the imposition of the constraint that the mass flux across any lateral section of the channel flow is conserved. It is within this framework that internally heated parallel shear flow with a Poiseuille component<sup>4</sup> is also examined. The critical Grashof number is determined by a linear stability analysis for various values of the Prandtl number. In our numerical study the angle of inclination of the channel is taken into account and we find that in each case studied, with the exception of a horizontal layer of fluid with vanishing applied constant pressure gradient, the basic flow loses stability in a Hopf bifurcation. Following the linear stability analysis our numerical studies focus on the emerging secondary flows and their stability, in order to identify possible bifurcation points of tertiary flow. Of particular interest is the competition between hexagonal convection cells and convection rolls oriented either in the longitudinal or the transverse direction with respect to the mean flow.

---

\*Chemical Engineering and Applied Chemistry, Aston University, Birmingham B4 7ET, UK E-mail: s.c.generalis@aston.ac.uk .

†Institute of Physics, University of Bayreuth, D-95440 Bayreuth, Germany E-mail: busse@uni-bayreuth.de .

<sup>1</sup>F.H. Busse, *J. Fluid Mech.* **30**, 625 (1967).

<sup>2</sup>S.C.Generalis et al., *ASME Journal of Heat Transfer* **125**, 795 (2003).

<sup>3</sup>A. Schluter et al, *J. Fluid Mech.* **23**, 129 (1965).

<sup>4</sup>U. Ehrenstein et al, *J. Fluid Mech.* **228**, 111 (1991).

### Yield-stress drops.

Guy German<sup>a</sup> and Volfango Bertola<sup>a</sup>

Liquid drops and their behaviour during detachment from a nozzle, free-fall, impact and subsequent spreading provide an interesting framework for experimentation. Not only is it a complex fluid dynamics problem, it is also present in a diverse number of industrial applications such as ink-jet printing, spray painting and cleaning, agrochemical spraying and fire extinguishment. Whilst extensive research into drop detachment and impact dynamics of Newtonian fluids has been completed and summarised<sup>1,2</sup>, more contemporary research has focused on complex fluids. Currently significant research has been completed on fluids with a polymer additive<sup>3,4</sup>, however relatively little has been performed on viscoplastic fluids that exhibit a measurable yield-stress. Existing work has included computational studies of yield-stress fluid pendant drop formation<sup>5</sup> and an experimental investigation of the impact behaviour and sessile state of drops of vaseline<sup>6</sup>. To build upon our current knowledge of viscoplastic fluid behaviour, experimental work has been completed with the aim of understanding how fluid yield-stress can influence drop dynamics. From this research, evidence has been obtained that supports the hypothesis that fluid yield-stress can alter drop detachment dynamics, inhibit spherical drop formation during free-fall, influence drop impact during the inertial expansion phase and can inhibit drop retraction and spreading. Drop impact dynamics and subsequent sessile drop shape appear to be controllable through careful selection of the fluid rheology and this has the potential for industrial spraying applications in processes where the maximisation of contact area is required whilst using a minimum amount of fluid.

---

<sup>a</sup> School of Engineering and Electronics, University of Edinburgh

<sup>1</sup> Rein, Fluid Dyn. Res. **12**, 61 (1993)

<sup>2</sup> Eggers, Rev. Mod. Phys. **69**, 865 (1997)

<sup>3</sup> Bergeron, Comptes rendus. Physique **4**, 211 (2003)

<sup>4</sup> Crooks and Boger J. Rheol. **44**, 973 (2000)

<sup>5</sup> Davidson and Cooper-White, Appl. Math. Model. **30**, 1392 (2005)

<sup>6</sup> Nigen, J. Atomiz. and Spray. **15**, 103 (2005)

## Nature-inspired porous airfoils for sound reduction

Thomas Geyer\*, Ennes Sarradj\*, Christoph Fritzsche\*

Owls are commonly known for their quiet flight. Fundamental studies by Graham<sup>1</sup>, Kroeger<sup>2</sup> and Neuhaus<sup>3</sup> found three basic mechanisms to be responsible for this quiet flight: The leading edge comb, the trailing edge fringe and the downy upper surface of the feathers. The presented research focusses on the third mechanism and its transfer to technical applications: The noise reduction achieved by porous airfoils in an airflow compared to nonporous airfoils.

To gain quantitatively differentiable properties of the plumage of different species and to assign them to material parameters, measurements were conducted on the feathers and wings of silent flying birds to determine the air permeability. This was done by measuring the air flow resistance which quantifies the air permeability of homogeneous media. The results were compared to other birds. Specimen of barn owl and tawny owl were representatives for the silent flying birds while specimen of pigeon and buzzard represented the not silent flying birds. The results show that the resistance of the feathers of pigeon and buzzard is indeed remarkably higher than that of the owls.

The effect of sound reduction that is based, among others, on the air permeability of the wings inspires the use in technical applications. Therefore, experimental studies on Low-Re-airfoils, made of different porous materials and one nonporous material, were performed in the aeroacoustic open jet wind tunnel of the BTU Cottbus<sup>4</sup>. The sound emission that occurs when the airfoils are exposed to an air flow was measured by the use of a 32-channel microphone array. The aerodynamic parameters were measured simultaneously. The different porous materials are acoustically characterized by their porosity  $\sigma$ , their airflow resistivity  $\Xi$  and their tortuosity  $\tau$ . The airflow resistivity is assumed to be the material parameter that has the biggest effect on the noise generation of the airfoils. Hence, in a first step the studies concentrated on the airflow resistivity of the porous material. Results are presented that show the influence of the airflow resistivity on the noise emission at the trailing edge of different airfoils. All the airfoils have the same size and shape but are made of different open porous materials with varying airflow resistances  $\Xi$  and one nonporous material. It turns out that to some extent the use of porous materials for technical airfoils enables a noise reduction, while the aerodynamic performance is influenced, too.

The physical process of the noise reduction with regard to the properties of the porous materials is examined. Finally, a first approach for a model describing the dependence of the sound emission on the parameters of the open porous materials is proposed.

\*Juniorprofessur Aeroakustik, Brandenburgische Technische Universität Cottbus.

<sup>1</sup>R. Graham, *Journal of the Royal Aeronautical Society* **286**, 837 (1934).

<sup>2</sup>R.A. Kroeger et al.: Low speed aerodynamics for ultra-quiet flight, *Air Force Flight Dynamics Laboratory Technical Report*, (1971).

<sup>3</sup>W. Neuhaus et al., *Biologisches Zentralblatt*, **92**, 495 (1973).

<sup>4</sup>E. Sarradj, T. Geyer, *Proceedings of the 13th AIAA/CEAS Aeroacoustics Conference*, (2007).



### Critical behaviour in granular segregation

Katharine J. Giannasi\*

Spontaneous segregation is ubiquitous in mixtures of granular materials. It has previously been shown that the segregation of a horizontally vibrated binary monolayer occurs above a critical packing fraction. The system exhibits behaviour which can be interpreted as *gaseous*, *liquid* or *solid* with increasing packing fraction,  $C$ , where  $C$  is the non-dimensionalised measure of the tray surface area containing granular material. In previous work a critical value of  $C$  was identified and this was established to be  $C_c = 0.647 \pm 0.049$ . The critical point occurs between the gaseous and liquid states and closely resembles a continuous phase transition.

The final states of our experimental runs are achieved from an initial condition of a homogeneous dispersion of the binary material, as shown in the top left hand photograph of the figure below. A low packing fraction produces the gaseous state as shown in the top right of the figure. Increasing packing fraction through the transition produces firstly a liquid state and then a solid state, as depicted in the lower left and right hand sides of the figure respectively.

Here we present experimental results showing the dependence of critical packing fraction when we now vary quantities of *both* particle types. Furthermore, we demonstrate the effects of particle shape on the segregation, with specific interest on the effects of anisotropy.



Figure 1: Depicted in the top left hand photograph are initial conditions from which we achieve our final states. Shown to the top right is a gaseous state. To the lower left and right are shown the liquid and solid states respectively.

\*Manchester centre for nonlinear dynamics, University of Manchester, Oxford Road, Manchester, M13 9PL, UK.

## More on the low frequency mode of a rotating cylinder

Flavio Giannetti\*, Jan Pralits\*, Paolo Luchini\*

Flows behind bluff bodies, may sustain synchronised periodic oscillations in a suitable parameter range. Under these conditions the whole flow field behaves like a global oscillator ("global mode"). In the context of a fully twodimensional linear stability analysis, a novel technique apt to study the characteristics of the global mode was introduced by<sup>1</sup>, who determined the location of the "wavemaker" for the flow past a cylinder using the properties of the adjoint equations. Recently this approach was extended by<sup>2</sup> to study the nonlinear, finite-amplitude vortex shedding and to assess how unsteadiness and saturation modify the numerical results obtained in a linear context.

In this contribution we apply this approach to study the case of the flow around a rotating cylinder. Previous work by<sup>3</sup> has shown that besides the classic vortex street, a second shedding mode exists at higher rotation rates. This new mode is characterized by a much lower frequency. This was further investigated in the work by<sup>4</sup> who computed the critical rotation rates for the first and second shedding modes at  $60 \leq Re \leq 200$ . According to<sup>3</sup> the second shedding mode is caused by a strong concentration of vorticity in a region of recirculating flow located in the vicinity of the stagnation point.

This was confirmed by<sup>5</sup> who applied the approach developed by<sup>1</sup> to study the flow around a rotating cylinder. There it was shown that the maximal sensitivity of the first unstable mode is located in the downstream wake of the cylinder, across the recirculation bubble as in the case of the non-rotating cylinder. For the second shedding mode, however, it was found to be located near the cylinder surface in the vicinity of the stagnation point.

Here we will show how these results are modified by nonlinear effects. The technique developed by<sup>2</sup> has been applied to the finite amplitude vortex shedding behind a rotating cylinder. The characteristics of the direct and adjoint modes have been analysed for different shedding regimes. The regions of the flow more sensitive to localized feedback from velocity to force will be shown and implications for flow control highlighted. The location of the nonlinear wavemaker will be presented for different Reynolds number and rotation rates. Finally, the sensitivity of the shedding frequency with respect to variations of the mean flow will be discussed.

---

\*DIMEC, Università di Salerno, Italy.

<sup>1</sup>Giannetti & Luchini, *J. Fluid Mech.* **581**, 167 (2007).

<sup>2</sup>Luchini et al., *Proc. IUTAM Symposium on unsteady separated flows and their control*, 18-22 June, Corfu, Greece (2007).

<sup>3</sup>Mittal & Kumar, *J. Fluid Mech.* **476**, 303 (2003).

<sup>4</sup>Stojković et al., *Phys. Fluids* **15**:5, 1257 (2003).

<sup>5</sup>Brandt et al., *Presentation at APS DFD 2007, Salt Lake City*.

## An energy approach for triple flame.

Léo Glangetas\*

We are interested in the study of triple flame propagation in a strained mixing layer formed between a fuel stream and an oxidizer stream. This flame is composed of a curved flame front followed by a one-dimensional diffusion flame. We consider the thermo-diffusive model within the framework of a constant-density and a single irreversible reaction. Lewis numbers are taken to be unity and the flame is symmetric. The speed of propagation of triple flame has been demonstrated by Dold, Hartley and Green<sup>1</sup> to be positive or negative under some assumptions. The effect of unequal diffusivities has been studied by Daou and Liñan<sup>2</sup>. From the work of Ghosal and Vervish<sup>3</sup>, for high activation energy and using some parabolic approximation, there are analytical formulas for the speed.

We introduce a Lyapunov energy  $\mathcal{E}$  for which the stable one-dimensional diffusion flame is a ground state and the unstable one is a saddle point and we derive an expression for the velocity  $U$  of the travelling wave for the corresponding triple flame:

$$U \times (\text{positive term}) = -\mathcal{E}.$$

Therefore the sign of the velocity depends only of the diffusion-flame part of the triple flame. The energy is negative for high Damkhöler number, is null when the Damkhöler number is equal to a critical value  $\lambda_0$  and positive below.

For high activation energy, we derive from asymptotic analysis an implicit formula for the speed:

$$\frac{U}{U_d} \times K\left(\frac{U}{U_d}\right) \approx \frac{\lambda}{\lambda_0} - 1$$

where  $\lambda$  is the Damkhöler number,  $U_d = \sqrt{D_T a}$ ,  $D_T$  is the diffusion coefficient of the heat,  $a$  is the strain rate and  $K$  is a positive function which depends only on the geometry of the vector field of the counterflow streams.

Parts of this work were done in collaboration with Luc Vervisch and Gregory Sagon.

---

\*Laboratoire de Mathématiques Raphaël Salem, University of Rouen, France

<sup>1</sup>Dold et al., *IMA Vol. Math. Appl.* **35**, 83 (1991).

<sup>2</sup>Daou et al., *Comb. Theory and Modelling* **2**, 449 (1998).

<sup>3</sup>Ghosal et al., *J. Fluid Mech.* **415**, 227 (2000).

## Noise generation in an unstable boundary-layer flow over a flexible wall

M.-L. Gobert<sup>\*,†</sup>, U. Ehrenstein<sup>‡</sup>, J. A. Astolfi<sup>\*</sup> and P. Bot<sup>\*</sup>

The prediction of the self-noise received by a sonar antenna, due to pressure fluctuations in the boundary-layer flow along the dome wall, is based on models, which in general take only partially into account its flexibility. The present work readdresses the problem of hydrodynamic noise, considering the geometrically simplified model of a two-dimensional unstable boundary-layer along an elastic plate with clamped ends.

Plate vibrations interact with convective instabilities generated by an upstream oscillatory forcing at unstable frequencies. A time-dependent coordinate transformation is performed to solve the incompressible Navier-Stokes equations in a cartesian domain, using a mixed finite differences - Chebyshev collocation discretization. A fractional step method enables the full coupling of the elastic plate model with the fluid system. Simulations over plates of various materials are carried out. The influence of the wall flexibility on the coupled system is analysed with regard to resonance, added mass phenomena and effects on the convective flow instability.

Radiated sound is then evaluated from wall pressure and boundary-layer velocity fluctuations in the framework of the Lighthill's analogy: acoustic pressure fluctuations beyond the boundary layer ( $y \geq 0$ ) are computed from the Lighthill tensor Fourier transform, using an appropriate cartesian Green function. Contributions of the plate vibrations to the radiated noise are highlighted, in particular at the plate's natural frequencies: large spatial structures due to the plate motions are superimposed on smaller ones linked to the convective instabilities, as shown in figure 1.

This work is supported by Thales Underwater System and DCNS.

<sup>\*</sup>IRENav, BP 600, 29240 Brest Armées.

<sup>†</sup>Thales Underwater Systems, 525 route des Dolines, BP 157, 06903 Sophia Antipolis.

<sup>‡</sup>IRPHE, 49 rue Joliot-Curie, BP 146, 13384 Marseille Cedex 13.

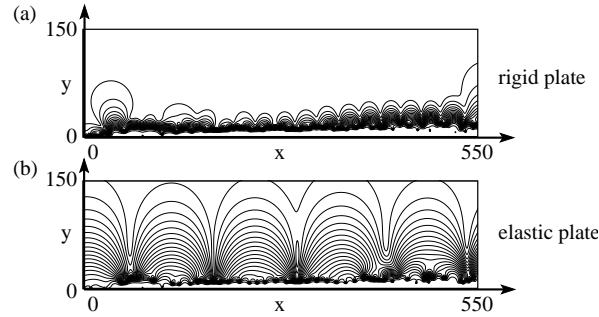


Figure 1: Isocontours of the pressure amplitude  $|\hat{p}(\omega_3, x, y)|$  in the acoustic far field at the third natural frequency  $\omega_3$  of the plate for the boundary layer along (a) the rigid wall, (b) the elastic plate.

## Anomalous statistics of rotating stably stratified turbulence

Alexandre Delache, Fabien S. Godeferd, Claude Cambon\*

Isotropic turbulence receives a continuous effort for an increasingly refined description, but complex effects modify the dynamics of turbulence, and are poorly understood. Instances of distorted turbulence by external body forces are present throughout natural and industrial flows, as in geophysical flows submitted to the Earth's rotation, and to density or temperature stratification. We focus here on the effects of stable stratification and solid body rotation on the dynamics and structure of homogeneous turbulence. We perform high resolution Direct Numerical Simulations (DNS), to characterize the 3D structure of anisotropic turbulence and its Lagrangian properties. Vertical structures appear in rotating turbulence, or a layering in stably stratified turbulence, depending on the rotation rate and the density gradient, parameters that are varied in our simulations.<sup>1</sup>

We first study the Lagrangian dispersion properties. In the DNS, particle trajectories are computed, yielding statistics of one-particle dispersion and two-particle separation in the horizontal and vertical directions. The standard Taylor laws are modified, and establishing their link with the anisotropic Eulerian structure of rotating stably stratified high Reynolds number turbulence is a fundamental question.

Different anomalous turbulent diffusion rates are observed. For instance, in the stratification dominated cases, one-particle diffusion reaches a plateau in the vertical direction, a consequence of the thin layering of the Eulerian velocity field.

Second, we study the structure of the flow by computing moments of the velocity and of the Lagrangian acceleration fields. Probability density functions (pdf) of the velocity components, and of the Lagrangian acceleration components, show an unexpected result: whereas the pdfs of the velocity components are anisotropic, the pdfs of the Lagrangian acceleration components do not exhibit any observable anisotropy (see figure). Whence this question: how is the Eulerian field anisotropy related to the Lagrangian one? This question and others pertaining to the occurrence of strong anisotropy in different statistics of rotating stably stratified turbulence will be addressed during the presentation at EFMC7.

\*LMFA UMR 5509, Université de Lyon, France

<sup>1</sup>Liechtenstein et al., *J. of Turb.*, **6**, 1 (2005)

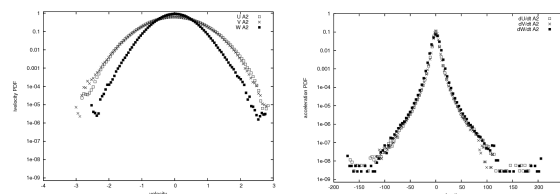


Figure 1: Pdf of: (left) velocity components, horizontal  $U$  and  $V$ , vertical  $W$ ; (right) normalized Lagrangian acceleration (case: strongly stratified turbulence, DNS  $1024^3$ ).

## Symmetry breaking of the vortex street produced by a flapping foil

R. Godoy-Diana, C. Marais, J.-L. Aider & J. E. Wesfreid \*

The symmetry breaking of the reverse Bénard-von Kármán (BvK) vortex street that has been observed in flapping-foil experiments <sup>1,2</sup> and numerical simulations <sup>3</sup> has been conjectured as a possible part of the manoeuvring techniques of animals using flapping-based propulsion. Analyzing PIV measurements from hydrodynamic tunnel experiments with a flapping foil, we have built a semi-empirical model based on the observation that the symmetry breaking of the reverse BvK vortex street is triggered by the production of dipolar structures that deviate the mean propulsive jet (see figure 1, left).

An estimate of the self-advection of such dipoles is given by  $v_{\text{dipole}} = \frac{\Gamma}{2\pi\xi}$  considering a dipole made of two point vortices of circulations  $\pm\Gamma$  separated by a distance  $\xi$ . A plot of  $v_{\text{dipole}}$  as a function of the Strouhal number  $St = fD/U$ , where  $f$  is the flapping frequency,  $D$  is the foil width and  $U$  is “cruise speed” (actually the upstream speed in the hydrodynamic tunnel), for three different flapping amplitudes  $A$  ( $A_D = A/D$ ) is shown in figure 1 (right). A semi-empirical model of the form  $v_T \propto \frac{\xi A_D}{T \cos \alpha}$ , where  $T$  is the flapping period and  $\alpha$  measures the orientation of the dipole with respect to the horizontal, allows to describe a threshold for the appearance of asymmetric wakes.

\*PMMH UMR7636 CNRS, ESPCI, Paris 6, Paris 7, Paris, France

<sup>1</sup>K. D. Jones, et al., *AIAA J.*, **36**(7), 1240 (1998).

<sup>2</sup>R. Godoy-Diana, et al., *Phys. Rev. E*, **77**(1), 016308 (2008).

<sup>3</sup>G. C. Lewin and H. Haj-Hariri, *J. Fluid Mech.*, **492**, 339 (2003).

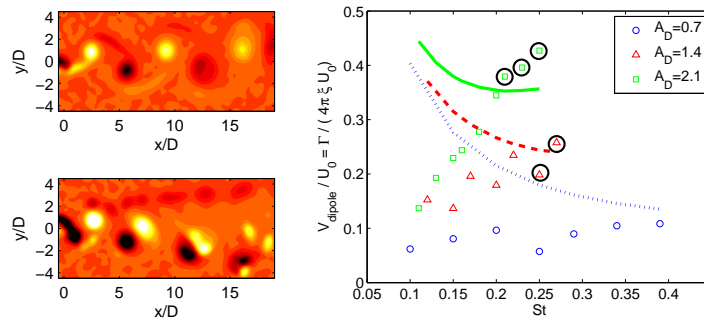


Figure 1: Left: vorticity fields in the wake of the flapping foil at  $Re = 255$ ,  $St = 0.15$  and  $A_D = 1.4$  (top) and  $2.1$  (bottom). Right: Estimate of the translation speed of the initial dipoles as a function of  $St$  and  $A_D$ . Circled points correspond to asymmetric wakes. The lines correspond to a semi-empirical model (dotted, dashed and solid lines correspond respectively to  $A_D = 0.7, 1.4$  and  $2.1$ ).

## Influence of density step on the local structure of a strain flow

M. Gonzalez\* and P. Paranthoën\*

The alteration of local flow structure induced by a density step is studied by addressing the problem in which an interface separating two regions with different constant densities is stabilised within a straining flow (figure 1). For this purpose, we consider the analytic solution for the flow field resulting from stabilisation of an infinitely thin flame by a stagnation-point flow<sup>1</sup>. The analytic solution for this two-dimensional incompressible flow field allows the exact derivation of the velocity gradient tensor and of parameters describing the local flow topology.

It is shown that the density step causes anisotropy of the pressure Hessian tensor which brings about rotation of the local strain principal axes. The Okubo-Weiss parameter does not feel this effect and indicates prevailing strain whatever the value of the density ratio. The ratio of effective rotation (vorticity plus strain axes rotation) to strain intensity rigorously defines a strain persistence parameter<sup>2</sup> which reveals a more subtle behaviour. In particular, it shows that for large values of the density ratio effective rotation prevails over strain in a restricted area past the interface.

Local alignment of a passive scalar gradient and relating stirring properties of the flow are derived from the strain persistence parameter. Even for moderate values of density ratio, the difference between the compressional direction and the equilibrium orientation of the scalar gradient resulting from the competing effects of strain and effective rotation is significant over most of the flow field beyond the interface. The growth rate of the gradient norm is thus noticeably lessened in this flow area (figure 2) which indicates weaker stirring properties than in the unaltered straining flow.

\*CNRS, UMR 6614/CORIA, University of Rouen.

<sup>1</sup>Y. D. Kim and M. Matalon, *Combust. Flame* **73**, 303 (1988).

<sup>2</sup>G. Lapeyre et al., *Phys. Fluids* **11**, 3729 (1999).

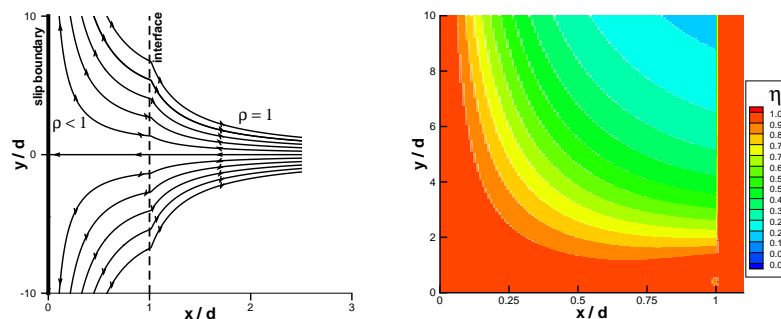


Figure 1: Strain flow with a density step; Figure 2: Local growth rate,  $\eta$ , of a passive scalar gradient; density ratio = 6.

## Satellite bubbles in the collapse of axisymmetric cavities and high speed Worthington jets

José Manuel Gordillo\*

When a bubble or gas-filled cavity breaks, the inward radial motion of the liquid near the minimum radius needs to be deflected, at some point, towards the axial direction. Recently, it has been visualized, among others by <sup>1</sup>, that in the high liquid Reynolds number regime satellite bubbles appear naturally in the breakup of axisymmetric gas-filled cavities as a consequence of the finiteness of gas inertia. Here, we propose a link between the formation of satellites and the ejection of the type of Worthington jets observed in the breakup of axisymmetric bubbles which can be considered, near the minimum radius, locally symmetric with respect to a plane perpendicular to the axis of symmetry. Our main conclusion is that the generation of satellite bubbles is promoted not only by gas density but also by liquid viscosity and, more importantly, by gas viscosity. The existence of satellites provides with finite liquid velocities at the length scale of satellite formation, and this imposes a scale for the axial velocity of the liquid jets that are usually observed as a consequence of a void collapse.

The theoretical analysis is performed assuming that the local shape of an axisymmetric bubble near the minimum radius is *slender*, possess mirror symmetry around the plane  $z = 0$  and can be locally described by  $f(z, t) = R_o(t) + r_1(t) z^2$ , with  $R_o$  and  $r_1$  the dimensionless minimum radius and axial curvature respectively.

We will show that, in the limit  $s \gg 1$ ,  $R_o r_1 \ll 1$  ( $s = -\ln R_o$ ), the local dynamics of the bubble is given by:

$$-\ln(R_o r_1) \frac{d \ln(R_o \dot{R}_o)}{ds} + 1 - \Lambda \frac{P}{(R_o r_1)} - 4/(R_o \dot{R}_o Re) - 2 R_o / [(R_o \dot{R}_o)^2 We] = 0, \quad (1)$$

$$\ln(R_o r_1) \frac{d \ln R_o r_1}{ds} - 1 + 1/2 \Lambda \frac{P}{(R_o r_1)} + 4/(R_o \dot{R}_o Re) + R_o / [(R_o \dot{R}_o)^2 We] = 0, \quad (2)$$

with  $Re$ ,  $We$  and  $\Lambda = \rho_g/\rho_l$ , the Reynolds, Weber and density ratio respectively;  $P$  is the dimensionless gas pressure at  $z = 0$ . Note that Eq. (1) represents a balance between the local liquid acceleration (first term on the left), the convective liquid acceleration (since Eq. (1) has been obtained by normalizing with  $1/2 \dot{R}_o^2$ , the second term from the left (+1) represents the convective acceleration), pressure difference between  $z = 0$  and the reference pressure ( $-\Lambda P/(R_o r_1)$ ), the normal viscous stress at the interface ( $4/(R_o \dot{R}_o Re)$ ) and the pressure drop associated to surface tension ( $-2 R_o / [(R_o \dot{R}_o)^2 We]$ ). Equation (1) is, therefore, a 2D Rayleigh-type equation but in which the factor  $\ln R_o r_1$  multiplying the local acceleration term needs to be calculated through the differential equation (2).

The scaling for the satellite size will be determined in the presentation by the condition that the gas pressure at  $z = 0$  becomes of the order of the liquid convective acceleration, finding good agreement with numerical simulations.

\*Área de Mecánica de Fluidos, Universidad de Sevilla, SPAIN.

<sup>1</sup>S.T. Thoroddsen et al, *Phys. Fluids* **19**, 042101 (2007).



## Vorticity dynamics in the vortex ring state of a descending rotor

R.B. Green\*, Ö. Savaş†, F.X. Caradonna ‡

The vortex ring state (VRS) is a potentially hazardous operating condition relevant to a helicopter rotor in descent. In the VRS the vortices that usually trail below the rotor disk to form a helical wake collapse into a ring-like structure around the plane of the disk, and the formation and subsequent breakdown of this ring-like vortex is accompanied by large, periodic thrust excursions. The fluid mechanics are fascinating but poorly understood, and this paper describes an extension of the experimental studies of <sup>1</sup> and <sup>2</sup> to investigate how the thrust excursions are coupled with the vorticity dynamics. The major difficulty with experimentation is the spatial extent and unsteadiness of the phenomenon. A series of tests on a model rotor in simulated descent were conducted in the towing tank at the University of California, Berkeley, USA, and time-resolved Particle Image Velocimetry (PIV) was used to measure the wake velocity field. Rotor thrust data were recorded simultaneously. Figure 1 shows the thrust and integrated vorticity for the flow over the leading and trailing edges of the rotor disk respectively. Thrust extrema coincide with accumulations of positive vorticity (trailed from the rotor tip) and negative vorticity (trailed from the rotor root). Furthermore the vorticity impulse theorem <sup>3</sup> may be used to help explain the role of the vorticity dynamics in the VRS. Presentations of experimental results will include movies of the time-changing vorticity field, where vortex filaments can be seen accumulating into vortex rings before breaking away from the rotor disk.

\*Department of Aerospace Engineering, University of Glasgow, UK.

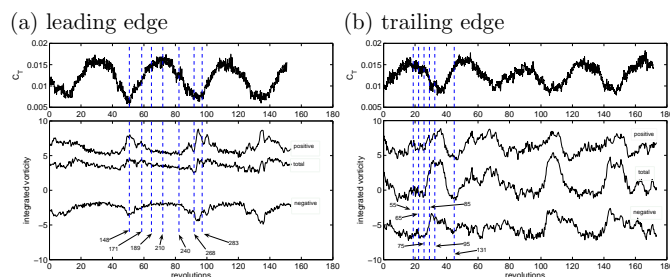
†Department of Mechanical Engineering, University of California at Berkeley, USA.

‡Army/ NASA Rotorcraft Division, Ames Research Center, California, USA

<sup>1</sup>Stack et al. *J. A.H.S* **50**, 279-288 (2005).

<sup>2</sup>Green et al. *J. Fluid Mech.* **534**, 237-261 (2005).

<sup>3</sup>J. Lighthill "An informal introduction to theoretical fluid mechanics" Clarendon Press, Oxford, 1986



## Oceanographic Coastal Currents Over Bottom Slopes

S. O. Gregorio\*, P. J. Thomas\*, M. A. Brend\*, I. H. Ellingsen<sup>†</sup> and P. F. Linden<sup>‡</sup>

Laboratory experiments simulating gravity-driven oceanographic coastal surface currents are described. Results from three complementing studies are discussed and compared to a new geostrophic model<sup>1</sup>. The first study was conducted in a small-scale (1m diameter) water-filled rotating tank. The other two studies were carried out at the large-scale Coriolis turntables at Grenoble<sup>2</sup> (13m tank diameter) and Trondheim<sup>3</sup> (5m tank diameter). The height, the width and the length of the currents are studied as a function of the relevant independent experimental parameters. The small-scale experiments and the Grenoble study focused on currents flowing along a vertical coastline in an effectively infinitely deep ocean. The Trondheim study generalized these results by investigating how the dynamics are affected when the currents flow along inclined coastlines with different bottom slopes. The data for vertical-wall and inclined-wall currents are compared to each other. Preliminary results obtained from computational simulations of the currents employing the SINMOD model<sup>4</sup> developed at SINTEF<sup>5</sup> are presented. A typical current as observed in a small-scale experiment is shown in Figure 1 and a simulated current is displayed in Figure 2. It can be seen that experiment and computation are already in good qualitative agreement.

\*Fluid Dynamics Research Centre, School of Engineering, University of Warwick, Coventry, UK.

<sup>†</sup>SINTEF Fisheries and Aquaculture, 7465 Trondheim, Norway.

<sup>‡</sup>Department of Mechanical and Aerospace Engineering, University of California, San Diego, La Jolla, CA 92093-0411, USA.

<sup>1</sup>Thomas and Linden, *J. Fluid Mech.* **578**, 35 (2007).

<sup>2</sup>Coriolis Facility, web site <http://www.coriolis-legi.org>

<sup>3</sup>Coriolis Laboratory, web site <http://www.ntnu.no/trondheim-marine-RI>

<sup>4</sup>Slagstad and McClimans, *J. Marine Syst.* **58**, 1 (2005).

<sup>5</sup>SINTEF Fisheries and Aquaculture Institute, website <http://www.sintef.dk/>

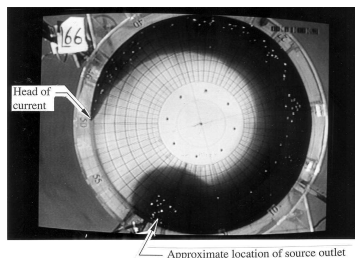


Figure 1: Visualization of typical current in an experiment (in circular tank).

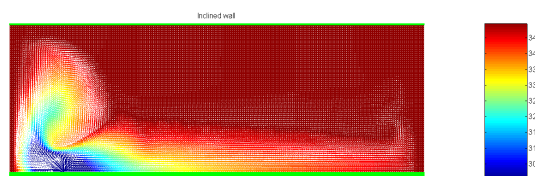


Figure 2: Computational simulation using SINMOD model (current flowing along straight wall).

### Multiphase-Electrospinning of colloidal nanofibers

F. Grossmann\*, A. Stoiljkovic<sup>†</sup>, T. Schneider\*, A. Greiner<sup>†</sup> and B. Eckhardt\*

Electrospinning of polymeric solutions allows to produce fibers with diameters on nanometer scales. For industrial applications multiphase electro-spinning, where either two liquids or colloidal suspensions are spun, have been studied. The final states reached during electrospinning of polystyrene colloids dispersed in an aqueous polyvinylalcohol solution show a remarkably rich structure of regular and irregular arrangements of the colloidal particles<sup>1</sup>. Depending on the concentration of particles, thin single-stranded chains, straight and twisted multiple stranded chains, as well as various irregular arrangements of particles can be observed. The numerical modelling of the process by gradient dynamics of colloids with short range attraction in an cylindrically contracting potential that models the evaporation of the solvent during electrospinning allows to reproduce structures, the magical concentrations where only a few regular arrangements are possible, as well as many of the disordered structures. The modelling reveals the significance of the evaporation for the formation of the chains. The theoretical results are in remarkable agreement with the experimental findings<sup>2</sup>.

\*Fachbereich Physik, Philipps-Universität Marburg, 35032 Marburg, Germany.

<sup>†</sup>Fachbereich Chemie, Philipps-Universität Marburg, 35032 Marburg, Germany.

<sup>1</sup>Aleksandar Stoiljkovic et al. *Polymer* **48**, 3974 (2007).

<sup>2</sup>Florian Grossmann et al. *in preparation*

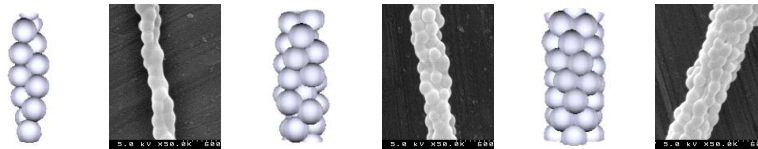


Figure 1: Comparison between theoretical and experimental findings.

## Particulate pipe flow

Élisabeth Guazzelli\*

Particulate multiphase flow involves the mechanics, flow, and transport properties of mixtures of fluid and solids. These mobile multiphase systems are encountered in a variety of industrial and natural situations. Examples include landslides and avalanches, sediment transport and dune formation, hydrate and sand issues in oil production, granular flow in food or pharmaceutical industries. The physical understanding of these flows offers problems of far greater complexity than found in single-phase flows. This leads to many new and intriguing flow phenomena absent in the single phase flows.

This talk will be concerned with the flow of solid particles in a pipe going from viscous to turbulent regimes. The first part of the talk will focus on neutrally buoyant particles. It will review some results on (i) collective migration of particles at low Reynolds number and (ii) lateral inertial migration of single particles as a function of the Reynolds number, and (iii) it will show that particles can modify the transition to turbulence that occurs in a single-phase flow. The second part of the talk will examine a bed constituted of sediment particles submitted to a pipe flow. It will discuss (i) critical condition for incipient motion of the grains, (ii) bed-load transport, and (iii) it will show that the evolution of the particle bed exhibits different dune patterns as the flow is increased from laminar to turbulent regimes.

Our work on these various problems has been done in collaborations with P. Aussillous, J. Chauchat, V. Glezer, J.-P. Matas, M. Medale, J. F. Morris, M. Ouriemi, Y. Peysson.

---

\*IUSTI CNRS Aix-Marseille Université.

## CFD study of biologically inspired flapping/oscillating foils in forward motion

Joel Guerrero<sup>a</sup>

Nature relies on reciprocating motions for locomotion and propulsion on land, in the air and the sea; legs for walking, flapping wings for flying and oscillating fins for swimming. These refined and optimized forms and motions used by nature, may serve engineers and scientists as an inspiration model, with the hope of finding a way to provide better and greater propulsive efficiencies and manoeuvrability than propellers and rotors at low Reynolds numbers in human built vehicles, such as; MAVs (micro aerial vehicles) and AUVs (autonomous underwater vehicles). The fluid dynamics of many swimming and flying animals involves the generation and shedding of vortices into the wake. In the present paper, we use an overlapping grids based incompressible flow solver to numerically study the unsteady dynamics of these vortices shed by two-dimensional flapping/oscillating foils that models an animal wing, fin or tail in forward motion. The study is done for several shapes and harmonic and non-harmonic kinematics, at a corresponding Reynolds number of the order of 1000 (such values are relevant for typical swimming and flying animals). Some numerical aspects of the overlapping grids method and preliminary three-dimensional results are also presented.

---

<sup>a</sup> Dipartimento di Ingegneria delle Costruzioni, dell'Ambiente e del Territorio (DICAT), University of Genova.

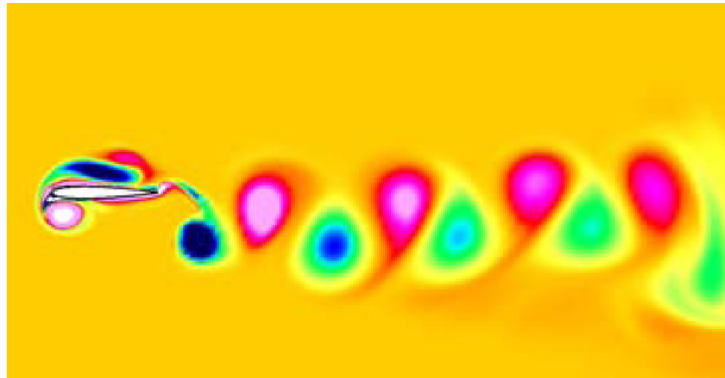


Figure 1: Vortex Street generated by a heaving airfoil.

## Micro-vascular networks pressure distribution in the brain

Romain Guibert<sup>\*†</sup>, Franck Plouraboué<sup>\*</sup> and Caroline Fonta<sup>†</sup>

The blood supply of the brain and its regulation by vessels of small sizes are important fundamental biological and clinical issues<sup>1</sup>. Resulting flows are highly dependent on the heterogeneous networks architecture and variations in blood composition. In such heterogeneous networks, it is known that penetrating arterioles which perfuse the grey matter are the main pillars of a hierarchical network which branches itself into a “mesh like” capillary network<sup>2</sup>. Recent experimental observations have shown that these penetrating arterioles are the bottleneck<sup>3</sup> in the neocortex perfusion. Strokes spatial extension is directly related to the hemodynamics region of influence of those penetrating arterioles. It is also known that these arterioles play a major role in normal tissues for the adaptation of hemodynamics response to the metabolism needs of neural activity. Nevertheless, very few quantitative estimation of pressure distribution in micro-vascular cortical networks have been previously proposed.

The purpose of this contribution is to provide a quantitative evaluation of blood pressure distribution through large micro-vascular cortical networks in healthy tissues.

Networks are obtained using an original experimental setup. Tissues samples are injected with a contrast agent and imaged using 3D synchrotron high-resolution computed micro-tomography<sup>4</sup>. It permits to obtain ten millimeter cube scans over the entire depth of cortical gray matter with micron resolution. Images processing follows classical steps for binerisation and skeletonization<sup>5</sup>. Discontinuities related to injection defaults are filled using a tensor voting method<sup>6</sup>.

Since the aspect ratio (radius over length) of vascular segments is in average close to 1/20, the lubrication approximation offers an interesting framework for the fluid description. The specific behavior of red blood cells in vessels whose diameter is close to their size leads to diameter dependent apparent blood viscosity which have been well documented in previous *in vitro* and *in vivo* studies<sup>1</sup>. Such models can be used for a local flux/pressure drop description of the flow integrated along each vessel segment. The resulting fluid description only involves solving the pressure at each network nodes on the entire three dimensional connected networks. The fluid incompressibility leads to flux conservation at any node of the network (Kirchhoff's law). The boundary condition on the pressure are imposed on arteries and veins (top and bottom faces of the volume). Periodic pressure boundary conditions are used on lateral faces. Solving this large sparse linear problem, using optimized libraries, provides the pressure distribution for a fixed network geometry. Some illustrative examples will be presented.

<sup>\*</sup>Institut de Mécanique des Fluides, UMR 5502, University of Toulouse, France.

<sup>†</sup>Centre de Recherche Cerveau et Cognition, UMR 5549, University of Toulouse, France.

<sup>1</sup>Popel et al., *Annu. Rev. Fluid Mech.* **37**, 43 (2005).

<sup>2</sup>H.M. Duvernoy, *Eds. Springer-Verlag*, (1995).

<sup>3</sup>Nishimura et al, *Proc. Natl. Acad. Sci. U.S.A.*, **104**, 365 (2007).

<sup>4</sup>Plouraboué et al., *J. Microsc.* **215**, 139 (2004).

<sup>5</sup>Risser et al., *J. Cerebr. Blood F. Met.* **27**, 293 (2006).

<sup>6</sup>Risser et al., *IEEE T. Med. Imaging*, In press.

## Dynamics of Band Drift in Particle-Laden Rimming Flow

E. Guyez<sup>a</sup> and P.J. Thomas<sup>a</sup>

In Refs. [1,2] we described a new pattern formation process associated with the flow inside a horizontal rotating cylinder that is partially filled with a particle-laden fluid. The pattern is observed to form as the particles segregate and agglomerate to form circumferential bands with high particle concentrations. Any two neighbouring granule bands are separated from one another by regions of liquid with low particle concentrations or, in some cases, regions entirely free of particles. A typical such pattern is shown in Fig. 1. Our most recent experiments [3] have revealed that the system can display an extremely rich, often highly symmetric, spatiotemporal behaviour that emerges over days or weeks as the patterns drift very slowly along the axis of rotation. A typical spatiotemporal plot is shown in Fig. 2. The plot was assembled by extracting pixel lines (see Fig. 1) from successive photos and composing these into a single figure. In Fig. 2 the presence of a band is identified in black whereas regions of low granule concentrations are represented in white. It can be seen that the bands drift from locations  $L > 0$  towards the cylinder end walls at  $L = 0$  cm and  $L = 27$  cm. For other experimental conditions bands can drift from the end walls towards the cylinder centre, they may display entirely irregular drift characteristics, or they may not drift at all. We discuss long-term observations of the system and focus on effects induced by a density difference between the particles and the ambient liquid. The key non-dimensional parameters governing the system are identified. It is found that a suitably defined Stokes number enables characterizing parameter regimes with drifting and stationary bands.

<sup>a</sup> Fluid Dynamics Research Centre, School of Engineering, University of Warwick, Coventry, UK.

<sup>1</sup> O.A.M. Boote and P.J. Thomas, *Phys Fluids*, **11**, 2020 (1999)

<sup>2</sup> P.J. Thomas *et al.*, *Phys. Fluids* **13**, 2720 (2001)

<sup>3</sup> E. Guyez and P.J. Thomas, *Phys. Rev. Lett.* **13**, publication scheduled for 22 Feb. 2008.

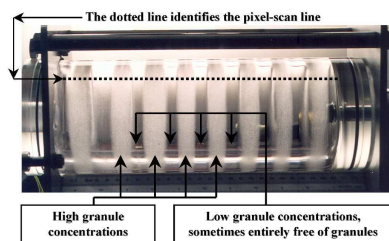


Fig. 1: Segregation banding pattern in horizontal circular cylinder viewed head-on.

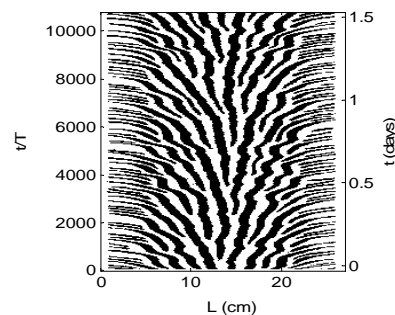


Fig. 2: Typical Spatiotemporal plot illustrating the drift of the granule bands.

### Solitary 3-D waves on free falling liquid films

V.V. Guzanov<sup>a</sup>, S.V. Alekseenko<sup>a,b</sup>, S.M. Kharlamov<sup>a</sup>  
and D.M. Markovich<sup>a,b</sup>

3-D wavy regimes are the last stage of wave evolution for falling liquid films at low and moderate Reynolds numbers  $Re$  of film flow. In case of such regimes the film surface is covered by numerous nonlinear horseshoe-shaped waves which interact with each other in a random fashion.

The most recent essential achievement in the theoretical investigation of 3-D waves after discovery of stationary solution of KS (Kuramoto-Sivashinsky) equation (valid for  $Re \sim 0$ ) in the form of traveling horseshoe-shaped wave<sup>1</sup> is the numerical construction of stationary 3-D waves for moderate  $Re$  on the base of Kapitsa-Shkadov model<sup>2</sup>. Also, experimental proof of the existence of stationary 3-D waves at small  $Re$  has recently been obtained<sup>3</sup>.

In this work we present the results of a systematic experimental study of 3-D waves evolution on vertically falling liquid films at low and moderate  $Re < 25$ . Laser induced fluorescence method<sup>2</sup> was used to register wave patterns. Stationary 3-D waves were registered for a wide range of  $Re$ . Whereas the amplitude and velocity of the registered stationary waves are close to the theoretically predicted values for low  $Re$ , with the grows of  $Re$  systematic divergence between theory and experiment has been observed. Additional set of experiments was made to investigate the interaction of 3-D waves with regular 2-D waves. Stability of 3-D waves at least to the high frequency regular 2-D waves has been shown experimentally.

<sup>a</sup> Institute of Thermophysics, Russian Academy of Sciences, Siberian Branch

<sup>b</sup> Novosibirsk State University, Novosibirsk

<sup>1</sup> V. I. Petviashvili and O. Yu. Tsvetodub, *Dokl. Acad. Nauk. SSSR* **238**, 1321 (1978).

<sup>2</sup> Demekhin et al., *Phys. of Fluids*, **19**, 114104 (2007).

<sup>3</sup> Alekseenko et al., *Phys. of Fluids*, **17**, 121704 (2005).

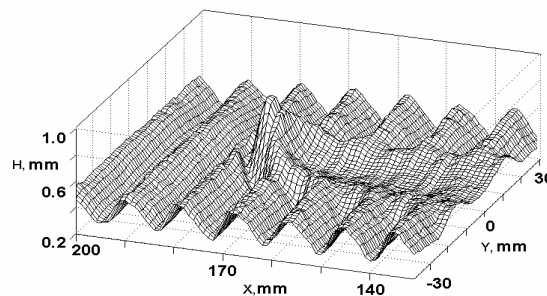


Figure 1: The shape of 3-D wave interacting with high frequency 2-D wave. X – downstream distance from the point of 3-D wave excitation.



## Pulsating spray-flame interacting with acoustics

Pierre HALDENWANG, Colette NICOLI <sup>\*†</sup>

Two-phase combustion is known to be sensitive to its coupling with acoustics, by way of proof the noise and instabilities observed in engines with liquid injection. The precise understanding of this phenomenon is still an open problem. Various mechanisms, as droplets inertia, latent heat of vaporisation, chemical kinetic modifications, have been put forward to explain how combustion heat release and acoustic field can cooperate positively. Our numerical/theoretical recent works <sup>1 2 3</sup> have shown that spray-flames can propagate with an oscillatory mode. Experiments recently conducted in micro-gravity <sup>4</sup> have also noted a pulsating propagation of two-phase flames. These natural oscillations should trigger acoustic waves <sup>5</sup>. We have investigated the dynamics of spray-flames using the simplest model of two-phase combustion; it shows that oscillatory propagation results from an intrinsically two-phase mechanism (independent of latent heat; it occurs with unity Lewis number). It predicts that pulsating flame exists in (heavy) alkane spray, as soon as the liquid loading is sufficiently large. We presently investigate spray-flame propagation in the presence of a small amplitude acoustic wave. It is found that the Rayleigh criterion (for thermo-acoustic instabilities) is satisfied for realistic parameters: intrinsic oscillations can convert some combustion energy into acoustic energy. In the figure, we observe that the heat power converted into acoustic energy is very sensitive to Zeldovich number. In other words, energy transfer strongly depends on the frequency fit between acoustic resonator and natural oscillations (the latter being governed by Zeldovich number). Further investigations show that the mechanism of energy transfer is of resonant type.

<sup>\*</sup>M2P2 (Modélisation en Mécanique et Procédés Propres), UMR CNRS 6181;

<sup>†</sup>38, Rue Joliot-Curie; F-13451 Marseille; haldenw@L3M.univ-mrs.fr, nicoli@L3M.univ-mrs.fr

<sup>1</sup>S. Suard, P. Haldenwang, C. Nicoli, *C.R. Acad. Sc. Mecanique (Paris)* **332**, pp. 387-396 (2004).

<sup>2</sup>C. Nicoli, P. Haldenwang, S. Suard, *Combust. and Flame* **143**, 299-312 (2005).

<sup>3</sup>C. Nicoli, P. Haldenwang, S. Suard, *Combust. and Flame* **149**, 295-313 (2007).

<sup>4</sup>H. Hanai, K. Maruta, H. Kobayashi, T. Niioka, *Proc. Combust. Inst.* **27**, 2675-2681 (1998).

<sup>5</sup>F. Atzler et al., *Comb. Sc. Techn.* **178**, 2177-2198 (2006).

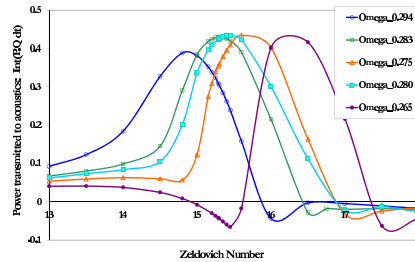


Figure 1: Growthrate of acoustic energy w.r.t. Zeldovich number, for a maximal liquid loading and various acoustic normalized frequencies ( $\omega$ ).

## On the instability of vortices embedded in shear flows

Philip Hall

Institute for Mathematical Sciences  
Imperial College of Science, Technology & Medicine  
London SW7 2BZ, UK

.....

February 13, 2008

Streamwise vortices in shear flows can be generated by a variety of instability mechanisms. For example centrifugal instabilities generate Taylor or Gortler vortices whilst convection produces similar structures in heated shear flows; Inviscid perturbation to a shear flow  $U(y, \lambda z)$  satisfy

$$P_{yy} + P_{zz} - \alpha^2 P - \frac{2U_y P_y}{U - c} - \frac{2U_z P_z}{U - c} = 0.$$

Here  $\alpha$  and  $c$  are the wavenumber and wavespeed of the inviscid wave superimposed on the vortex shear flow and  $\lambda$  represents a typical wavenumber of the vortex. The one-dimensional form of this equation is the 'pressure' form of the well-known Rayleigh equation for which the presence of inflection points is known to play a key role. For the two-dimensional case there are no related results concerning the necessary and sufficient conditions on the velocity field to produce instability.

We discuss flows where the above pde is relevant and investigate the nature of the different modes of instability by investigating the solution of the 2D eigenvalue problem associated with the above equation and the boundary conditions relevant to the particular flow under consideration. We show that the two types of modes associated with this instability (varicose and sinuous) correspond to situations when the spanwise variation of the flow is relatively slow or fast respectively and we derive asymptotic solutions of the above pde in those situations. We give asymptotic and numerical solutions of the pde for the most interesting physical situations and draw some conclusions for more general flows.

## Flow structure in an inclined and confined gravity current

Y. Hallez & J. Magnaudet\*

We investigate numerically the spreading of a gravity current confined in an inclined tube or channel with no-slip walls. A detailed analysis of the flow structure reveals the development of spanwise rolls issued from a Kelvin-Helmholtz-type instability, followed by that of pairs of streamwise counter-rotating vortices stretched and bent by the former rolls and the walls (figure 1(a)). We observe that these vortices have a strong influence on the transverse mixing between the two counterflowing currents. In order to clarify whether the streamwise vortices are generated by the interaction of the currents with the lateral walls or by a more generic three-dimensional flow instability, we also carry out simulations in a wider channel with periodic spanwise boundary conditions. As shown in figure 1(b), these additional computations indicate that the corresponding flow structure is close to that of a planar mixing layer involving no lateral wall effects (<sup>1</sup>). From this combination of computations, we conclude that the streamwise vortices seen in confined inclined gravity currents mostly result from a generic secondary three-dimensional Kelvin-Helmholtz instability, even though their spatial characteristics may be altered by the presence of the lateral walls. Interestingly, the typical lobe-and-cleft pattern is also recovered in the unconfined simulation and is found to be the first type of three-dimensional eddies that grows inside the flow domain, in line with a stability analysis performed in the head of a horizontal gravity current<sup>2</sup>.

\*Institut de Mécanique des Fluides de Toulouse, UMR CNRS/INPT/UPS 5502, Toulouse, France

<sup>1</sup>Bernal & Roshko, *J. Fluid Mech.* **170**, 499 (1986)

<sup>2</sup>Härtel et al., *J. Fluid Mech.* **418**, 189 (2000)

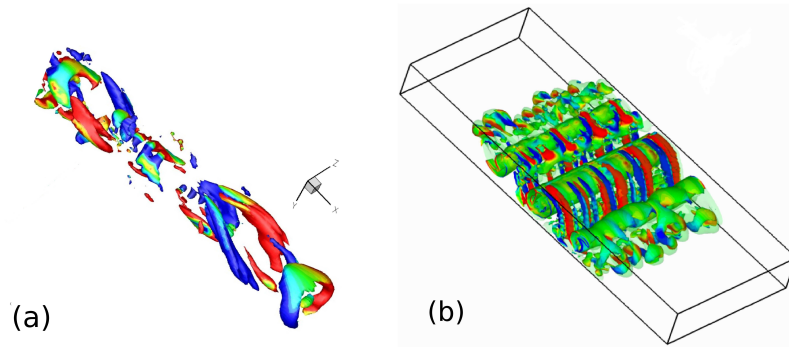


Figure 1: (a): Gravity current in a cylindrical tube inclined at 30° from vertical; (b): Gravity current in a (4:1) channel tilted at 40° from vertical. The surface shown in the figures is an iso-surface of the swirling strength colored by the streamwise vorticity. The Atwood and Reynolds numbers are 0.004 and 660 in both cases.

## Absence of small-scale fluctuations of high-Prandtl number buoyant scalars in stratified turbulence

Hideshi Hanazaki\* and Takehiro Miyao\*

It is well known that the fluctuations of scalars with small molecular diffusivities (Prandtl number  $Pr > 1$ ) can survive at length scales  $l$  smaller than the Kolmogorov scale  $l_K$  ( $l_B < l < l_K$ ), where the smallest scale  $l_B$  ( $= l_K/Pr^{1/2}$ ) is the Batchelor scale. This has been predicted in the theory intended for a passive scalar<sup>1</sup>, although the title of the paper contains the word *temperature*. Then, it has often been implicitly assumed that the similar results would be applied to every high-Prandtl number scalar. In this study, however, we demonstrate that the prediction would not be applied to buoyant/active scalars such as heat and salt, whose distribution affects the fluid motion. Results of direct numerical simulations for stratified turbulence with high- $Pr$  ( $Pr = 6$ ) buoyant scalar show that the fluctuations of high- $Pr$  scalar disappear nearly at the Kolmogorov scale. The vanishing of small-scale scalar fluctuations has been observed also in double-diffusive system where two active scalars constitute density stratification, since the phenomenon has its origin in the exchange between kinetic energy and potential energy. This implies that the fluctuations of heat ( $Pr = 6$ ) and salt ( $Pr = 600$ ) in the ocean might disappear at much larger scales than have been expected.

For example, when the active/stratifying scalar has a large Prandtl number of  $Pr = 6$  and the coexisting passive scalar has a low Prandtl number ( $Pr = 1$ ), high- $Pr$  active scalar has the dissipation scale similar to the low- $Pr$  passive scalar (Figure 1). This is very different from the theoretical prediction, but would occur since the active scalar exchanges its potential energy with the kinetic energy, and the length scale of the active scalar would be determined by the length scale of velocity.

---

\*Department of Mechanical Engineering and Science, Kyoto University, Japan

<sup>1</sup>G. K. Batchelor, *J. Fluid Mech.* **5**, 113 (1959).

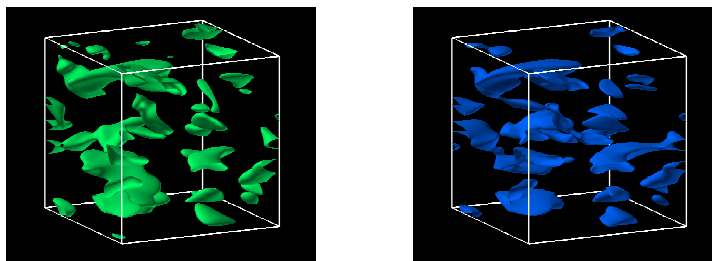


Figure 1: Contour surfaces of the dissipation rates of a high- $Pr$  active scalar ( $Pr = 6$ ) (left) and a low- $Pr$  passive scalar ( $Pr = 1$ ) (right) at large time ( $Nt/2\pi = 6$ ,  $N$ : Brunt-Vaisala frequency).

## A Novel Mathematical Model for Turbulent Fluid Flow

David Harris\*

A similarity between attempts to obtain, using classical continuum mechanics, mathematical models for (on the one hand) the deformation and flow of granular materials and (on the other hand) of turbulent fluid flows is that both problems have been successfully resistant to simple and elegant solutions. The problem appears to be related, in both cases, to the rotational part of the flow.

In the case of granular materials the author has found it helpful to extend the notion of a continuum to one that may be described as a reduced Cosserat continuum in which the concepts of micro-inertia and intrinsic spin are present but in which the usual ingredient of Cosserat theory, namely couple-stress, is absent. In a reduced Cosserat continuum the equation of rotational motion is an expression for the evolution and spatial variation of the anti-symmetric tensor (or its associated vector) of intrinsic spin and consequently the Cauchy stress tensor is not necessarily symmetric. The frame indifferent kinematic tensor appropriate for use in constitutive equations turns out to be the difference between the velocity gradient tensor and the intrinsic spin tensor and it is this non-symmetric kinematic tensor which the constitutive equation relates to the Cauchy stress. Within this framework the author has been able to propose realistic equations for the flow of granular materials which are well-posed, whereas classical continuum models have either physically unrealistic properties or are ill-posed.

We tentatively explore the possibility of whether or not a reduced Cosserat continuum could be an appropriate framework from which to propose simple mathematical models for turbulent flows. The natural extension of a Newtonian fluid has three viscosity parameters (the usual bulk and shear viscosities together with what may be called the rotational or eddy viscosity). A crucial difference between the translational and rotational momentum equations is that whereas the former contains the divergence of the stress, the latter contains the stress directly. As a consequence, the analogue of the Navier-Stokes equations contains only the gradient of the intrinsic spin (i.e. the first order spatial derivatives but not the second), while the balance of rotational momentum again contains first order partial derivatives (but not second order) and includes the vorticity. Thus, the physical properties of the intrinsic spin included in the model are a local acceleration and convection but the intrinsic spin does not itself diffuse, although the velocity field which may be generated by the intrinsic spin is diffusive. The resulting field equations for an incompressible such fluid are a coupled set of non-linear partial differential equations for the velocity, intrinsic spin and pressure in which the convection terms are the only non-linearity.

In this talk we investigate the possibility that the formation of eddies may be triggered by the intrinsic spin and that it may be possible to model the transition from laminar to turbulent flow in this way.

---

\*School of Mathematics, University of Manchester.

## Symmetry-breaking in two-dimensional, diverging-channel flow

Andrew Hazel\*, Philip Haines\* and Richard Hewitt\*

We present finite-element calculations for the flow of an incompressible Newtonian fluid in a (finite) two-dimensional diverging channel and compare the results to the Jeffrey–Hamel similarity solution, in which the velocity field has the assumed form  $\hat{\mathbf{u}} = \frac{\hat{f}(\theta)}{r} \mathbf{e}_r$  in plane polar coordinates  $(r, \theta)$ . Results will be presented for a number of wall-separation angles  $2\alpha$ , Reynolds numbers  $Re$  and ratios of inlet/outlet radii,  $\Gamma$ . In particular, we solve the two-dimensional eigenvalue problem and apply continuation methods to find a set of nested neutral curves in the  $Re - \alpha$  plane that correspond to symmetry breaking (about the mid plane of the channel), see figure 1 for typical results.

The precise behaviour of the system is found to depend on the choice of inlet boundary condition, but the first bifurcation is always found at parameter values close to those predicted by the similarity solution. In general, however, the bifurcation has a different criticality (supercritical rather than subcritical). We discuss this somewhat surprising result, but also demonstrate that there is a (rather specialised) class of inlet conditions for which subcritical behaviour can be achieved and for which it is possible to replicate the similarity solution bifurcation structure exactly. The temporal dynamics of the finite-domain problem will also be discussed with particular emphasis on regions in which the steady solution is unstable.

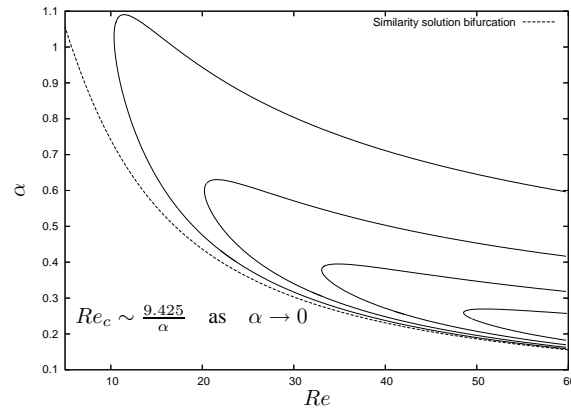


Figure 1: Location of symmetry-breaking bifurcations in the  $(Re, \alpha)$  plane for a radius ratio  $\Gamma = 100$ . Parabolic flow is applied at the inlet and the Neumann condition  $\frac{\partial \mathbf{u}}{\partial r} = 0$  is applied at the outlet. The location, and asymptotic behaviour, of the similarity solution pitchfork is also shown.

\*School of Mathematics, University of Manchester, UK.

## Observations on the wave number spectrum and evolution of an internal wave attractor

Jeroen Hazewinkel<sup>a,b</sup>, Pieter van Breevoort<sup>b</sup>, Stuart B. Dalziel<sup>a</sup> and Leo. R. M. Maas<sup>b</sup>

Reflecting internal gravity waves in a stratified fluid preserve their frequency and thus their angle with the gravitational direction. At boundaries that are neither horizontal nor vertical, this leads to a focusing or defocusing of the waves. Previous theoretical and experimental work has demonstrated how this can lead to internal wave energy being focused onto 'wave attractors' in relatively simple geometries. We present new experimental and theoretical results on the dynamics of wave attractors in a nearly two-dimensional trapezoidal basin. In particular, we demonstrate how a basin-scale mode forced by simple mechanical excitation develops an equilibrium spectrum. We find a balance between focusing of the basin-scale internal wave by reflection from a single sloping boundary and viscous dissipation of the waves with higher wave numbers. Theoretical predictions using a simple ray-tracing technique are used to explain the observed behaviour of the wave attractor during the initial development, steady forcing, and the surprising increase of wave number during the decay of the wave field after the forcing is terminated.

<sup>a</sup> Department of Applied Mathematics and Theoretical Physics, University of Cambridge, UK

<sup>b</sup> Royal Netherlands Institute for Sea Research, the Netherlands.

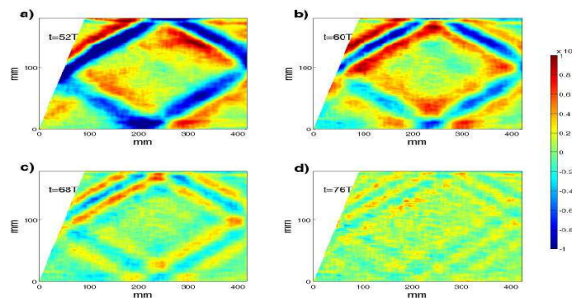


Figure 1: The gradient density perturbation field at four different times after the forcing is terminated. Note the decrease in wavelength.

## Absolute instability of co-flow mixing layers

J. J. Healey\*

This paper is concerned with the propagation and stability characteristics of inviscid linearised disturbances to plane mixing layers. In a study of a plane mixing layer that played an important role in bringing the concepts of absolute and convective instabilities to the attention of the hydrodynamics community, Huerre & Monkewitz<sup>1</sup> found that absolute instability only occurs when the counter-flow between the two streams is greater than a threshold value. Although the value for this threshold depends on the details of the model velocity profile, it seems to be generally believed that only counter-flow mixing layers can become absolutely unstable.

Absolute instability can be determined using Briggs' method in which the 'pinch-point' is located in the complex wavenumber plane. This is the dominant saddle-point that can be used to estimate the large-time asymptotic behaviour of an impulsive disturbance to the flow. Huerre & Monkewitz noted in the co-flow mixing layer (both streams in the same direction) that if the difference in velocities of the two streams is smaller than a certain value (compared with the mean velocity of the two streams) then the pinch point crosses into the left half of the complex wavenumber plane. This is problematic because in the left half-plane waves grow exponentially with distance from the shear layer, and so seem to violate homogeneous boundary conditions, which are satisfied by choosing solutions that decay exponentially with distance from the shear layer. Pinch-points have been found to enter the left half-plane in a number of different flows, but, until recently, they were considered to be unphysical.

However, Healey<sup>2</sup> has shown that they do have physical significance. They correspond to a new type of convective instability in which a disturbance grows exponentially with distance from the shear layer behind a propagating front, beyond which the flow is undisturbed, and homogeneous boundary conditions apply. Furthermore, Healey<sup>3</sup> has shown that the absolute instability characteristics of this class of flows with left half-plane modes is very sensitive to the nature of the boundary condition far from the shear layer. Changing this condition from one of exponential decay, to zero normal perturbation velocity at a finite distance from the shear layer, which models confinement by an impermeable plate, can lead to increased absolute instability however far the plate is from the shear layer, i.e. the confined problem in the limit of a very distant plate can have different behaviour from the unconfined problem.

We show that the plane mixing layer is a member of this newly identified class of flows and that it does become more absolutely unstable when confined by plates placed parallel to the flow for certain ranges of confinement parameter. A long-wave theory has been developed for the saddle-points created by confinement, which gives qualitative information on how changes to the basic flow will affect the absolute instability. This leads us to present, for the first time (to our knowledge), an example of an absolutely unstable co-flow mixing layer.

---

\*Department of Mathematics, Keele University

<sup>1</sup>P. Huerre & P.A. Monkewitz, *J. Fluid Mech.* **389**, 151 (1985).

<sup>2</sup>J.J. Healey, *J. Fluid Mech.* **560**, 279 (2006).

<sup>3</sup>J.J. Healey, *J. Fluid Mech.* **579**, 29 (2007).



# Transient growth in vortices with axial flow

C. J. Heaton\*

We look at linear transient growth in high Reynolds number and inviscid vortices. Many vortices do not possess strong classical exponential instabilities, but are still observed to be unstable (e.g. the trailing line vortex for  $q > 2.31$ ). Our computations show that large transient growth is typical, in agreement with previous studies, which might suggest a ‘bypass’ route to vortex instability analogous to the bypass transition of 2D shear flows.

We find transient growth which relies on inviscid mechanisms, specifically the inviscid algebraic instability possessed by vortices<sup>1</sup>. Based on the continuous-spectrum theory of the algebraic instability we find new scalings for the transient growth, which are verified numerically. The scalings are different from those known for 2D shear flows<sup>2</sup>, but the growth is analogous in several ways. Typically the rate of the transient growth is greater in a vortex flow than a 2D shear flow, although the amplitude reaches a maximum sooner because viscous damping is stronger.

The Batchelor (trailing line) vortex, which occurs in aeronautics, and spiral Poiseuille flow are used as case studies. We give calculations showing the level of transient growth from the inviscid mechanism, and discuss the competition between this effect and viscous instability modes (analogues of the Tollmein-Schlichting waves in 2D). For spiral Poiseuille flow experimental data are available<sup>3</sup>, and we find that transient growth leading to bypass transition is consistent with the transition observed in high Reynolds number and high Taylor number regimes.

\*Department of Applied Mathematics and Theoretical Physics, University of Cambridge.

<sup>1</sup>C. J. Heaton & N. Peake, *J. Fluid Mech.* **587**, 271 (2007).

<sup>2</sup>P. J. Schmid & D. S. Henningson, *Stability and transition in shear flows* (2001).

<sup>3</sup>D. L. Cotrell *et al.*, *J. Fluid Mech.* **509**, 353 (2004).

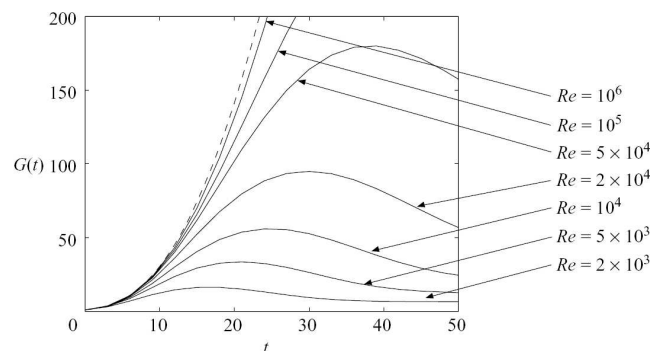


Figure 1: Transient growth for a Batchelor vortex: the inviscid case is shown by a dashed line, and controls the growth at finite Reynolds number (solid lines).

## Flow-induced, self-excited oscillations of collapsible tubes

Matthias Heil\*, Jonathan Boyle\*

Many fluid-conveying vessels in the human body are susceptible to fluid-elastic instabilities that lead to the development of flow-induced, large-amplitude oscillations. Examples include wheezing during forced expiration and the development of Korotkoff sounds during sphygmomanometry. Most theoretical and experimental studies of this phenomenon have been performed on variants of the so-called Starling resistor, sketched in Fig. 1. A thin-walled, elastic tube is mounted on two rigid tubes and enclosed in a pressure chamber that allows the external pressure,  $p_{ext}$ , to be controlled independently of the fluid pressure. When fluid is driven through the tube, oscillations tend to develop when the flow rate exceeds a certain threshold.

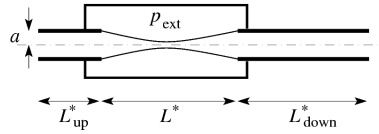


Figure 1: Sketch of the Starling resistor, a thin-walled, elastic tube, mounted on two rigid tubes and enclosed in a pressure chamber.

Following a brief overview of recent work<sup>1</sup> on the theoretical analysis of an instability mechanism that explains the onset of these oscillations in a particular parameter regime, we present the results of direct numerical simulations of the large-amplitude oscillations that develop subsequently. We demonstrate that the character of the oscillations depends strongly on the tube's initial degree of collapse, and that oscillations develop much more readily from steady-state configurations in which the tube is buckled non-axisymmetrically, rather than from axisymmetric equilibrium configurations. This is in pleasing agreement with the predictions from the theoretical model and with experimental observations.

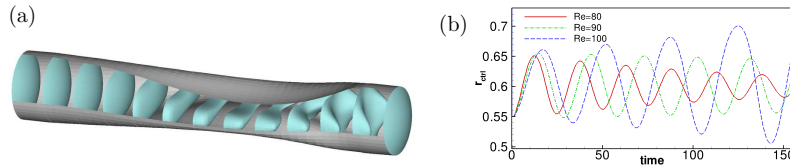


Figure 2: (a) Axial velocity profiles for steady flow in a strongly-buckled collapsible tube. (b) Evolution of the radius of a control point on the elastic tube wall, following a perturbation (applied at  $t = 0$ ), for three different Reynolds numbers.

\*School of Mathematics, University of Manchester.

<sup>1</sup>Joint work with Robert Whittaker and Sarah Waters from the University of Oxford, and Oliver Jensen from the University of Nottingham.

## Flow control applied to transitional flows

Dan Henningson  
Linné FLOW Centre, KTH Mechanics  
100 44 Stockholm Sweden

The dynamics and control of disturbances in the spatially evolving boundary layer on a flat-plate are investigated from an input-output viewpoint. From the linearized Navier-Stokes equations with inputs (disturbances and actuators) and outputs (objective function and sensor) controllable, observable and balanced modes are extracted using the snapshot-method and a matrix-free time-stepper approach. A balanced reduced-order model is constructed and shown to capture the input-output behaviour of linearized Navier-Stokes equations. This model is used to design a LQG-feedback controller to suppress the growth of perturbations inside the boundary layer, see figures 1 and 2. Finally, an overview of recent work applying these concepts to more complicated flows are given.

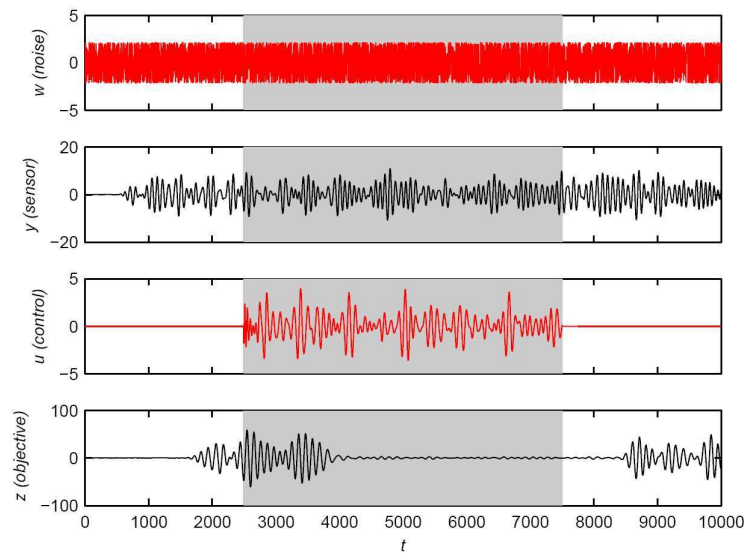


Figure 1. Input and output signal of the closed-loop system; a) the random forcing  $w$ ; b) measurement signal  $v$ ; c) control signal  $u$ ; d) the objective function  $z$ . The controller is active between  $t=2500$  and  $7500$ , marked with the grey area.

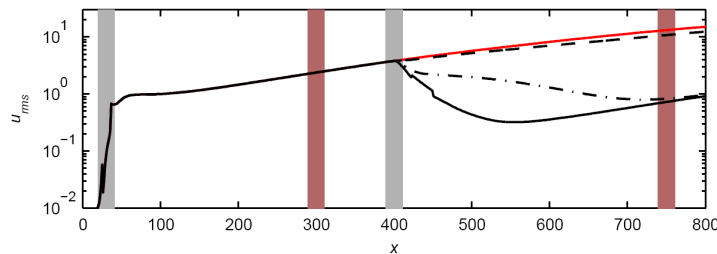


Figure 2. The rms-values of the uncontrolled system (red line), cheap controller (solid black), moderate controller (dashed-dotted line) and expensive controller (dashed line). The grey bar represent the size and location of the inputs, whereas the red bars correspond to the outputs.

## Flow transitions in side-heated cavities and their control by magnetic field

Daniel Henry\*, Hamda BenHadid\*, Anne Juel† and Slim Kaddeche‡

The determination of the flow transitions in a cavity heated from the side in low-Prandtl-number fluids has been a challenge for many years. The interest for such studies comes from the fact that the flows in this situation are considered as representative of those which arise in the melt during directional solidification of crystals and are suspected to be at the origin of defects (as striations) in the crystal. Contrarily to the Rayleigh-Bénard situation, the transitions in such situation occur in already very intense convective flows, and the problem has been up to now mainly treated in two-dimensional situations. Thanks to a numerical method which allows the direct determination of the bifurcation points, the thresholds corresponding to the first flow transition in a three-dimensional parallelepipedic cavity have been determined for a wide range of aspect ratios and Prandtl number values<sup>1</sup>. The map of the transitions thus obtained shows that the evolution of the thresholds is not regular. This is due to the very frequent change of stability branches when the aspect ratios or the Prandtl number are changed, and indicates that different flow structures, either steady or oscillatory, breaking different symmetries of the problem, are triggered at the thresholds. Another interesting point concerns the influence of the Prandtl number  $Pr$ : it is shown that the transition obtained in the limit case  $Pr = 0$  is not valid beyond  $Pr = 10^{-4}$ , i.e. this limit case is not representative of what can be obtained with realistic liquid metals.

The application of a magnetic field is common in modern growing facilities because of its overall damping effect on the convective flows. In fact, two different aspects can be distinguished: the braking effect on the steady flows, and the damping of the oscillations leading to the increase of the transition thresholds. If the braking effect has been much studied during the last 15 years, the influence on the thresholds is less considered. Our study focuses on the directional effect of the magnetic field on the oscillatory thresholds in a parallelepipedic enclosure. A strong influence of the magnetic field on the thresholds is observed: the thresholds scale exponentially with the intensity of the magnetic field for the three principal orientations of the magnetic field. The vertical field, however, has the best efficiency, followed by the transverse field and the longitudinal field. These results agree very well with those obtained by Hof *et al.* in a recent experiment<sup>2</sup>. Insight into the damping mechanism is gained from the fluctuating kinetic energy budget associated with the time-periodic disturbances at threshold.

\*Laboratoire de Mécanique des Fluides et d'Acoustique, Université de Lyon/CNRS, France.

†Manchester Centre for Nonlinear Dynamics, University of Manchester, UK.

‡Unité de Recherche Matériaux, Mesures et Applications, INSAT, Tunisie.

<sup>1</sup>D. Henry, H. Ben Hadid, *Phys. Rev. E* **76**, 016314 (2007).

<sup>2</sup>B. Hof *et al.*, *J. Fluid Mech.* **545**, 193 (2005).

## Gas transfer through the air-water interface with far-field homogenous turbulence in the water phase

Herlina<sup>a</sup>, Jan Wissink<sup>b</sup>, G.H. Jirka<sup>a</sup>

Transfer processes of weakly soluble gases across the air-water interface play a central role in many environmental and industrial systems. Reaeration in polluted rivers and the absorption of greenhouse gases, notably carbon dioxide into the ocean are two important examples of gas transfer processes in the environment. The difficulty in understanding the gas transfer problem of weakly soluble gases (e.g. O<sub>2</sub>, CO<sub>2</sub>) stems from the fact that the process is concentrated within a very thin layer on the liquid side (10-1000  $\mu\text{m}$ ). The turbulent mass transport term  $\epsilon'w'$ , which combines the information from the fluctuating turbulent part of concentration and velocity, is still typically not known and has to be modeled. Here, we will present results obtained from our experimental and numerical studies focusing on the gas transfer problem with far-field homogenous turbulence. In the experiments, gas transfer induced by grid-stirred turbulence in the water phase was investigated using a combined Particle Image Velocimetry - Laser Induced Fluorescence (PIV-LIF) technique. The techniques allowed visualization of the velocity and concentration fields with good spatial and temporal resolution and thus provided good insight into the gas transfer mechanisms. The PIV-LIF system also enabled direct quantification of the molecular diffusive transport term  $Dd\epsilon/dz$  and the turbulent mass flux  $\epsilon'w'$ . The results show that the contribution of the turbulent mass flux to the total gas flux is indeed significant ( $\epsilon'w'/j \approx 1$ )<sup>1</sup>. However, the apparent success of the simultaneous PIV-LIF still faces difficulties in resolving the uppermost diffusive layer. In order to overcome this problem, we are performing direct numerical simulations (DNS) using an adapted version of the "LESOCC" (Large Eddy Simulation On Curvilinear Coordinates) code<sup>2</sup>. The numerical code solves the incompressible 3D Navier-Stokes equations and the transport equations of passive scalars. The geometry of the simulation is in accordance with the experiments. The grid resolution is of the order  $100 \times 10^6$  cells. At the free boundaries of the calculation domain in the longitudinal and transverse direction, periodical boundary conditions are employed. In the vertical direction, a symmetry boundary condition is applied at the water surface, while at the bottom the background turbulence is introduced. This is performed by using the results of a separate LES simulation of isotropic turbulence in a periodic box which enters the domain at a fixed diffusion velocity. In the simulations, a rigid lid shear-free surface is assumed. First results of the DNS simulations will be presented and compared with the results from the experiments.

---

<sup>a</sup> Institute for Hydromechanics, University of Karlsruhe, Germany.

<sup>b</sup> School of Engineering and Design, Brunel University, UK.

<sup>[1]</sup> Herlina and Jirka, *J. Fluid Mech.* **594**, 183 (2008).

<sup>[2]</sup> Breuer, and Rodi, *Notes Numer Fluid Mech* **52**, 258 (1994).

## Inertial wave collapse

Wietze HERREMAN, Stéphane LE DIZES, Patrice LE GAL. \*

The violent breakdowns of the non linear evolution of inertial wave systems are well known phenomena that demand for a theoretical understanding. We discuss this strongly nonlinear dynamics, and derive low-dimensional dynamical systems capable of reproducing these collapses in the context of the elliptical instability of the confined vortex system<sup>1</sup>.

Our approach is based on a spectral analysis of the dynamics, using viscous eigenmodes in the expansions. This family of analytic solutions includes the viscous analogues of the Kelvin-waves and geostrophic flow. The low dimensional nonlinear models are derived as Galerkin projections of the exact system of elliptico-polar equations<sup>2</sup>.

Weakly non linear saturated states are found close to the linear instability threshold and are successfully compared to previous results. Further beyond linear instability threshold, we find intermittent signals which are similar to the experimentally observed growth relaminarisation cycles (see Fig. 1.a). Much of this complex dynamics can be understood in terms of a fixed point analysis and by studying some minimal models. We discuss an ill known frequency detuning effect, which may lead to sub-critical instability, and we demonstrate the role of triad resonances and geostrophic instabilities in the transition to complex nonlinear dynamics (see Fig. 1.b).

\*IRPHE, Université de Provence, France

<sup>1</sup>Eloy, Le Gal, Le Dizès, *J. Fluid Mech.*, **476**, 357-388 (2006)

<sup>2</sup>Mason, Kerswell, *J. Fluid Mech.*, **396**, 73-108 (2001)

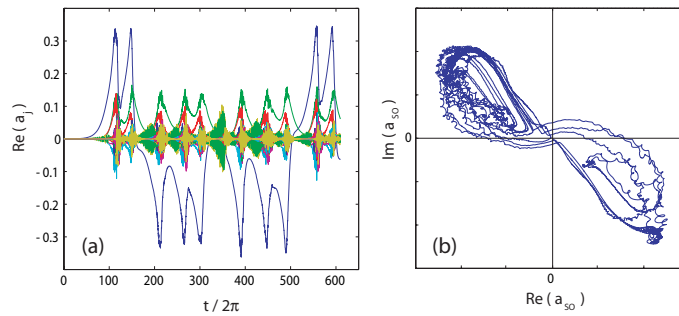


Figure 1: (a) Intermittent nonlinear dynamics due to elliptical instability. We show the real part of the amplitudes  $a_j(t)$  of the most important modes in the expansion, (b) Corresponding phase portrait for the (largest) complex spinover mode amplitude. Long period cycles around the three fixed points are the consequence of a geostrophic instability. Noise triggered by triad resonances decorrelates the cycles, and leads to intermittency.

## Spin-up in a torus

R.E. Hewitt\*, R.J. Clarke†, C. del Pino‡, J. Denier†, T. Mullin§

We consider the spin-up of fluid in a toroidal container with an axis of rotation coincident with the axis of rotational symmetry. Our motivation is to study a fully nonlinear spin-up flow in which the global readjustment mechanism is distinct from those already established in the literature<sup>1</sup>. A toroidal geometry is an ideal case to study because it strongly couples the global response of the contained fluid to critical phenomena in the unsteady boundary layer.

Initially the fluid and container rotate as a rigid body at an angular frequency  $\Omega_i$ . This initial state is altered such that the container rotation rate is  $\Omega_f = \Omega_i + \Delta\Omega$ , where the Rossby number  $Ro = \Delta\Omega/\Omega_f$  is an  $O(1)$  parameter. In general, in addition to  $Ro$ , the system is controlled by the Ekman number  $Ek = \nu/(a^2\Omega_f)$  and the container's curvature  $\delta = a/L$ ; here  $\nu$  is the kinematic viscosity of the fluid,  $a$  is the cross-sectional radius of the torus and  $L$  is the centreline radius of the torus. This case was first discussed experimentally for spin-up from rest ( $Ro = 1$ ) by Madden and Mullin<sup>2</sup>; we generalise their work to cover the full range of the Rossby numbers.

The spin-up problem is fully nonlinear and a multi-stranded approach is taken to describing the evolution of the system through a combination of finite- $Ek$  (axisymmetric) computations, boundary-layer theory and laboratory experiments. In this talk we emphasise the boundary-layer analysis and show that, near the inner/outer equatorial points of the flow, the boundary layer may exhibit non-uniqueness of steady states and finite-time breakdowns. We describe the conditions on the Rossby number for finite-time breakdowns to be observed and make quantitative comparisons between unsteady and steady boundary-layer solutions with both finite- $Ek$  numerical results and laboratory data. We show that a dramatic eruption of fluid at the equatorial points of the torus (as observed both experimentally and numerically) can be quantitatively correlated to the beginnings of the breakdown in the boundary-layer equations.

---

\*School of Mathematics, Univ. of Manchester.

†School of Mathematical Sciences, Univ. of Adelaide

‡ESTII, Univ. of Malaga, Spain

§MCND, Univ. of Manchester

<sup>1</sup>Benton & Clark, *Ann. Rev. Fluid Mech.*, **6**, 257.

<sup>2</sup>Madden & Mullin, *J. Fluid Mech.*, **265**, 217

### Pulse propagation in the pulmonary and systemic arteries

N.A. Hill\*, G.V. Vaughan\*, M.S. Olufsen†, M. Johnson‡ and C. Sainsbury§

The model of Olufsen<sup>1,2</sup> has been extended to study periodic pulse propagation in both the systemic and the pulmonary arterial trees. The systemic and pulmonary arteries are treated as separate, bifurcating trees of compliant and tapering vessels. Each model is divided into two coupled parts: the larger and smaller arteries. Blood flow and pressure in the larger arteries are predicted from a nonlinear 1D cross-sectional area-averaged model for a Newtonian fluid in an elastic tube. The initial cardiac output is obtained from magnetic resonance measurements.

The smaller blood vessels are modelled as asymmetric structured trees with specified area and asymmetry ratios between the parent and daughter arteries. For the systemic arteries, the smaller vessels are placed into a number of separate trees representing different vascular beds corresponding to major organs and limbs. Womersley's theory gives the wave equation in the frequency domain for the 1D flow in these smaller vessels, resulting in a linear system. The impedances of the smallest vessels are set to a constant and then back-calculation gives the required outflow boundary condition for the Navier–Stokes equations in the larger vessels. The flow and pressure in the large vessels are then used to calculate the flow and pressure in the small vessels. This gives the first theoretical calculations of the pressure pulse in the small ‘resistance’ arteries which control the haemodynamic pressure drop.

We study the effects, on both the forward-propagating and the reflected components of the pressure pulse waveform, of the number of generations of blood vessels, the compliance of the arterial wall, and of vascular rarefaction (the loss of small systemic arterioles) which is associated with type II diabetes. We discuss the possibilities for developing clinical indicators for the early detection of vascular disease.

---

\*Department of Mathematics, University of Glasgow, U.K.

†Department of Mathematics, North Carolina State University, USA

‡Scottish Pulmonary Vascular Unit, Western Infirmary, Glasgow, U.K.

§BHF Glasgow Cardiovascular Research Centre, University of Glasgow, U.K.

<sup>1</sup>M.S. Olufsen et al., *Ann Biomed Eng.* **28**, 1281–99 (2000)

<sup>2</sup>M.S. Olufsen, *Am J Physiol.* **276**, H257–68 (1999)

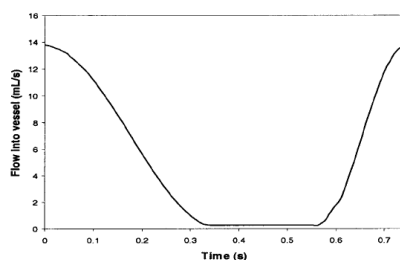


## Instability analysis of blood flows in stenosis with compliant walls

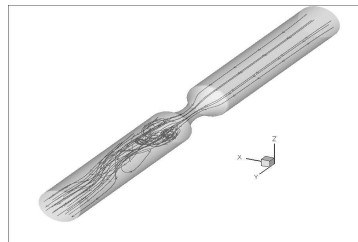
Y. Hoarau<sup>a</sup>, M. Braza<sup>b</sup>, Y. Ventikos<sup>c</sup>

Stenoses, or geometry constrictions, play an important role in a multitude of pathophysiologic conditions. Aortic coarctation, atherosclerotic depositions, vasospasm etc. are only some of the specific situations where the interaction of a moving liquid with a geometry restriction gives rise to important biomechanical conditions. The study of stenotic flow is gaining momentum in the last few years, yet there are still several unanswered questions concerning such flows, some of them being at the very centre of the mechanics involved. We have examined the effect of axisymmetry of the stenosis on the mode emergence connected. It has been shown that perfectly axisymmetric configurations, under certain conditions, are led to symmetry breaking via the emergence of non-axisymmetric instability modes. We have explored the level of the stenosis necessary to significantly change the spontaneous bifurcation scenarios observed in blood flows under pulsatile inflow condition. We ended this investigation by including compliance in the solid boundaries of our configurations. For the majority of problems of biological/medical relevance, this feature is indispensable and introduces complication and richness of phenomena that should not be overlooked. The deformability of live tissue, especially under pulsatile or unstable flow conditions introduces additional vibration modes and contributes significantly to the damping of otherwise unconstrained oscillations.

The multiphysics software suite CFD-ACE has been used to solve the unsteady incompressible Navier-Stokes equations in stenosed blood vessel as well as for the fluid-structure interaction. A smoothed pulsatile waveform is used in all the calculations corresponding to a physiologically realistic pulsatile wave form in the carotid artery. The period of pulsatility is 0.743 seconds, corresponding to a Womersley number in the common carotid of 4.9. The vessel is 7mm in diameter and 2cm long. Three levels of stenosis have been studied: 25%, 50% and 75%.



Pulsatile inlet



Flow pattern for the 75% stenosis

<sup>a</sup> Institut de Mécanique des Fluides et des Solides de Strasbourg, CNRS/ULP UMR n°7507, Strasbourg, hoarau@imfs.u-strasbg.fr

<sup>b</sup> Institut de Mécanique des Fluides de Toulouse, CNRS/INPT UMR n°5502, Toulouse

<sup>c</sup> Fluidics and Biocomplexity Group, Department of Engineering Science, University of Oxford

## Sensitivity of the compliant channel flow

Jérôme Hoepffner\*, Julien Favier† &amp; Alessandro Bottaro†

Compliant walls were extensively studied as a possible mean of preventing wall-bounded shear flow instabilities<sup>1</sup>. Effective reduction of the instability growth rate could postpone the transition to turbulence, thus help decreasing the skin-friction drag of air and water vehicles. Besides eigenmode analysis, the potentiality of transient energy growth of perturbations should also be considered for flows subject to external disturbances<sup>2</sup>. Indeed, if the flow sensitivity is large, subcritical transition to turbulence might be induced from the amplification of these external disturbances. In the present paper, we perform this analysis for a channel flow with compliant walls. We report various mechanisms arising from the dynamic interaction between the flow and the walls.

\*Department of Mechanical Engineering, Keio University, Yokohama, Japan.

†DICAT, Università di Genova, Genova, Italy.

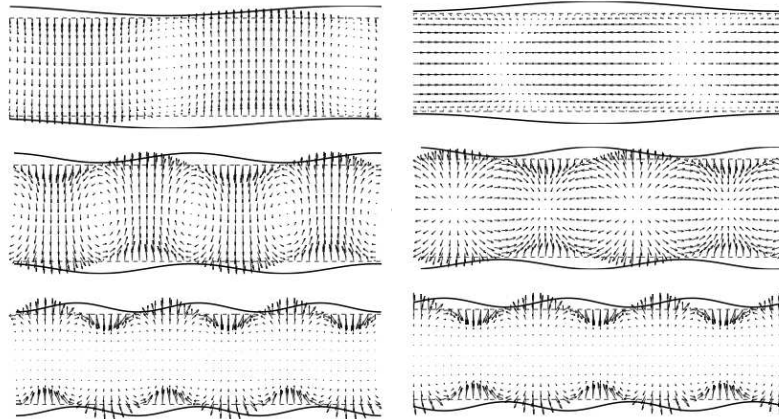
<sup>1</sup>Riley et al, *Annual Review of Fluid Mechanics*, **20**, 393 (1988).<sup>2</sup>Schmid & Henningson, *Springer* (2000).

Figure 1: Eigenmodes of the compliant channel with zero base flow. Velocity field for *left*) sinuous mode and *right*) varicose mode, for three wave numbers.

### An experimental investigation of turbulence in pipe flow.

Björn Hof<sup>a</sup>

Turbulent pipe flow is studied in the transitional regime for  $1500 < \text{Re} < 4000$ . Tomographic particle image velocimetry is applied to visualize localized turbulent structures (puffs and slugs) in pipe flow. In this Reynolds number regime velocities can be spatially and temporally fully resolved in a volume of about 4 pipe diameters in length. Our investigation focuses on the occurrence of axially and azimuthally periodic segments within the turbulent flow<sup>1</sup> and their role in the transition process. The main aim of this study is to characterize and quantify the occurrence of such periodic states and to rationalize their role in turbulent puffs and slugs. The three-dimensional velocity information allows to determine the wavelength as well as the phase velocity of these states. Indeed we find good quantitative agreement for the propagation velocity, wavelength and the streak vortex interaction with exact travelling wave solutions<sup>2,3</sup>. Although the overall dynamics are very similar, there are also clear differences between the velocity profiles of the experimental and the numerical waves. The wall friction as well as the overall velocity profiles show quantitative differences.

The time resolved velocity information also enables us to make a connection between the overall structure of turbulent puffs and slugs and the occurrence of spatially periodic segments within them.

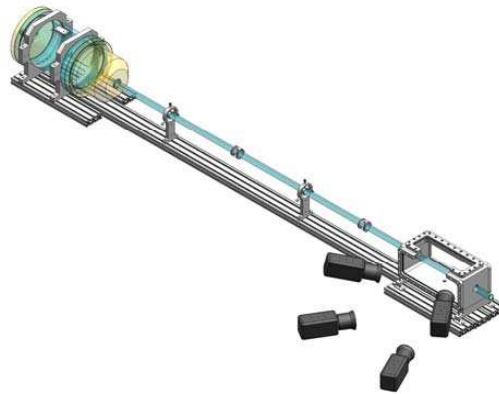


Figure 1: Experimental setup. Water enters the pipe through a specially designed inflow section. Turbulence can be triggered at injection points along the pipe. Volume resolved velocity measurements are carried out using a high speed (480Hz@4Mpixel) LaVision Tomographic PIV system.

<sup>a</sup> Max Planck Institute for Dynamics and Self-Organization, Göttingen, Germany.

<sup>1</sup> Hof et al., *Science* **389**, 169 (1999).

<sup>2</sup> Eckhardt et al., *Annu. Rev. Fluid Mech.* **39**, 447 (2008).

<sup>3</sup> Kerswell Nonlinearity **18**, R17 (2005)

## Instabilities of Stewartson Layers and Taylor Columns

Rainer Hollerbach\*

Consider a rapidly rotating spherical shell, with additionally a (small) differential rotation imposed on the inner sphere. Due to the Taylor-Proudman theorem, the flow aligns itself along *cylinders*, singling out the so-called tangent cylinder  $\mathcal{C}$ , the cylinder just touching the inner sphere and parallel to the axis of rotation. Outside  $\mathcal{C}$  the fluid co-rotates with the outer sphere; inside  $\mathcal{C}$  it rotates at a rate intermediate between the rotation rates of the inner and outer spheres. The detailed structure of the free shear layer that resolves the jump in angular velocity across  $\mathcal{C}$  was deduced by Stewartson<sup>1</sup>.

Now suppose that the imposed differential rotation of the inner sphere is gradually increased, until eventually non-axisymmetric instabilities occur, basically Kelvin-Helmholtz modes. Stewartson layer instabilities of this type have been studied experimentally<sup>2,3</sup>, asymptotically<sup>4</sup>, and numerically<sup>5</sup>. Hollerbach<sup>5</sup> in particular focused attention on the difference between positive and negative Rossby numbers  $Ro = \Delta\Omega/\Omega$  — that is, whether the inner sphere rotates slightly faster or slower than the outer sphere — which turn out to yield quite different instabilities.

Finally, suppose that the fluid is not only rotating, but also stably stratified, with Brunt-Vaisala frequency  $N$ . It is well known that in this case a Taylor column — which is essentially what the entire region inside the tangent cylinder is — no longer extends indefinitely in  $z$ , but is instead gradually reduced in height as the stratification is increased. Figure 1 shows an example of how the original Stewartson layer is compressed into an increasingly short Taylor column as the stratification parameter  $S = Pr N^2/\Omega^2$  is increased.

In this talk I will discuss not only this transition from Stewartson layers to Taylor columns, but also the resulting non-axisymmetric instabilities, and how they vary with the stratification  $S$ , the Prandtl number  $Pr$ , and again considering both positive and negative  $Ro$ .

---

\*Department of Applied Mathematics, University of Leeds, Leeds, LS2 9JT, United Kingdom.

<sup>1</sup>Stewartson, *J. Fluid Mech.* **26**, 131 (1966)

<sup>2</sup>Hide & Titman, *J. Fluid Mech.* **29**, 39 (1967)

<sup>3</sup>Früh & Read, *J. Fluid Mech.* **383**, 143 (1999)

<sup>4</sup>Busse, *J. Fluid Mech.* **33**, 577 (1968)

<sup>5</sup>Hollerbach, *J. Fluid Mech.* **492**, 289 (2003)

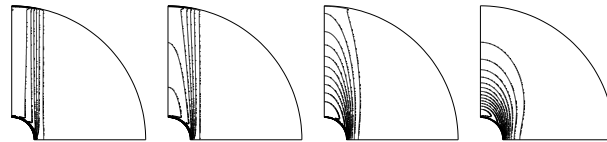


Figure 1: Contours of the angular velocity, with a contour interval of  $1/15$ . From left to right the stratification parameter  $S = 0, 0.01, 0.1$ , and  $1$ . Note the transition from a Stewartson layer for  $S = 0$  to a strongly compressed Taylor column for  $S = 1$ .

## Optimization of unflagellate and biflagellate locomotion

A. E. Hosoi\* and Daniel Tam†

The past decade has seen a number of engineering innovations that make construction of devices of micro- and even nanometric dimensions feasible. Hence, there is a growing interest in exploring new and efficient ways to generate propulsion at these small scales. Here we explore optimization of one particular type of low Reynolds number propulsion mechanism – flagella. Beyond the general challenges associated with optimization, there are a number of issues that are unique to swimming at low Reynolds numbers. At small scales, the fluid equations of motion are linear and time-reversible, hence reciprocal motion – *i.e.*, strokes that are symmetric with respect to time reversal – cannot generate any net translation (a limitation commonly referred to as the Scallop Theorem). One possible way to break this symmetry is through carefully chosen morphologies and kinematics.

One symmetry-breaking solution commonly employed by eukaryotic microorganisms is to select nonreciprocal stroke patterns by actively generating torques at fixed intervals along the organism. Hence, we will address the question: For a given morphology, what are the optimal kinematics? In this talk we present optimal stroke patterns using biologically inspired geometries such as single-tailed spermatozoa and the double-tail morphology of *Chlamydomonas*, a genus of green alga widely considered to be a model system in molecular biology.

In locomotion studies, the *geometry* of the system cannot be decoupled from the *kinematics*, hence the two must be optimized simultaneously. For spermatozoa, we find that if geometry and kinematics are optimized concurrently, predicted optimal tail lengths match those observed in mammalian sperm across a wide range of species.

\*Department of Mechanical Engineering, Massachusetts Institute of Technology.

†Department of Aeronautics and Astronautics, Massachusetts Institute of Technology.

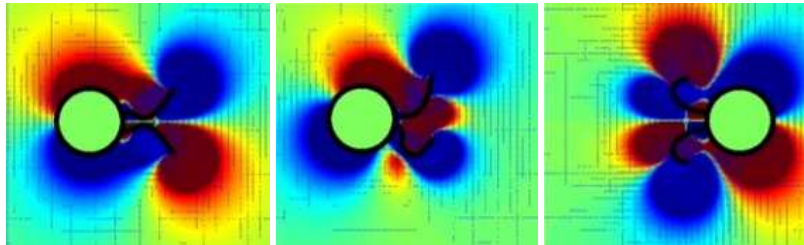


Figure 1: Snapshots of optimal stroke patterns for biflagellate low Reynolds number swimmers.

## Wake interaction between two long, tandem, flexible cylinders in a stepped current

F. J. Huera Huarte\*, P.W. Bearman†

Experiments on the interaction between two vertical long flexible cylinders pin jointed at their ends, were conducted during summer 2007 at the water flume of the Department of Aeronautics at Imperial College London. The figure below shows the experimental set up with the two riser models in tandem arrangement. The design of the riser models was based on that used for the Delta Flume Campaign in 2003<sup>1</sup> but at a reduced scale.

The aim was to investigate the dynamic response of the two bodies subjected to Vortex-Induced (VIV) and Wake-Induced Vibrations (WIV). The water flume at Imperial College allowed the generation of uniform currents, and by submerging the lower 40% of the riser model into water, a stepped current was obtained. Initially a single riser configuration was studied but additionally, a configuration consisting of a tandem of two riser models aligned with the flow direction, was also tested. The flow structures in the wake of the models for each one of the different configurations were investigated by using Digital Particle Image Velocimetry (DPIV).

---

\*Department of Mechanical Engineering, Universitat Rovira i Virgili (URV), SPAIN

†Department of Aeronautics, Imperial College London, UK

<sup>1</sup>J.R. Chaplin, P.W. Bearman, F.J. Huera Huarte and R.J. Pattenden. *J. Fluids & Structures* **21**, 3-24 (2005).

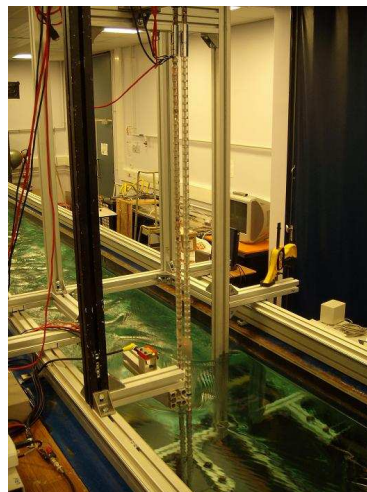


Figure 1: Experimental set up

## Sound radiation from self-sustained oscillations in a hot jet

Patrick Huerre,<sup>\*</sup> Lutz Lesshafft<sup>†</sup> and Pierre Sagaut<sup>‡</sup>

When subsonic jets are heated beyond a critical temperature ratio with respect to the ambient air, they bifurcate to a regime of intrinsic self-sustained oscillations in the form of regularly spaced ring vortices<sup>1</sup>. These oscillations may be described theoretically as a *nonlinear global mode* that exists due to absolute instability<sup>2,3</sup>. The acoustic far field radiated by such vortex streets in a hot jet will now be discussed, based on results from direct numerical simulations that resolve the aerodynamic near field and the acoustic far field simultaneously.

According to these simulations, visualized in figure 1, the acoustic field generated by the global mode in a hot jet at low subsonic Mach number  $Ma = 0.1$  is that of a *compact dipole*. The apparent source location within the jet corresponds to the region of nonlinear vortex roll-up. The dominant aeroacoustic source mechanisms within the jet are identified via analyses of Lighthill's and Lilley's equations: in the context of classical Lighthill source terms, the acoustic dipole field is demonstrated to arise from non-isentropic perturbations in the jet near field.

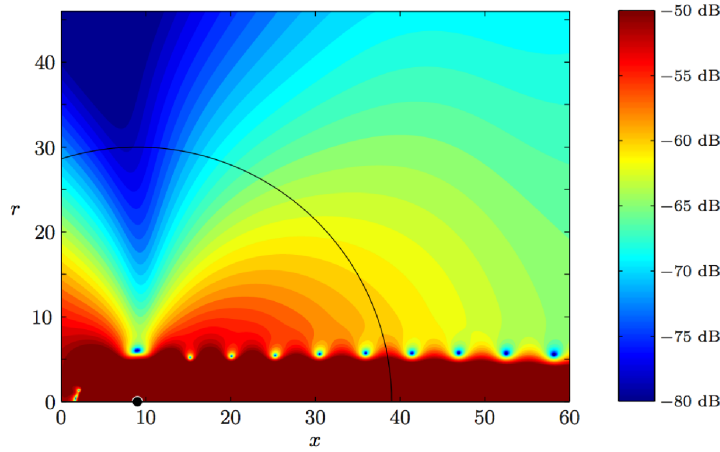


Figure 1: Far field pressure fluctuation amplitude in the DNS: the upper half plane is shown, the jet axis is at  $r = 0$ . The coordinates are scaled with the jet radius. A black dot marks the apparent source location.

<sup>\*</sup>Laboratoire d'Hydrodynamique, CNRS-École Polytechnique, Palaiseau (France).

<sup>†</sup>Department of Mechanical Engineering, University of California at Santa Barbara (USA).

<sup>‡</sup>Institut d'Alembert, Université Paris 6 (France).

<sup>1</sup>Monkewitz et al., *J. Fluid Mech.* **213**, 611 (1990).

<sup>2</sup>Lesshafft et al., *J. Fluid Mech.* **554**, 393 (2006).

<sup>3</sup>Lesshafft et al., *Phys. Fluids* **19**, 054108 (2007).

## The crossflow instability of the boundary layer on a rotating cone

Z. Hussain\*, S. J. Garrett<sup>†</sup> and S. O. Stephen\*

Experimental studies have shown that the boundary-layer flow over a rotating cone is susceptible to crossflow and centrifugal instability modes of spiral nature, depending on the angle of sharpness of the cone nose. For half-angles ( $\psi$ ) ranging from propeller nose cones to rotating disks ( $\psi \geq 40^\circ$ ), the instability triggers co-rotating vortices; whereas for applications such as sharp spinning missiles ( $\psi < 40^\circ$ ), counter-rotating vortices are observed.

Physically, wide rotating cones (say  $\psi > 40^\circ$ ) may be considered as a first approximation to modelling, amongst other applications, the central nose rotor of an aeroengine fan. Relatively large half-angles are used to deflect any ensuing turbulent flow away from the turbofan core yet still provide a sufficient amount of airflow into the fan blades. Such physically relevant flows form the basis for our motivation and the aim of the present study is to investigate the effect of  $\psi$  on measurable aerodynamic quantities.

The influential study of <sup>1</sup> contains the first observation of the stationary crossflow vortex pattern on a rotating disk ( $\psi = 90^\circ$ ), which is closely related to the rotating cone. More recently, numerical solutions for the curves of neutral-stability are presented (see <sup>2</sup>) using a parallel-flow approximation, as well as including streamline curvature and Coriolis effects. It is shown that there exist two distinct neutral branches, which we term type I and II. These results have later been verified via a linear asymptotic investigation<sup>3</sup>, which has successfully recovered Stuart's type I solution along with the type II branch. We continue in this light and proceed to extend the neutral-stability curve comparisons from a rotating disk to a rotating cone of general half-angle.

In this presentation, we provide a mathematical description of the onset of co-rotating vortices for a family of cones rotating in quiescent fluid, with a view towards explaining the effect of  $\psi$  on the underlying transition of dominant instability. We investigate the stability to inviscid cross-flow modes (type I), as well as modes which arise from a viscous-Coriolis force balance (type II), using numerical and asymptotic approaches. The influence of  $\psi$  on the number and orientation of the spiral vortices is examined, with comparisons drawn between our two distinct methods, as well as with the previous experimental investigations of <sup>4</sup>.

Our results indicate that increasing  $\psi$  has a stabilizing effect on both the type I and type II modes. Favourable agreement is obtained between the numerical and asymptotic methods presented here and existing experimental results for  $\psi > 40^\circ$ . Below this half-angle we suggest that an alternative instability mechanism is at work which is not amenable to investigation using the formulation presented here.

\*School of Mathematics, University of Birmingham.

<sup>†</sup>Department of Mathematics, University of Leicester.

<sup>1</sup>Gregory, Stuart & Walker, *Phil. Trans. R. Soc. Lond. A* **248**, 155 (1955).

<sup>2</sup>Malik, *J. Fluid Mech.* **164**, 275 (1986).

<sup>3</sup>Hall, *Proc. R. Soc. Lond. A* **406**, 93 (1986).

<sup>4</sup>Kobayashi & Izumi, *J. Fluid Mech.* **127**, 353 (1983).



## Segregation of heavy particles in a turbulent flow

Rutger H. A. IJzermans\*, Michael W. Reeks\*

The segregation of heavy particles in turbulence is studied by calculating the compression of the particle phase in a kinematic simulation. Particles are advected by Stokes drag in a flow field composed of 200 random Fourier modes, with an energy spectrum chosen in accordance with Kraichnan<sup>1</sup>. The flow field is smoothly varying in time and space and mimicks many features of real turbulence like the presence of regions of non-zero vorticity and non-zero strain. Suitable choices for the wavenumbers assure periodicity in space. We consider the deformation of an infinitesimal volume of particles along the trajectories of individual particles which are assumed to have the same velocity as the carrier flow at time  $t = 0$ . The volume occupied by the particles centered around a position  $\mathbf{x}$  at time  $t$  is denoted by  $J \equiv \det(J_{ij})$ , where  $J_{ij} \equiv \partial x_i(\mathbf{x}_0)/\partial x_{0,j}$ , where  $\mathbf{x}_0$  denotes the initial position of the particle. The particle-averaged compression,  $d\langle \ln |J| \rangle / dt$ , gives a measure for the change of the total volume occupied by the particle phase<sup>2</sup>. Numerical results show that the particle-averaged compression decreases continuously if the value of the Stokes number (the dimensionless particle relaxation time) is below a threshold value  $St_{cr} \simeq 0.7$  (see Fig. 1), indicating that the segregation of these particles continues indefinitely. If, on the other hand, the particle Stokes number is larger than  $St_{cr}$ , the particles are ‘mixed’. We show analytically that the long time limit of  $d\langle \ln |J| \rangle / dt$  is proportional to the Stokes number squared for sufficiently small values of  $St$ , and that the probability density function of  $\ln |J|$  tends to a Gaussian distribution, with both the mean and variance proportional to time and to the Stokes number squared. These results are consistent with the observation that the radial distribution function (RDF) approaches the form  $g(r) \sim r^{-\alpha}$  (see Fig. 1; also Chun et al.<sup>3</sup>), i.e. the RDF becomes infinite at  $r = 0$ . The present tools are ready to be used in a particle-laden DNS.

\*School of Mechanical and Systems Engineering, University of Newcastle-upon-Tyne, UK.

<sup>1</sup>Kraichnan, *Phys. of Fluids* **13**, 22 (1970).

<sup>2</sup>M.W. Reeks, *Proc. of IUTAM Symposium on Disperse Multiphase Flows*, Chicago IL, (2004).

<sup>3</sup>Chun et al., *J. Fluid Mech.* **536**, 219 (2005).

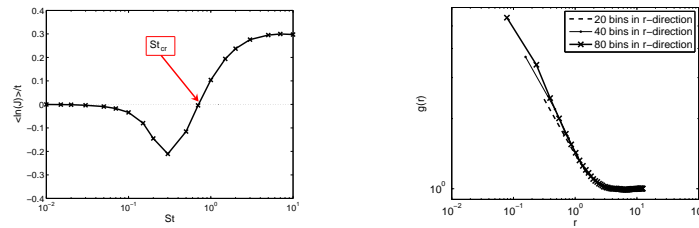
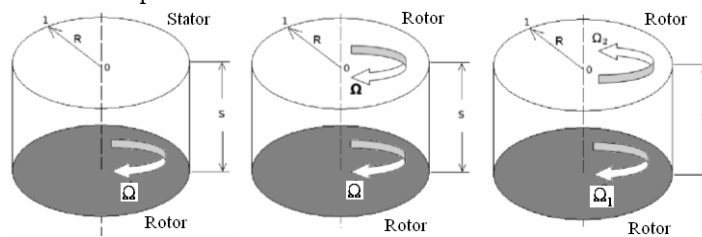


Figure 1: Left: time-converged results for the compression of the particle phase,  $t^{-1} \langle \ln |J| \rangle$ , as a function of the Stokes number  $St$ . Right: RDF for three different resolutions in  $r$ -direction, for  $St = 0.5$ .

## The computation of unsteady turbulent flow structures in rotating cavities

H. Iacovides<sup>a</sup>, B. E. Launder<sup>a</sup>, and A. Zacharos<sup>a</sup>.

Flows inside rotating cavities are relevant to geophysical flows, flows in cavities between turbine discs and flows inside computer disc drives. They have consequently been the subject of many investigations. As can be seen in Owen and Rogers<sup>1</sup>, most experimental and computational studies of cavities such as the ones in Figure 1, have assumed that flow conditions remain steady and axisymmetric. Recent numerical studies of laminar flows in co-rotating cavities, Tucker and Long<sup>2</sup> and also flow visualisation studies of turbulent flows in rotor-stator systems, Figure 1a, Czarny et al<sup>3</sup>, show that large-scale 3-D and unsteady structures are also present.



a) Rotor-Stator Cavity    b) Co-Rotating Cavity    c) Counter-Rotating Cavity

**Figure 1.** Rotating cavity configurations studied

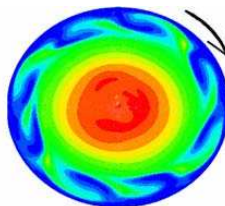


**Figure 2.** Vorticity contours for co-rotating cavity

This study explores whether economical, relative to LES, unsteady RANS methods, can be used to capture these unsteady, 3-D features. A set of 3-D unsteady flow computations has been produced, for the three cases shown in Figure 1; rotor-stator cavities, co-rotating cavities with a stationary outer shroud and also counter-rotating cavities. To minimize grid requirements, the high-Reynolds-number  $k-\epsilon$  model has been employed. For wall boundary conditions instead of the conventional, log-law-based, wall function, a more advanced, analytical wall function of Craft et al<sup>4</sup>, extended to 3-D, general-geometry flow solvers, is used. The paper will focus on the co- and counter-rotating cavities. It will show that the high-Re  $k-\epsilon$  with the analytical wall-function, as shown in Figure 2 for the co-rotating case, returns 3-D unsteady flow structures. Comparisons with measured time-averaged velocity profiles will be included as well as frequency spectra of the velocity and pressure fluctuations. Flow animations resulting from this work can be accessed from <http://tmgflows.mace.manchester.ac.uk/>.

<sup>a</sup> School of Mechanical, Aerospace and Civil Engineering, University of Manchester.

<sup>b</sup> <sup>1</sup>J.M. Owen and R.H. Rogers.. John Wiley & Sons, 1989.

<sup>2</sup>P.G. Tucker and C.A. Long. Int. Comm. Heat Mass Transfer, 22(5):639-648, 1995.

<sup>3</sup>O. Czarny, H. Iacovides and B. E. Launder, Fl., Turb. & Comb., Vol 69, pp 51-61, 2002.

<sup>4</sup>T. J. Craft, A. Gerasimov, H. Iacovides and B.E. Launder, Int. J. of Heat and Fl. Flow, 23, 148-16, 2002

## Boundary layers in high Reynolds number flows through a domain with permeable boundary

Konstantin Ilin\*

We study the effect of small viscosity on nearly inviscid flows of an incompressible fluid through a given domain. In contrast with the standard situation where the boundary of the flow domain is impermeable, we consider flows in which the fluid can flow into the domain through one part of the boundary (the inlet) and leave the domain through the other part (the outlet). We employ the Vishik-Lyusternik method to construct an asymptotic expansion of solutions to the Navier-Stokes equations in the limit of vanishing viscosity (high Reynolds number). In the leading order the velocity is the sum of two terms. The first term is a solution of the Euler equations and describes the flow everywhere in the domain except for a thin boundary layer near the outlet. The second term represents a boundary layer correction to the inviscid solution and is a solution of boundary layer equations which, in contrast with Prandtl's boundary layer, are linear and can be solved analytically in general case. An interesting feature of these boundary layer equations is that the corresponding initial boundary value problem is over-determined, but nevertheless has a unique solution provided that the initial and boundary conditions for the velocity in the original problem are consistent. It turns out that in order to satisfy the initial condition for the  $O(\nu)$  terms of the expansion, we have to impose an additional consistency requirement on the initial and boundary conditions for the tangent velocity at the outlet. It is shown that the asymptotic expansion can be continued up to terms of arbitrary order in  $\nu$ , and each successive approximation requires a new consistency condition.

Also, we construct an asymptotic expansion in the case of inconsistent initial and boundary conditions. Such mathematical problems can be used to describe real fluid flows produced by a sudden change in the tangent velocity at the outlet. In this case, the asymptotic solution includes a rapidly decaying component which describes the relaxation of the initial discontinuity. It is interesting that, in general, the inconsistency in initial and boundary conditions at the outlet results in the appearance of a boundary layer at the inlet in  $O(\nu)$  and higher order terms, which is in sharp contrast with the case of consistent initial and boundary conditions where there is no boundary layer at the inlet in all orders of the asymptotic expansion. In both cases, to verify the validity of the expansion, a number of simple examples are presented. The examples demonstrate that asymptotic solutions are in quite good agreement with exact or numerical solutions<sup>1</sup>.

---

\*Department of Mathematics, University of York.

<sup>1</sup>K. Ilin, *Eur. J. Mech. B/Fluids*, doi:10.1016/j.euromechflu.2007.10.003 (2007).

## Statistics of the interaction of the isotropic turbulent fields

D.Tordella\*, M.Iovieno\*

The interaction of two isotropic turbulent fields of equal integral scale but different kinetic energy is the simplest kind of inhomogeneous turbulent field. Numerical experiments show that the presence of a turbulent energy gradient is sufficient for the appearance of intermittency and open the way to the hypothesis that the presence of a gradient of turbulent energy is the minimal requirement for Gaussian departure in turbulence<sup>1</sup>. Two time decaying isotropic fields of kinetic energies  $E_1$  and  $E_2$  initially match over a narrow region<sup>1,2,3</sup>. Within this region the kinetic energy varies as a hyperbolic tangent. The following temporal evolution produces a shearless mixing.

In this work the anisotropy and intermittency of velocity and velocity derivative statistics is observed (the  $Re_\lambda$  of the high turbulent energy field is 45). The asymptotic behavior as a function of the ratio  $E_1/E_2 \rightarrow \infty$  is observed. This limit corresponds to the maximum observable turbulent energy gradient for a given  $E_1$  and is obtained through the limit  $E_2 \rightarrow 0$ . Within the mixing the intermittency is very high. The asymptotic values with respect to the ratio of the turbulent energies are nearly equal to 2.3 for the velocity skewness and to 11 for the velocity kurtosis. These values rise to -5 and 55 for the longitudinal velocity derivative skewness and kurtosis, respectively, which indicates a high intermittency on the small scales. Anisotropy was found to be mild for the velocity second order moments. On the contrary it was very intense in third order velocity moments (0.55 in the mixing direction, 0.225 in the normal directions, i.e. 5/9, 2/9, 2/9). The anisotropy observed through the third and fourth order moments of the velocity derivatives (longitudinal and transverse) also shows an horizontal asymptote in the limit  $E_1/E_2 \rightarrow \infty$ . However in this case the anisotropy is milder, see the figure below. The values are: 0.428 in the mixing direction, 0.286 in the normal directions (i.e. 3/7, 2/7, 2/7). At the small scales level the anisotropy is damped to nearly the 60% of that observed at the larger scales.

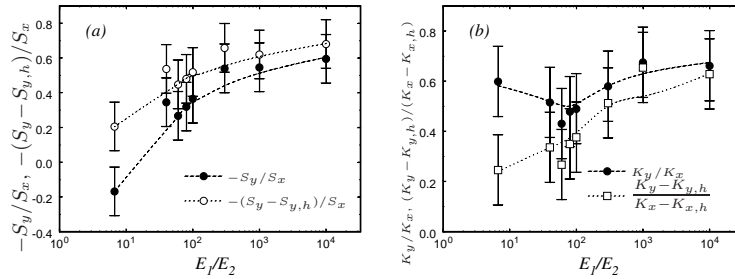


Figure 1: Ratios of the transversal and longitudinal normalized velocity derivative moments versus the energy ratio within the mixing: (a) derivative skewness; (b) derivative kurtosis. The bars represent the amplitude of the fluctuations of these ratios.  $S_{y,h}$ ,  $K_{x,h}$  and  $K_{y,h}$  are the values of  $S_y$ ,  $K_x$  and  $K_y$  in the homogeneous regions external to the mixing, initially equal to -0.4, 3.61 and 3.53, see ref.1.

\*Dipartimento di Ingegneria Aeronautica e Spaziale, Politecnico di Torino.

<sup>1</sup>Tordella et al., *Phys. Rev. E* **77**, 016309 (2008)

<sup>2</sup>S.Veeravalli, Z.Warhaft, *J. Fluid Mech.* **207**, 191 (1989).

<sup>3</sup>D.Tordella, M.Iovieno, *J. Fluid Mech* **549**, 441 (2006).

**Shear zones and wall slip in the capillary flow of concentrated colloidal suspensions**

Lucio Isa<sup>1</sup>, Rut Besseling<sup>1</sup> and Wilson C K Poon<sup>1</sup>

We image the flow of a nearly random close packed, hard-sphere colloidal suspension (a 'paste') in a square capillary using confocal microscopy. The flow consists of a 'plug' in the center while shear occurs localized adjacent to the channel walls, reminiscent of yield-stress fluid behavior. However, the observed scaling of the velocity profiles with the flow rate strongly contrasts yield-stress fluid predictions. Instead, the velocity profiles can be captured by a theory of stress fluctuations originally developed for chute flow of dry granular media [1]. We verified this both for smooth and rough walls. Moreover we present results for different channel sizes which help highlight the difference between the behavior of colloidal systems and dry grains.

[1] L Isa, R Besseling and W C K Poon, "Shear Zones and Wall Slip in the Capillary Flow of Concentrated Colloidal Suspensions", Physical Review Letters 98, 198305 (2007)

---

<sup>1</sup> SUPA & School of Physics, The University of Edinburgh, James Clerk Maxwell Building, The Kings Buildings, Mayfield Road, Edinburgh EH9 3JZ, UK

## A bifurcation study for large-scale motion in channel flow

Tomoaki Itano,\* Sadayoshi Toh,<sup>†</sup> Kai Sato<sup>‡</sup> and Sotos C. Generalis<sup>‡</sup>

Coherence in turbulent shear flows has attracted much attention of investigators for the last decades. The recent numerical studies based on bifurcation analysis<sup>1 2</sup> have been providing convincing evidence for the relevance of the coherence to unstable and finite-amplitude equilibrium states represented by travelling wave and periodic solutions. In the previous studies, the bifurcation analysis is however carried out mostly by imposing a few symmetries on a solution, which could restrict the range of our investigation.

Here, we will present an interesting case in which the alternation of a symmetry enables us to pursue for an unexplored and important class of coherent structures. The solution of channel flow obtained by Waleffe<sup>3</sup> is known to contain coherent structures typical in the near-wall region of turbulent channel flow, that is, a low-speed streaky structure and a couple of vortical structures. However, the reflection symmetry on the channel mid-plane prevents the solution from representing coherent structures possibly developing over the channel mid-plane, which have been actually reported in experiments, for example, “large-scale motion”<sup>4 5</sup>. Searching for travelling wave solutions in channel flow by adopting “upside-down reflection with spanwise shift” as an alternative symmetry, we obtained a nontrivial solution.

The bifurcation diagram of the obtained solution in the  $(c_x, Re_p)$  space is shown in figure (a) below, where  $c_x$  is the streamwise phase speed of the solution normalized by the laminar midplane velocity. The travelling wave solution previously obtained in Ref.3 is also calculated, which is shown as a reference by a dashed curve in the figure.

\*Faculty of Engineering Science, Kansai University.

<sup>†</sup>Department of Physics and Astronomy, Graduate School of Science, Kyoto University.

<sup>‡</sup>Division of Chemical Engineering and Applied Chemistry, Aston University.

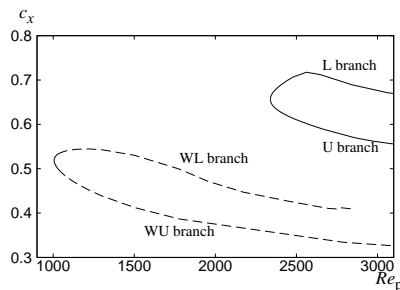
<sup>1</sup>H. Wedin and R. R. Kerswell, *J. Fluid Mech.* **508**, 333 (2004)

<sup>2</sup>J. Wang et al. *Phys. Rev. Lett.* **98**, 204501 (2007)

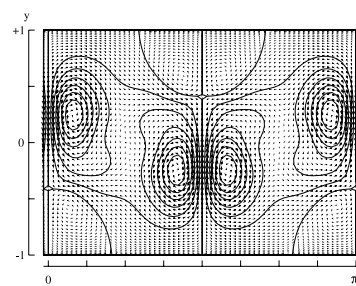
<sup>3</sup>F. Waleffe, *Phys. Rev. Lett.* **81**, 4140 (1998)

<sup>4</sup>R. J. Adrian, *Phys. Fluids* **19**, 41301 (2007)

<sup>5</sup>S. Toh and T. Itano, *J. Fluid Mech.* **524**, 249 (2005)



(a) The bifurcation diagram for our solution at the streamwise and spanwise wavelengths,  $(\alpha, \gamma) = (2, 2)$ .



(b) The cross-sectional view of the streamwise-independent component of streamwise vortices of our solution at  $Re_p = 2400$  and  $(\alpha, \gamma) = (2, 2)$ .

## Nonlinear thresholds of development of unsteady Görtler vortices. Experiment and theory.

A.V. Ivanov<sup>a</sup>, A.V. Boiko<sup>a</sup>, Y.S. Kachanov<sup>a</sup> and D.A. Mischenko<sup>a</sup>

Görtler instability represents one of not enough studied phenomena of the laminar-turbulent transition problem. Until now, mainly steady Görtler vortices are investigated, especially at linear stages of their evolution, while unsteady Görtler-instability plays also important role in practical applications. Moreover, the applicability of linear stability theory to description of experimental results remained often opened, since their amplitudes were very large (up to 10% and more). This problem is aggravated by low accuracy of steady-mode measurements associated with: (i) strong wall-normal mean-velocity gradients at a restricted accuracy of maintenance of the wall-normal probe positioning and (ii) an influence of the disturbance-source near-field effects (the non-modal, transient-growth effects).

New experimental and theoretical approaches developed recently gave us the possibility to overcome all these problems and to obtain reliably *all* characteristics of *linear* Görtler instability of a boundary layer on concave wall<sup>1</sup>. In particular, a very good quantitative agreement between experimental and theoretical disturbance amplification rates was obtained for the first time for steady Görtler vortices as well as for essentially unsteady ones. As far as the linear behaviour has been established reliably, a study of nonlinear thresholds of evolution of these modes becomes possible. Such investigation is carried out experimentally and theoretically. The main goal of the present work was to apply the approaches mentioned above to investigation of weakly nonlinear effects of development of boundary-layer perturbations belonging to the first (most unstable) Görtler mode in both steady (at quasi-steady approach) and unsteady cases. An example of amplitude dependence of streamwise behaviour of the fundamental Görtler mode and its second harmonic is illustrated in Fig. 1 for one of studied regimes.

This work is supported by the Russian Foundation for Basic Research (grant N 06-01-00519).

<sup>a</sup> Institute of Theoretical and Applied Mechanics of Siberian Branch of Russian Academy of Sciences.

<sup>1</sup> Boiko A.V. et al. *Proc. XIII Intl Conf. Methods Aerophysical Research, Part III.* – Novosibirsk: “Parallel”, 2007, p. 33–38.

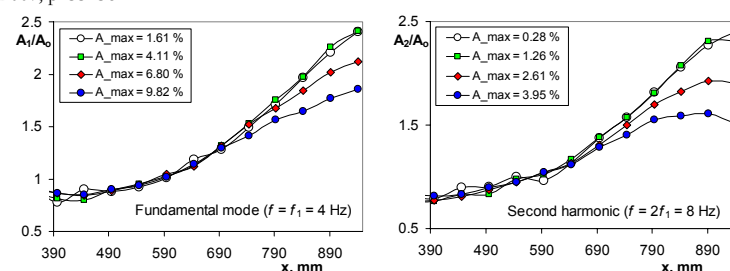


Figure 1: Nonlinear evolution of fundamental Görtler-vortex mode (a) and its second harmonic (b).

## Backward-facing step flow applied to transverse current flow on ship hulls in shallow water

Ken-Robert G. Jakobsen\*, Bjørnar Pettersen\*, Helge I. Andersson†

The focus of the presented work is motivated by phenomena exhibiting in transverse current flow on ship hulls, or vessels in transverse motion in shallow water. Naturally, there are many different aspects concerning such a topic. One example is *squat*. Squat is frequently studied due to its potential danger when a ship travels at forward speed in the vicinity of a seabed or a canal wall. It is defined as the maximum sinkage and trim along the ship's keel. This is a well-known effect caused by a pressure drop on the bottom of the vessel due to the accelerated water from the passing hull. As a result, the hull experiences an increased resistance in terms of hydrodynamic forces and moments, which can severely deteriorate the manoeuvrability of the ship. In order to study the viscous aspect of this, we are however limiting the problem to transverse flow only. There have been numerous experimental and numerical investigations to find hydrodynamic forces on ship sections subjected to transverse current, but the topics of interest in the current work are the details in the viscous flow itself rather than overall drag coefficients. We focus on only a small part of the section close to the bilge area illustrated by the dashed quadrate in figure 1, and several simplifications of the transverse flow have to be introduced to come down to a feasible case for numerical investigation. In this sense and due to its popularity in the literature, we have used the backward-facing<sup>1</sup> step as starting point for our calculations. To further approach the flow configuration in figure 1, a step with a rounded edge, the so-called smoothly-contoured ramp (SCR), is investigated. Very little work is done on the latter, apart from a few experimental and numerical investigations where the rounded edge is only a small part of a quarter circle<sup>23</sup>. Thus, the SCR is the main focus of the presented work. The Spalart-Allmaras one-equation turbulence model<sup>4</sup> is used for the flow modeling. Here, the Reynolds stress tensor in the 2D RANS equations is closed by solving a single transport equation for the turbulent eddy viscosity. Further work will also include 3D calculations using the Spalart-Allmaras model (URANS).

\*Department of Marine Technology, Norwegian University of Science and Technology (NTNU).

†Department of Energy and Process Engineering, NTNU.

<sup>1</sup>Driver and Seegmiller, *AIAA Journal* **23**, 163 (1985).

<sup>2</sup>Song et al., *Int. J. of Heat and Fluid Flow* **21**, 512 (2000).

<sup>3</sup>Wasistho and Squires, *2nd Int. Symp. on Turbulence and Shear Flow Phenomena* **3**, 405 (2001).

<sup>4</sup>Spalart and Allmaras, *La Recherche Aerospatiale (1)* **1**, 5 (1994).

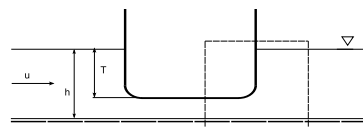


Figure 1: Transverse current flow on a ship section. The area of interest is illustrated by the dashed quadrate.



## Shear-driven two and three-dimensional capillary-gravity waves in a horizontally oscillating two-liquid flow

Shreyas V. Jalikop\*, Anne Juel\*

When a closed vessel containing two stably stratified, immiscible liquids is oscillated sinusoidally in the horizontal direction, the flat interface between the two liquids loses stability to two-dimensional ‘frozen waves’ through a mechanism analogous to that of the Kelvin–Helmholtz instability<sup>12</sup>. The onset of ‘frozen waves’ occurs through a supercritical pitchfork bifurcation, but for larger values of the forcing parameters, a qualitative change in the wave growth takes place. In terms of the vibrational Froude number,  $W$  (ratio of vibrational to gravity forces, proportional to the square of the forcing velocity), there is a critical value,  $W_c$ , beyond which the experimental data collapses onto a single curve that exhibits a linear dependence on  $W$ . We find that this collapse is indicative of a bifurcation to an inviscid solution at  $W_c$ . Our investigation of the evolution of the interface shape suggests that this second bifurcation is associated with a transition from gravity to capillary dominated waves, which is consistent with the wavelength reaching a minimum for  $W = W_c$ . For larger values of the forcing parameters, the two-dimensional array of waves becomes unstable to three-dimensional oscillatory waves through a sub-critical bifurcation. The response frequency of the three-dimensional oscillatory waves is found to be locked to the forcing frequency. Secondary transition to three-dimensional waves underpin the dynamics of a variety of fluid flows, e.g. the oscillatory instability of rolls in thermal convection and the formation of streamwise vortices in mixing layers. We characterise the secondary instability of our oscillating interface by comparison with these systems and discuss the physical mechanism that leads to the onset of three-dimensional waves.

---

\*Manchester Centre for Nonlinear Dynamics and School of Mathematics, University of Manchester.

<sup>1</sup>E.Talib, S.V. Jalikop & A. Juel, *J. Fluid Mech.* **584**, 45 (2007).

<sup>2</sup>E.Talib & A. Juel, *Phys. Fluids* **19**, 092102 (2007).

## History-dependent cell and microbead adhesion under varying shear

O.E. Jensen\*, S.Reboux\* & G. Richardson\*

Cell adhesion to surfaces via specific receptor-ligand bonds is central to the inflammatory response. Motivated by this and related applications, we consider a simple theoretical model of a cell or microbead adhering to a plane surface under the influence of an external shear flow (figure 1). The cell is modelled either as a rigid cylinder (in 2D) or a sphere (in 3D). Adhesion forces arise through intermolecular bonds between receptors on the wall and their ligands on the cell, which form flexible tethers that can stretch and tilt as the base of the cell moves past the wall. Binding kinetics is assumed to follow a standard model for slip bonds. By introducing a finite resistance to bond tilting, we use the model to explore the territory between previous theoretical models that allow either for zero or infinite resistance to bond rotation.

A microscale calculation (for two sliding plates) reveals a nonlinear force-speed relation arising from bond formation, tilting and breakage. This model is then coupled to a macroscale model of the cell or microbead in shear flow.

In 2D, modelling the cell as a cylinder and assuming binding kinetics is rapid in comparison to typical flow transit times, two distinct types of cell motion are predicted. Either bonds adhere strongly and the cell rolls (or tank treads) over the wall without slipping, or the cell moves near its free-stream speed with bonds providing weak frictional resistance to sliding. The model predicts bistability between these two states, implying that at critical shear rates the system can switch abruptly between rolling and free sliding.<sup>1</sup>

In 3D, modelling the cell as a sphere and accounting for non-equilibrium binding kinetics, a third state is identified in which the cell is almost completely arrested. This arises because of the extended lifetime of tilted bonds at the rear of the cell, which can exert a torque not present in the 2D model. We identify conditions under which there are hysteretic transitions between all three states (firm arrest, rolling and free sliding). We discuss the relevance of these findings to experimental observations of history-dependent cell and microbead adhesion under varying shear.

\*School of Mathematical Sciences, University of Nottingham

<sup>1</sup>Reboux et al. *Proc. R. Soc. A* **464**, 447 (2008).

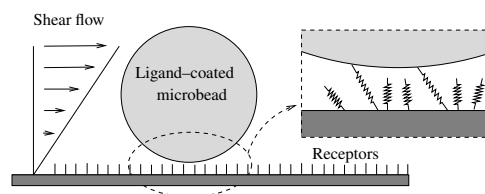


Figure 1: A ligand-coated bead or cell moving in a shear flow past an array of bonds that can stretch and tilt.

## A receptivity approach to predicting boundary layer transition.

Mark W. Johnson<sup>a</sup>

Accurate prediction of transition has become a pacing item in the development of CFD in many engineering applications (e.g. gas turbine blades and helicopter rotors). Current methods have limited accuracy as they rely on empirical correlations for 2-d (usually flat plate) boundary layers and hence the real effects on transition of typical 3-d engineering geometries are ignored. The objective of current work by the author is to obtain a fuller understanding of the flow processes leading to bypass transition and to use this knowledge to develop a more generic approach to transition prediction.

In this paper a CFD procedure is presented for predicting the response of a laminar boundary layer to freestream turbulence. Freestream turbulence can be considered as a collection of perturbation waves of varying wavelength and orientation. The boundary layer response to waves with a single wavelength and orientation is considered and hence the wave forms with the highest receptivity, which therefore dominate the transition process, are identified. The results show that the boundary layer is most receptive to wave forms which have long streamwise wavelengths ( $20-100 \delta$ ), but much lower cross stream spatial wavelengths ( $1-2 \delta$ ). Mirror sets of such waves, which constitute an array of streamwise vortices in the freestream, lead to the streamwise streaky structures (Figure 1) frequently observed in transition experiments.

The paper concludes with a discussion of how receptivity methods can be implemented within current CFD codes to improve 3-d boundary layer transition prediction.

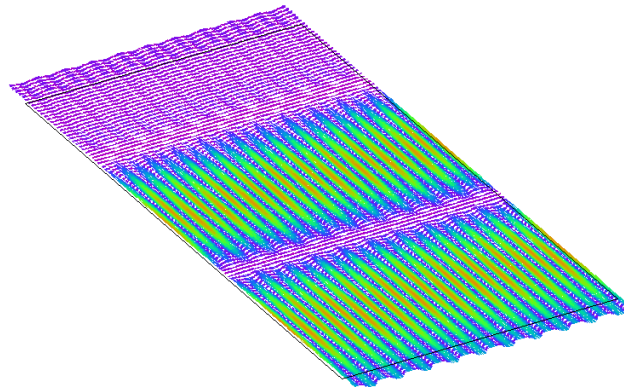


Figure 1: Streaky structures (velocity vectors).

---

<sup>a</sup> Department of Engineering, University of Liverpool, UK.

## Anomalous bubble propagation in elastic tubes

Anne Juel\*, Alexandra Heap\*

We present an experimental study of the reopening mechanics of a liquid-filled elastic tube in the limit of strong initial collapse<sup>1</sup>. The experiment is a simple mechanical model of pulmonary airway reopening<sup>2</sup>. The level of collapse is measured in terms of the collapsed cross-sectional area relative to its undeformed value,  $A/A_0$ , which decreases as the level of collapse is raised. For moderate levels of collapse, where the facing boundaries of the tube are not in contact,  $A/A_0 > (A/A_0)_{\text{owc}}$ , the propagating bubbles are consistently parabolic-tipped and symmetric about the vertical centre-plane of the tube. When the tube is collapsed more strongly so that opposite wall contact occurs,  $A/A_0 \leq (A/A_0)_{\text{owc}}$ , novel bubble shapes are observed, including asymmetric, double-tipped and pointed bubbles. These three bubble types appear to be generic, but further combinations are found for the strongest levels of collapse, where pointed bubbles appear at the tips of a double-tipped bubble. The asymmetric bubble occurs for low values of the capillary number,  $Ca$  (dimensionless bubble speed), and/or limited collapse beyond the first point of opposite wall contact. As  $Ca$  and/or the level of collapse are increased (i.e.  $A/A_0$  decreases), successive bifurcations are observed to double-tipped and pointed bubbles, which appear to be disconnected states. We investigate and discuss the physical origin of these anomalous bubbles in terms of the balance between surface tension, viscous and elastic forces, as well as the strongly non-uniform geometry of the cross-section of the tube. Whereas the pressure varies continuously at the transition between the asymmetric and double-tipped bubbles, the pointed bubble lies on a disconnected, lower pressure branch, and exhibits a pressure gap that depends on  $A/A_0$ . This state could be of relevance in the lung, where it is essential to reopen airways quickly without incurring damage.

---

\*Manchester Centre for Nonlinear Dynamics and School of Mathematics, University of Manchester.

<sup>1</sup>A. Heap, PhD Dissertation, University of Manchester (2008).

<sup>2</sup>A. Juel & A. Heap, *J. Fluid Mech.* **572**, 287 (2007).

## Dipole-wall collision in a shallow fluid layer

L.P.J. Kamp\*, A.R. Cieřlik\*, H.J.H. Clercx\* and G.J.F. van Heijst\*

Recent experimental studies of freely evolving quasi-two-dimensional dipolar vortices in shallow fluid layers have revealed complex three-dimensional (3D) flows, including strong frontal recirculations<sup>1,2</sup>. In this contribution we address the collision of such a dipole with a vertical no-slip wall, and the subsequent rebound from the wall. Stereoscopic-PIV (SPIV) has been used to measure the 3D velocity field at a few different horizontal levels. Using a finite element code the electromagnetic generation and evolution of the dipolar flow has been simulated for various fluid-layer depths. These 3D simulations provide details of the distribution of horizontal vorticity that cannot be extracted from the SPIV measurements in the current set-up.

We show that the dipole-wall collision and rebound is not only strongly determined by vertical vorticity production at the no-slip wall, well-known from classical 2D dipole-wall collisions<sup>3</sup>, but also by stretching and squeezing of horizontal vortex tubes.

The experimental results show indeed an increasingly complex vertical structure as the dipole approaches the no-slip wall, both in the vortex cores and the frontal recirculation. It has been found that during the collision vertical velocities increase irrespective of the fluid-layer thickness, a signature of the special role of the frontal recirculation: the horizontal vortex tubes seem to be stretched and squeezed.

The numerically obtained velocity fields at different horizontal levels agree with the SPIV results, although increasing discrepancies are observed just before and during impact of the dipole with the sidewall. These may be attributed to free-surface deformations in the experiments which are not accounted for in the simulations. Vertical snapshots of the velocity field (see fig. 1) confirm the role of stretching and squeezing of the horizontal vortex tubes during the dipole-wall collision.

\*J.M. Burgerscentre and Fluid Dynamics Laboratory, Dept. of Applied Physics, Eindhoven University of Technology, P.O. Box 513, 5600 MB Eindhoven, The Netherlands.

<sup>1</sup>D. Sous et al., *Phys. Fluids* **16**, 2886 (2004).

<sup>2</sup>R.A.D. Akkermans et al., *Europhys. Lett.* submitted.

<sup>3</sup>P. Orlandi, *Phys. Fluids A* **2**, 1429 (1990).

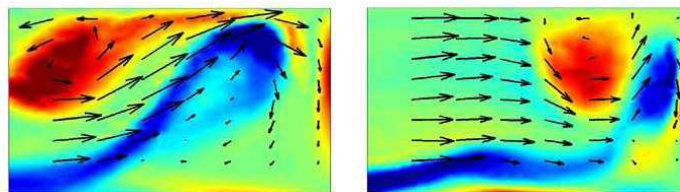


Figure 1: Snapshots of the horizontal component of the vorticity parallel to the wall in the vertical symmetry plane (perpendicular to the wall) of the dipole, obtained from simulations of the dipole-wall collision just before (left panel) and during (right panel) the collision. Colors represent the magnitude of the vorticity component, while the arrows represent the velocity field in the cross-sectional plane.

## Vortex rings in a viscous fluid: Asymptotic theory and numerical simulations

F. Kaplanski\*, Y. Fukumoto†, S.S. Sazhin‡

Extending the earlier study<sup>1</sup>, an initial value problem for an axisymmetric vortex ring in a viscous fluid was solved based on the linearised equation for vorticity<sup>2</sup>. The substitution of the vorticity and streamfunction, obtained from this solution, into the Helmholtz-Lamb transformation formula enabled us to obtain analytically the vortex-ring translational velocity, as the velocity of the vorticity centroid. The validity of this procedure was proven in reference<sup>3</sup>. By asymptotic analyses, the leading-order terms of the short- and long-time expansions for the obtained translational velocity and the kinetic energy are shown to coincide with Saffman's and Rott-Cantwell formulae, respectively<sup>4</sup>. Moreover, our velocity formula well compares with the Saffman's second formula<sup>4</sup> (taking into account the effects of non-constant ring's radius) and available experimental data. The form of the velocity formula is not very sensitive on the Reynolds number. In the present study, the vortex-ring evolution is simulated numerically taking into account the nonlinear terms, assuming the initial linear vorticity distribution. It is shown that the vorticity structure moves and extends depending on the Reynolds number. This leads to a noticeable difference of vorticity distribution, predicted by the numerical analysis, in comparison with the one predicted based on the linear approximation (see Fig 1(a)). However, the velocity and the energy do not exhibit considerable difference (see for example Fig1(b)). These results are applied to the modeling of laminar vortex-ring formation.

\*Tallinn University of Technology, Estonia

†Kyushu University, Japan

‡The University of Brighton, UK

<sup>1</sup>Kaplanski and Rudi, *Phys. Fluids* **17**, 087101 (2005).

<sup>2</sup>Fukumoto and Kaplanski, *Phys. Fluids*, Submitted for publication (2007).

<sup>3</sup>Rott and Cantwell, *Phys. Fluids* **A5**, 1443 (1993).

<sup>4</sup>Saffman, *Stud. Appl. Math.* **449**, 371 (1970).

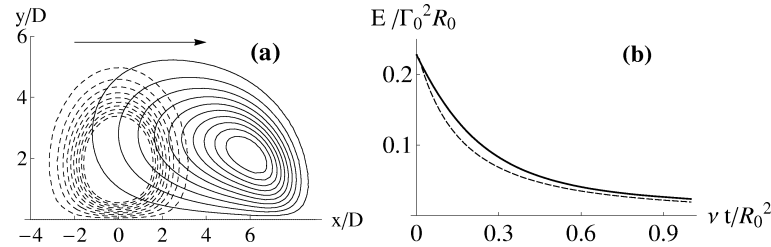


Figure 1: (a) Contours of vorticity distribution at  $\nu t/R_0^2 = 0.7$  for Reynolds number  $Re=1500$  and ring's thickness equal to 2. The arrow shows the direction of the vortex ring's movement. (b) Normalised kinetic energy versus time. Results obtained with and without nonlinear terms are shown by solid and dashed curves, respectively.

## Gravity currents near the temperature of maximum density

Anthony Kay\*, David Leppinen†

We consider lock-exchange flows of fresh water, in which the water in the lock is above the temperature of maximum density ( $T_{md} \approx 4^\circ\text{C}$ ), while the receiving water is below  $T_{md}$ . If the lock water is warm enough to be positively buoyant, it forms a gravity current along the upper surface of the receiving water, which may be either a free surface or a no-slip lid. Mixing near the head of the current then creates water closer to  $T_{md}$  than either of the unmixed waters. This dense water then descends in plumes, thus eroding the gravity current. Eventually, the current is completely starved of warm water, so cannot proceed beyond a final “run-out distance”.

The gravity currents proceed similarly to currents without maximum-density effects for a considerable time, and then slow down rather abruptly as they approach their final extent. We have determined how this run-out distance depends on the initial temperatures. Our experiments are supported by numerical simulations, although run-out distances tend to be slightly longer in the numerical simulations, possibly because of unavoidable initial mixing when the lock-gate is withdrawn in the experimental tank.

---

\*Department of Mathematical Sciences, Loughborough University.

†School of Mathematics, University of Birmingham.

**Simulation of flow in an idealised thoracic aorta:  
Influence of flow parameters on wall shear stress patterns  
and its relation to atherosclerotic lesions**

A. Kazakidi\*, P. Weinberg\* and S. Sherwin\*

Blood flow in the thoracic aorta near side branches is computed using high-order unstructured spectral/*hp* element methods. The objective is to study the role of different haemodynamic parameters in the localization of atherosclerosis. The patchy distribution of atherosclerosis in regions of arterial curvature and branching is consistent with haemodynamic stresses exerting a controlling influence on its rate of development. Patterns of lesion prevalence around the origins of intercostal arteries in the thoracic aorta are known to vary with age and species. We test the hypothesis that these variations could reflect differences in the pattern of shear stress exerted on the wall by the flow of blood.

The emergence of an intercostal artery from the aorta, which has a 10-fold larger diameter, is modelled as a cylindrical tube emerging perpendicularly from a flat plate (figure 1a); the idealised geometry simplifies interpretation of effects of the Reynolds number and side branch flow rate. Using the Newtonian incompressible Navier-Stokes equations, steady and pulsatile flow computations are performed and flow and wall shear stress (wss) patterns are analysed. In addition, the study is extended to examine flows in more realistic geometries, such as paired intercostal arteries and geometries approximating those seen in histological sections and corrosion casts.

This study shows that patterns of flow and wss are strikingly dependent on haemodynamic conditions. Both the Reynolds number and the side branch flow rate alter the wss distribution in steady flow (figure 1b). With increasing Reynolds number, stresses are lowered at the sides of the branch ostium and increased upstream and downstream. Increased flow into the side branch moves the low-shear side lobes and stagnation region downstream. Under unsteady flow conditions and for non-reversing side branch flow, the effect of pulsatility is small. However, significantly different wss patterns are generated when the side branch flow is made to reverse for part of the cycle. Arterial geometrical features appear to have little influence on the wall shear stress pattern. Aspects of the patterns observed in this study correlate well with, and may explain, lesion patterns seen in human, rabbit and mouse aortas.

\*Departments of Aeronautics and Bioengineering, Imperial College London.

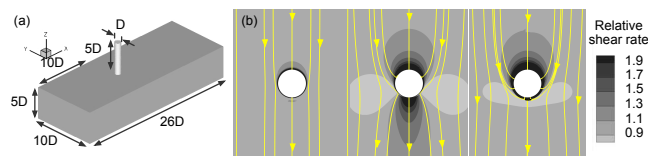


Figure 1: (a) Model of intercostal artery. (b) Wall shear stress maps.



### 3D Euler Circulation about a 2D Symmetry Plane

Robert M. Kerr\*, Miguel D. Bustamante\*

Results from new calculations of interacting anti-parallel Euler vortices are presented with the objective of understanding the origins of singular scaling in early calculations<sup>1,2</sup> and the lack thereof more recently<sup>3</sup>. Core profiles designed to reproduce the two results are presented and more robust analysis is proposed. Circulation conservation is introduced as a criteria for numerical convergence and compared with classical resolution studies and spectral convergence tests. Most of the analysis is on a  $1024 \times 256 \times 2048$  mesh. The particular core profile<sup>3</sup> combined with the hyperviscous filter violates circulation conservation at early times. If there is a finite-time singularity with enstrophy growth like  $\Omega \sim (T_c - t)^{-\gamma_\Omega}$  and vorticity growth like  $\|\omega\|_\infty \sim (T_c - t)^{-\gamma}$ , the new analysis would then support  $\gamma_\Omega \approx 1/2$  and  $\gamma > 1$ . These represent modifications of earlier conclusions<sup>1,2</sup>. In particular, it suggests that circulation in the symmetry plane is preserved within the collapsing structure. Figure 1 shows the full 3D structure at an early time and figure 2 shows the structure in the symmetry plane at a later time to demonstrate the degree to which the circulation remains concentrated, which will be further demonstrated by scaling analysis.

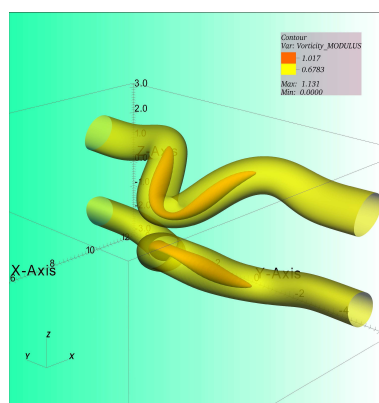


Figure 1: Isosurfaces of vorticity at  $t = 2.51$ . Half of the domain in the vertical  $z = -\pi$  to  $\pi$  is shown. Yellow corresponds to  $|\omega| = 0.6 \sup |\omega|$ . Orange corresponds to  $|\omega| = 0.9 \sup |\omega|$ .

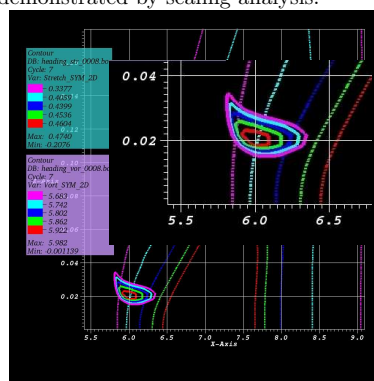


Figure 2: Contours of the deformed vortex core in the symmetry plane ( $y = 0$ ) are superposed on top of contours of the stretching out of the plane at  $t = 7.5$ . The inset is a blow-up of the left-bottom corner. Vertical domain is  $z = 0 - 0.18$ .

\*Department of Mathematics, University of Warwick.

<sup>1</sup>R.M. Kerr, *Phys. Fluids* **5**, 1725 (1993).

<sup>2</sup>R.M. Kerr, *Phys. Fluids* **17**, 075103 (2005).

<sup>3</sup>T.Y. Hou & R. Li, *J. Nonlin. Sci* **16**, 639 (2006).

## Investigation of the three-dimensional flow field around an artificial owl wing

Stephan Klän\*, Thomas Bachmann†, Hermann Wagner† and Wolfgang Schröder\*

Noise generation and propagation is one of the major problems in the vicinity of airports. Therefore, flying silently will require further efforts to sufficiently reduce aircraft noise in the future. That is, more research is necessary on the aerodynamic mechanisms generating noise. A good biological example for silent flight is the owl. Therefore, the flow field over a novel airfoil, the shape of which is related to that of an owl wing, is investigated to understand the aerodynamic mechanisms effecting the suppression of noise generation.

Special structures on the owl wing have been identified<sup>1</sup>, including the geometry of the wing, velvet-like upper surface of the wing feathers, and the leading edge serrations. To construct an artificial owl wing for wind tunnel tests, dead barn owls have been prepared under approximated gliding flight conditions. Three-dimensional surface scans of wings of several barn owls have been performed to obtain digital models. Using mathematical algorithms<sup>2</sup>, a quasi-2D and a fully three-dimensional wing model for wind tunnel tests have been developed.

One special feature of the owl wing is the velvet-like surface. The influence of structured surfaces on the surrounding flow has intensively been studied before. The most famous example is probably based on the impact of riblets on the flow field, the geometry of which is related to the skin of sharks. Drag reduction due to special surface structures could be shown by several researchers<sup>3</sup>. First measurements showed the flow field of the quasi-2D wing model and the influence of the velvet-like surface on the flow structures (fig. 1). Using three-component particle-image velocimetry, the three-dimensional flow field of the artificial owl wing will be recorded. Thereafter, the wing will be equipped with a surface structure similar to the owl feathers and its influence on the flow field will be analyzed. The change in the three-dimensional flow field and the influence on the vortex structures will be scrutinized and the impact on the overall aerodynamic performance will be discussed.

\*Institute of Aerodynamics, RWTH Aachen University.

†Institute of Biology II, RWTH Aachen University

<sup>1</sup>Graham, *J. R. Aeronaut. Soc.* **38**, 837 (1934)

<sup>2</sup>Liu et al., *AIAA Journal* **44**, 954 (2004)

<sup>3</sup>Bechert et al., *J. Fluid Mech.* **338**, 59 (1997)

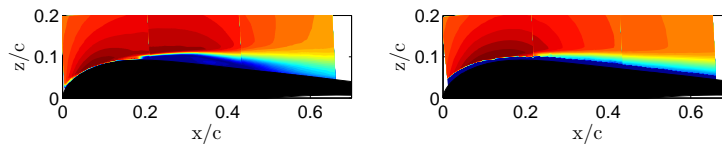


Figure 1: Velocity field at  $Re_c = 60,000$  and  $\alpha = 3^\circ$  for the clean surface (left) and the modified surface (right) of the quasi-2D wing.

### Riblet surfaces in turbulent evolving boundary layers

S.Klumpp\*, M.Meinke\* and W.Schröder\*

Surface structures, so-called riblets, which were inspired by shark skin, consist of tiny grooves aligned with the main flow direction. Numerical<sup>1</sup> and experimental<sup>2</sup> investigations confirm the potential of the riblet structure to reduce friction drag in turbulent flows if the riblet spacing  $s^+$  in wall units remains in a certain range, where a varying  $s^+$  from the optimum means less drag reduction and at a certain point even drag increase compared to clean surface. Even though the drag reduction capability is well known until now only very few investigations concerning practical applications, i.e., the flow over compressor blades of gas turbines or airplane wings, were performed. The current work investigates the transfer of the basic concept of drag reduction by riblets to technical applications with a special focus on reducing the drag under the condition of an evolving boundary layer while preserving the surface structure's feasibility. The chosen basic geometry consists of blunt riblets whose feasibility was already shown<sup>3</sup>. It will be shown in this work by a numerical analysis of a fully developed turbulent channel flow with one clean and one riblet wall that the new surface has a drag reducing capability of about 5%.

Due to evolving boundary layers along the surfaces of technical applications, which cause a locally changing flow state, the physical riblet spacing must be adapted in order to preserve the non dimensional riblet spacing. Since manufacturing an optimum adaption, at which the physical riblet spacing is continuously adapted to the local flow state to achieve a maximum drag reduction at every point, is extremely difficult the drag reduction potential of stepwise changing riblets is investigated. In this way the local  $s^+$  remains near the optimum along the entire surface and the manufacturing is extremely simplified. Due to discontinuous transitions in the riblet scales extra drag occurs even when well shaped transitions are considered. To determine the stepwise riblet spacings' optimum distribution the extra drag of each transition must be known. Therefore, two large-eddy simulations (LES) of a spacing transition are performed with a respective spacing ratio of 2.0 and 1.05. Using these data an estimate of the extra drag of a transition with arbitrary spacing ratio is given. Using these results a riblet distribution along the suction side of a CDA profile, which is a typical profile for compressor blades, is found. It will be evidenced that the achieved drag reduction is remarkably higher compared to the drag reduction of a surface with an optimal but constant physical riblet spacing. A detailed discussion of the physical reasons will be given.

---

\*Institute of Aerodynamics, RWTH Aachen University.

<sup>1</sup>Choi et al., *J. Fluid Mech.* **255**, 503 (1993).

<sup>2</sup>Bechert et al., *J. Fluid Mech.* **338**, 59 (1997).

<sup>3</sup>Klocke et al., *2nd ICNFT Bremen, Germany* (2007).

## Onset of instabilities in the wake of a fixed sphere in the mixed convection – configurations of assisting and opposing flow

Miroslav Kotouč\*, Gilles Bouchet\* and Jan Dušek\*

The scenario of axisymmetry breaking and transition to chaos in the wake of a fixed heated sphere immersed in a forced cold stream is investigated numerically for two configurations of the mixed convection problem – the assisting and opposing flow, in which buoyancy, respectively, adds to or acts against the forced stream (see Fig. 1 for the problem description). The study is carried out in a  $Ri - Re$  parameter plane ( $Ri = \pm \beta g(T_s - T_\infty)d/u_\infty^2$  and  $Re = u_\infty d/\nu$  being, respectively, the Richardson number and the Reynolds number) for a fixed value of Prandtl number  $Pr = \nu \rho c_p/\lambda = 0.72$  ( $\approx$  air). The positive value of  $Ri$  denotes, by consensus, assisting flows, whereas negative  $Ri$  stand for opposing flows. A linear stability analysis is employed to obtain the thresholds of the primary bifurcation, fully three-dimensional simulations are then carried out to investigate different steady and unsteady flow patterns, including chaotic flows.

It is shown that, for  $Ri > -0.13$ , the flow loses its axisymmetry via a regular bifurcation, whereas for  $Ri \leq -0.13$  via a Hopf bifurcation. The heating stabilizes the flow in the configuration of assisting flow (the critical Reynolds number  $Re_c$  of the onset of three-dimensionality increases with  $Ri$ ) and has the opposite effect in the opposing flow. For  $-0.07 \leq Ri \leq 0.2$ , the scenario of transition to turbulence for constant  $Ri$  and increasing  $Re$  is similar to that of a non-heated sphere (see e.g.<sup>1</sup>) and passes through four stages as illustrated in Fig. 2. For  $Ri \geq 0.3$  and higher Reynolds numbers ( $> 800$ ) a slow oscillation or rotation of the bifid wake (a in Fig. 2) has been evidenced. For  $Ri \leq -0.09$ , apart from two ordered regimes with planar symmetry (periodic and quasiperiodic vortex shedding with zero average lift), a rich variety of non-planar quasiperiodic three-dimensional regimes preceding the chaos, never reported so far, has been observed.

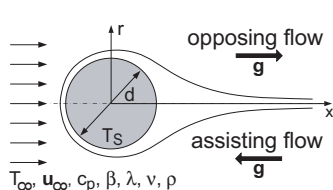


Figure 1: Problem description and coordinate system.

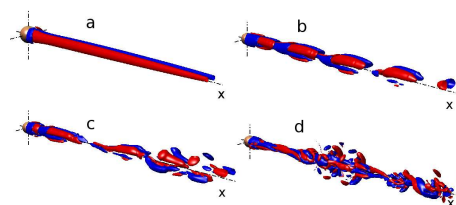


Figure 2: Isosurfaces of axial vorticity at a level  $\omega_x = \pm 0.1$  at  $Ri = 0.1$ : a) steady bifid wake with planar symmetry ( $Re = 300$ ), b) periodic vortex shedding ( $Re = 400$ ), c) quasiperiodic vortex shedding ( $Re = 550$ ), d) chaotic flow ( $Re = 800$ ).

\*Institut de Mécanique des Fluides et des Solides, UMR 7507 ULP/CNRS, 2 rue Boussingault, 67000 Strasbourg, France

<sup>1</sup>B. Ghidersa and J. Dušek, *J. Fluid Mech.*, **423**, 33 (2000).

## Low reynolds number instabilities induced in a channel with wavy walls

T.A. Kowalewski<sup>a</sup>, J. Szumbariski<sup>b</sup>, S. Błoński<sup>a</sup>

Enhancement of mixing in the laminar regime is of fundamental importance in numerous applications in microfluidics, biotechnology, medicine and heat transfer. Significant improvement of mass and/or heat transfer can be achieved only if sufficiently complex and time-dependent vortex structures are present. Such structures can be triggered by various geometric modifications (like wall waviness or the applications of surface-mounted obstacles), external forcing (like an oscillations of a driving pressure gradient) or the combination of both. Unfortunately, in most cases the mixing improvement is accompanied by large increase of hydraulic resistance.

The current work describes the mixing-enhancement method based on the idea of forced chaotic convection in the channel with appropriately shaped and transversely oriented wall waviness. The method is based on results of linear stability analysis of the simple, unidirectional flow in wavy channel<sup>1,2</sup>. It was shown that for properly tuned waviness geometry the channel flow can spontaneously loose stability at the Reynolds numbers as low as 60. The unstable mode of disturbances has the form of a vortex array, which travels downstream. The remarkable feature is that the most destabilizing waviness does not introduce any additional flow resistance.

Following this idea three- dimensional numerical simulations of viscous flow through wavy channel are performed both for the infinite flow domain (periodic boundary conditions) and for the channel bounded by side walls. The positive outcome of the numerical model gave us confidence to the theoretical predictions, necessary to design microchannel mixer.

Finally flow structures are investigated experimentally for laminar flow of water in a 70 mm long 33 mm wide and 0.7 mm high microchannel with 20 streamwise rows modulating one of the walls. Microscopic flow analysis using fluorescent tracers is used to identify emerging flow instabilities. Quantitative flow field evaluation is performed using micro-PIV technique. It appears that spanwise flow components can be identified for flow Reynolds number about 100. These flow disturbances are generated across the whole channel width interacting in a complex way with all 20 corrugations.

---

<sup>a</sup> IPPT PAN, Polish Academy of Sciences, Warsaw, Poland.

<sup>b</sup> Warsaw University of Technology, Poland

<sup>1</sup> J. Szumbariski, J.M. Floryan, *J. Fluid Mech.* **568**, 243 (2006).

<sup>2</sup> J. Szumbariski, *JTAM* **45**, 659 (2007).

## Lifetime of turbulence in pipe flow

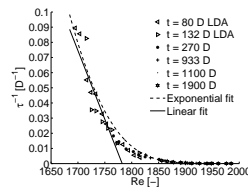
Dirk Jan Kuik\*, Björn Hoff†, Christian Poelma\* and Jerry Westerweel\*

Understanding the flow physics of pipe flow is one of the last unsolved problems in fluid mechanics. Especially the transition process from laminar to turbulent flow is unclear. Therefore Peixinho and Mullin<sup>1</sup> devised an experiment to investigate the reverse process: the relaminarisation of concentrated turbulent disturbances (puffs). In their experiments they found that the life times of puffs is proportional to  $(Re_c - Re)^{-1}$ . This implies that the lifetime of the disturbances diverge at a finite, critical, Reynolds number. Later A.P. Willis and R.R. Kerswell<sup>2</sup> confirmed this relation by direct numerical simulations. However experiments performed by B.Hof et. al<sup>3</sup> demonstrated that the life time of disturbances does not decay according to  $1/(Re_c - Re)$ , but rather exponentially. This implies that the lifetimes of turbulence does not diverge at a finite Reynolds number but remains a transient.

The present paper presents results from a new experiment to quantitatively determine the life time of puffs. For the investigation a 690 diameter long glass pipe was constructed with a diameter of 10 mm. The flow of water was gravity driven and passes a constriction before entering the pipe. This constriction causes a large pressure drop ensuring a constant mass flow independent of the flow state in the pipe. A carefully designed pipe entrance ensured a laminar flow beyond Reynolds number of  $9 \cdot 10^3$ . To measure the lifetimes of turbulent puffs the flow was disturbed by injecting fluid through a small port normal to the pipe wall. At different locations downstream of the disturbance the centerline velocity was measured as function of time by laser Doppler anemometry (LDA). The resulting velocity of all injected disturbances was recorded and a puff was considered to have survived if the turbulence intensity was above a certain threshold. The ratio of survived puffs over decayed puffs was determined at each location as function of Reynolds number. Figure 1 shows the life time of turbulent puffs determined from the ratio found, together with two fits. It is clear that the life times do not reach zero for a finite Reynolds number but approaches it asymptotically.

\*Laboratory for Aero &amp; Hydrodynamics, Delft University of Technology, The Netherlands.

†Max-Planck-Institut für Dynamik und Selbstorganisation, Göttingen, Germany.

<sup>1</sup>J. Peixinho & T. Mullin, *Phys. Rev. Lett.* **96**, 094501 (2006).<sup>2</sup>A.P. Willis & R.R. Kerswell, *Phys. Rev. Lett.* **98**, 014501 (2007).<sup>3</sup>B. Hof et al., *Nature* **443**, 59 (2006).Figure 1: Measured reciprocal life time  $\tau^{-1}$  as a function of Reynolds number

## DNS of Rotating Convection in a Cylinder

Rudie Kunnen<sup>\*</sup>, Bernard Geurts<sup>†\*</sup> and Herman Clercx<sup>\*†</sup>

The turbulent motion of a fluid driven by a destabilising temperature gradient working against gravity and modulated with rotation is relevant for many geophysical, astrophysical as well as industrial problems. We study turbulent rotating convection in a cylinder under axial rotation with direct numerical simulation (DNS). Our prime interest is the dependence on rotation-rate of the convective heat flux, in dimensionless form represented by the Nusselt number  $Nu$ . In particular, the focus is on a nontrivial *increased* heat flux under moderate rotation, found in numerical<sup>1</sup> and experimental<sup>2</sup> studies.

A series of simulations is carried out at constant Rayleigh number (dimensionless temperature gradient)  $Ra = 1 \times 10^9$ , and constant Prandtl number (characterising diffusivities of the fluid)  $\sigma = 6.4$  for water. The rotation-rate (in dimensionless form: Taylor number  $Ta$ ) is varied between the runs. The Rossby number  $Ro = \sqrt{Ra}/(\sigma Ta)$  directly indicates the relative importance of buoyancy and Coriolis forces: it takes values from  $Ro = \infty$  (no rotation) to  $Ro = 0.045$  (rotation-dominated flow).

We also wish to assess the influence of rotation on the organisation of the flow into coherent structures. In the simulations it is found that for  $Ro \gtrsim 1$  the flow is organised into a single domain-filling circulation cell [fig. 1(a)]. At  $Ro \lesssim 1$ , however, vertical tube-like structures possessing considerable vorticity are the dominant structures, cf. fig. 1(b). The vorticity, produced close to the walls, provides an additional vertical transport mechanism: the so-called Ekman pumping. Heat transfer is enhanced by up to 15% at appropriate rotation rates [fig. 1(c)];  $Nu$  attains a maximum at  $Ro \approx 0.2$  in our simulations. At lower  $Ro$  the flow is stabilised by rotation and there is less vertical transport of heat and fluid.

<sup>\*</sup>Dept. of Applied Physics & J.M. Burgers Centre for Fluid Dynamics, Eindhoven University of Technology, P.O. Box 513, 5600 MB Eindhoven, The Netherlands.

<sup>†</sup>Dept. of Applied Mathematics & J.M. Burgers Centre for Fluid Dynamics, University of Twente, P.O. Box 217, 7500 AE Enschede, The Netherlands

<sup>1</sup>Kunnen et al., *Phys. Rev. E* **74**, 056306 (2006); Oresta et al., *Eur. J. Mech. B/Fluids* **26**, 1 (2007).

<sup>2</sup>Rossby, *J. Fluid Mech.* **36**, 309 (1969); Liu and Ecke, *Phys. Rev. Lett.* **79**, 2257 (1997).

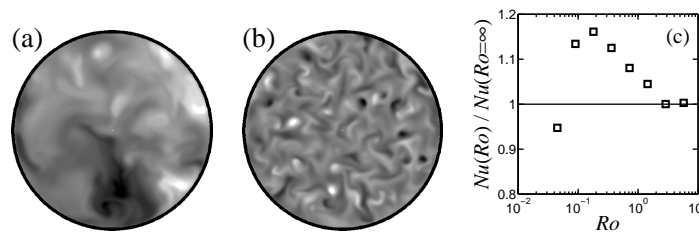


Figure 1: Vertical-velocity slices at half-height for (a)  $Ro = 5.76$ , (b)  $Ro = 0.09$ . (c) The heat flux  $Nu(Ro)$  relative to its value without rotation  $Nu(Ro = \infty)$ .

## Boundary layer flow studies on undulatory wall motion

Ch. Brücker<sup>a</sup>, S.Kunze<sup>b</sup>

The goal of this cooperation project between the Technical University of Freiberg and the University of Bonn is to understand the dynamic interaction between the sensory and actuator system during the fish motion. In detail the fluid dynamic mechanisms and the dynamic adaptation of the swimming stroke are investigated in consideration of efficient locomotion. Therefore the swimming behaviour of a trout (*Onchorhynchus mykiss*) and a goldfish (*Carassius auratus*) was analysed in an undisturbed flow and a cylinder wake flow at the University of Bonn. At the University of Freiberg a mechanical model of an undulatory moving wall was developed to simulate the swimming behaviour of a fish at different flow parameters, see figure 1.

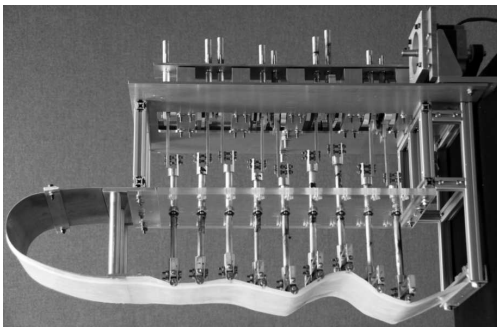


Figure 1: Photograph of the mechanical model, expected incoming flow  $U$  from the left side

The undulatory moving wall is generated via nine lifters, which are driven by a camshaft at the top of the model. The stroke of these lifters rises linear from 3mm at the front of the model up to 70mm at the downstream end of it. The wavelength of the undulatory moving wall was preset at 30mm, therefore 1.5 wavelengths were represented over the whole length of the model of 45mm. The wave speed  $V$  of the moving wall depends on the rotational speed of the camshaft and was varied between  $0.9 \leq V/U \leq 1.1$  against the velocity of the incoming flow  $U$ . Figure 2 illustrates time exposure pictures of the boundary layer flow along the wall. The flow along the steady wall ( $V/U=0$ ) is used as a reference measurement and one can see clearly the separation at the wave crest on the left picture, indicated by the red circle. On the right-hand side the flow is illustrated for a ratio of wave speed to incoming flow velocity of  $V/U=1$ . There is no visual flow separation noticeable at the wave crest, which corresponds to previous findings in experimental<sup>1</sup> and numerical investigations<sup>2</sup>. Further measurements were down for turbulent boundary layer conditions indicating the interactions of the coherent structures with moving wall.

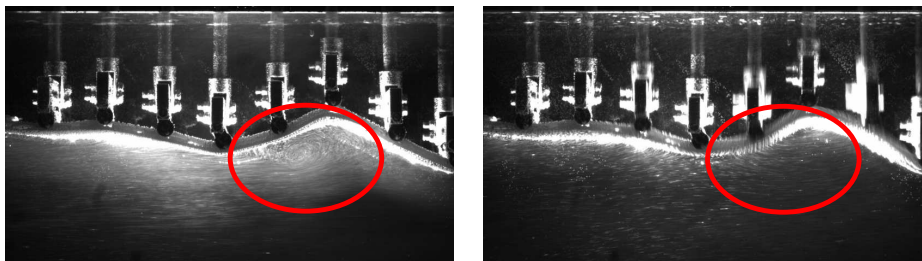


Figure 2: Flow visualisation with 200ms duration of exposure left: unmoving wall ( $V/U=0$ ), right: moving wall ( $V/U=1$ )

<sup>a, b</sup> Institut für Mechanik und Fluidodynamik, TU Bergakademie Freiberg

<sup>1</sup> Taneda et al. J. Phys. Soc. Japan **36**, 1683 (1974)

<sup>2</sup> Shen et al., J. Fluid Mech. **484**, 197 (2003).



# Effect of surface roughness and FST\* on crossflow instability

T. Kurian<sup>†</sup>, J.H.M. Fransson<sup>†</sup>

In industrial applications knowledge about transition criteria is highly sought after, but still not well understood. Currently, the  $e^N$ -method is widely used even in cases where surface roughness is present and the free stream is affected by background noise. Today, this is known to trigger a different transition scenario with algebraic disturbance growth at sub-critical Reynolds numbers considering classical stability theory. More experiments are needed to enhance the fundamental knowledge of the receptivity mechanisms, which can lead to the establishment of receptivity coefficients.

To this end an experimental investigation has been undertaken to study the growth of crossflow instabilities over a swept flat plate under different receptivity mechanisms, namely: surface roughness and FST. The experiments were carried out in the MTL wind tunnel at KTH Mechanics. The leading edge of the flat plate was a modified super-ellipse at a sweep angle of  $25^\circ$ . Taking into account the expected growth of the crossflow mode as well as the thickness of the boundary layer a bump, designed to give a strong acceleration with a Hartree parameter,  $\beta = 0.19$ , was built. FST levels were varied by placing different turbulence generating grids upstream of the leading edge. By changing both the position as well as the actual grid (thus the mesh and bar widths), it is possible to vary the incoming free stream turbulence intensity as well as the characteristic length scales. Surface roughness was introduced by means of discrete roughness elements. Measurements were done with a single hot-wire that could be slanted in the flow to obtain both the streamwise and spanwise mean velocities as well as their variances and the covariance. Figure 1 shows that the contour lines of the base flow are parallel with the sweep angle up to approximately one metre from the leading edge and that the acceleration along the centreline matches with  $\beta = 0.19$ . Disturbance energy evolution inside the boundary layer will be presented. This investigation has been performed within the project TELFONA (TEsting for Laminar Flow On New Aircraft) under contract number AST4-CT-2005-516109.

\*Free Stream Turbulence

<sup>†</sup>Linné Flow Centre, KTH Mechanics, SE-100 44, Stockholm, Sweden.

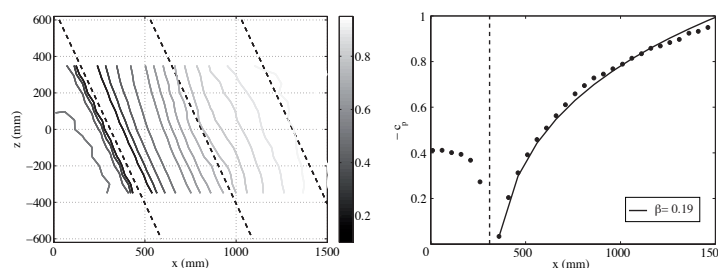


Figure 1: Pressure coefficient of the base flow.

## Deposition of cohesive sediment from turbulent plumes

G F Lane-Serff<sup>a</sup>

A model for the deposition of cohesive sediment from turbulent buoyant plumes is described. The cohesive sediment is made up of small particles that aggregate to form larger “flocs,” which are in turn broken up by turbulent shear. The equilibrium floc size (and thus the equilibrium fall speed) is a function of the turbulent dissipation rate and the sediment concentration. The flows are modelled using integral plume models, with dissipation related to bulk flow properties. It is shown that there is a well-defined equilibrium fall speed at the virtual origin (despite the infinite concentration and velocity there) and that the fall speed changes relatively slowly in the initial, momentum-dominated part of the plume. Assuming the flocs adjust instantaneously to their equilibrium size, an integral model for a turbulent plume carrying cohesive sediment can be described in terms of two parameters: the angle between the plume and the horizontal at the virtual origin and the non-dimensional fall speed there. Next, a typical time scale for flocs to adjust to their equilibrium size is identified and the model is extended to include an equation for the rate of change of the mean floc size along the plume. In this non-equilibrium model a further non-dimensional parameter is identified,  $B$ , which is proportional to the ratio of a typical plume time scale to the typical floc size adjustment time scale. When  $B$  is large, the flocs adjust almost instantaneously to the equilibrium size while when  $B$  is very small the flocs remain close to their size at the source (see Figure 1).

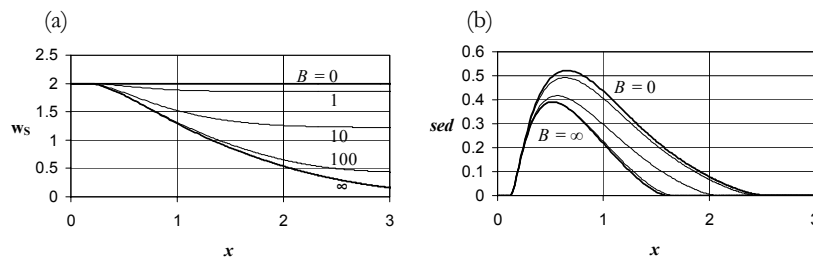


Figure 1. (a) Non-dimensional floc fall speed and (b) sediment deposition, from buoyant plumes injected horizontally with initial non-dimensional fall speed  $w_{s0} = 2$ , and various values of the parameter  $B$  ( $= 0, 1, 10, 100, \infty$ ).

Whatever the value of  $B$ , the local adjustment time scale always tends to zero approaching an idealised source (virtual origin), so that the equilibrium model is always valid there. In addition to a number of results for turbulent plumes, the equilibrium model is also applied to two-dimensional and axisymmetric gravity currents and turbidity currents.

<sup>a</sup> School of Mechanical, Aerospace and Civil Engineering, University of Manchester

## Computational Fluid Dynamics analysis of low speed transitional wind turbine flows

S.S. Latorre\* and M.S. Campobasso\*

Two important features peculiar to horizontal axis wind turbine (HAWT's) make HAWT Computational Fluid Dynamics (CFD) assessments particularly challenging. One arises because of the quite exceptional sizes of these blades, which yields a large variation of the relative flow conditions along the blade span. Near the hub, the flow has a very low speed, with Mach numbers of the order 0.01 and often close to stagnation. Moving towards the tip, on the other hand, the relative fluid velocity increases substantially. In turn, this large velocity variability induces large variations of the Reynolds number from hub to tip. At the hub, the value of this parameter is well below the subcritical threshold. The flow is therefore transitional over a large fraction of the blade height. The other complex feature is that the flow is strongly unsteady because of several factors, including variability of atmospheric conditions, skewed wind (i.e. misalignment of wind velocity and normal to the rotor plane) and dynamic stall induced by excessive incidence.

In order to tackle all these complex modelling issues, the ISAAC CFD code implemented by J. H. Morrison has been used as a starting platform<sup>1</sup>. Preliminary CFD investigations of HAWT aerodynamics performed by the authors<sup>2</sup>, point to the suitability of ISAAC to cope with the complexity of this problem. This paper will report further enhancements of this CFD tool in view of the analysis of the most difficult operating conditions. In order to handle the whole range of variation of the Mach number, a time-derivative preconditioning algorithm, which is suitable also for viscous flows, has been introduced, following Choi and Merkle's guidelines<sup>3</sup>.

In order to handle turbulent phenomena of HAWT flows, a transition model is being introduced in the CFD code. Such a model is going to be coupled with the existing and validated variants of the  $k-\varepsilon$  and  $k-\omega$  closures.

The first stage of the validation of the ISAAC code for wind turbine flows is being carried out based on a number of wind turbine airfoils the performance of which has been experimentally determined. This paper will demonstrate the improvements achieved by introducing the free-transition model and the low-speed treatment. The former will be first validated by selecting suitable test cases from the ERCOFTAC experimental database. Thereafter, both the low-speed algorithm and the free-transition model will be validated by considering the low-speed transitional unsteady flow past wind turbine airfoils. Turning on or off the low-speed preconditioner, we expect to find significant differences in the unsteady flow prediction, as reported by Le Pape<sup>4</sup>. The two solutions obtained will be compared to unsteady flow measurements<sup>5</sup> (e.g. hysteretic force loops), which will establish the superior quality of the solution computed by using the low-speed preconditioner and the free transition model.

\* Aerospace Engineering, University of Glasgow.

<sup>1</sup> J. H. Morrison, <http://isaac-cfd.sourceforge.net>, (2001).

<sup>2</sup> M. S. Campobasso, *Submitted to Applied CFD Conference* (2008).

<sup>3</sup> Choi et al., *J. Computational Physics* **105**, 207-223 (1993).

<sup>4</sup> Le Pape et al., *Wind Energy* **7**, 309-324 (2004).

<sup>5</sup> P. Fuglsang et al., *Risø National Laboratory Tech. Rep. R-1041(EN)*, (1998).

## Vorticity Production in Shock Bubble Interaction

N. A. Adams\*, X.Y. Hu\* and C. Schmitt†

The interaction of a shock with a cylindrical material interface constitutes an important generic configuration for the investigation of shock-induced mixing. For mixing the production of vorticity is important, which can occur due to the slip-line effect, primary baroclinic production (at the interface) and secondary baroclinic production (in the bulk). In this paper we perform a systematic analysis of shock-material-interface interaction, based on the experiment of Zoldi<sup>1</sup>. A series of two-dimensional computations is carried out where we use a conservative sharp-interface model<sup>2</sup>. Unlike previous computations our objective is not only to represent the initial period of interaction accurately, but also to analyze the different vorticity production mechanisms. For this purpose we perform simulations (i) PGNSV, for a perfect-gas equation of state with suitable parameters for the heavy and the light gas and representing all possible exchange effects (friction in the bulk, friction at the interface), (ii) PGNSI, where viscous interactions at the interface are dropped, (iii) PGEUV, and (iv) PGEUI, where friction in the bulk is dropped. Furthermore, in a second series of simulations we replace the perfect-gas equation of state by a polytropic equation of state, so that there is no baroclinic vorticity production in the bulk (BGNSV, BGNSI, BGEUV, BGEUI). A grid-resolution study with PGNSV confirms that we reproduce the experiment with acceptable accuracy. Vorticity contours at several time instants for PGNSV and PGNSI illustrate the significance of interface friction. In the final paper we will show that several significant conclusions can be drawn from a detailed analysis of the simulation results. These are, for instance, that the main roll-up is caused by the slip-line effect, that no significant secondary baroclinic production occurs, and that friction in the bulk has almost negligible effect.

\*Institute of Aerodynamics, Technische Universität München.

†Flow Physics and Computation, Stanford University.

<sup>1</sup>C.A. Zoldi, *Ph.D. Thesis*, State University of New York (2002).

<sup>2</sup>X.Y. Hu et al., *J. Comput. Phys.* **219**, 553-578 (2006).

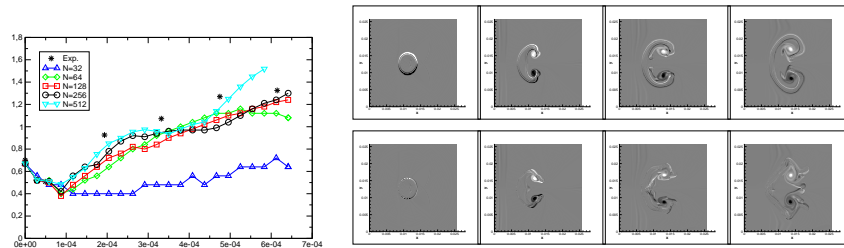


Figure 1: Left: Evolution of the bubble width for PGNSV at different resolution in comparison to the experiment. Right: Time series for vorticity, upper row PGNSV, lower row, PGNSI.

## Variations on the Scallop Theorem

Eric Lauga\*

Fluid mechanics plays a crucial role in many cellular processes. One example is the external fluid mechanics of motile cells such as bacteria, spermatozoa, and essentially half of the microorganisms on earth. These organisms typically possess flagella, slender whiplike appendages which are actuated in a periodic fashion in a fluid environment, thereby giving rise to propulsion.

The type of periodic actuation which cannot be exploited for locomotion was established in 1977 by Purcell, and is referred to as the Scallop theorem<sup>1</sup>: it states that, due to the linearity of Stokes's equations of motion, time-reversible movement (i.e. movement that is identical under time-reversal) cannot not lead to any average locomotion.

In this talk, we ask the following question: what ingredients are necessary to escape the constraints of the Scallop theorem? We first demonstrate that the theorem breaks down in a continuous fashion with inertia, both with the inertia of the fluid and with the inertia of the swimmer. We then consider locomotion in non-Newtonian fluids, and show that the Scallop theorem breaks down in this case by displaying a number of counter-examples. Application to biological systems will be discussed.

---

\*Department of Mechanical and Aerospace Engineering, University of California, San Diego, 9500 Gilman Drive, La Jolla CA 92093-0411, USA.

<sup>1</sup>E. Purcell, *Am. J. Phys.* **45**, 3 (1977).

## The structure and efficiency of mixing in complex density profiles

Andrew G.W. Lawrie<sup>a</sup> and Stuart B. Dalziel<sup>a</sup>

Mixing between miscible fluids is ubiquitous in the natural environment, and is an important, often performance-limiting aspect of many industrial applications. Here, we focus on understanding the mixing process, and attempt to quantify the dynamical behaviour of fluid systems where the kinetic energy for mixing is converted from potential energy by Rayleigh-Taylor instability across an unstable density interface.

An experimental technique, based on Planar Laser Induced Fluorescence, has been developed to directly visualise mixing at a molecular level as it evolves, by using a fluorescent dye that changes its emission wavelength sharply in response to changes in pH. Image analysis yields statistical data that characterises the structure of the mixing region, particularly the scaling between iso-surfaces of volume fraction and the volume of fluid already mixed. Figure 1, below, illustrates the degree of molecular mixing that occurs in the early stages of the Rayleigh-Taylor instability.

In many naturally occurring Rayleigh-Taylor unstable situations there exists an underlying stable stratification, and this case is modelled experimentally in the laboratory and compares well to a hierarchy of analytical and one-dimensional numerical models. Geometric constraint of the mean eddy size in the turbulence significantly affects the evolution of the Rayleigh-Taylor instability, and this is also considered in the theoretical modelling.

Detailed measurements of the stratification before and after an experiment allow us to calculate the mixing efficiency of the Rayleigh-Taylor process when it takes place within an underlying stable stratification. While conventionally it is believed that Rayleigh-Taylor instability achieves close to the maximum mixing efficiency possible, results herein suggest that the actual value is somewhat less.

Three-dimensional incompressible numerical simulations using an Implicit Large Eddy Simulation methodology complement this study and appear to corroborate these findings.

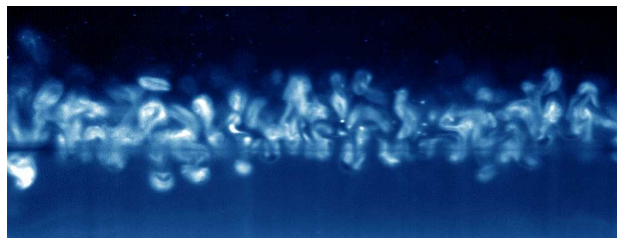


Figure 1. Direct Visualisation of Rayleigh-Taylor Instability

---

<sup>a</sup> Department of Applied Mathematics and Theoretical Physics, The University of Cambridge.

### Law of spreading of the crest of a breaking wave

M. Le Bars <sup>a</sup>, Y. Pomeau <sup>b</sup>, T. Jamin <sup>a</sup>, P. Le Gal <sup>a</sup> and B. Audoly <sup>c</sup>

In a wide range of conditions ocean waves break. This can be seen as the manifestation of a singularity in the dynamics of the fluid surface, moving under the effect of the fluid motion underneath. We show that, at the onset of breaking, the wave crest expands in the span-wise direction as the square root of time. This is first derived from a theoretical analysis of the 2D Burgers equations, considered as a generic model for this type of singularity. Then we show theoretically that the same breaking process occurs in 'real' water wave, in the approximation of long wave, relatively small amplitude and negligible dispersion. We finally present experimental observations of the spreading of the crest of breaking-wave in a laboratory set-up (figure 1) allowing accurate measurements in shallow water, this showing a remarkable agreement with the theoretically predicted exponent (figure 2).

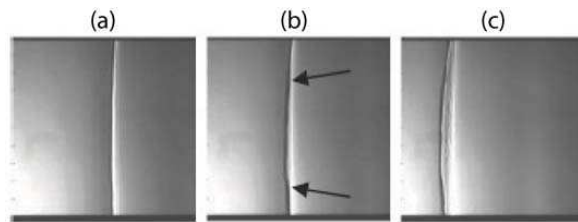


Figure 1: shadowgraph of a wave breaking recorded by a high speed camera. t = 25 ms, b) t = 100 ms, c) t = 250 ms. The arrows indicate the location of the singularities that progress along the transverse direction y.

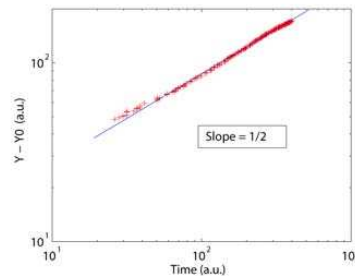


Figure 2: logarithmic representation of the progression in time of the singularity along the lateral y axis.

<sup>a</sup> IRPHE, UMR 6594, CNRS & Aix-Marseille Université, France.

<sup>b</sup> LPS, Ecole Normale Supérieure, France.

<sup>c</sup> LMM, UMR 7607, Université Pierre et Marie Curie, France.

## Flow of a particle along a rotating wall

A. Le Quiniou\*, F. Rioual † Y. Lapusta ‡

We present an experimental and numerical study of the flow of a single spherical particle along a rotating wall. A typical trajectory consists in a succession of rebounds followed by a permanent contact of the particle along the vane. We proposed recently a model to account for this trajectory <sup>1</sup>. We showed in particular that the rolling/sliding motion of the bead is an important issue.

We present here an extensive experimental work on the characterisation of the trajectory. Using image analysis, we conducted a statistical analysis of the velocities, the spins and the trajectories of the particle along the wall as a function the rotation velocity  $\Omega$ , the distance of release  $x_0$  and the mechanical properties of the surface of the rotating wall (friction, restitution). The specific role of the air flow around the rotating wall on the trajectory is addressed.

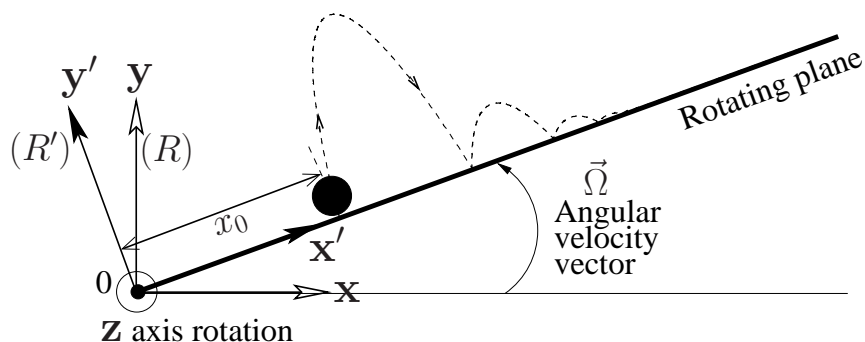
We also explored the dynamics for model and real non spherical particles of different shapes which are relevant in applications. We discuss the new physical features that have to be taken into account for models in this case.

\*TSCF, Cemagref Clermont-Ferrand, France

†TSCF, Cemagref Clermont-Ferrand, France

‡Institut Français de Mécanique Avancée, Clermont-Ferrand, France

<sup>1</sup>A. Le Quiniou et F. Rioual, accepted in *Europhys. Lett.*, (2008)





## Experimental evidence of the Strato-Rotationnal Instability

P. Le Gal<sup>a</sup> and M. Le Bars<sup>a</sup>

In 2001, Molemaker et al.<sup>1</sup> predicted that cylindrical Couette flow in a stratified fluid may become unstable under the Rayleigh line, i.e. in the stable Couette regime of pure fluid co-rotating flow. Moreover, and contrary to the classical Taylor vortices, the most unstable modes should be non-axisymmetric. The theoretical analysis of Molemaker et al.<sup>1</sup> was then continued in an astrophysical context by Shalybkov and Rüdiger<sup>2</sup> and extended to the stability of accretion disk Keplerian flows by Dubrulle et al.<sup>3</sup>. No experimental validation of these theoretical predictions have been published yet, apart from a short comment in Withjack and Chen<sup>4</sup> and a stability curve in Boubnov and Hopfinger<sup>5</sup>. We present here the first experimental evidence of this so-called Strato-Rotationnal Instability and its expected helicoidal modes. Kalliroscope visualizations of the flow are performed in a classical Couette device. A salt stratification is obtained via the double bucket technique and the Froude number is chosen equal to 0.5 which is the classical value met in accretion disk studies. The particularity of our study comes from the possibility to rotate separately both cylinders and therefore to reach the new regime. Non axisymmetric helicoidal modes are indeed observed under the Rayleigh line (figure 1). Moreover, our experimental determination of the Strato-Rotationnal Instability threshold is in excellent agreement with the theoretical value proposed by Shalybkov and Rüdiger<sup>2</sup>.

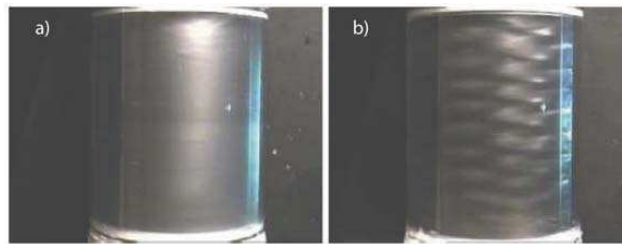


Figure 1: Kalliroscope visualization of the stable Couette flow in pure water (a) and of the SRI in the vertically stratified salt water with  $Fr = 0.5$  (b) at the same Reynolds number  $Re = 1155$ . The braid pattern of the SRI is formed by the superimposition of two identical helicoidal waves (azimuthal wavenumber  $m = 4$ ) propagating in opposite vertical directions.

<sup>a</sup> IRPHE, UMR 6594, CNRS & Aix-Marseille Université, France.

<sup>1</sup> Molemaker et al., *Phys. Rev. Lett.* **86**, 5270 (2001).

<sup>2</sup> Shalybkov et al., *J. Phys.* **14**, 128 (2005).

<sup>3</sup> Dubrulle et al., *Astron. Astrophys.* **429**, 1 (2005).

<sup>4</sup> Withjack et al., *J. Fluid Mech.* **66**, 725 (1974).

<sup>5</sup> Boubnov et al., *Sov. Phys. Dokl.* **42**, 312 (1997).

**Experimental investigation of state variables in a dense granular layer.**Frederic Lechenault<sup>1</sup>, Karen Daniels<sup>1</sup>

Stationary states in dense granular systems lack a predictive statistical description, as kinetic theory approaches fail when the interactions significantly deviate from binary collisions. In particular, because of the degeneracy of geometric states due to friction forces, it has been argued that a comprehensive theory of such dense granular systems must incorporate additional state variables associated with constraint fluctuations. We investigate the relevance of various ensembles in a dense mixture of disks laid on a horizontal air table and driven into steady states by random kicks at the boundaries. We study how microscopically defined intensive parameters affect the macroscopic response of the system, and clarify the equilibration properties of these parameters.

---

<sup>1</sup> North Carolina State University, Physics Department.

## Bubble-induced wall friction enhancement

Dominique Legendre\* and Catherine Colin\*

In many practical situations bubbles can be generated and stay on a wall. Bubble formation can result from phase change in a boiling system or by desorption of gas under saturation condition. The presence of bubbles is known to have an influence on the wall friction since micro-bubbles are injected in some applications to reduce the skin friction<sup>1</sup>.

In this study we consider the modification of the wall friction induced by bubbles located on a wall. The zero shear stress condition at a bubble surface suggests a priori that locally the shear is reduced. But a bubble modifies the velocity field and experiences a drag force parallel to the wall. The three-dimensional flow around a hemispherical bubble fixed on a wall in a viscous linear shear flow is solved using direct numerical simulation<sup>2</sup>. We first determine the drag and lift forces experienced by a hemispherical for shear Reynolds numbers in the range  $0.01 \leq Re_\alpha = 2R^2\rho\alpha/\mu \leq 2000$  where  $\rho$  and  $\mu$  are the density and viscosity of the fluid,  $R$  is the bubble radius and  $\alpha$  is the velocity gradient. The drag force acting on the bubble is found to be always larger than  $\pi\mu R^2\alpha$  the drag acting in the absence of the bubble on the surface  $\pi R^2$  occupied by the bubble.

To determine the induced effect on the wall friction, we define the local wall drag  $D(a)$  by integrating the wall shear stress on a disc of radius  $a$  centered on the bubble. The normalized drag  $D^* = D/\mu\pi a^2\alpha$  is found to be significantly larger than 1 and to increase with the shear Reynolds number, indicating that the wall friction is increased by the presence of the bubble for all the shear Reynolds number considered. In the limit  $Re_\alpha \rightarrow 0$ ,  $D^*$  reaches the analytical solution obtained by calculating the creeping flow solution that gives  $D^* = 1 + R^2/a^2$ . The evolution of  $D^*$  versus  $(R/a)^2$  is found to be linear for all the shear Reynolds number and directly linked to the drag force  $F_D$  experienced by the bubble. A very simple description of the drag wall evolution is proposed as  $D^* = 1 + [C_D Re_\alpha/8 - 1] R^2/a^2$  where  $C_D = 4F_D/\pi\rho R^4\alpha^2$  is the drag coefficient.

Finally, if we consider an uniform distribution of hemispherical bubbles on a wall, the parameter  $(a/R)^2$  can be interpreted as the surface fraction occupied by the bubbles on the wall. Our numerical simulations show that the drag wall increases linearly versus the concentration of bubble on the wall. This result suggests that the presence of bubbles at a wall (for example for micro-bubble injected to reduce the wall friction) has a influence of the global wall friction balance.

\*Institut de Mecanique des Fluides de Toulouse

<sup>1</sup>Madavan et al., *J. Fluid Mech.* **156**, 237 (1985) - Xu et al., *J. Fluid Mech.* **468**, 271 (2002) - Ferrante & Elghobashi, *J. Fluid Mech.* **503**, 345 (2004) - Sanders et al., *J. Fluid Mech.* **552**, 353 (2006)

<sup>2</sup>Legendre & Magnaudet, *J. Fluid Mech.* **368**, 81 (1998).

## The onset of three-dimensionality in inclined film flows

VL. Leontidis<sup>a</sup>, M. Vlachogiannis<sup>b,a</sup>, and V. Bontozoglou<sup>a</sup>

The three-dimensional (3-D) characteristics of solitary waves in laminar film flow are studied experimentally in a 3 m long by 0.5 m wide facility, under small inclination angles  $\varphi$ . The fluorescence imaging technique<sup>1</sup> is used to record the spatio-temporal evolution of the free surface, and in particular provide information on the development of transverse and longitudinal free surface structures. A disturbance of constant frequency is introduced at the inlet, resulting downstream in a periodic array of events. Transverse disturbances are induced statically, as in Park & Nosoko<sup>2</sup>. By the above procedure, the initial stages of nonlinear growth are bypassed and the resulting regular wave-train is more easily studied. It is noted that, in all Re examined, these regular waves are very similar to the irregularly spaced solitary waves observed at long fetch in film flow subjected only to random noise<sup>3</sup>.

Diverse 3-D phenomena are documented with increasing Re: The first is the variation along the crest-line of a nominally 2-D solitary wave. The fact that experimental waves are never truly 2-D has been occasionally invoked as the source of inconsistencies between theory and experiment<sup>4</sup>, but appears not to have been studied in detail. We observe that the crest-line is parabolic (with maximum curvature that depends on Re,  $\varphi$  and channel width) and that both the wave height and the capillary characteristics vary in the transverse direction.

The second 3-D phenomenon investigated is the transition, with increasing Re, to small-scale three-dimensionality in front of the main hump. The outcome is a fully stationary main hump, characterised by a front-running 3-D capillary structure with pronounced regular depressions in the transverse direction. This wave is stable to imposed transverse disturbances and appears as a robust feature of liquid films weakly inclined from the horizontal.

With further increase in Re, large-scale three-dimensionality is manifested. The first events occur close to the side walls, with intermediate humps being created by radiation of capillary energy from the tails of the main hump. At even higher Re, the parabolic crest-line of the main hump becomes unstable to transverse disturbances with length significantly shorter than the channel width, and this instability gives rise to isolated horseshoe waves. The onset of horseshoe waves has been well-documented in vertical films<sup>2</sup>, but the preceding sequence of events could only be observed at small inclinations, where the evolution with fetch is significantly slower.

---

<sup>a</sup> Mechanical Engineering, University of Thessaly, Volos, Greece.

<sup>b</sup> Technological Educational Institute of Larissa, Greece.

<sup>1</sup> M. Vlachogiannis & V. Bontozoglou, *J. Fluid Mech.* **435**, 191 (2001).

<sup>2</sup> C.D. Park & T. Nosoko, *AIChE J.* **49**, 2715 (2003).

<sup>3</sup> J. Liu et al, *Phys. Fluids* **7**, 55 (1995).

<sup>4</sup> B. Scheid et al, *J. Fluid Mech.* **562**, 183 (2006).

## Sediment waves: Coupled flow/sediment-bed instability in turbidity currents

Lutz Lesshafft\*, Brendon Hall\*, Eckart Meiburg\* and Ben Kneller†

*Sediment waves* are a commonly encountered phenomenon in sedimentary rock formation on the ocean floor: the bedform of sediment that is deposited from *turbidity currents* in these cases exhibits sinusoidal long-wavelength variations, with crest lines perpendicular to the flow direction. These waves are reminiscent of very large ripples, with wavelengths on the order of  $10^2$  to  $10^3$  meters and amplitudes of several meters. A typical class of sediment waves is frequently observed along the backslopes of channel levees. These waves are assumed to arise from turbidity currents that form during an overflow from the channel<sup>1</sup>. A peculiar feature of such sediment waves is their apparent *upstream* propagation in the sedimentary record, against the flow direction of the turbidity current. As a consequence, their occurrence has often been attributed to nonlinear *antidune* formation processes.

We propose a new interpretation of sediment wave formation, based on a linear stability analysis of the bottom boundary layer in a turbidity current. The analysis is performed on the 2D Navier-Stokes equations for the fluid, and it accounts for the coupled interaction of fluid and suspended particle motion with the erodible bed below. Wavy perturbations of the bottom topography may either be amplified or levelled out under the competing effects of sediment deposition and erosion. Results of temporal and spatial analyses indicate that unstable long-wavelength perturbations exist in the coupled flow-bedform system, and that the associated eigenmodes travel at *negative* phase velocities over parameter regimes that are typical of turbidity currents.

Instability occurs in situations where the concentration of suspended sediment in the base flow decays more slowly away from the sediment bed than does the shear stress within the current. Under such conditions, an upward protrusion of the sediment bed will find itself in an environment where erosion decays faster than sediment deposition, therefore it will keep growing. Conversely, a local valley in the sediment bed will see a stronger increase in erosion than in sediment deposition, which again will amplify the initial perturbation. This criterion is similar to observations in the context of *channel formation* due to cross-stream instabilities in turbidity currents<sup>2</sup>.

The base flow effect on the stability of the bedform is modulated by the perturbation eigenmodes of sediment deposition and of erosive shear stress. The phase relation between these two perturbation fields influences the total growth rate and determines the phase velocity of waves in the bed-fluid interface. Upstream-traveling waves are dominantly caused by preferred erosion of sediment into the flow along the *downslope* of the interface wave, in qualitative agreement with existing experimental and numerical investigations<sup>3</sup>.

---

\*Department of Mechanical Engineering, University of California at Santa Barbara (USA).

†Department of Geology and Petroleum Geology, University of Aberdeen (Scotland).

<sup>1</sup>Faugères et al., *Mar. Geol.* **162**, 1 (1999).

<sup>2</sup>Hall et al., submitted to *J. Fluid Mech.* (2007).

<sup>3</sup>Kubo & Nakajima, *Mar. Geol.* **192**, 105 (2002).

## The effect of acoustic forcing on heat release in self-excited round jet diffusion flames

Larry K.B. Li<sup>a</sup>, Matthew P. Juniper<sup>a</sup> and Joseph W. Nichols<sup>b</sup>

In many combustion devices, the coupling between unsteady heat release and acoustics can produce damaging pressure oscillations, a problem known as combustion instability. The aim of this work is to investigate whether this coupling can be weakened by a global shear instability – that is by the presence of self-excited hydrodynamic oscillations that are relatively insensitive to external pressure perturbations.

Experiments were conducted on two globally unstable jets: a non-reacting low-density helium jet (density ratio 0.14) and a methane jet diffusion flame (cold density ratio 0.55). Both flows were produced in a round convergent nozzle and at a Reynolds number of 1100. Regions of local absolute instability at the base of the flows triggered strong self-excited bulging oscillations at well-defined natural frequencies, as indicated by high-speed schlieren imaging. Moreover, high-speed OH natural emission measurements in the diffusion flame revealed heat release oscillations at the same frequency as the natural global mode.

When acoustic forcing was applied upstream at frequencies around the natural mode, the oscillation frequency of the non-reacting jet locked into the forcing frequency relatively easily. When the same forcing was applied to the diffusion flame, however, very large forcing amplitudes (of order of the mean jet velocity) were required to make the heat release lock into the forcing frequency. In the main body of the flame, even at large forcing amplitudes, the majority of the heat release occurred around the natural frequency rather than the forcing frequency (Fig. 1). This suggests that it may be possible to exploit global instability in flames to weaken the coupling between pressure perturbations and heat release, hence mitigating combustion instability.

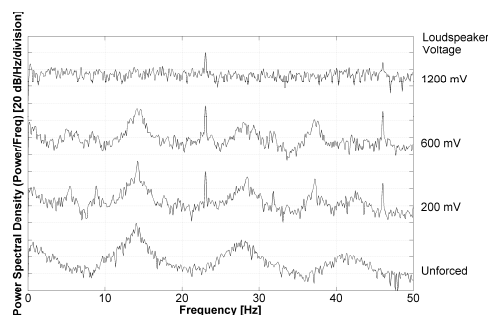


Fig. 1: Power spectral density of OH emission intensity for a methane jet diffusion flame forced acoustically at 23 Hz. The natural global mode, at around 14 Hz, is quite robust and is overwhelmed only at the highest forcing amplitude.

<sup>a</sup> Engineering Department, University of Cambridge, CB2 1PZ, United Kingdom

<sup>b</sup> Laboratoire d'Hydrodynamique (LadHyX), CNRS-École Polytechnique, 91128 Palaiseau, France

## An DNS analysis of inter-scale interaction in helicity cascade

Yi Li\*

Helicity, defined as the  $h(\mathbf{x}, t) = \mathbf{v} \cdot \boldsymbol{\omega}$ , is an inviscid invariant of fluid flows<sup>1</sup>. While some of its effects are contended, it is well-established that the presence of mean helicity in isotropic turbulence tends to suppress energy cascade<sup>2</sup>. It has also been shown that the existence of a helicity-like inviscid invariant in shell models is crucial for them to display the anomalous scaling behaviors observed in Navier-Stokes turbulence<sup>3</sup>. Moreover, helicity is also of much interest in the study of magnetohydrodynamic turbulence.<sup>4</sup>

In turbulence with sustained mean helicity input, it has been proposed and found numerically that there are simultaneous energy and helicity cascade, and helicity cascade displays many different features compared with energy cascade<sup>5</sup>. In the context of large-eddy simulation, it has been shown *a priori* that the traditional Smagorinsky model tends to underpredict sub-grid scale helicity dissipation to a significant portion<sup>6</sup>. Helical sub-grid scale models are proposed to reproduce, with some success, more realistic results. In a parallel work, the same problem is considered within a general framework of multi-scale gradient expansion of sub-grid scale stress<sup>7</sup>. A nonlinear-type model is suggested, and is illustrated in a model flow field.

Given the possible significance of helicity in many applications, we will in this talk present an *a priori* analysis of the nonlinear-type helical model. After briefly reviewing related works, derivation of the model expression is introduced. A DNS dataset of stationary isotropic helical turbulence is then used to compare the model expression with the real sub-grid scale stress. Correlation between the stresses, sub-grid scale helicity dissipations, and some other quantities are calculated. Comparison with previous models is also made. The results show that, over all, the nonlinear-type model expression provides better parameterization of the sub-grid scale stress in helical turbulence.

---

\*Department of Applied Mathematics, University of Sheffield, Sheffield, UK

<sup>1</sup>Moffatt and Tsinober, *Annu. Rev. Fluid Mech.*, **24**, 281(1992).

<sup>2</sup>Polifke and Shtilman, *Phys. Fluids A*, **1**, 2025 (1989).

<sup>3</sup>Biferale, *Annu. Rev. Fluid Mech.*, **35**, 441 (2003).

<sup>4</sup>See Ref. 1 and Davidson, *An Introduction to Magnetohydrodynamics*, CUP, 2001.

<sup>5</sup>Brissaud *et. al.*, *Phys. Fluids*, **16**, 1366 (1973). Chen *et. al.*, *Phys. Fluids*, **15**, 361 (2003). Borue and Orszag, *Phys. Rev. E*, **55**, 7005 (1997).

<sup>6</sup>Li *et. al.*, *Phys. Rev. E*, **74**, 026310 (2006).

<sup>7</sup>Eyink, *J. Fluid Mech.*, **549**, 159 (2006).

Communication proposed to  
EFMC7, 14/18 september 2008,  
Manchester.

### Shape transitions of drops sliding down a plane.

I. Peters, A. Daerr and L. Limat

*Laboratoire Matière et Systèmes Complexes, UMR 7057 du CNRS, Université Paris 7 - Denis Diderot, 10 rue  
Alice Domon et Léonie Duquet, F-75025 Paris cedex 13, France.*

A drop sliding down an incline exhibits different shape changes when its velocity is progressively increased [1,2]: (1) rounded drops, (2) formation of a “corner” at the drop rear in which two inclined contact lines are meeting in a singular point (conical interface), (3) evolution towards a cusp with droplet deposition (“pearling”). We here discuss two questions:

- what limitates the conical singularity in the corner regime, i.e. how does evolve the curvature of the contact line that edges the tip of the cone? Recent measurements that we have obtained suggest an exponential variation of the curvature upon capillary number. This result is reminiscent of what is observed on other singularities, but seems inconsistent with models that we have built upon the lubrication approximation [3,4]. We show that, at least for this subtle problem of curvature selection, the velocity gradients in the direction parallel to the plane are to be taken into account, and not only the dissipation linked to the friction of the liquid on the solid plate.

- how does pearling occur, and at which value of the capillary number? We will here propose a rough modeling that extends the one recently introduced by Snoeijer et al. [5] to arbitrary slenderness ratio, the price to paid being a loss of accuracy. We confront both approach with available data.

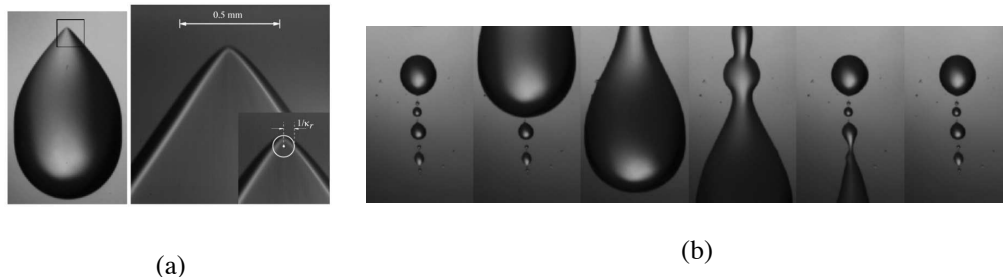


**Figure:** (a) At high enough velocity a silicon oil drop sliding down a plane coated with fluoropolymers displays a “corner” which tip remains rounded at small scale; (b) At even higher velocities, trains of “cornered” drops destabilize leading to deposition of smaller droplets (“pearling”).

### Bibliography.

- [1] Podgorski, T., Flesselles, J.-M. and Limat, L., 2001. Corners, cusps and pearls in running drops, *Phys. Rev. Lett.* **87**, 036102(1).
- [2] N. Le Grand, A. Daerr, and L. Limat, 2005. *J. Fluid Mech.* **541**, 293.
- [3] L. Limat and H. A. Stone, 2003. *Europhys. Lett.* **65**, 365.
- [4] J. H. Snoeijer, E. Rio, N. Le Grand, and L. Limat, 2005. *Phys. Fluids* **17**, 072101.
- [5] J. H. Snoeijer, N. Le Grand, L. Limat, H.-A. Stone and J. Eggers, 2007. *Phys. Fluids*. **19**, 042104.



## Centrifugal instabilities in wake-dominated curved compressible mixing layers

Li Lin\* and Sharon O. Stephen†

This investigation is concerned with the linear development of Görtler vortices in the high-Reynolds-number laminar compressible wake behind a splitter plate which is aligned with the centreline of a curved mixing layer system. The Görtler vortices may be beneficial to mixing in applications such as scramjet engines. This study follows the study of<sup>1</sup> who showed that Görtler modes exist within curved compressible mixing layers. Two distinct modes were found. One is for the case of an ‘unstably’ curved compressible mixing layer, where the centreline curves towards the faster stream. An additional mode was found for the case of a ‘stably’ curved compressible mixing layer driven by the temperature profile and referred to as ‘thermal’ modes.

The effect of a wake on the growth rate and location of the modes is determined in the limit of large Görtler number and high wavenumber. Results will be presented for two analytic models of the basic wake flow near the trailing edge of a splitter plate: (i) a Gaussian wake and (ii) a composite model for two supersonic laminar streams<sup>2</sup>.

A new ‘wake’ mode is identified which occurs for the ‘stably’ curved case but behaves differently to the ‘thermal’ modes. The growth rate of these modes can become comparable with those existing in the ‘unstably’ curved case.

Results will also be presented from the numerical solution of the governing basic flow equations for a compressible wake flow behind a splitter plate.

---

\*Schlumberger, Abingdon Technology Centre.

†School of Mathematics, University of Birmingham.

<sup>1</sup>Owen et al., *Phys. Fluids* **9**, 2506 (1997).

<sup>2</sup>Liang et al., *Phys. Fluids* **8**, 3253 (1996).

## Buoyancy Driven Convection in Vertically Shaken Granular Matter: Experiment, Numerics, and Theory

Peter Eshuis <sup>\*</sup>, Meheboob Alam <sup>†</sup>, Stefan Luding<sup>\*</sup>,  
Devaraj van der Meer<sup>\*</sup>, Ko van der Weele <sup>‡</sup>, Detlef Lohse<sup>\*</sup>

Granular material is vertically vibrated in a 2D container: above a critical shaking strength, and for a sufficient number of beads, a crystalline cluster is elevated and supported by a dilute gaseous layer of fast beads underneath. We call this phenomenon the granular Leidenfrost effect. The experimental observations are explained by a one-dimensional hydrodynamic model featuring three dimensionless control parameters: the energy input  $S$ , the number of particle layers  $F$ , and the inelasticity of the particle collisions  $\epsilon$ . The  $(S, F)$  phase diagram, in which the Leidenfrost state lies between the purely solid and gas phases, shows accurate agreement between experiment and theory<sup>1</sup>.

For large aspect ratio and sufficiently strong shaking, this Leidenfrost states gets unstable and counter-rotating convection rolls form with pronounced density variations, see figure 1. These rolls are also found in molecular dynamics simulations. The onset of convection is *quantitatively* explained through a linear stability analysis of the above hydrodynamic continuum model.

Finally, we experimentally explore<sup>2</sup> the full phase diagram of the vertically shaken granular bed in the quasi 2-D container in the  $(S, F)$  phase space: Next to the (1) Leidenfrost state and the (2) convection rolls we find a (3) bouncing bed state, (4) undulations, and (5) a granular gas state.

---

<sup>\*</sup>Physics of Fluids, University of Twente

<sup>†</sup>Engineering Mechanics, Jawaharlal Nehru Center, Bangalore

<sup>‡</sup>Department of Mathematics, University of Patras

<sup>1</sup>Eshuis, van der Weele, van der Meer, Lohse, *Phys. Rev. Lett.* **95**, 258001 (2005).

<sup>2</sup>Eshuis, van der Weele, van der Meer, Bos, Lohse, *Phys. Fluids* **19**, 123301 (2007).

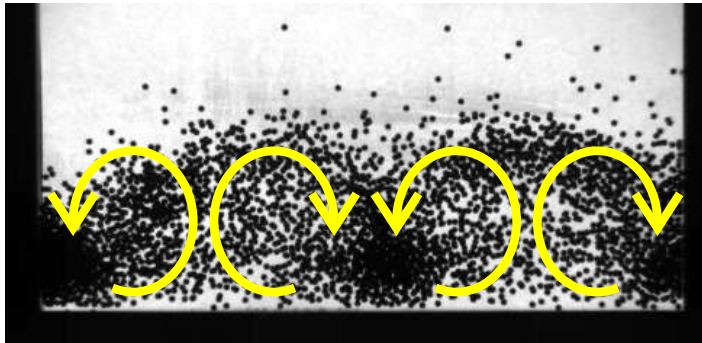


Figure 1: Convection rolls in vertically and strongly shaken granular matter.

## On the capabilities of a POD-based flow estimation technique.

Edoardo Lombardi<sup>\*,†</sup>, Matteo Gabbani<sup>\*,†</sup>, Marcelo Buffoni<sup>\*</sup>,  
Maria Vittoria Salvetti<sup>†</sup> and Angelo Iollo<sup>\*</sup>

The capabilities of a POD-based non-linear observer for unsteady flow estimation using a limited number of measurements are investigated.

A description and application of such a technique to two- and three-dimensional test cases have been made in our previous works<sup>1</sup>. It was shown that the non-linear observer outperforms preexisting static estimation techniques such as classical Least Squares or Linear/Quadratic Stochastic Estimation in two-dimensional periodic flows.

When more complex dynamics appear in the flow, the estimation procedure gives an accurate prediction only for the POD modes that are related to the vortex shedding. For the remaining modes, the accuracy is lower. Nevertheless, the instantaneous velocity fields are reconstructed with an accuracy close to the best possible, which is the one that would be obtained by projecting the DNS fields on the retained POD modes. It appears that for flows characterized by complex dynamics, the major limitation of all estimation techniques based on POD is indeed the ability of the retained POD modes to adequately representing the flow field<sup>2</sup>.

In order to increase the accuracy of the POD modes, two filtering procedures of the high frequency dynamics of the velocity fields used to obtain the POD basis are performed. The first method is based on the idea of a time average of the flow evolution; the new velocity fields  $\mathbf{v}^*(\mathbf{x}, t)$ , are obtained by the time convolution between the actual velocity fields and a given time filter kernel.

$$\mathbf{v}^*(\mathbf{x}, t) = \mathbf{v}(\mathbf{x}, t) * f(t)$$

In the second technique the new smoothing filtered velocity field  $\mathbf{v}^*(\mathbf{x}, t^*)$  is achieved by the spatial convolution between the actual velocity field at time  $\mathbf{v}(\mathbf{x}, t^*)$  and a given spatial filter kernel  $\mathbf{G}(\mathbf{x})$ .

$$\mathbf{v}^*(\mathbf{x}, t^*) = \mathbf{v}(\mathbf{x}, t^*) * \mathbf{G}(\mathbf{x})$$

In the present work, it is shown that an improvement of the POD representation is obtained if the POD basis is built from the filtered (either in time or in space) snapshots. Then, these POD bases are used within the non-linear observer method and an application of such a technique to a three-dimensional unsteady flow past a confined square cylinder is presented.

<sup>\*</sup>Institut de Mathématiques de Bordeaux UMR 5251 CNRS, Université Bordeaux 1 and INRIA  
Projet MC2, 351, Cours de la Libération, 33405 Talence cedex, France

<sup>†</sup>Dipartimento di Ingegneria Aerospaziale, Università di Pisa, 56122 Pisa, Italy

<sup>1</sup>Buffoni et al., *J. Comp. Phys.* **227**, 2626 (2008)

<sup>2</sup>Buffoni et al., *J. Fluid Mech.* **569**, 141 (2006).

## Universal Gelation of Particles with Short-ranged Attraction

Peter J. Lu \*

Nanoscale or colloidal particles are exceptionally important in many realms of science and technology. They can dramatically change the properties of materials, imparting solid-like behavior to a wide variety of complex fluids, from yoghurt to cast ceramics. This behavior arises when particles aggregate to form mesoscopic clusters and networks. The essential component leading to aggregation is an interparticle attraction, which can be generated by many physical and chemical mechanisms. In the limit of irreversible aggregation, infinitely strong interparticle bonds lead to diffusion-limited cluster aggregation (DLCA), long-understood as a purely kinetic phenomenon, which can form solid-like gels at arbitrarily low particle volume fraction,  $\phi$ . Far more important technologically are systems with weaker attractions, where gel formation requires higher  $\phi$ . Numerous scenarios for gelation have been proposed, including DLCA, kinetic or dynamic arrest, phase separation, percolation, and jamming. No consensus has emerged, and despite its ubiquity and significance, gelation is far from understood; even the location of the gelation phase boundary is not agreed upon. Here we show that gelation of spherical particles with isotropic short-ranged attractions is initiated by spinodal decomposition; this thermodynamic instability triggers the formation of density fluctuations, leading to spanning clusters that dynamically arrest to create a gel. This simple picture of gelation does not depend on microscopic system-specific details, and should thus apply broadly to any short-ranged attractive particle system. Our results suggest that gelation, often previously considered a purely kinetic phenomenon, is in fact a direct consequence of equilibrium liquid-gas phase separation. Without exception, we observe gelation in all of our samples predicted by theory and simulation to phase separate; this suggests that it is phase separation, not percolation, that corresponds to gelation in models for attractive spheres.

Collaborators:

Emanuela Zaccarelli, Fabio Ciulla and Francesco Sciortino, Universita Roma I "La Sapienza", Rome

Andrew Schofield, University of Edinburgh, Scotland

David A. Weitz, Harvard University, Cambridge, Mass. USA

---

\*Department of Physics, Harvard University

## Gravity Wave Turbulence in the Laboratory Flume

S. Lukaschuk\*, P. Denissenko† and S. Nazarenko ‡

Statistics of a sea surface roughness determine characteristics of many physical processes at the atmosphere-sea interface. The random roughness is the result of wave turbulence which received energy from wind, tides and currents. These energy sources are most effective at large scales, and to dissipate the energy should pass to the small scales such that an universal range of scales is formed between the energy source and dissipation scales. Knowledge of the wave elevation statistics in the universal range is important both for practical applications and fundamental science.

There are two most celebrated mechanism of wave energy transport towards the small scales - the wave breaking<sup>1</sup> and the nonlinear wave interactions<sup>2</sup>. Both mechanisms lead to the universal energy spectrum  $E_\omega \propto \omega^{-\nu}$ ,  $E_k \propto k^{-\alpha}$ , but with different exponents  $\nu$  and  $\alpha$ . The point-like breaks in space result in  $E_\omega \propto \omega^{-5}$  and  $E_k \propto k^{-4}$  spectrum. The breaks developing along the line give the spectra<sup>3</sup>  $E_\omega \propto \omega^{-4}$  and  $E_k \propto k^{-4}$ . Similar slopes are predicted by the weak turbulence theory considering four-wave interactions,  $E_\omega \propto \omega^{-4}$  and  $E_k \propto k^{-7/2}$ . One may expect that for relatively low amplitude the weak turbulence mechanism is prevailed while for higher wave amplitudes the breaks contribution is more significant.

Many statistical characteristics of gravity waves were obtained in field experiments. These results are difficult to compare with theories since they consist a great deal of uncertainty in environmental conditions. Laboratory wave experiments are usually well controlled but were mainly performed in long channels and thus are effectively one dimensional. Here we report the results of a "two-dimensional" experiment with gravity waves performed in a flume with the aspect ratio close to one and dimensions 12 x 6 x 1.5 m. To understand the mechanisms of wave turbulence we study  $k$ - and  $\omega$ - spectra of wave elevations. The waves were generated by a wavemaker enabling to mix an initial state as a sum of waves with different wave vectors. Multiple wave reflections from the flume boundaries make the wave field isotropic. Surface elevations were measured simultaneously as a function of time at two fixed points using capacitance gauges and as a function of  $r$ -coordinate along the line on the surface using a laser fluorescent technique. The results are presented in terms of the energy spectra, the elevation PDFs and structure functions both in  $t$ - and  $r$ -domains. We found that at large wave intensities the universal range in the spectra reaches one decade in  $\omega$  and  $k$ . Though the spectrum slopes,  $\nu$  and  $\alpha$ , are not universal, they depend on the mean wave energy and change from -6 to about -4 for  $\nu$  and from -4.2 to -3 for  $\alpha$ . We explain these trends in terms of different mechanisms of energy transport including finite size effects. The PDFs and structure functions of finite differences of the wave elevations demonstrate intermittent character of wave turbulence.

---

\*Department of Engineering, University of Hull.

†Department of Engineering, University of Warwick.

‡Mathematics Institute, University of Warwick.

<sup>1</sup>O.M. Phillips, *J. Fluid Mech.* **4**, 426 (1999).

<sup>2</sup>V.E. Zakharov et al., *Sov. Phys. Dokl.* **11**, 881 (1967).

<sup>3</sup>E.A. Kuznetsov, *JETP Letters* **80** 83 (2004).

## The Cascade Structure of Linear Instability in Collapsible Channel Flows

X.Y. Luo<sup>a</sup>, Z.X. Cai<sup>b</sup>, W.G. Li<sup>a</sup> and T.J. Pedley<sup>c</sup>

The unsteady behaviour and linear stability of the flow in a collapsible channel is studied in a fluid-beam model. The solid mechanics is analyzed in a plane strain configuration, in which the principal stretch is defined with a zero initial strain. Two approaches are employed: unsteady numerical simulations solving the nonlinear, fully coupled fluid-structure interaction problem, and the corresponding linearized eigenvalue approach solving the Orr-Sommerfeld equations modified by the beam. The two approaches give good agreement with each other in predicting the frequencies and growth rates of the perturbation modes, close to the neutral curves. For a given Reynolds number in the range of 200-600, an interesting cascade of instabilities is discovered as the wall stiffness (or effective tension) is reduced<sup>1</sup>. Under small perturbation to steady solutions for the same Reynolds number, the system loses stability by passing through a succession of unstable zones, with mode number increasing as the wall stiffness is decreased. It is found that this cascade structure can, in principle, be extended to many modes, depending on the parameters. A puzzling “tongue” shaped stable zone in the wall stiffness – Re space turns out to be the zone sandwiched by the mode-2 and mode-3 instabilities. Self-excited oscillations dominated by modes 2-4 are found near their corresponding neutral curves. These modes can also interact and form period-doubling oscillations. Extensive comparisons of the results with existing analytical models are made, and a physical explanation for the cascade structure is proposed.

---

<sup>a</sup> Department of Mathematics, University of Glasgow, Glasgow, UK

<sup>b</sup> Department of Mechanics, Tianjin University, China

<sup>c</sup> Department of Applied Mathematics and Theoretical Physics, University of Cambridge, UK

<sup>1</sup> Luo et al. *J. Fluid Mech.* (**in press**).

## Grain motion and shearing in confined granular flows

J-F. Métayer<sup>\*</sup>, P. Richard, J. Crassous, R. Delannay

Although kinetic theory captures the behavior of dilute granular flows, the theoretical attempts made to describe dense granular flows, and in particular the necessity to take into account enduring contacts<sup>1,2</sup> are still matter of debate. Pouring continuously grains at the top of a granular heap allows one to observe all the states of granular matter: from gaseous state (close the the free surface) to a quasistatic state (deep inside the flow). It is thus the ideal experiment to test existing theories or to inspire new ones.

Using a smart imaging method Komatsu et al.<sup>3</sup> show that in such type of experiments two regions can be considered : a flowing region close to the surface flow and below this region a creeping flow region characterized by an exponential decay of the mean velocity. Thus, the grains below the surface flow are not frozen but exhibit a slow motion.

Influence on the behavior of the grain in the bulk region is lacking. Here, we report a careful experimental study on this point

Our experimental set-up consists of two  $1200 \times 1200$  mm parallel and vertical glass plates separated by width  $W$ . Granular medium we used is glass-beads of diameter  $d = (500 \pm 100) \mu\text{m}$ . By combining two experimental methods (particle tracking and dynamic light scattering) we are able to obtain the streamwise velocity profile over 10 decades. This confirms the exponential character of the velocity decay in the creeping region and clearly shows the existence of two characteristic lengths : one for the flowing region (where the shear rate is found to be rather constant) and the other one for the creeping region. These two lengths are correlated, indicating that although the frontier between the two regions is rather clear, they are in strong interaction.

In the flowing region, velocity profiles are almost linear (except close to the free surface for large angles of inclination). The shear rate is found to be independent of the inclination angle.

---

<sup>\*</sup>IPR, UMR CNRS 6251, university of Rennes.

<sup>1</sup>P.C. Johnson et al., *J. Fluid Mech* **176**, 67 (1987)

<sup>2</sup>M. Y. Louge, *Physical rev. E* **67**, 061303 (2003)

<sup>3</sup>Komatsu et al., *Physical review letters* **86**, 1757 (2001)

## Coalescence of droplets on a wall with contact-angle hysteresis

Marco Maglio\*, Hang Ding†, Dominique Legendre\* and Peter D. M. Spelt†

Previous experimental work<sup>1</sup> has shown strong differences between the coalescence of freely-suspended drops, and the coalescence of almost-perfectly-wetting drops on a wall (which has applications in e.g. spray painting and condensation processes<sup>2</sup>). Specifically, the width of the liquid bridge between two coalescing wetting drops on a surface turned out to increase as  $t^{1/2}$ , which could be explained from a mass conservation model in conjunction with a lubrication approximation. A similar behaviour has been observed for almost-non-wetting drops<sup>3</sup> for mercury drops. Furthermore, in Ref.3, the experiments were supplemented by a more or less favourable comparison of numerical simulations with the experiments. Although a power-law regime resulted from the simulations, the exponent showed some deviation from the experimental value. More recently<sup>4</sup>, experimental results have been reported for partially wetting drops, showing additional oscillatory behaviour in the height of the bridge, arguably resulting from inertial effects.

We revisit this problem here, primarily to investigate the effect of contact-angle hysteresis. Numerical methods are used for this purpose. Not only can the window of contact-angle hysteresis readily be varied in simulations, simulations also provide an opportunity to shed further light on the coalescence process. Finally, results of two different numerical methods are presented here, these corresponding to different methods in which the stress singularity at a moving contact line is resolved. Both methods solve the full Navier-Stokes equations for two-phase flows; in one, a VOF method is used to track the interface<sup>5</sup>, whereas the second method is a diffuse-interface method<sup>6</sup> that has recently been compared with a level-set method<sup>7</sup> and been used for other flows wherein contact-angle hysteresis plays an important role<sup>8</sup>.

We first report on the results of a convergence study on a system that facilitates relatively high grid resolution, the coalescence of 2D cylindrical droplets that are initially just touching. This system also provides a solid basis on which to further build our understanding of the 3D flow, especially regarding the tendency in the results towards power-law behaviour of the liquid bridge height versus time, in the viscous and inertial regimes – and the occurrence of very strong oscillations in the inertial regime. The results for the fully 3D case are shown to be partially related to the 2D system, but to be rather sensitive to contact-angle hysteresis, with the partially coalesced drops suddenly grinding to a halt. Finally, results are presented for two spreading (and initially non-touching) drops that coalesce.

---

\*IMFT, Toulouse, France

†Department of Chemical Engineering, Imperial College London

<sup>1</sup>Ristenpart et al., *Phys. Rev. Lett.* **97**, 064501 (2006)

<sup>2</sup>Andrieu et al., *J. Fluid Mech.* **453**, 427 (2002)

<sup>3</sup>Menchaca-Rocha et al., *Phys. Rev. E* **63**, 046309 (2001)

<sup>4</sup>Kapur and Gaskell, *Phys. Rev. E* **75**, 056315 (2007)

<sup>5</sup>Bonometti and Magnaudet, *Int. J. Mult. Flow.* **33**, 109 (2007)

<sup>6</sup>Ding and Spelt, *Phys. Rev. E* **75**, 046708 (2007)

<sup>7</sup>Ding and Spelt, *J. Fluid Mech.* **576**, 287 (2007)

<sup>8</sup>Ding and Spelt, *J. Fluid Mech.* **599**, 341 (2008, in press)



## Laboratory Scale Experimentation and Large Eddy Simulation of Crown Fire Initiation in Shrublands by Surface Fire

S. Mahalingam<sup>a</sup>, W. Tachajapong<sup>a</sup>, J. Lozano<sup>a</sup>, and D. R. Weise<sup>b</sup>

### Abstract

Parameters that influence fire dynamics including canopy height, crown base height, and crown bulk density may be very different in shrublands as compared to conifer forests. In California, crown fires occurring in shrublands cause extensive damage annually. There is thus a need to better understand the process of crown fire initiation, and to develop a predictive model to enable management of fire risk in these areas. The evolution of a surface fire burning through dead fuel, leading to ignition of elevated live fuel was studied through laboratory scale experiments and large eddy simulations (LES). A fixed mass of aspen (*Populus tremuloides*) excelsior evenly distributed over a 0.80 m × 1.80 m flat bed, was used to represent the surface fuel. A fuel bed depth of 0.10 m was chosen so that the resulting flame height ranged from 0.15 m to 0.45 m. The crown fuel was arranged in a volume with dimensions 0.30 m × 0.30 m × 0.80 m in height, depth and width. It comprised of live chamise (*Adenostoma fasciculatum*) with foliage diameter of  $\approx 0.50$  mm and branch diameter of approximately  $\approx 3.50$  mm. The effects of varying crown base height (0.2 to 0.4 m), mean wind speed (0 to 1.8 m/s), and crown fuel bulk density (0.75 to 1.75 kg/m<sup>3</sup>) was investigated in detail. Experimental results indicate that ignition of crown fuel occurs when the crown base height is located within either the continuous, or intermittent flame regimes. LES modeling results suggest that increasing crown fuel bulk density enhances retention of thermal energy inside the crown fuel matrix while reducing convective cooling to the surrounding, thereby promoting crown fire initiation.

---

<sup>a</sup> Department of Mechanical Engineering, University of California, Riverside, CA 92521, USA

<sup>b</sup> Forest Fire Laboratory, Pacific Southwest Research Station, USDA Forest Service 4955 Canyon Crest Drive, Riverside, CA 92507, USA

## Linear Analysis of Drag Reduction in Channel Flow by Wall Heating/Cooling

Hiroya Mamori\*, Koji Fukagata\*, Jérôme Hoepffner\* and Shinnosuke Obi\*

Reduction of the skin friction drag in turbulent flows is of significant importance for effective energy utilization. In fully developed channel flows, the increment of the skin friction drag from the laminar value ( $\Delta D$ ) is expressed<sup>1</sup> as

$$\Delta D = \frac{3}{2} \text{Re} \int_{-1}^1 (-\overline{u'v'})(-y)dy. \quad (1)$$

Here,  $\text{Re}$  is the Reynolds number based on the laminar centerline velocity and the channel half-width, and  $-\overline{u'v'}$  is the Reynolds shear stress.

Recently, Min et al.<sup>2</sup> have reported that a traveling wave-like surface blowing and suction can reduce the skin friction drag by producing a negative Reynolds shear stress in the region near the wall. Similar effect can be expected with body forces. The objective of this study is to make a linear analysis on the possibility of drag reduction by using a traveling wave-like surface heating and cooling.

The linearized and Fourier-transformed continuity, Navier-Stokes and energy equations can be expressed as matrix equation, i.e.,  $\mathbf{A}\hat{\mathbf{q}} = \mathbf{b}$ . Here,  $\mathbf{A}$  is the system matrix discretized by using the Chebyshev collocation,  $\hat{\mathbf{q}}$  contains the discretized velocity, pressure and temperature, and  $\mathbf{b}$  is the vector including the boundary condition. From the solution,  $\hat{\mathbf{q}}$ , the velocity and temperature fluctuations and the Reynolds shear stress distribution can be determined.

Figures 1 and 2 are sample results obtained by the present analysis. Increment of drag ( $\Delta D$ ) is shown in Fig. 1 as a function of  $c$ , where  $c$  is the wavespeed of the traveling wave. It shows that  $\Delta D$  is negative when the wave travels downstream ( $0 \leq c \leq 0.47$ ). Figure 2 illustrates this mechanism. The buoyancy force is created by the temperature distribution from surface traveling wave (Fig. 2(a)), and the velocity fluctuations are induced so as to make the Reynolds shear stress nominally negative in the region near the wall (Fig. 2(b)).

\*Department of Mechanical Engineering, Keio University.

<sup>1</sup>K. Fukagata et al., *Phys. Fluids* **14**, L73-L76 (2002).

<sup>2</sup>T. Min et al., *J. Fluid Mech.* **558**, 309-318 (2006).

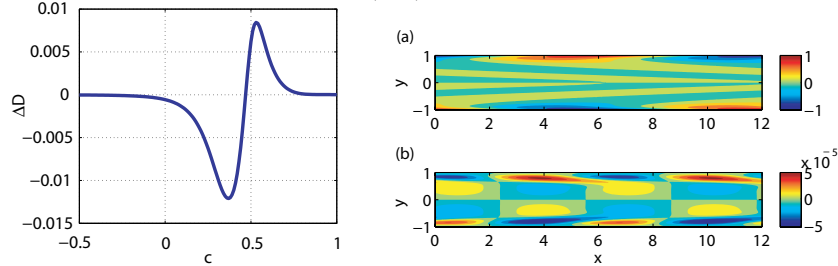


Figure 1: Increment of friction drag,  $\Delta D$ , Figure 2: Distribution of fluctuation: (a) temperature; (b) Reynolds shear stress.

Plane Couette flow at the laminar-turbulent transition as a spatiotemporal process

Paul Manneville, Ladhyx, Ecole Polytechnique, 91128 Palaiseau

Plane Couette flow at the laminar-turbulent transition has been studied via numerical simulations of a model focusing on the in-plane  $(x,z)$  space dependence of a few velocity amplitudes with reduced cross-stream  $(y)$  dependence. The model appears well suited to the study of the low- $R$  transitional range. I shall present my most recent findings and discuss in particular the fact that the spatio-temporal perspective taken seems to give a better understanding of processes at work in extended systems than the classical viewpoint in terms of chaotic transients characteristic of the low-dimensional dynamical system approach.

## Impulse response in a subcritical cylinder wake

C. Marais, R. Godoy-Diana, D. Barkley and J.E. Wesfreid \*

We study experimentally the impulse response of a cylinder wake in the subcritical regime, in a hydrodynamic tunnel, using two-dimensional particle image velocimetry (PIV). Previous experimental works<sup>1</sup> have used the spatiotemporal evolution of streak lines from dye visualizations to analyze qualitatively the evolution of a perturbation. Here we obtain quantitative measurements in the wake of the cylinder using PIV, which allow us to accurately describe the evolution of the wave packet produced by a small perturbation to the subcritical wake. We disturb the flow by imposing a very short rotary motion of amplitude  $\delta\theta$  to the cylinder. The strength of the rotation is chosen such that the duration of the perturbation (nondimensionalized by the convection time) is kept constant. For each experiment we determine, using spatiotemporal diagrams of the cross stream velocity field (see figure 1.a) the position in time and space of the maximum perturbation amplitude and the group and phase velocities of the wave packet. The energy gain (see figure 1.b) as a function of time allows to get a clear view of the time scales involved in the evolution of the convectively unstable packet as a function of the Reynolds number. Finally, we compare the experimental results with numerical simulations (2D DNS).

\*PMMH, Equipe Instabilités, Contrôle et Turbulence, CNRS ESPCI, Univ. Paris 6 et Paris 7.

<sup>1</sup>V.Croquette and P.Le Gall, *Physical Review E* **62**, 3 (2000).

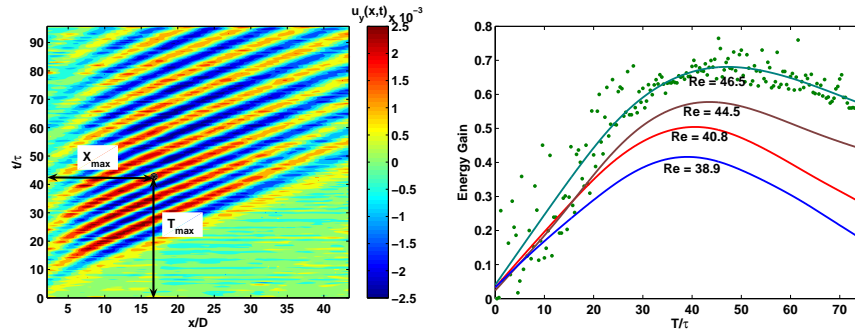


Figure 1: (a) Spatiotemporal diagram for a Reynolds number equal to 46.3.(b) Energy gain  $G(t)$ : each curve corresponds to a different Reynolds number. For the highest Reynolds number the data points are shown together with a fitted curve.

## Lagrangian Dispersion of Inertial Particles in Turbulent Swirled Flow

Cristian Marchioli\*, Francesco Zonta\* and Alfredo Soldati\*

Swirling flows gained an increasing interest in the last decade due to their importance in the oil industry, where high-pressure pneumatic conveying in large piping systems are often encountered. These flows are of particular importance in technical applications such as axial separators or hydrocyclones, where gas-solid, gas-liquid or liquid-liquid mixtures are separated by a centrifuging swirler.

The mechanisms controlling axial separation in such devices are closely related to the interactions between dispersed phase dynamics and turbulent transport and mixing<sup>1</sup>. In two-phase turbulent flows without swirl, separation can be regarded as the outcome of a three-stage process<sup>1</sup>: first, the dispersed phase (constituted here by inertial particles or droplets) is segregated into clusters localized around the large vortical structures of the flow; then clusters are transported by the instantaneous realizations of the fluid Reynolds stresses towards the wall, where deposition occurs; once at the wall, particles/droplets remain trapped by turbulence in the viscous sublayer, where particle concentration eventually increases.

When a swirling flow is superposed to the mean axial flow, an additional wall-ward centrifugal effect acts on the particles and favours separation by increasing particle deposition rates. However, the swirl motion imparted to the fluid may also disrupt the near-wall turbulence structures, thus being detrimental for particle trapping. Separation efficiency, which is the key parameter for optimized separator performance, will increase or decrease depending on which of these two opposite mechanisms will prevail. Deep understanding and detailed knowledge of the physical mechanisms controlling particle dispersion in turbulent swirled flows are thus fundamental if one seeks to maximize the separation efficiency. Accurate numerical simulations are a useful tool to improve current understanding of complex flow physics associated with swirling flow phenomena: unfortunately, little effort has been taken in this direction so far<sup>2</sup>.

In this paper, we present results obtained from a Direct Numerical Simulation of turbulent particle dispersion in gas-solid swirled pipe flow at Reynolds number  $Re = 5000$ , based on the bulk velocity (the corresponding shear Reynolds number being  $Re_\tau = 170$ ). The model we used to develop the swirling flow is the so-called Batchelor concentrated vortex, which produces a rotation characterized by axially-decaying intensity and concentrated near the pipe center<sup>2</sup>. The fluid is air, assumed to be incompressible and Newtonian. Three large samples of micrometer size particles, characterized by Stokes numbers  $St = 0.1, 1$  and  $10$  (corresponding to diameters  $d_p = 6.8, 21.4$  and  $67.8 \mu m$ , respectively) are tracked following the Lagrangian approach.

The instantaneous features of the turbulent flow field and particles dispersion are discussed from a qualitative mechanistic viewpoint to analyze the role of the decaying swirl motion on the separation process and its effect on axial separation efficiencies. Quantitative velocity and dispersion statistics are also provided.

---

\*Dipartimento di Energetica e Macchine, University of Udine.

<sup>1</sup>A. Soldati, *ZAMM - J. of Applied Mathematics and Mechanics* **85**, 683 (2005)

<sup>2</sup>S. Muntean et al., *Transactions on Mechanics* **50**, 77 (2005).

### Three-dimensional linear stability analysis of lid-driven cavity flow

Luca Marino\*, Paolo Luchini†

In this paper we present the numerical analysis of an incompressible flow in a 3-D lid-driven cavity. The stability analysis is classically carried out by a linear approach and the flow field is given by a stationary base flow and a time dependent small amplitude perturbation. Both the base flow and the fluctuating field are three-dimensional.

The two dimensional case has been extensively investigated by many authors in the past while, recently, has been studied<sup>1, 2</sup> the three dimensional linear stability of a 2-D base flow.

The fully three dimensional flow is still considered both for numerical benchmarks and vortex analysis purposes and represents a challenging goal from the numerical point of view.

The governing equation for the base flow and the stability problem are formulated in primitive variables and discretized on a staggered mesh by means of a second order finite differences scheme. An iterative algorithm, based on the multigrid technique, is adopted for the solution of the base flow and the linearized stability equations.

With reference to Fig. 1, the geometry considered corresponds to a square cavity of side  $L$  the with aspect ratio  $A$  in the span direction  $z$ . The flow is driven by the motion along the  $x$ - axis of the lid located at  $y = L$ .

The first instability has been studied for different values of the span aspect ratio of the cavity and for two set of boundary conditions. The first set corresponds to no-slip and no-penetration conditions for the velocity field at all the walls of the cavity. In the second set periodic boundary condition are given along the  $z$  direction.

The neutral curve is obtained for different values of the aspect ratio and for the two boundary conditions. In particular the analysis of the influence of the rigid endwalls in the spanwise direction has been investigated in a large range on  $A$  in so extending the results published<sup>3</sup> for  $A = 6.55$ .

\*Department of Aeronautics and Mechanics, University of Rome "Sapienza".

†Department of Mechanical Engineering, University of Salerno.

<sup>1</sup>S. Albensoeder et al., *Phys. Fluids* **13**, 121 (2001).

<sup>2</sup>V. Theofilis et al., *J. Fluid Mech.* **505**, 249 (2004).

<sup>3</sup>S. Albensoeder et al., *J. Fluid Mech.* **569**, 465 (2006).

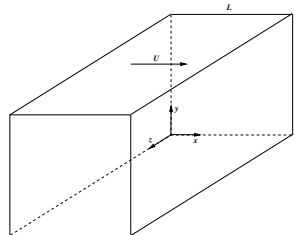


Figure 1: Geometry of the lid-driven cavity.

# Microfluidic with foams: interplay between the drag and the arrangement of bubbles

Philippe Marmottant, Jan-Paul Raven\*

We present an experimental study of the flow of 2D microfoams, resulting from the agglomeration of microbubbles. We use the flow-focusing method to produce the foam bubble by bubble, inside a microfluidic chip. The size can be controlled by the input gas pressure and liquid flow rate. Because bubble sizes are identical, they arrange in crystal patterns.

The foam flow rate in a microchannel depends non-linearly on the applied pressure. Large discontinuities appear when the topological arrangement of bubbles changes. Indeed for the same bubble volume, several patterns are possible. The simpler pattern is when there is only one bubble across the channel (bamboo looking pattern, named F1, bottom figure). When two bubbles are in the channel, we call the pattern a foam F2. We observe that rheology is strongly dependant on the arrangement of bubbles in the channel <sup>1</sup>.

The transition between the arrangements of bubbles provides a rich dynamical behavior in the rheology. We observe three types of transition: i) spontaneous oscillations between the structures, with a pulsation of the flow rate <sup>2</sup>, ii) coexistence of two phases in the channel, a structure being changed in the other at a fixed transition location, the flow rate is stable iii) advection and coexistence of two phases.

Looking at the video recording we evidence the occurrence of wave of rearrangements that goes upstream, the structure F1 being energetically less favorable than F2. According to the imposed velocity of the foam, the transitions reported previously can be classified in three types of non-linear instabilities: i) absolute when the wave of rearrangement is faster than the foam, ii) stationary when the wave has the same velocity and iii) convective when the wave goes slower. The speed of bubble rearrangement is thus crucial to determine the stability of the oscillator.

\*both at Laboratoire de Spectrométrie Physique, CNRS - Université Grenoble I, B.P. 87, F-38402 St Martin d'Hères Cedex, France

<sup>1</sup>J.P. Raven, P. Marmottant, F. Graner, *Eur. Phys. J. B*, **51**,137-143 (2006)

<sup>2</sup>J.P. Raven, P. Marmottant, *Phys. Rev. Lett.*, **97**, 154501 (2006)

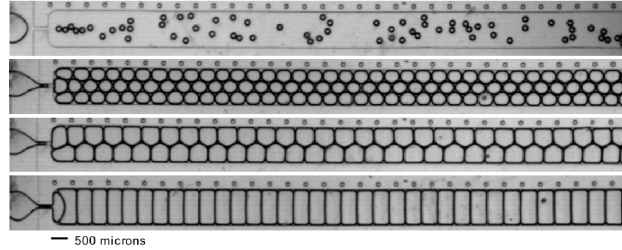


Figure 1: From bubbly flow (top) to microfluidic foams (F3, F2, F1).

## Influence of wall modes on the onset of bulk convection in a rotating cylinder

Francisco Marques\*, Juan M. Lopez<sup>†</sup> and Antonio Rubio<sup>‡</sup>

The onset of thermal convection in an enclosed rotating cylinder is greatly influenced by the interaction between the Coriolis force and the cylinder sidewall. For temperature differences between the hot bottom and the cool top that are too small to sustain convection throughout the entire cylinder, convection sets in as pairs of wall-bounded hot thermal plumes ascend and cold thermal plumes descend in the sidewall boundary layer, the so-called wall modes of rotating convection. Over an extensive range of parameter space, several wall modes with different numbers of thermal pairs coexist stably, and this multiplicity of states leads to very rich nonlinear dynamics as the temperature difference is increased to a level supporting thermal convection throughout the bulk of the cylinder<sup>1</sup>. The bulk convection takes on characteristics of Küppers-Lortz spatio-temporal chaos (see figure 1a), but its interaction with the persistent wall modes also leads to further flow complications (like the square patterns in figure 1b) which are explored here via numerical simulations<sup>2</sup>. The effects of the centrifugal buoyancy, that tends to decrease the azimuthal wave number of the wall modes and delay the bifurcations to larger Rayleigh numbers, are also discussed.

\*Applied Physics, Universitat Politècnica de Catalunya, 08034, Barcelona, Spain.

<sup>†</sup>Department of Mathematics and Statistics, Arizona State University, Tempe, AZ 85287, USA.

<sup>1</sup>Lopez, J.M., Marques, F., Mercader, I. & Batiste, O., *J. Fluid Mech.*, **590**, 187 (2007)

<sup>2</sup>Marques, F. & Lopez, J.M., *Phys. Fluids*, in press (2008)

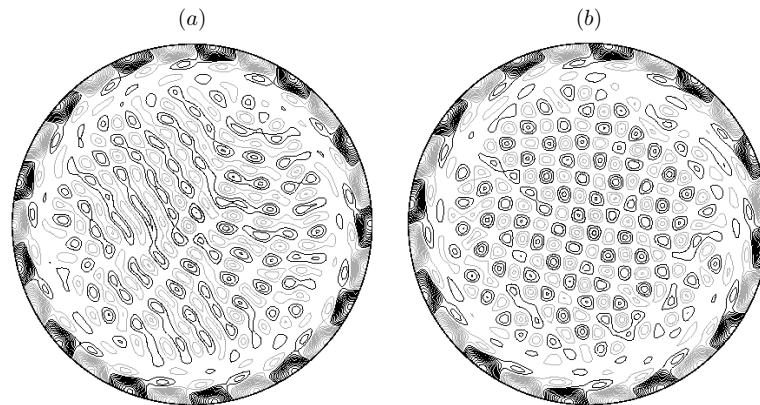


Figure 1: Bulk convection and wall modes at  $Ra = 10^5$ , aspect ratio 4, Prandtl number 7 and Coriolis number 625. (a) shows an  $m=13$  wall mode with Küppers-Lortz chaos, (b) shows an  $m=12$  wall mode with a square pattern and defects.



## Corner waves downstream a partially submerged vertical plate

Martínez-Legazpi, P.<sup>\*</sup>; Rodríguez-Rodríguez, J.<sup>†</sup>; Lasheras, J.<sup>‡</sup>

The flow downstream the corner of a partially submerged vertical plate is experimentally studied. In this flow configuration (see figure 1), a steady wave remains attached to the corner of the plate. Both the amplitude and slope of the wave front increase with the downstream distance until, depending on the value of a properly defined Froude number, the wave breaks giving birth either to a spilling or a plunging breaker.

The evolution and subsequent breakage of this wave resembles in many aspects that of two-dimensional deep-water breakers. This is a consequence of the slender nature of the flow, as the streamwise velocity is much larger than the other two components. The most interesting similarity is the existence of two different breaker configurations: spilling breakers and plunging breakers.

The velocity field and free surface have been measured for a number of flow configurations, with the aim at understanding the physical mechanism behind the breaking.

Using these experimental measurements as a guideline, a criterion to predict which configuration will exhibit the above described wave is proposed based on the idea that, once a plunging breaker is formed, the resulting plane jet follows a ballistic trajectory. In addition, a model for the jet range, and thus impact velocity, is obtained. It is worth noticing that the ability to model the behavior of this flow constitutes a tool to predict the air exchange between the waves, either generated by this configuration or not, and the ocean. This work has been partially supported by the ONR through grant N00014-05-1-0121.

<sup>\*</sup>Universidad Carlos III de Madrid.

<sup>†</sup>Universidad Carlos III de Madrid.

<sup>‡</sup>University of California San Diego

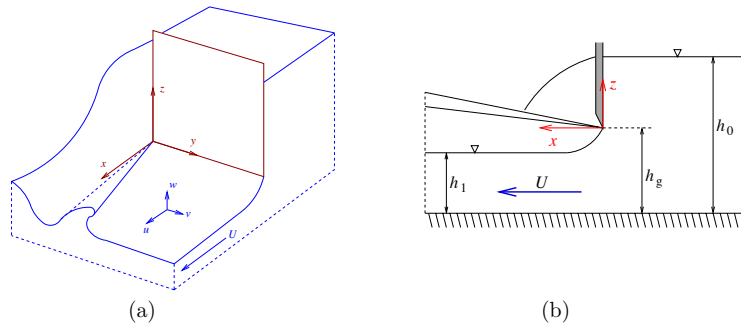


Figure 1: Sketch of the flow.

## Buoyancy Effects in the Process of Jet Formation

Marugán-Cruz, C.<sup>\*</sup>, Rodríguez-Rodríguez, J.<sup>\*</sup>, Martínez-Bazán, C.<sup>\* †</sup>

Starting jets, usually generated by the displacement of a piston that pushes the liquid through a hole or nozzle into a quiescent atmosphere, have been extensively studied. The boundary layer rolls up into a vortex ring, which moves at a certain velocity followed by a trailing jet. The effects of the length stroke, the shape of the nozzle, the velocity program and the velocity profile at the jet exit have been already understood by previous experimental, numerical or theoretical works<sup>1</sup>. In relation to jets with different densities important efforts have been carried out to study the dynamics of plumes and thermals, where the buoyancy effects are related with the different temperatures between the jet and the ambient fluid. Nevertheless, to our knowledge, some important aspects of buoyant jets, with density differences not related to temperature variations, still have not been addressed. In this work we have studied numerically and experimentally the formation of a negatively buoyant jet in a miscible liquid. The experimental set-up consists of a piston that injects the fluid into a tank filled with a denser fluid. The cases studied correspond to Reynolds numbers,  $Re = \rho_j U_j D / \mu_j$ , ranging from 300 to 3000, where  $\rho_j$  and  $\mu_j$  are density and viscosity of the light fluid,  $D$  is the diameter of the nozzle and  $U_j$  is the mean velocity of the jet at the exit of the nozzle. The present work is restricted to density differences such that  $\Delta\rho/\rho \ll 1$ , where we report evidences of the evolution of these jets and its dependence on the densimetric Froude number,  $Fr = \rho_j U_j^2 / \Delta\rho g D$ . For Froude numbers smaller than a critical value,  $Fr_c$ , no jet is formed and the vortex head remains close to the wall for all times. On the other hand, for Froude numbers larger than  $Fr_c$  two regimes have been found with a smooth transition between them. For  $Fr$  moderately larger than  $Fr_c$  the vortex ring detaches but it does not have enough energy to penetrate the heavier fluid whereas for larger  $Fr$  the vortex ring travels distances much larger than the diameter. Figure 1 shows the vorticity contours for the same non-dimensional time for three different Froude numbers ( $Fr = \infty$ ,  $Fr > Fr_c$  and  $Fr < Fr_c$ ). Comparison between experiments and numerics are shown. Finally an attempt is made to theoretically model the behavior of the flow near the critical Froude number.

<sup>\*</sup>Universidad Carlos III, Madrid.

<sup>†</sup>Área de Mecánica de Fluidos, Dep. Ingeniería Mecánica y Minera, Universidad de Jaén, Spain

<sup>1</sup>Gharib et al., *J. Fluid Mech.* **360**, 121 (1998).

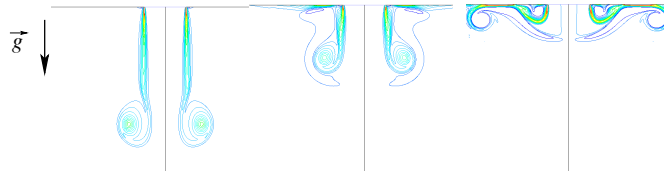


Figure 1: Vorticity contours for a)  $Fr = \infty$ , b)  $Fr > Fr_c$  and c)  $Fr < Fr_c$ .

## Numerical and experimental study of wavelength selection of Görtler vortices

Kouhei Baba\*, Noritaka Aota\*, Masaharu Matsubara\*

In a boundary layer on a concave wall, longitudinal vortices, so-called Görtler vortices, are generated due to a centrifugal-type instability mechanism. In spite of many studies on Görtler vortices, investigation on the spanwise wavelength selection of Görtler vortices are limited. An open questions on it is disagreement of the wavelength observed by experiments with that predicted by linear stability theory. In this work, the spanwise wavelength of the Görtler vortices fully developed in an asymptotic suction boundary layer on the concave porous wall is determined by means of numerical simulations and experiments. A benefit of this flow field is in ease to compare between the linear theory and experimental results because of a consistent boundary layer thickness.

In numerical simulations, Fourier-Galerkin method for spanwise direction, Chebychev-collocation method for normal-to-wall direction have been employed to discretize spatially. The boundary condition on the wall is non-slip condition and on the spanwise bound is periodic condition. The disturbance equations can be solved by marching in streamwise coordinate by means of second-order backward difference scheme. The experimental setup consists of a straight porous wall followed by a concave porous wall. The air is homogeneously sucked through both porous walls to realize an asymptotic suction boundary layer.

Figure 1 shows comparison of the calculation result in the case of multi mode initial disturbance including ten different wavelength modes with the naturally generated Görtler vortices in experiments. Height and spacing of low velocity regions forming mushroom-like shapes are in good agreement with the experimental result. This is suggesting well performance of calculation. The non-dimensional wavelengths  $U_\infty \lambda / \nu$  decrease with increase the non-dimensional curvature radius  $\nu / U_\infty R$ , and they fall in a narrow band on the line  $(\nu / U_\infty R)^{-0.8}$ . This results is also confirmed for previous experimental results in Görtler vortices on an a developing boundary layer. It is concluded that the spanwise wave selection of Görtler vortices has a certain physical mechanism.

\*Shinshu University. 4-17-1 Wakasato, Nagano, 380-8553, Japan.

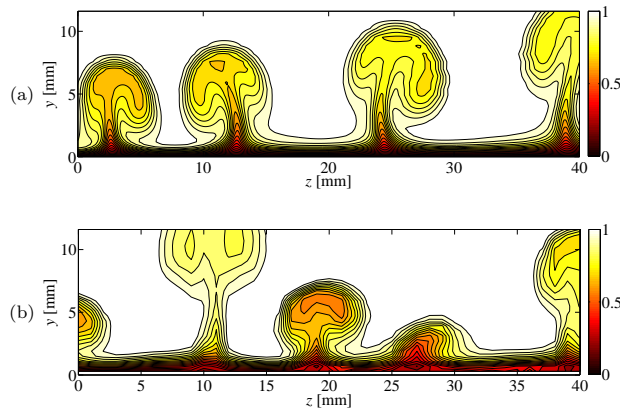


Figure 1: Contour maps of streamwise velocity. (a) Numerical simulation, (b) Experiment.

## Pipe flow critical trajectories and underlying solutions

F Mellibovsky\*, A Meseguer

Pipe flow undergoes transition to turbulence despite the linear stability of its basic laminar solution. Finite amplitude solutions in the form of travelling waves<sup>1</sup>, coexisting with the basic flow, have been identified in the last few years. While they have been proved to play a certain role in the turbulent dynamics<sup>2</sup>, their involvement in the transition process seems to be simply ungrounded. Furthermore, some recent experimental results point at a transitory nature of turbulence<sup>3</sup>, thus questioning the mere existence of a well defined critical threshold. The region of phase space dominated by turbulent dynamics would then be constituted by a surging amount of bifurcating complex solutions as the Reynolds Number is increased, acting as an attractor most of the time, but always retaining some probability that any trajectory finds its way back to laminarity. However transient may turbulence be, the notion of a threshold separating initial conditions that lead to transition from others that end up decaying still applies. It suffices to define the threshold as the point where the perturbation lifetime seems to diverge, possibly not to infinity if turbulence is a transient phenomenon, but still abruptly. Then, the threshold regains interest, and the question can be asked of how a solution wandering about criticality<sup>4</sup> would look like. Starting from different initial conditions, and through accurate refinements, trajectories on the edge between turbulence and laminarity can then be analysed to elucidate which properties of a solution determine whether it belongs to the laminar or the turbulent basin of attraction. We analyse these trajectories to try and understand transition. Using an adapted Newton method we systematically search for travelling wave solutions underlying the dynamics of these critical trajectories (Fig 1).

\*Dept. Física Aplicada, Universitat Politècnica de Catalunya.

<sup>1</sup>H. Faisst and B. Eckhardt, *Phys. Rev. Lett.* **91**(22), 224502 (2003).

<sup>2</sup>B. Hof et al., *Science* **305**, 1594 (2004).

<sup>3</sup>B. Hof et al., *Nature* **443**(7107), 59–62 (2006).

<sup>4</sup>T. Schneider et al., *Phys. Rev. Lett.* **99**(3), 034502 (2007).

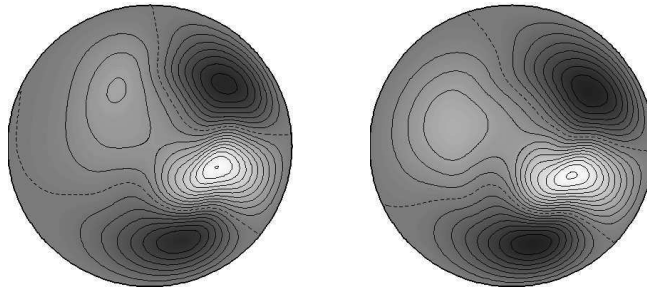


Figure 1: Axial velocity contours on a cross-section. Left: critical trajectory based on the streak-breakdown scenario. Right: converged exact travelling wave solution.

## Numerical exploration of subcritical instabilities in small gap Couette-Taylor problem

Alvaro Meseguer\*; Fernando Mellibovsky\*

The phenomenon of subcritical transition in a fluid confined between counter-rotating cylinders will be studied numerically. The exploration is carried out for a small gap case  $\eta = a/b = 0.882$ , where  $a$  and  $b$  are the inner and outer radii of the cylinders, respectively. This problem has been addressed experimentally in the past<sup>1</sup>. The investigation intends to identify turbulent transient bursts resulting from finite amplitude perturbations of selected azimuthal and axial periodicity. This procedure is carried out close to the part of the Couette-Taylor diagram where spiral turbulence and hysteretic effects have been identified<sup>2</sup>. The study provides time-scale analysis of the transient bursts and tries to identify secondary flows responsible for the intermittency.

---

\*Dept. Applied Physics, Universitat Politècnica de Catalunya.

<sup>1</sup>Coles, D., *J. Fluid Mech.* **21**, 385 (1965).

<sup>2</sup>Hegseth et al., *Phys. Rev. Lett.* **62**(3), 257 (1989).



## Instabilities of a Braginsky fluid

Jonathan Mestel<sup>\*</sup>, Steve Cowley<sup>†</sup> and Alex Schekochihin<sup>‡</sup>

When plasma is permeated by a sizable magnetic field its behaviour is strongly influenced by the Lorentz force. Even when the magnetic field is so weak that the Lorentz force is negligible, however, individual ions have a tendency to gyrate around the local field direction,  $\mathbf{b}$ . This gives rise to an anisotropic viscosity in the stress tensor, which in most applications dominates the usual viscosity. Standard homogeneity and isotropy arguments are then shown to give rise to the modified Navier-Stokes equations

$$\rho \frac{D\mathbf{u}}{Dt} = -\nabla p + \beta \nabla \cdot (\Gamma \mathbf{b} \mathbf{b}) \quad \nabla \cdot \mathbf{u} = 0,$$

where

$$\Gamma = \mathbf{b} \cdot \nabla \mathbf{u} \cdot \mathbf{b}.$$

The unit vector  $\mathbf{b}$  is itself advected by the conducting fluid according to

$$\frac{D\mathbf{b}}{Dt} = \mathbf{b} \cdot \nabla \mathbf{u} - \Gamma \mathbf{b}.$$

These coupled evolution equations were first obtained by Braginsky<sup>1</sup> using a kinetic approach.

In this paper we investigate a class of exact solutions to the Braginsky equations which are  $O(1)$  perturbations of a simple straining flow,

$$\mathbf{b} = \mathbf{b}(x, t) \quad \mathbf{u} = (\lambda_2 x, \lambda_1 y, -(\lambda_1 + \lambda_2)z) + (0, v(x, t), 0).$$

It is shown that some nonlinear solutions lose smoothness in a finite time, less than a typical eddy-turnover time of a large-scale flow. Solutions with the field direction parallel to the compression axis, which would be expected to be unstable on the eddy-turnover time, are shown in fact to have super-exponential growth.

The theoretical predictions are compared with numerical simulations and the implications for the large-scale structure of turbulent flow are discussed.

---

<sup>\*</sup>Mathematics Dept, Imperial College London.

<sup>†</sup>Physics Dept, Imperial College London.

<sup>‡</sup>S.I. Braginsky, *Rev. Plas Phys.* **1**, 285.





### Falling clouds of particles in viscous fluids

Bloen Metzger\*, Maxime Nicolas\* and Elisabeth Guazzelli\*

We have investigated both experimentally and numerically the time evolution of clouds of particles settling under the action of gravity in an otherwise pure liquid at low Reynolds numbers. We have found that an initially spherical cloud containing enough particles is unstable. It slowly evolves into a torus which breaks up into secondary droplets which deform into tori themselves in a repeating cascade. Due to the fluctuations in velocity of the interacting particles, some particles escape from the cloud toroidal circulation and form a vertical tail. This creates a particle deficit near the vertical axis of the cloud and helps in producing the torus which eventually expands. The rate at which particles leak from the cloud is influenced by this change of shape. The nature of the break-up of the torus is found to be intrinsic to the flow created by the particles when the torus aspect-ratio reaches a critical value.

---

\*IUSTI-CNRS UMR 6595

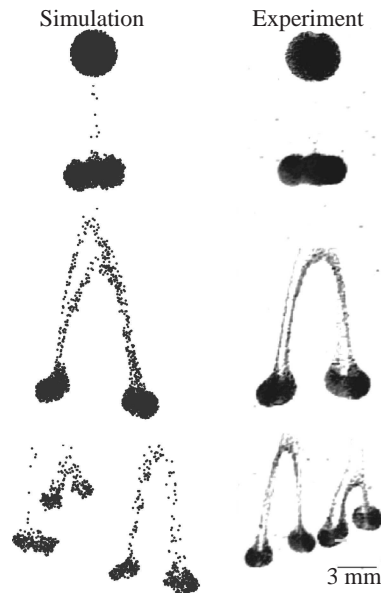


Figure 1: Snapshots of a falling cloud: point-particle simulation with  $N_0 = 3000$  (left) and experiment using glass beads of  $100\ \mu\text{m}$  in silicon oil (right).

### Dynamics of a fluid inside a precessing cylinder

Romain Lagrange\*, Patrice Meunier\*, François Nadal† & Christophe Eloy\*

The dynamics of a fluid inside a precessing cylinder is addressed theoretically and experimentally. Such a motion is found for example in aeronautics (precession of flying objects with liquid propellant) and in geophysics (terrestrial precession, influence on its liquid core).

It is well known<sup>1</sup> that precession forces hydrodynamics waves called Kelvin modes whose structure and amplitude are predicted by a linear and inviscid theory. When a Kelvin mode is resonant (i.e when the cylinder height is an odd number of half wavelength) its amplitude diverges and it is necessary to consider viscous<sup>2</sup> and non-linear effects. We have shown that this amplitude saturates at a value which scales as  $Re^{1/2}$  for small Reynolds numbers and as the precessing angle to the one third for large Reynolds numbers<sup>3</sup>.

For sufficiently large Reynolds numbers, this flow becomes unstable<sup>4,5</sup>. By a linear stability of analysis we have established a formal expression of the growth rate when a Kelvin mode forced by precession resonates with two free Kelvin modes. Figure 1 shows the vorticity, in transverse sections, of these free Kelvin modes. The interaction between three Kelvin modes (triadic resonance) is realized thanks to the non-linear term of the Navier–Stokes equation. From the expression of the growth rate we have determined the precessing angle for which the flow becomes unstable. Predictions are in good agreement with experimental measurements obtained by PIV.

\*Institut de Recherche sur les Phénomènes Hors Équilibre, Université de Provence, France.

†Commissariat à l'énergie Atomique, CESTA, France.

<sup>1</sup>McEwan, A.D. (1970). *J. Fluid Mech.* **40**(3) 603-640

<sup>2</sup>Gans, R. F. (1970). *J. Fluid Mech.* **41**(4) 865-872

<sup>3</sup>Meunier et al. (2007). *J. Fluid Mech.* **599** 405-440

<sup>4</sup>Manasseh, R. (1996). *J. Fluid Mech.* **315** 151-173

<sup>5</sup>Kobine, J.J. (1996). *J. Fluid Mech.* **319** 387-406

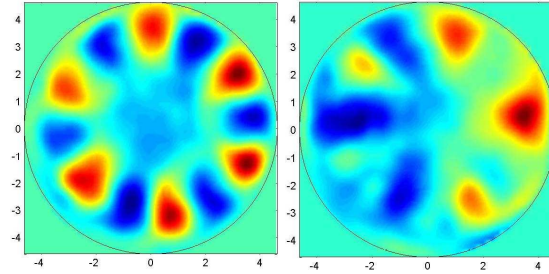


Figure 1: Experimental vorticity fields of the instability inside a precessing cylinder at two different transverse sections: mid-height section (left) and quarter-height section (right)

## Exact solutions for a turbulent buoyant plume rising from a circular source in an unstratified quiescent environment

Ghislain Michaux\* and Olivier Vauquelin\*

We consider a turbulent round plume which is formed by the steady release of a buoyant isothermal fluid into a quiescent environment. The environment is assumed to be unconfined and unstratified. The purpose of this study is to establish exact analytical expressions for the evolutions with height of the main plume variables (radius, vertical velocity and density).

Initial works were proposed by Morton *et al.*<sup>1</sup> who established the time-averaged conservation equations in terms of *top-hat* variables. The authors derived similarity solutions for the mean plume variables with the Boussinesq approximation (density variations neglected except in the buoyancy term). More recently, Delichatsios<sup>2</sup> and Rooney & Linden<sup>3</sup> shown that similarity solutions can also be obtained in the general non-Boussinesq case. Similarity solutions are based on point source of buoyancy assumption whereas, in many cases of practical interest, real sources have finite area with initial radius, velocity and density. Nevertheless, Morton<sup>4</sup> demonstrated that the flow above a source of finite area can be related to an equivalent plume rising from a buoyant point source via the introduction of a virtual origin correction. However, with such a correction, the similarity theory may be sufficient to describe the plume in the far-field region but is not suitable close to the source. As an example, the use of similarity solutions does not allow to characterize the possible occurrence of particular flow features in the near-field region such as a neck (point of minimum cross-section) and a velocity peak<sup>5</sup>.

This study extends the previous theoretical works by providing exact analytical solutions for all plume variables (radius, vertical velocity and density deficit) at any height (near-field and far-field) and for both the Boussinesq and non-Boussinesq cases. At first, using a particular set of variables, governing equations are re-written under a form which encompasses both the Boussinesq and non-Boussinesq cases. We also introduce the *plume function*  $\Gamma(z)$  which extends the source parameter initially defined by Morton<sup>4</sup> and known to inform about the plume regime (*lazy*, *pure* or *forced*)<sup>6</sup>. Then, we derive analytical expressions for all plume variables in terms of  $\Gamma$  only. Finally, we show that, for known source conditions, the plume function  $\Gamma$  (and subsequently, all plume variables) can be evaluated at any distance above the source via two integral functions which are defined separately for lazy and forced plumes. In addition, exact expressions for the maximum velocity and the plume neck as well as for their locations above the source are derived from the analytical solutions.

\*IUSTI, University of Aix-Marseille, France.

<sup>1</sup>Morton et al., *Proc. Roy. Soc.* **243**, 1 (1956).

<sup>2</sup>M.A. Delichatsios *Comb. Sc. Tech.* **24**, 191 (1981).

<sup>3</sup>G.G. Rooney and P.F. Linden *J. Fluid Mech.* **318**, 237 (1996).

<sup>4</sup>B.R. Morton, *J. Fluid Mech.* **5**, 151 (1959).

<sup>5</sup>T.K. Fannelp and D.M. Webber, *J. Fluid Mech.* **497**, 319 (2003).

<sup>6</sup>B.R. Morton and J. Middleton, *J. Fluid Mech.* **58**, 165 (1973).

## Wildfire Simulation and Challenges in Modelling Heat Transfer Behaviour

George Milne and Paul Johnston, University of Western Australia

A wildfire spread simulator takes as inputs the current position of the fire, the spatial variation of fuel types and topography, the temporal variation of fuel moisture and weather conditions and fire suppression activities. Fire simulation is a mathematical and computational task which applies existing fire behaviour models to the input data and projects the fire position forward through time.

Challenges face us when developing a simulator based on the transfer of discrete packets of heat across the landscape, where the landscape is divided into irregular polygons to avoid introducing directional bias. However, we are challenged by lack of knowledge of heat dissipation to the atmosphere and the rate of generation and consumption of energy by the burning and unburnt polygons, respectively. We currently adopt the traditional propagation delay approach to simulate the spread of fire. The advantage of this approach is that fire behaviour models input directly into the simulation engine and there is no need for further calibration.

The most important feature of the simulator technology is its extreme efficiency. Simulations that previously required several minutes to run now complete in less than a second. This quantum leap in performance allows us to rapidly perform hundreds of simulation experiments of the same fire with different input data, allowing us to factor in uncertainties in forecast weather, fuel state and the current state of a fire.

## Wave processes in a viscous shock layer and problem of pulsations control

S. G. Mironov<sup>a,b</sup>, A. N. Kudryavtsev<sup>a</sup>, A. A. Maslov<sup>a,b</sup>,  
T. V. Poplavskaya<sup>a,b</sup> and I. S. Tsyryulnikov<sup>a</sup>

The paper describes a work on numerical and experimental study of the characteristics of disturbances generated in the hypersonic shock layer on a flat plate by free-stream disturbances, and of disturbances entered into the shock layer from a surface were carried out. The method of the active (interference) control of pulsations intensity in the shock layer was proposed. This method has been confirmed by the direct numerical simulation<sup>1</sup> and realized experimentally.

The computational investigations were performed with the direct numerical simulation method based on full two-dimensional unsteady Navier-Stokes equations with the use of high-order shock-capturing scheme<sup>2</sup>. In the free-stream the disturbances were specified as plane waves, the disturbances from the surface were specified with a finite-size “blow-suction” source. The numerical simulation is performed within the wide range of stream parameters and parameters of disturbances-shock layer interaction. In particular, the receptivity of the shock layer to the acoustic waves in the free-stream and “blow-suction” pulsations was studied with the varying amplitude and frequency of disturbances at Mach numbers of 12 and 21, Reynolds number based on free-stream parameters and plate length equal to  $Re_L = 1.44 \cdot 10^5$ ,  $2.88 \cdot 10^5$ ,  $4.32 \cdot 10^5$  and the surface temperature factor range being from 0.08 to 0.5.

The experiments were performed in the hypersonic nitrogen wind tunnel T-327A based in ITAM SB RAS at Mach number 21, Reynolds number  $Re_L = 1.44 \cdot 10^5$  and the surface temperature factor range being from 0.08 to 0.5. The measurements in the shock layer were carried out with the electron-beam fluorescence method. It was obtained the data on the mean flow and pulsations characteristics produced in the shock layer by the natural (uncontrolled) disturbances of the free-stream of the wind tunnel, and with the periodical controlled disturbances entered into the free-stream and shock layer. In the wind-tunnel experiments, the pulsations generated in the shock layer by the acoustic waves of the external flow, were suppressed/amplified by the disturbances generated by an oblique-cut gas-dynamic whistle with the controlled phase shift relative to the external disturbances. Comparing the data of the direct numerical simulation and measurement data at the realization of control of pulsation intensity has demonstrated good agreement between the computational and experimental results.

The work has been financially supported by the Russian Foundation for Basic Researches (Grant No. 05-08-33436).

---

<sup>a</sup> Khristianovich's Institute of Theoretical and Applied Mechanics SB RAS, Novosibirsk, Russia.

<sup>b</sup> Novosibirsk State University, Novosibirsk, Russia.

<sup>1</sup> Fomin et al., *Rep. RAS*, **414**(2), 190 (2007).

<sup>2</sup> Kudryavtsev et al., *Appl. Mech. & Techn. Phys.* **47**(5), 617 (2006).

## Dynamics and rheology of vesicle and red blood cell suspensions

Chaouqi Misbah\*

Giant vesicles are closed bilayer membranes suspended in an aqueous solution. They are believed to represent a simple model for red blood cells. We discuss several features out of equilibrium. For example, under a shear flow a vesicle is known to exhibit four different behaviors that will be discussed here. The most known dynamics are tankreading (TT) and tumbling (TB). TT corresponds to the situation where the vesicle makes a constant angle with the flow while its (fluid) membrane undergoes a tank-reading-like motion. If the viscosity contrast between the interior and the exterior exceeds a certain critical value there is a bifurcation from TT to TB. Both analytical and numerical results will be presented. We shall make a link between microscopic dynamics and rheology. It will be shown that the microscopic dynamics is encoded in some rheological signatures. For example, at the TT-TB bifurcation point the effective viscosity exhibits a minimum, while the normal stress differences undergo a collapse. The rheology of vesicles<sup>1,2</sup>, markedly differs from that of droplets (emulsion)<sup>3</sup>. As a way of example, the effective viscosity of vesicle suspensions decreases with the viscosity contrast in the TT regime, while the opposite is found for emulsions. We shall also discuss some recent experiments on vesicles and red blood cells. The behavior is in agreement with theoretical predictions obtained for vesicles.

---

\*Laboratoire de Spectrométrie Physique-UMR 5588, CNRS - Université Joseph Fourier, Grenoble I, BP 87, 38402 Saint Martin d'Hères, France

<sup>1</sup>C. Misbah, Phys. Rev. Lett. **96**, 028104 (2006)

<sup>2</sup>G. Danker and C. Misbah, Phys. Rev. Lett. **98**, 088104 (2007)

<sup>3</sup>G.I. Taylor, Proc. Royal Soc. A **146** 501 (1934)

### Three component miscible viscous fingering of finite sample with linear adsorption

M. Mishra<sup>†,\*</sup>, M. Martin<sup>†</sup> and A. De Wit<sup>‡</sup>

Viscous fingering between miscible fluids of different viscosities can affect the dispersion of finite samples in porous media<sup>1</sup> and the adsorption of retained solutes onto the porous matrix<sup>2</sup>. Here, we investigate numerically (using a pseudo-spectral method<sup>3</sup>) on the basis of a three component model the influence of such viscous fingering due to a difference between sample solvent and eluent viscosities on the spreading of a solute initially dissolved in the sample and undergoing adsorption-desorption processes on the porous matrix. The model equations are governed by Darcy's law coupled to the convection-diffusion evolution equation for the concentration of the sample solvent and to a mass balance equation for the solute concentration. A linear adsorption isotherm model for the solute adsorption onto the porous matrix is considered. The influence of various parameters that control viscous fingering and especially of the retention parameter  $\kappa'$  are shown (see Fig. 1; at successive times in a frame moving at the velocity of eluent with log mobility ratio  $R = 2$ ). The possible disengagement of the retained solute zone with respect to the sample solvent zone as a function of  $\kappa'$  explains the effects of the sample solvent on the peak shape of analytes eluted in liquid chromatography experiments as discussed recently in the literature<sup>4</sup>. It is found that the larger the retention parameter  $\kappa'$ , the quicker the separation of both analyte and sample solvent plugs.

\*LSTM-Erlangen, Friedrich-Alexander Universität Erlangen-Nürnberg, Erlangen, Germany

<sup>†</sup>PMMH, Ecole Supérieure de Physique et de Chimie Industrielles, Paris, France

<sup>‡</sup>Nonlinear Physical Chemistry Unit, Université Libre de Bruxelles, Brussels, Belgium

<sup>1</sup>G. M. Homsy, *Ann. Rev. Fluid Mech.* **19**, 271 (1987).

<sup>2</sup>Mishra et al., *Phys. Fluids* **19**, 073101 (2007)

<sup>3</sup>C. T. Tan and G. M. Homsy, *Phys. Fluids* **29**, 3549 (1986)

<sup>4</sup>Keunchkarian et al., *J. Chromatogr. A* **1119**, 20 (2006)

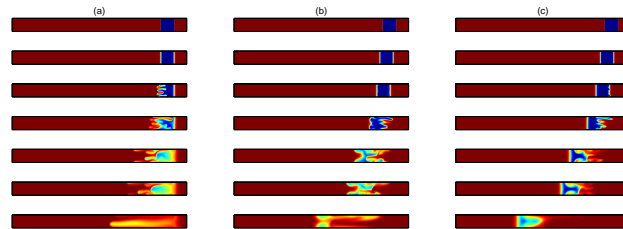


Figure 1: Density plots of the mobile phase concentration of the solute; (a)  $\kappa' = 0$  (b)  $\kappa' = 0.3$ , (c)  $\kappa' = 0.5$ .

## LES of Physiological Pulsatile Flow in a Model Stenosis

Md. Mamun Molla\*, Manosh C Paul\* and Giles Roditi †

A Large Eddy Simulation (LES) is performed to investigate the transition of physiological pulsatile (PP) flow through a 3D model of arterial stenosis. The computational domain is chosen as a simple channel with a biological type stenosis formed eccentrically on the top wall and the physiological pulsation is generated at the inlet using the fourth harmonic of the Fourier series of pressure pulse<sup>1</sup>. It is found that the presence of stenosis in the wall causes the flow laminar to turbulent at the post stenotic region where a high level of recirculation is achieved. Some interesting features of the flow physics are attained which will be presented in details in terms of the velocity vectors, vortices, velocity distribution, wall pressure and shear distribution, turbulent kinetic energy, velocity and pressure turbulent fluctuations as well as their energy spectra. The medical significances of these simulation results will also be explained physically.

In LES, the large scale flows are resolved fully while the unresolved sub-grid scale (SGS) motions are modelled using the Germano-Lilly dynamic model<sup>2</sup>. An assessment of using the LES for modelling the PP flow is made through the predictions of the SGS energy dissipation into the flow. The LES code used here is in-house developed and second-order accurate in both time and space. The physiological inlet velocity profile and the spanwise-averaged vorticity for  $Re = 2000$  are shown in Figures 1 and 2 respectively. The structure of the vortices and their break-down nature towards the downstream are captured well in the simulation.

\*Department of Mechanical Engineering, University of Glasgow, Glasgow, G12 8QQ, UK.

†Department of Radiology, Glasgow Royal Infirmary, 16 Alexandra Parade, G31 2ER, UK.

<sup>1</sup>Nichols *et al.*, *McDonald's Blood Flow in Arteries: Theoretical, Experimental and Clinical Principles*, 4th Edition, Oxford University Press (1998).

<sup>2</sup>D. K. Lilly, *Phys. Fluids A*, **2**(2), 633 (1992).

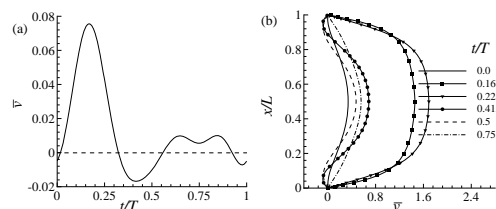


Figure 1: (a) Physiological velocity and (b) Inlet velocity profiles at different time.

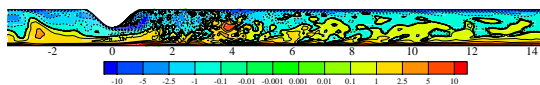


Figure 2: Spanwise-averaged vorticity at the peak pulsation.



## MODELLING THE EFFECT OF FLOW PULSATION ON TURBULENT FLOW IN A $10^\circ$ PLANE DIFFUSER

Tim Craft, Hector Iacovides, Parham Momeni \*

Flows involving detachment and reattachment are found in a range of engineering systems such as vehicles and planes. The  $10^\circ$  diffuser flow considered here sees gradual change in the mean flow, which makes it challenging to model. The separation point here is not geometrically fixed, so the effect of separation control can then be investigated for both the flow detachment and reattachment processes. The subject of this investigation is the response of the flow to the imposed unsteadiness arising from a periodic injection / suction upstream of the reattachment point. The test case examined is that studied experimentally by Masuda et al.<sup>1</sup> shown in Figure 1. There are considerable modelling challenges in computing flows exhibiting even steady detachment and reattachment. In order to minimize computing times there is a desire to employ relatively simple RANS models of turbulence. However, simple linear eddy-viscosity models are known to perform badly in separated flows, and even non-linear eddy-viscosity models do not all produce accurate and reliable results. In a recent study, Craft et al.<sup>2</sup> introduced refinements to a non-linear eddy-viscosity model and showed that this performed quite successfully in predicting the steady flow and heat transfer through a sudden pipe expansion. The present work tests the two-equation linear  $k - \epsilon$  scheme<sup>3</sup>, and the modified two-equation non-linear model.

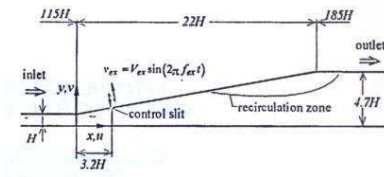


Figure 1: The Masuda et al.  $10^\circ$  diffuser

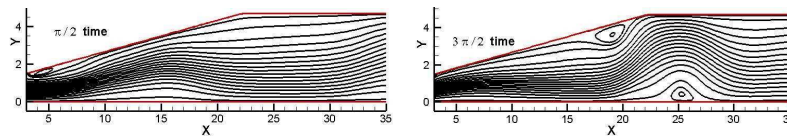


Figure 2: Computed streamlines at two time phases ( $\pi/2$  and  $3\pi/2$ )

Figure 2 shows predicted instantaneous streamlines for the forced case (at a Strouhal number  $St_H = fH/U_{inlet}$  of 0.005) at two phase times ( $\pi/2$  and  $3\pi/2$ ), demonstrating the significant temporal variations that occur. Further details and analysis will be presented in the final paper.

\*School of Mechanical, Aerospace and Civil Engineering, University of Manchester.

<sup>1</sup>Masuda et al., *Turbulence Control - ASME***193**, (1994).

<sup>2</sup>Craft et al., *UK Heat transfer conference, Manchester*, (2005).

<sup>3</sup>Launder, B. E. and Sharma, B.I., *Lett. Heat Mass Transfer***1**,(1974).

## The development of turbulent pipe flow

J. P. Monty\*, M. S. Chong\*, J. Doherty\* and P. Ngan\*.

The paper presented aims to determine the length required of a circular pipe before turbulent fluid flowing through it reaches a ‘fully developed’ state. The definition of ‘fully developed’ flow has been somewhat unclear to date, but is commonly thought to exist when the flow is statistically streamwise invariant; usually mean velocity is the statistic of choice due to ease of measurement. However, most investigations into turbulent pipe flow either dismiss the issue of length by constructing very long pipes, or make measurements at a limited number of streamwise locations (often only two). This work was initiated as part of the international effort to construct a high Reynolds number pipe flow facility at the Center for International Cooperation in Long Pipe Experiments (CICLoPE). A major issue in the design of this facility is the pipe length — or, more pertinently, the length of the laboratory — needed in order to achieve fully developed flow. Using a novel hot-wire probe carriage and an external magnetic guide (figure 1), measurements were made in the University of Melbourne pipe flow facility at intervals of  $2.5D$  (where  $D$  is pipe diameter) spanning from the pipe entrance to a distance of  $228D$  downstream. Development of all streamwise velocity statistics and, importantly, energy spectra with distance from the pipe inlet will be presented. An example of the contour plot of pre-multiplied spectra is shown in figure 2.

\*Dept. of Mechanical Engineering, The University of Melbourne.



Figure 1: Scale diagram of magnetically positioned probe support mounted in pipe.

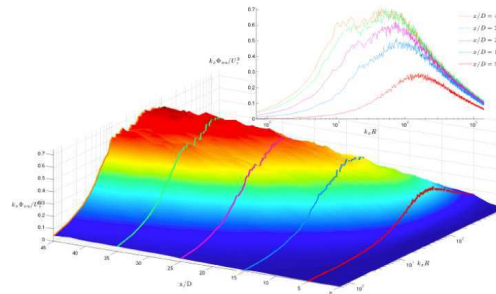


Figure 2: Plot of energy spectra (z-axis) against streamwise position and wavenumber. Inset is a plot of energy spectra vs wavenumber at selected streamwise locations.

## On the Continuity of Neumann Condition at Fluid-Porous Interfaces

A. Khalili\*, M.R. Morad†

The first contribution to the interfacial velocity slip condition between a fluid and the underlying porous layer goes back to Beavers and Joseph <sup>1</sup>. Assuming the continuity of interfacial shear stress, later, Neale and Nader <sup>2</sup> solved the governing flow equations in the both regions. Since then, many theoretical studies on this subject were conducted. Nevertheless, the lack of a clear consensus has given rise to misinterpretation of some classical solutions. To describe the influence of gradient-based interfacial conditions and resulting differences between exact solutions of flow equations, we considered two different scenarios: *a*) continuous shear stress, *b*) continuous velocity gradient at the interface, and employ Brinkman's equation below a permeable interface in a Poiseuille flow configuration (see figure 1a). The Beaver and Joseph slip coefficient was obtained to be the root of the ratio of either effective to fluid or fluid to effective viscosity depending on whether the interface condition *a* or *b* has been taken. The analytically obtained solutions were compared to preceding experimental results from porous medium made of multisized fibers obtained by Gupte and Advani <sup>3</sup> (see figure 1b). Due to an erroneous generalization of the slip condition, experimental results were misinterpreted. To demonstrate this, a set of new experiments with polydispersed porous samples were also performed.

\*Max Planck Institute for Marine Microbiolog, Celsiusstr. 1, 28359 Bremen, Germany.

†Max Planck Institute for Marine Microbiolog, Celsiusstr. 1, 28359 Bremen, Germany.

<sup>1</sup>G.S. Beavers, D.D. Joseph, *J. Fluid Mech.* **30**, 197 (1967).

<sup>2</sup>G. Neale, W. Nader, *Can. J. Chem. Eng.* **52**, 475 (1974).

<sup>3</sup>S.K. Gupte, S.G. Advani, *Exp. in Fluids* **22**, 408 (1997).

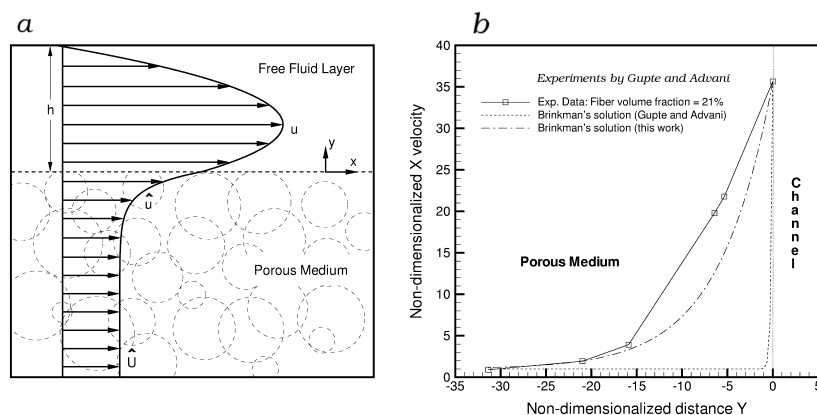


Figure 1: **a.** Flow with permeable interface. **b.** Velocity profile below the interface

## Development of a high-order numerical method to simulate flows over surface discontinuities

Laia Moret-Gabarro\*, Christophe Airiau\* and Patricia Cathalifaud\*

The objective of this study is to develop an adequate numerical tool to simulate a compressible flow over a 2D rectangular cavity of industrial interest. It has been carried out by Direct Numerical Simulation of Euler and Navier-Stokes equations using a sixth order compact finite-difference scheme<sup>1</sup>. A new interblock connectivity method is used to compute the derivatives of the fluxes<sup>1</sup>. Ghost cells are used to simulate the solid boundaries while the non-reflecting boundary conditions are characteristics.

Test cases of increasing complexity have been selected. The first problem consists of an acoustic pulse in an uniform flow impacting against a wall. It is taken from a CAA workshop<sup>2</sup>, whose analytical solution is used for validation. The corner treatment has been tested in isolation in a problem consisting of an acoustic pulse impacting against a corner<sup>3</sup>, with no incoming flow. An analytical solution has been derived in order to validate the results, shown in figure 1. Euler equations have been used for both problems, which are currently being extended to Navier-Stokes equations to include the viscous effects. Finally, to test the overall performance of the code in a multiblock configuration, an incompressible flow over a backward-facing-step will be simulated and validated against available studies in the literature.

The results obtained from the Euler equations are in very good agreement with the analytical solutions, proving its suitability for aeroacoustic problems.

\*Institut de Mécanique des Fluides de Toulouse.

<sup>1</sup>Guaus, *PhD Thesis*, University of Toulouse III (2008).

<sup>2</sup>Hardin et al., *NASA*, NASA/CP-3300 (1995).

<sup>3</sup>Rona et al., *AIAA paper*, AIAA 2008-0056 (2008).

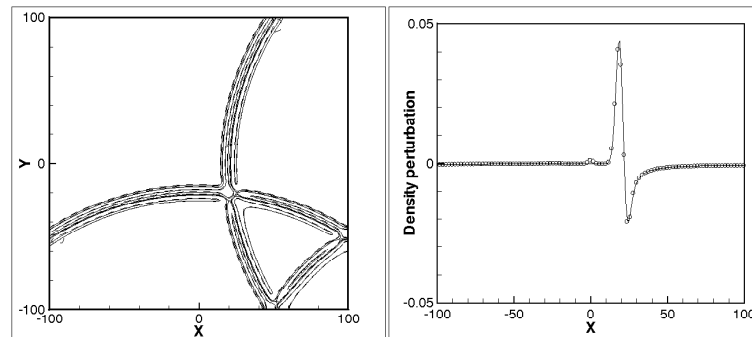


Figure 1: Results for a pulse reflected against a corner. Left plots: non-dimensional density contours, contour levels -0.02, 0.01, 0.02, 0.04; (—) analytical solution, (---) numerical prediction. Right plots: Normalized density distribution, along the x-axis, (—) analytical solution, (o) numerical prediction

## On uniqueness in the linear problem of ship waves

O.V. Motygin\*, P. McIver†

In the work we consider uniqueness question for the classical linear problem of ship waves. The problem appears in the framework of the surface wave theory and describes motion of rigid bodies  $B$  with a constant speed  $U$  in an unbounded heavy fluid  $W$  having a free surface. The direction of motion (along  $x$ -axis, with our choice of coordinate system) is orthogonal to direction of gravitational forces ( $y$ -axis). The fluid is assumed to be ideal and incompressible; its motion is steady-state and irrotational. We consider both 2D and 3D problems and the case when the contours of ships are totally submerged.

The mathematical problem consists in finding the velocity potential  $u$  which satisfies  $\nabla^2 u = 0$  in  $W$  ( $\nabla^2 = \partial_x^2 + \partial_y^2 + \partial_z^2$  in 3D case, where  $z$  is the second horizontal coordinate), the Neumann condition  $\partial_n u = U \cos(n, x)$  on  $S = \partial B$ , and the boundary condition  $\partial_x^2 u + \nu \partial_y u = 0$  on the unperturbed free surface  $F = \{y = 0\}$ , where  $y$ -axis is directed upwards,  $\nu = g/U^2$  and  $g$  is acceleration due to gravity. The problem should be completed with conditions at infinity. It is notable that despite the problem's long history, the conditions are not fully understood. For example, in very thorough mathematical investigation of the problem<sup>1</sup> the conditions were formulated in terms of  $u$  (not the velocity  $\nabla u$ ), which makes unclear their physical interpretation.

By proving a new uniqueness theorem for motion of empty layer we formulate conditions at infinity as follows:  $\sup_W |\nabla u| < \infty$  (2D, 3D) and  $|\partial_x u(x, 0)| \rightarrow 0$  (2D),  $\int_{-\infty}^{\infty} |\nabla_{x,z} u(x, 0, z)| dz \rightarrow 0$  (3D), as  $x \rightarrow +\infty$ . For this statement of the problem we are able to derive Green's identity and boundary Fredholm integral equation on  $S$  and to show its equivalence to the boundary-value problem. This allows us to use the approach<sup>2</sup> (suggested for water wave problem) to obtain uniqueness criteria for the problem in question, valid for bodies of arbitrary shape ( $S \in C^{1,\alpha}$ ,  $0 < \alpha < 1$ ), without any assumptions on finiteness of Dirichlet energy integral over  $W$ .

For this we introduce a self-adjoint operator  $\mathcal{T} = T + T^* - T^*T$ , combined from operator of integral equation  $T$  (direct value of the double layer potential), and consider  $\lambda_1 = \max\{\lambda_i\}$ , where  $\lambda_i \leq 1$  are eigenvalues of  $\mathcal{T}$ . Then, we prove that the uniqueness in the problem is equivalent to the condition  $\lambda_1 < 1$ , and the homogeneous problem has non-trivial solutions at points of the discrete set  $\{\nu : \lambda_1 = 1\}$ . This criterion allows us to formulate sufficient conditions of uniqueness based on approximations of operator  $T$  and to obtain a numerical algorithm for verification of uniqueness.

Another new criterion of uniqueness has the form  $\langle (I - T)\mu_1, \mu'_1 \rangle = 0$ , where  $\langle \cdot, \cdot \rangle$  means scalar product in  $L_2(S)$  and  $\mu_1$  and  $\mu'_1$  are eigenfunctions, corresponding to the maximum eigenvalues  $\lambda_1$  and  $\lambda'_1$  for the operators  $\mathcal{T}$  and  $\mathcal{T}' = T + T^* - TT^*$  (it is shown that  $\lambda_1 = \lambda'_1$ ). Numerical algorithms based on this criterion allow us to recognize convincingly if for a given geometry non-uniqueness occurs at some  $\nu$ .

The work is supported by INTAS YSF grant, no. 06-1000014-6343.

\*Institute of Problems in Mech. Engineering, Russian Academy of Sciences, St.Petersburg, Russia.

†Mathematical School, University of Loughborough, UK.

<sup>1</sup>N. Kuznetsov *et al.* Linear water waves. Cambridge Univ. Press (2002).

<sup>2</sup>O.V. Motygin, Proc. 21th IWWFEB. Loughborough, UK (2006).

## Simulations of turbulent transition in long pipes

David Moxey\*, Dwight Barkley\*

Motivated by recent progress in understanding turbulent transition in pipe flow<sup>1</sup> and, in particular, experimental studies of long pipes of many hundreds of diameters<sup>2,3</sup>, we have undertaken the direct numerical simulation of turbulence in long pipes at transitional Reynolds numbers. We have employed high-performance parallel computations using a spectral-element code to solve the Navier-Stokes equations in a Cartesian geometry<sup>4</sup>. This code uses a spectral-element discretization along circular cross-sections of the pipe, with a Fourier expansion in the remaining streamwise direction (necessitating the use of a periodic boundary condition). The flow is driven by use of a body-force in order to simulate a constant pressure gradient, although simulations for a fixed flow rate are also possible.

With these techniques we estimate that we will be able, for the first time with direct numerical simulation, to obtain results for pipe lengths of several hundred diameters. We report on preliminary findings from these studies up to  $Re \simeq 5000$ . Figure 1 shows some initial results from simulations of fully-developed turbulence at this Reynolds number.

---

\*Mathematics Institute and Centre for Scientific Computing, University of Warwick.

<sup>1</sup>B. Hof et al., *Science* **305** 1594 (2004).

<sup>2</sup>J. Peixinho, T. Mullin, *J. Fluid Mech.* **582** 169 (2007).

<sup>3</sup>B. Hof, B. Eckhardt et al., *Nature* **443** 59 (2006).

<sup>4</sup>D.M. McIver, H.M. Blackburn et al., *ANZIAM J* **42**(E) C954 (2000).

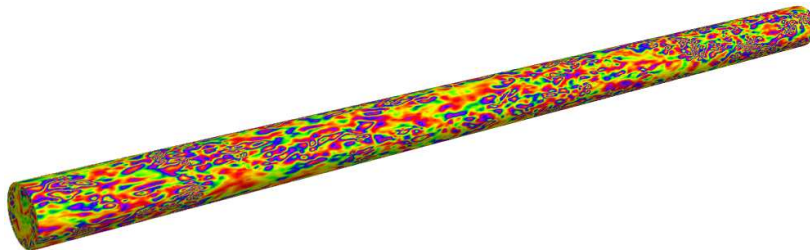


Figure 1: Streamwise vorticity in numerical simulations of turbulent pipe flow at  $Re \simeq 5000$ .

### Numerical simulation of laminar flow instabilities in tubes with wire coil inserts

D. Muñoz-Esparza<sup>a</sup>, J. Pérez-García<sup>a</sup>, E. Sanmiguel-Rojas<sup>b</sup>, A. García<sup>a</sup>,  
and J.P. Solano<sup>a</sup>

Numerical simulations of steady incompressible laminar 3D fluid flow in smooth round tubes of diameter  $d$ , with wire coil inserts, have been accomplished. A set of wire coils with different geometrical characteristics of dimensionless pitch ( $p/d$ ) and wire-diameter ( $e/d$ ) has been analysed using the finite volume method. A detailed study for different Reynolds numbers,  $Re$ , in the laminar region has been carried out. Numerical results allow us to determine the internal flow structure, to identify the critical Reynolds number,  $Re^*(e/d, p/d)$ , of oscillating laminar flow and to obtain practical correlations of the Fanning friction factor,  $f(Re, e/d, p/d)$ . These results have been compared with experimental data obtained by García et al.<sup>1</sup> and a good agreement is reached.

The wire coil induces a swirl to the main flow and produces a recirculation zone just downstream of the wire. Therefore, the friction factor increases in reference to smooth tube for the same Reynolds number. In addition, the size of the recirculation zone enlarges and becomes unstable when the critical Reynolds number is exceeded. These instabilities advance the transition region to lower Reynolds numbers, depending on the geometrical characteristics. 3D path lines over the wire coil are shown in Fig. 1, (a) for a purely laminar flow ( $Re=200$ ) with a steady recirculation, and (b) the destabilization of the recirculation zone for a  $Re$  lightly higher than  $Re^*$ .

<sup>a</sup> Área de Mecánica de Fluidos. Universidad Politécnica de Cartagena. Cartagena, Spain.

<sup>b</sup> Área de Mecánica de Fluidos. Escuela Politécnica Superior, Universidad de Jaén. Jaén, Spain.

<sup>1</sup> García et al., *J. Heat and Mass Transfer*. **48**, 4640 (2005).

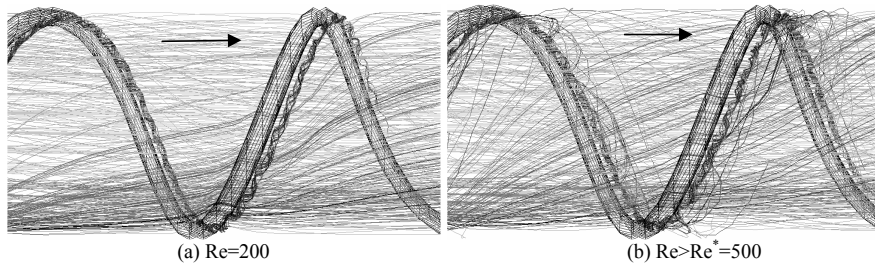


Figure 1: Internal 3D path lines across a duct with a wire coil insert.

The deformation of an elastic ring by surface forces.

T Mullin

Manchester Centre for Nonlinear Dynamics,  
Department of Physics and Astronomy,  
Manchester University,  
Manchester, M13 9PL.

**Abstract**

We present the results of experimental investigations into instabilities in an elastic ring floating on a fluid. An initially circular ring sits on the surface of a fluid filled cone and is compressed as the liquid is drained away. The compressive forces give rise to buckling instabilities in the ring and these can be related to results for the compression of solid rings within cylinders. The effects of outer boundary shapes have been explored where anisotropic forcing has produced interesting cases.



## Sliding of a drop on a wall and pinch-off by shear flow

Mohammad N. H. Gilani\*, Hang Ding\* and Peter D. M. Spelt\*

We report here on the various flow regimes that result when a three-dimensional droplet on a wall is exposed to a shear flow. A diffuse-interface method is used for this purpose, which circumvents the stress singularity at the moving contact line, and allows for a density and viscosity contrast between the fluids. Previous tests and applications have been published in earlier work<sup>1,2,3</sup>. Contact-angle hysteresis is represented by the prescription of a receding contact angle  $\theta_R$  and an advancing contact angle value  $\theta_A$ . A moderate contact-angle hysteresis window of  $\theta_A = \pi/2$  and  $\theta_R = 2\pi/9$  is used in all cases. The initial shape of the droplet is assumed to be a spherical cap that is specified by the contact angle  $\theta_0$  ( $\theta_R \leq \theta_0 \leq \theta_A$ ).

The critical conditions for the onset of motion of a three-dimensional droplet on a wall in shear flows at moderate Reynolds number will be summarized briefly, these having been published already by us<sup>4</sup>, following earlier work on the creeping-flow problem by e.g. Dimitrakopoulos & Higdon<sup>5</sup>. The results could be summarized in a critical Weber number that depends on the Reynolds number, the density and viscosity ratios, and the initial condition used for the shape of the drop.

We focus here on the conditions beyond the onset of motion. The results show that, at intermediate values of a Weber number, the droplet reaches a constant velocity and shape. It is found that an apparent contact angle can be defined at the downstream end of the drop, and that results for different flow parameters can be collapsed onto a single curve, versus a capillary number based on the contact-line speed.

Part of the droplet is sheared off beyond a second critical value of the Weber number. Results are presented for the dependency of this critical Weber number on the Reynolds number, both for a pinned contact line and for moving drops. It is found that even at rather large values of a Reynolds number (based on the shear rate and the initial drop height), this critical Weber number is still more or less proportional to the Reynolds number, indicating that viscous stresses rather than inertial forces dominate the onset of entrainment.

The final part of the presentation investigates the entrainment process in great detail. Results are presented for the ligament length (that subsequently breaks off from the droplet) versus time. These results are compared with a theory by Marmottant & Villermaux<sup>6</sup> who analysed the successive steps of atomization of a liquid jet when a fast gas stream blows parallel to its surface. Finally, the pinch-off process itself is investigated. Results are presented for the minimum neck radius versus time to rupture, and a power-law regime appears to be approached. The relation of these results to the self-similar pinch-off regime<sup>7</sup> is discussed.

\*Department of Chemical Engineering, Imperial College London

<sup>1</sup>Ding et al. *J. Comput. Phys.* **226**, 2078, (2007)

<sup>2</sup>Ding and Spelt *Phys. Rev. E* **75**, 046708 (2007)

<sup>3</sup>Ding and Spelt *J. Fluid Mech.* **576**, 287, (2007)

<sup>4</sup>Ding and Spelt *J. Fluid Mech.*, **599**, 341, (2008, in press)

<sup>5</sup>Dimitrakopoulos and Higdon *J. Fluid Mech.* **395**, 181 (1999)

<sup>6</sup>Marmottant and Villermaux *J. Fluid Mech.* **498**, 73 (2004)

<sup>7</sup>Lister and Stone *Phys. Fluids* **10**, 2758 (1998)

## Reduced order model based control of subsonic cavity flows

Kaushik Kumar Nagarajan\*, Christophe Airiau\*, Laurent Cordier ‡ and Peirre Comte †

The aim of this study is the reduced order modelling based control of highly subsonic cavity flows. A Direct Numerical Simulation (DNS) of the compressible Navier-Stokes equation at regimes of low subsonic flows has been carried out using an explicit 4<sup>th</sup> order accurate scheme in space and time. The flow is allowed to stabilize in frequency before an ensemble of snapshots are generated to cover sufficient number of flow cycles. A reduced order model based on Proper Orthogonal Decomposition (POD) is constructed on these ensemble to extract the most energetic flow structures<sup>1</sup>.

The grid convergence to verify the validity of the DNS is studied using the POD technique see figure <sup>1</sup>, where the dominant eigen values representing the large scale pattern in the flow structures are preserved with progressive grid refinement, as also the smallest eigen values which represent the dissipative scales. There is however a range where the eigen values do not match with progressive grid refinement and this represent the intermediate scales of turbulence. In this study we focus on the large scale structures represented by the larger eigenvalues. A Galerkin projection reconstruction code has been developed by projecting the governing equations on the subspace spanned by the POD modes thereby resulting in a system of ordinary differential equations also termed as the Reduced Order Model (ROM). The obtained ROM is calibrated to predict the DNS data accurately so that it can be actively used in control application problems. Finally we propose to develop an adjoint technique based POD-ROM code to introduce control in the flow simulation where the obtained control is introduced back into the DNS solver to demonstrate the validity of a ROM based control<sup>2</sup>

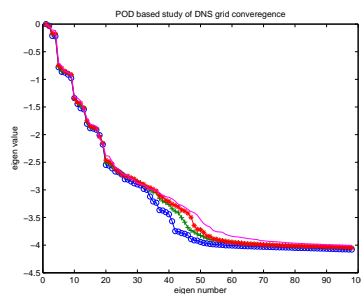


Figure 1: A study of the DNS grid convergence using POD, for progressive grid refinement

\*Institut de Mécanique des fluides de Toulouse

†CEAT/LEA Poitiers.

‡Rowley, Physica D, 142,1-19,2000

<sup>2</sup>Bruno Spagnoli, PhD thesis, INP Toulouse, 2006

## The Taylor-Bénard problem

M. Nagata\* and T. Okuno\*

The thermal convection realized in the narrow gap limit of a fluid flow between differentially rotating coaxial cylinders is considered, where both cylinders are kept at different temperatures and gravity acts only through the centrifugal force in the radial direction. We extend the linear and weakly nonlinear analyses by Kropp & Busse<sup>1</sup> and Auer & Busse<sup>2</sup> to a fully nonlinear case.

Our numerical investigation based on a bifurcation theory shows that the two two-dimensional secondary flows, namely axisymmetric longitudinal roll solution (LR) and axially-independent transverse roll solution (TR), interact with each other in some parameter region for a fluid with the Prandtl number  $Pr = 7$ , and a mixed mode solution is produced as a three-dimensional tertiary flow. The mixed mode solution connects the points on the two-dimensional solution branches where the solutions change their stability properties (see Figure 1). For  $Pr = 0.7$  we are able to identify a parameter region where two distinct three-dimensional states, *spirals* and *ribbons*, bifurcate directly from the basic state simultaneously due to three-dimensional instabilities (see Figure 2). We shall discuss the physical properties of these flows in detail.

\*Department of Aeronautics and Astronautics, Graduate School of Engineering, Kyoto University.

<sup>1</sup>Kropp, M. & Busse, F. H. *Geophys. Astrophys. Fluid Dynamics* **61**, 127 (1991).

<sup>2</sup>Auer, M. & Busse, F. H., *Phys. Fluids* **10**, 318 (1998).

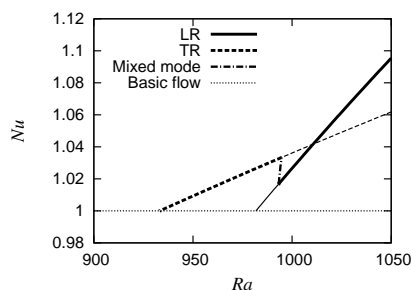


Figure 1: The bifurcation diagram in the Rayleigh number,  $Ra$ , and the Nusselt number,  $Nu$ , space. The thick/thin part of the lines indicates a stable/unstable branch.  $Pr = 7$ .

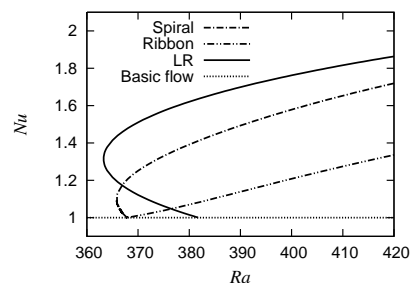


Figure 2: The bifurcations of spiral and ribbon in the  $Ra - Nu$  space.  $Pr = 0.7$ .

## Structural Transitions in Swirled Compressible Flows

A. Ni<sup>a</sup>

Vortex breakdown is a phenomenon observed in swirled flows. Its onset is manifested as an abrupt flow structural transition accompanied by formation of stagnation zone. Vortex breakdown is an important flow element in technical devices. It is used in power generation technology for flame stabilization in combustors, in cyclone devices etc. Transonic rotating flows are of interest in connection with supersonic compressors and oil processing industry<sup>1</sup>. It plays also a negative role being a source of hydrodynamic losses in turbo-machinery.

In our paper Benjamin's method developed for swirled incompressible flows<sup>2</sup> is extended to compressible transonic quasi one-dimensional flows in ducts both in cylindrical and annular geometries. The flow analysis is reduced to eigen value problem for a system of three ordinary differential equations expressing conservation of total enthalpy, total pressure (entropy), and circulation  $H_0(\xi), p_0(\xi), \Gamma(\xi)$  along streamlines  $r(\xi)$  ( $\xi$  -Lagrangian coordinate):

$$u \frac{du}{d\xi} = -\Gamma \Gamma' \frac{1}{r^2} + \left( \frac{p}{p_0} \right)^{\frac{\gamma-1}{\gamma}} \frac{\gamma-1}{\gamma} \frac{H_0}{p_0} \frac{dp_0}{d\xi} - \left[ \left( \frac{p}{p_0} \right)^{\frac{\gamma-1}{\gamma}} - 1 \right] \frac{dH_0}{d\xi}$$

radial equilibrium condition

$$\frac{dp}{d\xi} = \rho \frac{\Gamma^2}{r^3} \frac{dr}{d\xi}$$

and mass conservation

$$\rho u r \frac{dr}{d\xi} = R(\xi) U(\xi) \xi = j(\xi)$$

with  $u, p, \rho, v$  - axial velocity, static pressure, density, and azimuthal velocity,  $R(\xi), U(\xi)$  -density and axial velocity given at the duct inlet. Transitions from subsonic to supersonic flow regimes and back as well as formation of stagnation zones are studied in frameworks of the suggested model. Stability of rotating flows relative to three dimensional perturbation is investigated.. It is shown that losses strongly influence the flow structure and its stability.

---

<sup>a</sup> ALSTOM Power Technology Center, Zentralstrasse 40, 5242 Birr, Switzerland

<sup>1</sup> Offshore Magazine. Twister application hints at subsea separation Volume 64 Issue 6, June 2004

<sup>2</sup> Benjamin, J. Fluid Mech.14, 593(1962)

## Rotating annulus convection with large aspect ratio

Takashi Noguchi\*, Kotaro Naruo\* and Masato Nagata\*

We investigate the stability of the basic flow produced by imposing radial temperature gradient in a rotating annulus, theoretically and experimentally. Linear stability analysis shows that the rotation destabilize the basic flow and leads to spiral vortex flows with different slope: nearly horizontal at low rotation rate, whereas nearly vertical at high rotation rate (Figure 1). For each of the two regimes, we obtain nonlinear secondary flows and consider their linear stability. Tertiary flow for nearly-vertical spiral mode is also obtained. We observed the nearly-vertical spiral mode in the experiments using a rotating annular tank with radius ratio of 0.9 and aspect ratio of 56. The spiral vortices are always transient and eventually develop into nonstationary kinked vortices (Figure 2). When the Grashof number (temperature difference across the annular gap) is small, characteristics of the spiral vortex at the initial stage is in good agreement with theoretical results.

\*Graduate School of Engineering, Kyoto University.

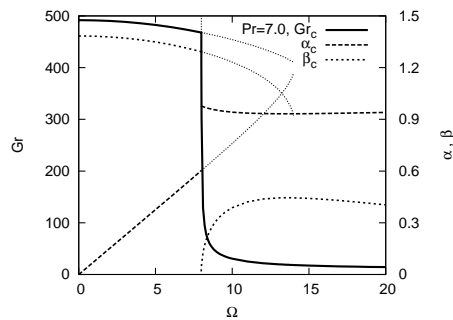


Figure 1: Linear critical Grashof number and critical wavenumber for water ( $Pr=7.0$ ), where  $\alpha$  and  $\beta$  denote wavenumbers in azimuthal and vertical directions respectively.

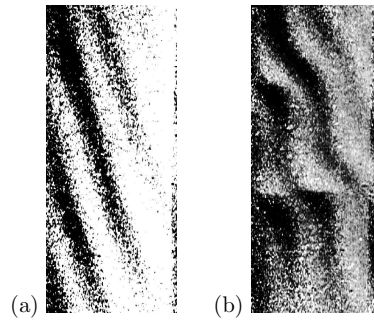


Figure 2: Liquid crystal visualization of thermal structure of the spiral vortices for: (a) initial stage, (b) mature kinked stage.

## Laminar-turbulent transition in pipe flow for yield-stress fluids.

A. Esmael and C. Nouar\*

Understanding the mechanism of transition from laminar to turbulent flow of Newtonian fluids has been an ongoing quest for more than a century. It is only during this last decade that considerable advances have been made with the discovery of new numerical solutions. Based on the self-sustained process theory developed by Waleffe<sup>1</sup> and a subsequent continuation approach<sup>2</sup>, a family of three-dimensional travelling waves (TW) have been discovered by Faisst and Eckhardt<sup>3</sup> and Wedin and Kerswell<sup>4</sup>. These TW are characterized by pairs of downstream vortices and streaks and are very similar to the coherent structures observed experimentally in equilibrium puffs<sup>5</sup>. Concerning the transition to turbulence for non-Newtonian fluid flows very little is known, probably because of the inherent complexities involved. However the existing literature reveals an interesting and as yet unexplained result: In the transitional regime, the flow presents a stable asymmetry, while in the laminar and turbulent regimes the flow is axisymmetric. Independent observations of this asymmetry has been made by Escudier and Presti<sup>6</sup> and Peixinho *et al.*<sup>7</sup> These two groups have recently jointly published these, and additional observations<sup>8</sup> to highlight this effect. The aim of the current communication is to provide a three-dimensional description of this asymmetry. First of all, we recall that the fully developed laminar flow of a yield stress is characterized essentially by the existence of a central unyielded zone and an annular sheared region where the effective viscosity varies nonlinearly. The linear stability analysis indicates that the Hagen-Poiseuille flow of a yield stress is linearly stable for all Reynolds number and the optimal perturbation is a travelling wave with an azimuthal and axial wavenumbers  $m = 2$  and  $\alpha = 1.2$  respectively. From experimental point of view, the fluid used is a 0.2 wt % aqueous solution of Carbopol 940. It is a shear thinning fluid with a yield stress. Measurements of the mean, i.e., time-averaged, axial velocity profiles as well as the rms of the axial velocity fluctuations were performed using Dantec FlowLite Laser system at three axial locations  $z = 20 D$ ,  $54 D$  and  $122 D$  where  $D$  is the diameter of the test section and at four azimuthal positions. The results show that the inlet flow is symmetric and the asymmetry increases along the pipe. The obtained mean velocity profiles are then written as the superposition of an azimuthal average velocity profile  $\bar{U}(r, z)$  and a streak  $U_s(r, \theta, z)$ . It is then shown that the azimuthal variation of  $U_s$  can be described by:  $U_s \propto \cos(\theta + \phi)$ . This result suggests the existence of a robust coherent structure characterized by two counter-rotating longitudinal vortices.

\*LEMTA UMR 7563 CNRS Nancy-Université, 2 Avenue de la Forêt de Haye, BP 160, 54504 Vandoeuvre, France.

<sup>1</sup>Waleffe, Phys. Fluids **9**, 889 (1997)

<sup>2</sup>Waleffe, Phys. Rev. Lett. **81**, 4140 (1998)

<sup>3</sup>Faisst and Eckhardt, Phys. Rev. Lett. **91**224502 (2003).

<sup>4</sup>Wedin and Kerswell, J. Fluid. Mech. **508**, 333 (2004).

<sup>5</sup>Hof *et al.*, Science **305**, 1594 (2004).

<sup>6</sup>Escudier and Presti, J. non-Newtonian Fluid Mech. **62**, 291 (1996).

<sup>7</sup>Peixinho *et al.*, J. non-Newtonian Fluid Mech. **128**, 172 (2005).

<sup>8</sup>Escudier *et al.*, J. non-Newtonian Fluid Mech. **127**, 143 (2005).

# Experimental study of the relaminarization in a two-dimensional channel flow

T. Numano\*, T. Okumura\* and M. Matsubara\*

A two-dimensional channel flow can maintain turbulence even under critical Reynolds number for an infinitesimal disturbance predicated by a linear theory stability. The purpose of this study is to reveal about flow around Reynolds number which is the minimum Reynolds number for any disturbance. Relaminarization was made by decreasing Reynolds number by means of expansion of the end wall distance. The flow visualization was made for observation of a process of relaminarization, and hot-wire measurements were made to do a quantitative evaluation of disturbances appeared around the minimal Reynolds number.

The flow visualization shows that the relaminarization is not rapidly but gradually with decreasing Reynolds number. The spatial ratio of disturbed regions in the flow decreases with decrease of Reynolds number, and the flow is totally laminar when Reynolds number is 1300. Turbulence energy measured by the hot-wire anemometer was decreasing exponentially in the streamwise direction from  $Re=1220$  to  $Re=1470$ . If we define non-dimensional streamwise distance of which the turbulence energy come to half as half life  $\tau$ , it was increasing rapidly with increasing Reynolds number as shown Fig.1. The Reynolds number at which the inverse of the half life goes to zero, is estimated as 1490. This is the minimal Reynolds number for a turbulent channel flow.

YYYY

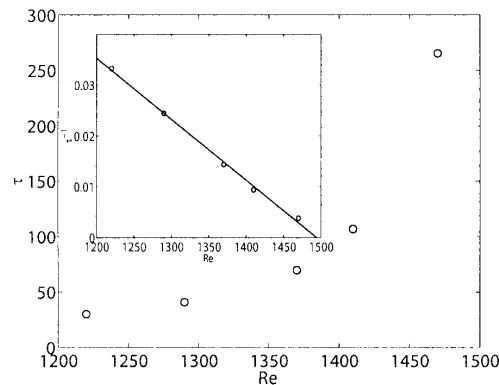


Figure 1: Variation of the decay rate as a function of  $Re$  and the inset is the inverse half life versus  $Re$  and a linear fit.

\*Shinshu Univ.Mechanical systems engineering,Wakasato 4-17-1,380-8553 Nagano,Japan.

## Interfacial wave motion in turbulent stratified channel flow

Lennon Ó Náraigh\*, Omar Matar\*, Peter Spelt\*, and Tamer Zaki†

We consider the motion of a deformable interface that separates a fully-developed turbulent gas flow from a thin layer of laminar liquid. We outline a family of linearised models to describe the interaction between the turbulent gas flow and the interfacial waves; this consists of the Orr–Sommerfeld equation with the appropriate turbulent mean flow profile, together with a turbulent stress closure scheme. This approach permits us to determine numerically the growth rate of the wave amplitude, as a function of the relevant dimensionless system parameters and turbulence closure relations. It also extends previous work by accounting for the effects of the thin liquid layer on the dynamics.

The simplest possible closure model is the mixing-length model of Van Duin and Janssen<sup>1</sup>, appropriate for slow waves. We find that the incorporation of turbulent stresses through this model enhances the growth rate of the interfacial mode, while the growth rate of the internal mode is suppressed, and becomes negative at all wavenumbers for Reynolds numbers typical of pipe flow. The inclusion of the Reynolds stresses therefore gives rise to a significant correction in the wave growth rates. We shall report a comparison between this simple turbulence closure scheme and other, more involved closures, such as the damped mixing-layer model<sup>2</sup>, and the  $k$ – $\epsilon$  model<sup>3</sup>.

---

\*Department of Chemical Engineering, Imperial College London.

†Department of Mechanical Engineering, Imperial College London.

<sup>1</sup>C.A. Van Duin and P.A.E.M. Janssen, *J. Fluid Mech.* **236**, 197 (1992).

<sup>2</sup>J.E. Cohen and S.E. Belcher, *J. Fluid Mech.* **386**, 345 (1999).

<sup>3</sup>G. Ierley and J. Miles, *J. Fluid Mech.* **435**, 175 (2001).



## Study of high-symmetric 3D Euler flows with Clebsch potentials

Koji Ohkitani

*School of Mathematics and Statistics, The University of Sheffield,  
Hicks Building, Hounsfield Road, Sheffield S3 7RH, U.K.*

The Kida-Pelz vortex is a highly-symmetric, periodic solution of the 3D incompressible Euler equations

$$\frac{\partial \mathbf{u}}{\partial t} + (\mathbf{u} \cdot \nabla) \mathbf{u} = -\nabla p, \quad \operatorname{div} \mathbf{u} = 0,$$

which starts from an initial condition

$$\mathbf{u} = \begin{pmatrix} \sin x (\cos 3y \sin z - \cos y \sin 3z) \\ \sin y (\cos 3z \sin x - \cos z \sin 3x) \\ \sin z (\cos 3x \sin y - \cos x \sin 3y) \end{pmatrix}.$$

It is one of candidates of flows which may lead to singularity formation in finite time. This flow is simple in that it has a single pair of Clebsch representation [1]:

$$\mathbf{u} = f \nabla g - \nabla \phi, \quad \boldsymbol{\omega} = \nabla f \times \nabla g,$$

where we may take the potentials material as

$$\frac{Df}{Dt} = \frac{Dg}{Dt} = 0.$$

A number of choices of initial Clebsch potentials are given explicitly. All of them are found to have unphysical singularities.

We trace the time evolution of the Clebsch potentials by numerical simulations, paying attention to how nonlinearity depletion, in the sense of  $\nabla f \parallel \nabla g$  introduced in [1], may be observed in this representation. Also, some attempts are made to constrain possible singularities by this method.

As initial potentials, we may take for example

$$f = 2 \frac{(\cos x)^{3/2} (\cos^2 y - \cos^2 z)}{(\cos y \cos z)^{1/2}}, \quad g = 2 \frac{(\cos y)^{3/2} (\cos^2 z - \cos^2 x)}{(\cos z \cos x)^{1/2}}$$

in  $0 \leq x, y, z < \pi/2$ . Note that  $\phi \neq 0$ , but

$$\phi = 2 \cos x \cos y \cos z (\cos^2 x + \cos^2 y - \cos^2 z) - \frac{2 \cos^3 x \cos^3 y}{\cos z}.$$

Another choice is

$$\tilde{f} = \frac{\cos^2 y (\cos^2 z - \cos^2 x)}{\cos^2 z (\cos^2 y - \cos^2 x)}, \quad h' = -2 \frac{(\cos z)^3 (\cos^2 x - \cos^2 y)^2}{\cos x \cos y},$$

$$\phi_2 = 2 \cos x \cos y \cos z (\cos^2 y + \cos^2 z - \cos^2 x) - \frac{2 \cos^3 y \cos^3 z}{\cos x},$$

where  $\mathbf{u} = \tilde{f} \nabla h' - \nabla \phi_2$ .

## References

- [1] K. Ohkitani "A geometrical study of 3D incompressible Euler flows with Clebsch potentials – a long-lived Euler flow and its power-law energy spectrum," *Physica D* (2008), to appear.

# Linear and nonlinear analyses of rotating plane Couette flow subject to a spanwise translational oscillatory boundary motion

S. Okino\* and M. Nagata\*

The effect of a translational spanwise boundary oscillation on the linear stability of rotating plane Couette flow (see Figure 1) is studied numerically by applying Floquet theory. It is found that the critical states, determined by longitudinal perturbations as in the case without oscillation, are delayed, and that the response to the oscillation is synchronous in all the parameter ranges examined. We shall compare our findings in the plane geometry with those in the annulus case investigated by Marques et al.<sup>1</sup>.

Also, we examine a subsequent nonlinear development of the flow by a two-dimensional direct numerical simulation. When the frequency,  $\omega$ , of the spanwise oscillation and the system rotation,  $\Omega$ , are fixed, the momentum transport in the streamwise direction,  $\tau_x$ , is gradually reduced from the value,  $\tau_{xB}$ , without oscillation as the amplitude,  $R_y$ , of the spanwise oscillation is increased as shown in Figure 2. For a large amplitude we detect a window on the  $R_x$ -axis ( $R_x$  denotes the Reynolds number of the basic Couette flow) where the response to the oscillation ceases to be synchronous as indicated by the lack of a curve for  $R_y = 50$  in Figure 2. For this  $R_y$ , as  $R_x$  is increased from the lower edge of the window, the synchronous secondary flow first loses its stability to a synchronous flow with a travelling wave component propagating in the spanwise direction followed by a double-periodic flow and finally a chaotic state. As  $R_x$  is increased further the chaotic state ceases to exist and the flow with the synchronous response is recovered.

\*Department of Aeronautics and Astronautics, Graduate School of Engineering, Kyoto University.

<sup>1</sup>Marques et al, *J. Fluid Mech.* **348**, 153 (1997).

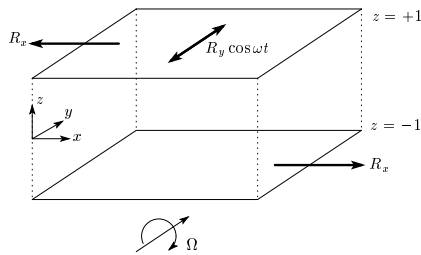


Figure 1: The configuration of the problem.

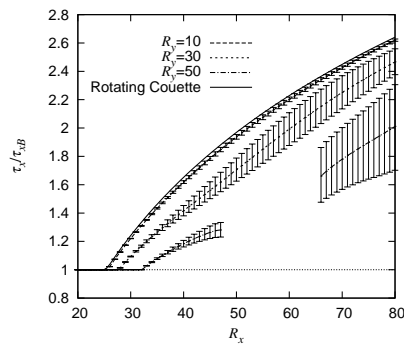


Figure 2: The bifurcation diagram.

## Appearance of vortex multiplets in lid-rotated cavity flow

Okulov V.L.<sup>a</sup>, Sørensen J.N.<sup>a</sup> and Naumov I.V.<sup>b</sup>

This paper presents results of a laboratory experiment aimed at studying the appeared multiplets in confined swirling flow driven a lid in a cylindrical cavity. Two optical techniques – laser Doppler anemometry (LDA) and particle image velocimetry (PIV) have been used simultaneously. By extending the range of the flow parameters studied earlier [1, 2] clearly pronounced vortex multiplets (vortex triplet, double vortex triplet, double vortex duplet and quadruplet) have been discovered (Fig. 1). The extended instability branch was originally obtained as a byproduct of previous investigations. If the well-known instability branch (for  $1.7 \leq H/R \leq 3.2$ ) is basically determined by axial oscillations of axisymmetric vortex breakdown, the new one (for  $3.2 \leq H/R \leq 5.5$ ) is totally fixed by a rotation of the vortex multiplets.

<sup>a</sup> Department of Mechanical Engineering, DTU, DK-2800 Lyngby, Denmark

<sup>b</sup> Institute of Thermophysics, SB RAS, Novosibirsk, 630090, Russia

<sup>1</sup> M.P.Escudier, *Exp. Fluids*, **2**, 189 (1984)

<sup>2</sup> J.N. Sørensen, I.V. Naumov, and R. Mikkelsen, *Exp. Fluids*, **41**, 425 (2006)

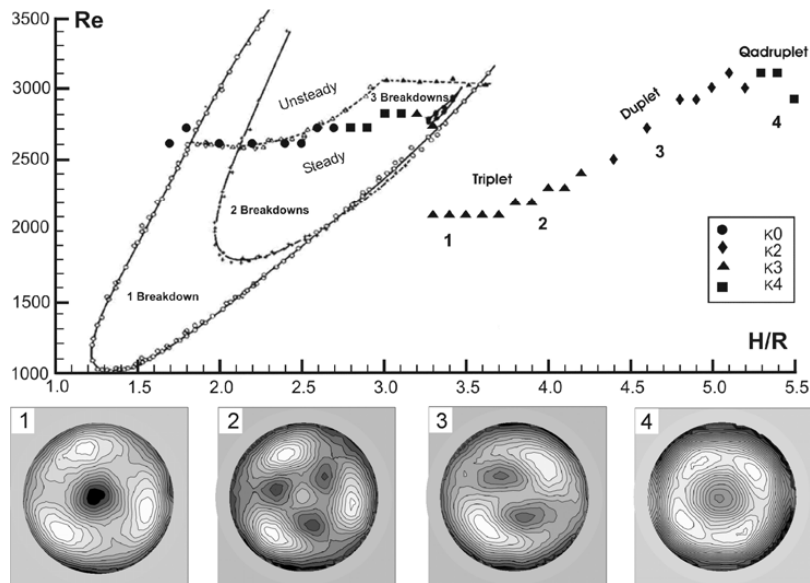


Figure 1: Original Escudier's diagram (small symbols and lines - [1]) and two branches of the flow stability (large symbols - present) with typical flow patterns - vortex triplet (1), double triplet (2), double duplet (3) and quadruplet (4) indicated the deviations of the axial vorticity component from Gaussian distributions.

## Dynamic Measurements on an Airfoil Using Acoustic Forcing

W.F.J.Olsman\*, A. Hirschberg\*, R.R. Trieling\* and G.J.F. van Heijst\*

Knowledge of the unsteady forces on a wing is crucial for successful wing design. For conventional profiles the unsteady linearized potential theory of Theodorsen & Sears<sup>1</sup> has been successful in predicting the unsteady forces on a two dimensional thin airfoil in subsonic flow. Our current research effort is focused on predicting and measuring the influence of a cavity on the unsteady forces for a thick airfoil (NACA0018), see fig. 1. The cavity is intended to prevent flow separation and massive vortex shedding. Numerical simulations have indicated that the dynamic behaviour of an airfoil with cavity can show significant deviations from linear theory for a flat plate. The work is part of the European project VortexCell2050<sup>2</sup>. Measurements of the unsteady forces on an airfoil are typically carried out using complex mechanical systems to displace the airfoil with respect to the main flow. We present a new method where the airfoil is fixed with respect to the wind tunnel and we displace the flow rather than the airfoil.

The airfoil was mounted in the center of the wind tunnel and a transversal acoustic standing wave was generated using two speakers in the side walls of the tunnel. The frequency was tuned to the first transversal resonance frequency. The standing wave generated velocity fluctuations in the center of the wind tunnel which are perpendicular to the main flow. In these experiments we move the flow rather than the airfoil, avoiding a complex mechanical system to dynamically displace the airfoil. Currently acoustic velocity fluctuations up to 1.5% of the main flow are generated. At three locations near the leading edge, dynamic pressure transducers were mounted to record the pressure. Initial tests have been carried out with a NACA0018 airfoil without cavity, the results of these measurements agree within 30% to unsteady linear potential theory for a flat plate. We will repeat the measurements with a NACA0018 airfoil with cavity and compare the results with two-dimensional Euler simulations and a two-dimensional discrete vortex method.

---

\*Fluid Dynamics Laboratory, Eindhoven University of Technology.

<sup>1</sup>Sears W.R., Von Karman Th., *J. Aeronaut. Sci.* **5**, 379 (1938).

<sup>2</sup>[www.vortexcell2050.org](http://www.vortexcell2050.org)

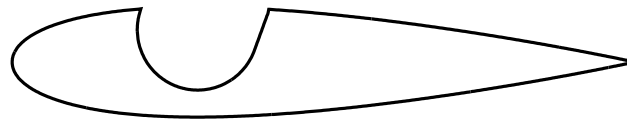


Figure 1: NACA0018 airfoil with cavity.

## The Computation of Buoyant Flows in Differentially Heated Cavities

S.A.Omranian<sup>a</sup>, H. Iacovides<sup>a</sup>

Natural convection flows are often encountered both in nature and also in engineering applications. Turbulent natural convection flows, even in geometrically simple systems, can be physically very complex. The buoyant force, depending on the orientation of the temperature gradients, can either enhance or suppress turbulence. Earlier numerical studies of such flows, based on RANS<sup>1</sup>, found it necessary to use low-Reynolds-number models of turbulence, which need fine near-wall grids.

This study explores the potential of a recently developed wall-function strategy for the economical and reliable prediction of natural convection flows. This strategy, AWF<sup>2</sup>, involves the use of large near-wall control volumes and the analytical solution of boundary-layer forms of the momentum and enthalpy equations, to provide wall boundary conditions for momentum, temperature and the turbulence parameters. The conventional wall-function strategy, based on the log-law, is also used for base-line comparisons. The turbulent stresses are approximated through high-Reynolds-number turbulence models, which include the  $k-\epsilon$  and 2<sup>nd</sup>-moment closures. In 2<sup>nd</sup>-moment closures, elaborate, approximations are employed for the modeling of the turbulent heat fluxes, extending to solution of equations for the temperature fluctuation and its dissipation rate.

The proposed paper will include comparisons between RANS predictions that result from the use of these models and experimental data, for several cavities. One case is that of a square cavity<sup>3</sup> with differentially heated vertical walls, Fig. 1. Nusselt number comparisons, such as those of Fig. 2, suggest that as the AWF provides a cost-effective alternative to low-Reynolds number models.

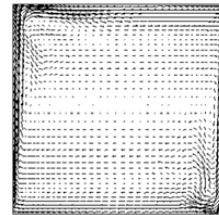


Figure 1. Square Cavity<sup>3</sup>

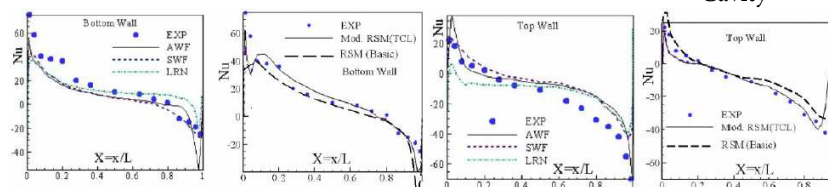


Figure 2. Local Nusselt number comparisons over the walls of the square cavity.

<sup>a</sup> School of Mechanical, Aerospace and Civil Engineering, University of Manchester.

<sup>1</sup> Ince N Z and Launder B E, Int. Journal of Heat and Fluid Flow, 10, Np 2, pp 110-117, 1989

<sup>2</sup> Craft T. J., Gerasimov A V, Iacovides H. and Launder B.E., International Journal of Heat and Fluid Flow, 23, 148-16, 2002

<sup>3</sup> Ampofo, F. and Karayiannis, T.G., Int. J. of Heat and Mass Transfer 46, pp. 3551-3572, 2003.

## Suppression of the Rayleigh-Taylor instability of thin liquid films by the Marangoni effect

Alexander Oron\*, and Alexander Alexeev†

We carry out an investigation of the dynamics of thin liquid films subjected to the Rayleigh-Taylor instability (RTI) coupled with the Marangoni effect in the setting of the experimental study<sup>1</sup>. Our goal is twofold: first, to compare between the solutions obtained from the original Navier-Stokes (NS) equations and the evolution equation derived in the framework of the long-wave (LW) theory and to show that suppression of the RTI by the Marangoni effect and creation of stable steady states are possible. Second, we attempt to compare between the solutions of the NS and LW equations and between them and the experimental results<sup>1</sup>. Both the NS and LW equations are solved in two and three dimensions. In the 2D case we find that the film evolution leads to formation of a steady state for larger values of the temperature drop across the film  $\Delta T$  or to competition between the touchdown at the bottom and rupture at the top for lower temperature differences. In the case of steady-state formation, a good agreement between the solutions of the NS and LW equations in the wide range of  $\Delta T$  with respect to the maximal film thickness of the steady state is revealed. The difference between the solutions increases with a decrease of the temperature drop and some morphological differences such as secondary humps appear. Despite these differences the critical event of the touchdown occurs in both theoretical approaches at the temperatures within the interval of 1 K. A good qualitative agreement is found also between the steady states obtained from the axisymmetric NS and the 3D LW equations. The occurrence of the touchdown at the bottom is found to match between both theoretical approaches. The results of this comparative study provide a new validation for the LW approach and its predictions. The emergence of steady states, where the RTI is saturated by the Marangoni effect first shown by Deissler and Oron<sup>2</sup> via minimization of an appropriate free-energy functional, is now confirmed following the film evolution in the framework of both NS and LW evolution equations. As for the comparison between the theory and experiments<sup>1</sup>, the experimental result of film stabilization at  $\Delta T = 9.7$  K was under scrutiny. Unfortunately, the description of film stabilization was not documented in detail<sup>1</sup>. If the fact of remaining the film interface flat is meant by film stabilization there, then the theoretical results show a mismatch. The discrepancy of more than 5 K between the instability threshold predicted by the linear theory and the experimental results constitutes a difference of 30% and cannot be due to the effect of boundary conditions at the sidewalls. This is based on the fact that different boundary conditions used for the NS and LW equations lead to similar results that weakly depend on the boundary conditions, especially for films of aspect ratio 400.

A.O. was partially supported by the Technion President Fund and the Fund for Promotion of Research at the Technion.

\*Department of Mechanical Engineering, Technion-Israel Institute of Technology, Haifa, ISRAEL.

†Department of Mechanical Engineering, Georgia Institute of Technology, Atlanta, Georgia, USA.

<sup>1</sup>J. M. Burgess et al., *Phys. Rev. Lett.* **86**, 1203 (2001).

<sup>2</sup>R. J. Deissler and A. Oron, *Phys. Rev. Lett.* **68**, 2948 (1992).

## Evolution of the particle concentration profile in a dilute suspension flow through the entry region of a channel

Andrei A. Osipov<sup>a</sup> and Evgeny S. Asmolov<sup>a,b</sup>

Within the two-fluid approach, an asymptotic model of a dilute suspension flow through the entry region of a plane channel or a circular pipe is constructed. The interphase momentum exchange is due to the Stokes drag force and the Saffman lift force, the latter taken with a correction factor for a bounded flow at an arbitrary shear rate.<sup>1</sup> The channel Reynolds number is high, the particle velocity relaxation length is comparable to the channel width, and the fluid-to-particle density ratio is of order unity. The solution is constructed using the matched asymptotic expansions method. The problem of finding the far-downstream cross-channel concentration profile is reduced to solving the equations of the fluid-particle boundary layer developing on the channel walls. The Full Lagrangian approach<sup>2</sup> is used to study the evolution of the cross-flow particle concentration profile in the boundary layer (Fig. 1). The asymptote and the jump of the concentration profile (curve 2 in Fig. 1) correspond to the lower and the upper boundaries of the fold in the Lagrangian volume of the particulate medium. Thus the shear-induced particle migration results in particle accumulation on two symmetric planes (an annulus) distanced from the walls, with a non-uniform concentration distribution between the planes (inside the annulus) and particle-free layers near the walls. The numerical results are discussed in comparison with the tubular pinch effect observed in experiments,<sup>3</sup> and a qualitative agreement is found.

<sup>a</sup> Schlumberger Moscow Research, Moscow, Russia.

<sup>b</sup> Central Aero-Hydrodynamics Institute, Zhukovsky, Moscow Region, Russia.

<sup>1</sup> J.B. McLaughlin, *J. Fluid Mech.* **246**, 249 (1993).

<sup>2</sup> A.N. Osipov, *Astrophys. Space Sci.* **274**, 377 (2000).

<sup>3</sup> Guazzelli et al., *J. Fluid Mech.* **515**, 171 (2004).

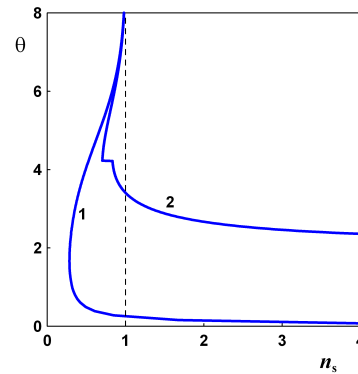


Figure 1: Particle number concentration  $n_s$  vs. the nondimensional coordinate  $\theta$  measured from the wall for the classical (1) and corrected (2) Saffman lift force.

### The Effects of Surface Roughness on the Motion of a Sphere in a Stokes Flow Near a Wall

Otto, C.\*

The results of an experimental investigation of the effects of surface roughness on the motion of a solid sphere in a rotating horizontal drum fully filled with very viscous fluid are reported. Our results for smooth spheres are in agreement with theory over a range of sphere densities. Roughened spheres exhibit a particle-boundary contact, which smoothly crosses over to a non-contact regime as the drum's rotational speed is increased. This non-contact regime is in agreement with theory. It is well known that cavitation is an important ingredient in this flow and we observe this in our experiments both for smooth and rough spheres (as shown in Figure 1). On the other hand cavitation is not found for almost neutrally buoyant spheres and the speed ratio is greater than predicted by theory.

---

\*Manchester Centre for Nonlinear Dynamics, University of Manchester.

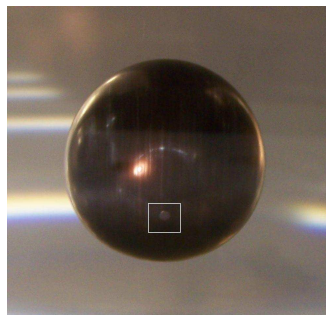


Figure 1: Photograph of sphere and cavitation bubble.



## Jamming and flows of dense noncolloidal suspensions

G. Ovarlez\*, S. Rodts\* and F. Bertrand\*

We present an experimental study of the local behavior of dense suspensions of noncolloidal particles<sup>1</sup> in a Couette geometry based on a combination of local velocity and concentration profiles measurements through Magnetic Resonance Imaging techniques, and macroscopic rheometric experiments. From steady rheometric measurements (Fig. 1a), the generally accepted picture is that these dense suspensions behave as dry granular systems at low shear rates (the shear stress is constant), and as viscous materials at intermediate shear rates.

We find that the flow is localized at low velocities, and also at concentrations above 60.5%: the material is partially jammed<sup>1</sup>. Surprisingly, by studying the response to a velocity step (Fig. 1a), we find that dense suspensions have a purely viscous behavior<sup>1</sup> whatever the shear rate is, even when the flow is localized: there is no observable influence of a yield stress nor granular friction. Shear localization may then be the result of a change in the suspension configuration as there must be a frictional contact network in the jammed zone to support stresses without flowing.

We also show that the particle distribution in the suspension is heterogeneous<sup>1</sup> under shear, and that the shear-induced migration process at the origin of this heterogeneity is almost instantaneous and unavoidable, in contradiction with previous observations. From the concentration and velocity profiles, we are nevertheless able to provide for the first time local measurements of the maximum packing fraction and of the viscosity/concentration relationship<sup>1</sup>, based on the real local shear rate and the real local concentration (Fig. 2). We find a Krieger-Dougherty law  $\eta(\phi) = \eta_0(1 - \phi/\phi_m)^{-2}$  to apply with  $\phi_m = 0.605$ . We finally propose a simple constitutive law based on a purely viscous behavior to account for all the macroscopic and local observations.

\* Université Paris-Est, UR Navier, Laboratoire des Matériaux et Structures du Génie Civil, France

<sup>1</sup>G. Ovarlez et al., *J. Rheol.* **50**, 259 (2006).

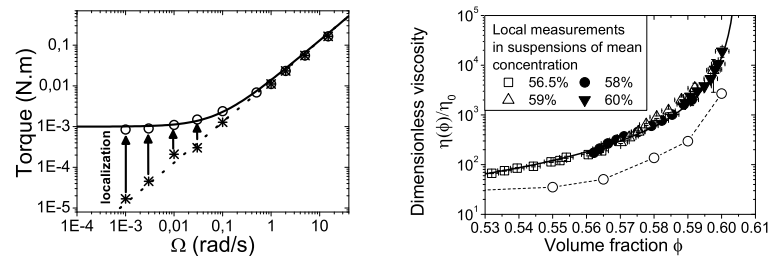


Figure 1: a) Torque vs. rotational velocity for the Couette flows of a 58% suspension: steady flows (open circles); instantaneous response to a velocity step (stars). The dotted line is a viscous line. b) Local viscosity vs. local concentration from MRI measurements; the line is a Krieger-Dougherty law. Macroscopic measurements based on the mean shear rate and the mean concentration would result in the open circles.

## Global mode analysis in the development region of a rotating Hagen-Poiseuille flow.

L. Parras\*, C. del Pino\*, E. Sanmiguel-Rojas†

The problem of a Rotating Hagen-Poiseuille (hereafter referred as RHP) has been widely studied, because contrary to its non-rotating counterpart, the flow is known to be unstable to infinitesimal perturbations for moderate Reynolds numbers<sup>1</sup>. Later studies also show that there is a transition from convective to absolute instabilities<sup>2</sup>. For this reason, this unstable problem is suitable to be used as a benchmark for global modes analysis.

Global mode analysis has increased its interest in the recent years because it can provide a way to apply general stability theory to more applied control problems<sup>3</sup>. In all these works, a set of boundary conditions provide the existence and properties of global modes, which are those that maintain self-sustained oscillations. These boundary conditions are useful only in the cases where the non-parallel effects are important as it happens in sudden expansions flows (backward facing step, sudden expansion from a pipe, etc), cavities or bumps. In this study, usual boundary conditions used in control problems are not longer valid, because they cannot provide the local spectrum in the limit of the parallel base flow, so a different set of boundary conditions are studied and analysed.

On the other hand, in this work we have studied the three-dimensional global stability of the development region from a non-swirling uniform flow to a RHP at moderate Reynolds numbers and several swirl parameters. In this area of interest, non parallel effects must be taken into account in the base flow to analyse the spatial stability<sup>4</sup>. Finally, we compare three different approximations (local, non parallel and global) to study the flow stability of this simple problem.

---

\*E.T.S.I. Industriales, Universidad de Málaga.

†E.T.S.I. Industriales, Universidad de Jaén.

<sup>1</sup>P. A. Macrodt, *J. Fluid. Mech.*, **73**,153-164 (1976)

<sup>2</sup>R. Fernandez-Feria, C del Pino, *Phys. Fluids*, **14**, 3087-3097, (2002)

<sup>3</sup>Akervik et al. *J. Fluid. Mech.*, **579**, 305-314, (2007)

<sup>4</sup>C del Pino, et al, *Fluid Dynamic Research*, **32**, 261-281, (2003)

## Direct Numerical Simulation of the linear stability of a free convective boundary layer flow

M. C. Paul\*, D. A. S. Rees†

Direct Numerical simulations are performed to investigate the linear stability of a two-dimensional incompressible free convective flow from a vertical semi-infinite heated flat plate. A small-amplitude local temperature disturbance with a slowly increasing frequency is introduced on the surface near to the leading edge in order to generate disturbance waves within the boundary layer. In other engineering contexts such a disturbance is described as a sine-sweep. Examples of its use lie in the fields of acoustics<sup>1</sup>, dynamic testing<sup>2</sup>, flutter testing<sup>3</sup>, structural analysis<sup>4</sup>, and crack detection<sup>5</sup>.

The aim of this paper is to compare the response of the thermal boundary layer with that obtained by selecting discrete frequencies of disturbance<sup>6</sup>. In the present study, air is considered to be the working fluid for which the value of the Prandtl number is taken to be  $Pr = 0.7$ .

The computational results show that the disturbance decays initially until it reaches a critical distance which depends on the effective current frequency of the disturbance. Thereafter the disturbance grows, but the growth rate also depends on the effective frequency of the disturbance.

To our knowledge, it is the first time that the sine-sweep technique is used to assess the stability characteristics of a thermal boundary layer. Comparisons with previous work using constant disturbance frequencies show that the sine-sweep technique is an effective method for analysing the instability of convectively unstable boundary layers.

---

\*Department of Mechanical Engineering, University of Glasgow.

†Department of Mechanical Engineering, University of Bath.

<sup>1</sup>P. Fausti, A. Farina, *J. Sound Vib.* **221**, 331 (1990).

<sup>2</sup>Kowalski et al., *J. Automobile Eng.* **216**, 373 (2002).

<sup>3</sup>M. Marchitti, *Mech. Sys. and Sig. Proc.* **20**, 757 (2006).

<sup>4</sup>Y.F. Guo, J.H. Zhang, *Shock and Vib.* **11**, 521 (2004).

<sup>5</sup>Biemans et al., *J. Intelligent Material Sys. and Structures.* **12**, 589 (2001).

<sup>6</sup>Paul et al., *Int. J. Ther. Sci.* doi:10.1016/j.ijthermalsci.2007.10.017 (2007).

# Mathematical modelling of blood flow in curved arteries with elastic walls

Sevil Payvandi\*, Jennifer Siggers\*, and Kim Parker\*

The progression of atherosclerosis in arterial endothelial cells is governed by a complex interaction of the mechanics of the arterial wall, the stress induced by nearby blood flow, and the physiological factors within the blood and interstitial environment, which is found to lead to a non-uniform plaque distribution. This study seeks to understand and characterise the steady flow in an idealised model of a weakly-curved artery with elastic walls. The governing parameters of the model are the Dean number,  $D$ , which is proportional to the Reynolds number of the flow multiplied by the square root of the curvature,  $\delta$ , and the non-dimensional compliance of the wall,  $\epsilon$ . In the limit of small  $\delta$ ,  $D$  and  $\epsilon$ , asymptotic analysis is used to obtain solutions to the governing equations, with the driving pressure gradient and velocity assumed to be slowly varying in the axial direction. Figure 1 displays the coordinate system used.

The effects of the Dean number on flow in a weakly-curved rigid pipe have been extensively researched by previous authors; however, the effects of compliance are less well studied, even though the diameter of large arteries can vary by up to 5% during the cardiac cycle<sup>1</sup>. The particular aim of this research is to find what effect compliance has on the wall shear stress distribution because of the relevance of shear stress to atherogenesis. We model the artery as being curved because of the prevalence of atherosclerosis in highly curved arteries such as the aorta and the coronary arteries.

We found that increasing compliance reduces the shear stress (low wall shear stress is often cited as a factor in atherogenesis). In addition, further vortices are found to appear in the secondary flow near the wall in both hemispheres of the pipe (Figure 2, where I and O mark the inside and outside of the pipe bend). These additional vortices give rise to flow reversal regions, which could have important implications on particle mixing and residence time, and hence on atherogenesis.

\*Department of Bioengineering, Imperial College London.

<sup>1</sup>D.A.McDonald, *Blood Flow in Arteries*, Edward Arnold London (1974).

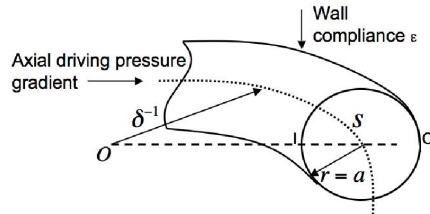


Figure 1: The nondimensionalised coordinate system.

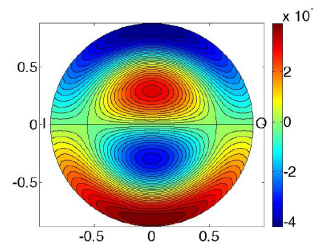


Figure 2: Contours of  $O(\epsilon)$  nondimensional secondary flow in the pipe cross-section.

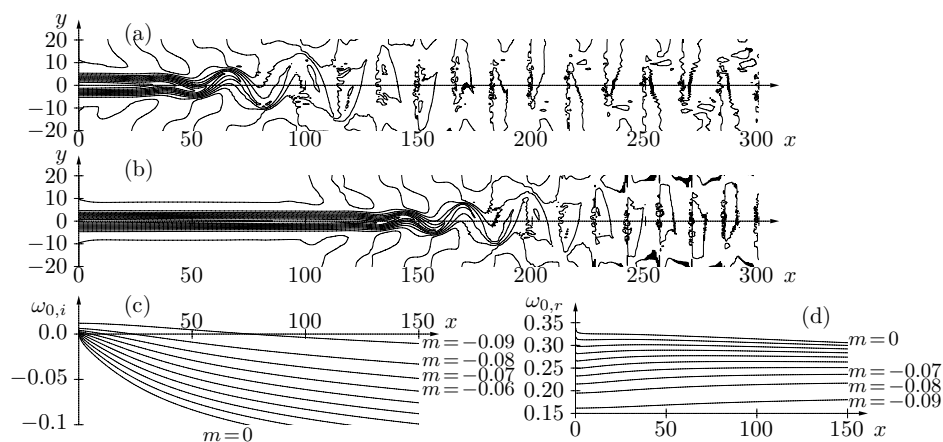
## Global nonlinear dynamics of thin airfoil wakes

Benoît PIER\* and Nigel PEAKE†

In the present investigation of thin airfoil wakes we compare the global nonlinear dynamics, obtained by direct numerical simulations, to the associated local instability features, derived from linear stability analyses.

In the numerical implementation, we consider a semi-infinite flow domain corresponding to the region downstream of the airfoil trailing edge, where a symmetric velocity profile is imposed represented by the double-Falkner–Skan boundary layer solutions with negative pressure gradient  $m$ . The parameter  $m$  is varied from  $m = 0$  (double-Blasius wake) to  $m = -0.09$  (near flow separation); Reynolds numbers up to  $Re = 5000$  are considered. It is found that the wake gives rise to self-sustained vortex shedding provided the Reynolds number and the adverse pressure gradient are large enough. Snapshots of streamwise velocity contours in the fully developed régime at  $Re = 4000$  for (a)  $m = -0.09$  and (b)  $m = -0.08$  are shown below; the associated global frequencies are  $\omega = 0.170$  and  $\omega = 0.198$ .

Local stability features are computed from the corresponding basic flows. At  $Re = 4000$ , the local absolute growth rates  $\omega_{0,i}$  and frequencies  $\omega_{0,r}$  are given in figures (c) and (d). It is seen that absolute instability prevails in the near wake and that the spatial variations of  $\omega_{0,i}$  strongly depend on  $m$ : the largest absolutely unstable domains and the weakest spatial variations are obtained at large (negative) values of  $m$ . The global frequency predictions<sup>1</sup> derived from these curves are  $\omega = 0.162$  for  $m = -0.09$  and  $\omega = 0.195$  for  $m = -0.08$ , in excellent agreement with the above direct numerical simulations. Another feature of interest is that nonlinear saturation may occur well downstream of the absolutely unstable domain.



\*Laboratoire de mécanique des fluides et d'acoustique; CNRS—Université de Lyon; École centrale de Lyon; 36 avenue Guy-de-Collongue ; F-69134 Écully cedex.

†Department of Applied Mathematics and Theoretical Physics; University of Cambridge; Wilberforce Road; Cambridge CB3 0WA; UK.

<sup>1</sup>Chomaz, *Annu. Rev. Fluid Mech.* **37**, 357 (2005).

An infinite, uniform suspension of swimming micro-organisms can become unstable in a variety of ways. If the cells are denser than water and swim upwards, there is a gyrotactic instability, leading to bioconvection plumes, as analysed by Pedley et al in 1988 and 1990. If the cells are neutrally buoyant and do not have a preferred swimming direction then the intrinsic stresslets of their swimming motions cause an instability whether they are pushers (thrust generated behind the body) or pullers (in front), as found by Simha & Ramaswamy in 2002 (SR). Here the analysis is repeated for the general case in which the cells may or may not be denser than water or subject to an orienting torque. The main findings are that the SR instability may be suppressed by rotational diffusion or by a large enough orienting torque, but a new mode of instability arises from the fact that the intrinsic stress is non-zero, though non-uniform, in the basic state. The results are applied to suspensions of algae, bacteria and spermatozoa.

## Instability of the interface of a rising bubble in a vertical slowly diverging pipe

J. Peixinho\* , S. Takeuchi\* , S. Takagi\* and Y. Matsumoto\*

Experiments on an air bubble rising in liquid-filled vertical slowly diverging pipes will be presented. This work was motivated by the understanding of wave occurrence and propagation of surface waves on rising Taylor bubbles and their interface instability in an expanding domains.

The experiment consists on diverging pipe with angles of 4 or 6 degrees. A bubble is generated at the bottom by a quasi-static injection of air. Initially, the liquid is quiescent and the top is closed. The bubble is large compared to the tube diameter and fills up the space leaving a liquid film between the air bubble and the wall. The bubble is pulled up by gravity and the liquid film goes down and becomes unstable. Further, the bubbles may exhibit various shapes and remarkable spatio-temporal patterns. The rising velocity, the bubble aspect ratio and the interface shape are analysed for several bubble volumes and different liquids with different viscosities and surface tensions. In the case bubbles exhibit surface waves, the growth rates of the amplitude is measured. Interestingly, the frequency of the waves is constant and the amplitude grows as the bubble propagates. This instability controls the detachment process which can be encountered in applications. A simple model and a tentative numerical work will be also presented.

This work was supported by the Japanese Society for the Promotion of Science

---

\*Department of Mechanical Engineering, University of Tokyo, Japan

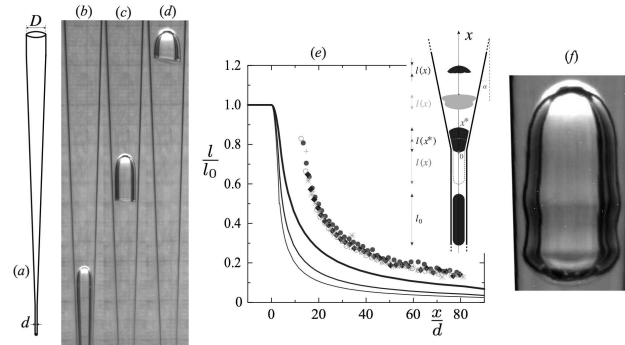


Figure 1: (a) Schematic of the apparatus. (b, c and d) Sequence of photographs of the rising air bubble in a silicone oil 100 times more viscous than water. (e) Axial bubble size evolution of the rising bubble versus its position along the pipe. The lines represent a model based on volume conservation principles for  $\alpha = 1, 2$  and  $3$  degrees and symbols are measurements. The inset is a schematic with the co-ordinate system. (f) Picture of an unstable air bubble in water.

## Magnetic Field Effects on Three Dimensional Stability of Natural Convection Flows in Differentially Heated Cavities

N. A. Pelekasis<sup>a</sup>, D. Dimopoulos<sup>a</sup>

Three dimensional stability analysis is conducted, of 2d steady state solutions obtained for free convection in a long square duct subject to a magnetic field with a temperature gradient perpendicular to the direction of gravity. For completeness sidewall conductivity is also accounted for. The base flow solution<sup>1</sup> is characterized by two recirculation cells that extend along the longitudinal direction of the duct. Beyond a certain threshold value of Gr it loses stability to a 2d time periodic solution. The wave-number k for which neutral stability with respect to 3d periodic longitudinal disturbances is achieved, is sought for. The numerical methodology for eigenvalue calculations via the Arnoldi method is optimised and different options are tested. In the absence of magnetic field and at low Pr=0.032 the base flow is seen to be more unstable to three dimensional perturbations, smaller threshold value of Gr compared to 2d disturbances, leading to a stationary arrangement that is periodic in the longitudinal direction and dominated by small wavenumbers. The emergence of three dimensional structures with the vortices aligned with the magnetic field, also developing periodically in the longitudinal direction, is investigated. In particular, the effect of increasing Hartman number is of interest in the context of a base configuration with the temperature gradient aligned with the direction of gravity, as indicated by relevant experiments<sup>2</sup>.

---

<sup>a</sup> Dept. of Mechanical and Industrial Engineering, University of Thessaly, Volos 38334, Greece.

<sup>1</sup> N. Pelekasis, *Phys. Fluids*, **18**(3), 1-23 (2006).

<sup>2</sup> U. Burr & U. Müller, *J. Fluid Mech.* **453**, 345-369 (2002)



## Dynamics of a falling film with solutal Marangoni effect

Antonio Pereira\* and Serafim Kalliadasis\*

We investigate the dynamics of a thin liquid film on an inclined planar substrate in the presence of an insoluble surfactant on its free surface. The governing equations are: (i) continuity and Navier-Stokes subject to the no-slip/no-penetration boundary conditions on the wall and the normal/tangential stress balances and kinematic boundary conditions on the free surface; (ii) transport equation for the surfactant in the free surface. With regards to this equation, in particular, we point out the ambiguity of the partial time derivative for the surfactant concentration in the transport equation obtained by Stone<sup>1,2</sup>.

We consider both the linear and nonlinear regimes. The linear regime is examined through the Orr-Sommerfeld eigenvalue problem of the full Navier-Stokes/concentration and wall/free-surface boundary conditions. The nonlinear regime is investigated through two different models. The first one is obtained from the classical long-wave expansion and the second one through an integral-boundary-layer approximation combined with a simple Galerkin projection. Although accurate close to the instability threshold, the first model fails to describe the dynamics of the system far from criticality. On the other hand, the second model not only does it capture accurately the behavior close to the instability threshold, but is also valid far from criticality. Analytical and numerical results on the role of the surfactant on the free-surface dynamics are presented. In the linear regime, the Marangoni stresses induced by the surfactant reduce the domain of instability for the base flow. In the nonlinear regime, the system evolves into solitary pulses for both free surface and surfactant concentration as shown in figure 1. The amplitude and velocity of these pulses decrease as the Marangoni effect becomes stronger.

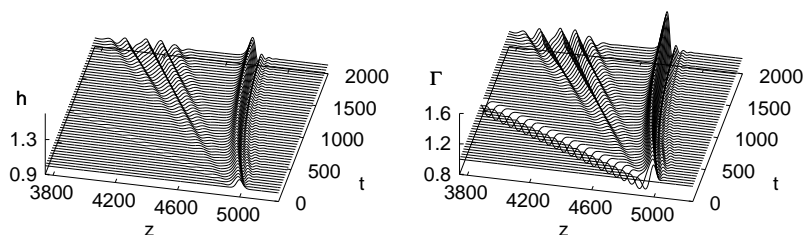


Figure 1: Time evolution of the surface deflection  $h$  and surfactant concentration  $\Gamma$ .

\*Department of Chemical Engineering, Imperial College London

<sup>1</sup>Stone, *Phys. Fluids* **2**, 111 (1990).

<sup>2</sup>Pereira et al., *Phys. Fluids* **19**, Art. No. 112102 (2007).

## Similarity solutions of the boundary-layer equations for flow along a curved wall

K P Pereira\*

The boundary-layer equations are obtained that approximate the steady flow of a viscous incompressible fluid along a body with a moderately curved surface. Using a group theoretic approach, a similarity transformation is constructed to convert the boundary-layer equations from a system of partial differential equations to a system of ordinary differential equations involving a curvature parameter  $\Omega$ . The system of ordinary differential equations is integrated numerically and we obtain a similarity solution of the boundary-layer equations for the flow past a 'curved' wedge. Unlike previous work<sup>1 2</sup> it is shown that for  $|\Omega| > 10^{-2}$  the curvature of the body becomes too large and the boundary-layer equations cease to be valid. Furthermore, in certain cases the similarity solution is not unique.

---

\*School of Computational and Applied Mathematics, University of the Witwatersrand.

<sup>1</sup>J.S. Murphy *AIAA*, **3**, 2043, (1965)

<sup>2</sup>B.S. Massey et al *Trans ASME J Basic Eng*, **87**, 483, (1965)

## Numerical simulation of Faraday waves

Nicolas Perinet\*, Damir Juric† Laurette S. Tuckerman\*

Faraday<sup>1</sup> first described in 1831 the pattern of standing waves generated at the surface of a vertically oscillated fluid layer; the corresponding linear stability analysis was carried out in 1954 for inviscid fluids<sup>2</sup> and in 1994 for viscous fluids<sup>3</sup>. The experimental observation in 1992 of quasicrystalline patterns<sup>4</sup> has inspired an abundance of experimental<sup>5</sup> and theoretical<sup>6</sup> research, but has not been accompanied by realistic numerical computations. Here, we report on the first fully three-dimensional and nonlinear simulations of Faraday waves.

Our numerical method solves the 3D incompressible Navier-Stokes equations in the two bulk fluids and incorporates a front-tracking method for the interface<sup>7</sup>. The velocity and pressure fields are obtained by a projection method on a MAC finite difference mesh. A separate Lagrangian mesh tracks the interface and provides geometric quantities required for the calculation of the surface tension force, which is subsequently distributed to the MAC mesh via an immersed boundary approach<sup>8</sup>.

Preliminary calculations for the three-dimensional nonlinear two-phase Navier-Stokes equations have successfully reproduced the theoretical instability threshold<sup>3</sup>. Various lattice patterns – lines, squares and hexagons – are known to appear in single-frequency forcing. In figure 1 we show the interface computed by our simulation, following an experiment<sup>9</sup> in which a hexagonal pattern was observed. We also investigate more exotic patterns such as quasicrystalline and superlattice patterns.

\*PMMH-ESPCI-CNRS, France

†LIMSI-CNRS, France

<sup>1</sup>Faraday, *Phil. Trans. R. Soc. Lond.* **52**, 319 (1831).

<sup>2</sup>Benjamin, Ursell, *Proc. R. Soc. Lond. A* **225**, 505 (1954).

<sup>3</sup>Kumar, Tuckerman, *J. Fluid Mech.* **279**, 49 (1994).

<sup>4</sup>Edwards, Fauve, *J. Fluid Mech.* **278**, 123 (1994).

<sup>5</sup>Kudrolli, Gollub, *Physica D* **97**, 133 (1996); Arbell, Fineberg, *Phys. Rev. E* **65**, 036224 (2002).

<sup>6</sup>Rucklidge, Silber, *Phys. Rev. E* **75**, 055203R (2007); Chen, Viñals, *Phys. Rev. E* **60**, 559 (1999).

<sup>7</sup>Shin, Juric, *J. Comput. Phys.* **180**, 427 (2002).

<sup>8</sup>Peskin, *J. Comput. Phys.* **25**, 220 (1977).

<sup>9</sup>Kityk, Embs, Mekhonoshin, Wagner, *Phys. Rev. Lett.* **72**, 036209 (2005).

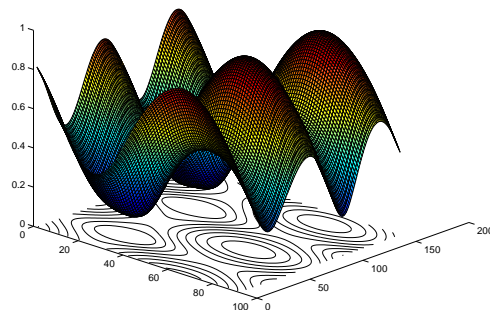


Figure 1: Pattern obtained from fluid dynamical simulation.

### Problem of steady-state flow over a step in the shallow-water approximation

A.S. Petrosyan<sup>a</sup> and K.V. Karelsky<sup>a</sup>

The study is aimed at solving the problem of a steady-state fluid flow over a step in the shallow-water approximation. The shallow –water equations are an approximation of the Euler equations for inviscid fluid with a free surface in the gravity field and hence, inherit all restrictions adopted in deriving these initial equations, in particular the condition of simple connectedness of the region occupied by the fluid in the neighborhood of the step. In this work, taking into account this condition made it possible to find the new steady-state flow regimes. The limitations on the possible flows depending on the flow direction are considered. All flow regimes characterized by the ratio of the fluid depth to the step height and the flow direction is found. Analytical expressions for the limitations imposed on the hydrodynamic flow parameters are obtained for each flow regime.

The classical shallow –water equations coincide to within the notation with compressible-gas equations, the Prandtl number now plays the role of the Mach number and, depending on its absolute value, the flow is called subsonic or supersonic. We obtained three flow regimes, namely, (1) subsonic flow ahead of the step and supersonic or subsonic flow behind the step, (2) supersonic flow ahead of the step and supersonic or subsonic flow behind the step, (3) supersonic flow ahead of the step and sonic flow behind the step. Regimes analysis showed that there exist two kinds of non-uniqueness of the solution. The first kind is attributable to the existence of two solutions with the same parameters to the left (or to the right) of the step. The second kind is related to the fact that the equations admit the transition from supersonic to subsonic flow unlimited number of times both ahead of and behind the step. The non-uniqueness of both kinds is the drawback of the shallow-water model.

In the complete solution obtained in our work with account for the flow direction, for each range of variation of the fluid depth ahead of the step, two values of the fluid depth behind the step exist. They correspond to subsonic and supersonic flows (non-uniqueness of the first kind). Only one of two possible equation roots corresponds to the physically meaningful solution: if ahead of the step the flow is supersonic and the fluid depth only slightly differs from the step height then the step is a significant obstacle sufficient for transition to the subsonic regime. In this case, behind the step the flow is subsonic. If ahead of the step the flow is supersonic and the fluid depth is much greater than the step height, then the step is an insignificant obstacle and the flow behind the step remains supersonic. In this case, to the right of the step we chose the supersonic solution. In this manner, we eliminate the non-uniqueness of the first kind in the cases of significant and insignificant influence of the step. The way to eliminate non-uniqueness of the second kind is also discussed.

---

<sup>a</sup> Space Research Institute, Russian Academy of Sciences.

## Generation of hairpin vortices and their decay in pipe flow

Jimmy Philip\* and Jacob Cohen\*

In recent years there has been a renewed interest in studies concerning transition in pipe flow<sup>1</sup>. It is well known that flow in a pipe is stable to linear disturbances at all Reynolds numbers ( $Re$ ). However, it has been found that the initial (normalized) disturbance ( $v_0$ ) needed to initiate turbulence decreases with  $Re$  as  $v_0 \sim Re^{-1}$ .<sup>2</sup> Moreover, it has been observed that finite amplitude disturbances decay in pipe even after the flow has become turbulent, given a sufficiently long pipe, where the turbulence decay has been found to be extremely dependent on the initial conditions<sup>3</sup>.

Most of the previous studies have used long pipes (the maximum having a length to diameter ( $X/D$ ) ratio of 7500) and with various criteria for detecting turbulent flow. We here follow the evolution of hairpin vortices assuming they characterize the nonlinear stage of transition<sup>4</sup>. Continuous, metered and dyed disturbances are injected into the pipe and various coherent structures are observed (as shown by two perpendicular views in figure 1 for  $Re = 1050$ ). Figure 1(a) shows a small disturbance with a single low velocity region (left view), which increases to become a streak with increasing injection rate (figure 1(b)). An increase of the disturbance level leads to the formation of an array of hairpins (figure 1(c)) which further intensifies into stronger vortices (figure 1(d)) at even higher levels of disturbance. Preliminary results in our (relatively short pipe of  $X/D=120$ ) facility indicate that a similar scaling law of  $v_0 \sim Re^{-1}$  can be obtained and that  $v_0$  or the scaling law is a function of the downstream distance. This is plotted in figure 1(e), which seem to coincide with the  $v_0 \sim Re^{-1}$  only at the length  $X/D=0$  (the red line showing a slope of -1).

\*Faculty of Aerospace Engineering, Technion - Israel Institute of Technology, Haifa 32000, Israel.

<sup>1</sup>Eckhardt et al., *Annu. Rev. Fluid Mech.* **39**, 447 (2007).

<sup>2</sup>Hof et al., *Phys. Rev. Letts.* **91**, 244502 (2003).

<sup>3</sup>Hof et al., *Nature* **443**, 59 (2006).

<sup>4</sup>Philip et al., *Phys. Rev. Letts.* **98**, 154502 (2007).

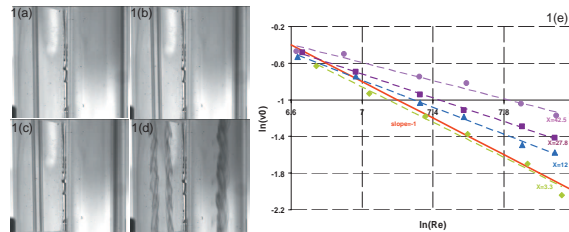


Figure 1: (a-d) Evolution of hairpin vortices as the injection velocity is increased at  $Re = 1050$ , (e) Plot of variation of scaling law with increasing downstream distance.

**Start and stop of an avalanche in a granular medium subjected to an inner water flow**

P. Philippe

Cemagref, Aix-en-Provence, France

(pierre.philippe@cemagref.fr / tel: 33(0)442669955)

Gravitational stability of a soil is a major concern either for civil engineering structures or for natural hazards since slope failures can trigger large surface avalanches, massive landslides or potentially devastating debris flows. Such events occur in subaerial as well as in subaqueous environment and, for instance, landslides are frequently observed on the seafloor, even on very slight inclines. For fully saturated soils, ground water flow affects soil stability and, according to streamlines orientation versus gravity, can possibly lead to fluidization or to slope failure. Downstream face sliding on an earth dam, submarine landslide or quicksand are some related examples of gravitational instabilities induced by groundwater flows.

This contribution deals with the situation of an immersed granular medium submitted to an inner water flow with a constant pressure drop, either in upward or downward direction in respect to its free surface normal. The main question is to understand how the drag force exerted on the grains by the flow will enhance or reduce the overall stability of the medium. In the specific case of granular media, the stability threshold is simply determined by the maximum stable slope inclination also called *avalanche angle*. The aim of this study is to focus both theoretically and experimentally on the influence of a steady inner water flow on the avalanche angle of a granular medium and on its subsequent dynamics. To tackle this issue, granular physics, soil slope stability and hydrodynamics in porous media must be brought together.

We report experimental results on the *avalanche angle* of a granular medium as a function of the applied non dimensional pressure drop  $i$ , called *hydraulic gradient*. A unique avalanche threshold is derived by two alternative theoretical developments, namely a continuum and a discrete approach, and is successfully confronted to many measurements in a large experimental range. A qualitative analysis of the instability triggering reveals different dynamical behaviours depending on the direction of the internal water flow, namely *stabilizing* versus *destabilizing* regime. The repose surface of the sample following an avalanche is not linear as in the purely hydrostatic situation because the hydraulic gradient is no more constant in the medium. A simple model is proposed that can satisfactorily predict the post-avalanche height profile as well as its subsequent evolution for higher inclinations.

## Experimental characterization of near transition region in rotating-disk boundary layer

Benoît PIER\*, Lionel LE PENVEN\*, Julian SCOTT\*,  
Alexandre AZOUZI\*, Patrick DUTHEIL\*, Roger MICHELET\*

The flow due an infinite disk rotating in otherwise still fluid has served as the archetypical configuration for the study of three-dimensional boundary layers and is known to display a sharp transition from laminar to turbulent flow at a nondimensional critical radius  $R \simeq 510$ . Using linear stability analysis, this location was found by Lingwood<sup>1</sup> to precisely coincide with the onset of local absolute instability at  $R^{ca} \simeq 507$ . More recently<sup>2</sup>, a fully nonlinear analysis and a secondary stability analysis have further contributed to the understanding of the complex dynamics prevailing near the transition station.

The present experimental investigation has been undertaken to confront these theoretical results with detailed observations of the transition region.

The experimental arrangement consists of a 50 cm diameter disk that is rotated at constant angular speeds, up to 1500 rpm. Time-resolved local measurements of the azimuthal velocity component are performed by a constant temperature hot wire probe mounted on a two-axes traversing mechanism, achieving displacements in the radial and axial directions with a precision of  $20 \mu\text{m}$  and  $2 \mu\text{m}$  respectively.

Spectral analysis of the azimuthal velocity time series confirms that transition from the laminar boundary layer (flat spectra) to the turbulent régime (characteristic power laws) occurs near the radial location  $R \simeq 510$ . However, an intermediate weakly nonlinear régime has also been identified, characterized by a harmonic spectrum. This régime is observed in the lower part of the boundary layer, close to the disk surface, starts around  $R \simeq 470$  and survives up to  $R \simeq 530$  (plots (1a) and (1b)). In contrast, above this near wall region, towards the outer edge of the boundary layer, the transition from laminar to turbulent régimes is seen to occur very suddenly over  $500 < R < 510$  (plot 1c). An interpretation of this intermediate régime in terms of linear and nonlinear instability waves will be proposed.

\*Laboratoire de mécanique des fluides et d'acoustique; CNRS—Université de Lyon; École centrale de Lyon; 36 avenue Guy-de-Collongue ; F-69134 Écully cedex.

<sup>1</sup>Lingwood, *J. Fluid Mech.* **299**, 17 (1995).

<sup>2</sup>Pier, *J. Fluid Mech.* **487**, 315 (2003).

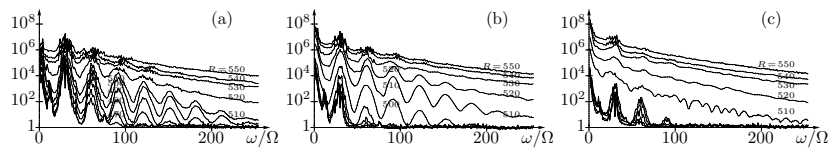


Figure 1: Fourier power spectra of velocity time series at  $R = 460, 470, \dots, 550$  for different positions within the boundary layer: (a)  $Z = 2$ , (b)  $Z = 3.5$ , (c)  $Z = 5$ .

## Falling jets of particles in viscous fluids

Florent Pignatel\*, David Saintillan†, Maxime Nicolas\*  
and Élisabeth Guazzelli\*

We have investigated the time evolution of a jet of non-Brownian particles falling under the action of gravity in a viscous liquid at low Reynolds number. We have found that the jet is unstable and presents modulation of its diameter (see figure 1). Different regimes have been observed depending upon the volume fraction and the particle-to-jet diameter ratio. The dominant wavelength and saturated amplitude are measured versus volume fraction. A scaling for the jet velocity coming from a continuous model is proposed. A simple numerical simulation using point-particles is able to capture the instability (see figure 1).

---

\*IUSTI CNRS Polytech Marseille.

†Mechanical Science and Engineering, University of Illinois, Urbana Champaign.



Figure 1: On the left of the figure, we can see a photograph of a jet of particules for a volume fraction of 10 % and a particle-to-jet diameter ratio of 22. On the right, we can see a picture of the simulation of a jet of point-particules.



## Unexpected unsteady instability in DNS computations dedicated to 3D localized receptivity

Estelle Piot\*, Grégoire Casalis\*

The present work deals with a Direct Numerical Simulation of the crossflow waves induced by micro-roughness elements placed on a swept cylinder along a line parallel to the leading edge. The incoming flow velocity is 50 m/s, the sweep angle  $60^\circ$  and the radius of the cylinder 10 cm. The roughness elements are periodically placed in the spanwise direction. According to different experiments<sup>1</sup>, steady crossflow vortices are generated with the same spanwise period as the spacing between the roughness elements. Consequently a DNS investigation can be limited to a domain around a single roughness element. It is performed using the code SabrinA<sup>2</sup>.

The roughness element has a parallelepipedic shape, its typical height is  $\delta/10$  with  $\delta$  the leading edge boundary layer thickness. The roughness is meshed, with no-slip conditions upon its different faces. Computations are performed in two steps, first without roughness, then with it. A steady flow is obtained at the end of the first step and is used as initial flow for the second step. This initialization induces an unsteady behavior as shown by time evolutions of a sensor placed downstream of the roughness, see figure 1. Two cases are shown corresponding to two chordwise positions of the roughness element. For the upstream position, the unsteady behavior seems to remain permanently, whereas the flow becomes steady for the downstream one. In the first case, the expected steady crossflow modes are altered by nonlinear interactions induced by the unsteady perturbation due to its rather large amplitude, whereas in the second case the steady modes are well defined w.r.t. the linear stability after the damping of the unsteady part.

A detailed analysis, which will be presented during the conference, shows that the unsteady fluctuation is an unsteady crossflow mode induced by a "quasi" absolute instability mechanism. For the upstream location, the absolute instability is nearly neutral whereas it is stable for the downstream one.

\*Aerodynamics and Energetics Modeling, ONERA, Toulouse, FRANCE

<sup>1</sup>Reibert et al. , *AIAA-97-1816*, 1997.

<sup>2</sup>M. Terracol, *Technical Report RT 5/07383*, ONERA, 2003.

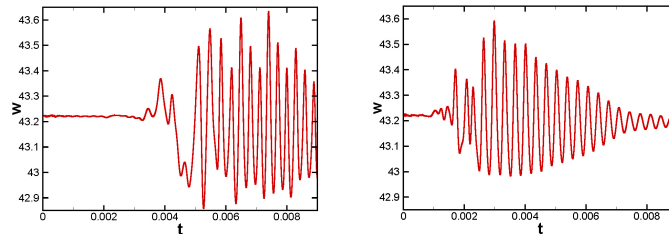


Figure 1: Spanwise velocity component vs time at the chordwise position  $\theta = 20^\circ$ . The roughness element is placed at  $\theta_r = 8^\circ$  (left graph) and  $\theta_r = 14^\circ$  (right graph).

## Marangoni instability in binary fluids and nanofluids.

A. Podolny\*, A. A. Nepomnyashchy†, A. Oron‡

Investigation of the Marangoni convection in binary fluids in the framework of linear stability theory was started several decades ago. Recently a new class of fluids, nanofluids, has been successfully applied in heat transfer devices. Nanofluids are suspensions of nanoparticles in the size range of about 10 to 50 nm in a carrier fluid. Nanofluids have significantly higher thermal conductivity and heat transfer coefficients than their base fluid. Also, typical nanofluids are characterized by an extremely small Lewis number.

In order to develop a realistic two-component model for transport phenomena in nanofluids it is important to understand the mechanisms by which the nanoparticles can develop a slip velocity with respect to the base fluid. It is shown that Brownian diffusion and thermophoresis may become important as slip mechanisms while gravity settling is negligible.

We consider relatively thick fluid layer under terrestrial gravity conditions subjected to a transverse temperature gradient. Concentration gradient is induced due to the Soret effect. The layer is exposed to the ambient gas phase at its non-deformable free surface. Surface tension is assumed to depend on both temperature and solute concentration, so both Marangoni, thermo- and soluto -capillary effects are taken into account. So, in such layers, a combination of Rayleigh and Marangoni convection takes place.

The talk presents a unified theoretical description of Marangoni convection, which can be applied for both binary solutions and nanofluids.

We study the case of the long-wave instability of the system with poorly conducting boundaries in the limit of asymptotically small Lewis numbers. The behavior of the critical Marangoni number depends on the relationship between small parameters of the problem. Two kinds of the small-parameter approaches can be applied to the solution of this problem. In the first one we choose Biot number  $Bi$  as the basic small parameter, consider different cases for smallness of the wave number  $k$ , and only afterwards the Lewis number  $L$  becomes small, which corresponds to  $L \gg k, Bi$ . In the second one  $L$  is considered as a basic small parameter while the smallness of  $k$  and  $Bi$  with respect to  $L$  can be different. The second approach is novel and it gives potentially the whole picture for small- $L$  fluids. It leads to the essential difference in the structure of equations governing the monotonic and oscillatory instability and the shape of the eigenfunctions. Thus, the consideration of the nanofluids, even in the framework of the binary-fluid model, demands solving new non-trivial mathematical problems. In the framework of the new approach typical behavior of monotonic and oscillatory instability boundaries is investigated in distinct limits of parameters.

---

\*Department of Mathematics, Technion, Haifa 32000 Israel.

†Department of Mathematics, Technion and Minerva Center for Nonlinear Physics of Complex Systems, Technion- Israel Institute of Technology, Haifa 32000 Israel.

‡Department of Mechanical Engineering, Technion, Haifa 32000 Israel.

## Circular and spiral waves in a Batchelor flow between a rotating and a stationary disk

Sébastien Poncet,<sup>\*</sup> Éric Serre <sup>\*</sup>, Marie-Pierre Chauve <sup>†</sup> and Patrice Le Gal<sup>‡</sup>

A three-dimensional direct numerical simulation is combined with flow visualizations to study the transition to turbulence of the flow enclosed between a rotating and a stationary disk. The numerical approach is based on a pseudo-spectral technique using Chebyshev polynomials in the radial and axial directions with Fourier series in the azimuthal direction. The rotor-stator cavity can be defined by this aspect ratio  $G = b/h = 7$  and this curvature parameter  $1 \leq R_m = (a+b)/(a-b) \leq 8.33$ , where  $a$  and  $b$  are the inner and outer radii of the rotating disk and  $h$  is the interdisk spacing. The flow is also governed by the rotational Reynolds number  $Re = \Omega b^2/\nu \leq 8 \times 10^4$ , with  $\Omega$  the rotation rate and  $\nu$  the kinematic viscosity of water.

For Batchelor-like flows, Schouveiler *et al.*<sup>1</sup> observed a first instability, which appear as circular rolls (RC) propagating towards the center of the cavity along the stator. Above a second threshold, an Eckhaus instability develops at the periphery of the stator as spiral rolls (RS1), which coexist with the RC patterns. These two instabilities have been here studied both numerically and experimentally and a closed agreement has been obtained on the thresholds and on the characteristics of these patterns. We show in particular that the circular rolls (Fig.1a,b) are a convective instability, which confirms the experiments of Gauthier *et al.*<sup>2</sup>. This instability appears to be self-sustained in the present experiment as in the one of Schouveiler *et al.*<sup>1</sup> by an experimental noise. At  $Re = 24630$ , the circular rolls disappear after 20 turns and the flow gets stable again in the calculation. So, we introduce a small sinusoidal perturbation to get the RS1 patterns (Fig.1c), whereas the two instabilities coexist in the experiment (Fig.1d). By changing the boundary condition on the external cylinder, we show that the RS1 patterns are a shear layer instability due to the destabilization of the Stewartson layer along the shroud. Finally, the influence of the curvature parameter on the route to turbulence has also been highlighted experimentally.

<sup>\*</sup>Laboratoire M2P2, UMR 6181 CNRS - Univ. Aix-Marseille.

<sup>†</sup>IRPHE, UMR 6594 CNRS - Univ. Aix-Marseille.

<sup>1</sup>Schouveiler *et al.*, *J. Fluid Mech.* **443**, 329-350 (2001).

<sup>2</sup>Gauthier *et al.*, *J. Fluid Mech.* **386**, 105-126 (1999).

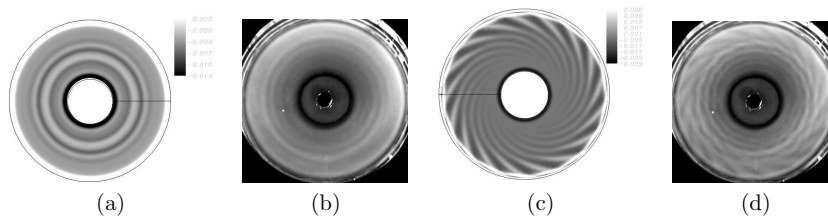


Figure 1: Circular (a,b) and spiral (c,d) rolls obtained respectively at  $Re = 15000$  and  $Re = 24630$  by DNS (a,c) and flow visualizations (b,d) for  $R_m = 1.8$ .

## Inertia-induced adiabatic structures in time-periodic laminar flows

Z. Pouransari<sup>a</sup>, M.F.M. Speetjens<sup>b</sup>, H.J.H. Clercx<sup>a</sup>

Mixing quality in unsteady incompressible laminar flows can be greatly enhanced by three-dimensional (3D) chaotic advection. A significant issue for mixing applications is the response of invariant surfaces, which the non-inertial limit ( $Re=0$ ) of such flows may admit, to fluid inertia ( $Re>0$ ). We have studied topological properties of a viscous incompressible time-periodic flow in a square cylindrical domain. In particular we have focused on the response of the one-action state to the inertial perturbations for the general two-step volume preserving maps. Previous investigations indicate formation of one coherent structure consisting of two incomplete adiabatic surfaces and two tubes with transversal motion in between, i.e. resonance-induced merger (RIM) for a specific forcing protocol (one step forward in  $x$ -direction followed by one step forward in  $y$ -direction)<sup>1</sup>. Here the adiabatic surfaces are remnants of perturbed invariant surfaces and tubes are centred upon elliptic segments of periodic lines. In this study we have validated and examined the formation of such coherent structures by RIM for any arbitrary two-step volume preserving map. Fundamental topological characteristics of the general two-step forcing protocol (as the building block for future protocols) have been examined numerically (Fig1-a) and the so called 'RIM' phenomena has been detected in the neighborhood of parabolic borders (Fig1-b,c). Key aspects of numerical simulation results are validated by means of an experimental visualization method.

Furthermore the above analytical and numerical studies have been extended to the three-step closed loop map, i.e. bottom wall is translated while following a triangle. This enables infinite repetition in a laboratory set-up using finite walls and thus facilitates detailed experimental analysis of RIM.

<sup>a</sup> Fluid Dynamics Laboratory, Department of Applied Physics, Eindhoven University of Technology, P.O. Box 513, 5600 MB Eindhoven, The Netherlands, (E-mail: [z.pouransari@tue.nl](mailto:z.pouransari@tue.nl))

<sup>b</sup> Energy Technology Laboratory, Department of Mechanical Engineering, Eindhoven University of Technology, P.O. Box 513, 5600 MB Eindhoven, The Netherlands

<sup>1</sup> Speetjens et al, *J. Fluid Mech.* **514**, 77 (2004), Speetjens et al, *Phys Fluid.* **18**, 083603 (2006).

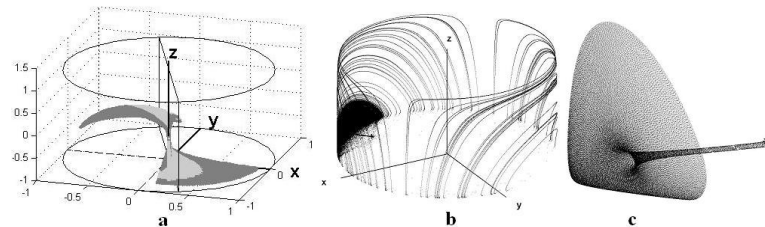


Figure 1: (a) Elliptic (dark) and hyperbolic (bright) segments of the surface formed by the periodic lines of two-step protocol while the 2<sup>nd</sup>-step angle is changing,  $0<\theta<180$  (b) Poincaré section (320000 periods), star points to the initial position of the tracer (c) Close view of RIM, tube structure merges to the neighborhood adiabatic surface.

## High Rayleigh Number High Prandtl Number Natural Convection mimicking Mantle Convection

Vivek N. Prakash<sup>a</sup>, K. R. Sreenivas<sup>a</sup>, Jaywant H. Arakeri<sup>b</sup>

Convection in the Earth's Mantle is responsible for volcanism, plate-tectonics and orography. The condition under which convection occurs in the mantle corresponds to a large Rayleigh number and in a medium of large Prandtl number<sup>1</sup>. Using concentration difference to drive the convection<sup>2</sup>, we simulate large Rayleigh number convection and study the effect of Prandtl number on the dynamics of convection and its structures. The experimental set up consists of a square-cross section tank having two parts, lower and upper sections, separated by a permeable-membrane that allows a through-flow. A layer of high-density sugar solution is in the upper section, which is resting over a layer of fresh water in the lower section and the permeable membrane separates these two layers. To achieve high Schmidt numbers (which is a proxy for the Prandtl number) in our experiments the viscosity of the medium is enhanced using Sodium CarboxyMethylCellulose (Na-CMC). Buoyancy flux is controlled by the rate of through-flow across the membrane with the help of a valve connecting the lower section of the tank to an external reservoir.

The Rayleigh numbers (Ra) covered in the present study are in the range of  $10^9$  to  $10^{11}$  and Schmidt numbers (Sc) are in the range of  $10^3$  to  $10^5$ . At low Sc, the near-membrane flow structures consist of sheet plumes. The plan forms of these sheet plumes show a marked change in morphology as the viscosity of the upper fluid layer is increased (Figure 1). With the increase in viscosity the plume spacing increases and also there is a transition from sheet plumes to discrete blobs. In our full paper, we will present the parametric dependence of these changes on the viscosity.

<sup>a</sup> EMU, Jawaharlal Nehru Centre for Advanced Scientific Research, Bangalore - 560064, INDIA

<sup>b</sup> Mechanical Engineering Department, Indian Institute of Science, Bangalore – 560012, INDIA

<sup>1</sup> C. Lithgow-Bertelloni et al., *J. Fluid Mech.* **434**, 1 (2001).

<sup>2</sup> B.A. Puthenveetil et al., *J. Fluid Mech.* **542**, 217 (2005).

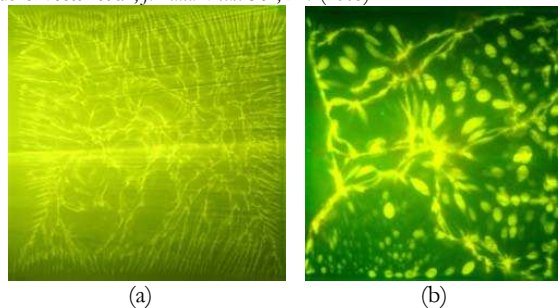


Figure 1: Plan views of plume structures in convection-system driven by concentration variation (a) in a medium having no viscosity contrast between plume and medium (b) in a medium of high viscosity in which plumes have lower viscosity.

## Algebraic versus exponential spatial growth in swept-wing flow

Jan Pralits\*, Raffaele Donelli†, Paolo Luchini\*

Transition from laminar to turbulent flow in boundary layers on swept wings is usually caused by perturbations with infinitesimal amplitude which grow as they propagate downstream. These perturbations are, insofar as convective instabilities, commonly analysed using spatial linear stability theory (LST) in order to obtain their respective growth rate and amplification. The growth rate is used to obtain from a multiple-scale approximation or parabolic stability equation, the integrated amplification over a spatial span and predict the point of transition. It is well known that in swept-wing flow the perturbations which first attain an amplification level which can cause transition are of inviscid type and usually denoted as crossflow vortices (CFV). These perturbations are due to the inflection point in the crossflow component of the mean flow which is caused by the influences of sweep and pressure gradient present in the flow. The CFV manifest themselves as stationary vortices aligned to within a few degrees of the local inviscid streamlines, on which travelling waves might be superimposed. The growth rate of the leading normal mode of the CFV, obtained using the Orr-Sommerfeld equation, in many cases manages well to compare with experiments. However, when the integrated amplification is sought, there are obvious doubts that a high frequency approximation, such as either multiple-scale analysis or parabolic stability equation is, can be applied to this type of perturbations which are inherently low or zero frequency. Nevertheless both modal and algebraic growth were studied by<sup>1</sup> in their investigation concerning optimal perturbations in swept-wing flows. They used the temporal framework with the mean flow approximated by Falkner-Skan-Cooke similarity solutions and showed that the most amplified disturbances take the form of vortices almost aligned with the external streamline, and later evolve into streaks. They also reported, for certain cases of adverse pressure gradient, that the wavenumber region of maximum algebraic growth coincides with a region of maximum exponential growth.

The aim of the current work is twofold. First, to analyse the order of magnitude of the errors of a multiple-scale approximation as applied to crossflow instabilities and give a sounder theoretical basis to its use in transition prediction. Second, to apply an approach similar to<sup>1</sup> in a spatial framework and discuss the relative importance of algebraic and exponential contributions to the growth as far as transition prediction is concerned in Falkner-Skan-Cooke boundary layers.

The authors wish to acknowledge the support of CIRA (Italian Aerospace Research Center) within the national research project ACADEMIA.

---

\*DIMEC, Università di Salerno, Italy.

†CIRA (Italian Aerospace Research Center), Capua, Italy.

<sup>1</sup>Corbett & Bottaro, *J. Fluid Mech.* **435**, 1 (2001).

**Coherent Structures on the Laminar/Turbulent Boundary**C.C.T. Pringle\*, Y. Duguet\* and R.R. Kerswell \*

Transition to turbulence in shear flows remains an outstanding problem in fluid mechanics, with the earliest rigorous study carried out in pipe flow by Osborne Reynolds (1883). While pipe flow is now known to be linearly stable, it is unstable to finite-amplitude disturbances. This means there must be a boundary in phase space separating perturbations to the laminar flow which relaminarise and those that trigger transition. Trajectories confined to this boundary are now known to undergo an intermediate form of chaotic dynamics (neither relaminarising nor becoming fully turbulent) in which it is possible to identify transient coherent structures. We will discuss the nature of these coherent states and comment on their relevance to transition.

---

\*Department of Mathematics, University of Bristol.

## On the influence of the boundary condition on stability of Hagen–Poiseuille flow

Vít Průša\*

We analyze influence of choice of boundary condition (no-slip and Navier’s slip boundary conditions) on linear stability of Hagen–Poiseuille flow. Although the slip boundary condition is not very common in the classical fluid mechanics, it seems to be the right effective boundary condition for flows past “infinitesimally” structured walls (like chemically patterned surfaces<sup>1</sup>, infinitesimally ribbed surfaces<sup>2</sup> and other infinitesimal structures frequently occurring in nanotechnology).

It is well known that linear stability of Hagen–Poiseuille flow is highly sensitive to the experimental setup like exact shape of the pipe’s cross-section<sup>3</sup>, therefore the question whether the flow is stabilized or destabilized by Navier’s slip boundary condition immediately arises. The standard linearized equations for disturbance  $\mathbf{v}$  are in this case the following

$$\begin{aligned} \frac{\partial \mathbf{v}}{\partial t} + [\nabla \mathbf{V}] \mathbf{v} + [\nabla \mathbf{v}] \mathbf{V} &= -\nabla p + \frac{1}{\text{Re}} \Delta \mathbf{v}, \\ \nabla \bullet \mathbf{v} &= 0, \\ \mathbf{v} \bullet \mathbf{n}|_{r=1} &= 0, \\ \theta \mathbf{v} \bullet \mathbf{t} + (1 - \theta) 2\Gamma \mathbf{D} \mathbf{n} \bullet \mathbf{t}|_{r=1} &= 0, \\ \mathbf{v}|_{t=0} &= \mathbf{v}_0, \end{aligned}$$

where  $\Gamma$  is a parameter describing “strength” of the slip,  $\theta \in (0, 1]$  is a governing parameter that allows to continuously transform the boundary condition from no-slip ( $\theta = 1$ ) to Navier’s slip ( $\theta = \frac{1}{2}$ ),  $\mathbf{D} = \frac{1}{2}(\nabla \mathbf{v} + (\nabla \mathbf{v})^\top)$ ,  $r \in [0, 1]$  is the dimensionless pipe radius, and  $\mathbf{t}$  and  $\mathbf{n}$  are (unit) tangent and normal vector to the boundary. The only difference between this setting and the standard one is in the boundary condition, and in the formula for the (dimensionless) base flow  $\mathbf{V}$  that now contains an additional term due to the slip on boundary—the velocity component in the direction of the pipe’s axis is now  $V^z = (1 - r^2) + 4\frac{1-\theta}{\theta}\Gamma$  instead of  $V^z = (1 - r^2)$ .

Several heuristic arguments based on detailed analysis of spectrum of the Stokes operator are given, and it is concluded that Navier’s slip boundary condition should have a destabilizing effect on the flow. Finally the linear stability problem is solved by numerical means, and quantitative results confirming the heuristic prediction are obtained. It is shown that the destabilization is not strong enough to maintain an unstable disturbance, and that the significant destabilization effects of Navier’s slip boundary condition are restricted to small values of the Reynolds number. As a byproduct we obtain explicit formulas for eigenfunctions of the Stokes operator subject to Navier’s slip boundary condition, and furthermore we derive (by purely analytical means) a sufficient condition on monotone linear stability of the flow.

\*Mathematical Institute, Faculty of Mathematics and Physics, Charles University, Sokolovská 83, Prague 8, 186 75, Czech Republic.

<sup>1</sup>Quian et al., *Phys. Rev. E* **72**, 022501 (2005).

<sup>2</sup>Bucur et al., to appear in *Proc. Edinburgh Math. Soc.*

<sup>3</sup>A. Davey, H. Salwen, *J. Fluid Mech.* **87**, 357 (1994).



### Instabilities in papermaking: a local and global approach

S. J. Rees\*, O. Tammisola†, F. Lundell†, M. P. Juniper\* and D. Söderberg† ‡

A range of confined co-flow viscous jets and wakes are considered, which are characterized by the parameters: shear, confinement and Reynolds number. At certain parameter values the flows are particularly unstable and beat back and forth at a distinct frequency, characteristic of a global mode. The developing base flow is produced by solving the equations of motion and is then analyzed using both local and global instability methods. A global analysis is conducted on the developing flow in order to determine the properties of the global instability. A local analysis is conducted on the base flow at stream-wise intervals in order to determine their local instability properties. Of particular interest is whether the local instability properties of the base flow, in particular the first location of local absolute instability, dictate the properties of this global instability. The focus of this study is to better understand such instabilities with a view to improving the paper production process. In modern papermaking the paper sheet is formed in a continuous process. The initial step is to shape the pulp-fibre suspension into a thin planar liquid jet using a nozzle. The jet from the nozzle impinges between two moving wire mesh conveyors, which trap the fibres while allowing water to drain. The wet web that is formed is then pressed and dried. Instabilities appearing in the jet close to the nozzle have detrimental effects on the process efficiency as well as on the properties of the final product. The stability of the jet can be controlled through modification of nozzle geometry, co-blowing and confinement.

\*Department of Engineering, University of Cambridge, UK.

†Linn FLOW Centre, KTH Mechanics, Sweden.

‡STFI-Packforsk AB, Sweden.

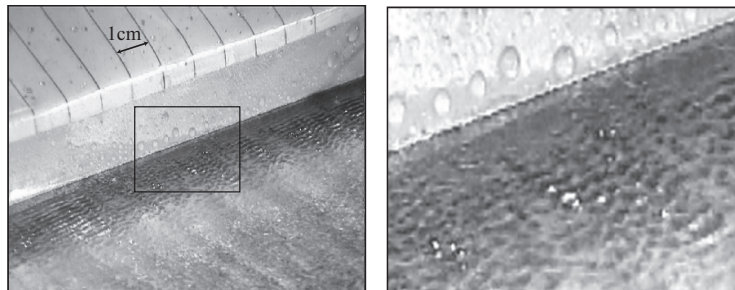


Figure 1: Jet issuing from a paper machine nozzle. Nozzle and jet with a visible centimeter scale (left) and a close-up with visible waves (right).

## Steady streaming in a periodically rotating sphere

Rodolfo Repetto<sup>†\*</sup>, Jennifer Siggers<sup>†</sup> and Alessandro Stocchino<sup>‡</sup>

We consider the motion of a viscous fluid within a spherical cavity subject to periodic rotations. The work is motivated by the motion of the vitreous humour inside the eye. In the case of vitreous liquefaction, a physio-pathological condition affecting large proportion of the elderly population, or after vitreous replacement (vitrectomy), the vitreous chamber may be occupied by a purely viscous fluid. In this case eye rotations produce fluid movement within the eye ball which generates fluid mixing and shear stresses on the retina, both worth attention from the bio-mechanical point of view.

We approach the problem theoretically by assuming eye rotations of small amplitude  $\varepsilon$  and seek a perturbation solution of the Navier-Stokes equations. At leading order ( $\varepsilon$ ) the velocity at each point is periodic in time and velocity vectors lie on planes orthogonal to the axis of rotation. At second order ( $\varepsilon^2$ ) the non-linear terms produce a steady streaming flow on planes containing the axis of rotation. Such a streaming is important from the physiological point of view as it produces fluid mixing over long time scales. An example of the steady streaming flow is reported in figure 1a. The intensity of the streaming is found to be strongly dependent on the Womersley number of the flow,  $\alpha$  (figure 1b).

Theoretical predictions are corroborated by experimental results. We employ an 8 cm diameter sphere, filled with glycerol and set in rotation by a computer controlled motor. P.I.V. measurements of the steady streaming are taken both on the equatorial plane and on a plane containing the axis of rotation. The agreement between theoretical predictions and experimental results is satisfactory, both in terms of streaming intensity (see figure 1b) and velocity profiles.

\*Department of Water, Structures and Soil, University of L'Aquila, Italy. On sabbatical at the Department of Bioengineering, Imperial College of London, UK.

<sup>†</sup>Department of Bioengineering, Imperial College of London, UK.

<sup>‡</sup>Department of Constructions and Environmental Engineering, University of Genoa, Italy.

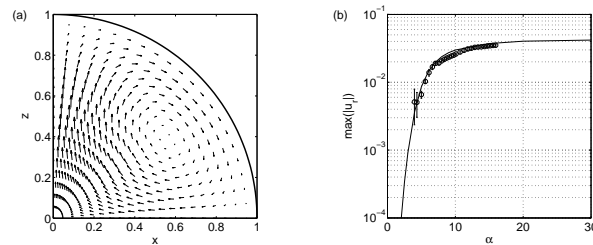


Figure 1: (a) Steady streaming cell. The axis of rotation is at  $x = 0$  ( $\alpha = 5$ ). (b) Comparison between theoretical and experimental results: maximum streaming velocity on the equatorial plane vs the Womersley number of the flow,  $\alpha$ .

## Drag reduction effects in a turbulent channel flow induced by spanwise wall oscillations

Pierre Ricco\*, Maurizio Quadrio<sup>†</sup>

We have conducted direct numerical simulations to investigate a turbulent channel flow with sinusoidal spanwise wall oscillations. The linear relation between the drag reduction and a scaling parameter<sup>1,2</sup>, related to the oscillating Stokes layer acting on the near-wall turbulence, is exploited for gaining insight into the drag reduction characteristics of the flow.

For a fixed maximum wall velocity  $W$ , this parameter is proportional to the maximum streamwise vorticity of the oscillating spanwise layer at a critical distance from the wall between the quasi-streamwise vortices and the low-speed streaks. This finding illustrates the idea that drag reduction is achieved when an efficient shearing motion is imposed onto these coherent structures. The relevance of the Stokes layer on the disruption of the self-sustaining turbulence-producing cycle is thus highlighted.

The difference between the periods of oscillation  $T$  which guarantee the maximum drag reduction for a given maximum wall displacement and for a maximum  $W$  is outlined for the first time. The scaling parameter is used to determine the net energy saving (see figure 1), computed by taking into account the power spent to move the walls, and very good agreement is found with our highly-accurate DNS results. The dependence of the drag reduction on the Reynolds number is investigated and the drag reduction data in the literature are compared with the prediction given by the scaling parameter, thus attaining a comprehensive view of the state of the art.

\*Department of Mechanical Engineering, King's College London.

<sup>†</sup>Dipartimento di Ingegneria Aerospaziale, Politecnico di Milano.

<sup>1</sup>Choi et al., *AIAA J.* **40** (5), 842 (2002).

<sup>2</sup>P. Ricco, M. Quadrio, *J. Fluid Mech.* **521**, 251 (2004).

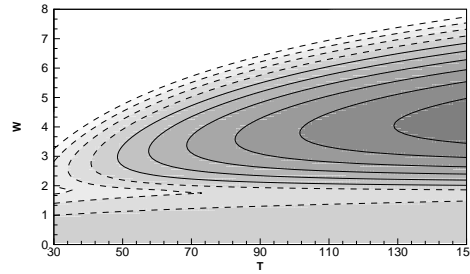


Figure 1: Contours of the percent net energy saving as function of  $W$  and  $T$ , scaled by inner viscous units of the fixed-wall case. Darker colours indicate a higher net energy saving, contour increments are by 1% and dashed lines are for negative values (only values for  $P_{net} \geq -4\%$  are shown).

## Radiative instability of a stratified Lamb-Oseen vortex

Xavier RIEDINGER\*, Stéphane LE DIZÈS\*, Patrice MEUNIER\*

Le Dizès and Billant<sup>1</sup> have shown that a Lamb-Oseen vortex with a strong stratification along the vortex axis is inviscidly unstable. The unstable modes are radiative and extend far from the vortex core. In this work, our objective is to analyse the effects of viscosity and stratification on these unstable modes. A linear temporal stability analysis is performed using a Chebychev collocation spectral code. The equations are the linearized Navier-Stokes equations with Boussinesq approximation. The parameters are the Froude number  $F = \Omega_{max}/N$  and the Reynolds number  $Re = \Gamma/(2\pi\nu)$  with  $\Omega_{max}$  the maximal angular velocity of the vortex,  $N$  the Brunt-Väisälä frequency,  $\Gamma$  the vortex circulation and  $\nu$  the kinematic viscosity.

For fixed  $m$  (azimuthal wavenumber),  $k$  (axial wavenumber),  $F$  and  $Re$  the spectral code provides the complex frequency  $\omega$  of the eigenmodes. By maximising the growth rate  $Im(\omega)$  over the axial wavenumber, we obtain typical growth rate curves of the form illustrated in fig.1(a). This plot shows that the instability is the strongest for a Froude number around one and that the vortex remains unstable for all Reynolds numbers. We shall explain that the stabilization for small Froude number is due to the scaling in  $F$  of the most unstable wavenumber and that the stabilization for large Froude number is linked to the appearance of a critical layer.

For intermediate Froude numbers, another instability mechanism responsible for growth rate oscillations (see figure 1(b)) has been discovered. This new instability which will be explained in detail is due to resonances between radiative modes and Kelvin modes.

\*I.R.P.H.E., Marseille.

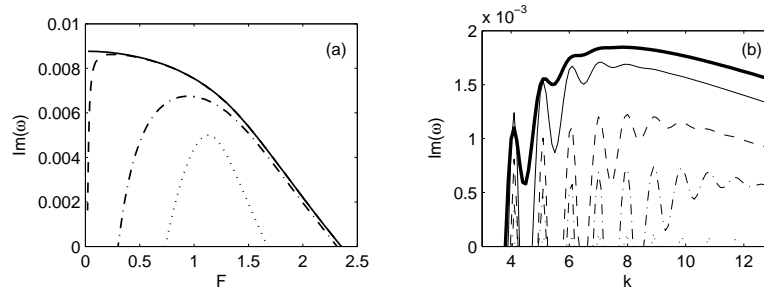
<sup>1</sup>Le Dizès and Billant, *Radiative instability of a stratified vortex*, submitted to *Phys. Rev. Letters*. (2008).

Figure 1: (1) Maximal growth rate versus the Froude number for  $m = 1$ ,  $Re = \infty$  (solid line),  $Re = 10^6$  (dash),  $Re = 3000$  (dash-dot),  $Re = 200$  (dotted). (2) Growth rate versus the axial wavenumber for  $m = 1$ ,  $Re = \infty$ ,  $F = 2.5$  (thick solid line),  $F = 3$  (solid),  $F = 4$  (dash),  $F = 5$  (dash-dot),  $F = 7$  (dotted).

## Stochastic modelling of turbulent reactive flows with particle formation with the species-number density pdf approach

Giovanni Di Veroli<sup>a</sup>, Stelios Rigopoulos<sup>a</sup>

Polydispersed particles (e.g. crystals, droplets) are characterised by a Particle Size Distribution (PSD) which must be predicted by a Population Balance Equation (PBE), essentially an additional transport equation for the particle number density. The presence of turbulence, however, poses important theoretical problems with respect to the coupling of the PBE to fluid dynamics. A transported Probability Density Function (PDF) approach that operates on both reactive species and particle number density is put forward as a solution to the problem<sup>1</sup>.

The high dimensionality of the joint pdf transport equation excludes conventional methods (finite difference/elements). In this work we present a Lagrangian Monte-Carlo method that resolves the PDF field via an ensemble of notional particles. In this context, the evolution of a stochastic particle in physical and phase space is modelled by:

$$d\mathbf{x} = [\mathbf{u} + \nabla \Gamma_{turb}(\mathbf{x}, t)]dt + (2\Gamma_{turb}(\mathbf{x}, t))^{1/2} \cdot d\mathbf{w} \quad (1)$$

$$dY_a = \left[ \frac{C_\phi}{2} \frac{1}{\tau_u} (<Y_a>(t) - Y_a) + \dot{w}(Y_1, Y_2, \dots, Y_m) \right] \cdot dt \quad (2)$$

$$dN_i = \left[ \frac{C_\phi}{2} \frac{1}{\tau_u} (<N_i>(t) - N_i) - G_1(Y_1, Y_2, \dots, Y_m, v_i) \cdot N_i(x, t) + \right. \\ \left. + G_2(Y_1, Y_2, \dots, Y_m, v_i) \cdot N_{i-1}(x, t) \right] dt \quad (3)$$

Here  $Y_a$  are the chemical species, while  $N_i$  are the number densities arising from a discretisation of the continuous PSD carried out prior to the derivation of these equations,  $G_1$  and  $G_2$  are functions arising from this discretisation, while  $d\mathbf{w}$  is the increment of the Wiener process.

The test case consists of  $\text{BaSO}_4$  reactive precipitation in a tubular reactor. The flow field is computed via a standard RANS turbulence model ( $k-\epsilon$ ). Monte Carlo simulations are then carried out to simulate the evolution of the pdf comparisons are made with results from the literature<sup>2,3</sup>. The method allows us to obtain an extensive range of results, including the full PSD, not obtained with moment methods.

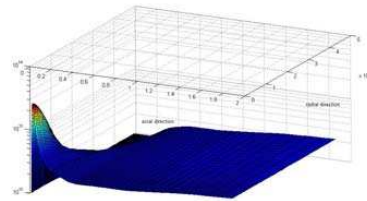


Figure 1: 0th moment field

<sup>a</sup> School of MACE, University of Manchester.

<sup>1</sup> Rigopoulos, Chem. Eng. Sci. **62**, 6865 (2007)

<sup>2</sup> Marchisio et al., Ind. Eng. Chem. Res. **40**, 5132 (2001)

<sup>3</sup> Baldyga et al., Chem. Eng. Sci. **56** (7), 2435 (2001)

## Modelling of a dense granular flow in centrifugal spreading

F. Rioual\*, Pierre A. Gremaud,<sup>†</sup>

Dense gravity driven granular flows have received a considerable interest recently because of the puzzling problem of their rheology as they are encountered in a wide range of industrial applications as environment (see <sup>1</sup> for a recent review). However in some practical applications, gravity is not the only driving force of the flow. Hence in spreading or coating applications <sup>2,3</sup>, the centrifugal force created by a rotating boundary is able to transport the granular material at a high velocity (see figure 1 below). We are interested here in the permanent dense granular flow along the rotating boundary. Using a Discrete Element Method (DEM) and some preliminary experimental data, we present some physical properties for the flow along the rotating vane as a function of the friction properties at the boundary.

Following the analysis of Savage and Hutter <sup>4</sup>, the Saint-Venant equations have been introduced successfully in the context of the modelling of dense granular flows. We present here a depth averaged hydrodynamic modelling for the flow considering a constant solid friction at the basis. We discuss the possibility for this kind of approach to capture the main characteristics of the flow.

\*Cemagref, Clermont-Ferrand

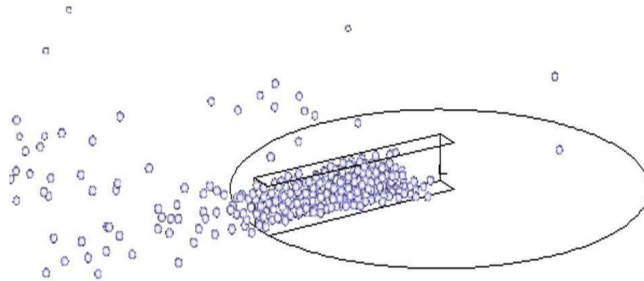
<sup>†</sup>Dept. of Mathematics, North Carolina Southern University<sup>1</sup>O. Pouliquen et al, *Ann. Rev. of Fluid Mech.* (2008)<sup>2</sup>F. Rioual et al, *Appl. Phys. Lett.* **389**, 169 (2007)<sup>3</sup>A. Le Quiniou et al, to be published in *Europhysics Lett.*, (2008)<sup>4</sup>Hutter and Savage, *J. Fluid Mech.* **389**, 169 (1990).

Figure 1: Example of a dense flow in centrifugal spreading

## Wake attenuation in large Reynolds number dispersed two-phase flows

F. Risso\*, V. Roig\*, Z. Amoura\*, G. Riboux\* and A.-M. Billet†

The dynamics of high-Reynolds number dispersed two-phase flow strongly depends on the wakes generated behind the moving bodies that constitute the dispersed phase. The length of these wakes are considerably reduced compared to those developing behind isolated bodies. In this paper, this wake attenuation is studied from several complementary experimental investigations with the aim of determining how it depends on the body Reynolds number and the volume fraction  $\alpha$ . It is first shown that the wakes inside a homogeneous swarm of rising bubbles decay exponentially with a characteristic length that scales as the ratio of the bubble diameter  $d$  to the drag coefficient  $C_d$ , and surprisingly does not depend on  $\alpha$  for  $10^{-2} \leq \alpha \leq 10^{-1}$ . The wake attenuation in a fixed array of spheres randomly distributed in space ( $\alpha = 2 \times 10^{-2}$ ) is observed to differ radically from the wake of an isolated sphere in a turbulent incident flow (fig. 1), but follows the same trend as in the bubble swarm. It thus appears that the wakes in dispersed two-phase flows are controlled by multi-body interactions, which cause a much faster decay than turbulent fluctuations having the same energy and integral length scale. A decomposition of the velocity fluctuations into a contribution related to temporal variations and a contribution associated to the random character of the body positions is proposed as a perspective for studying the mechanisms responsible of multi-body interactions.

\*Institut de Mécanique des Fluides de Toulouse, UMR 5502 CNRS-INP-UPS.

†Laboratoire de Génie Chimique, UMR 5503 CNRS-INP-UPS.

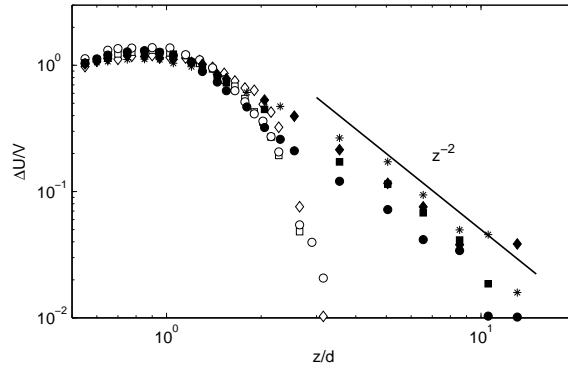


Figure 1: Velocity defect against the distance from a sphere in either an incident turbulence ( $Re = *$  110,  $\diamond$  230,  $\blacksquare$  670,  $\bullet$  1090) or in a random array of spheres ( $Re = \diamond$  235,  $\square$  700,  $\circ$  1120).

## Experimental Characterization of the Separated Flow over a Cylindrical Cavity

F. Rodriguez Verdugo<sup>a</sup>, R. Camussi<sup>a</sup>, E. Mariani<sup>a</sup>, A. Di Marco<sup>a</sup> and P. Yao<sup>a</sup>

The scope of this investigation is to characterize the flow over a cylindrical cavity. Even if this subject has many aeronautical applications, e.g. landing gear wells, few works have followed this direction.

Tests were carried out in the closed-circuit low-speed wind tunnel of the Aerodynamics laboratory of the DIMI (Industrial and Mechanical Engineering Department of the university "Roma TRE") and ENEA (Italian Agency for New Technology, Energy and Environment) cooperation. The studied cavity of radius 105mm and depth 285mm was realized in Plexiglas in order to allow optical measurements inside the cavity. The experimental set-up is shown in figure 1.

Hotwire measurements have been done in order to characterize the turbulent boundary layer of the approaching flow and to obtain the velocity profiles in 16 positions above the cavity and in the wake. Two measurement campaigns have been carried out, for two different free stream velocity magnitudes (20 and 40 m/s). The resulting mean flow field is asymmetric in spanwise direction as reported in Dybenko et al.<sup>1</sup> and Hiwara et al.<sup>2</sup>. The power spectra analysis shows the presence of coherent structures near the cavity trailing edge at  $St \approx 0.8$  for both velocities.

Further Laser Doppler Anemometry (LDA) and acoustic measurements are planned. The fluctuating pressure will be acquired by 22 flush-mounted microphones installed on the cavity surface: 12 on the side wall and 10 on the cavity base. The cavity will be rotated to measure the pressure in 10 angular positions (each  $10^\circ$  step between  $0^\circ$  and  $90^\circ$ ). The two components LDA system will be synchronised with the acoustic measurements in order to correlate the noise and the fluid dynamics.

<sup>a</sup> DIMI: Industrial and Mechanical Engineering Department of the University 'Roma Tre', Rome.

<sup>1</sup> Dybenko et al., *Canadian Society of Mechanical Engineering Forum*, Kananaskis, Canada 21-24 May (2006)

<sup>2</sup> Hiwara et al., *Bulletin of the JSME* **26**, 1744 (1983).



Figure 1: Experimental set-up.



### Self-excited oscillations in a buoyant confined bubbly shear layer

Roig Véronique<sup>a</sup>, Larue de Tournemine Amaury <sup>a</sup>

We have performed experiments on the dynamics of ascendant bubbly shear layers developing in a vertical channel from a non uniform injection of gas volume fraction at the inlet (figure 1). Depending on the inlet conditions (velocities  $U_{10}$ ,  $U_{20}$ ; void fraction  $\alpha_{20}$ ) a great variety of 2D flows may be observed. From the analysis of the time evolution of the frontier between the bubbly side of the flow and the single-phase side, we have classified the flows as having unstable (fig. 1-a) or stable (fig. 1-b) frontier. The development of the flows depends on the non-dimensional numbers  $\lambda_0 = \Delta U_0 / 2U_{m0}$ ,  $Fr_0^2 = (U_{10}^2 + U_{20}^2) / (\alpha_{20} g b)$  and on the  $sign(U_{20} - U_{10})$  where  $\Delta U_0 = |U_{10} - U_{20}|$ ,  $U_{m0} = (U_{10} + U_{20})/2$ ,  $g$  and  $b$  are the gravity acceleration and the half width of the channel. Due to the buoyancy-induced acceleration of the mean flow, a counter-current flow may appear in this system of finite length for specific inlet conditions. This explains the transition between usual convective instability (CI) of the shear layer and self-excited oscillations associated to absolute instability (AI)<sup>1,2,3</sup>.

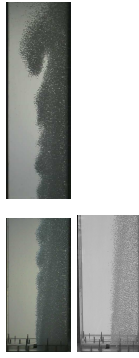


Figure 1 : Flow visualizations  
(a) run 4 (b) run 14

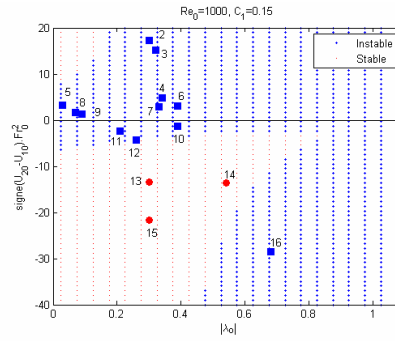


Figure 2: Map of CI (red o) and AI (blue □) regimes

#### References

- Huerre P., Monkewitz A., J. Fluid Mech., vol. 159, 1985.
- Monkewitz P. A., Bechert D. W., Barsikow B., Lehmann B, J. Fluid Mech., vol. 213., 1990.
- Strykowski P.J., Niccum D.L., J. Fluid Mech., vol. 227, 1991

<sup>a</sup> Institut de Mécanique des Fluides de Toulouse, av. Prof. C. Soula, 31400, Toulouse.

## Parametrically forced patterns and quasipatterns

Alastair Rucklidge<sup>\*</sup>, Mary Silber<sup>†</sup>

The classic Faraday wave experiment consists of a horizontal layer of fluid that spontaneously develops a pattern of standing waves on its surface as it is driven by vertical oscillation with amplitude exceeding a critical value. Faraday wave experiments have consistently produced patterns with remarkably high degrees of symmetry. Quasipatterns, which are quasiperiodic in any spatial direction, are particularly interesting since there is, as yet, no satisfactory theoretical understanding of their formation. We use multi-frequency parametric forcing to investigate the formation of patterns and approximate quasipatterns in a model partial differential equation, which plays the same role for the Faraday wave experiment that the Swift–Hohenberg equation plays for convection. We exploit three-wave resonant interactions to design forcing functions that ought to produce complex patterns, and make quantitative comparisons between weakly nonlinear predictions and the solutions of the PDE. This comparison reveals the limitations of the theory, and we explore ways in which these limitations can be addressed.

---

<sup>\*</sup>School of Mathematics, University of Leeds.

<sup>†</sup>Engineering Sciences and Applied Mathematics, Northwestern University, USA.

## Velocity profile influence on spiral vortex breakdown in diffuser

P. Rudolf<sup>a</sup>

Flow in diffuser with circumferential velocity component is accompanied by spiral vortex breakdown for large diffuser divergence angles. This phenomenon, although being investigated for almost fifty years<sup>1,2</sup>, is not fully understood yet. Study of this problem is essential for example for design of hydraulic turbine draft tubes operating in part load conditions, where vortex breakdown causes severe pressure pulsations.

It is well known that tangential velocity profile plays important role in origin and character of the vortex breakdown<sup>3</sup>. Aim of this paper is to find influence of tangential velocity profile on spiral vortex breakdown, not only in terms of swirl number, but also in terms of velocity profile shape.

Experiment was carried out for diffuser divergence angle 11.6 degrees. Inlet circumferential velocity profile was provided by swirl generator with fixed blades. Velocity field was measured with LDA and pressure was recorded on the diffuser walls to obtain frequency spectra of the vortex rotation. This set of data was used for the initial verification of the computation. Analysis of the vortex breakdown for different inlet velocity profiles was carried out numerically with finite volume method. The results point to relationship between vortex breakdown characteristics (rotational frequency, helix slope, pressure decrease within the vortex) and inlet velocity field. The results are also correlated with other quantities like vorticity and helicity.

This outcome is not only important for deeper insight into vortex breakdown phenomenon, but also brings important knowledge for the turbine design.

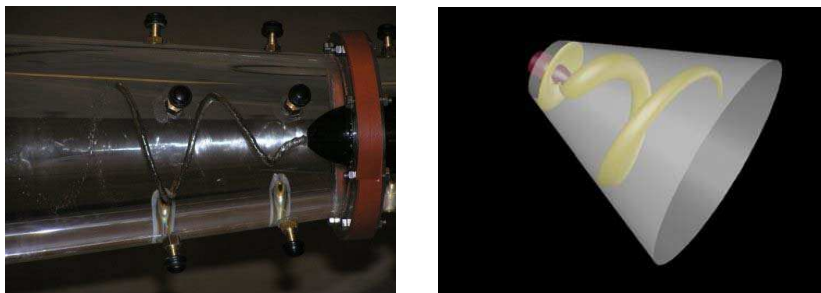


Figure 1: Spiral vortex breakdown in diffuser visualized by (a) cavitation in experiment (b) pressure contour in computation.

---

<sup>a</sup> Brno University of Technology, Faculty of Mechanical Engineering, Czech Republic

<sup>1</sup> T.B. Benjamin, *J. Fluid Mech.* **14**, 593 (1962).

<sup>2</sup> S. Leibovich, *Ann. Rev. Fluid Mech.* **10**, 221 (1978).

<sup>3</sup> O. Lucca-Negro and T. O'Doherty, *Progr. Energ. Combust. Sci.* **27**, 431 (2001).

## Experimental investigation of bubbly two-phase flow in an open capillary channel under microgravity conditions

Abdelkader Salim\*, Catherine Colin†, Michael Dreyer\*

An open capillary channel is used to investigate the wall shear stress as well as the interaction of the bubbles with each other and the free surface in laminar bubbly flow. The channel offers the unique possibility to observe the pressure by observing the curvature of the free surface. The experiment is performed in a compensated gravity environment to avoid any influence of hydrostatic pressure and buoyancy.

An open capillary channel is a configuration in which capillary forces allow a free surface flow and essentially influence the flow structure. The single phase flow in this configuration was investigated by Rosendahl et al.<sup>1</sup>, Haake et al.<sup>2</sup>, and Rosendahl and Dreyer<sup>3</sup>. It was found that for an internal pressure lower than ambient pressure the free liquid surface is bent inwards and concave at any cross section. The pressure decreases in flow direction and the curvature of the free surface increases, thus the flow path constricts. A steady flow is only obtained for a liquid flow rate below a critical value. For that case the differential pressure is compensated by the capillary pressure of the free surface. Beyond the critical flow rate, the liquid surface collapses at the channel outlet and the flow transits from steady single-phase flow to unsteady two-phase flow. We want to extend this research to two-phase flows with a low void fraction.

The present work investigates bubbly two-phase flow in open capillary channels under microgravity conditions aboard the sounding rocket TEXUS 45. The channel consists of two parallel plates of distance  $a = 1$  cm, depth  $b = 2.5$  cm and a free surface on one side with length  $l = 8$  cm. The other surface is closed by a solid, thus the geometry is similar to a groove. The bubbles are injected at the inlet nozzle of the capillary channel via 6 capillary tubes of  $100\text{ }\mu\text{m}$  in inner diameter. The diameter was chosen with regard to the required bubbles size, its frequency, and the gas (air at 0.25 to 0.7 ml/s) and liquid flow rates (FC-72 at 5 to 7 ml/s). The void fraction ranges between 0.05 and 0.10.

Similar to the single phase flow in open capillary channels, the free surface curvature is a signature of the differential pressure between the fluid mixture and the ambient pressure, and the pressure along the flow path can be deduced from the free surface curvature. Then, a one-dimensional flow model is developed in which the pressure in the gas liquid mixture is related to the capillary pressure at the free surface. This device allows a very accurate measurement of the wall shear stress in bubbly flow.

\*Center of Applied Space Technology and Microgravity, University of Bremen.

†Institut de Mécanique de Fluides de Toulouse, University of Toulouse.

<sup>1</sup>Rosendahl et al., *J. Fluid Mech.* **518**, 187 (2004).

<sup>2</sup>Haake et al., *Ann. N.Y. Acad. Sci.* **1077**, 443 (2006).

<sup>3</sup>Rosendahl & Dreyer, *Exp. Fluids*. **42**, 683 (2007).

### Flow structures, sediment transport and controls at river bifurcations: a laboratory flume experiment

SD Sandbach<sup>a</sup>, DR Parsons<sup>a</sup>, GM Keevil<sup>a</sup>, JL Best<sup>b</sup>, SN Lane<sup>c</sup>, RE Thomas<sup>a</sup>, and R J Hardy<sup>c</sup>

River bifurcations are key nodes within fluvio-deltaic systems and in braided rivers, the mechanics controlling the flow and sediment partitioning at such sites being the key controls on dynamics of river braiding and distributary systems that have broad implications for river management, engineering and flooding. Recent research has shown that certain geometrical configurations induce instabilities that lead to downstream mid-channel bar formation. However, to date, we have a poor process understanding of flow dynamics within and through channel bifurcations and their downstream distributary channels and we know very little on the flow division process and its overall controls. This paper presents results of a series of experiments from a flume laboratory study that were conducted in a dedicated facility in the Sorby Environmental Flow Dynamics Laboratory at the University of Leeds.

The flume has an equal width, symmetrical 40 degree, channel bifurcation 2.25 metres into the model section, with upstream and downstream channel widths being 0.5 and 0.25 metres respectively. A constant head was produced using a pump providing a constant discharge ( $20 \text{ L s}^{-1}$ ) that provided flow at depths of 0.08 metres throughout the model. A series of experiments were conducted where detailed three-dimensional velocity measurements were obtained at a total of 10 cross sections through the flume model. The water surface slope was controlled by varying the weir heights in each of the bifurcated channels, providing a range of conditions of flow division at the bifurcation. The results indicate that flow division occurs close to the point of bifurcation in all experimental conditions. Results also indicate that the influence of the downstream water elevations are very significant in the flow dynamics; dividing the flow farther upstream than in the equal weir height case and significantly altering the flow structures and shear stresses through this zone. Results also indicate that secondary flows induced at the bifurcation and just upstream that have an opposite sense of helicity at the bifurcation point, moving towards the outer banks at the bed in both distributary channels.

---

<sup>a</sup> University of Leeds, Woodhouse Lane, Leeds, LS29JT, United Kingdom

<sup>b</sup> University of Illinois, Green Street, Urbana, IL 61801, United States

<sup>c</sup> University of Durham, University Road, Durham, D217LE, United Kingdom

## Global stability analysis of base-bleed as a wake control mechanism at supercritical Reynolds numbers

E. Sanmiguel-Rojas\*, A. Sevilla\*, C. Martínez-Bazán\* and M.A. Burgos†

The flow around a slender body with a blunt, trailing edge is unstable in most situations of interest. Usually the flow instabilities are generated within the wake behind the bluff body, which give rise to normal modes with well-defined frequencies that are independent of the ambient noise. Such instabilities produce fluctuating forces on the body, resulting in oscillations in the drag and lift coefficients, and introduce the possibility of resonance mechanisms with the risk they imply. In the present research, we investigate the instability properties of the flow using global stability analysis, based on the Newton-Free-Jacobian method, with the aim at studying the efficiency of base-bleed as a mechanism to control the wake. In particular we will describe the flow instability characteristics as a function of the Reynolds number,  $Re$ , the boundary layer thickness at the trailing edge,  $\theta/D$ , where  $D$  is the diameter of the body, and the bleed coefficient, defined as the bleed-to-freestream velocity ratio  $C_b = u_b/u_\infty$ , when the density of the bleed fluid is the same as that of the ambient fluid. Numerical simulations of the basic flow will be used to describe the dependence of the critical bleed coefficient, for which the recirculating bubble generated behind the body is blown away, on the Reynolds number and  $\theta/D$ ,  $C_b^c(Re, \theta/D)$  (see fig1). In addition a global stability analysis will be performed to determine the sequence of bifurcations taking place in the near field of the wake depending on the values of  $Re$ ,  $\theta/D$ , and  $C_b$ . These results will be compared with those obtained by Sevilla et al.<sup>1</sup> using local stability analysis.

This work has been supported by the Spanish Ministry of Education under project number DPI2005-08654-C04-01. E.S.R. also acknowledges the Ramón y Cajal program.

\*Área de Mecánica de Fluidos. Escuela Politécnica Superior, Universidad de Jaén. Jaén, Spain.

†E.T.S.I. Industriales, Universidad Politécnica de Cartagena. Cartagena, Spain.

<sup>1</sup>A. Sevilla and C. Martínez-Bazán, *Phys. Fluids*, **16**, 3460-3469 (2004).

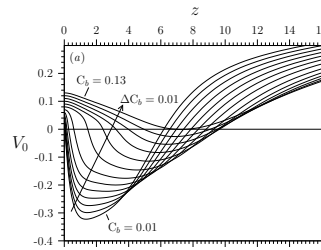


Figure 1: Evolution of the axial velocity along the axis,  $V_0$ , for different values of  $C_b$  at  $Re = 1200$ . The figure shows that, in this particular case, the recirculating bubble disappears for  $C_b = 0.13$ .

## The effect of the surrounding gas velocity on the stability of a plane liquid sheet

A. Sasaki\*, Y. Wakabayashi\*, O. Tammisola† L.D. Söderberg‡  
F. Lundell† and M. Matsubara\*

Instability of a thin liquid sheet, which is related to industrial applications such as atomization, has been studied experimentally and theoretically. This instability is due to aerodynamic interaction of the liquid sheet with its surrounding gas medium<sup>1</sup>. The present study focuses on the effect of the velocity of the surrounding gas. A plane liquid sheet is plunged from a two-dimensional nozzle, and the surrounding gas velocity is changed by blowing air parallel to the liquid sheet. The liquid sheet oscillates with a certain streamwise wavelength and eventually breaks down as it moves downstream. In order to control the disturbance frequency, an initial disturbance is introduced by a loudspeaker. As shown in figure 1, surface oscillation amplitude increases exponentially downstream, if the liquid sheet moves in a stationary gas. When the gas velocity reaches the sheet velocity, the amplitude is extremely small and no collapse is observed yet. For estimation of the growth rate of the disturbance, the surface gradient was measured by detecting the laser reflection on the liquid surface. By measuring the amplitude evolution of the surface gradient in the streamwise direction, it was shown that the growth rate depends on the streamwise wave number of the initial disturbance. The wave number dependence of the growth rate is compared to linear stability calculations including the effect of surface tension<sup>2</sup>. This result will be discussed in connection with the velocity profile of the gas.

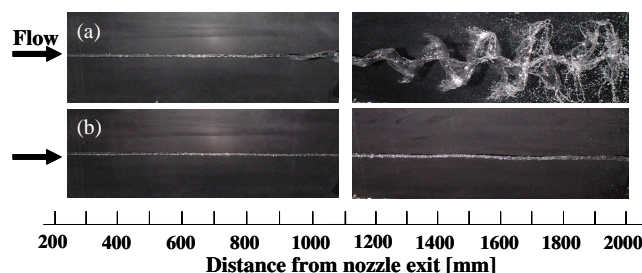


Figure 1: Surface oscillation with different gas velocities. Liquid sheet thickness is 1.2 mm and liquid velocity at the nozzle exit is 6 m/s. The initial disturbance frequency is 40 Hz. The gas velocity at the nozzle exit is (a) 0 m/s (stationary gas), (b) 5 m/s.

\*Shinshu University, Wakasato 4-17-1, Nagano 380-8553, Japan.

†Linné FLOW Centre, KTH Mechanics, SE-10044 Stockholm, Sweden.

‡STFI-Packforsk AB, Box 5604, SE-114 86 Stockholm, Sweden.

<sup>1</sup>Li and Tankin, *J. Fluid Mech.* **226**, 425 (1991).

<sup>2</sup>Söderberg, *J. Fluid Mech.* **493**, 89 (2003).

### 3D Monte Carlo Simulations of Internal Aggregate Structures in a Colloidal Dispersion composed of Rod-like Particles for Application of Large Magneto-rheological Effect

A. Satoh<sup>a</sup>

We have treated a suspension composed of ferromagnetic rod-like particles with a magnetic moment normal to the particle axis in order to investigate aggregation phenomena of such a suspension by means of cluster-moving Monte Carlo simulations. In the present study, we have considered a three-dimensional mono-dispersed model system composed of such rod-like particles. Internal structures of self-assembled clusters have significant influences on rheological properties of such a suspension under circumstances of an applied magnetic field. Hence, these self-assembled clusters have been discussed quantitatively in terms of radial distribution, pair correlation, etc.

Rod-like particles tend to aggregate to form raft-like clusters along the magnetic moment direction more significantly with magnetic particle-particle interactions. In such raft-like clusters, the direction of each particle axis has a tendency to incline in parallel formation, but is not so parallel as in a two-dimensional dispersion. For the case of strong magnetic particle-particle interactions, sufficiently long raft-like clusters are formed along the magnetic field direction, even if the influence of an external magnetic field is of the same order of that of the thermal energy. However, rod-like particles in such clusters do not necessarily incline in significantly parallel formation along a certain direction. Self-assembled tube-like clusters are formed when magnetic particle-particle interactions are much more dominant than the rotational Brownian motion under circumstances of rod-like particles inclining in a certain direction.

a. Faculty of System Science and Technology, Akita Prefectural University, 84-4, Ebinokuchi, Tsuchiya-aza, Yuri-honjo 015-0055, Japan

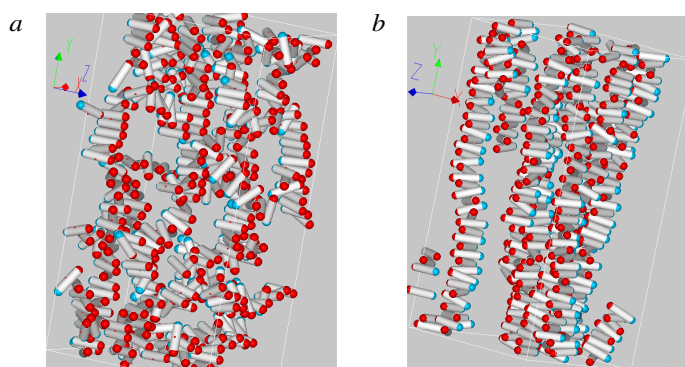


Fig. 1. Aggregate structures of magnetic rod-like particles : (a) for no field and (b) for a strong applied magnetic field.



## Temporal variation of non-ideal plumes with changes in driving-source conditions

M. M. Scase\*, C. P. Caulfield<sup>†‡</sup> and S. B. Dalziel<sup>‡</sup>

The classical bulk models for isolated jets and plumes due to Morton, Taylor & Turner<sup>1</sup> are generalized to allow for time dependence in the various fluxes driving the flow. These new systems model the spatio-temporal evolution of both Boussinesq and non-Boussinesq jets and plumes in unstratified and uniformly stratified fluids<sup>2,3</sup>. Separable time-dependent similarity solutions for plumes and jets have been found. These similarity solutions are characterized by having time-independent plume or jet radii, with appreciably smaller spreading angles than either constant source buoyancy flux pure plumes or constant source momentum flux pure jets. Recent experiments indicate good agreement with these models<sup>4</sup> in the case of a reduction in source strength. In particular we note that established plumes are very robust to reductions in their source strength.

Motivated by the success of the model in predicting reductions in source strength we consider the industrially and environmentally important problem of dramatic increases in source strength. We find strong evidence that the height of the new highly buoyant fluid region increases with  $F^{1/4}t^{3/4}$  where  $F$  is the buoyancy flux and  $t$  is the time. We also consider how our model copes with starting plumes and whether the horizontal entrainment assumption is adequate.

\*School of Civil Engineering, University of Nottingham.

<sup>†</sup>BP Institute, University of Cambridge.

<sup>‡</sup>Department of Applied Mathematics and Theoretical Physics, University of Cambridge.

<sup>1</sup>Morton et al., *Proc. Roy. Soc. Lon. A* **234**, 1–32 (1956).

<sup>2</sup>Scase et al., *J. Fluid Mech.* **563** 443–461.

<sup>3</sup>Scase et al., *J. Fluid Mech.* **563** 463–472.

<sup>4</sup>Scase et al., *J. Fluid Mech.* **600** *In Press*

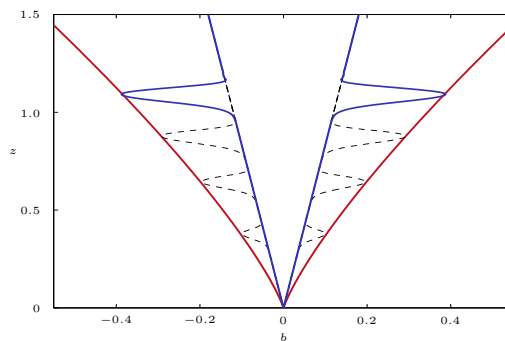


Figure 1: Figure showing the evolution of a pulse rising up an established plume due to a significant increase in the source buoyancy flux. Classical steady plume (blue) pulse envelope (red).

## Structural Rearrangements that govern Flow in Colloidal Glasses

*Peter Schall, University of Amsterdam*

Amorphous colloidal suspensions are known to be powerful models for studying dynamical processes in glasses. The individual colloidal particles – around a micrometer in size - can be tracked in three dimensions and real time with confocal microscopy, which offers a unique microscopic window at glassy structure and dynamics.

We focus on three-dimensional structural rearrangements in a slowly flowing colloidal glass. Several ten thousand particles are followed in time, and their trajectories are used to determine the distribution of local shear strain. We observe shear localization in ‘shear transformation zones’, and we visualize the thermally activated formation of these zones. Correlations in the formation of these zones, mediated through their long-range stress field, result in flow, which is homogeneous on a macroscopic length scale.

## Edge of chaos and the turbulence transition in pipe flow

Tobias M. Schneider\* and Bruno Eckhardt\*

In pipe flow and some other shear flow situations the laminar profile is linearly stable and triggering turbulence requires finite amplitude perturbations. Much insight into the non-linear transition mechanism has recently been gained by applying methods from dynamical systems theory and exploring the systems' state space<sup>1</sup>. Regions of laminar and turbulent dynamics coexist at the same parameter values. They are separated by the *edge of chaos*,<sup>2,3</sup> which extends the concept of basin boundaries to situations with transient turbulence<sup>4</sup>.

Embedded in the *edge of chaos* are locally attracting objects, termed *edge states*. Using a recently developed iterated bracketing technique, we can numerically trace out the dynamics in the edge and reconstruct the edge state in various systems. We will present results for pipe flow, both in a symmetry reduced subspace and in the full space, plane Couette flow and for a low-dimensional model, to illustrate the variety of relative invariant attractors that can occur. Regarding the relation of the dynamically attracting edge state and known exact solutions to the underlying Navier-Stokes equations such as fixed points in plane Couette or travelling waves in pipe flow, we will argue that these states can only act as an edge state provided that they only have a single unstable direction. Only then their stable manifold is a hypersurface of codimension 1 that locally separates state space. Since in unconstrained pipe flow all known exact travelling wave solutions have at least two unstable directions, there are additional unstable directions within the edge giving rise to a chaotic edge state<sup>5</sup> shown in Fig. 1.

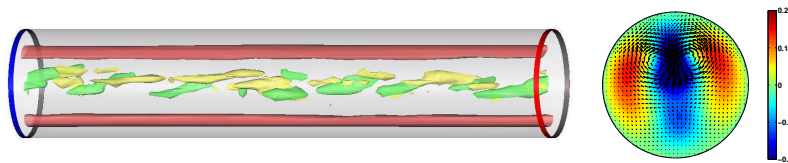


Figure 1: The chaotic edge state flow field in unconstrained pipe flow. Left: Instantaneous snapshot showing the elongated low speed streaks and constantly active vortical structures in the center region. Right: time-averaged flow field characterized by a pair of counter-rotating vortices located off-center.

The significance of the edge states lies in their governing role for the transition to turbulence. Our iterated edge tracing technique allows to numerically construct flow structures in-between laminar and turbulent dynamics. Thus, it should be possible to design turbulence control strategies based on the topology of the edge state.

\*Fachbereich Physik, Philipps-Universität Marburg, Germany.

<sup>1</sup>Eckhardt et al., *Annu. Rev. Fluid Mech.*, **39**, 447–468 (2007).

<sup>2</sup>Skufca et al., *Phys. Rev. Lett.*, **96**, 174101 (2006).

<sup>3</sup>Schneider et al., *Phys. Rev. Lett.*, **99**, 034502 (2007).

<sup>4</sup>Hof et al., *Nature*, **443**, 59–62 (2006).

<sup>5</sup>Schneider and Eckhardt, *Chaos*, **16**, 041103 (2006).

## Measurements of oscillating flow in flexible pipes

S. Große\*, S. Burgmann\*, W. Schröder\*

In most biomechanical flows, e.g., respiratory and vascular flows, the flexibility of the walls is expected to possess significant effects on the evolving flow field.<sup>1</sup> The simplifications in the geometry and structural mechanics of the models that have been used so far showed to only roughly allow the investigation of realistic biomechanical flows. Measurements in a realistic, transparent - but rigid - silicon model of the upper human airways already showed the flow case to be highly complex and three-dimensional and different from the flow cases in more simplified models.<sup>2</sup> As such, for a deeper understanding of the flow in real biomechanical systems, it is necessary to also account for the high degree of flexibility of the walls. Unfortunately, the experimental realization represents an intrinsic task and demands for the adaptation of existing measurement techniques.

As a first step towards a more realistic modeling in terms of fluid-structural interaction (FSI) the flow field of a pulsatile pipe flow with flexible walls is investigated by means of time-resolved PIV.

The pipe is made of an elastic silicone and has an inner diameter of  $D = 24 \text{ mm}$  and a material thickness of  $h = 1.6 \text{ mm}$ .<sup>3</sup> The model has been adapted regarding fluid mechanical and structure mechanical aspects (e.g., longitudinal constraints, vessel compliance/pulse-wave velocity, viscoelastic parameters) to resemble realistic physiological flows. Measurements are performed using a refractive-index adapted PIV system. Furthermore, the dilatation of the flexible wall  $\tilde{\epsilon} = (D - D_{ref})/D_{ref}$  at different Reynolds and Womersley numbers is investigated. Additionally, pressure sensors will be installed to also detect the temporal evolution of the pressure gradient and the local pressure at the measurement position.

First exemplary results are given in figure 1. The temporal developments of the pipe dilatation  $\tilde{\epsilon}$  and the velocity show a phase lag between the two distributions at the chosen Reynolds and Womersley number.

\*RWTH Aachen University

<sup>1</sup>Eguchi et al., *Memoirs Fac. Eng. Kyushu Univ.*, **63**, 161 (2003)

<sup>2</sup>Grosse et al., *Exp. Fluids*, **42(6)**, 955 (2007)

<sup>3</sup>Grosse et al., *submitted to journal*, (2008)

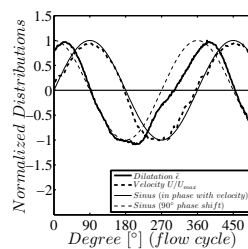


Figure 1: Pipe dilatation  $\tilde{\epsilon}$  and the velocity.

### Periodic states in pipe flow

James R. T. Seddon\* and Tom Mullin\*

The transition to turbulence in pipe flow remains as one of the most intriguing problems in fluid mechanics. Laminar flow is linearly stable, yet turbulence is readily produced at even modest Reynolds numbers. Certain structured features have been detected within turbulent flow, including travelling waves and hairpin vortices. However, the transition to turbulence is generally catastrophic and the underlying physical processes involved remain equivocal.

Here we discuss results of an experimental investigation into the formation of hairpin vortices in transitional pipe flow. The flow is perturbed by a small jet of fluid (0.12% of the pipe mass flux) injected perpendicularly to the flow through a side wall. This creates a family of hairpin vortices which move steadily downstream. We investigate how the critical *amplitude* of perturbation for vortex creation varies with  $Re$ , as well as showing the variation in the number of vortices as a function of perturbation *time*.

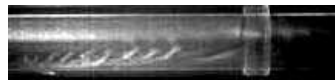


Figure 1: A series of hairpin vortices travelling downstream in transitional flow.

---

\*Manchester Centre for Nonlinear Dynamics, University of Manchester, Oxford Road, Manchester, M13 9PL, UK.

## Lattice Boltzmann simulation of relaminarization from turbulence in channel flow

Daisuke Seki\* and Masato Yoshino†

Numerical simulations of relaminarization from turbulence in channel flow are carried out using the lattice kinetic scheme<sup>1</sup> which is an improved method of the original lattice Boltzmann method.<sup>2</sup> Calculated turbulent energy in the relaminarization shows an exponential decay for  $600 \leq \text{Re} \leq 1500$ , where  $\text{Re}$  is the Reynolds number based on the streamwise velocity at the centerline and the half width of the channel. In these cases, we investigate a half-lifetime of turbulence,  $\tau$ , which is defined as time when the initial turbulent energy is reduced to half. As shown in Figure 1, the inverse of the half-lifetime indicates exponential decrease up to  $\text{Re} \approx 1000$ , and above the value it asymptotically converges to 0 with the Reynolds number. Also, in comparison with the previous studies by Peixinho et al.<sup>3</sup> and by Hof et al.,<sup>4</sup> it is expected that the process of relaminarization from turbulence in channel flow has much similarity to that in pipe flow.

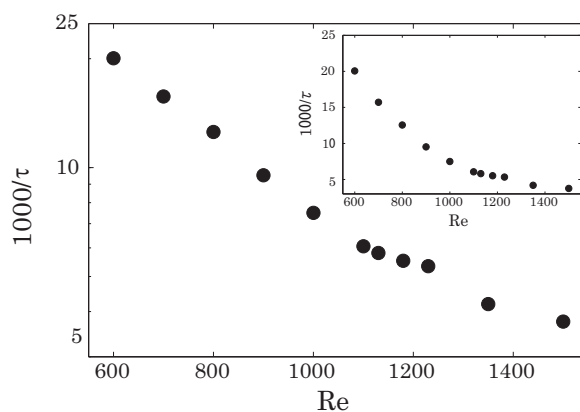


Figure 1: Relation between the inverse of half-lifetime and Reynolds number.

\*Department of Mechanical Systems Engineering, Interdisciplinary Graduate School of Science and Technology, Shinshu University.

†Department of Mechanical Systems Engineering, Shinshu University.

<sup>1</sup>T. Inamuro, *Phil. Trans. R. Soc. Lond. A* **360**, 477 (2002).

<sup>2</sup>S. Chen and G. D. Doolen, *Annu. Rev. Fluid Mech.* **30**, 329 (1998).

<sup>3</sup>J. Peixinho and T. Mullin, *Phys. Rev. Lett.* **96**, 094501(2006).

<sup>4</sup>B. Hof et al., *Nature* **443**, 59 (2006).

## Internal Flow Dynamics of Aneurysms – Validation of Numerical Simulations and Impact of Stent

S. Seshadhri<sup>a</sup>, G. Janiga<sup>a</sup>, R. Bordás<sup>a</sup>, B. Preim<sup>b</sup>,

G. Rose<sup>c</sup>, M. Skalej<sup>d</sup>, D. Thévenin<sup>a</sup>

University of Magdeburg “Otto von Guericke”, Magdeburg (Germany)

The treatment of cerebral aneurysms is a major challenge for neurosurgery and neuro-radiology due to its complexity and to the resulting, high hazard ratio. Future improvements require a better knowledge of unsteady blood flow patterns in complex 3D geometries. Since in vivo measurements are extremely difficult and therefore limited, complementary model-based investigations considering a realistic configuration are essential, as presented in the present work.

In a first step an aortic aneurysm (Fig.1, left) is analyzed, since it involves a simpler geometry and larger vessels. It is thus a perfect prototype on the way towards more complex cerebral aneurysms. The present study relies on quantitative comparisons between simulations and experiments based on an identical, realistic geometry (physical phantom) allowing for a meaningful comparison. The numerical results are obtained with Computational Fluid Dynamics (CFD) relying on the industrial software FLUENT 6.3, using a three-dimensional unstructured grid. The validation experiments rely on in situ, Laser-Doppler Velocimetry (LDV) measurements in a 1:1 inverse silicon model. A complex liquid mixture (composed of water, glycerine, xanthan-gum and sodium thiocyanate) has been specifically developed for the present investigation. It shows physical properties very similar to real blood, but leads to a refraction index perfectly matched to that of the silicon model (Fig. 1, middle). This allows accurate velocity measurements within the model and a direct comparison with CFD (Fig. 1, right) using identical, non-Newtonian fluid properties. Detailed comparisons will be shown at the Conference along with first results concerning flow modifications induced by stents.

- a. Lab. of Fluid Dynamics and Technical Flows  
 b. Visualization Research Group  
 c. Medical Telematics & Medical Engineering Group  
 d. Institute for Neuro-Radiology, Medical Department

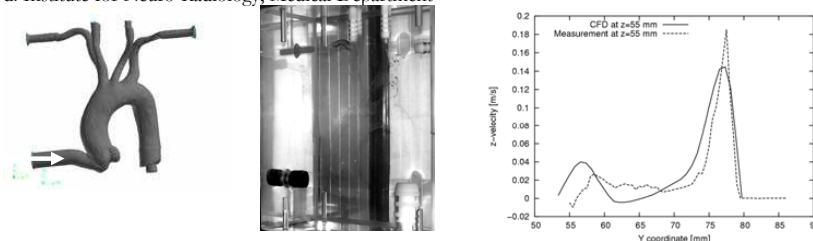


Figure 1: geometry of an aortic artery with aneurysm (left), corresponding inverse silicon model with refraction index matching (middle, barely visible), example of velocity profile comparison between LDV and CFD (right)

## Interaction of a shock wave with multiple gas bubbles in water

Stephen J. Shaw\*, Peter D. M. Spelt\* and Omar K. Matar\*

The propagation of both strong and weak shock waves through water containing a number of compressible gas bubbles is considered numerically. Assuming both the gas and liquid phases are inviscid and compressible, the compressible Euler equations together with suitable equations of state are utilised. In each phase the pertinent equations are solved using a third order Eno-Roe scheme to evaluate spatial derivatives whilst quantities are evolved temporally using a third order TVD Runge-Kutta method<sup>1</sup>. The interface between the two phases is tracked using a level set function. Accurate interfacial boundary conditions are imposed using the Ghost Fluid method together with the isobaric fix technique<sup>1,2</sup>. Our scheme is employed to consider bubble/shock interactions in 2D cartesian, axisymmetric and fully 3D cartesian coordinates.

When the shock front impacts an individual bubble, due to the large acoustic impedance mis-match between water and the gaseous contents of the bubble, most of the shock wave is reflected. For multi-bubble scenarios, resultant interactions between reflected and transmitted shock fronts gives rise to complex pressure and velocity fields between the bubbles. Interactions between rarefactions also give rise to potential regions of secondary cavitation. Under the assumption of uncontaminated water, no such cavitation occurs for the pressures considered. In the presence of contamination, nucleation sites exist, which, we speculate, may give rise to an array of micro-cavities.

In the case of 'weak' shock waves (for example, a strength of 10MPa), no liquid jets thread any of the bubbles, but they do undergo collapse. For stronger strength shock waves (for example, 100MPa), as well as bubble collapse, liquid jets are observed, the direction of which depend on relative bubble orientations, relative bubble sizes and initial shock strengths. A thorough parametric study is conducted for all three geometry types considered, in order to quantify these observations. Comparisons are made with compressible Rayleigh-Plesset type equations to access for what shock strengths significant deviations occur<sup>3</sup>. The temperature fields inside the respective bubbles throughout the shock impact and subsequent interaction processes is also examined.

---

\*Department of Chemical Engineering, Imperial College London

<sup>1</sup>Fedkiw et al. *J. Comp Phys.* **153**, 457 (1999)

<sup>2</sup>Fedkiw et al. *J. Comp Phys.* **148**, 545 (1999)

<sup>3</sup>Watanabe and Prosperetti *J. Fluid Mech.* **274**, 349 (1994)



## Investigations of vortex shedding processes at the end of the parallel-plate stack in the oscillatory flow

Lei SHI<sup>a</sup>, Zhibin YU<sup>a</sup> and Artur J. JAWORSKI<sup>a,\*</sup>

A typical standing-wave thermoacoustic system consists of a thermoacoustic “stack” sandwiched between the cold and hot heat exchangers, the whole assembly located in an appropriately designed acoustic resonator. The role of the stack is to either consume externally supplied acoustic power to facilitate heat pumping from the cold to hot heat exchanger or to generate acoustic power due to the temperature gradient imposed by them. Parallel-plate arrays are used as a basic stack configuration. In high-amplitude standing-wave acoustic field, the flow structures at the end of the stack or the heat exchangers are very complex due to the discontinuities of the cross sectional area and the nature of the oscillating flow. Clearly, the energy transfer taking place within the thermoacoustic stack will be affected by the flow phenomena such as turbulence generation or shedding of coherent vortex structures (the latter usually referred in acoustics language as non-linear acoustics processes).

In the ejection stage of an acoustic cycle (i.e. fluid flowing out of the stack) flow structures analogous to von Karman street are observed. In order to estimate Strouhal number – **St** (here based on the plate thickness and the local velocity amplitude) standard hot-wire anemometry is used to detect velocity fluctuations due to the vortex shedding at the end of stack. The hot-wire signal is analyzed using Fast Fourier Transform (FFT), the vortex shedding frequency obtained from the frequency spectra.

By changing the intensity of acoustic excitation and the stack configuration (plate thickness and plate spacing), the dependence of the vortex shedding **St** number on the Reynolds number (based on the plate thickness) can be carefully studied. The plate thickness used was 0.5, 1, 2, 3, 4 and 5 mm, while the plate spacing varied from about 1 to a 20 mm. It is shown that the obtained **St** numbers tend to fall within two clear ranges. For the stacks with relatively thin plates (0.5 and 1 mm), the resulting **St** numbers range between 0.08 and 0.11. For stacks with thicker plates (2, 3, 4 and 5 mm) **St** numbers tend to fall in the range 0.18 – 0.21. Some explanations of these processes will be provided using phase-locked PIV measurements.

---

<sup>a</sup> School of MACE, University of Manchester, PO BOX 88, Manchester M60 1QD, UK

\* Corresponding author, e-mail: [a.jaworski@manchester.ac.uk](mailto:a.jaworski@manchester.ac.uk); Tel: 01612754352; Fax: 08701307474

## Free-surface singularity in convergent flow: Cusp, corner or an ‘apparent’ phenomenon?

Y.D. Shikhmurzaev\*

As we know from experiments<sup>1</sup>, a sufficiently strong convergent flow near a liquid-gas free surface leads to the formation of what looks like a singularity in the free-surface curvature. Furthermore, the transition from a smooth free-surface profile to this singular structure is accompanied by a qualitative change in the flow’s kinematics — the fluid particles that initially belong to the free surface no longer stay there at all time; instead, they are now being swept through the singularity into the interior<sup>2</sup>. Even a casual glance at the phenomenon raises a number of questions. Can the experiments be explained in the framework of the standard fluid mechanics model, either directly or by incorporating additional physical effects, like the entrainment of the gas into the moving liquid? If not, what is the mechanism of this phenomenon? Is it a ‘one-off’ effect or a particular case from a sufficiently wide class of flows? Irrespective of theoretical arguments, is there an experimental analogue of this phenomenon that could help to investigate it qualitatively?

In this work, we analyze free-surface singularities in convergent flows allowing for the process of interface formation<sup>3</sup>. This approach embeds the standard fluid mechanics model into a more general context and helps to understand when the standard approach is no longer applicable. We show that the interface formation model allows one to make sense of the experimentally observed features of this phenomenon and indicates that (i) the free-surface curvature is indeed singular and (ii) this singularity is a corner, not a cusp. A direct analogy with the so-called hydrodynamic assist of dynamic wetting<sup>4</sup> is discussed.

---

\*School of Mathematics, University of Birmingham.

<sup>1</sup>Joseph *et al.*, *J. Fluid Mech.* **223**, 383 (1991).

<sup>2</sup>Jeong and Moffatt, *J. Fluid Mech.* **241**, 1 (1992).

<sup>3</sup>Y.D. Shikhmurzaev, *Capillary Flows with Forming Interfaces*, Taylor & Francis, 2007.

<sup>4</sup>Blake *et al.*, *Phys. Fluids* **11**, 1995 (1999).

## Measurement of Velocity and Acceleration in Turbulent Jet with a Laser Doppler Velocity Profile Sensor

K. Shirai\*, C. Bayer\*<sup>†</sup>, A. Voigt\*, L. Büttner\* and J. Czarske\*

Jet is one of the fundamental flows in fluid mechanics. Turbulent jet is faced in a number of situations in industry such as for mixing, cooling and propulsion. The main feature of a turbulent jet is described with its wide range of scale distribution in a field without solid boundary. The mechanism of turbulent jets has been extensively investigated with different techniques. Particularly the large scaled structure and the interface of turbulent/non-turbulent regions are studied with non-invasive techniques such as particle image velocimetry (PIV) and laser induced fluorescence (LIF). However, their accuracy of measurement is not as high as one-point technique such as laser Doppler anemometry (LDA). On the other hand, LDA is limited to point-by-point measurement of local flow velocity.

Laser-Doppler velocity-profile sensor has been developed as an extension of LDA for clarifying turbulent phenomena with its high spatial resolution. It utilizes a pair of fan-like fringe systems in a single measurement volume, and both velocity and position of single tracer particles are determined from the measured Doppler frequency pairs. Since it has a spatial resolution inside the measurement volume, it can be considered as a one-dimensional measurement technique which compensates the spatial resolution of LDA and the accuracy of PIV/LIF. We<sup>1</sup> have reported that the resolution of the sensor is in the range of a few micrometers and the relative accuracy of velocity measurement is in the order of  $10^{-3}$ . These values are much higher resolution and accuracy compared with LDA. The feasibility of turbulent flow was reported in the measurements of two-dimensional turbulent channel flow up to fourth order moment<sup>1</sup>. The sensor is currently extended for the measurement of multiple particles at nearly the same time. It is expected to provide further information of turbulence such as instantaneous velocity-gradient and two-point spatial correlation with a single sensor.

In the present study we report on the further development of the sensor and its application to turbulent jet. The sensor was extended to measure the spatial distribution of acceleration as well as velocity. The feasibility of the measurement of local acceleration and tilted trajectory has already been investigated with a velocity profile sensor<sup>2,3</sup>. Turbulent jet faces strong acceleration and deceleration due to the discharge of fluid with high momentum to inviscid still fluid in the surrounding and the entrainment process from the surrounding region. The jet measured in the present study is the one from a smooth contraction nozzle. The fluid is air at a normal room temperature and tracer particles with sub-micrometer size is used to guarantee the tractability to the local fluid acceleration. The velocity profile sensor is applied to investigate the discharge and the entrainment process of turbulent jet by measuring velocity/acceleration field. The measurement is carried out from the self-similar region and detailed investigation will be taken place in the near-field.

\*Chair of Measurement and Test Techniques, Dresden University of Technology

<sup>†</sup>now at Fraunhofer Institute for Photonic Microsystems

<sup>1</sup>Shirai et al. *European J. Mech. -B/Fluids*, in print (2008).

<sup>2</sup>Büttner and Czarske, *J. Opt. Soc. Am. A* **23**, 444 (2006).

<sup>3</sup>Bayer et al., submitted to *Meas. Sci. Technol.*

## High-resolved simulations of turbulent thermal convection in domains with interior boundaries

Olga Shishkina\*, Claus Wagner\*

To simulate turbulent flows in complicated enclosed three-dimensional domains a fast finite-volume high-order method based on the Chorin ansatz was developed. The Poisson solver, which is applied to compute the pressure, uses the capacitance matrix technique<sup>1</sup> together with the separation of variables<sup>2</sup>. The developed numerical method generally allows to use computational meshes, which are non-equidistant in all three directions and non-regular in any two directions. The method was successfully used in the Direct Numerical Simulations of turbulent thermal convection with high Rayleigh numbers ( $Ra$ ) in three-dimensional domains with interior boundaries, which ambient domains can be cubical as well as cylindrical (see figure 1). For these flows turbulent statistics was investigated as well as the local heat fluxes<sup>3</sup> and the thermal plumes<sup>4</sup>.

\*German Aerospace Center (DLR), Institute for Aerodynamics and Flow Technology, Göttingen

<sup>1</sup>U. Schumann, R.A. Sweet, *J. Comput. Phys.* **20**, 171 (1976).

<sup>2</sup>O. Shishkina et al., *J. Comput. Appl. Maths* submitted (2008).

<sup>3</sup>O. Shishkina, C. Wagner, *Phys. Fluids*, **19**, 085107 (2007).

<sup>4</sup>O. Shishkina, C. Wagner, *J. Fluid Mech.* **599**, 383 (2008).

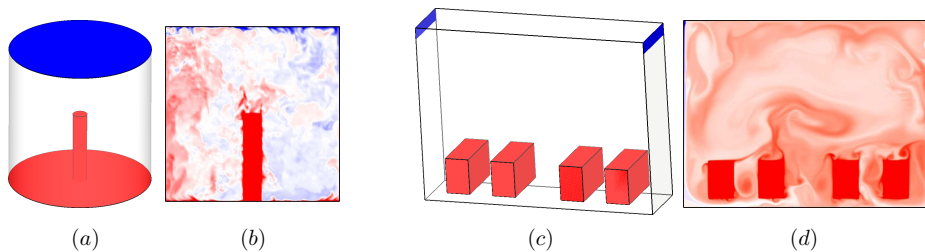


Figure 1: Domains with the temperature boundary conditions (a, c) and the corresponding temperature distributions inside these domains for  $Pr = 0.7$ ,  $Ra = 10^9$  (b) and  $Ra = 2.5 \times 10^9$  (d). Warm (cold) walls and fluid are given in red (blue).

## Reconstruction of the droplet size distribution in flows with single or multi-component condensation

R. Sidin\* and R. Hagmeijer\*

We investigate the evolution of the droplet size distribution in rapidly expanding flows, where homogeneous nucleation and droplet growth are the governing mechanisms. As condensation releases latent heat into the flow, there is potentially a strong two-way coupling between the liquid and vapor phases, so that the population balance equation (PBE) for the droplets needs to be solved simultaneously with the Fluid Dynamic equations (FDE). Use of this exact two-way coupling is computationally very expensive, and is practically not feasible for large scale industrial applications. A viable alternative to this approach has been introduced by Hagmeijer *et al.*<sup>1</sup> in the form of an approximated two-way coupling, where the interaction between the flow dynamics and the condensation process are first approximated by using the Method of Moments (MOM), whereafter the droplet size distribution is reconstructed along fluid trajectories. Previous evaluation of the method for cases of low liquid mass fractions, with droplets consisting of only one chemical component, has shown favorable results<sup>2</sup>. In this presentation we extend our evaluation of this computational method to cases of high liquid mass fractions, and to droplets which consist of multiple chemical components. We show that in the case of multi-component condensation, reformulation of the multi-component PBE is vital in order to devise a numerical scheme to predict the droplet composition distribution. With respect to the influence of the liquid mass fraction, we show that in the case of high liquid loading, the solutions for the flow field and the droplet size distribution are substantially corrupted by the closure error in the MOM (see figure 1) .

\* University of Twente, PO Box 217, 7500AE Enschede, the Netherlands.

<sup>1</sup>R. Hagmeijer *et al.*, *Phys. Fluids* **17**, 056101 (2005).

<sup>2</sup>R. Sidin *et al.*, *ICMF 2007*, S4.Thu.D.61 (2007).

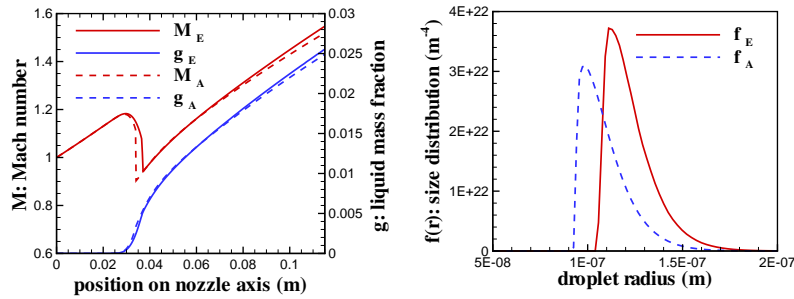


Figure 1: Comparison of numerically obtained flow field solutions (left) and droplet size distributions (right) for a quasi-one-dimensional nozzle flow: index E and A respectively refer to exact and approximate two-way coupling

## Oscillating flow in a deformed sphere: application to motion of the vitreous humour

Jennifer Siggers\*, Rodolfo Repetto†\*

Fluid motion of the vitreous humour (the fluid filling the posterior chamber of the eye) can be driven by saccades of the eyeball. Drugs to be delivered to the retina may be injected into the vitreous humour, and subsequent paths of the drug particles will be affected by the fluid motion. The occurrence of retinal detachments may be promoted by large shear stresses at the retinal surface, caused by fluid motion in the vitreous humour.

We model saccades as sinusoidal oscillations about the superior-inferior axis of the eye, and the vitreous humour as a Newtonian fluid. Assuming the posterior chamber to be a sphere, in the limit of small amplitude oscillations the flow is entirely in the azimuthal direction, but as the amplitude increases a flow correction must be made, the largest contribution of which includes a steady streaming component. This streaming consists of flow from the region near the equator towards the centre of the sphere, then along the axis of oscillation towards the poles, and finally back towards the equator near to the surface. Although it only appears at second order, the streaming dominates the long-time behaviour of the fluid particle paths.

In reality the posterior chamber deviates from a spherical shape predominately due to the presence of the lens. Introducing a small indentation in the sphere gives rise to a correction in the flow field, which is oscillatory at leading order, and includes a circulation structure just behind the indentation. During the period the structure moves towards the centre of the sphere and is annihilated. The next correction to the flow (which arises due to increasing oscillation amplitude) has a steady streaming component, in which there are two counter-rotating circulations. We briefly discuss implications of these results for the pressure and wall shear stress distributions.

\*Department of Bioengineering, Imperial College London.

†Department of Engineering of Structures, Water and Soil, University of L'Aquila, Italy.

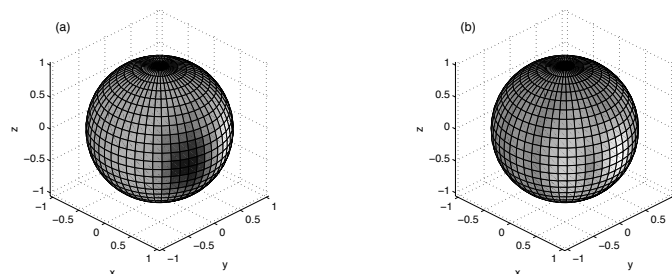


Figure 1: Correction in the (a) pressure and (b) wall shear stress due to non-sphericity. The lens is centred at  $(1, 0, 0)$ .

## Dynamics of two-layer non-isothermal films

A. A. Nepomnyashchy, I. B. Simanovskii

Department of Mathematics, Technion – Israel Institute of Technology,  
32000 Haifa, Israel

In the past few decades, the development of microfluidics and nanotechnology led to a significant progress in the exploration of thin film flows. The dynamics of ultra-thin (but still macroscopic) films, with the thickness less than 100 nm, is of special interest. In the case of ultra-thin films, it is necessary to take into account the long-range intermolecular forces (first of all, van der Waals forces) acting between molecules of the liquid and substrate. These forces can either stabilize the film or create a longwave instability leading to the film rupture through the formation of holes. The wetting properties of the interfaces can be significantly changed by the creation of two-layer films, which reveal much richer dynamics than one-layer films.

In the present work, the evolution of a two-layer film under a joint action of thermocapillary effect and intermolecular forces, is considered. The appearance of the Marangoni oscillations has been predicted by the linear stability theory and confirmed by nonlinear simulations. We have found that for moderate values of the Biot number, heating from below leads to the acceleration of the decomposition, decrease of the characteristic lateral size of structures, and the increase of the droplets heights. Heating from above leads to slowing down the instability rate and eventually to a complete suppression of the instability.

We have observed a nontrivial change of the droplet shape in the presence of the Marangoni effect, which manifests itself as the deformation of a “plateau” into an “inkpot”. It is shown that in a certain region of parameters, under the joint action of van der Waals forces and thermocapillary effect, the nonlinear evolution of the monotonic instability leads to a specific type of nonlinear oscillations.

Decomposition of ultra-thin two-layer films under the joint action of the van der Waals forces and Marangoni stresses in the presence of an inclined temperature gradient, is investigated. Under certain conditions, we have observed also a spontaneous ordering of the system of droplets, secondary instabilities creating “splashes”, as well as different kinds of ordered and disordered wavy motions.

## Dynamics of Flexible Fish Manoeuvres

Kiran Singh \*, Timothy J. Pedley

DAMTP, University of Cambridge  
February 14, 2008

Flexible fish swimming is characterised by a travelling wave passing down the length of the body. Symmetric transverse body undulations generate thrust which propel the fish forward. Turning can be generated by an asymmetric transverse body deflection. Of interest to this work are C-turns, a type of lateral manoeuvre frequently observed in fish that involves a C shaped flexure of the body. Prior work on this topic studied manoeuvres as a coupled inertial-hydrodynamic system [1]. We extended classical forward swimming methods ([2, 3]) to develop the generalised theory to analyse flexible body manoeuvres. The theory was used to validate the three-dimensional discrete vortex numerical methods that were developed to analyse arbitrary fish bodies.

In this work we extend the approach to examine the role of internal body mechanics on flexible body manoeuvres. By the methods developed by Cheng et al [4] we model the body as a beam, consisting of a composite of biological materials, the visco-elastic muscle and skin and the stiff bone. The body structural dynamic model is implemented using Euler beam theory and is coupled to the original inertial-hydrodynamic swimming model. This methodology allows us to compute body bending-moment distribution and the influence of body structural properties on the turn capabilities of fish. The numerical methods also allow us to examine variations in body composition as well as geometry. With these methods we may interpret the effects of body flexibility and compare turn performance between different species. It is thus possible to understand the physiological implications of differences in body structure on swimming and manoeuvring performance.

## References

- [1] K. Singh and T.J. Pedley. The hydrodynamics of flexible body manoeuvres in swimming fish. *Physica D, Special Issue as Proceedings of the Conference EE250*, 2008. Accepted for publication.
- [2] M.J. Lighthill. Note on swimming of slender fish. *Journal of Fluid Mechanics*, 9, Part2:305–317, 1960.
- [3] T.Y.T. Wu. Swimming of a waving plate. *Journal of Fluid Mechanics*, 10:321–344, 1961.
- [4] J.Y. Cheng, T.J. Pedley, and J.D. Altringham. A continuous dynamic beam model for swimming fish. *Philosophical Transactions of Royal Society London B.*, 353:981–997, 1998.

---

\*kiran.singh@damtp.cam.ac.uk



## Experimental and theoretical investigation of sperm motility in viscous and viscoelastic liquids

David J. Smith<sup>\*†§</sup>, Eamonn A. Gaffney<sup>†§‡</sup>, John R. Blake<sup>‡§</sup>  
and Jackson C. Kirkman-Brown<sup>§\*</sup>

Modelling provides insight into the mechanisms by which sperm swim in nearly zero Reynolds number liquids<sup>1</sup> and how internal mechanisms couple with viscous and elastic forces to produce the flagellar waveforms observed experimentally<sup>2345</sup>. Our research builds on previous studies by taking into account: (1) rheological properties of the liquids sperm encounter, such as viscoelastic cervical mucus; (2) detailed characterisation of the movement of the flagellum, including three-dimensionality; and (3) consideration of species-specific physiology, most notably the shape of the sperm head. Human sperm flagellar waves are imaged using high-speed digital video and negative phase contrast microscopy. The shape and movement of the flagellum is then captured using an image analysis algorithm. The force densities, bending moments and instantaneous power of beating are calculated using a recent implementation of slender body theory<sup>6</sup> combined with the boundary integral method to represent the physiological sperm head<sup>7</sup>. We also generalise slender body theory to take account of linear viscoelasticity, and discuss the use of the FEM for more general rheology. Finally we discuss the effect of increased liquid viscoelasticity on the waveform, forces and moments, and also the surface accumulation and migration behaviour of human sperm, which may be important in understanding in vivo fertilisation.

<sup>\*</sup>Reproductive and Child Health, Medical School, University of Birmingham, Edgbaston, Birmingham, B15 2TT, UK

<sup>†</sup>Mathematical Institute, University of Oxford, 24-29 St. Giles', Oxford, OX1 3LB, UK

<sup>‡</sup>School of Mathematics, University of Birmingham, Edgbaston, Birmingham, B15 2TT, UK

<sup>§</sup>Centre for Human Reproductive Science, Birmingham Women's Health Care NHS Trust, Edgbaston, Birmingham B15 2TG, UK

<sup>1</sup>Gray & Hancock, *J. Exp. Biol.* **32**, 802 (1955)

<sup>2</sup>Dillon et al. *Ann. N. Y. Acad. Sci.* **1101** 494 (2007)

<sup>3</sup>Brokaw *Cell Motil. Cytoskel.* **53** 101 (2002)

<sup>4</sup>Lindemann *Ann. N. Y. Acad. Sci.* **1101** 477 (2007)

<sup>5</sup>Gueron & Levit-Gurevich *Proc. R. Soc. Lond.* **268** 599 (2001)

<sup>6</sup>Smith et al. *Bull. Math. Biol.* **69**, 1477 (2007)

<sup>7</sup>Pozrikidis *A practical guide to boundary-element methods with the software library BEMLIB* Chapman & Hall (2002)

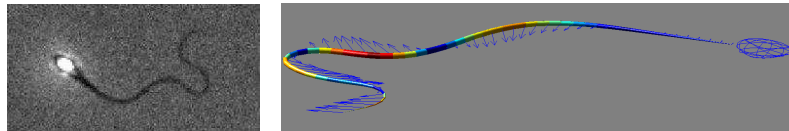


Figure 1: Left—imaging data of a human sperm in viscoelastic liquid. Right—force and bending moment analysis of the same cell.

## Direct Numerical Simulation of Turbulent Heat Transfer Modulation in Micro-Dispersed Channel Flow

Alfredo Soldati<sup>\*</sup>, Francesco Zonta<sup>\*</sup> and Cristian Marchioli<sup>\*</sup>

Heat transfer enhancement is a fascinating subject with extremely interesting possibilities for application. One option to increase heat transfer is to devise a new concept of heat transfer media constituted by a base fluid in which suitably-chosen heat transfer agents, precisely micro and nano particles, are injected. In this way, the fluid can be a standard fluid characterized by simplicity of use and well-known properties, like water, and the heat transfer agents can be heavy-metal, high-heat-capacity, dispersed particles (e.g. copper, gold or platinum).

Current literature trends show the potentials of such heat transfer media, called nanofluids; yet the complicacy and the cost of experimental methods make it hard to understand the intricacy of the mechanisms which govern the dynamics of the turbulent heat transfer among the fluid and the particles. Current open questions range from the optimal size of the particles, to the optimal concentration and practical solutions in real applications. Further complicating effects are represented by the particle inertia and the particle thermal inertia, which are additional parameters.

The present study represents a first effort made in the frame a broader project on the numerical simulation of heat transfer in nanofluids. Our strategic object is to investigate the heat transfer mechanisms in nanofluids and to devise a suitable numerical methodology to analyse their behavior. In this paper, preliminary results obtained from DNS of two-phase gas-solid and liquid-solid turbulent flow in a channel with heat transfer are presented. Hydrodynamically fully-developed, thermally-developing flow conditions have been considered to investigate on heat transfer modulation produced by the dispersion of micrometer sized particles. One value of the shear Reynolds number,  $Re^* = 150$ , and two values of the Prandtl number,  $Pr = 0.71$  and  $Pr = 3$ , have been considered. Two different sets of particles are considered, which are characterized by dimensionless inertia response times equal to  $St = 1.56$  and  $St = 6.24$  and by dimensionless thermal response times equal to  $St_T = 0.5$  and  $St_T = 2$ , respectively.

The instantaneous features of the velocity field, the temperature field and particles dispersion are discussed from a qualitative mechanistic viewpoint to analyse the role of particles as heat transfer enhancement agents. Preliminary results on velocity and temperature statistics for both phases show that, with respect to single-phase flow, heat transfer fluxes at the walls increase by roughly 2% when the flow is laden with the smaller particles ( $St = 1.56$ ), which exhibit a rather persistent stability against non-homogeneous distribution and near-wall concentration. An opposite trend (slight heat transfer flux decrease) is observed when the larger particles ( $St = 6.24$ ) are dispersed into the flow. These results are consistent with previous experimental findings and are discussed in the frame of the current research activities in the field.

---

<sup>\*</sup>Dipartimento di Energetica e Macchine, University of Udine.

## Rarefaction Effects in Micronozzles

Pier Giorgio SPAZZINI\*, Renzo ARINA†

The objective of the present work is to discuss some peculiarities of internal rarefied flows. The problem is becoming of interest within the framework of micropropulsion as the requirements for low thrust, fine-tunable propulsors evolve towards more stringent standards. Several kinds of propulsors may be affected by rarefaction effects in the exhaust pipe; the most important problems are expected to appear within cold-thrusters, i.e. propulsors based on fluid dynamical phenomena connected to gas expansion<sup>1</sup>.

The usual nozzle theory states that the specific impulse provided by a nozzle should depend only on the thermodynamical conditions at the nozzle entrance and exit. Recently, experimental observations showed a reduction of nozzle specific impulse when the mass flow rate through the nozzle is very small<sup>2</sup>. This fact has technological relevance as it implies a decay of the effectiveness of low-thrust propulsors.

A simple test nozzle has been numerically analyzed, with the direct simulation Monte Carlo method (DSMC)<sup>3</sup> in order to clarify some of the phenomena taking place within the rarefied internal flow. The performance of the nozzle has been analyzed as a function of gas density, and the specific impulse reduction was confirmed (Fig. 1). The computational data clearly display the physical origin of the performance loss. It has been observed that, while the translational temperature evolves throughout the nozzle (Fig. 2), the rotational temperature tends to be frozen at values that increase as the rarefaction increases, until for the lower densities, it is locked to the value at the throat. This freezing locks part of the gas energy which is therefore no more available to be converted in kinetic energy.

\*INRIM Fluid Dynamics Unit, C/o DIASP, Politecnico di Torino, C.so Duca degli Abruzzi 24 - 10129 TORINO (Italy).

†DIASP, Politecnico di Torino, C.so Duca degli Abruzzi 24 - 10129 TORINO (Italy).

<sup>1</sup>R.Shyne, *NASA TM 2002-211977*, (2002)

<sup>2</sup>R.Bayt and K.Breuer, *AIAA-2001-0721*, (2001)

<sup>3</sup>G. Bird, *Molecular Gas Dynamics and the Direct Simulation of Gas Flows*, Clarendon Press., (1994).

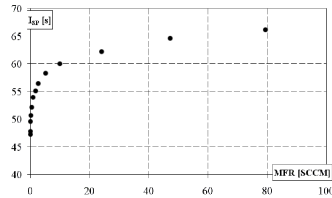


Figure 1: Specific impulse from a micronozzle as a function of mass flow rate (thermodynamic conditions upstream and downstream held constant).

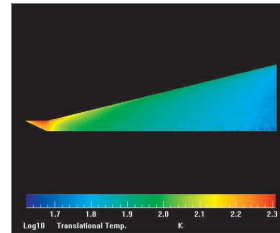


Figure 2: Translational temperature map within a micronozzle, mass flow rate  $\approx 1$  SCCM.

## Fluid and scalar transport: a unified Lagrangian approach

M.F.M. Speetjens\*

The advective transport of fluid by a flow field  $\mathbf{u}$  is in the Lagrangian representation described by the position  $\mathbf{x}(t)$  and density  $\rho(\mathbf{x}(t), t)$  of fluid parcels, governed by  $\dot{\mathbf{x}} = \mathbf{u}(\mathbf{x}, t)$  and  $\partial\rho/\partial t + \nabla \cdot (\rho\mathbf{u}) = 0$ . The advective-diffusive transport of a scalar  $\phi$  is in Eulerian representation governed by  $\partial\phi/\partial t + \nabla \cdot (\phi\mathbf{u} + \mathbf{q}) = 0$ , with  $\mathbf{q} = -\alpha\nabla\phi$  the diffusive flux and  $\alpha$  the diffusion coefficient. Reformulation into the “continuity equation”  $\partial\phi/\partial t + \nabla \cdot (\phi\mathbf{u}_\phi) = 0$ , with  $\mathbf{u}_\phi = \mathbf{u} - \alpha\nabla(\ln\phi)$  the *total* scalar flux, gives a form mathematically equivalent to the continuity equation for fluid transport. Thus scalar transport fundamentally is the transport of “parcels” with “density”  $\phi$  by the *total* advective-diffusive scalar flux  $\mathbf{u}_\phi$  in an analogous way as fluid motion is the transport of fluid parcels by the flow  $\mathbf{u}$ . This analogy naturally leads to

$$\frac{d\mathbf{x}}{dt} = \mathbf{v}(\mathbf{x}, t), \quad \frac{\partial\theta}{\partial t} + \nabla \cdot (\theta\mathbf{v}) = 0, \quad \mathbf{v} = \mathbf{u} - \alpha\nabla(\ln\theta), \quad (1)$$

as unified Lagrangian transport formalism (ULTF) for fluid and scalar transport, with  $\mathbf{x}$  and  $\theta$  the position and “density” of a parcel released in the flux field  $\mathbf{v}$ .<sup>1</sup>

The ULTF is demonstrated for the fluid and heat transfer within a 2D channel confined by a hot bottom and cold top wall. (Here  $(\theta, \alpha) = (\rho, 0)$  and  $(\theta, \alpha) = (T, Pe^{-1})$  for fluid and heat transport, respectively, with  $T$  temperature and  $Pe$  the Péclet number.) The flow is set up by two counter-rotating point vortices<sup>2</sup> that may oscillate horizontally with an amplitude  $\epsilon$ . Vanishing  $\epsilon$  implies steady conditions and, consequently, a stream function for both fluid and heat transport.<sup>1</sup> Figure 1 (left) shows the (fluid) streamline portrait, consisting of two adjacent islands (one per vortex) that entrap and circulate fluid. Figure 1 (right) shows the “thermal streamline portrait” for a given  $Pe$ , consisting of two islands separated by channels connecting the bounding walls. The islands, phenomenologically similar as before, entrap heat and thus form thermally-isolated regions; the channels constitute the thermal path that facilitates wall-wall/wall-fluid heat exchange. Non-zero  $\epsilon$  implies unsteady conditions and effectuates progressive disintegration of the coherent structures in Figure 1 in favour of chaotic regions. This breakdown of Lagrangian structures in the transport topologies is the universal mechanism that underlies both chaotic fluid and heat transport.<sup>1</sup>

\*Energy Technology Laboratory, Eindhoven University of Technology, The Netherlands.

<sup>1</sup>M.F.M. Speetjens, *Phys. Rev. E* **77** (2008) (in press).

<sup>2</sup>V. V. Meleshko, *Phys. Fluids*, **6**, 6 (1994).

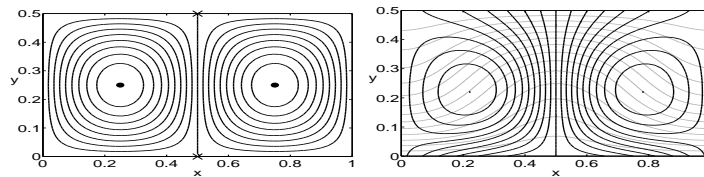


Figure 1: Fluid streamline portrait (left) and thermal streamline portrait (right). Gray curves in right panel correspond with isotherms.

## Spherically converging and diverging shock waves in collapsing bubbles

Peter D. M. Spelt\*, Stephen J. Shaw and Omar K. Matar

The numerical simulations of Moss *et al.*<sup>1, 2</sup> of the flow inside a collapsing bubble clearly indicate the formation of a shock wave that propagates radially inwards. Moss *et al.*<sup>2</sup> predict that the shock reaches the bubble centre, from which it is subsequently reflected, forming a diverging, i.e., radially outward propagating, shock wave. Their simulations also indicate the bubble reaches minimum volume around this time. Moss *et al.*<sup>1,2</sup> merely presented some sample results, specifically chosen with sonoluminescence in mind. In the present work, our aim is to determine the extremity of the conditions inside collapsing bubbles, as well as providing a detailed study of the shock propagation behaviour. We employ a recently developed shock-capturing two-fluid compressible solver for this purpose<sup>3</sup>. The numerical method employs the method of lines, the spatial fluxes being calculated by first projecting along respective characteristics and then using a third-order ENO-Roe scheme, whilst a third-order TVD RK method is employed for the temporal fluxes. The two fluids are coupled using a ghost-fluid method. Results of 3D and spherically symmetric systems will be presented.

A first issue specifically investigated here is to determine the conditions for which a self-similar regime may be observed. Such self-similar solutions for the conditions behind converging shocks can be found in e.g. Landau & Lifschitz<sup>4</sup>. Earlier numerical work by Van Dyke & Guttman<sup>5</sup> used an expansion of the global solution in powers of time for the case of a spherical piston that moves radially inward at constant velocity. This approach was successful in even locating the shock close to the instance of collapse. However, the system studied by Van Dyke & Guttman is possibly not directly applicable to collapsing bubbles, as the bubble radius does not converge linearly with time. Also, the physical conditions during the collapse were not studied.

Results will be presented for the temperature values generated at the bubble centre, and the conditions under which plasma might be formed will be discussed (see Flannigan & Suslick<sup>6</sup>).

---

\*Department of Chemical Engineering, Imperial College London

<sup>1</sup>Moss *et al.*, *Phys. Fluids* **6**, 2979 (1994)

<sup>2</sup>Moss *et al.*, *Phys. Rev. E* **59**, 2986 (1999)

<sup>3</sup>Shaw *et al.*, in preparation (2008)

<sup>4</sup>Landau and Lifshitz, *Fluid Mechanics* (1987)

<sup>5</sup>Van Dyke and Guttman *J. Fluid Mech.* **120**, 451 (1982)

<sup>6</sup>Flannigan and Suslick, *Nature* **434**, 4.4.2005, 52 (2005)

## Some aspects of drops impacting on solid surfaces

J.E. Sprittles\*, Y.D. Shikhmurzaev\*

The impact and spreading of liquid drops on solid surfaces is the key element of many industrial processes. Examples include ink-jet printing of images, spray cooling of surfaces, crop spraying and spray coating<sup>1</sup>. An exciting new area of research is the ink-jet printing of electronic circuits<sup>2</sup> which provides a cheap alternative to traditional fabrication methods. Despite the widespread industrial interest in the phenomena of drop impact and spreading, and a huge body of experimental results, existing theoretical approaches fail to account for experimental results<sup>3</sup>.

The spreading of liquid drops falls into a class of flows in which a liquid-gas interface moves across a solid surface. In such circumstances it is well known that classical fluid mechanics fails to provide a solution<sup>4</sup>. The standard remedy to this problem, offered by the so-called ‘slip models’, is (i) to relax the no-slip condition near the liquid-gas-solid contact line, and (ii) specify the angle formed between the liquid-solid and liquid-gas interface, known as the contact angle, as a function of the contact-line speed and material properties of the system. Significantly, the latter is in direct conflict with recent experimental findings<sup>5</sup>. In particular, for a drop impact problem it has been found experimentally<sup>6</sup> that the dependence of the contact angle on the contact-line speed varies with the size of the impacting drop. An alternative, and more mathematically challenging approach, is to use the interface formation theory<sup>7</sup> to describe the dynamics of the interface. Here, as with experiments, the contact angle is determined by the flow field and consequently the model has been able to describe a wide range of physical phenomena in which the standard approach fails<sup>8</sup>.

To investigate drop impact and spreading phenomena we have developed a finite element based multi-purpose computational code, that uses the spine method designed by Scriven and co-workers<sup>9</sup>. This code incorporates both the standard slip models and the interface formation theory, allowing us to test different approaches to the drop impact problem in a wide range of parameters. Of particular interest is the impact of the micron size drops used by ink-jet printers. It is expected that for such flows, where the fluid’s large surface-to-volume ratio leads to a greater significance of interfacial effects, the differences between the two model’s predictions will be most striking. In the present work we show some of the results obtained using this multipurpose code and pay particular attention to when the impacting drop becomes toroidal or, alternatively, rebounds completely off the substrate.

---

\*School of Mathematics, University of Birmingham.

<sup>1</sup>Yarin, *Annu. Rev. Fluid Mech.* **38**, 159 (2006).

<sup>2</sup>Calvert, *Chem. Mater.* **13**, 3299 (2001).

<sup>3</sup>Sikalo et al., *Exp. Therm. Fluid Sci.* **25**, 503 (2002).

<sup>4</sup>Huh and Scriven, *J. Colloid Interface Sci.* **35**, 85 (1971).

<sup>5</sup>Clarke and Stattersfield, *Phys. Fluids* **18**, 048106 (2006).

<sup>6</sup>Bayer and Megaridis, *J. Fluid Mech.* **558**, 415 (2006).

<sup>7</sup>Shikhmurzaev, *Int. J. Multiphase Flow* **19**, 589 (1993).

<sup>8</sup>Shikhmurzaev, *Capillary Flows with Forming Interfaces* (2007).

<sup>9</sup>Kistler and Scriven, *Computational Analysis of Polymer Processing - Coating flows* (1983).

## Parametric dependence of lift in a flapping flight

Devranjan Samanta<sup>a</sup> and K R Sreenivas<sup>a</sup>

In recent times, research in the area of flapping flight has attracted interest with an aim to use this for lift & thrust generation in Micro Air vehicles (MAVs). Identification of a simple and efficient wing kinematics will improve the capacity to carry higher payloads and longer flight-endurance by MAVs. We earlier, using experiments and discrete vortex method (DVM) simulations, have shown that simple *asymmetric-flapping* could generate sustained lift<sup>1</sup>. In this paper, we present results from DVM simulations of flapping-flight indicating the effect of wing flexibility, flapping-amplitude and wing-inclination on the lift coefficient. By taking different flexural rigidity (EI) in the first and 2<sup>nd</sup> half of the wing, and considering wing as a cantilever-beam with a varying load proportional to  $\rho\omega^2x^2/2$ , we could mimic the wing - deflection of a flapping-bird. We have carried out simulations for various values of flexural rigidity ratios, wing inclinations and flapping-amplitudes. Results indicate that for a given flapping-amplitude (80°) and mean wing inclination (-25° to horizontal) maximum lift is generated when the flexural rigidity ratio is around 5.5 (fig. 1). For the flexural rigidity ratio of five, lift coefficient increases with increase in flapping amplitude (fig. 2). Figure 2 also indicates the dependence of lift on the mean inclination of the wing. In our presentation we present various parameters governing lift generation in flapping flight.

<sup>a</sup> Engineering Mechanics Unit, Jawaharlal Nehru Centre for Advanced Scientific Research, Bangalore, INDIA.

<sup>1</sup> JV Shreyas and KR Sreenivas, *Proc. Eleventh Asian Fluid Mechanics Congress*, 930 (2006).

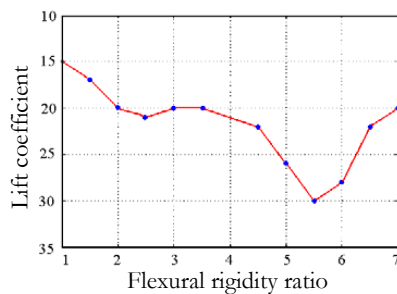


Fig. 1: Variation of lift coefficient with flexural rigidity ratio.

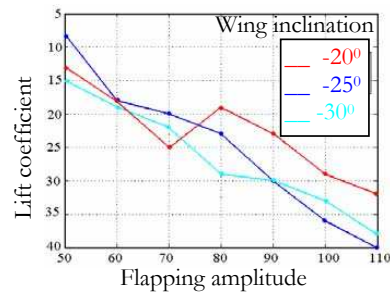


Fig. 2: Variation of lift coefficient with flapping amplitude and wing inclination

## Stability of the boundary layer on a compliant rotating disc

Sharon O. Stephen\* and Jo-Anne L. John\*

Transition to turbulence of the three-dimensional boundary layer on a rotating disc can be preceded by the emergence of crossflow vortices that are stationary with respect to the disc. These result from an inviscid instability mechanism associated with an inflexion point within the boundary layer velocity profile or a mechanism induced by the balance between viscous and Coriolis forces.

Research into the hydrodynamic stability of flow over flexible boundaries has revealed that a compliant response can have a beneficial effect on certain types of instability. In particular for two-dimensional boundary layers the spatial growth rates of Tollmien-Schlichting instabilities may be reduced. However, instabilities due to the flexible surface can also be induced. Thus, a correct balance of physical parameters within the problem must first be attained before any possible delay in transition can be achieved. There have been fewer studies on the effect of compliance on the instabilities formed within three-dimensional boundary layers. This is an important problem because these occur in many physical situations ranging from swept wings to rotating machinery. The investigation of<sup>1</sup> computationally modelled the effects that compliance had on both the stationary and travelling modes of the rotating disc. The experimental study carried out by<sup>2</sup> investigated the laminar to turbulent transition of the boundary layer over a rotating compliant disc. It was found that compliance had a stabilising effect on the inviscid (Type I) instability in the frequency range but an overall destabilising effect on the boundary layer flow. The more recent experiments of<sup>3</sup> have verified the results of<sup>1</sup> that compliance can destabilise viscous (Type II) disturbances on a rotating compliant disc.

We consider the linear stability of flow over a compliant rotating disc. The disc is considered to be of finite thickness, in contrast to the infinite thickness investigated by<sup>1</sup>. Numerical solutions of the linear stability equations will be presented for larger Reynolds numbers than the study of<sup>1</sup>. Growth rates and neutral solutions will be presented showing some interesting features for the wavenumber and orientation of both inviscid and viscous modes. Asymptotic solutions for the neutral inviscid and viscous modes (Type I and Type II) for large Reynolds numbers will also be discussed. The results obtained suggest that the inviscid mode of instability will be stabilised by compliance but the viscous mode will be greatly destabilised.

---

\*School of Mathematics, University of Birmingham.

<sup>1</sup>A. J. Cooper and P. W. Carpenter, *J. Fluid Mech.* **350**, 231 (1997).

<sup>2</sup>Colley et al., *Phys. Fluids* **11**, 3340 (1999).

<sup>3</sup>Colley et al., *Phys. Fluids* **18**, 054107 (2006).



## Rotating Rayleigh-Bénard convection: the influence of rotation on thermal boundary layers

Richard Stevens <sup>\*</sup>, Chao Sun <sup>\*</sup>, Herman Clercx <sup>†</sup>, Detlef Lohse <sup>\*</sup>

For Rayleigh-Bénard (RB) convection, the Rayleigh- and Prandtl number dependence of the heat transfer and the turbulence strength can satisfactorily be described within the Grossmann-Lohse (GL) theory <sup>1</sup>. It heavily builds on the Prandtl-Blasius laminar boundary layer (BL) theory, according to which the thermal BL thickness  $\lambda_\theta$  scales as  $Pr^{-1/2}$  in the low  $Pr$  regime and with  $Pr^{-1/3}$  in the high  $Pr$  regime.

In an attempt to extend the GL theory to the rotating RB case, we first study the influence of rotation on the thermal BL thickness in von Kármán flow, i.e., in flow above an infinite rotating disk (angular speed  $\Omega_D$ ) and no rotation of the fluid infinity. While rotation does not modify the Pr-scaling of  $\lambda_\theta$  in the large Pr regime, it does so in the low Pr regime, where now  $\lambda_\theta/L \sim Pr^{-1}$  is obtained, see fig. 1a.

Building on ref. <sup>2</sup>, the analysis is generalized to flow in which fluid at infinity rotates with an angular velocity  $\Omega_F = s\Omega_D$ ,  $0 < s < 1$ . Figure 1b reveals that the scaling of the thermal BL thickness is independent of  $s$ . The inset shows the crossover between the high and the low Pr regime against  $s$ . For increasing  $s$  the low Pr regime becomes more and more favored. Finally, we show that the thermal BL thickness decreases with increasing rotation, thereby explaining the experimentally <sup>3</sup> and numerically <sup>4</sup> observed increase in  $Nu$  (as compared to RB without rotation) at slow rotation rates.

<sup>\*</sup>Physics of Fluids, University of Twente

<sup>†</sup>Department of Physics, Eindhoven University; Department of Mathematics, University of Twente

<sup>1</sup>Grossmann and Lohse, *J. Fluid Mech.* **407**, 27 (2000); *Phys. Fluids* **16**, 4462 (2004).

<sup>2</sup>Rogers and Lance, *J. Fluid Mech.* **7**, 617 (1960).

<sup>3</sup>Rosby, *J. Fluid Mech.* **36**, 309 (1969)

<sup>4</sup>Oresta, Stingano, Verzicco, *Eur. J. Mech.* **26**, 1 (2007); Kunnen, Clercx, Geurts, *Phys. Rev. E* **74**, 056306 (2006).

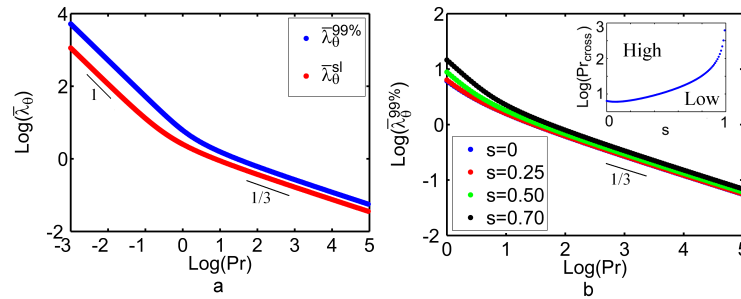


Figure 1: a) The thermal BL thickness scales with  $Pr^{-1/3}$  in the high  $Pr$  regime and with  $Pr^{-1}$  in the low  $Pr$  regime for von Kármán flow ( $s = 0$ ). b) Thermal BL thickness as a function of  $s$ . Inset: Crossover between the high and the low  $Pr$  regime.

## Local and global instabilities of flow in a flexible-walled channel

Peter S. Stewart\*, Sarah L. Waters†, John Billingham\* and Oliver E. Jensen\*

Self-excited oscillations can arise when a flow is driven sufficiently rapidly through a flexible-walled tube. These oscillations have numerous physiological applications, including Korotkoff sound generation in sphygmomanometry and wheezing in lung airways.

We consider the motion of high-Reynolds-number flow through a long, finite-length planar channel, where a segment of one wall is replaced by a membrane held under longitudinal tension. The flow is driven by a fixed pressure difference across the full length of the channel and is described using an integral form of the unsteady boundary-layer equations, which is reduced to an approximate, spatially one-dimensional model by assuming a parabolic velocity profile. This provides an overview of parameter space that is a useful guide to two and three dimensional models.

The basic flow state, for which the channel has uniform width, exhibits static and oscillatory global instabilities and rich nonlinear dynamics.

In the limit of large membrane tension the basic flow state becomes unstable to a high frequency instability, with a balance between membrane tension and fluid inertia at leading order. A mechanism for this instability has been described previously<sup>1</sup> by considering the full two-dimensional problem. We deduce an equivalent mechanism, with a slight discrepancy caused by the assumption of a parabolic flow profile. Now 12/19 (compared to 2/3) of the net flux of kinetic energy extracted from the mean flow is lost to viscous dissipation in the oscillation, with the remainder balanced by increased dissipation in the mean flow. This alteration of the mean flow by oscillations makes the primary instability subcritical. By linearising about the basic flow state, we demonstrate that this primary global oscillatory instability is a combination of travelling wave flutter and static divergence modes, each of which is convectively stable (in the absence of boundaries), and that amplification comes entirely from wave reflections with the rigid parts of the system.

The basic flow state can also become unstable to various spatially non-uniform static configurations for low membrane tension, which can subsequently become unstable to lower frequency oscillations as the Reynolds number increases. These instabilities resemble those observed in previous numerical studies of the system<sup>2</sup> and experiment. Using numerical simulations, we contrast energy transport during these oscillations with that arising in the high frequency case.

---

\*School of Mathematical Sciences, University of Nottingham.

†OCIAM, University of Oxford

<sup>1</sup>Jensen & Heil, *J. Fluid Mech.* **481**, 235 (2003).

<sup>2</sup>Luo & Pedley, *J. Fluid Mech.* **314**, 191 (1996).

## Two-layer obliquely-rotating shallow water equations with complete Coriolis force

Andrew Stewart\*, Paul Dellar\*

We derive equations to describe the flow over topography of two thin, superposed layers of inviscid, incompressible fluid with a free surface in a rotating frame. We include components of the Coriolis force arising from the locally horizontal component of the Earth's rotation vector. Our work therefore improves upon the standard shallow water equations that neglect this component, the so-called traditional approximation.

Our first derivation averages the three-dimensional rotating Euler equations over each of the layers. We also consider a Hamiltonian form, averaging a Lagrangian under the assumption of columnar motion in each layer. Both approaches lead to the inclusion of a number of additional terms in the two-layer obliquely-rotating shallow water equations that do not appear in the traditional two-layer shallow water equations. We obtain conservation properties for the potential vorticity, momentum, and energy. The momentum and potential vorticity include additional terms that are related to the additional horizontal component of the Coriolis force.

Despite the success of traditional shallow-water models for geophysical fluids in approximating the behaviour of ocean flow, their incomplete treatment of the Coriolis force means that they are of questionable validity in the Earth's equatorial regions. Existing models are commonly regularised using empirical friction<sup>1</sup> to balance pressure gradients at the equator, where the traditional component of the Coriolis force vanishes.

Recent work<sup>2</sup> has lead to the derivation of the obliquely-rotating shallow water equations for a single thin layer of inviscid, incompressible fluid in a rotating frame. By extending these equations for the case of two superposed layers of fluid, we obtain an improved model for the behaviour of the equatorial oceans, and one that is particularly useful for studying the flow of deep currents in these regions. This model does not need empirical friction to regularise it at the equator.

---

\*Mathematical Institute, University of Oxford.

<sup>1</sup>Choboter & Swaters, *J. Geophys. Res.* **109**, C03038 (2004).

<sup>2</sup>Dellar & Salmon, *Phys. Fluids* **17**, 106601 (2005).

## Modelling of fluctuations in turbulent two-phase flow by stochastic processes

Tobias Strömngren\*, Geert Brethouwer\*, Gustav Amberg\*  
and Arne V. Johansson\*

Stochastic differential equations have previously been used to model turbulence and subgrid scale motions<sup>1</sup>. We apply a set of stochastic differential equations to describe fluid and particle velocities in isotropic turbulent gas-particle flows and study the particle kinetic energy  $K_p$ . The system of equations reads

$$dU = -\frac{U}{T_L}dt + \phi \frac{V - U}{\tau_p}dt + \left(\frac{2\sigma^2}{T_L}\right)^{\frac{1}{2}}dW_f(t) \quad (1)$$

$$dV = -\frac{V - U}{\tau_p}dt + CdW_p(t) \quad (2)$$

where  $U$  is the fluid velocity,  $V$  is the particle velocity,  $T_L$  is the Lagrangian time scale of the turbulence,  $\sigma^2 = \frac{2}{3}K_f$  where  $K_f$  is the fluid turbulent kinetic energy,  $dW_f$  and  $dW_p$  are Wiener processes for the fluid and particles, respectively. The model takes into account particle diffusion due to particle-particle collisions (the last term in (2), where  $C$  is a collisional parameter depending on e.g. a collisional time scale), the turbulence influence on the particles by drag (the first term on the right hand side of (2),  $\tau_p$  is the particle response time), and the feedback from the particles on the fluid phase (the second term on the right hand side of (1),  $\phi$  is the particle volume fraction). The following relation between  $K_p$  and  $K_f$  is obtained by solving (1) and (2) using Itô calculus

$$\kappa = \frac{K_p}{K_f} = \frac{1 + \frac{C^2\tau_p}{2\sigma^2}(1 + \frac{\tau_p}{T_L} + 2\phi + \phi^2\frac{T_L}{\tau_p})}{1 + \frac{\tau_p}{T_L} + \frac{C^2\tau_p}{2\sigma^2}\phi^2\frac{T_L}{\tau_p}} \quad (3)$$

If we assume no particle-particle collisions ( $C=0$ ), (3) reduces to the same expression as derived by Hinze<sup>2</sup>. However, particle-particle collisions can have a significant effect. Our expression shows that  $\kappa$  increases for increasing particle-particle collisions and that increasing particle response times decreases  $\kappa$ .

It is studied, through model simulations, how the new expression for  $\kappa$  affects turbulent gas-particle flows. To do this (3) is implemented into an Eulerian-Eulerian model for turbulent gas-particle channel flow that we have developed<sup>3</sup>. The effect of particle-particle collisions and the gradient in the turbulence intensity near the wall on the preferential concentrations of particles is studied by combining our Eulerian-Eulerian model and expression (3).

---

\*Linné Flow Centre, Department of Mechanics, Royal Institute of Technology, Stockholm.

<sup>1</sup>Marstorp et al., *Phys. Fluids* **035107**, 19 (2007).

<sup>2</sup>J.O. Hinze, *Turbulence*, McGraw-Hill (1959).

<sup>3</sup>T. Strömngren et al., submitted to *AIChE J.*

### Fluid mechanical study on the material exchange across microvessel walls

Masako Sugihara-Seki<sup>a</sup>, Takeshi Akinaga<sup>a</sup> and Tomoaki Itano<sup>a</sup>

One of the most important functions of the blood circulation is the material exchange between circulating blood and surrounding tissues across microvessel walls. The luminal surface of vascular endothelial cells is covered by a layer of macromolecules referred to as the glycocalyx, and it was hypothesized that the glycocalyx is a major structure as a molecular sieve, or a solute transport barrier. In the present study, we have developed a mathematical model for the exchange of solutes and water across microvessel walls, based on the latest detailed ultrastructural studies of the endothelial surface glycocalyx<sup>1</sup> and the intercellular cleft between adjacent endothelial cells<sup>2</sup>. We analyzed the motion of solutes and the suspending fluid numerically, and examined the role of the endothelial surface glycocalyx in the transcapillary exchange.

For the solute transport across the endothelial surface glycocalyx, we assumed a hexagonal arrangement of core proteins with 12 nm diameter and characteristic spacings of 20 nm<sup>1</sup>, and made fluid mechanical computations on the motion of spherical solutes of 2 – 4 nm radius and the suspending fluid across the glycocalyx<sup>3</sup>. The predicted values of the diffusive permeability to solutes decline with solute size, known as “restricted diffusion”, and show a reasonable agreement with experimental observations. The reflection coefficient to solutes corresponding to serum albumin is predicted to be as high as 0.8, accounting satisfactorily for the observed molecular filtering of the microvessel wall. These results conform to the hypothesis that the endothelial surface glycocalyx forms the primary size selective structure to solutes in microvascular permeability.

With regard to the water transport, on the other hand, it was indicated that the hydraulic conductivity, which is defined as the ratio of the flow rate to the pressure drop, can not be accounted for by the glycocalyx property alone, and a 3-D flow analysis is necessary across the whole microvessel wall. We adopted a continuum medium approach for the whole pathway consisting of the endothelial glycocalyx and the interendothelial cleft with tight junction strands and their discontinuous leakages<sup>2</sup>, where the Brinkman equation was used as the governing equation of the fluid flow and the Darcy permeability for the glycocalyx was determined based on the regular arrangement of the core proteins mentioned above<sup>4</sup>. The present study predicts the hydraulic conductivity close to the experimental values for rat mesentery microvessels. It was suggested that the interendothelial cleft, rather than the endothelial surface glycocalyx, could be a major determinant of the hydraulic conductivity.

---

<sup>a</sup> Dept. of Pure and Applied Physics, Kansai University

<sup>1</sup> J.M. Squire, et al., *J. Struct. Biol.* **136**, 239 (2001).

<sup>2</sup> R.H. Adamson, et al., *J. Physiol.* **557**, 889 (2004).

<sup>3</sup> M. Sugihara-Seki, *J. Fluid Mech.* **551**, 309 (2006).

<sup>4</sup> M. Sugihara-Seki, et al., *J. Fluid Mech.* in press (2008).

### Branches: obstacles or springboards for samaras

Takeshi Sugimoto<sup>a</sup>, San'ei Ichikawa<sup>b</sup>, Shigekatsu Saitou<sup>b</sup>,  
Keiichi Kawase<sup>b</sup> and Masashi Mimura<sup>b</sup>

Field observations reveal that the average flight range of the samaras is significantly larger than the conventional estimate:  $R > Hw_T/U$ , where  $R$ ,  $H$ ,  $w_T$ , and  $U$  designate the flight range, the height of releasing the samaras, the terminal velocity of the samaras, and the speed of the transverse wind, respectively; the excess is up to 10-20 % of the conventional estimate. The most important point that the former works have neglected is the existence of the transverse winds. The samaras will not be scattered without the transverse winds faster than the terminal velocity of the samaras. We have carried out experiments in the transverse winds; we find that high lift acts on the samaras and that they fly farther than the conventional estimate<sup>1</sup>.

The next point is the existence of branches in the woods. The test section of our blow-down wind tunnel is 0.6m high, 0.6m wide, and 1.8m long; we model the branch by a circular cylinder with 16mm diameter placed transversely 0.34m high from the floor and 1.5m upstream from the end of the test section; we drop plastic spheres with 15mm diameter through the hole on the wind tunnel ceiling where is 0.26m high and 0.3m upstream from our branch; wind velocity is fixed at  $U = 5.0\text{m/s}$ .

The result is that our branch acts as a springboard rather than an obstacle: the flight range without the branch is on average 0.625m with 0.037m standard deviation, whilst the flight range with the branch is on average 1.11m with 0.604m standard deviation. Figure 1 shows some typical flight trajectories. Spheres, collided with the branch at the angle larger than  $\tan^{-1}(w_T/U)$ , leap markedly, although the coefficient of restitution for the plastic spheres is found to be as low as 0.347. Figure 2 shows the histogram of the flight range with the branch. It is apparent there are two peaks that stand for the flight ranges with leaps upward and downward.

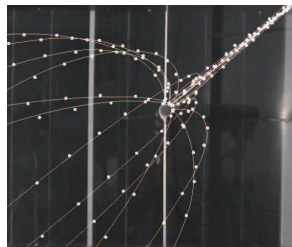


Figure 1: Trajectories.

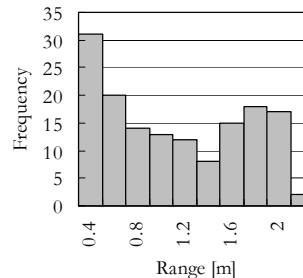


Figure 2: Flight range with the branch.

<sup>a</sup> Faculty of Engineering, Kanagawa University.

<sup>b</sup> Japan Wildlife Research Center.

<sup>1</sup> S. Ichikawa et al., *Theor. & Appl. Mech.*, **56**, 189 (2008).

## Growth and collapse of a vapor bubble in a microtube

C. Sun\*, E. Can\*, R. Dijkink\*, D. Lohse\*, and A. Prosperetti\*

The growth and collapse of a vapor bubble inside a narrow tube has recently been studied both theoretically and numerically<sup>1</sup>. Here we present systematic *experimental measurements* on this phenomenon. The vapor bubble is created by a laser pulse focussed in a cylindrical glass tube filled with water, similarly as in earlier experiments in our lab<sup>2</sup>. Both ends of the axisymmetric glass tube were connected to reservoirs with constant pressure. The inner diameter of the tube is  $50\ \mu\text{m}$  and the aspect ratio  $\Gamma = \text{length}/\text{diameter}$  varies from 80 to 1020. Next to the aspect ratio, the second main control parameter of the system is the energy of the laser pulse.

Figure 1 (a) shows the time evolution of the bubble length ( $L$ ) at fixed laser energy ( $0.5\ \text{mJ}$ ) for various values of  $\Gamma$ . The expansion and collapse are almost symmetric for  $\Gamma = 120$ . For larger  $\Gamma \geq 380$  the collapse becomes slower than the expansion. This observed trend is qualitatively consistent with the numerical simulation (Fig.2 in Ref. 1) of Ory *et al.*<sup>1</sup>, who have demonstrated that the motion proceeds by inertia after the initial phase change occurring on a very short time scale. The present large  $\Gamma$  case corresponds to their small Reynolds number case. Figure 1 (b) shows the time evolution of the bubble length at a fixed large aspect ratio,  $\Gamma = 540$ , for various laser energies. The expansion of the bubble is faster than the collapse for this large  $\Gamma$ . A robust and visible feature in figure 1(b) is the *linear* bubble collapse during the final phase. One possible reason is that the collapsing motion is dominated by viscosity. However, the linear collapse could also be explained by assuming that vapor condensation dominates the shrinkage of the bubble. Ongoing work is disentangling inertial, viscous, and thermal effects to arrive at a quantitative understanding of the vapor bubble growth and collapse in a narrow tube.

\*Physics of Fluids, University of Twente, the Netherlands.

<sup>1</sup>E. Ory, H. Yuan, A. Prosperetti, S. Popinet and S. Zaleski *Phys. Fluids* **12**, 1268 (2000).

<sup>2</sup>E.V. Zwaan, S. Le Gac, K. Tsuji, and C.D. Ohl, *Phys. Rev. Lett.* **98**, 254501 (2007).

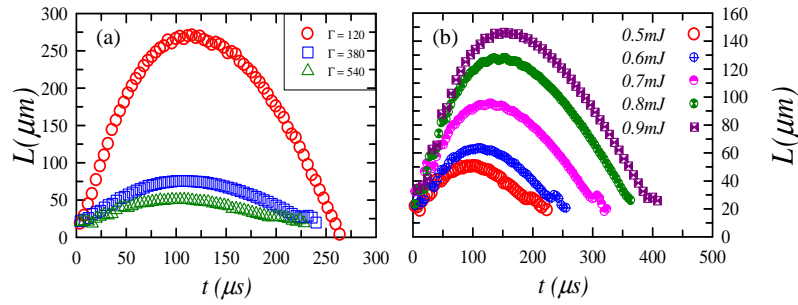


Figure 1: Bubble length vs. time for (a) varying  $\Gamma$  at fixed laser energy  $0.5\ \text{mJ}$  and (b) for fixed  $\Gamma = 540$  at varying laser energies.

# Global linear stability of plane confined wakes and jets

Outi Tammisola\*, Fredrik Lundell\* and Daniel L. Söderberg\*,<sup>†</sup>

Self-sustained oscillations in plane wakes and jets are studied numerically with 2D temporal global modes. Many different parameters can influence the stability of these flows. Some examples are confinement, inlet velocity profile, inlet Reynolds number and in the special case of two immiscible fluids - Weber number (describing the relative importance of surface tension).

Studies based on local velocity profile indicate that confinement has a considerable effect on global stability of plane 2D jets and wakes<sup>1</sup>. For a given inlet velocity profile and confinement, the base flow can be calculated for domains of arbitrary extent. The global mode is then obtained as the 2D eigenmode for oscillations around this baseflow. However, since the disturbance amplitude distribution is unknown a priori, the upstream and downstream boundary conditions for the disturbance are non-trivial. This presents a first challenge that has to be addressed. It is shown that the results are independent of the streamwise boundary conditions.

The global mode distributions (amplitude and phase) together with the corresponding growth rates in unconfined and confined cases are compared with each other. We focus on the influence of confinement on the stability based on the physics of the problem, *e.g.* inlet profile modifications, boundary layer development and disturbance boundary conditions on the walls. Two extreme cases will be studied in detail - a plane wake with no density gradient and no surface tension between the layers, and a capillary water jet in air with surface tension. These particular choices are motivated by the needs to understand global instabilities occurring in papermaking process.

\*Linné Flow Centre, KTH Mechanics, Royal Institute of Technology, S-100 44 Stockholm, Sweden

<sup>†</sup>STFI-Packforsk AB, Stockholm, Sweden

<sup>1</sup>M.Juniper, *J. Fluid Mech.* **565**, 171 (2006).

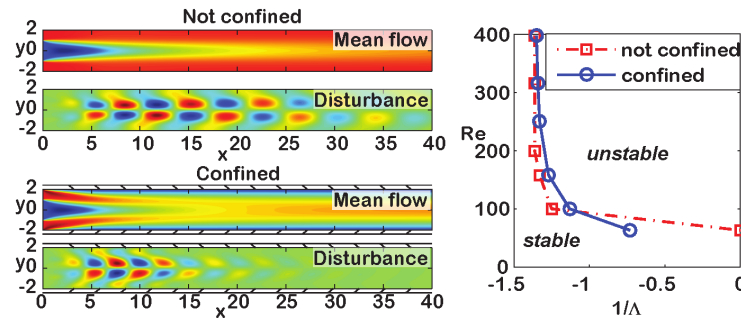


Figure 1: Left: Mean streamwise velocity and real part of the streamwise disturbance velocity. The colorscale goes from black via white to black. Right: Critical value of  $Re$  for shear ratio  $1/\Lambda < 0$ ,  $\Lambda = (U_1 - U_2)/(U_1 + U_2)$  where index 1 and 2 refer to the velocity of the jet/wake and surrounding stream at the inlet, respectively.



### Analysis of Flow Disturbances in Diseased Arteries using Two-Equation Transitional and Turbulence Models

Felicia Tan<sup>a</sup>, Nigel Wood<sup>a</sup>, Simon Thom<sup>b</sup>, Alun Hughes<sup>b</sup> and Yun Xu<sup>a</sup>

Blood flow is typically laminar, especially in non-diseased vessels, except in larger vessels in exercise. However, in the presence of sufficiently severe stenosis, the flow in the post-stenotic region decelerates and becomes unstable, with separation, recirculation and possible transition to turbulence. Disturbance and turbulence in blood flow influence physiological parameters and processes, such as pressure distribution, wall shear stress (WSS), flow regulation, wall remodelling, inflammation and mass transport from the blood to the vessel wall. Of potential interest here are the effects of disordered and turbulent flow on the resultant forces acting on the walls of a stenosed carotid bifurcation and a thoracic aortic aneurysm (TAA).

Following a validation study for pulsatile flow in an axisymmetric stenosed tube, magnetic-resonance (MR) image-based models of a 70% stenosed carotid bifurcation and a TAA were reconstructed. Patient-specific conditions such as velocity waveforms were used in pulsatile flow simulations. Laminar flow and a correlation based transitional version of Menter's hybrid  $k-\epsilon/k-\omega$  Shear Stress Transport (SST) model<sup>1</sup> were implemented in a finite volume method program, ANSYS CFX 11. Velocity profiles, WSS and turbulence intensities throughout a cardiac cycle were analysed.

In the validation study with well established experimental measurements<sup>2, 3</sup>, the transitional version of SST is shown to give a better overall agreement with experimental data than its standard counterparts. For the carotid bifurcation model, wall shear stress analysis showed discernable differences between the laminar flow and SST transitional model. Preliminary results for the TAA model demonstrated that the transitional model gave better overall agreement with MRI velocity data. Velocity profiles showed disturbed flow and recirculation within an anterior bulbous region of the aneurysm.

The validation results presented for the present application give credence to the application of the comprehensive engineering correlations incorporated in the transition model, to physiological flow conditions. This study demonstrated the possible superiority of such a transitional model over the conventional laminar flow assumption and full turbulence models in capturing the flow phenomena in moderate to severe stenosed carotid arteries and aortic aneurysms. This approach can provide an individual evaluation of the stresses on the diseased arterial wall that requires no invasive measurement and if combined with wall mechanics, it would represent an improved risk predictor for plaque or aneurysm rupture.

---

<sup>a</sup> Department of Chemical Engineering, Imperial College London

<sup>b</sup> International Centre for Circulatory Health, Imperial College London

<sup>1</sup> Menter et al., *ASME-GT-2004-53452* (2004).

<sup>2</sup> Ahmed, S. A., *Exp. Therm. Fluid Sci.*, **17**(4), 309 (1998).

<sup>3</sup> Ahmed et al., *J. Biomech.*, **17**(9), 695 (1984).

# Multiscale combination of microfluidic and structure-continual studies of stress state in dilute suspensions

E. Yu. Taran<sup>a</sup> and V. A. Gryaznova<sup>a</sup>

In this paper, we present a structure-phenomenological theory of stressed state in gradient flows of dilute suspensions of rigid axially symmetric elongated particles with the Newtonian carrier fluid. It is assumed that the studied suspensions satisfy assumptions of Einstein<sup>1</sup>, in particular, the double inequality  $l \ll d \ll L$  is fulfilled. Here,  $d$  is the characteristic dimension of suspended microparticles;  $l$  is the molecular dimension of the carrier fluid;  $L$  is the characteristic dimension of macroflow region of the suspension. Due to such correlation of the scales, a multiscale combination of *microfluidic* and *structure-continual* studies of the considered suspensions is used in order to obtain within the frames of *structure-phenomenological approach* the constitutive equation for stress arising in gradient flows of suspensions.

The inequality  $l \ll d$  allows us to model the carrier fluid by *the classical continuum* and consider the interaction of suspended microparticles with the carrier fluid as a hydrodynamic one. An ellipsoid of revolution is used as hydrodynamic models of suspended microparticles. Such a modeling allows to perform *the microfluidic study* of the hydrodynamic interaction of the Newtonian carrier fluid with suspended microparticles *in the microscale* of them using dynamic method of Landau<sup>2</sup>.

At the same time, *in the macroscale* of suspension macroflow region, the inequality  $d \ll L$  allows us to model considered suspensions by a *structure continuum* with two internal microparameters defining orientation and relative angular velocity of suspended particles. In this case, the rheological macrocharacteristics of the modeled suspensions are defined within the framework of *the structure-continual study*. So, the constitutive equation for stress in the suspension is postulated phenomenologically as function of deformation rate tensor and internal microparameters of the structure continuum that model considered suspension. In order to obtain theoretically phenomenological rheological constants entered in the postulated constitutive equation for stress, we combine the microfluidic and structure-continual studies of suspensions within the framework of *the structure-phenomenological approach*<sup>3</sup>. As a result of such combination we obtain the general constitutive equation for stress arising in arbitrary gradient flows of the dilute suspension of ellipsoidal particles. Further investigations show that the derived constitutive equation may be used in order to obtain the constitutive equations for stress in gradient flows of dilute suspensions with Brownian and non-Brownian, magnetically neutral and magnetically sensitive suspended particles. The obtained results give a chance to unite into a general structure-phenomenological theory the separate results obtained up to date in mechanics of dilute suspensions of rigid axially symmetric elongated particles.

<sup>a</sup> Faculty of Mechanics and Mathematics, National Taras Shevchenko University of Kyiv.

<sup>1</sup> A. Einstein, *Ann.Physik* **19**, 289 (1906).

<sup>2</sup> L.D. Landau, E.M. Lifshitz, *Fluid Mechanics*, Addison Wesley, Reading, Massachusetts (1959).

<sup>3</sup> E.Yu. Taran, DSc (Physics and Mathematics) thesis, Kharkov State University, Kharkov (1994).

## Electromagnetic Flow Measurement

André Thess<sup>a</sup>, Christian Karcher, Yurii Kolesnikov

Measuring the velocity in liquid metals is a notoriously difficult problem because these materials are opaque and often hot and aggressive. Especially when liquid metals reach high temperatures, as in metallurgy, the development of reliable, robust, and contactless velocity measurement methods has far-reaching consequences. The goal of the present communication is twofold. First, we will provide an overview of the history of electromagnetic flow measurement starting from Michael Faraday's experiments in 1832. Second, we will describe a novel flow measurement technique in which the problem is reduced to a force measurement that does not require any mechanical contact between the measurement system and the melt. The technique, which we term Lorentz force velocimetry (LFV) [1], [2], is based on exposing the fluid to a magnetic field and measuring the force acting upon the magnetic-field-generating system. We illustrate the physical principles of LFV and report results of comprehensive laboratory experiments which characterise the sensitivity of LFV. We then present results of an industrial test of the technique in the aluminium industry which demonstrates that LFV performs well under harsh industrial conditions. We finally outline some future developments and argue that LFV, if properly designed, has a wide range of potential applications.

- [1] A. Thess, E. Votyakov, Y. Kolesnikov, Lorentz Force Velocimetry, *Phys. Rev. Lett*, vol 96 (2006) 164501.
- [2] A. Thess, E. Votyakov, B. Knaepen, O. Zikanov, Theory of the Lorentz Force Flowmeter, *New J. Phys.*, vol. 9 (2007) 299.

---

<sup>a</sup> Department of Mechanical Engineering, Ilmenau University of Technology, P.O. Box 100565, 98684 Ilmenau, Germany, Email: [thess@tu-ilmenau.de](mailto:thess@tu-ilmenau.de)

## Micro Ripples, Sand Ripples and their Universal Wavelength Scaling

P. J. Thomas<sup>a</sup>, F. Zoueshtiagh<sup>b</sup>, A. Merlen<sup>b</sup> and V. Thomy<sup>c</sup>

Results from experiments investigating oscillatory motion of a fluid carrying suspended micron-sized particles in a capillary tube (diameter:  $288\text{ }\mu\text{m}$ ) are summarized - the experimental set up is illustrated in Fig. 1. The oscillatory fluid motion is driven by a computer-controlled syringe pump and filmed with two video cameras A and B; for details refer to Ref. 1. The experiments show that initially uniformly distributed particles can segregate and accumulate to form regularly spaced micron-sized particle clusters within the capillary tube (Fig. 2). As far as we are aware these represent the smallest ripple structures that have hitherto been reported.

The wavelength of the micro clusters is compared to wavelength data for macroscopic sand-ripple patterns from the literature for studies conducted over a wide range of substantially different experimental conditions. It is found that the wavelength of the micro ripples follows the same universal scaling that was obtained in Ref. 2 for the wavelength of the macroscopic sand-ripple patterns.

This agreement of the scaling suggests that relevant local scales on the surface of the granular layer, where the ripples form, govern the ripple-formation mechanism. Hence, all global scales and global flow features are irrelevant. Prompted by this conclusion a dimensional and asymptotic analysis is performed<sup>1</sup> yielding a power-law scaling exponent that agrees to within 4% with that found in Ref. 2 from experimental data. This very good agreement theoretically supports the universality of the scaling obtained in Ref. 2 on a purely experimental basis.

- <sup>a</sup> Fluid Dynamics Research Centre, School of Engineering, University of Warwick, Coventry, UK.  
<sup>b</sup> Laboratoire de Mécanique de Lille UMR CNRS 8107, Bd. Paul Langevin, 59655 Villeneuve d'Ascq, France  
<sup>c</sup> Institute d'Electronique et de Microélectronique et Nanotechnologie UMR CNRS 8520, Avenue Poincaré, 59652 Villeneuve d'Ascq, France

<sup>1</sup> F. Zoueshtiagh, P.J. Thomas, V. Thomy and A. Merlen, *Phys. Rev. Lett.*, **100**, 054501 (2008).

<sup>2</sup> F. Zoueshtiagh and P.J. Thomas, *Phys. Rev. E*, **67**, 031301 (2003).

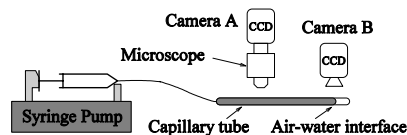


Figure 1: Sketch of the experimental set up.

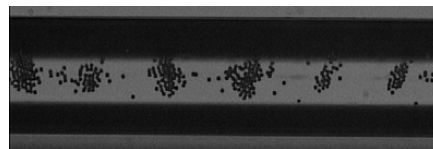


Figure 2: Micro-ripple pattern for particles with average diameter of  $10\text{ }\mu\text{m}$ .

## The Interaction of Swimming Microorganisms With Flow: Modelling Motile Phytoplankton in Turbulence

Dr. Graeme J. Thorn\*

It is important to study the interaction of swimming phytoplankton and typical ocean flow conditions in order to understand how the spatial distribution evolves due to the dispersive properties of turbulence. Many harmful algal bloom-forming species are motile,<sup>1</sup> hence such a study will provide insights into how blooms develop once formed. For a gyrotactic microorganism, whose preferred motile behaviour is to swim upwards, this interaction is non-trivial as turbulence can alter this behaviour by preventing its reorientation to this preferred direction due to rapid changes in the local flow on its Lagrangian particle path.

As the swimming of phytoplankton typically occurs on length scales (of the order of 1-100  $\mu\text{m}$ ) some orders of magnitude below the Kolmogorov scale for ocean turbulence (of the order of 1 cm), a model for the swimming behaviour in arbitrarily-oriented simple flows can be used to parameterise the effects of the smallest eddies on the mean swimming velocity. This result can then be incorporated into a population-level equation which will describe the time evolution of the spatial distribution of a patch of phytoplankton. This advection-diffusion model extends previous work which has concentrated on developing models for population dispersal in linear homogeneous flows using the macroscopic generalised Taylor dispersion method.<sup>2</sup>

This talk will begin with a description of the advection-diffusion model, by showing how it is built up from the simple flow model, and will proceed to comparisons of this population-level model with simulations of individuals in turbulent flows.

---

\*Department of Mathematical Sciences, University of Liverpool.

<sup>1</sup>Horner et al., *Limnol. Oceanogr.* **42**(5), 1137 (1997).

<sup>2</sup>N.A. Hill and M.A. Bees, *Phys. Fluids* **14**(8), 2598 (2002).

## Modelling of particle size segregation and its applications to geophysical problems

A. Thornton\*, Prof. J.M.N.T Gray\*, Prof. P. Kokelaar†

It is important to be able to predict the distance to which a hazardous natural flow (e.g. snow slab avalanches, debris-flows and pyroclastic flows) might travel, as this information is vital for accurate assessment of the risks posed by such events. In the high solids fraction regions of these flows the large particles commonly segregate to the surface, where they are transported to the margins to form bouldery flow fronts (figure 1 : left, right). In many natural flows these bouldery margins experience a much greater frictional force, leading to frontal instabilities<sup>1</sup>. These instabilities create levees that channelize the flow vastly increasing the run-out distance.

A similar effect can be observed in dry granular experiments, which use a combination of small round and large rough particles. When this mixture is poured down an inclined plane particle size segregation causes the large particles to accumulate near the margins. Being rougher, the large particles experience a greater friction force and this configuration (rougher material in front of smoother) can be unstable. This instability causes the uniform flow front to break up into a series of fingers<sup>2</sup>.

A recent model for particle size-segregation<sup>3</sup> has been coupled, through a particle concentration dependent friction law, with existing avalanche models<sup>4</sup>. In this talk numerical solutions of this coupled system are presented and compared to both large scale experiments carried out at the USGS flume (figure 1 : left) and more controlled small scale laboratory experiments (figure 1 : middle). These simulations and experiments show good agreement and the numerical model allows the whole of parameter space to be sampled in a systematic way. Additionally the numerical model can be used to analyse the effect of individual assumptions, leading to a better understanding of the key mechanisms which drive the observed phenomena.

\*School of Mathematics, University of Manchester.

†Department of Earth Science, University of Liverpool

<sup>1</sup>Iverson *Reviews in Geophysics* **35**, 245 (1997)

<sup>2</sup>Pouliquen & Vallance *Chaos* **9**(3), 621 (1997)

<sup>3</sup>Gray & Thornton *Proc. Royal Soc. A* **461**, 1447 (2005)

<sup>4</sup>Savage & Hutter *Acta Mech.* **86**, 201 (1991)

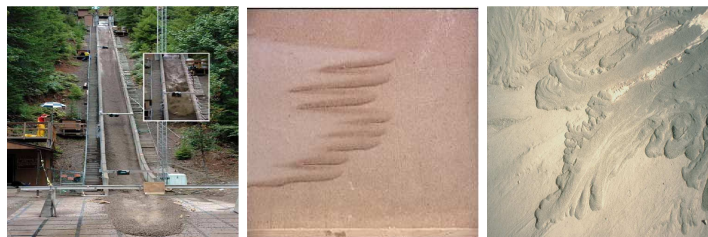


Figure 1: Left: USGS debris-flow flume. Middle : Small scale laboratory experiment showing the formation of fingers. Right : Small volume pyroclastic density current with lobate terminals.

## Global ALE Method for Stratified Richtmyer-Meshkov Instability

Baolin Tian<sup>a</sup>, Weidong Shen<sup>a</sup>, Shuanghu Wang<sup>a</sup>

Richtmyer-Meshkov(RM) instability<sup>1</sup> arises when a material interface is accelerated impulsively by shock waves. It plays an important role in many fields, such as ICF, supernova and so on. In this work, a novel arbitrary Lagrangian-Eulerian method, global ALE method (GALE), was developed for stratified RM instability.

Unlike traditional ALE methods<sup>2</sup>, where rezoning and remapping are performed just in the internal of one material region, and material interfaces are tracked by Lagrangian mesh lines, the GALE method attempts a compromise by combining the merits of both ALE and Eulerian methods. In the GALE method, modern Eulerian methods, such as mass fraction model, level set method, are coupled with a Godunov-type ALE method. Thus all the meshes can be moved arbitrarily no matter whether they are material interface or not. In the simulation of multi-material flows using GALE, Lagrangian or Eulerian interface treatment can be selected according to the degree of interface distortion or other standard. Some benchmark problems, such as gas-liquid shock tube problem, RM instability with small initial perturbation in planar geometry, were computed by the GALE to verify the method, and the numerical results agree well with exact solution or theoretical model.

The previous numerical studies for RM instability are mainly performed in the case with single interface in plane geometry by Eulerian methods. In this work the GALE method was used to simulate the stratified RM instability with two or more material interfaces in planar, cylindrical and spherical geometries. The unperturbed interface was tracked in Lagrangian mode and the perturbed interface was captured in Eulerian mode by mass fraction model. The interface evolution process was studied and compared in different geometry cases based on simulation results. As shown in Fig.1, the spikes in planar and cylindrical geometries are narrower and longer than those of spherical case, and the roll-up of spikes seems more manifest. These discrepancies can be contributed to the stronger implosive compressibility in converged geometry. More detailed analysis will be made in the future work.

Acknowledgement: This work was supported by the National Basic Research Program(Grant No.2005CB321700), and Key Lab Foundation (9140C690201060C69).

<sup>a</sup> The Institute of Applied Physics and Computational Mathematics, Beijing, China, 100084.

<sup>1</sup> M. Brouillette, *Annu. Rev. Fluid Mech.*, **34**, 445(2002).

<sup>2</sup> D. J. Benson, *Comput. Methods Appl. Mech. Eng.* **99**, 235 (1992).

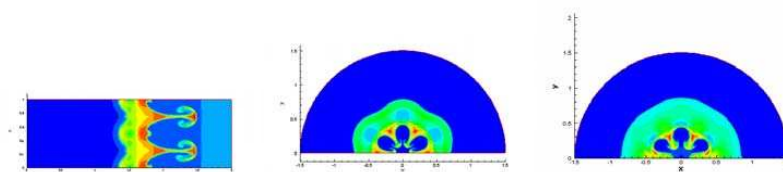


Figure 1: Stratified RM instability in planar, cylindrical and spherical geometry.

## Experimental investigation of the near-wall flow behind a backward-facing step

J. Tihon<sup>a</sup>, V. Penkavova<sup>a</sup>

This experimental study of backward-facing step flow is focused on the transient flow regime. An unsteady flow pattern with several regions of flow separation downstream the step was first described in the classical work by Armaly et al. (1983). Our objective is to study the near-wall flow organization by measuring the wall shear rate fluctuations behind the step. The electrodiffusion method is used for this purpose with the aim to assess the influence of two different parameters: channel geometry ( $ER=1.4, 2, 2.5, \text{ and } 4$ ) and inlet flow forcing ( $f=0-3 \text{ Hz}$ ). The investigation is carried out for the Re number ranging from 20 to 4000.

The movable step configuration with two flush-mounted wall probes is used to measure the wall shear rate profiles along the bottom and roof of the water channel (see Fig.1). The application of two-strip sensors provides information also on the local direction of near-wall flow and thus enables us to detect the position of mean reattachment point (III). The near-wall extent of secondary recirculation zones (corner eddy (V), roof eddy (VII), temporary secondary recirculation at the step wall) is determined as well. These results provide some insight into the flow rearrangement due to the change in flow rate or step configuration and suggest a general scaling for the reattachment length.

The near-wall flow behind the step is found to be very unsteady, with strong low-frequency oscillations, even at moderate Re numbers. The high level of skin friction is observed inside the reverse flow region. The spectral analysis of fluctuating wall shear rate reveals that low frequencies corresponding to  $St_h$  from 0.1 to 0.2 are dominated in the reattachment region at natural flow conditions. The inlet flow forcing strongly affects the overall flow structure. Up to 70% reduction of the reattachment length is achieved by applying flow pulsations at the most effective frequency. This frequency is determined by two observed instability modes. The “step” mode dominates under the laminar flow regime, whereas the “shear layer” mode at transient flow conditions.

<sup>a</sup> Institute of Chemical Process Fundamentals, Academy of Sciences of the Czech Republic, Rozvojová 135, 16502 Prague 6, Czech Republic (e-mail: [tihon@icpf.cas.cz](mailto:tihon@icpf.cas.cz)).

This work was supported by the Grant Agency of the Czech Republic under the project No.101/08/0428.

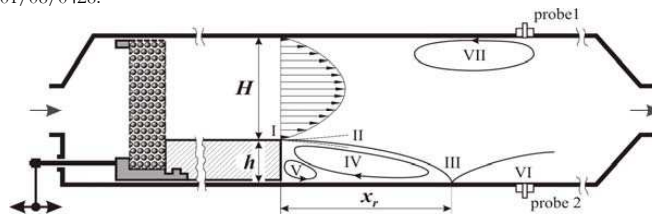


Figure 1: Backward-facing step channel with the schema of inside flow pattern.



## Thermo-fluid Dynamics of the unsteady channel flow

Renato Tognaccini\*, Amilcare Pozzi\*

Unsteady laminar flows in pipes have been widely studied since the classical paper of Szymanski<sup>1</sup>, in which the author proposed the exact analytical solution describing the incompressible, laminar flow arising in a circular pipe initially at rest and accelerated by a sudden jump of the pressure gradient to a constant value. This is among the few exact analytical solutions of the unsteady Navier-Stokes equations of physical relevance. A renewed interest in the analytical analysis of these problems can be found in literature in these years, see<sup>2</sup>. Nonetheless, studies devoted to the analysis of two-dimensional unsteady channel flows are only a few due to the difficulty of the involved inverse Laplace transforms. The problem is further complicated when the thermal field in the fluid is studied: no exact solution exists for the thermal field including the effects of the dissipation of kinetic energy (Eckert number different than zero).

In this paper we present two new exact explicit analytical solutions for both the velocity and thermal field including the effect of the Eckert number. The first one is the incompressible, laminar, fully developed flow of a fluid accelerated from rest in a two-dimensional channel with flat, parallel walls, by assigning a general time law for the pressure gradient (unsteady Poiseuille flow). In the second problem the motion of the fluid, initially at rest, is generated prescribing a general time law for the velocity of the upper wall in the direction of the channel axis (unsteady Couette flow). For the thermal field a constant wall temperature along the channel is assumed.

Both solutions have been found by the Laplace transform technique. The inverse Laplace transforms have been obtained using some interesting properties of the Jacobi's  $\theta_2$  and  $\theta_3$  functions leading to series in terms of the well known error functions rapidly converging to the solution of the problem.

The presence of a complex non-homogeneous term in the energy equation makes its integration very difficult when the Eckert number is taken into account. However, in the present paper a simple analytical expression of a particular integral of the non-homogeneous equation has been found that enables to easily obtain an analytical solution. Therefore, explicit relations for the axial velocity and temperature profiles across the channel, shear stress and Nusselt number have been derived.

The local analysis for small time values, reveals the existence of two regions in the flow: near the wall a self-similar *Rayleigh type layer*, far from the wall a *potential region*, where the velocity is constant across the channel, zero in the case of the unsteady Couette flow and proportional to a power of the nondimensional time for the unsteady Poiseuille flow.

The method of solution can be easily applied when the time law imposed for the pressure gradient or upper wall velocity is of polynomial type and a number of applications are proposed with the analysis of the effects of the involved parameters discussed by means of suitable diagrams.

---

\*Dipartimento di Ingegneria Aerospaziale, Università di Napoli Federico II.

<sup>1</sup>Szymanski, *J. Math. Pures Appl.*, **11**, 67 (1932).

<sup>2</sup>Drazin and Riley, *Cambridge University Press*, (2006).

# Multiscale analysis of long three-dimensional perturbation waves in shear flows

S. Scarsoglio\*, D. Tordella\* and W. O. Criminale†

In spatially developing flows different scales can be selected. In some flow configurations, it is observed that long waves can be destabilizing. An example of this behaviour is the three-dimensional cross-flow boundary layer. In such instances, when instability occurs, the perturbation wavenumber  $k$  is much less than  $O(1)$ . Thus, a regular perturbation scheme can be adopted, defining as the small parameter the polar wavenumber  $k$ . Two spatial scales, a short one -  $y$  - and a long one associated to the perturbation -  $Y = ky$  - can be introduced ( $y$  is the coordinate normal to the base flow direction). For the temporal dynamics, three temporal scales, the fast one -  $t$  - and the slow ones -  $\tau = kt$  (perturbation) and  $T = k^2t$  (diffusion) - can be identified.

The formulation is carried on in terms of velocity and vorticity<sup>1</sup> by imposing initial arbitrary conditions in terms of the elements of the trigonometrical Schauder basis in the  $L^2$  space. A combined Laplace-Fourier transform is performed<sup>2</sup>. We introduce the wavenumber  $\alpha_r$  and the spatial damping  $\alpha_i \geq 0$  in the evolution direction  $x \geq 0$ , and the wavenumber  $\gamma$  in the direction  $z$  normal to the base flow. The initial perturbation has a zero or positive spatial damping because its kinetic energy must be finite. Here the perturbative equations are solved up to order  $O(1)$  for the case of the two-dimensional non parallel wake. The base flow is approximated using the longitudinal as well as the transversal components of an asymptotic Navier-Stokes expansion<sup>3</sup>, so that a trace of the transversal dynamics (in particular of the entrainment) is included in the stability analysis. A section of the intermediate wake ( $x_0 = 10$  body scales, region where absolute instability pockets were found by recent modal analyses<sup>4-5</sup>) is considered. In Fig. 1 an example of short and long term growth of the normalized kinetic energy density  $G$  of the perturbation<sup>6</sup> is shown. An interesting result is that, by changing the order of magnitude of  $\alpha_i$ , perturbations that are more rapidly damped in space (Fig. 1a) lead to an immediate and monotone non decreasing growth in time (Fig. 1b).

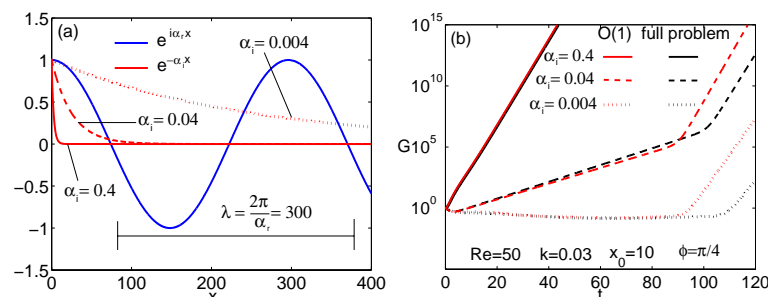


Figure 1: Effect of the spatial damping rate  $\alpha_i$ . (a) projection of perturbation wave in the  $x$  direction and (b) normalized kinetic energy density  $G$  as function of time. Comparison between the multiscale and full problem ( $\phi$  is the disturbance angle of obliquity with respect to the base flow plane, the inputs are asymmetric).

\*Dipartimento di Ingegneria Aeronautica e Spaziale, Politecnico di Torino, 10129 Torino, Italy.

†Department of Applied Mathematics, University of Washington, Seattle, WA 98195-2420, USA.

<sup>1</sup>Criminale and Drazin, *Stud. in Applied Math.* **83**, 123 (1990)

<sup>2</sup>Scarsoglio et al., *Proc. 11th Euromech* **117**, 221 (2007)

<sup>3</sup>Tordella and Belan, *Phys. Fluids* **15**, 1897 (2003)

<sup>4</sup>Tordella et al. *Phys. Fluids*, **18**, 054105 (2006)

<sup>5</sup>Belan and Tordella, *J. Fluid Mech.* **552**, 127 (2006)

<sup>6</sup>Criminale et al., *J. Fluid Mech.* **339**, 55 (1997)

## The importance of leading-edge vortices in dragonfly flight

Cam Tropea\*, David Rival†

In classical rotorcraft aerodynamics the leading-edge vortex (LEV) has been shown to be of primary importance in the dynamic stall process<sup>1</sup>. For steady forward flight, the formation of a strong LEV over the dragonfly's forewing has been revealed using the smoke-visualization technique<sup>2</sup>. The formation of the LEV on the forewing has been identified as a quasi two-dimensional process across most of the wingspan and body. This LEV is stabilized by finely controlling the instantaneous effective angle of attack over the wing, as well as by out-of-phase hindwing movement. In order to examine these effects in detail, an experimental tandem-airfoil facility for the Eiffel-type low-speed wind tunnel at the Institute of Fluid Mechanics and Aerodynamics has been developed. By using airfoils with a pitch/plunge motion the problem has been simplified to the two-dimensional case, which is advantageous both for the time-resolved lift and moment measurements as well as for the smoke-visualizations and time-resolved particle image velocimetry (PIV) measurements. In Figure 1, a clearly-defined LEV can be seen rolling over the surface of the airfoil at a point midway through the downstroke. The convection of this vortex is responsible for a sharp increase in lift as well as a strong pitch-down moment. Near the end of the downstroke the LEV is shed from the trailing edge thus reducing the lift until the beginning of the following downstroke in which a subsequent LEV is formed. Further results from these studies are presented including the effect of non-sinusoidal kinematics as well as various out-of-phase hind-airfoil movements.

\*Institute of Fluid Mechanics and Aerodynamics, Technische Universität Darmstadt, Germany

†Institute of Fluid Mechanics and Aerodynamics, Technische Universität Darmstadt, Germany

<sup>1</sup>McCroskey, *Ann. Rev. Fluid Mech.* **14**, 285-311 (1982).

<sup>2</sup>Thomas *et al.*, *J. Exp. Biol.* **207**, 4299-4323 (2004).

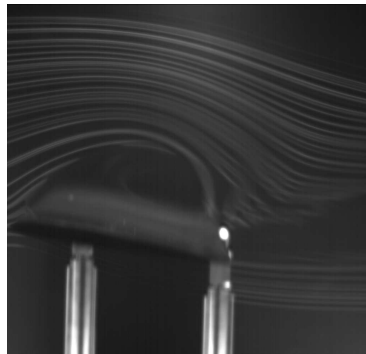


Figure 1: Smoke visualization of LEV convecting over airfoil surface midway through the downstroke.

## The dynamics of droplet impact upon carbon nanofibre jungles

Peichun Tsai\*, Leon Lefferts† and Detlef Lohse\*

We experimentally investigate the rapid dynamics of droplet impact on carbon nanofibre jungles (CNFJs). Different from the paradigmatic studies of droplet impact process on flat surfaces<sup>1</sup> or micro-textured substrates<sup>2</sup>, catalytically generated carbon nanofibre jungles exhibit inhomogeneous, multiscaled roughness of both micron and nano scales (see Fig. 1). Fig. 2 shows snapshots of a droplet of distilled water impinging on a hydrophobic CNFJ with a static contact angle of  $142 \pm 2^\circ$ , revealing a similar impact phenomenon to that for some conventional microstructured surfaces<sup>3</sup>. The aim of this study is to clarify whether the wetting property of the surface in terms of contact angle is the only relevant control parameter for such droplet impact experiments; i.e., we perform a detailed comparison of impact events on both micropatterned surfaces and CNFJs of multiscaled roughness. Ongoing research includes experiments under reduced ambient pressure to scrutinize the effects of air on the fast droplet impact processes on heterogeneous surfaces, with both CNFJs and microstructured materials.

\*Physics of Fluids Group, Department of Applied Physics, University of Twente, the Netherlands.

†Catalytic Processes and Materials Group, University of Twente, the Netherlands.

<sup>1</sup>A. L. Yarin, *Annu. Rev. Fluid. Mech.*, **38**, 159 (2006).

<sup>2</sup>M. Reyssat et al., *Europhys. Lett.* **74**, 306 (2006).

<sup>3</sup>D. Bartolo et al., *Europhys. Lett.* **74**, 299 (2006)

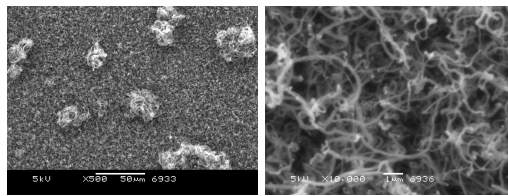


Figure 1: Scanning electron microscope (SEM) images of a CNFJ, showing its intrinsic multiscaled surface roughness. Clusters of carbon nanofibres (right) display profound porosity and a surface roughness of tens of microns (left). We gratefully acknowledge Sergio Pacheco<sup>†</sup> for providing the CNFJ samples and the SEM images.



Figure 2: Droplet impact dynamics on the hydrophobic CNFJ shown in Fig.1. Right after the impingement, the droplet quickly expands in the radial direction. However, the hydrophobicity of the surface then retracts the liquid, eventually bounding of the droplet. Subsequently, the droplet re-hits the surface with a lower kinetic energy and turns to a sticky vibrating ball on the surface, as displayed in the last two marked figures. The time interval is 1 ms between two successive images, except the last two marked images which are snapshots after the bouncing droplet re-impacted the surface. Here the impact velocity is 48.5 cm/s, and the droplet radius is about 1 mm.

## Two-phase gas-particle flow through a set of moving and stationary cascades of blades

Yury Tsirkunov\*, Denis Romanyuk\* and Sergei Panfilov\*

The present study deals with computational simulation of two-phase gas-particle flow through a set of two, moving and stationary, airfoil cascades. This flow can be considered as a model of flow in the inlet stage of an axial turbomachine. The presence of dispersed particle in a flow results in some new effects which more often than not, are undesirable. Specifically, it causes the erosion of blades and energy losses<sup>1</sup>. The purpose of this work is to study the behaviour of solid particles in the time-dependent high-speed subsonic 2D-flow in both cascades.

A dusty gas flow with very low particle mass load is considered. The inter-particle collisions and the effect of the dispersed phase on the carrier gas flow are assumed to be negligible. In this case, the problem of two-phase flow simulation can be reduced to the sequential solving of two problems: (i) computation of the carrier gas flow field, and (ii) calculation of the particles' motion in this flow field.

Flow of a compressible gas through the set of cascades is described by the complete Navier-Stokes equations. At the airfoil surface, the no-slip condition and the constant-temperature wall condition are enforced. At the inflow boundary of the calculational domain, the stagnation enthalpy  $h_0$  and the entropy function  $\vartheta = p/\rho^\gamma$  are given. At the outflow boundary of the set of cascades, the pressure  $p_{out}$  is taken equal to  $1.2 p_{in}$  that corresponds to some experimental data.

The Navier-Stokes equations were solved numerically using a finite-volume method of the second order, and the results were compared with those obtained for the Euler equations to estimate the role of viscosity in forming vortex wakes behind blades. It was found that the vortex wakes produced a complex pattern of weak pressure waves.

The momentum and angular momentum equations for particles together with the kinematic relations for the particle coordinates were solved numerically. In the most of computations, the particles were assumed to be spherical, however non-spherical particles were also considered to estimate the effect of particle scattering in particle-wall collisions which can be significant in some cases<sup>2</sup>. In the model of gas-particle interaction, the drag force, the lift Magnus force and the damping torque were taken into account. The last two factors play an important role when particles acquire high rotational velocity in the process of particle-blade impact interaction.

The input data in computations (flow properties, speed of a moving cascade, airfoil sizes, etc.) were taken close to those in the flow through an axial compressor of an aircraft turbojet engine. Flow fields of the carrier gas and the dispersed phase were visualized computationally by tracing of massless markers and solid particles. Flow patterns of particles of different sizes in both, moving and stationary, cascades are discussed and analyzed.

This study has been supported by the RFBR through Grant No. 05-08-50075.

\*Dept. of Plasma- and Gasdynamics, Baltic State Technical University, Saint Petersburg, Russia

<sup>1</sup>M.F. Hussein and W. Tabakoff, *J. Aircraft* **10**, 543 (1993).

<sup>2</sup>Yu. Tsirkunov and S. Panfilov. *Proc. 6th Int. Conf. on Multiphase Flow*, Leipzig, Germany, July 9-13, 2007

### A flow field investigation on crown-shaped nozzles

D. Tsovolos<sup>a</sup> and T. H. New<sup>a</sup>

The near-field vortex interactions emanating from crown-shaped nozzles under forced conditions (Strouhal number=0.5) have been investigated. Digital particle-image velocimetry (DPIV) and flow visualisation techniques were used to examine the near-field flow characteristics. Two crown-shaped nozzles were used: one in which the peaks/troughs have included-angle of  $30^\circ$  and another where the included-angle was  $60^\circ$ . Each nozzle consisted of four peaks and four troughs and furthermore, two out of the four peaks were smooth rather than sharp. The aim here is to investigate whether the exact geometry of the peaks affect the vortex dynamics significantly and influence the jet-mixing mechanism. Flow visualisation, velocity and vorticity field results have been obtained and compared with the circular reference nozzle (with no nozzle-lip modifications), in order to elucidate any flow differences. Typical examples of flow visualisation results obtained for the crown-shaped nozzles are shown in Figure 1. It can be observed that in both cases, forced flow conditions lead to the formation of shear layer instabilities that follow the nozzle lip contour very closely, which in turn result in highly three-dimensional vortex structures. Part of the reason is the persistent formation of streamwise vortices at the peak locations. Additionally, it appears that regardless of whether the peaks are smooth or sharp, the nature of the resultant streamwise vortices remains very similar even when the overall nozzle sharpness has varied. As the jet convects further downstream, the jet shear layer can be seen to roll up and form relatively distorted azimuthal ring-vortices. Lastly, due to the inherent instability of the distorted ring-vortices, transition to turbulence takes place much faster when compared to the circular reference nozzle. More flow field information will be presented during the conference to elaborate further.

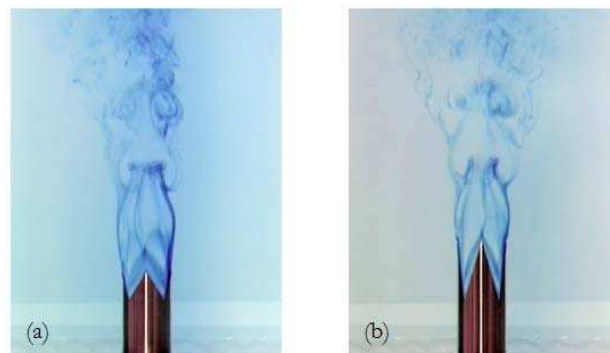


Figure 1: Flow visualisations of (a)  $60^\circ$  and (b)  $30^\circ$  crown-shaped nozzles.

<sup>a</sup> Department of Engineering, University of Liverpool

## Roll cells in turbulent plane Couette flow with system rotation

Takahiro Tsukahara<sup>\*†</sup>, Nils Tillmark<sup>\*</sup> and P. Henrik Alfredsson<sup>\*</sup>

To determine the flow in a rotating reference frame, as in the case of rotating fluid machinery or geophysical flows, the effect of system rotation must be clarified. It is known that system rotation gives rise to a Coriolis force, which may substantially affect the flow stability, transition between laminar and turbulent flow as well as the mean flow pattern. If there is a rotation-vector component that is parallel (anti-parallel) to the mean flow vorticity, the Coriolis effect may lead to stable (unstable) ‘stratification’ of the flow field. Previous theoretical<sup>1</sup> and experimental<sup>2</sup> studies on plane Couette flow (PCF) with spanwise system rotation indicate that when the destabilizing rotation is imposed, a tertiary flow in form of a 3D roll-cell state occurs via transition from a secondary flow with a 2D roll cell. These studies show that such a stable 3D roll-cell structure may exist within a limited low-Reynolds-number range up to  $Re = 150$ , where  $Re$  is based on half the relative wall speed  $U_w$  and the channel half-width  $h$ . In the present work, experiments on the rotating PCF are carried out for a rather wide  $Re$  range, and we have observed 3D roll cells even in turbulent flow.

Our PCF apparatus has been used in a number of reported experiments<sup>1,3</sup>. The flow is governed by  $Re$  and the rotation number  $\Omega = 2\Omega_0 h^2/\nu$ , with  $\Omega_0$  the angular velocity of the PCF apparatus itself, and  $\nu$  the kinematic viscosity of water as the working fluid. Visualization of the pattern is accomplished by the addition of light-reflecting platelets. Figure 1 (a) shows rather homogeneous fine-scale turbulent structures, while the time-averaged (a long exposure time) flow field reveals the coexistence of 3D roll cells [see (b)] of a much larger scale. The observed spanwise wavelength of these structures resembles that in laminar flow, but the streamwise wavelength is about twice of that observed in the laminar case. For high rotation numbers ( $\Omega > 25$  at  $Re = 600$ ), the 3D roll cells are more distinct, whereas for  $\Omega < 15$ , the turbulent flow instead contains stable 2D roll cells.

<sup>\*</sup>Linné Flow Centre, KTH Mechanics, Royal Inst. of Tech., SE-100 44 Stockholm, Sweden.

<sup>†</sup>Dept. of Mech. Eng., Tokyo Univ. of Science, 2641 Yamazaki, Noda, Chiba 278-8510, Japan.

<sup>1</sup>M. Nagata, *J. Fluid Mech.* **358**, 357 (1998).

<sup>2</sup>K. Hiwatashi et al., *Phys. Fluids* **19**, 048103 (2007).

<sup>3</sup>N. Tillmark and P.H. Alfredsson, *J. Fluid Mech.* **235**, 89 (1992).

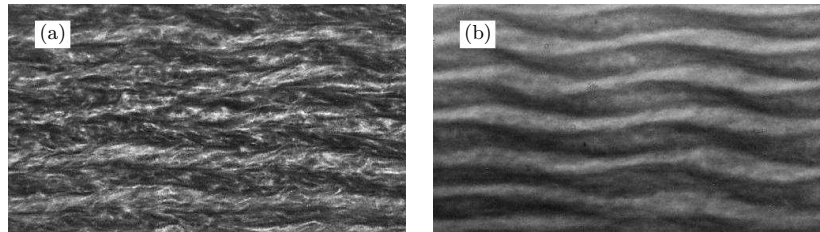


Figure 1: The 3D roll cell in turbulent background, for  $Re = 600$  and  $\Omega = 24.4$ . The exposure time of the camera is set to  $1/25$  sec in (a), and  $3.0$  sec in (b). Each picture displays nearly simultaneous observations in an area of  $24.8 \times 14.3$  cm<sup>2</sup>, i.e.  $52h \times 30h$ .

## Order parameter for turbulent-laminar banded patterns in plane Couette flow

Laurette S. Tuckerman\*, Dwight Barkley†, Olivier Dauchot‡

In large-aspect-ratio plane Couette flow, a pattern of oblique bands, alternating between turbulent and laminar flow, is the intermediate regime between uniform turbulence and simple laminar flow<sup>1</sup>. We have reproduced these patterns numerically<sup>2</sup> and have shown that the mean flows corresponding to these patterns are represented almost perfectly by a single trigonometric function along the direction of the pattern wavevector (which we denote by  $z$ ). In order to quantify the transition between uniform turbulence and turbulent-laminar patterns, we analyze timeseries of the modulus of the Fourier transform of the spanwise velocity along the  $z$  direction. These spanwise spectra show a very prominent feature: the Fourier component  $a \equiv |\text{span}_1|$  corresponding to the pattern wavelength 40 (in half-gaps).

The probability distribution functions of  $a$  for  $Re = 500$ , 410, and 350 are shown on the left part of figure 1. For  $Re \geq 440$ , when the turbulence is uniform, the most probable value is at  $a_{\max} = 0$  and  $\ln p(a) = c_0 + c_2 a^2$ , i.e.  $p(a)$  is Gaussian. As  $Re$  is lowered and a pattern appears,  $a_{\max}$  becomes positive. For  $Re = 350$ ,  $p(a)$  is fit fairly well by  $\ln p(a) = c_0 + c_1 a + c_2 a^2$ .

\*PMMH, ESPCI-CNRS

†University of Warwick

‡GIT, CEA-Saclay

<sup>1</sup>Prigent, Grégoire, Chaté, Dauchot & van Saarloos, *Phys. Rev. Lett.* **89**, 014501 (2002).

<sup>2</sup>Barkley & Tuckerman *Phys. Rev. Lett.* **94**, 014502 (2005); *J. Fluid Mech.* **576**, 109 (2007).

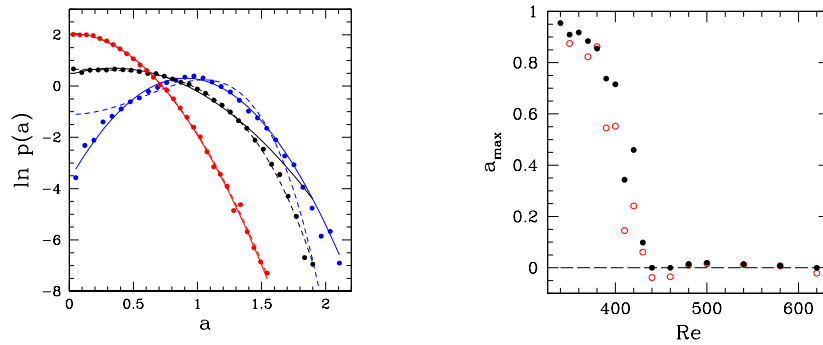


Figure 1: Left: probability distribution functions  $p(a)$  for  $Re = 500$  (red, highest at  $a = 0$ ),  $Re = 410$  (black), and  $Re = 350$  (blue, lowest at  $a = 0$ ). Right: Maximum  $a_{\max}$  of PDFs as a function of Reynolds number (solid black dots)



# Cat's eyes and neutral modes of a two-dimensional vortex

M. R. Turner\*, A. D. Gilbert\*, A. P. Bassom†

This work considers the relaxation of a smooth two-dimensional vortex to axisymmetry, after an instantaneous, weak external strain field is applied. In this limit the disturbance decays exponentially in time at a rate that is linked to a pole of the associated linear inviscid problem (known as a Landau pole). To model a typical vortex distribution that can give rise to cat's eyes, we consider distributions that have a basic Gaussian shape but whose profiles have been artificially flattened about some radius  $r_c$ . A numerical study of the Landau poles for this family of vortices shows that as both the location  $r_c$ , and the thickness of the flat region, are varied so the decay rate of the disturbance moves smoothly between poles as the decay rates of two Landau poles cross.

Cat's eyes which occur in the nonlinear evolution of a vortex lead to an axisymmetric azimuthally averaged profile with an annulus of approximately uniform vorticity, rather like the artificially flattened profiles investigated. It is found that finite thickness cat's eyes can persist (i.e. the mean profile has a neutral mode) at two distinct radii, and in the limit of a thin flattened region the result that vanishingly thin cat's eyes only persist at a single radius is recovered. The decay of non-axisymmetric perturbations to these flattened profiles for larger times is investigated and a comparison with the result for a Gaussian profile is made.

\*Mathematics Research Institute, School of Engineering, Computing and Mathematics, University of Exeter, Exeter EX4 4QF, U.K.

†School of Mathematics and Statistics, University of Western Australia, Crawley 6009, Australia.

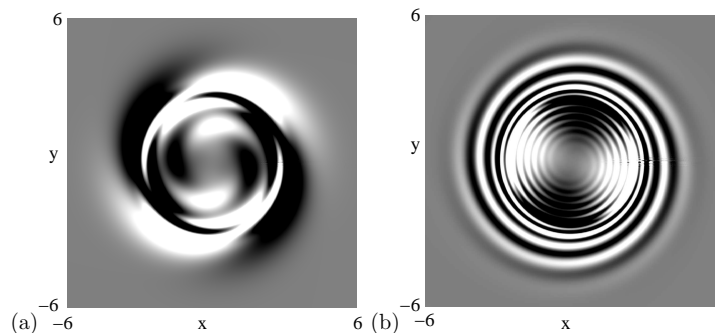


Figure 1: A neutral mode perturbation disturbance, with azimuthal wavenumber 2, on a vortex with a flat region at  $r_c = 2.85$  at (a)  $t = 200$  and (b)  $t = 1000$ . The azimuthal wavenumber 2 structure can be seen to persist for long times in (b) rather than winding up into a fine-scale structure. The scale of this figure is white/black where the vorticity is greater/less than 0.5 times the maximum/minimum vorticity.

## Microfluidics of Cytoplasmic Streaming and its Implications for Intracellular Transport

Idan Tuval\*, Jan-Willem van de Meent\* and Raymond E. Goldstein\*

Ever since Bonaventura Corti's discovery<sup>1</sup> in 1774 of the persistent circulation of the cytoplasm of plant cells, the phenomenon now known as *cytoplasmic streaming* or *cyclosis* has been conjectured to play an important role in metabolism. It occurs in organisms as diverse as amoebae, algae and terrestrial plants, and fungi. In plants it is driven by multitudes of the motor protein myosin moving along bundled actin at the boundary of the cytoplasm, carrying microscopic particles or organelles, and entraining fluid.

In the more than two centuries since its discovery, streaming has frequently been conjectured to aid in transport and mixing of molecular species in the cytoplasm, and, by implication, in cellular homeostasis, yet no theoretical analysis has been presented to quantify these processes. We show by a solution to the coupled dynamics of fluid flow and diffusion appropriate to the archetypal "rotational streaming" of algal species such as *Chara* and *Nitella* that internal mixing and the transient dynamical response to changing external conditions can indeed be enhanced by streaming, but to an extent that depends strongly on the pitch of the helical flow. The possibility that this may have a developmental consequence is illustrated by the coincidence of the exponential growth phase of *Nitella* and the point of maximum enhancement of those processes<sup>2</sup>.

\*Department of Applied Mathematics and Theoretical Physics, University of Cambridge.

<sup>1</sup>B. Corti, *Osservazione Microscopiche sulla Tremella e sulla Circolazione del Fluido in Una Planto Acquaguola*, (1774).

<sup>2</sup>R. E. Goldstein, I. Tuval, and JW. van de Meent, *Proc. Natl. Acad. Sci. (USA)* **in press**, (2008).

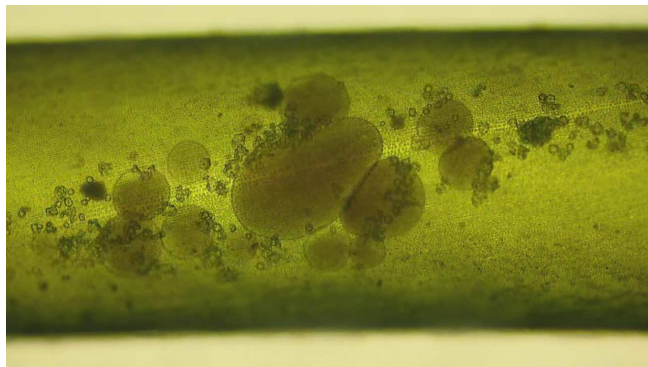


Figure 1: Aggregated globules streaming in the Characean Vacuole.

## Influence of free-stream turbulence scale and shape of leading edge on laminar-turbulent transition in boundary layer

M.V. Ustinov<sup>a</sup>, S.V. Zhigulev, A.A. Uspensky and V.G. Shumilkin

Influence of turbulence scale and shape of leading edge on laminar-turbulent transition in the flat plate boundary layer caused by free-stream turbulence was studied experimentally. It was obtained, that transition at blunt-nosed plate occurs more rapidly compared with transition on sharp-nosed one (see Figure 1). Amplification of pulsations and transition location on the sharp-nosed plate depend substantially on the integral scale of outer turbulence. Pulsations generated by turbulence of similar intensity may amplify and decay in boundary layer depending on turbulence scale. Maximal growth of disturbances was observed for intermediate scale comparable with boundary layer thickness. Transversal scale of boundary layer disturbances is almost independent from the scale of turbulence. Its longitudinal size depends from scale of turbulence and amplitude of pulsations. Based on measurement of probability density functions of velocity fluctuations it was shown, that streaks development become non-linear when their amplitude exceeds  $0.05 u_\infty$ . In the upper part of boundary layer the most probable velocity exceeds mean value and large negative velocity deviations are more probable that positive deviations of equal magnitude. Near the wall the trend is opposite.

The work was supported by Russian Foundation for Basic Researches (Grants No 05-08-50239, 08-01-00729, 08-08-00970)

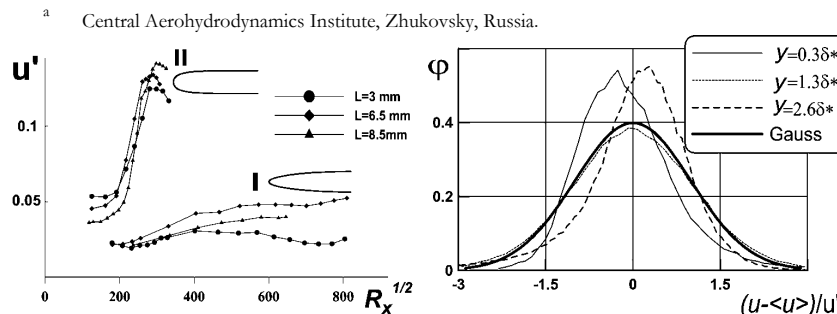


Figure 1: Pulsations in the boundary layer on the plate with sharp (I) and blunt (II) leading edge for  $Tu=1.3\%$  and different turbulence scale in free stream.

Figure 2: P.D.F. of velocity pulsations excited by free-stream turbulence in boundary layer in section where  $u' = 0.074u_\infty$

## Domain decomposition for high Reynolds number near-wall flows

Sergei V. Utyuzhnikov

School of Mechanical, Aerospace & Civil Engineering,  
University of Manchester, Manchester, M60 1QD, U.K.

s.utyuzhnikov@manchester.ac.uk

### Abstract

The modelling of near-wall high Reynolds number turbulent flows is a very time-consuming problem especially in the framework of DNS and LES. A domain decomposition approach is suggested to overcome the problem. The original computational domain is split into a near-wall (inner) subdomain and an outer subdomain. On the base of the Calderon–Ryaben’kii potential theory [1] it is possible to consider the near-wall (inner) problem independently on the external problem. The influence of the inner problem can exactly be represented by a pseudo-differential equation formulated on the intermediate boundary. In 1D case, it leads to the wall functions represented by Robin boundary conditions which can be determined either analytically or numerically [2], [3], [4]. It is important that the wall functions (or boundary conditions) are mesh independent and can be realized in a separate routine. No modification is required in the main code but the change of the boundary conditions. Thus, the original problem can only be solved in the outer domain using URANS or LES with some specific boundary conditions. In contrast to many existing approaches the suggested wall functions are based on a solid theoretical foundation, incorporate all important near-wall physical effects and do not include any free turning parameters. The approach can be extended to multidimensional formulations with nonlocal wall functions [5].

### References

- [1] V. S. Ryaben’kii, Method of difference potentials and its applications, 2002, Berlin, Springer-Verlag.
- [2] S. V. Utyuzhnikov, Some new approaches to building and implementation of wall-functions for modeling of near-wall turbulent flows. *Computers & Fluids*, 2005; **34** (7): 771–784.
- [3] S. V. Utyuzhnikov, Generalized wall-functions and their application for simulation of turbulent flows. *Int. J. Numerical Methods in Fluids*, 2005; **47** (10–11): 1323–1328.
- [4] S. V. Utyuzhnikov, The Method of Boundary Condition Transfer in Application to Modeling Near-Wall Turbulent Flows. *Computers & Fluids*, 2006; **35** (10): 1193–1204.
- [5] S. V. Utyuzhnikov, Robin-type wall Functions and their numerical implementation. *J. Applied and Numerical Mathematics*, 2008 (to appear).

## Dispersion of inertial particles in stratified turbulence

M. van Aartrijk\*, H.J.H. Clercx\*

The turbulent dispersion of particles plays an important role in stratified oceanic and atmospheric flows. In this work we focus on inertial particles and by means of DNS we study a model system: the dispersion of particles in statistically stationary homogeneous stably stratified turbulent flows. A constant, negative linear vertical density gradient is present in the flow, and large-scale forcing is applied to obtain a statistically stationary state<sup>1</sup>. The resulting flow typically displays large horizontal vortical structures and thin, sheared layers in vertical direction.

Three types of particles are tracked in this flow: fluid particles, light particles ( $\rho_p/\rho_f = \mathcal{O}(1)$ ) and heavy particles ( $\rho_p \gg \rho_f$ ). Particle trajectories are obtained from  $\frac{d\mathbf{x}_p}{dt} = \mathbf{u}_p$ . For fluid particles their velocities are derived from cubic spline interpolation of the velocity field at the particle position. The velocities of inertial particles (light + heavy) are obtained by solving the Maxey-Riley equation<sup>2</sup>.

Results for vertical and horizontal single-particle dispersion are shown in the figure. In vertical direction dispersion is suppressed compared to isotropic turbulence. For intermediate times a plateau<sup>3</sup> is found and for long times a transition toward a diffusive regime can be seen. With increasing Stokes number (measure of inertia) the long-time vertical dispersion increases. Horizontal dispersion in stratified turbulence is enhanced compared to isotropic turbulence<sup>1</sup>, and the influence of inertia on this result is limited.

Furthermore, we study the distribution of inertial particles over the domain. It is highly non-uniform, and the distribution reflects the anisotropy of the flow. Also the role of gravitational effects on particle dispersion will be discussed and the importance of the different forces acting on (especially light) inertial particles.

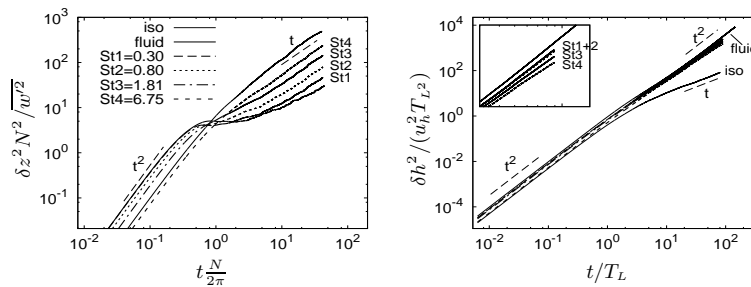


Figure 1: Vertical (left) and horizontal (right) single-particle dispersion as a function of time for buoyancy frequency  $N = 0.31 \text{ s}^{-1}$ . Results for fluid particles, heavy particles (four different Stokes numbers), and isotropic turbulence (graph shifted in the left plot) are shown.

\*Fluid Dynamics Laboratory, Department of Physics, Eindhoven University of Technology

<sup>1</sup>M. van Aartrijk et al., *accepted for publication in Phys. Fluids* (2008).

<sup>2</sup>M.R. Maxey, J.J. Riley, *Phys. Fluids* **26**(4), 883 (1983).

<sup>3</sup>Y. Kimura, J.R. Herring, *J. Fluid Mech.* **328**, 253 (1996).

## Bifurcation characteristics of the swirling annular flow in transition

Venkatesa I. Vasanta Ram\*, Jeanette Hussong<sup>†</sup> and Nikolaus Bleier<sup>‡</sup>

This paper addresses the question of bifurcation characteristics of the class of swirling flows in the annulus between two concentric circular cylinders when this flow is undergoing transition. Swirl in the class of flows of interest is maintained by an axial pressure gradient, acting simultaneously with rotation and axial translatory motion of one of the cylinders. The parameters influencing transition in this laboratory example of a swirling flow are, besides the geometrical parameter  $\epsilon_R = \frac{2H}{R_i + R_o}$  and the Reynolds number  $Re_{xp} = \frac{U_{ref xp} H}{\nu}$ , the swirl and wall-translation parameters  $S = \frac{U_{ref \varphi}}{U_{ref xp}}$  and  $T_{wx} = \frac{U_{ref tw}}{U_{ref xp}}$ . Here  $2H$  is the gap-width,  $R_i$  and  $R_o$  are the radii of the inner and outer cylinders respectively,  $U_{ref xp}$  the characteristic velocity derivable from the axial pressure gradient,  $\nu$  the kinematic viscosity, and  $U_{ref \varphi}$  and  $U_{ref tw}$  are the characteristic velocities due to rotation and of the axial motion of the cylinder respectively. With a judicious choice of the moderate number of parameters, this laboratory example offers the advantage of relative simplicity of analysis while preserving characteristic features of radial distribution patterns of the circumferential velocity (or of the pitch of the helical streamlines) typical of real fluid flows, features known to exercise a decisive influence on the transition characteristics of any swirling flow, hence its research interest. In particular, the nature of transition onset in the limiting cases of zero axial pressure gradient (Taylor-Couette flow) and zero circumferential velocity (plane channel flow), and the flow behaviour subsequent to bifurcation are known to possess saliently different features, and the object of the present work is to examine if and to what extent the relevant feature of the limiting case is modified by the presence of swirl.

We have approached the problem through examining the propagation of disturbances, not necessarily small, to the basic flow in question. Our initial step is formulating the set of equations for disturbances derivable from the equations of motion in which the nonlinear terms have been retained and which reduce to the forms taken for the corresponding problem in the Taylor-Couette flow and the plane channel flow when viewed in terms of suitable variables and the swirl parameter  $S$  is large or small. The next step is then obtaining solutions for the eigenvalue problem that results when this set is linearised for small amplitudes, which we have done by employing the spectral-collocation method using MATLAB. Following this step, we have studied the effect of nonlinearities through setting up amplitude evolution equations by the method described by Huerre and Rossi in <sup>1</sup>. The results draw attention to some salient differences in the effects of nonlinearities on the different flows studied.

\*Institut für Thermo- und Fluidodynamik, Ruhr Universität, Bochum, Germany

<sup>†</sup>formerly at Institut für Thermo- und Fluidodynamik, Ruhr Universität, Bochum, Germany, presently at TU Delft, Netherlands

<sup>‡</sup>formerly at Institut für Thermo- und Fluidodynamik, Ruhr Universität, Bochum, Germany, presently at Institut für Mechanik, Ruhr Universität, Bochum, Germany

<sup>1</sup>Godreche and Manneville. Hydrodynamics and Nonlinear Instabilities. Cambridge University Press, 1998

## Stochastic Coherent Adaptive Large Eddy Simulation (SCALES)

Oleg V. Vasilyev\* and Giuliano De Stefano†

In this talk we discuss the ongoing efforts in the development of the novel methodology called Stochastic Coherent Adaptive Large Eddy Simulation (SCALES).<sup>1</sup> SCALES is an extension of Large Eddy Simulation that uses a wavelet filter-based dynamic grid adaptation strategy to solve for the most *energetic* coherent structures in a turbulent flow field, while modelling the effect of the less energetic eddies. In order to realize the full benefits of the SCALES methodology for highly non-homogenous flows in complex geometries a localized SGS model is required. Two different families of local dynamic SGS model formulations have been explored:

1. Lagrangian Dynamic Model with path-line/tube averaging<sup>2</sup> and
2. Localized Dynamic Kinetic Energy based Models.<sup>3</sup>

The *Lagrangian dynamic path-line/tube averaging* approach consists of Smagorinsky eddy-viscosity model with the dynamic procedure based on statistical moving filtered averages over the trajectory of a fluid particle,  $\mathbf{x} = \mathbf{x}(t)$ :

$$\bar{\mathcal{I}}_i(\mathbf{x}, t) = \frac{1}{T} \int_{-\infty}^t \iiint_D e^{\frac{\tau-t}{T}} G(\mathbf{y} - \mathbf{x}(\tau), \mathbf{x}(\tau)) \mathcal{I}_i(\mathbf{x}(\tau), \tau) d\tau d\mathbf{y},$$

where  $G(\boldsymbol{\xi}, \mathbf{x})$  is the local low-pass filter moving together with fluid particle and  $\mathcal{I}_i$  ( $i = 1, 2$ ) are instantaneous quantities used by the local dynamic model. The *Localized Dynamic Kinetic Energy Models*, of both eddy-viscosity and non eddy-viscosity type, involve the solution of an evolution equation for the additional field variable that represents the kinetic energy associated to the unresolved motions. This way, the energy transfer between resolved and residual flow structures is explicitly taken into account by the modeling procedure without an equilibrium assumption, as in the classical Smagorinsky approach. Both families of local SGS models are explored together with the spatially variable wavelet thresholding strategy to ensure that only a priori specified fraction of subgrid scale dissipation or other statistical quantities of interest are resolved.

A number of numerical experiments for forced and decaying homogeneous turbulence are presented and discussed. Good results are obtained in terms of low order flow statistics, when compared to pseudo-spectral reference solutions, as well as grid compression, which is a fundamental parameter for wavelet-based numerical simulation of turbulence. In contrast to classical large-eddy simulation, where the energetic small scales are poorly simulated, the agreement holds not only in terms of global statistical quantities but also in terms of spectral distribution of energy and, more importantly, enstrophy all the way down to the dissipative scales.

\*Department of Mechanical Engineering, University of Colorado, CO 80309 Boulder, USA

†Dipartimento di Ingegneria Aerospaziale e Meccanica, Seconda Università di Napoli, I 81031 Aversa, Italy

<sup>1</sup>D. E. Goldstein and O. V. Vasilyev, *Phys. Fluids* **16**, 2497 (2004).

<sup>2</sup>O.V. Vasilyev, G. De Stefano, D.E. Goldstein, and N.K.-R. Kevlahan, *J. of Turbulence* in press (2008).

<sup>3</sup>G. De Stefano, O.V. Vasilyev, and D.E. Goldstein, *Phys. Fluids* in press (2008).

## Effect of radiation on temperature profiles in a radiatively participating medium

Mukund V<sup>a</sup> and K. R. Sreenivas<sup>a</sup>

In many problems involving a radiatively participating medium, radiation plays an important role in determining the temperature profile, as well as having a stabilizing effect on unstable layers<sup>1</sup>. Examples include heat transfer in stellar atmospheres, glass melts and vertical temperature profiles over the earth's surface. In the laboratory, for typical convective-conductive set-ups, involving a temperature difference between two parallel plates, such strong effects of radiation on the temperature profile are not seen due to a coupling of the convection-conduction and radiation boundary conditions. For example, in the classic experiments by Gille and Goody<sup>2</sup>, radiative effects resulted in a deviation from the conduction profile of about 0.02 K.

Here, we present results obtained in a laboratory set up where a decoupling of conduction-convection and radiative boundary conditions results in an easily measurable effect of radiation. A schematic of the set up is shown in figure 1. Using this set up experiments can easily be carried out to investigate the radiative effects in a variety of situations. In particular, the problem of radiation stabilization can also be addressed. In figure 2, we show a temperature profile obtained in this set up showing a marked deviation from the linear conduction profile. This was obtained using a (initially) stable stratification in the test section and low temperature for the radiation source. In the full paper, results will be presented showing the dynamical behaviour of such profiles and dependence of the temperature profile on the emissivity of the bottom boundary.

<sup>a</sup> Engineering Mechanics Unit, Jawaharlal Nehru Centre for Advanced Scientific Research, Bangalore INDIA.

<sup>1</sup>V. E. Larson, *Dynamics of Atmospheres and Oceans*, **34**(1), 45, (2001).

<sup>2</sup>J. Gille and R. Goody, *J. Fluid Mech.*, **20**, 47 (1964).

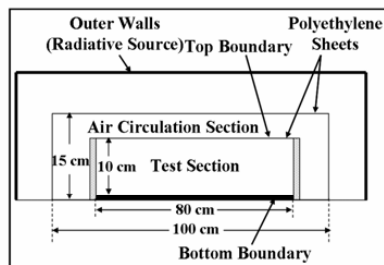


Figure 1: A schematic of the laboratory set up

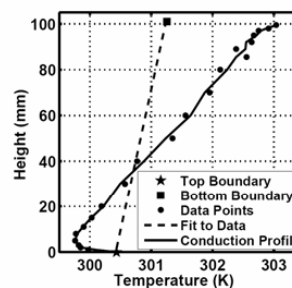


Figure 2: A typical temperature profile showing a marked deviation from linear profile



## Local helical symmetry of vortices created by vortex generators in a low Reynolds number boundary layer

Velte C.M.\*, Okulov V.L.\* and Hansen M.O.L.\*

Stereoscopic Particle Image Velocimetry (SPIV) experiments have been conducted in a low Reynolds number (free stream velocity  $U_0 = 1.0$  m/s) wall bounded flow downstream of vortex generators in order to study the flow processes generated by the devices<sup>1,2</sup>. Vortex generators are small winglets placed on a surface with an angle of attack to the oncoming flow that are designed to redistribute the momentum in the boundary layer to prevent separation. Results show that the vortex generators give rise to longitudinal vortices possessing local helical symmetry. I.e. the following relation is satisfied along lines radially outward from the vortex core.

$$u_z + \frac{r}{l}u_\theta = u_0 \equiv \text{const.}, \text{ or } u_z = u_0 - \frac{r}{l}u_\theta \quad (1)$$

$u_z$  is the axial velocity,  $u_\theta$  is the azimuthal velocity,  $u_0$  is the velocity tangent to the helical line,  $r$  is the radius and  $l$  is the helical pitch. Figures 1 and 2 show results for rectangular devices of height  $\delta$ . Figure 1 shows the mean velocity field in a plane downstream of a vortex generator pair in a counter rotating configuration. In-plane velocities are represented by arrows and the out-of-plane velocities by color contours. Testing of helical symmetry of vortex generator induced vortices is shown in figure 2.

\*Department of Mechanical Engineering, DTU, DK-2800 Lyngby, Denmark.

<sup>1</sup>Velte C.M. et. al., *Environ. Res. Lett.* **3**, (2008) 015006.

<sup>2</sup>Velte C.M. et. al., *Proceedings of The Second Conference on The Science of Making Torque from Wind*, (2007).

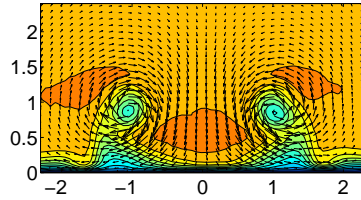


Figure 1: Velocity vector plot of the flow field downstream of a vortex generator pair in a counter rotating configuration. The arrows represent the in-plane velocities and the color represents the out-of-plane velocities. Every fourth vector is shown.

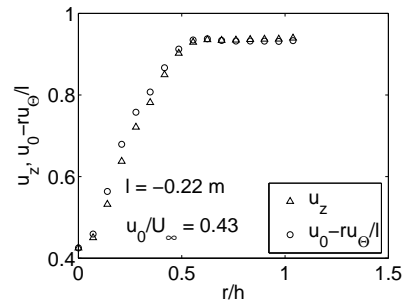


Figure 2: Testing of local helical symmetry of vortex generator induced vortices. The data is taken on the vortex to the right along a line from the center of the vortex and to the right.

## Numerical simulations of high Rayleigh number thermal convection

Roberto Verzicco\*

Thermal convection and it is being investigated for more than a century<sup>1</sup> owing to its relevance in Nature and technology; cooling processes and heat exchangers, geophysical flows and stellar convection are just few examples among many. The basic flow consists of a fluid layer vertically bounded by flat plates at different temperatures, the lower being hotter than the upper. The main control parameters are the Rayleigh ( $Ra$ ), and Prandtl ( $Pr$ ) numbers defined as:  $Ra = g\alpha\Delta h^3/(\nu k)$  and  $Pr = \nu/k$  where  $\Delta$  and  $h$  denote the temperature difference and the separation between the plates,  $g$  is the acceleration of gravity  $\alpha$ ,  $\nu$  and  $k$  are thermal expansion coefficient, kinematic viscosity and thermal diffusivity of the fluid. The output of the flow is the heat transfer between the plates  $\phi$  that, when normalized by the purely conductive value yields the Nusselt number ( $Nu$ ). Unfortunately the Rayleigh number depends on  $h^3$  thus a modest temperature difference in a big system is enough to yield a large Rayleigh number. In contrast experimental set-ups have small dimensions, because of cost and homogeneity constrains, and large  $\Delta$  are used to make up for the small  $h$ . The increase of  $\Delta$  however can not go beyond a limit ( $\alpha\Delta \approx 0.15$ ) in order to retain the Boussinesq approximation thus posing similarity problems<sup>2</sup>. The temperature boundary conditions are another cause of concern because in the ideal problem the temperature is strictly constant over the plates while in the practical realization materials of very high thermal conductivity are involved.

In the last decade, thanks to impressive advances of the CPU architectures and parallel computing, direct numerical simulation (DNS) of the Rayleigh-Bénard problem has become an attractive option<sup>3</sup>: Simulations can avoid the above technological limitations just discussed and provide baseline data with flow details inaccessible in experiments. DNS, on the other hand, requires that all the flow scales up to the smallest are properly resolved by a sufficiently fine grid and that their dynamics is integrated in time by small time steps. Both conditions become more restrictive as the Rayleigh number increases thus posing a limitation to the highest affordable  $Ra$ .

In the talk we present some results of high-Rayleigh number numerical simulations of confined turbulent thermal convection that we compare with analogous experimental investigations. Although experiments and numerics have several analogies there are also important differences that have been analysed by ad hoc numerical simulations. In particular, the effects of the finite thermal conductivity of side wall and plates, the roughness of the latter and the role of the temperature boundary conditions are discussed and, when possible, compared with the literature. Non-Boussinesq effects are also briefly discussed. It is concluded that numerical simulations have become a useful complementary tool to laboratory experiments although there are aspects in which the latter are the only practical possibility.

\*Dipartimento di Ingegneria Meccanica, Università di Roma 'Tor Vergata'.

<sup>1</sup>H. Bénard, *Revue Gen. des Sci. pures et appl.* **11**, 1261 (1900)

<sup>2</sup>E.D.Siggia *Ann. Rev. Fluid Mech.* **26**, 137 (1994)

<sup>3</sup>G. Amati *et al.*, *Phys. Fluids* **17**, 121701 (2005)

## Scaling laws for plane and axisymmetric turbulent boundary layer flows at pressure gradients

Igor Vigdorovich\*

We consider a two-dimensional incompressible turbulent boundary layer flow on a plane profile or an axisymmetric body. We show that in the general case, the turbulent shear stress is a function of the transverse gradient of the rotational part of the longitudinal mean velocity in the boundary layer as well as a functional of the specified potential velocity distribution on the body. This functional, in turn, can be represented in terms of a functional of an invariant curve on a phase plane, which is calculated on the basis of the potential velocity distribution. The closure condition is derived without invoking any special hypotheses on the nature of turbulent motion only from the reasoning of dimensional invariance<sup>1</sup>

The Reynolds-averaged Navier–Stokes equations along with the closure conditions give us a well-posed boundary-value problem for the mean velocity field. We rewrite the equations for a dimensionless stream function  $\Psi(\xi, \eta)$ , where  $\eta$  is the normalized distance from the wall and  $\xi$  is the logarithm of the Reynolds number based on the boundary layer thickness, and seek the solution as  $\xi \rightarrow \infty$ <sup>2</sup>. In this limit process, the derivatives with respect to  $\xi$  can be neglected and in the outer region of the boundary layer, the problem is reduced to an ordinary differential equation for a function related to the velocity deficit. The functional specifying the turbulent shear stress in this equation degenerates to a usual function of two variables.

The proposed mathematical formalism gives us a tool to describe equilibrium, according to Clauser's terminology, boundary layers and near-equilibrium ones.

The problem depends on a single parameter, which can be represented in terms of the well-known Clauser equilibrium parameter  $\Gamma$ . The solution has a singularity as  $\Gamma \rightarrow -\infty$ . In this case, the outer region of the boundary layer takes a two-layer structure. An intermediate region, where the velocity obeys the square root law, emerges above the logarithmic sublayer which is typical of the flows at strong adverse pressure gradients.

A velocity defect law for the outer region of the boundary layer is established in the form

$$\frac{U_e - u}{U_e \sqrt{c_f/2 - \delta^* d \ln U_e / dx}} = f(\Gamma, \eta) + O(\sqrt{c_f}), \quad \Gamma = \frac{2\delta^*}{c_f} \frac{d \ln U_e}{dx},$$

where  $U_e$  is the velocity at the outer edge of the boundary layer,  $c_f$  is the skin friction coefficient, and  $\delta^*$  is the displacement thickness. For both plane and axisymmetric cases, the velocity profiles can be described by the same one-parameter family of curves depending on  $\Gamma$ . In the case of a strong adverse pressure gradient ( $\Gamma \rightarrow -\infty$ ), the velocity profiles collapse to a single universal curve.

A universal friction law for near-equilibrium boundary layers, which makes it possible to represent the skin friction distributions corresponding to different Reynolds numbers and pressure gradients in terms of a function of one variable, is also established.

\*Institute of Mechanics, Moscow State University.

<sup>1</sup>Vigdorovich I. I., *J. Exp. Theor. Phys.* **104**(6), 972 (2007).

<sup>2</sup>Vigdorovich I. I., *J. Appl. Math. Mech.* **69**, 705 (2005).

## Travelling parabolic fronts and hyperbolic waves in unsteady boundary layers.

Gregory Vilenski, Anatoly Ruban\*

Obtained by Prandtl as early as 1905, the unsteady boundary-layer equations play an important role both theoretically and in applications. Dramatic advances in the field over the past decades are reflected in a number of textbooks and reviews<sup>1</sup>. However, despite the existence of exact solutions and success of the similarity techniques<sup>3</sup>, there is still a great need for a systematic theory.

This work is devoted to the mathematical study of 2D unsteady boundary layers. It reports a new nonlinear substitute which leads to the second-order parabolic equation (1) for the streamwise velocity component  $u(t, x, \eta)$  and the linear hyperbolic equation (2) for the unknown “diffusion coefficient”  $\psi(t, x, \eta)$ :

$$\frac{\partial u}{\partial t} + u \frac{\partial u}{\partial x} = -\frac{dp}{dx} + \psi \frac{\partial}{\partial \eta} \left( \psi \frac{\partial u}{\partial \eta} \right), \quad (1)$$

$$\frac{\partial \psi}{\partial t} + u \frac{\partial \psi}{\partial x} = \frac{\partial u}{\partial x} \psi, \quad (2)$$

where  $t$  and  $x$  are the time and the streamwise coordinate. The cross-stream coordinate  $y = \int_0^\eta d\eta' / \psi(t, x, \eta')$ . The pressure gradient  $dp/dx$  is known from the potential flow. The major advantage of this reduction is that it allows for explicit separation of the effects of the nonlinear parabolic front evolution due to the equation (1) from the effects due to the hyperbolic travelling wave (2).

When the “diffusion coefficient”  $\psi(t, x, \eta)$  is non-zero, equation (1) is qualitatively similar to the Burgers’ equation, i.e., the nonlinear steepening of the velocity profile  $u$  is compensated by the viscous diffusion. For  $\psi(t, x, \eta) = 1$  and  $dp/dx = 0$  we find a class of travelling parabolic fronts on which (1) reduces to the Burgers’ equation.

The situation changes dramatically, when  $\psi(t, x, \eta)$  approaches zero. This happens, for instance, if there is a region in the initial velocity profile  $u(t = 0, x, \eta)$ , where  $\partial u / \partial x < 0$ . The negative forcing on the right of (2) then results in the decrease in  $\psi(t, x, \eta)$ , reduction of the viscous term in (1) and the velocity steepening due to the convective term. This leads to the even more negative  $\partial u / \partial x$  and further drop in  $\psi$ . Ultimately,  $\psi(t, x, \eta)$  dips to zero, the nonlinear steepening of  $u$  becomes uncompensated in the absence of the viscous diffusion, and the singularity develops along the surface  $\psi(t, x, \eta) = 0$ .

This scenario is illustrated by a numerical example of a jet-type flow. If  $dp/dx = 0$ ,  $\psi(t, x, \eta)$  approaches zero asymptotically with time. Non-zero  $dp/dx$  either mediates the steepening process of the parabolic front with the singularity occurring at a finite time, or slows it down. Also described are the continuation of the solution beyond the singular wave front  $\psi(t, x, \eta) = 0$ , connections of the proposed approach with the Lagrangian formulation<sup>4</sup> and with the theory of nonlinear parabolic fronts.

\*School of Mathematics, University of Manchester.

<sup>1</sup>N. Riley, *Sci. Progress Oxford* **74**, 361 (1990).

<sup>2</sup>D.R. Telionis, *Unsteady Viscous Flows*. Springer, NY, (1981).

<sup>3</sup>D.K. Ludow, et al *Q. J. Mech. Appl. Math.* **53**, 175 (2000).

<sup>4</sup>L.L. Van Dommelen, *J. Fluid Mech.* **210**, 593 (1990).

## Numerical and experimental modelling of transonic flow in very narrow channels and gaps

J. Vimmr\*, M. Luxa†, O. Bublík\* and R. Dvořák‡

Mathematical modelling and experimental investigation of transonic flow in very narrow channels and gaps is one of the topical and demanding problems of internal aerodynamics. Clearance gaps in screw compressors represent one of many applications. Some experimental and numerical simulations of gas flow through a 2D model of the male rotor-housing gap (the sealing gap between the head of the male rotor tooth and screw compressor housing) have been already made<sup>1</sup>. All of those numerical computations were performed by CFD package Fluent.

In this study, research attention is focused on the modelling of a laminar compressible viscous fluid flow through 2D models of this clearance gap for various widths (100  $\mu\text{m}$ , 200  $\mu\text{m}$ , 350  $\mu\text{m}$  and 500  $\mu\text{m}$ ) and for various pressure ratios ( $p_2/p_{01} = 0.333$ ,  $p_2/p_{01} = 0.25$  and  $p_2/p_{01} = 0.2$ ).

Because of relatively low values of reference Reynolds numbers  $Re_{ref}$  in the considered cases of the male rotor-housing gap with various widths, the laminar flow model described by the non-linear conservative system of the 2D NS equations is assumed for our numerical computations. Making an orientation calculation of the Knudsen number  $Kn$  using  $Kn = (M/Re_{ref})\sqrt{\kappa\pi/2}$ , see<sup>2</sup>, the obtained values for all our computations are always lower than  $Kn < 6 \cdot 10^{-4}$ . Therefore, the fluid can be considered as a continuum and the application of the complete system of the compressible NS equations is acceptable.

The developed numerical code for the solution of the system of the NS equations is based on the cell-centred finite volume method on a structured quadrilateral grid. We consider the flux on a cell face of the control volume to be a sum of inviscid and viscous parts. For the spacial discretization of the inviscid part of the flux, the AUSM flux vector splitting scheme<sup>3</sup> is applied. The first order spatial accuracy of the AUSM scheme is improved to second order by linear reconstruction with minmod limiter. The viscous part of the flux is modeled using a finite volume version of central differences on dual cells. For time integration, we use the two stage second order Runge-Kutta algorithm.

All obtained numerical results are qualitatively compared with the experimental results. The optical and pneumatic measurements on the considered 2D models of the male rotor-housing gap are carried out. The modification of the Schlieren method is used for the flow visualisation.

The numerical and experimental results show that the occurrence of shock waves in the supersonic region of the considered 2D models of the clearance gap is dependent on the gap width and on the pressure ratio  $p_2/p_{01}$ .

---

\*Department of Mechanics, Faculty of Applied Sciences, University of West Bohemia.

†Institute of Thermomechanics, Academy of Sciences of the Czech Republic.

<sup>1</sup>Kauder et al., *Schraubenmaschinen* **8**, 5 (2000).

<sup>2</sup>Karniadakis et al., *Microflows and Nanoflows*. Fundamentals and Simulation (2005).

<sup>3</sup>M.-S. Liou and C.J. Steffen, *J. Computat. Phys.* **107**, 23 (1993).

## Non-modal instability of mixing layer flow

H. Vitoshkin<sup>a</sup>, A.Yu.Gelfgat<sup>a</sup>

Possibility of non-modal growth of three-dimensional disturbances in mixing layer is studied. Considering mixing layer flow in infinite domain we argue that all the eigenvectors of continuous spectrum lay outside the mixing zone. Since such disturbances are not of our interest we take into account the discrete spectrum only (Fig. 1).

The Orr-Sommerfeld and Squire equations are considered in an interval of the width  $2L$  and are discretized using second-order finite differences. The spectrum is calculated using the QR algorithm. After the spectrum is computed and its discrete part is extracted a possibility of non-modal growth is studied as described in [1]. The code is validated by comparison with published results for plane Poiseuille and Couette flows and for boundary layer Blasius profile. A series of test calculations for the mixing layer flow shows that converged and independent on the choice of  $L$  spectrum can be calculated using  $L=20$  and 1000 nodes grid strongly stretched near the symmetry plane.

It is found that a transient energy growth is possible at low Reynolds numbers for which linear modal theory predicts stable flow [2], and optimal disturbance is always three-dimensional. We show additionally how different optimal disturbances having same growth rate can be calculated by different orthogonal decompositions of the Gram matrix (Fig. 2).

<sup>a</sup> School of Mechanical Engineering, Faculty of Engineering, Tel-Aviv University.

1. Schmid P.J., Henningson D.S. Stability and Transition in Shear Flows., Springer, 2001, 572pp.
2. Gelfgat A.Yu. and Kit E. 2006. Spatial versus temporal instabilities in a parametrically forced stratified mixing layer. J. Fluid Mech, 552, 189-227.

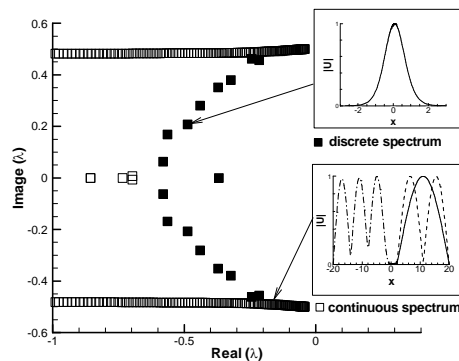


Fig. 1: Spectrum of mixing layer flow for  $Re=100$ ,  $\alpha=0.5$ ,  $\beta=2$  and examples of eigenvectors corresponding to the discrete and continuous parts of the spectrum.

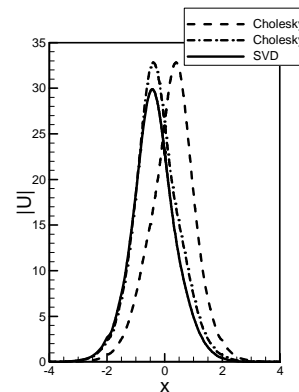


Fig. 2: Different optimal vectors for  $Re=100$ ,  $\alpha=0.5$ ,  $\beta=2$ , calculated by different orthogonal decompositions of the Gram matrix. Amplitude of all vectors grow in  $\approx 200$  times at  $t=4$ .

### Added mass for motion in density-stratified fluids

B. Voisin\*

In a density-stratified fluid, owing to the generation of internal gravity waves, the added mass of a moving body becomes anisotropic and frequency-dependent. Two definitions of added mass, equivalent in a homogeneous fluid<sup>1</sup>, become different: one based on the impulse of the fluid, and the other on the pressure on the body.

We start by deriving a Kirchhoff–Helmholtz integral for internal waves, extending earlier attempts<sup>2</sup>, and deduce from it the relation between the two definitions. We then calculate the motion of the fluid for oscillating spheres and cylinders, extending earlier results<sup>3</sup>, and deduce from it the coefficients of added mass, represented in figure 1(a) and consistent with experiment<sup>4</sup>. At frequencies large compared with the buoyancy frequency the coefficients take their values  $C_\infty$  in a homogeneous fluid (1/2 for the sphere and 1 for the cylinder); at frequencies smaller than the buoyancy frequency they become complex, of real part associated with added mass in the usual sense and imaginary part associated with wave drag. These variations are related by Fourier transformation to the free oscillations, represented in figure 1(b) and consistent with experiment<sup>5</sup>, of the bodies displaced from their neutrally buoyant levels then released.

\*I.E.G.I, CNRS–UJF–INPG, BP 53, 38041 Grenoble Cedex 9, France.

<sup>1</sup>Batchelor, *An Introduction to Fluid Dynamics*, Cambridge University Press, §6.4 (1967).

<sup>2</sup>Miropol'skii, *Izv. Atmos. Ocean. Phys.* **14**, 673 (1978); Simakov, *J. Fluid Mech.* **248**, 55 (1993).

<sup>3</sup>Lai and Lee, *Int. J. Engng Sci.* **19**, 1411 (1981); Hurley, *J. Fluid Mech.* **351**, 105 (1997).

<sup>4</sup>Ermanyuk and Gavrilov, *J. Fluid Mech.* **451**, 421 (2002), **494**, 33 (2003).

<sup>5</sup>Larsen, *Deep-Sea Res.* **16**, 587 (1969); Winant, *Deep-Sea Res.* **21**, 445 (1974).

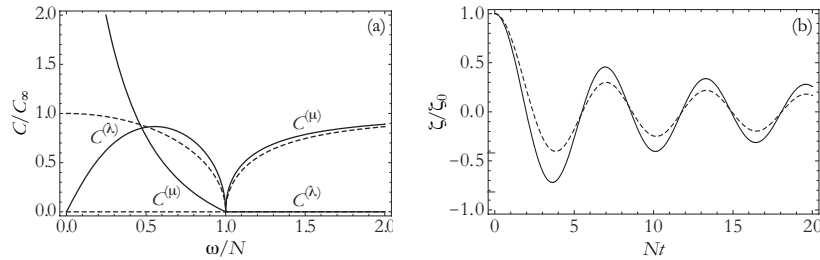


Figure 1: (a) Coefficients of added mass  $C^{(\mu)} = \text{Re } C$  and damping  $C^{(\lambda)} = (\omega/N) \text{Im } C$  of a sphere (solid lines) and horizontal circular cylinder (dashed lines) oscillating vertically at frequency  $\omega$  in a fluid of buoyancy frequency  $N$ . (b) Vertical displacement  $\zeta$  of a sphere (solid line) and horizontal circular cylinder (dashed line) displaced by  $\zeta_0$  from its neutrally buoyant level  $\zeta = 0$  then released at time  $t = 0$ .

## Instabilities and pattern formation in phase-separating fluids

J. Vollmer\*

Orographic precipitation occurs on the windward side of mountains and is caused by the rising air motion of a large-scale flow of moist air across the mountain ridge, resulting in adiabatic cooling and condensation.<sup>1</sup> However, the understanding of the physics involved in the formation of rain droplets is still elusive: the coarsening from nuclei to big droplets is orders of magnitudes faster than expected. We suggest that studies on instabilities and pattern formation in binary fluids, where phase separation is induced by a temperature ramp, can provide fresh insight into the interaction of strong convection, nucleation, coarsening and sedimentation also appearing in clouds.

The thermodynamic equilibrium of the fluid mixtures and their isothermal relaxation to equilibrium after a rapid temperature quench are well understood due to extensive experimental, numerical and theoretical studies in the past decades. In clouds and in many technological processes one is however confronted with phase-separating systems where the temperature is slowly drifting. In this case it is of interest to follow the evolution of the (local) composition also while the temperature is evolving. A simple estimate shows that even for very small drift the composition cannot quasi-statically (in the sense of local thermodynamic equilibrium) follow the change of temperature. The temporal evolution of the composition consequently becomes a problem of pattern formation: For small temperature drift nucleation and convection can arise,<sup>2</sup> and a large drift induces repeated waves of precipitation (fig. 1).<sup>3</sup>

We suggest a minimal theoretical model, which allows us to explicitly calculate the border of stability of the quasi-static phase-separation towards onset of nucleation and convection, and we suggest a mechanism for the repeated waves of precipitation. These theoretical findings are compared to experiments, and their relevance for clouds will be indicated.

\*MPI Dynamics & Self-Organization, Bunsenstr. 10, D-37073 Göttingen, Germany

<sup>1</sup>[http://en.wikipedia.org/wiki/Precipitation\\_\(meteorology\)](http://en.wikipedia.org/wiki/Precipitation_(meteorology))

<sup>2</sup>Cates et al., *Phil. Trans. Roy. Soc. (Lond.) Ser. A* **361**, 793 (2003).

<sup>3</sup>Vollmer et al., *Phys. Rev. Lett.* **98**, 115701 (2007).

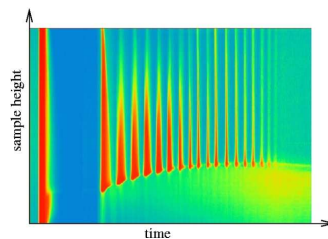


Figure 1: The turbidity of the mixture as a function of time and height. The colors range from blue for a transparent sample to red for a turbid (milk-like) appearance.



### Vortical flow past a semispherical cavity on a plate

G. Voropaev, V. Voskoboinick, N. Rozumnyuk, A. Voskoboinick

The paper presents the findings of the experimental research and numerical modeling of the flow past a semispherical cavity in the surface of a plate. In the experimental part of the research the flow was visualized, and the velocity and pressure fields were measured over the surface. The experimental results have shown that at small Reynolds number a recirculating flow is formed inside the cavity that spans almost the entire cavity volume. At a transient regime, when intensive low-frequency oscillations are observed in the oncoming flow, a large-scale asymmetrical vertical structure develops inside the cavity which breaks down and ejects into the boundary layer. The ejection happens very rarely and irregular. As a rule, the vorticity sense of the ejected vertical structure alternates. At the Reynolds number  $Re_d > 10^4$ , that corresponds to the turbulent regime of flow, a stable pair of longitudinal vortices forms in the cavity wake.

Numerical modeling on the basis of nonstationary Navier-Stokes equations in the velocity-pressure variables also shows that a big-scale vortex core exists inside the cavity, which is symmetrical relative the longitudinal cross-section of the cavity. The vortex core is curved as an arc which legs rest on the side walls in the bottom part and crest is located on the level of the cavity edge. Around the arc crest where the longitudinal vorticity has big magnitude (maximum velocity gradient), there are strong oscillations than leads to rupture of the arc vortex core when it is ejected into the boundary layer, and to formation of two counter rotating longitudinal vortices. Hence the transversal vorticity generated inside the cavity has been transformed into the longitudinal vorticity in the boundary layer on the pane surface behind the cavity. A pair of longitudinal vortices develops downstream.

Thus typical features of the vortical motion inside the cavity have been identified in dependence on the flow regime and geometry. Also revealed are resonance oscillations inside the cavity, ejections of vortical systems from the cavity and their functional dependencies on the flow conditions. Kinematical and dynamical characteristics of the vortical flow in the cavity and boundary layer over the plane surface about the cavity. Controlling the formation and development of the flow structure past a cavity can change the drag of a body and heat transfer over the body surface.

---

Institute of Hydromechanics of the National Academy of Sciences of Ukraine, Kyiv, Ukraine.

### Cross correlations between velocity and pressure fluctuations in the open cavity flow

A.V. Voskoboinick, G.A. Voropaev, A.A. Voskoboinick,  
V.A. Voskoboinick

Results of experimental researches of interaction between velocity and pressure fields which take place inside the streamlined open cavity are submitted. The open cavity had the hemispheric dimple form on a flat plate. Inside the cavity there was a three-dimensional unstable vortical flow on which it was imposed number resonant oscillations. Convection of the vortical structures and the pressure waves inside the cavity is caused formation of the determined and random fluctuations of velocities and pressures both inside the cavity, and on its streamlined surface. Interaction and correlation between unstable velocity and pressure fields which are generated inside a hemispherical cavity was studied by means of cross spectral and correlation analyses. Statistical processing of experimental results allowed to determine space-time dependences between velocity and pressure fluctuations, scales, a direction of movement and convective velocities of the coherent vortical structures forming the cavity flow.

Experimental researches were carried out in an open wind tunnel and in the hydrodynamic channel on hydraulic smooth plates which are settled down along a longitudinal axis of measuring sections of experimental plants. The velocity field was measured hot-wires and hot-film probes. The wall-pressure fluctuations and full pressure fluctuations were measured by small-scale pressure fluctuation transducers. Piezoceramic wall-pressure fluctuation transducers were established a flush with the streamlined cavity and plate surfaces. Hot-wire and hot-film probes, and also transducers of full pressure fluctuations are moved above a streamlined surface by means of the coordinate devices. In measurements up to 16 transducers were simultaneously used. Their electric signals by means of the analog-to-digital converter have acted on the personal computers. The researches in air were carried out for stream velocities from 3 m/s up to 16 m/s, and in water - from 0.03 m/s up to 0.5 m/s for which Reynolds's numbers corresponded  $Re_x=(1...6)*10^5$  and  $Re_D=(3...40)*10^3$ , the relationship of cavity diameter to momentum thickness was  $D/\theta=(20...60)$ .

Spectral dependences of velocity and pressure fluctuations in frequency and wave representations have shown presence of discrete peaks which are answered characteristic features of vortical movement inside a cavity and vortex break up outside a cavity in the boundary layer. It is established, that three-dimensional, wake and shear layer modes of the vortex flow oscillations are generated into the cavity which are caused by hydrodynamic mechanisms of the self-sustained fluctuations. Experimental results have shown enough high correlations between wall pressure fluctuations on a streamlined cavity surface and the deformed plate in various locations inside and close to the cavity. The correlation score between the velocity and pressure fields both near to a streamlined surface and directly on walls of the plate and the cavity is established. The group convection velocity of the vortical structures forming the shear layer makes up 50 % of the flow velocity, and recirculation flow velocity in bottom region of a hemispherical cavity does not exceed 15 % of the flow velocity. On the basis of short-time spectral and correlation analyses are determined non-stationary in time and non-uniform in space characteristics of coherent vortical systems forming vortex flow inside the open cavity and close to it.

---

Institute of Hydromechanics of the National Academy of Sciences of Ukraine, Kyiv, Ukraine.

## The Dynamics of the Swirling Flow with Open Boundaries

Elena Vyazmina<sup>a</sup>, Joseph Nichols<sup>a</sup>, Jean-Marc Chomaz<sup>a</sup> and Peter Schmid<sup>a</sup>

Incompressible swirling flows with open boundaries<sup>1</sup> are studied by means of linear stability analysis and direct numeric simulation (DNS). The effects of viscosity and external axial pressure gradient near critical axisymmetric swirling flow are investigated. In order to have insight to the behaviour of flow near to critical swirl, a small-disturbance analysis<sup>2</sup> has been generalized for the case of two different perturbation parameters. As shown before<sup>3</sup>, a small but finite viscosity breaks the transcritical bifurcation of the solution to the Euler equations at the critical swirl into two solution branches of the Navier-Stokes equations. For the viscous solutions near the critical swirl, a finite gap exists between the two branches, where there is no near-columnar axisymmetric state. The size of this gap is predicted to be proportional to the square root of viscosity<sup>2</sup>. Beyond this range, two equilibrium states may exist with the same boundary conditions. When a sufficient negative external pressure gradient is applied, however, this special behaviour changes into a branch of solutions with no fold allowing access to new stable or unstable branches corresponding to high swirl number, breakdown-free states<sup>4</sup>. Both the asymptotic solutions and the solutions branches obtained from DNS shown on figure 1 match the bifurcation diagrams from previous theoretical and numerical studies and extend their results.

<sup>a</sup> Laboratoire d'Hydrodynamique (LadHyX), Ecole Polytechnique

<sup>1</sup> Vyazmina et al., *Proc. 18<sup>th</sup> Congrès Français de Mécanique* electronic version (2007).

<sup>2</sup> S. Wang and Z. Rusak, *Phys. Fluids*, **9**, 1914 (1997).

<sup>3</sup> S. Wang and Z. Rusak, *J. Fluid Mech.* **340**, 177 (1997).

<sup>4</sup> Vyazmina et al., *Proc. 60<sup>th</sup> APS Meeting, Div. Fluid Dynamics*, **52**, 40 (2007).

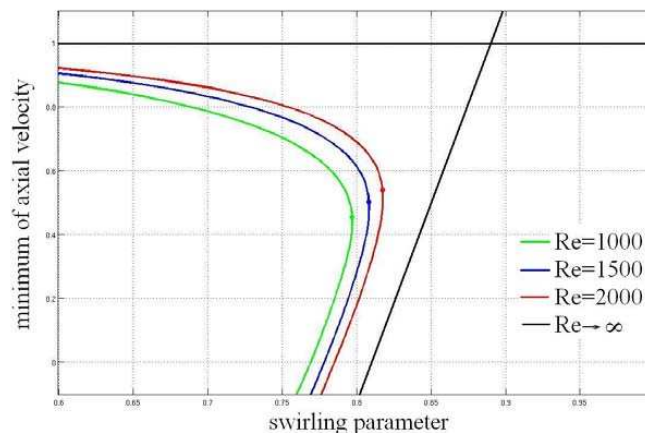


Figure 1: Bifurcation steady state diagram.

## Is turbulence what you think it is?

Fabian Waleffe\*

What is turbulence, really? Yes, it does help mixing milk and coffee, and yes, it is all around, even inside us. A few decades ago, there was hope that ‘Chaos theory’ and ‘strange attractors’ would provide a deeper understanding and better models for turbulence, but that hope remained largely unfulfilled. In practice, the guiding conceptual models of turbulence remain those of Prandtl and von Karman — where turbulence is the random collisions of eddies leading to an ‘eddy-viscosity’, and of Richardson and Kolmogorov — where turbulence is a cascade of energy from large to universal, isotropic small scales. Yet, neither conceptual model fits with the detailed experimental and numerical visualizations of turbulent shear flows that have been made in the last few decades. These visualizations have revealed a series of relatively long-lived ‘coherent structures’. Those observations prompted a search for the mechanisms able to sustain such structures and this has led to the discovery of a multitude of ‘exact coherent states’ — traveling wave and time-periodic solutions of the Navier-Stokes equations that capture all the key elements of observed coherent structures, as well as the statistics of turbulent flows, at least at low Reynolds’ numbers. We will review these recent results and speculate about their theoretical and practical implications.

---

\*Departments of Mathematics and Engineering Physics, University of Wisconsin, Madison, USA.

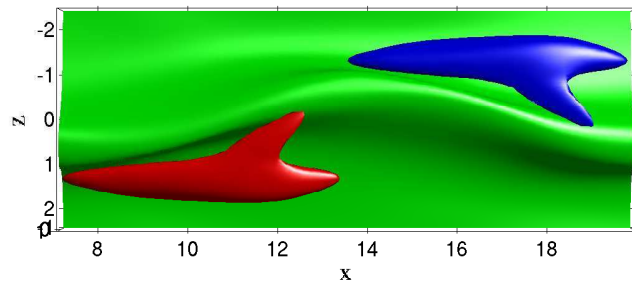


Figure 1: Minimal *Exact Coherent State* in Channel Flow consisting of wavy streaks (green) flanked by staggered quasi-streamwise vortices (red and blue) at scales  $L_x^+ = 274$ ,  $L_y^+ = 44$ ,  $L_z^+ = 106$  [F. Waleffe, *Phys. Fluids* **15**, 1517 (2003).]

### A 3D XFEM/Lagrange Multiplier based approach for fluid structure interaction

Wolfgang A. Wall\*, Ursula M. Mayer\* and Axel Gerstenberger\*

This talk illustrates the ongoing effort to develop an accurate, robust and efficient fixed grid fluid-structure interaction scheme that can be applied to the 3-dimensional interaction of most general structures with incompressible flows. As a core feature, the eXtended Finite Element Method (XFEM) in combination with stabilized, equal order (Q2Q2) elements is used to account for the moving interface on the fixed fluid grid. The commonly used Lagrangean structural formulation is not affected by the extended fluid formulation. Hence, no restrictions exist with respect to possible deformation modes or the choice of structural material models. Along the fluid-structure interface, Lagrange multiplier techniques ensure a consistent coupling between kinematic and kinetic variables of both fields allowing both monolithic and partitioned solution approaches<sup>1</sup>. For the examples given in this presentation, the extended Eulerian fluid field and the Lagrangian structural field are coupled using a partitioned, iterative approach that we have successfully applied to ALE methods before<sup>2</sup>.

While mathematically the extension of the XFEM and Lagrange multiplier formulations from 2d to 3d is straight forward, many challenges have to be met to allow an efficient and accurate 3d implementation. This includes among others, geometric questions like locating the interface on the fixed grids. In this presentation, we sketch our approach of finding and intersecting higher order fluid elements with curved structural surfaces in a parallel environment that is needed for 3-dimensional large scale problems. The closely related problem of properly integrating domain integrals in intersected elements as well as surface integrals along the FSI interface will be discussed as well. Finally, the presentation of fluid and FSI benchmark simulations shall verify the correctness of our approach.

---

\*Chair for Computational Mechanics, Technical University of Munich.

<sup>1</sup>Gerstenberger and Wall, *Computer Methods in Applied Mechanics and Engineering* doi:10.1016/j.cma.2007.07.002, (2007).

<sup>2</sup>Küttler and Wall, *Computational Mechanics* doi:10.1007/s00466-008-0255-5, (2008).

## Motion of a capsule in a simple shear flow: Coupling of finite element and boundary integral methods

Johann Walter\*, Anne-Virginie Salsac\*, Hakim Naceur†,  
Jean-Louis Batoz† and Dominique Barthès-Biesel\*

Bioartificial capsules consisting of an internal liquid protected by a thin membrane have potential therapeutic uses, such as drug delivery in the microcirculation and artificial blood design. Numerical models are necessary to predict their behaviour in the microflow conditions encountered during fabrication and transport. The strong fluid-structure coupling results in large deformations of the membrane due to the viscous flows of the internal and suspending liquids.

The objective of this study is to couple a finite element model that describes the capsule wall in large deformation with a boundary-integral formulation of the Stokes flow equations. In this model, the equilibrium of the capsule is given by the weak form of the virtual work principle. This approach thus differs from the methods commonly used in capsule studies, which rely on the local equilibrium equations. We first implement the method for a hyperelastic membrane.

The membrane is meshed using constant strain triangle elements (CST), with three degrees of freedom (the components of the displacement vector) at the three nodes. At a given time step, the elementary internal force vector is derived from the known displacement vector, using the Neo-Hookean law. The global internal force vector is assembled from the forces calculated on each element. The equilibrium of the membrane, expressed in its weak form, provides the external load on the elements.

The Stokes equations are then solved on the same mesh using a boundary integral method, which computes the velocity at the nodes from the distributed external forces on the membrane. At the following time step, the position of the nodes is updated through Lagrangian tracking by means of a second-order Runge-Kutta integration.

As a benchmark study, we focus on the case of an initially-spherical capsule suspended in a simple shear flow. The Reynolds number is assumed to be zero. The results found are consistent with previous studies.<sup>12</sup> In particular, we find three different types of behaviours depending on the strength of the flow relative to the elasticity of the membrane. For moderate flow strengths, a stationary shape can be attained. For larger values, two tips appear on the membrane along the direction of elongation and the computation does not reach a stable shape. Finally, for small flow strengths, compressive tensions appear and lead to numerical wrinkles, which render the computation unstable.

In conclusion this numerical method solves an explicit fluid-structure interaction problem, which couples a finite element model with a boundary integral method to solve the Stokes equations. The advantage is that we need only to mesh the capsule wall. These preliminary results establish the feasibility of this coupling procedure.

---

\*UMR6600, Université de Technologie de Compiègne.

†Laboratoire Roberval, Université de Technologie de Compiègne.

<sup>1</sup>Lac et al., *J. Fluid Mech.* **516**, 303 (2004).

<sup>2</sup>Ramanujan and Pozrikidis, *J. Fluid Mech.* **361**, 117 (1998).

### Interstitial fluid movement and its interaction with extracellular matrices in tissue deformation

Wen Wang<sup>a\*</sup>

Movement of the interstitial fluid in extracellular matrices not only affects mechanical properties of soft tissues and micro-mechanical environment for cells, but also facilitates the transport of nutrients and the removal of waste products. In tissues where there are limited or no blood supplies, the interstitial fluid is the sole carrier for solute transport. External mechanical loading affects cell function, viability and differentiation *in vivo* and *in vitro* [1, 2]. A quantitative understanding of mechanical stresses on the extracellular matrix and interstitial fluid movement under different loading conditions provides insights into the experimentally observed cell response to mechanical loading. In this presentation, confined tissue indentation is investigated as an example, where a poroelastic theory [3] is used to study the interstitial fluid movement in a tissue sample in a cylindrical chamber. Loading is applied on the top central surface of the specimen by a porous indenter. The interaction between the solid and the fluid is examined under ramp and cyclic loads. Fluid circulation, with opposite directions in the loading and unloading phases in the extracellular matrix is observed. Fluid pressurization arrives at equilibrium much faster than the solid matrix deformation. As the loading frequency increases, the location of the peak pressure oscillation moves closer to the indenter and the magnitude of the pressure oscillation increases. Concomitantly, the axial stress variation of the solid matrix is reduced. Interstitial fluid movement helps to alleviate severe strain of the solid matrix beneath the indenter. Further investigations have been carried out on effects of tissue heterogeneity, e.g. strain-dependent permeability and depth-dependent matrix aggregate module, which better represent tissue properties *in vivo*. Finally, the presentation reveals how dynamic loads affect the transport of solute of different sizes in the matrix. The study demonstrates that cyclic load and the associated interstitial fluid movement promote cell viability in regions of the tissue where solute transport by diffusion alone has limited accessibility. The study gives quantitative insights into the interstitial fluid movement in tissue deformation. It supports the view that dynamic tissue loading is essential to maintain tissue health and provides a strategy in promoting functional tissue repair.

---

<sup>a</sup> Medical Engineering Division, School of Engineering & Materials Science, Queen Mary, London.

<sup>\*</sup> Currently on sabbatical in Department of Chemistry and Chemical Biology, Harvard University and Department of Biological Engineering, Massachusetts Institute of Technology.

<sup>1</sup> P.F. Davies, *Physiol. Rev.* **75**, 519 (1995).

<sup>2</sup> T. Arisaka, *Ann NY Acad Sci.* **748**, 543 (1995).

<sup>3</sup> W. Wang, *J. Biomech. Engng.* **129**, 324 (2007).

**Self-sustained Flow States in a Square Duct**

Håkan Wedin<sup>\*</sup>, Damien Biau<sup>\*</sup>, Alessandro Bottaro<sup>\*</sup> and Masato Nagata<sup>†</sup>

The transition from laminar to turbulent flow in a square duct is an intriguing problem of hydrodynamics. The laminar profile of the flow in a square duct is linearly stable and it is hence conjectured that transition to turbulence is caused by the emergence of finite amplitude solutions of the Navier-Stokes equations. Recent evidence suggests that these alternative solutions, in the form of travelling waves and with no connection to the laminar flow, provide the skeleton around which time-dependent trajectories in phase space can orbit, preventing relaminarization of the flow for long times. Here we present nonlinear solutions or 'self-sustaining-states' to the Navier-Stokes equations, obtained with an approach initiated by Waleffe. The nonlinear flow that emerges when using such states as initial conditions in direct numerical simulations is studied.

---

<sup>\*</sup>University of Genova, Italy.

<sup>†</sup>University of Kyoto, Japan



### Flow instabilities in the wake of the sphere

J.E. Wesfreid<sup>a</sup>, A. Prządka<sup>b</sup>, S. Goujon-Durand<sup>a</sup>, J. Miedzik<sup>b</sup> and K. Gumowski<sup>b</sup>

We will present the results of an experimental investigation in a low velocity hydrodynamical tunnel, about the flow behind a solid sphere, in the range of  $150 < Re < 300$ .

With very well controlled PIV measurements, we characterized the structure of the first mode of the instability which breaks the axisymetry of the flow, producing two counter-rotating longitudinal streamwise vortex.

A special attention is payed to follow the second transition, including by POD decomposition, to an instationnary mode, which shows 3D oscillations of the two trailing vortices. This transition is observed before the hairpins sheddings occurs, at a threshold, lightly smaller that the usual Reynolds number used to characterized the hairpin apparition.

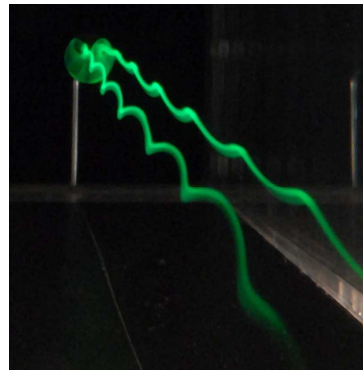


Figure 1: Flow visualisation showing 3D oscillations.

---

<sup>a</sup> PMMH – Ecole Supérieure de Physique et Chimie Ind. de Paris –ESPCI- , Paris, France

<sup>b</sup> Instt. of Aeronautics and Appl. Mechanics, Warsaw Inst. of Technology, Warsaw, Poland

## Oscillations in Flow Through a Flexible Tube

Robert J. Whittaker\*, Sarah L. Waters\*, Oliver E. Jensen†,  
Jonathan Boyle‡ and Matthias Heil‡

Experiments<sup>1</sup> show that steady flow along an elastic-walled tube can become unstable to large-amplitude oscillations involving both the tube wall and the fluid. We describe a theoretical analysis for the cases of axial flow driven by either a steady flux at the downstream end, or by a steady pressure difference between the ends.<sup>2</sup>

Building on 2D work by Jensen and Heil<sup>3</sup> and 3D work by Heil & Waters<sup>4,5</sup>, we consider a prescribed oscillatory wall motion as a first step to understanding the instability. The resulting fluid flow is calculated, and the energy budget is used to infer details about the likely stability of self-excited oscillations. We associate a net flux of energy to the tube walls as an indication that there is free energy available to drive an instability.

We consider small-amplitude high-frequency oscillations in a tube that is long compared with its diameter. This enables the use of long-wavelength approximations, ensures the leading-order problem is linear, and gives a solution structure that has an inviscid core with thin viscous boundary layers adjacent to the oscillating walls.

We construct a general asymptotic solution for an arbitrary initial tube profile and oscillation mode shape. We provide a general result for the critical flow rate at which the mean energy transfer to the walls is zero. This result can be expressed simply in terms of the fluid properties, initial tube shape, and the oscillation frequency and shape. Excellent agreement is found with numerical computations.

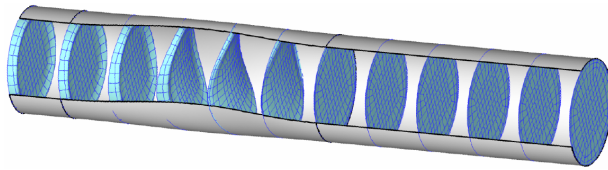


Figure: Numerically computed axial velocity perturbation in a tube with an oscillating wall.

The instability mechanism is found to be essentially unchanged from 2D,<sup>3</sup> and can be explained in terms of energy fluxes. The oscillations in the wall generate axial oscillatory flow, which increases the advective kinetic energy flux at the tube ends. A greater increase at the upstream end leads to a net input of kinetic energy. One third of this input is lost to an increase in work of the steady flow against the steady pressure gradient. If the remaining two thirds can overcome the additional dissipation due to the oscillations then there is free energy to drive the growth of the instability.

\*OCIAM, University of Oxford.

†School of Mathematical Sciences, University of Nottingham.

‡School of Mathematics, University of Manchester.

<sup>1</sup>C.D. Bertram, C.J. Raymond, & T.J. Pedley *J. Fluids Struct.* **4**, 125 (1990)

<sup>2</sup>R.J. Whittaker, S.L. Waters, O.E. Jensen, J. Boyle, & M. Heil *J. Fluid Mech.* In preparation.

<sup>3</sup>O.E. Jensen & M. Heil *J. Fluid Mech.* **481**, 235 (2003)

<sup>4</sup>M. Heil & S.L. Waters *J. Fluid Mech.* **547**, 185 (2006)

<sup>5</sup>M. Heil & S.L. Waters *J. Fluid Mech.* (2008) In press.

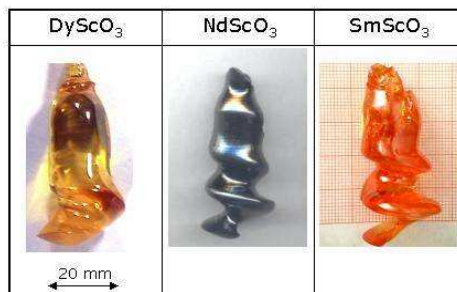
### Hydrodynamic instability during crystal growth from the melt

H. Wilke<sup>a</sup> and K. A. Cliffe<sup>b</sup>

The growth of single crystals from the melt has become a very important technology during the last decade. Crystal quality and yield strongly depend on the fluid motion in the molten crystalline material. The flow is driven by buoyancy and surface tension (Marangoni effect) as well as forced convection (crystal rotation). Oxide crystals with high melting points show a very intensive fluid flow in the melt. The corresponding crystals are excellent candidates for substrates of ferroelectric materials (FRAMs) and are also widely used in solid state lasers. Due to extremely high thermal gradients several types of hydrodynamic instability can occur during the growth process. Spoke pattern on free surfaces and striations frozen in grown crystals are examples of defects that are caused by fluctuations in the melt. However, we will focus on a morphological instability, known as spiral growth that arises via spontaneous symmetry breaking. The figure shows three examples grown at melting temperatures of about 2000°C using the Czochralski method. These high temperatures make internal measurements very difficult and numerical simulation is required to understand what is happening.

In our assumptions about the basic mechanism of spiral growth (corkscrew instability) the hydrodynamic interaction plays a significant role. It turns out that an analysis of the growth stability can be performed in terms of fluid flow behavior using a bifurcation study for the hydrodynamic parameters applied to the Navier-Stokes equations. The bifurcation points can be located exactly using an appropriate extended system of equations and an effective numerical branch following technique. Since the momentum equations are strongly coupled to the thermal conditions, the problem becomes complex and therefore only the most significant parameters have been taken into account.

The approach starts from a 2D axisymmetric solution and considers the stability with respect to the fluid flow interaction of the driving forces. Because the crystal rotation (forced convection) can be controlled from outside the growth process it is used as the primary bifurcation parameter. The results indicate a non-unique solution along the continuation path with typical S-shape and turning/limit points in the technologically relevant range. The location of the symmetry breaking bifurcation is determined by carrying out appropriate eigenvalue calculations that make use of the underlying symmetry to reduce the problem to be discretised from three to two dimensions. Once the bifurcation point has been located approximated, and appropriate extended system can be used to follow paths of bifurcation points. These paths determine the boundaries of parameter space within which the process can take place avoiding the onset of spiral growth and can, therefore, provide practical help to the crystal growers.



Three scandate oxide crystals showing spiral growth

<sup>a</sup> Leibniz-Institute for Crystal Growth (IKZ), Max-Born-Str. 2, 12489 Berlin, Germany

<sup>b</sup> School of Mathematical Sciences, University of Nottingham, UK

## Coherent structures in pipe flows

Ashley P. Willis\* and Rich R. Kerswell†

Laminar pipe flows have been achieved at flow rates at least 50 times beyond those considered to be ‘transitional’ for turbulence. Pipe flow therefore exhibits no relevant linear instability and the only known solutions of the Navier–Stokes equations for pipe flow are unstable. These travelling wave solutions (TWs) typically have only a handful of small unstable eigenvalues, however, suggesting that they may nevertheless be approached transiently. Despite some promising signs that this may indeed be the case, identification of coherent structures in real flows has remained somewhat of a challenge.

Recent theoretical evidence from ‘edge’ simulations<sup>1</sup> (achieved by bisection of nearby initial conditions leading to either turbulence or the laminar flow) and by shooting in opposite directions from TWs<sup>2</sup> suggest that the known solutions lie on a boundary between the laminar and turbulent states in the phase space. While confirming that TWs indeed play an important role in transition, this evidence has been gathered in periodic pipe models, typically of length 5-diameters<sup>3,4</sup>, and their relationship to real spatially-inhomogeneous flows has remained unclear.

In this talk I will discuss evidence of coherence drawn from experiments and via my own previous<sup>5</sup> and new simulations of pipe flow in long domains, full 3-dimensional calculations and from a reduced model<sup>6</sup>, which capture the changing spatial characteristic of pipe flows at different flow rates – localised ‘puffs’ and expanding ‘slugs’.

---

\*LaDHyX, École Polytechnique, Paris, France

†Department of Mathematics, University of Bristol, U.K.

<sup>1</sup>T. M. Schneider, B. Eckhardt and J. A. Yorke, *Phys. Rev. Lett.* **99**, 034502 (2007).

<sup>2</sup>R. R. Kerswell and O. R. Tutty, *J. Fluid Mech.* (2007).

<sup>3</sup>T. M. Schneider, B. Eckhardt and J. Vollmer, *Phys. Rev. E* **75**, 066313 (2007).

<sup>4</sup>Y. Duguet, A. P. Willis and R. R. Kerswell, *arXiv:0711.2175* (2008).

<sup>5</sup>A. P. Willis and R. R. Kerswell, *arXiv:0706.3330* (2008).

<sup>6</sup>A. P. Willis and R. R. Kerswell, *arXiv:0712.2739* (2008).

## Evaporating Droplets

S. K. Wilson\*, G. J. Dunn\*, B. R. Duffy\*, S. David† and K. Sefiane†

A mathematical model for the quasi-steady diffusion-limited evaporation of a pinned droplet which incorporates the dependence of the saturation concentration of vapour at the free surface of the droplet on temperature is formulated and solved both numerically and in various physically realistic asymptotic limits (such as, for example, in the limit of a thin droplet on a thin substrate, and in the limit of a highly insulating substrate). The predictions of the model are found to be in good agreement with the results of recent physical experiments by David et al.<sup>1</sup>, and incorporating two ad hoc improvements to the model (namely, a Newton's law of cooling on the unwetted surface of the substrate and the buoyancy of water vapour in the atmosphere) gives excellent quantitative agreement for all of the combinations of liquid and substrate considered.

\*Department of Mathematics, University of Strathclyde, Glasgow.

†School of Engineering and Electronics, University of Edinburgh, Edinburgh.

<sup>1</sup>S. David et al., *Colloids and Surfaces A: Physicochem. Eng. Aspects* **298**, 108 (2007).

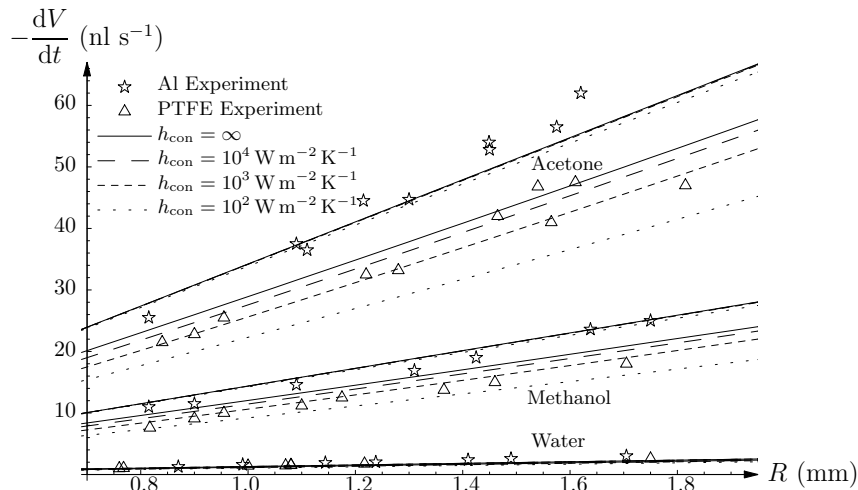
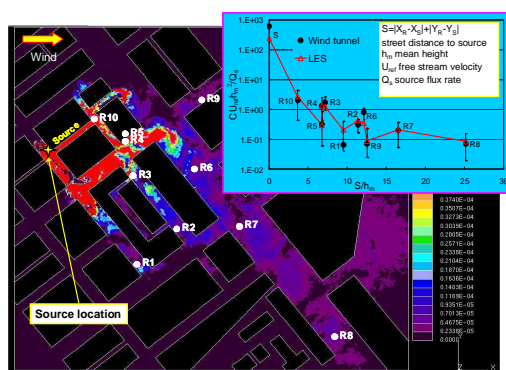


Figure 1: Comparison between experimentally measured and theoretically predicted values of the average total evaporation rate plotted as a function of droplet radius  $R$  for droplets of acetone, methanol and water on aluminium and PTFE substrates including the theoretical predictions for the improved model with a Newton's law of cooling with convective heat transfer coefficients  $h_{\text{con}} = \infty, 10^4, 10^3$  and  $10^2 \text{ W m}^{-2} \text{ K}^{-1}$ .

## Large-Eddy Simulation for Flow and Dispersion in Urban Streets

Zheng-Tong Xie<sup>a</sup> and Ian P Castro<sup>a</sup>

Understanding the mechanisms in flow through arrays of obstacles is directly beneficial to the understanding of building aerodynamics and urban meteorology<sup>[1]</sup>. This paper continues our previous work in this area<sup>[2,3]</sup>. A new inflow technique<sup>[2]</sup> has been applied in LES computations of turbulent flow and point source dispersion over the DAPPLE<sup>\*</sup> field site located at the intersection of Marylebone Rd and Gloucester Place in Central London. The (full scale) computational domain size was 1200m (streamwise) x 800m (lateral) x 200m, with a resolution down to approximately one meter. Attention was focused on two wind directions (-51.4° and -90° with Marylebone Rd direction). Mean velocity and Reynolds stress profiles at fourteen sites are in good agreement with wind tunnel data (EnFlo, University of Surrey). Sensitivity of the turbulence statistics to the wind direction (e.g. -51.4°±1°) has been investigated and numerical experiments, e.g. with varying wind direction, have been performed to investigate the differences between the full scale field experiments and the wind tunnel experiments. Tracers were released simultaneously at different locations upstream of the intersection of Marylebone Rd and Gloucester Pl. Mean concentration and relative concentration fluctuations were compared with data from the wind tunnel experiments. Time series of the different tracers were sampled at some typical stations. Correlations between the time series were studied. Currently more numerical simulations and further analysis are being undertaken and the latest pertinent results will be reported at the conference. Our main conclusion is that LES with the inflow technique is accurate and affordable for simulating flow and scalar dispersion within and above usefully-sized sub-domains of a city region.



Instantaneous concentration patterns at source height (2m in full scale). The inset shows comparisons between LES and wind tunnel (1:200 scale) data for mean, normalised concentration at the ten R-locations indicated.

\* Information on DAPPLE can be obtained at <http://www.dapple.org.uk/>

<sup>a</sup>School of Engineering Sciences, University of Southampton.

<sup>1</sup> Britter & Hanna, *Ann. Rev. Fluid Mech.*, **35** (2003).

<sup>2</sup> Xie & Castro, *Flow, Turbulence and Combustion*, to appear (2008).

<sup>3</sup> Xie et al, *Atmospheric Environment*, **41**, 16 (2007).

**Acknowledgments:** This project was supported by NCAS (NERC), under Grant No. DST/26/39.

## Numerical investigation of internal wave breaking near obstacles

S.N.Yakovenko, T.G.Thomas and I.P.Castro<sup>a</sup>

The objective is to explore the steady internal wave breaking observed in stably stratified flows past obstacles<sup>1</sup>. We use a numerical approach based on well-resolved Navier-Stokes DNS/LES methods using parallel multi-block architecture<sup>2</sup> with the Boussinesq approximation and sponge layer treatment to avoid wave reflection from upstream and downstream boundaries. As a test, good agreement was obtained with data from DNS/experiments of other authors<sup>3</sup> for the velocity and scalar field characteristics in turbulent channel flows with zero, passive and active scalars, for prescribed values of either the scalar or its flux at boundaries. Numerical experiments on the generation, development and breaking of internal waves in a stably stratified medium have been performed and analysed for  $Re_h \sim 4000$ . Internal waves are generated by means of “porous” 2D or 3D cosine-shaped obstacles emulated by insertion of corresponding drag terms into the governing equations.

Wave breaking is captured in the present numerical simulations (Figure 1) and is rather sensitive to particular parameters chosen, e.g. the Reynolds & Froude numbers, grid resolution, boundary conditions, obstacle parameterisation accuracy and geometry. Similar phenomena, followed by a downstream mixed region and an absence of trapped lee waves have previously been observed both in 2D DNS at  $Re_h = 200$  (but with free-slip boundary condition on both bottom and obstacle surface)<sup>4</sup>, as well as in towing tank experiments<sup>1</sup> at much higher  $Re$ . The paper will discuss the dynamics of the breaking regime and the resulting turbulent patch.

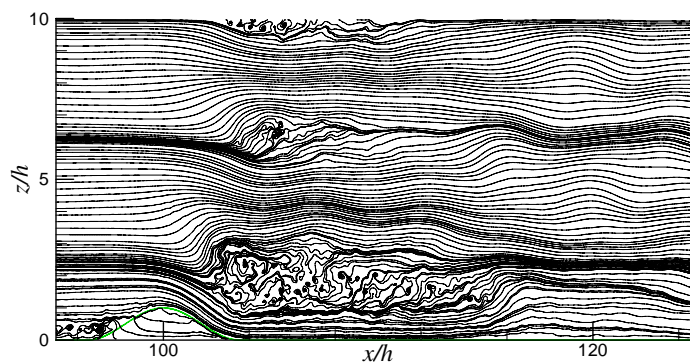


Figure 1: Fluid particle pathlines near 2D obstacle at  $Re_h = 4000$ ,  $F_h = 0.6$ ,  $Nt = 333$ .

<sup>a</sup> AFM Research Group, School of Engineering Sciences, University of Southampton.

<sup>1</sup>I.P. Castro, W.H. Snyder, *J. Fluid Mech.* **255**, 195 (1993).

<sup>2</sup>T.G. Thomas, J.J.R. Williams, *J. Wind Eng. Ind. Aero.* **67&68**, 155 (1997).

<sup>3</sup>N. Kasagi, M. Nishimura, *Int. J. Heat Fluid Flow* **18**, 88 (1997).

<sup>4</sup>Gheusi et al., *J. Fluid Mech.* **410**, 67 (2000).

## Application of the Finite-Volume Method to Fluid-Structure Interaction Analysis

M. N. Yates\*, T. J. Craft\*, H. Iacovides\*

The modelling of flow through constricted tubes is important to develop our understanding of physiological phenomena such as blood flow through stenosed arteries. Numerical simulations of such problems need to address a number of complex factors including: flow separation and re-circulation, transition to turbulence and fluid-structure interaction (FSI) effects.

The aim of this work is to simulate flow through a constricted tube with elastic walls using a coupled, finite-volume based numerical algorithm. On the solid modelling side, an in-house CFD code, STREAM, has been adapted to provide a stand-alone method for solving the steady state elasticity equations in 2D planar and axisymmetric coordinates. A number of validation cases have been carried out and the results have shown good agreement with the analytical solutions. The method has been numerically implemented in such a way as to allow simple coupling with existing in-house CFD codes. In addition to solving elastic body stress analysis problems, the method has proven itself to be capable of producing high quality numerical grids.

On the fluid side, the STREAM code has been used to simulate the flow of water through a rigid walled tube with a sinusoidal stenosis of 89% severity (by area reduction). The results from these simulations have been compared to the experimental data of Young and Tsai<sup>1</sup> to serve as a validation exercise before coupled FSI analyses are performed. Initial attempts using a laminar flow solver were successful only for Reynolds numbers in the range  $10 < Re < 300$ . The loss of convergence coincides with the experimentally observed start of transition. Subsequent simulations using a simple  $k-\epsilon$  turbulence model were successful for Reynolds numbers of greater than 1500. The comparison of pressure drop between the numerical and experimental results is shown in Figure 1. This leaves a range of intermediate Reynolds numbers which pose a significant challenge due to the numerical difficulties associated with accurately predicting transitional behaviour.

Current attention is focused on simulating the intermediate Reynolds number range for the rigid walled case and in coupling the newly developed finite-volume solid solver to the existing CFD code. Once this has been achieved, a fully coupled FSI simulation will be performed and the results will be compared to the experimental data of Stergiopulos<sup>2</sup>.

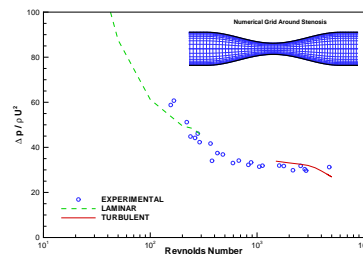


Figure 1: Comparison of pressure drop across the stenosis.

\*School of MACE, University of Manchester.

<sup>1</sup>D.F.Young and F.Y.Tsai, *J. Biomechanics* **6**, 395 (1973).

<sup>2</sup>N.Stergiopulos *et al.*, *Advances in Bioengineering* **BED-26**, 455 (1993).



## Identification of shedding mode II behind a rotating cylinder

I.Yildirim\*, C.C.M. Rindt \*, A.A. van Steenhoven\*, L. Brandt†,  
J. Pralits ‡ and F. Giannetti‡

The 2-D/3-D transition of the flow behind a circular rotating cylinder is investigated experimentally. For the two-dimensional flow at low Reynolds number two shedding modes have been identified previously <sup>1</sup>. Shedding mode I is appearing at low rotation rates whereas shedding mode II is observed around rotation rates of about  $\alpha \approx 5$ , where  $\alpha$  is defined as the ratio between the circumferential velocity at the cylinder surface and the incoming free-stream velocity. Mode I corresponds to the classic von Karman Vortex Street, which becomes asymmetric when the cylinder is rotating and is eventually quenched for values of  $\alpha \approx 2$ . Mode II, conversely, is associated with one-order-of-magnitude lower shedding frequencies and is found only in a narrow range of the parameter  $\alpha$ . The aim of the present work is to experimentally verify the existence of the shedding mode II and compare its main features with those obtained in the numerical studies <sup>2</sup>. For this set of measurements a fixed Reynolds number will be considered,  $Re = \mathcal{O}(100)$ . In addition, the focus of the experiments is to identify the 2-D/3-D transition for the flow around a rotating cylinder, displaying the three-dimensional patterns for the shedding mode II. It is not known at this stage above which Reynolds number the flow around a rotating cylinder can still be considered two-dimensional and whether the critical Reynolds number above which three-dimensional perturbations are amplified is dependent on the rotation rate.

Information about the flow physics is obtained from flow visualization experiments which are performed in a towing tank using electrochemical tin-precipitation method. Flow visualizations are performed in both 2-D and 3-D configurations.

\*Faculty of Mechanical Engineering, Eindhoven University of Technology. The Netherlands

†Linne Flow Center, KTH Mechanics, Sweden

‡DIMEC, University of Salerno, Italy

<sup>1</sup>Stojkovic et. al., *Phys. Fluids*. **15**, 1257 (2003).

<sup>2</sup>Mittal et. al, *J. Fluid Mech.* **476**, 303 (2003).



Figure 1: Flow visualization results for non-rotating circular cylinder at  $Re = 110$ .

## Prediction of bubble sliding and lift-off diameters at the wall in a shear flow

Harunori N. Yoshikawa\*, Catherine Colin\* and Dominique Legendre\*

The modelling of heat and mass transfers in convective boiling requires the determination of the bubble diameter at detachment, the frequency of bubble formation and the density of activated nucleation sites. In this study we are interested in the prediction of two characteristic bubble diameters: the sliding diameter corresponding to the diameter reached by the bubble when it departs from its nucleation site by sliding along the wall and the lift-off diameter when the bubble leaves the wall in the perpendicular direction, directly from the nucleation site (pool boiling) or after a sliding period. These characteristic diameters are often predicted in the literature by using force balance equations for a hemispherical or spherical bubble growing on the wall<sup>1,2</sup>. Predicting the bubble detachment radius is however not an easy task because no expression for the hydrodynamic forces does exist for a growing bubble with a truncated sphere shape in contact with a wall. Moreover the range of bubble Reynolds numbers experienced by a bubble during its growth and after its detachment is very large (10-1000). In most of the studies, the added mass force is estimated from the potential flow theory applied to a hemispherical bubble on the wall<sup>3</sup>, or a spherical bubble growing in the wall vicinity<sup>4</sup>. The expressions used for the drag and lift forces are those for a spherical bubble in an unbounded medium<sup>5</sup>. Another difficulty is the prediction of the capillary force, which depends on the surface contact area between the bubble foot and the wall and also on the contact angle at the triple line solid-liquid-vapour.

Recent results<sup>6</sup> of Direct Numerical Simulation around a hemispherical bubble fixed or sliding at the wall of a shear flow can be used to predict the bubble dynamics at the early stage of its growth. Namely, at the beginning of its growth, the bubble shape, controlled by inertia effects, is hemispherical. Then it has the shape of a truncated sphere during the major part of its growth and becomes more spherical before the lift off. The results concerning the values of the drag and lift forces on a hemispherical bubble are used in a force balance model to estimate the bubble sliding and lift-off diameters on horizontal and vertical walls. The predicted bubble diameters are in good agreement with those measured in different experimental studies<sup>7,8</sup>.

---

\*Institut de Mecanique des Fluides de Toulouse

<sup>1</sup>Thorncroft et al., *Multiphase Science Technology* . **13**, 35 (2001).

<sup>2</sup>Situ et al., *Int. J. Heat Mass Transfer* **48**, 5536 (2005).

<sup>3</sup>Klausner et al., *Int. J. Heat Mass Transfer* **36**, 651 (1993).

<sup>4</sup>Duhar et al., *Heat Mass Transfer* , DOI 10.1007/s00231-007-0287-y (2007).

<sup>5</sup>Legendre & Magnaudet, *J. Fluid Mech.* **368**, 81 (1998).

<sup>6</sup>Legendre et al., *Proc. Roy. Soc.* , to appear (2008).

<sup>7</sup>Zeng et al., *Int. J. Heat Mass Transfer* **36**, 2271 (1993).

<sup>8</sup>Thorncroft et al., *Int. J. Heat Mass Transfer* **41**, 3867 (1997).

## 2D inviscid transonic flow of perfect gas in the vicinity of a curvature-break point on a rigid body surface

D. Yumashev\*, A.I. Ruban\*

This work presents a theoretical analysis of a 2D inviscid transonic flow of perfect gas in the vicinity of a curvature-break point on a rigid body surface. It is assumed that a sonic point coincides with the curvature-break point, and that the oncoming flow is potential. The irregularity in the shape of the surface leads to singular pressure gradients  $dp/dx \sim G_{\mp}(\mp x)^{-1/3}$  upstream and downstream of the point respectively, which follows from an asymptotic analysis of Karman–Guderley equation. In order to obtain amplitude coefficients  $G_{\mp}$  (their signs in particular), one has to employ *hodograph method* and consider the so-called *phase portrait* of the flow.<sup>1</sup>

The upstream and downstream wall curvatures, denoted as  $\kappa_-$  and  $\kappa_+$  respectively, are assumed to be positive for convex walls. The local flow structure obviously depends on the ratio of the curvatures. In the symmetrical case  $\kappa_- = \kappa_+$  (no curvature break) the flow is simply a potential vortex outside a rotating cylinder. Taking this as a starting point, we can increase or decrease  $\kappa_+/\kappa_-$  slightly and work out the local flow. If  $\kappa_+/\kappa_- > 1$ , the flow upstream of the curvature-break point is subsonic and undergoes acceleration to become supersonic on the downstream wall. Both pressure gradients are favorable in this case. If  $0 < \kappa_+/\kappa_- < 1$ , the flow upstream of the curvature-break point is supersonic. However, it does not pass through the *limiting characteristic* and is somewhat inferior, allowing deceleration to subsonic speeds without a shock. Now both pressure gradients are adverse, which is likely to cause the boundary layer separation. These two main regimes are called *subcritical*, and their local flow structure is uniquely defined for a given ratio of the curvatures, being irrelative of the global flow. In particular, the wall pressure gradients can be expressed only via  $\kappa_+/\kappa_-$ .

Nevertheless, certain upstream supersonic flows, called *supercritical*, accelerate to pass through the limiting characteristic. It can be proved that this inevitably leads to a formation of a weak shock attached to the body surface. To obtain the proof, self-similar solutions near the sonic point in hodograph plane are used. The local structure of a supercritical flow, according to our analysis, depends on one extra parameter along with  $\kappa_+/\kappa_-$ , for example the upstream pressure gradient  $G_-$  (which appears to be adverse and stronger compared to the one in subcritical flows). In other words, the local flow is influenced by the global flow pattern. The downstream pressure gradient  $G_+$  can be expressed via  $G_-$  and  $\kappa_+/\kappa_-$  uniquely. Depending on these parameters, the flow behind the shock is either subsonic or supersonic, resulting in adverse or favorable downstream pressure gradients respectively. The ratio of the curvatures may take positive values  $0 < \kappa_+/\kappa_- < \infty$ , and can also be negative, corresponding to a concave downstream wall with  $\kappa_+ < 0$ . However, if  $|\kappa_+/\kappa_-|$  is large enough, the shock over a concave downstream wall becomes detached.

\*School of Mathematics, University of Manchester.

<sup>1</sup>Ruban et al., *J. Fluid Mech.* **568**, 387 (2006).

## **BOUNDARY-LAYER RECEPTIVITY TO EXTERNAL SOUND WAVES**

V.B Zametaev, M.A. Kravtsova

Central Aerohydrodynamics Institute (TsAGI), Zhukovsky, Moscow reg., 140180, Russia

The receptivity problem of laminar separated two-dimensional boundary-layer under influence of external acoustic waves is considered. Basic features of this theory were formulated by Ruban (1984) and then Goldstein (1985), but these investigations were limited by small perturbations of steady parallel flow only. Following these studies, we take flows with separated bubbles and at critical value of basic parameter. The steady flow near a corner point of profile is of considerable interest and a question naturally arises about the sensitivity of the separation bubble inside the boundary layer to external disturbances such as sound waves. Another question arises about the sensitivity of near critical base flow, namely if corner is concave there is a marginal angle which limits existence of such base flow. This fact usually is linked with sudden reconstruction of full flow pattern past a profile. Development of perturbations inside the interaction region may give some answers about the appearance of turbulence. Calculations have shown that linear response of sound wave inside the nonparallel interacting viscous layer contains wave packet of large amplitude. Numerical solution admits resonance frequencies at which amplitude rises very fast. As is usually viscous interaction problem essentially reduces to a study of the lower-deck equations. Present investigation considers also the raising downstream solution in the upper deck of viscous-inviscid interactive region to highlight the growing nature of the Tollmien-Schlichting waves.

## Numerical simulations of the interaction of an array of synthetic jets with a separating boundary layer

Jue Zhou and Shan Zhong

3D unsteady numerical simulations have been conducted using FLUENT to investigate the flow control effectiveness of a spanwise array of five synthetic jets in delaying laminar flow separation over a flap. The test conditions are identical to those used in a water flow experiment which is being undertaken in parallel. The freestream velocity is 0.1m/s and the boundary layer thickness at the location of actuators is about 10mm. The orifice diameter of the synthetic jet actuators is 2mm with a spacing of 6mm between the centres of consecutive orifices. The characteristics of the synthetic jets can be altered by changing the diaphragm vibrating frequency  $f$  and displacement  $\Delta$ . Two cases were selected which produced distinctly different vortical structures and shear stress footprints on the wall; i.e. Case A:  $\Delta=0.0395\text{mm}$ ,  $f=8\text{Hz}$ ; Case B:  $\Delta=0.079\text{mm}$ ,  $f=8\text{Hz}$ .

The formation and evolution of vortical structures and their interaction with the separated boundary layer are examined with the aid of  $Q$ -criterion, as shown in Figure 1. The preliminary results show that vortical structures in Case B are stronger and appear to persist beyond the separated region. The pattern of wall shear stress exhibits multi-peaks in the spanwise direction with the peak value occurring in the middle of adjacent orifices. The pattern of skin friction lines confirms that the array of synthetic jets has resulted in a considerable delay of flow separation in both cases. In comparison, the flow control effectiveness in Case B is greater with the separation bubble being almost completely suppressed in the central region of the array. On the other hand, the flow control effectiveness in Case B seems to decrease more rapidly towards the edge of the finite array due to the stronger interaction between the structures from adjacent orifices. In the following on study, the simulation results will be compared with experimental data and used to help the interpretation of the experimental finding.

School of Mechanical, Aerospace and Civil Engineering, University of Manchester.

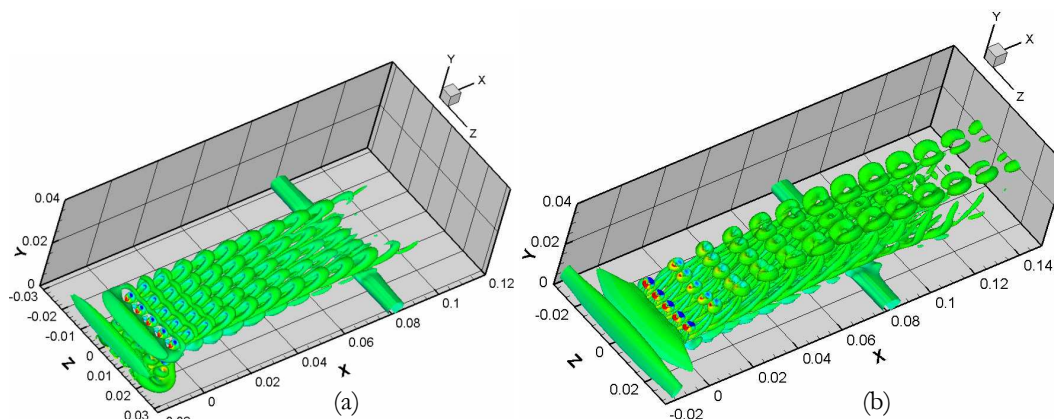


Figure 1 Instantaneous iso-surface of  $Q = 1$  of (a)  $f = 8$ ,  $L = 2$  and (b)  $f = 8$ ,  $L = 4$

## A non-local effect in the spread of a wildfire

Anna Zinoviev<sup>\*</sup>, John Dold<sup>\*</sup>, James Gould<sup>†</sup>

If a bushfire or wildfire is ignited at a point in open vegetation-covered terrain, empirical evidence from extensive field experiments<sup>1</sup> has shown that the head fire (the part that is supported by the ambient wind) does not advance at a constant speed. The overall fireline evolves in an elongated shape that grows in size as the head fire advances and becomes wider, as the flank fires (which spread laterally to the wind) move further apart. Burnt-out vegetation is left behind in the region between the flank fires, the head fire and the backing fire (which spreads against the wind). Only as the width of the head-fire grows increasingly large does its spread-rate approach a limiting value known as the potential spread-rate, for given wind and vegetation conditions.

In fact the phenomenon has a relatively simple physical basis in the action of the fire-plume, which starts off being strongly non-Boussinesq since flames raise the temperature to well above 1000°C. This entrains surrounding air into the plume above every part of the fireline; in effect, the flank fires take the wind out of the head fire. Experiments using strips of vegetation of finite width, so that flank fires were eliminated, did not show a significant effect of head-fire width on the spread rate<sup>2</sup>.

A relatively simple model for the effect focuses on the strongly non-Boussinesq entrainment which, above any section of the fireline, can be taken to be proportional to the intensity of burning at that part of the fire. In turn, the intensity may be taken, in its simplest form, to be proportional to the local rate of spread of the fireline, a description that is most accurate for a nearly steady linear fire front. A more sophisticated approach takes into account the thickness of the fireline which does not change instantaneously as the spread-rate of the leading edge changes<sup>3</sup>. Its response is determined mostly by the time of burning or residence time of the flame in the vegetation.

Taking the suction due to the entrainment to be focused along a path above the fireline, the effect on the ambient air (treated as an ideal fluid) is approximated as a line of sinks of strength proportional to the local fireline intensity. The contribution to air-flow arising from any small part of the fireline then follows an inverse square law so that, after integrating over an entire fireline, the deviation from ambient wind should scale inversely with the overall length-scale of the fire. The spread-rate of the head fire should thus be expected to approach its limiting value inversely with the head-fire width.

Simulations based on this relatively simple model formulation are found to be broadly in line with experimental field observations.

---

<sup>\*</sup>School of Mathematics, University of Manchester, U.K.

<sup>†</sup>Ensis-CSIRO Forest Biosecurity and Protection, Canberra, Australia.

<sup>1</sup>N.P. Cheney and J.S. Gould, *Int. J. Wildland Fire* **5**, 273–247 (1995).

<sup>2</sup>B.M. Wotton, R.S. McAlpine and M.W. Hobbs, *Int. J. Wildland Fire* **9**, 247–253 (1999).

<sup>3</sup>F.A. Albini, *Combustion Science and Technology* **29**, 225–241 (1982).

## The steady propagation of an air finger into a rectangular tube

Alberto de Lózar<sup>\*†</sup>, A. Juel<sup>†</sup> and Andrew L. Hazel<sup>†</sup>

The steady propagation of an air finger into a fluid-filled tube of rectangular cross-section is investigated. We focus primarily on the influence of the aspect ratio,  $\alpha$ , on the flow properties, but the effects of a transverse gravitational field are also considered. The three-dimensional interfacial problem is solved numerically using the object-oriented multi-physics finite-element library `oomph-lib` and the results agree with our previous experimental results<sup>1</sup> to within the  $\pm 1\%$  experimental error, see figure 1.

The pressure drops across the finger tip, wet fractions (the relative quantity of liquid that remains on the tube walls after the propagation of the finger) and finger widths are investigated as function of the aspect ratio. Our results indicate that the system is approximately quasi-two-dimensional when  $\alpha \geq 8$ , when we obtain quantitative agreement with the two-dimensional model of McLean and Saffman<sup>2</sup>.

For  $\alpha \geq 3$  a previously unobserved flow regime has been identified in which a small recirculation flow is situated in front of the finger tip, shielding it from any contaminants in the flow. In addition, for  $\alpha \geq 2$  the capillary number at which global recirculation flows disappear  $Ca_c$  has been observed to follow the simple empirical law:  $Ca_c^{2/3} \alpha = 1.21$ .

<sup>\*</sup>Max-Planck Institute for Dynamics and Self-Organization, Göttingen.

<sup>†</sup>School of Mathematics, University of Manchester.

<sup>1</sup>A. de Lózar et al, *Phys. Rev. Lett.* **99**, 234501

<sup>2</sup>J.W. McLean & P.G. Saffman, *J. Fluid Mech.* **102**, 455

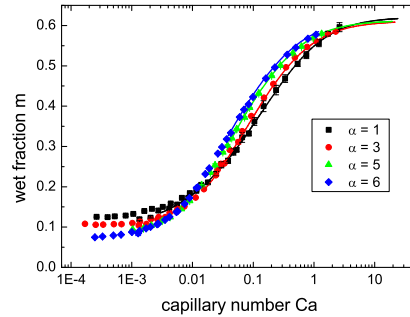


Figure 1: Wet fraction as a function of the capillary number (ratio of viscous to surface-tension forces) in rectangular tubes of aspect ratios  $\alpha = 1, 3, 5, 6$ : numerical study (lines) and previous experiments<sup>1</sup> (points). The gravitational force was included in the simulations for a direct comparison with the experiments.

## Numerical simulation of a confined swirling jet impinging onto a smooth wall\*

M.A. Herrada,<sup>†</sup> J. Ortega-Casanova<sup>‡</sup> and C. Del Pino<sup>‡</sup>

Motivated by its importance for many engineering applications, the behaviour of a swirling jets family emerging from a pipe and impinging into a smooth wall has been analyzed numerically. The wall is placed at a fixed distance and perpendicular to the pipe. We pay our attention to analyze the effect of the level of swirl, characterized by the swirl parameter  $S$ , the concentration of the vortex core (parameter  $\delta$ ) and the core velocity deficiency (parameter  $a$ ) on the structure of the flow. The results on the mechanical behaviour of the flow are obtained for a certain range of Reynolds numbers ( $Re$ ). For the non-swirling jets family with a core velocity deficiency ( $a > 1$ ), the results are in agreement to previous works<sup>1,2</sup>, which predict the appearance of stagnation recirculation bubbles in the impingement area. Our results also show that the introduction of the swirl has an important effect on the impingement process. Depending on the level of concentration of the vortex core and the Reynolds number, there is a critical swirl level above which recirculating vortex breakdown (VB) bubbles appear near the axis. The presence of these bubbles (like the ones that are depicted in figure 1 for three different values of the Reynolds number) produce a strong reduction of the pressure coefficient over the wall and enhance the transition from a steady state to a periodic regime when the Reynolds number is increased.

\*Supported by the European Commission, Grant No. COOP-CT-2005-017725.

<sup>†</sup>Escuela Superior de Ingenieros, Universidad de Sevilla, Camino de los Descubrimientos s/n, 41092, Spain

<sup>‡</sup>E. T. S. Ingenieros Industriales, Universidad de Málaga, Pza. El Ejido s/n, 29013, Spain

<sup>1</sup>A. Rubel, *AIAA journal* **21**, 351 (1983).

<sup>2</sup>D.J. Phares et al., *Physics of fluid* **12**, 20046 (2000).

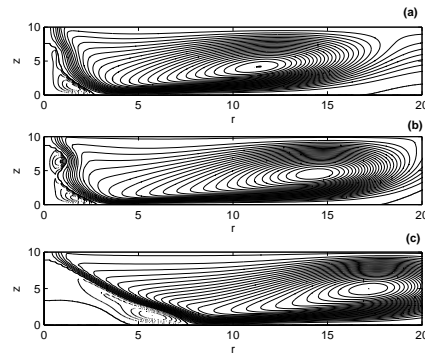


Figure 1: Streamlines for a swirling jet with  $S = 0.6$ ,  $\delta = 0.5$  and (a)  $Re = 100$ , (b)  $Re = 150$  and (c)  $Re = 200$ . Dashed lines represent the vortex breakdown bubble.



## Composite Two-Fluid–PDF Models for Particle Transport in Bounded Flows.

Peter van Dijk\* and David Swailes\*

A limitation of two-fluid models for disperse particle transport in bounded flows is the difficulty of attaching relevant boundary conditions that accurately capture the effects of particle-wall interactions: For all but the simplest cases it is practically impossible to incorporate the effect of such interactions in a physically precise way. The underlying pdf equation<sup>1 2</sup>, that may serve as a master equation to construct the particle continuum equations, still permits natural representations of complex particle-wall interactions<sup>3</sup>. However, the increased dimensionality of phase-space pdf's imposes significant computational demands in numerical treatments. In this respect two-fluid models offer a more natural and efficient framework for studying transport away from boundary regions. This prompts the idea of constructing a methodology that combines the two modelling approaches. In particular it seems natural to decompose the flow domain into two regions as in Figure 1: A near-wall region in which particle transport and wall interactions are modelled within a pdf framework, and a far-field region, in which the particle phase is treated in terms of mean-field properties such a number density  $\rho$ , mean velocity  $\bar{\mathbf{v}}$  and kinetic stresses  $\overline{\mathbf{c}\mathbf{c}}$  ( $\mathbf{c} = \mathbf{v} - \bar{\mathbf{v}}$ ), governed by transport equations within a two-fluid framework.

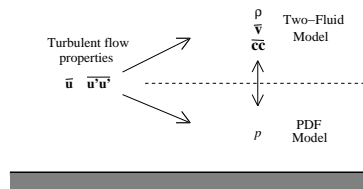


Figure 1: Composite Modelling.

Earlier work<sup>4</sup> showed that constructing composite models requires solving an ill-posed problem. That is the pdf at the interface between the two regions has to be estimated from the mean-field quantities. The employed coupling method, based on the maximum entropy principle, has, however, its limitations.

In the work presented here the continuum equations and the pdf equation are coupled in a more advanced way by introducing an overlap region where both models are solved. The resulting system is treated numerically for different Stokes numbers, and for a range of boundary conditions describing different particle-wall interactions. Discontinuous Galerkin schemes combined with multigrid methods are used to solve the two models efficiently. The effectiveness of this composite approach is assessed by reference to particle tracking simulations and the direct application of pdf models.

\*School of Mechanical and Systems Engineering, Newcastle University.

<sup>1</sup>Reeks, *Physics of Fluids* **3**, 446 (1991)

<sup>2</sup>Swailes, Darbyshire, *Physica A* **242**, 38 (1997)

<sup>3</sup>Swailes, Reeks, *Physics of Fluids* **6**, 3392 (1994)

<sup>4</sup>Van Dijk, Swailes, *Proc. ICMF 2007*, Leipzig, (2007)

## Index

- Abduljalil, A, 1  
Abkarian, M, 2  
Abou El-Azm Aly, A, 3  
Abramyan, A, 4  
Adhikari, D, 5  
Agueda, A, 6  
Akinaga, T, 7  
Akkermans, R, 8  
Alam, M, 9  
Amir, M, 10  
Anand, G, 11  
Andro, J, 12  
Aristov, V, 13  
Auguste, F, 14  
Avila , M, 15  
  
Baffico, L, 16  
Bagheri, S, 17  
Barkley, D, 18  
Baudoin, M, 19  
Bearon, R, 20  
Benilov, E, 21  
Bergognoux, L, 22  
Bienvenue , N, 23  
Billant, P, 24  
Billingham, J, 25  
Blount, M, 26  
Bokhove, O, 27  
Bolanos-Jimenez, R, 28  
Bonfigli, G, 29  
Bontozoglou, V, 30  
Boppana, V, 31  
Borkent, B, 32  
Borodulin, V, 33  
Boronin, S, 34  
Boronska, K, 35  
Bottaro, A, 36  
Boulesteix, S, 37  
Braun, C, 38  
Braun, S, 39  
Brinkmann, M, 40  
Burguete, J, 41  
Busse, F, 42  
Bustamante, M, 43  
  
Cadot, O, 44  
Camarri, S, 45  
Camussi, R, 46  
Cantwell, C, 47  
  
Carrière, P, 48  
Casalis, G, 49  
Caulfield, C, 50  
Cekli, H, 51  
Charru, F, 52  
Chateau, X, 53  
Cherdantsev, A, 54  
Chernoray, V, 55  
Cherubini, S, 56  
Chinappi, M, 57  
Chong, T, 58  
Chung, Y, 59  
Coenen, W, 60  
Conrath, M, 61  
Cookson, A, 62  
Coomaraswamy, I, 63  
Coppola, G, 64  
Culverhouse, N, 65  
  
Dalziel, S, 66  
Daou, J, 67  
Davies, P, 68  
de Lozar, A, 377  
del Pino, C, 378  
Delbende, I, 69  
Delbos, S, 70  
Deloze, T, 71  
Denissenko, P, 72  
Dergham, G, 73  
Derzho, O, 74  
Dias, F, 75  
Dold, J, 76  
Dollet, B, 77  
Domenichini, F, 78  
Donelli , R, 79  
Dowling, A, 80  
Dreyer, M, 81  
Duffy, B, 82  
Duguet, Y, 83  
Duran-Matute, M, 84  
  
Eckhardt, B, 85  
Eggers, J, 86  
Ehrenstein, U, 87  
Ekiel-Jezewska, M, 88  
El Khoury, G, 89  
Ellis, A, 90  
Eloy, C, 91  
Ern, P, 92

- Etling, D, 93
- Fabre, D, 94
- Fallenius, B, 95
- Fedosenko, N, 96
- Feldman, Y, 97
- Fiabane, L, 98
- Figuerola, B, 99
- Florens, E, 100
- Fontane, J, 101
- Foster, M, 102
- Fransson, J, 103
- Gadelha, H, 104
- Gaffney, E, 105
- Gajjar, J, 106
- Gamnitzer, P, 107
- Ganesan, S, 108
- Garbin, V, 109
- Gaudlitz, D, 110
- Gekle, S, 111
- Generalis, S, 112
- German, G, 113
- Geyer, T, 114
- Giannasi, K, 115
- Giannetti, F, 116
- Glangetas, L, 117
- Gobert, M, 118
- Godeferd, F, 119
- Godoy-Diana, R, 120
- Gonzalez, M, 121
- Gordillo, J, 122
- Green, R, 123
- Gregorio, S, 124
- Grossmann, F, 125
- Guazzelli, E, 126
- Guerrero, J, 127
- Guibert, R, 128
- Guyez, E, 129
- Guzanov, V, 130
- Haldenwang, P, 131
- Hall, P, 132
- Hallez, Y, 133
- Hanazaki, H, 134
- Harris, D, 135
- Hazel, A, 136
- Hazewinkel, J, 137
- Healey, J, 138
- Heaton, C, 139
- Heil, M, 140
- Henningson, D, 141
- Henry, D, 142
- Herlina, -, 143
- Herreman, W, 144
- Hewitt, R, 145
- Hill, N, 146
- Hoarau, Y, 147
- Hoepffner, J, 148
- Hof, B, 149
- Hollerbach, R, 150
- Hosoi, A, 151
- Huera-Huarte, F, 152
- Huerre, P, 153
- Hussain, Z, 154
- Iacovides, H, 156
- IJzermans, R, 155
- Ilin, K, 157
- Iovieno, M, 158
- Isa, L, 159
- Itano, T, 160
- Ivanov, A, 161
- Jakobsen, K, 162
- Jalikop, S, 163
- Jensen, O, 164
- Johnson, M, 165
- Juel, A, 166
- Kamp, L, 167
- Kaplanski, F, 168
- Kay, A, 169
- Kazakidi, A, 170
- Kerr, R, 171
- Klaen, S, 172
- Klumpp, S, 173
- Kotouč, M, 174
- Kowalewski, T, 175
- Kuik, D, 176
- Kunnen, R, 177
- Kunze, S, 178
- Kurian, T, 179
- Lane-Serff, G, 180
- Latorre, S, 181
- Lauer, E, 182
- Lauga, E, 183
- Lawrie, A, 184
- Le Bars, M, 185
- Le gal, P, 187
- Le Quiniou, A, 186
- Lechenault, F, 188
- Legendre, D, 189
- Leontidis, V, 190
- Lesshafft, L, 191

- Li, L, 192  
 Li, Y, 193  
 Limat, L, 194  
 Lin, L, 195  
 Lohse, D, 196  
 Lombardi, E, 197  
 Lu, P, 198  
 Lukaschuk, S, 199  
 Luo, X, 200  
  
 Métayer, J, 201  
 Maglio, M, 202  
 Mahalingam, S, 203  
 Mamori, H, 204  
 Manneville, P, 205  
 Marais, C, 206  
 Marchioli, C, 207  
 Marino, L, 208  
 Marmottant, P, 209  
 Marques, F, 210  
 Martinez-legazpi, P, 211  
 Marugan-Cruz, C, 212  
 Matsubara, M, 213  
 Mellibovsky, F, 214  
 Meseguer, A, 215  
 Mestel, J, 218  
 Metzger, B, 219  
 Meunier, P, 220  
 Michaux, G, 221  
 Milne, G, 222  
 Mironov, S, 223  
 Misbah, C, 224  
 Mishra, M, 225  
 Molla, M, 226  
 Momeni, P, 227  
 Monty, J, 228  
 Morad, M, 229  
 Moret-Gabarro, L, 230  
 Motygin, O, 231  
 Moxey, D, 232  
 Muñoz-Esparza, D, 233  
 Mullin, T, 234  
  
 N. H. Gilani, M, 235  
 Nagarajan, K, 236  
 Nagata, M, 237  
 Ni, A, 238  
 Noguchi, T, 239  
 Nouar, C, 240  
 Numano, T, 241  
  
 O Naraigh, L, 242  
 Ohkitani, K, 243  
  
 Okino, S, 244  
 Okulov, V, 245  
 Olsman, J, 246  
 Omranian, A, 247  
 Oron, A, 248  
 Osipstov, A, 249  
 Otto, C, 250  
 Ovarlez, G, 251  
  
 Parras, L, 252  
 Paul, M, 253  
 Payvandi, S, 254  
 Peake, N, 255  
 Pedley, T, 256  
 Peixinho, J, 257  
 Pelekasis, N, 258  
 Pereira, A, 259  
 Pereira, K, 260  
 Perinet, N, 261  
 Petrosyan, A, 262  
 Philip, J, 263  
 Philippe, P, 264  
 Pier, B, 265  
 Pignatell, F, 266  
 Piot, E, 267  
 Podolny, A, 268  
 Poncet, S, 269  
 Pouransari, Z, 270  
 Prakash N., V, 271  
 Pralits, J, 272  
 Pringle, C, 273  
 Prusa, V, 274  
  
 Rees, S, 275  
 Repetto, R, 276  
 Ricco, P, 277  
 Riedinger, X, 278  
 Rigopoulos, S, 279  
 Rioual, F, 280  
 Risso, F, 281  
 Rodriguez Verdugo, F, 282  
 Roig, V, 283  
 Rucklidge, A, 284  
 Rudolf, P, 285  
  
 Salim, A, 286  
 Sandbach, S, 287  
 Sanmiguel-Rojas, E, 288  
 Sasaki, A, 289  
 Satoh, A, 290  
 Scase, M, 291  
 Schall, P, 292  
 Schneider, T, 293

- Schroeder, W, 294  
 Seddon, J, 295  
 Seki, D, 296  
 Seshadhri, S, 297  
 Shaw, S, 298  
 Shi, L, 299  
 Shikhmurzaev, Y, 300  
 Shirai, K, 301  
 Shishkina, O, 302  
 Sidin, R, 303  
 Siggers, J, 304  
 Simanovskii, I, 305  
 Singh, K, 306  
 Smith, D, 307  
 Soldati, A, 308  
 Spazzini, P, 309  
 Speetjens, M, 310  
 Spelt, P, 311  
 Sprittles, J, 312  
 Sreenivas, K, 313  
 Stephen, S, 314  
 Stevens, R, 315  
 Stewart, A, 317  
 Stewart, P, 316  
 Strömgren, T, 318  
 Sugihara-seki, M, 319  
 Sugimoto, T, 320  
 Sun, C, 321  
  
 Tammisola, O, 322  
 Tan, F, 323  
 Taran, E, 324  
 Thess, A, 325  
 Thomas, P, 326  
 Thorn, G, 327  
 Thornton, A, 328  
 Tian, B, 329  
 Tihon, J, 330  
 Tognaccini, R, 331  
 Tordella, D, 332  
 Tropea, C, 333  
 Tsai, P, 334  
 Tsirkunov, Y, 335  
 Tsovolos, D, 336  
 Tsukahara, T, 337  
 Tuckerman, L, 338  
 Turner, M, 339  
 Tuval, I, 340  
  
 Ustinov, M, 341  
 Utyuzhnikov, S, 342  
  
 Van Aartsijk, M, 343  
  
 van Dijk, P, 379  
 Vasanta Ram, V, 344  
 Vasilyev, O, 345  
 Vasudevan, M, 346  
 Velte, C, 347  
 Verzicco, R, 348  
 Vigdorovich, I, 349  
 Vilenski, G, 350  
 Vimmr, J, 351  
 Vitoshkin, H, 352  
 Voisin, B, 353  
 Vollmer, J, 354  
 Voropaev, G, 355  
 Voskoboinick, A, 356  
 Vyazmina, E, 357  
  
 Waleffe, F, 358  
 Wall, W, 359  
 Walter, J, 360  
 Wang, W, 361  
 Wedin, H, 362  
 Wesfreid, J, 363  
 Whittaker, R, 364  
 Wilke, H, 365  
 Willis, A, 366  
 Wilson, S, 367  
  
 Xie, Z, 368  
  
 Yakovenko, S, 369  
 Yates, M, 370  
 Yildirim, I, 371  
 Yoshikawa, H, 372  
 Yumashev, D, 373  
  
 Zametaev, V, 374  
 Zhou, J, 375  
 Zinoviev, A, 376